The Dissertation Committee for Kyle Austin Riding Certifies that this is the approved version of the following dissertation:

Early Age Concrete Thermal Stress Measurement and Modeling

Committee:

Kevin J. Folliard, Supervisor

Maria C. G. Juenger, Co-Supervisor

David W. Fowler

Anton K. Schindler

Harovel G. Wheat

Early Age Concrete Thermal Stress Measurement and Modeling

by

Kyle Austin Riding, B.S.; M.S.E.

Dissertation

Presented to the Faculty of the Graduate School of

The University of Texas at Austin

in Partial Fulfillment

of the Requirements

for the Degree of

Doctor of Philosophy

The University of Texas at Austin

August 2007

Dedication

To my wife Marci, for her patience, support and unconditional love.

Acknowledgements

I would like to thank everyone that contributed to my education and helped make this dissertation possible. I would first like to thank my co-supervisors Dr. Maria C. G. Juenger and Dr. Kevin J. Folliard for their advice, guidance, and complete support of my personal and professional development. I would also like to thank my unofficial co-supervisor Dr. Anton K. Schindler, for his advice, guidance, and help in understanding concrete early age behavior. I am truly grateful for the many hours that they have spent helping me, many of which went beyond what would normally be expected from a supervising professor.

I am also indebted to Jonathan Poole. I have greatly enjoyed and benefited from his creativity, practical knowledge, work ethic, and humor. His help and experience has been essential to this dissertation and to my development. Working with Jonathan has made my time at the University of Texas a truly memorable experience. I would also like to thank Tyler Ley, Jason Ideker, John Hema, Thanos Drimalas, Eric Koehler, and Ryan Chancey. I would like to thank Rachel Lute for her meticulous calorimetry work, Sam Slatnik and Arnaud Thibonnier for their many hours of help performing cracking frame tests, and Carole Cummings for her help in mixing concrete and testing hardened concrete mechanical properties. I would also like thank Cuyler Smith for his endless puns and help in laboratory and field work and Paul Warfield for his help in mixing concrete and performing calorimetry. Jared Whigham and Jason Meadows at Auburn University have also greatly contributed to this dissertation with the rigid cracking frame tests they have performed. The help of Dr. Michael D.A. Thomas from the University of New Brunswick with developing the chloride service life module as part of this dissertation is greatly appreciated. Additionally, the work of Dr. Loukas Kallivokas and Sezgin Kucukcoban on the the concrete elastic stress module is acknowledged. The concrete early age stress analysis would not be possible without their help. I would further like to thank the staff at the Concrete Durability Center Michael Rung, Kerry Rothenbach, Dave Whtiney and Sherian Williams for their help, advice and patience.

I would finally like to thank my family for their years of help, support, love and encouragement. My parents, Don and Donna have been a great source of encouragement and love for me. My mother and father-in-law have also been a great source of encouragement and have leant their listening ears to help my cause. My daughters Rachel and Annie have also been a constant source of unconditional love and motivation for me. I would finally like to thank my sweet wife Marci, for her patience and kindness. Words cannot begin to express all the support and love she has given me.

Early Age Concrete Thermal Stress Measurement and Modeling

Publication No._____________

Kyle Austin Riding, Ph.D.
The University of Texas at Austin, 2007

Supervisors: Kevin J. Folliard and Maria C. G. Juenger

A large amount of heat can be liberated during cement hydration, causing very large temperature increases in mass concrete members. The non-uniform temperature field produced by the cement during curing can cause very high internal stresses that may crack the concrete. Concrete thermal cracking in very large structures is a well-known phenomenon and was studied extensively during the height of dam construction in the United States. In recent years concrete bridge member sizes have increased for structural and aesthetic reasons. Recent problems in San Antonio and Houston, Texas with thermal cracking and very high internal temperatures in mass concrete bridge members has renewed interest in studying early-age thermal cracking and its mechanisms. In order to predict the early-age thermal cracking risk of a concrete member, the temperature history, autogenous shrinkage, modulus development, tensile strength development, coefficient of thermal expansion development, creep behavior, and external restraint conditions must be known. A testing procedure has been developed to measure concrete heat of hydration, mechanical property development, and free shrinkage response at different curing temperatures. The concrete free shrinkage includes thermal and autogenous shrinkage components and is measured using a newly developed free shrinkage testing apparatus. The early age concrete creep is calculated from rigid cracking frame tests performed at different varying temperatures. Trends in early age creep behavior for different concrete mixtures common in mass concrete have been found and are used to develop a statistical model relating concrete mixture proportions and constituent material properties for use in mass concrete thermal stress modeling. The results from the test methods described are used in a new concrete early-age cracking risk and durability software package called ConcreteWorks.

Table of Contents

List of Tables

List of Figures

CHAPTER 1 INTRODUCTION

The transportation system in the United States is facing congestion and rapid deterioration that requires a major reinvestment in our infrastructure. Besides the significant number of new bridges and roads that need to be built to eliminate the estimated $200 billion economic impact caused by delays in our overtaxed infrastructure system (USDOT 2006), an estimated 27% of our existing bridges are deficient and need repaired or replaced (ASCE 2005). It is imperative that our newly constructed infrastructure be durable to avoid in the future this same level of crisis that our society is now facing.

Much of the needed infrastructure will be built of reinforced concrete. Portland cement, the main binder used in concrete, releases heat during hydration. The temperature rise caused by this heat release in the concrete during hydration has in some cases caused premature concrete degradation, reducing the intended service life of the structure. The non-uniform temperature profile that is created in the concrete member will create non-uniform stresses. When the tensile stresses in the member exceed the tensile strength of the member, cracking will occur. Concrete cracking reduces the expected service life of the concrete structure by allowing deleterious agents such as water, carbon dioxide, or chlorides from deicer salts to penetrate into the concrete, which may lead to corrosion of the reinforcing steel.

Thermal stress cracking has been observed for quite some time. A great amount of research on controlling the temperature rise in concrete was done in the 1930’s, during the period of extensive dam building in the United States. Hoover dam was built using the newly developed low heat of hydration cement, 9 in. maximum size aggregates, and embedded cooling pipes. Later on, the use of lower cement contents, supplementary cementing materials, and ice or liquid nitrogen to cool the fresh concrete became common practice in reducing concrete temperature rises (ACI 207 1996). Traditionally, however, the use of temperature control measures was limited to dams, locks, and other very large structures. Temperature control and thermal stress development in smaller concrete members, such as those used in bridge construction, were generally not considered. Recently, as bridge member size has increased for both structural and aesthetic reasons, thermal cracking in a few of these medium sized mass concrete members has caused concern among owners. Figure 1-1 shows an example of early age concrete cracking that occurred recently in a bridge column in Houston, Texas.

Temperature related issues are also a concern in pavements and bridge decks. Because bridge decks are subjected to heat transfer on both the top and bottom sides, they can reach freezing temperatures much sooner than pavements and other structures. Additionally, thermal stresses in bridge decks can be quite significant and cause cracking (Krauss and Rogalla 1996). Pavements may also experience large thermal stresses during curing, as well as delayed setting from cold weather (Schindler 2002).

There has been concern in recent years over cracking from delayed ettringite formation in mass concrete structures. Delayed ettringite formation may occur when the temperature exceeds 70°C (158°F) during the initial concrete curing, causing sulfate to be trapped in hydration products that will be released later to potentially form ettringite in the meso-pores. Expansive pressures may occur in these pores during ettringite formation, causing cracking. Figure 1-2 shows an example of cracking from delayed ettringite formation in a footing.

Besides chlorides penetrating into the concrete through cracks and causing corrosion, chlorides may also penetrate into the concrete through diffusion. Concrete is a porous material, with many interconnected pores that provide the chlorides with a path to the reinforcing steel. Although chloride ingress through diffusion is a slower mechanism than penetration through cracks, it is still very significant and can severely limit a structure's service life. Normally, the reinforcing steel is protected by an iron oxide layer that forms around the steel in the high ph environment of the concrete, dramatically slowing down the corrosion rate to an insignificant level. A sufficient quantity of chlorides at the steel can break down the protective passive layer, initiating corrosion. Corrosion induced concrete damage by chloride ingress is especially prevalent in marine structures, and in bridges and parking structures subject to deicer or industrial salts, (ACI 222 2001).

1.1 Designing for Durability

Concrete materials and construction practices can be optimized to control the concrete temperature development and consequent thermal stresses. Concrete early age cracking occurs when the concrete stress exceeds the strength. Because there are not many reliable, easy to use models available for determining the concrete early age stress development, most strategies focus on indirectly reducing the cracking probability by reducing the temperature difference and gradients in concrete. There are several recommended methods of reducing the temperature development in concrete members, and in many cases a combination of these methods is needed. The first method is to reduce the temperature rise in the concrete by using materials with a low heat of hydration. Many concrete mixtures contain much more cementing material than is necessary, with the ill-informed idea that more must be better. Chemical admixtures and well shaped and graded aggregates can help reduce the mixture water demand and consequently the amount of cementing materials needed to ensure good workability and meet the design compressive strength (Cannon et al. 1992). The total amount of heat released may also be reduced by replacing cement with supplementary cementing materials such as fly ash, ground granulated blast furnace slag, silica fume, metakaolin and other fillers. Additionally, the rate of heat released may also be reduced to limit the temperature rise by using coarser cements, supplementary cementing materials, or chemical admixtures.

Another way to reduce the temperatures developed in concrete structures is to reduce the placement temperature. Cooling the fresh concrete will not only reduce the placement temperature, but also the temperature rise. Because the rate of cement hydration is dependent on the temperature, reducing the placement temperature will slow down the reaction. The apparent activation energy of the cementing materials is a measure of the temperature dependence of this reaction (Poole et al. 2007a). The concrete can be cooled by shading or sprinkling aggregate stockpiles, using chilled mixing water, chipped ice as a mixing water replacement, or by dosing the concrete with liquid nitrogen during mixing (ACI 207 1996).

Concrete can be post-cooled by embedding cooling pipes in the concrete that circulate chilled water. This method of temperature control is very effective at controlling the temperature development on very large structures. Post-cooling can be very expensive, however and is generally not economical, especially in bridge members.

Construction methods may also be altered to reduce the risk of early-age cracking. Formwork insulation may be used to control the temperature gradients in the concrete. They should be left on for a sufficient enough time to avoid rapidly cooling the concrete surface, which thermally shocks the concrete (ACI 207 1996). Insulation is an excellent means of increasing the concrete rate of hydration and strength gain in cold weather, as well as providing protection against freezing the young concrete. The use of insulation should be carefully considered before construction because of the impact on formwork cycling of the longer curing period required. The time of concrete placement may also be changed to minimize fresh concrete cooling costs and minimize stress development.

The risk of concrete corrosion caused by chloride ingress can be minimized by limiting the chlorides that come in contact with the concrete, their rate of penetration, and the amount of chlorides at the steel level that initiates corrosion. Membranes and sealers can be effective in reducing the chloride surface concentration and increasing the amount of chlorides applied that are washed off. The rate of chloride ingress can be reduced by lowering the diffusivity of the concrete through the use of low w/cm concrete and supplementary cementing materials. The chloride threshold level that will initiate reinforcing steel corrosion can be increased by the use of alternative steels, such as stainless steel, and corrosion inhibitors that are mixed in with the concrete before placement.

1.2 Research Scope

In order to improve the durability of our built infrastructure, concrete temperature control and chloride ingress must be considered before the concrete is placed. If cracking occurs, or very permeable concrete is placed, repairs can be very expensive and may delay the project completion. Engineers, contractors, and material suppliers all have equal roles in building a durable structure. They need a tool that can help quantify the concrete performance before placement, so that the concrete may be optimized for durability.

The goal of this study was to develop a software tool that can be used to design concrete mixtures and construction sequences for durability. There are no existing models that can predict the concrete temperature development, thermal stress development and chloride service life in one software package that is user-friendly enough for engineers, contractors, and inspectors to use. The software developed as part of this research project, called ConcreteWorks, can estimate the concrete temperature development for mass concrete, pavements, bridge decks, and precast concrete beams, the early-age cracking probability of several mass concrete members, and the service life for mass concrete and bridge deck members. In order to make the software more user friendly, ConcreteWorks allows the user to select from a set of commonly used concrete member shapes and boundary conditions. This slightly limits the applicability of ConcreteWorks, but was judged a necessary trade-off for the increased user-friendliness.

Several areas where gaps in the state-of-the-art existed and where research was needed were identified. The three main areas of research identified were improvement to concrete temperature modeling, restrained concrete cracking probability quantification, and durability testing, as shown in **Figure 1-3**. The user manual written for ConcreteWorks is included in this dissertation, as it explains much of the background theory and assumptions that were used in developing the software.

The first section of this dissertation is on temperature modeling and contains two chapters, with additional data included in appendices. Chapter 2 discusses the development of a model for calculating the heat transfer boundary conditions for vertical concrete members. Chapter 2 was originally published in volume 104 in the July/August 2007 issue of the American Concrete Institute Materials Journal, and is reprinted in this dissertation with the authorization of the American Concrete Institute. The authors on this paper are Kyle A. Riding, Jonathan L. Poole, Anton K. Schindler, Maria C.G. Juenger, and Kevin J. Folliard. Chapter 3 discusses methods and uses of performing calorimetry performed at the job-site. Chapter 3 was originally published by the American Concrete Institute in the special publication 241 as paper 3 which was originally published in 2007. Chapter 3 is reprinted in this dissertation with the authorization of the American Concrete Institute. The authors on this paper are Kyle A. Riding, Jonathan L. Poole, Anton K. Schindler, Maria C.G. Juenger, and Kevin J. Folliard. A comparison is made between calorimetry performed at the laboratory to that in the field to investigate the effects of climate controlled conditions on the calorimeter, batch variability, and to concrete batches made from materials collected from field sites to and mixed in small laboratory mixers to that of concrete delivered on-site in ready mix concrete trucks. Appendix A contains nine technical memos that describe the field site investigations performed to collect temperature data from actual concrete members for use in calibrating the temperature prediction module in ConcreteWorks. Appendix B contains a technical memo on how to make temperature sensors with internal dataloggers that can be embedded in concrete and obtain these field data.

The second section in this report is the research performed to quantify concrete material stress relaxation behavior and cracking probability. Chapter 4 discusses the development of a combination of tests that together allow the concrete stress relaxation to be determined. Chapter 5 discusses experiments performed in the rigid cracking frame that were used to qualitatively assess the relative cracking potential of bridge decks due to thermal stresses using different concrete materials and placement times. Chapter 6 shows the development of an early age concrete creep model that is based on the mixture proportions and the cementing material properties used. The early age creep model used is a modified version of the Linear Logarithmic Model developed by Larson (2003) to include the effects of temperature on early age concrete creep. A statistical model is then developed that relates the mixture proportions and cement material properties to the early age concrete creep parameters using the Modified Linear Logarithmic Model obtained from rigid cracking frame testing and the concrete elastic modulus development. Chapter 7 discusses a simple allowable stress method for determining the probability of concrete cracking from the stress-to-strength ratio.

The third, durability testing, section of this dissertation centers around the development of a simplified version of the rapid chloride permeability test (RCPT) described in ASTM C 1202, and is explained in chapter 8. The RCPT method was simplified by performing the ASTM C 1202 testing on an uncut, laboratory cured specimen taken directly from the 100% relative humidity chamber. A correlation between the standard RCPT test and the simplified version was developed. It is hoped that this test may in the future be used as a simple, rapid, and cheap concrete quality control test.

The final section of the dissertation is made up of the ConcreteWorks user manual. The background theory, assumptions made, and model limitations of

ConcreteWorks are described in chapter 9. Appendix C is also part of the ConcreteWorks user manual, and describes how to operate the software.

Chapter 10 contains a short conclusion and summary of the work performed, and suggestions for future of research and improvements to ConcreteWorks.

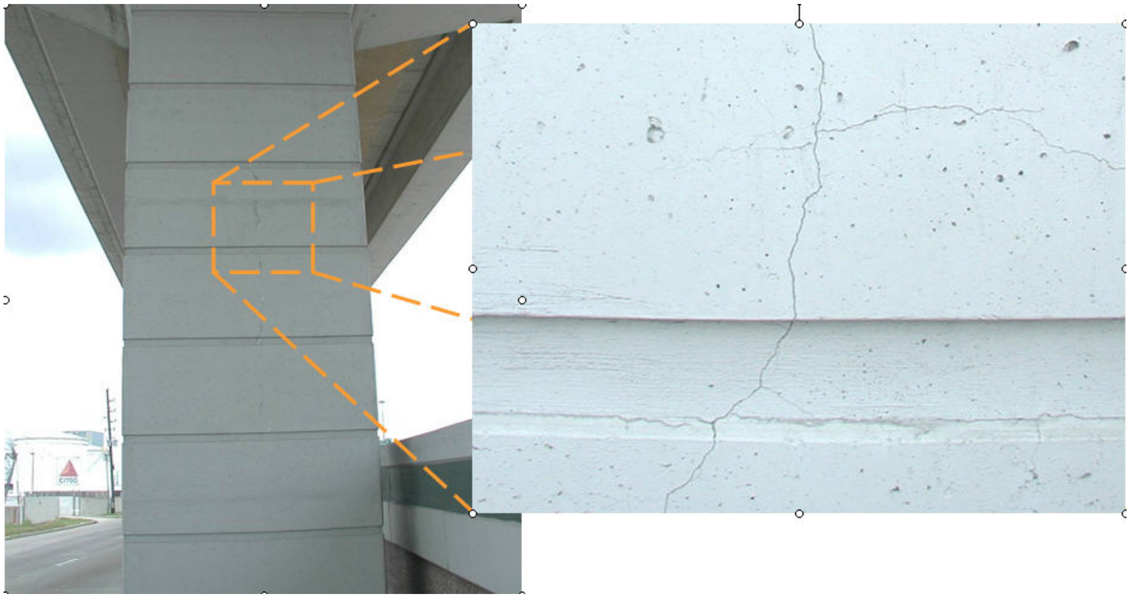

Figure 1-1 – Early-age cracking in a bridge column in Houston, Texas (Courtesy of J.C. Liu, TxDOT)

Figure 1-2 - Cracking caused by delayed ettringite formation in a footing (Picture courtesy of Ralph Browne, TxDOT)

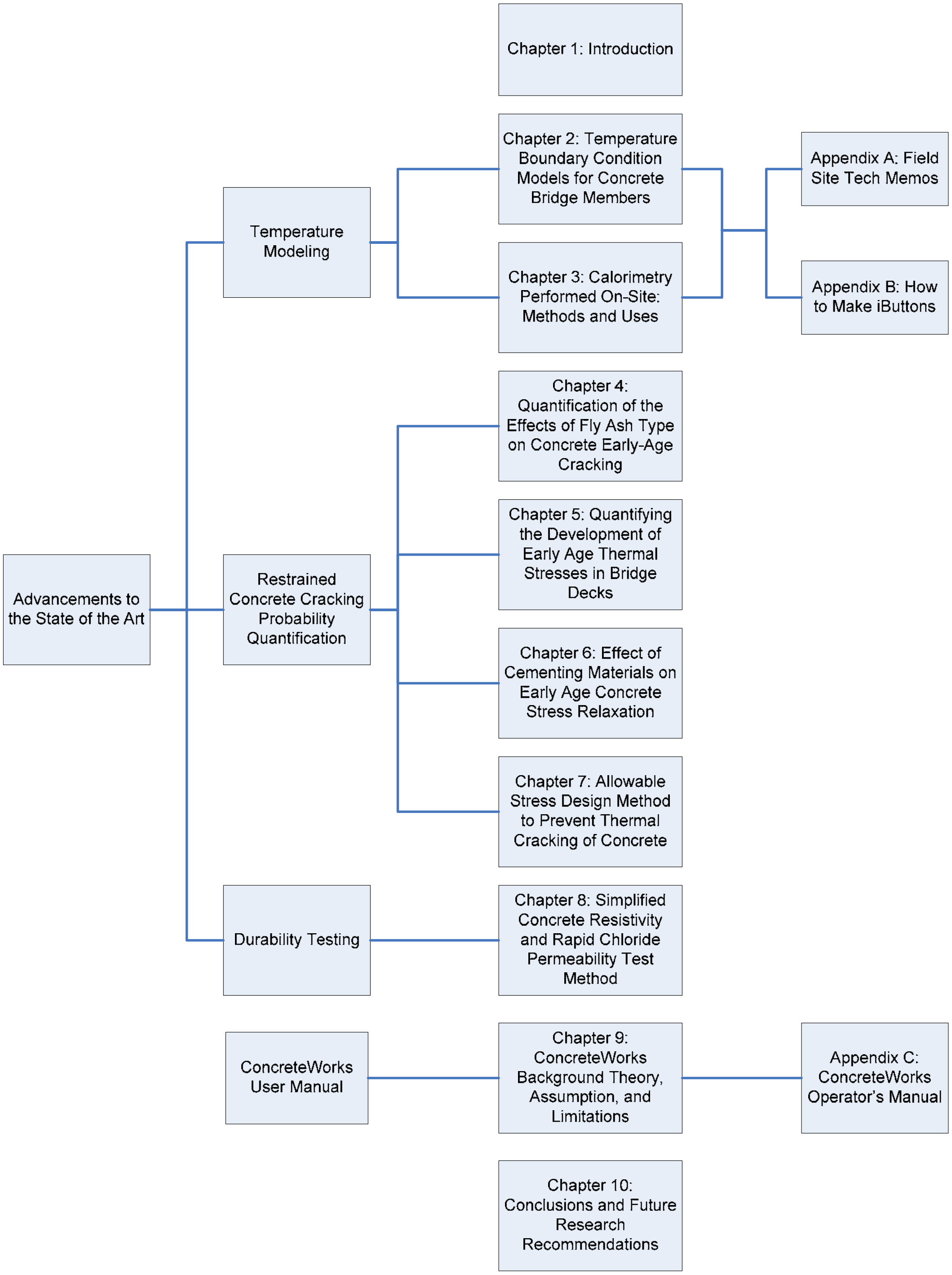

Figure 1-3 - Dissertation Outline

CHAPTER 2 TEMPERATURE BOUNDARY CONDITION MODELS FOR CONCRETE BRIDGE MEMBERS

The temperature development of mass concrete elements is strongly dependent on constituent materials and mixture proportions, as well as the formwork type, geometry, and environmental conditions. This paper presents a method to account for the effects of convection, radiation, and shading on the surface temperature of mass concrete. Solar radiation, atmospheric radiation, surface-emitted radiation, and formwork radiation exchange were considered. Wind speed, ambient temperature, and surface roughness were included in the convection model. The model described was incorporated into a mass concrete temperature prediction model. The predicted temperatures were then compared to measured near-surface concrete temperatures. The ability of the model to predict the maximum temperature and maximum temperature difference were also examined. The results show that the model accurately estimates the near-surface concrete temperatures, the maximum temperature, and maximum temperature difference of the 12 concrete members instrumented.

2.1 Introduction

Large quantities of heat are released during the exothermic hydration process in concrete, which in turn raises the concrete temperature. In recent years, larger bridge members, increased cement fineness, and greater amounts of cement in concrete mixtures have increased the temperature rise in concrete bridge members. Concern over thermal cracking and delayed ettringite formation (DEF) (Day 1992) in these members has spurred interest in developing temperature prediction models for mass concrete bridge members.

Heat transfer and temperature prediction of a concrete member involves a number of interrelated mechanisms, none of which has a closed-form solution. Each of these mechanisms must be modeled, and a solution determined iteratively. The analysis may be divided into three main components: the heat generation from the hydration process, the heat conduction in the concrete, and the heat exchanged at the boundary of the structural element. This paper will focus on the heat exchange with the environment and boundary conditions as they pertain to mass concrete elements.

There is a body of literature (Schindler and van Breugel 1998) that deals with methods to account for the heat generated by cement hydration. The most commonly used method combines the equivalent age maturity method and an exponential degree of hydration curve to characterize the rate of heat generation. This method is well documented in other papers, and is shown in Equation 2-1 (Schindler and van Breugel 1998).

$$Q_h(t) = H_u \cdot C_c \cdot \left(\frac{\tau}{t_e}\right)^{\beta} \cdot \left(\frac{\beta}{t_e}\right) \cdot \alpha_u \cdot \exp\left(-\left[\frac{\tau}{t_e}\right]^{\beta}\right) \cdot \exp\left(\frac{E}{R}\left(\frac{1}{273+T_r} - \frac{1}{273+T_c}\right)\right) \quad \textbf{Equation 2-1}$$

where Q_h is the rate of heat generation (J/hr/m^3), H_u is the total amount of heat generated at 100% hydration (J/kg), C_c is the total amount of cementitious materials (kg/m^3), τ is the hydration time parameter (hrs), t_e is the concrete equivalent age at the reference temperature (hrs), β is the hydration slope parameter, α_u is the ultimate degree of hydration (unitless), E is the activation energy (J/mol), R is the universal gas constant (J/mol/K), T_r is the reference temperature (°C), and T_c is the concrete temperature (°C).

The conductive properties of concrete are well covered in literature. Heat conduction in the concrete is dependent on the moisture content, density, specific heat, and thermal conductivity of the concrete. The specific heat and thermal conductivity of concrete is dependent on the mixture proportions, temperature and degree of hydration of the concrete (van Breugel 1998). Aggregates play an especially important role in the conductive properties of concrete.

The discussion of boundary conditions in literature is less thorough. Most of the work reported has been done on horizontal surfaces, mainly bridge decks and pavements (Wojcik and Fitzjarrald 2001, Wojcik Et al. 2003, Hermansson 2001). The boundary conditions of the concrete member are the most complex and variable portion of the heat transfer analysis. The modeling of the concrete heat exchange with the environment is dependent on the surrounding features such as walls and ground surfaces, formwork, curing blankets, ambient conditions, orientation of the element, and heat conduction from the concrete interior (Gilliland and Dilger 1997). Radiation and convection are especially dependent on these parameters. A review of the theory behind these heat transfer mechanisms is thus warranted and is provided in this paper.

Radiation exchange with the environment involves incoming and outgoing components. Solar radiation, radiation from the atmosphere, radiation from the surrounding surfaces, and radiation from the formwork bracing can all impact the surface temperature of the concrete and can be considered heat sources. Irradiation (radiation emitted by the formwork) and reflected radiation act as heat sinks. Figure 2-1 illustrates the different radiation and convection surface boundary conditions from the environment to the outside formwork of a column.

Convection transfer on the outside of concrete members consists of free and forced convection. Free convection is the heat transfer due to bulk fluid movement (due to buoyancy forces from the temperature differences in the air during heat exchange) and diffusion of the fluid (usually air or water for concrete members) around the member. Forced convection is the heat transfer from bulk fluid movement caused by the wind (Incropera and Dewitt 2002).

Despite the apparent complexity of temperature prediction, there is a systematic approach that produces an accurate solution. The heat transfer at boundary conditions may be calculated using the finite difference method. The finite difference method may be approached by using an energy balance for differential volumes; the sum of the energy in minus the sum of the energy out equals the change in energy (and thus temperature) of a control volume. The approach allows for the treatment of each boundary condition effect separately at each time step (Incropera and Dewitt 2002).

This paper reviews several models for calculating the heat transfer at concrete member boundaries, with emphasis placed on those for vertical surfaces. Next, the paper discusses the incorporation of these models into a mass concrete temperature prediction model. Finally, a comparison is made between the predicted temperatures from the temperature prediction model to measured temperatures from 12 concrete bridge structures.

2.2 Research Significance

Changing concrete member dimensions, mixture proportions and material properties in recent years have led to temperature-related problems in mass concrete bridge elements. Concrete temperature modeling is being used to help avoid any problems that may occur from excessive temperatures. Correct boundary condition modeling of concrete bridge members is an essential part of any temperature prediction model. This paper presents a model for temperature boundary condition modeling of mass concrete structures, focusing especially the vertical surfaces. Model results are also compared to measured temperatures from mass concrete bridge elements.

2.3 Experimental Methods

2.3.1 CONCRETE MEMBER INSTRUMENTATION

Twelve concrete members were instrumented to record the temperature during the first few days after concrete placement. The concrete members instrumented were selected to give a wide variety of geometries, materials, formwork, ambient conditions, and curing conditions. Table 2-1 shows a summary of the concrete member size and construction sequences. The Rectangular Bent Cap, T-shaped Bent Cap, and Pedestal were constructed with wood forms. Concrete was placed against the embankment in Footing 2. The remainder of the concrete members were built using un-insulated steel forms. Table 2-2 shows the concrete mixture proportions. Semi-adiabatic calorimetry was performed on-site for each concrete mixture; Table 2-3 shows the concrete hydration parameters as measured by semi-adiabatic calorimetry. Adiabatic temperature development curves were calculated from the semi-adiabatic tests using the procedure suggested by RILEM technical Committee 119 (RILEM 1998). Over 33,000 hours of temperature data from 137 temperature sensors were collected for comparison to the predicted concrete temperatures. Of the 137 temperature sensors, 66 were within 0.31 m (1 ft) of an exterior surface. The rest of the sensors were placed at varying distances from the surface to capture conduction effects of the concrete temperature development at different locations inside the concrete core.

2.3.2 INSTRUMENTATION PROCEDURE

A commercial on-site weather station that measured air temperature, humidity, wind speed, wind direction and solar radiation was used. The weather station was programmed to collect weather data each hour. All temperature sensors were programmed to record and log the temperature at 15 minute intervals. The procedures for modifying the sensors for access outside of the concrete member were similar to those used in an earlier study (Ramaiah Et al. 2002). Each temperature sensor was placed to best capture the core and edge temperatures in each concrete member. The location of each temperature sensor in the concrete member was recorded.

2.4 Analytical Methods

2.4.1 WEATHER DATA

The boundary conditions in concrete temperature prediction models are a function of the ambient conditions. The temperature prediction model contains weather files for 239 U.S. cities and data from these files are used in heat transfer calculations. The weather files contain hourly 30 year average weather data calculated from the National Climatic Data Center (NCDC) Solar and Meteorological Surface Observational Network (SAMSON) CDs (National Climatic Data Center 1993). The weather data used in the temperature prediction model uses the global horizontal solar radiation, extraterrestrial horizontal solar radiation, barometric pressure, dry bulb temperature, relative humidity, and wind speed data from this database in the calculations. The relative humidity, wind speed, and dry bulb temperature used in the calculations can be scaled by the user by manually inputting maximum and minimum daily values. Solar radiation values can be adjusted indirectly by changing average daily cloud cover values.

A linear relationship between cloud cover and solar radiation is assumed as shown in Equation 2-2 (Wojcik 2004, Freedman et al. 2001):

$$E_H = (0.91 - (0.7 * C)) * E_{TOA} \qquad \textbf{Equation 2-2}$$

where E_H is the surface horizontal solar radiation (W/m^2), C is the cloud cover fraction, and E_{TOA} is the extraterrestrial horizontal solar radiation (W/m^2).

2.4.2 RADIATION

Radiation may be defined as “energy emitted by matter that is at a finite temperature (Incropera and Dewitt 2002).” There are several different ways in which energy is given off or absorbed by a surface. These include solar radiation, radiation exchange between form elements, atmospheric radiation, ground radiation, and column irradiation. The following sections will discuss the theories used to model the different sources of radiation and irradiation.

2.4.2.1 Solar Radiation

The temperature prediction model uses the product of cloud cover factor and extraterrestrial solar radiation to calculate the surface horizontal solar radiation. This value is the total amount of direct and diffuse solar radiation that would strike a horizontal surface at ground level (National Climatic Data Center 2003). The amount of solar radiation incident on the vertical surfaces of a column is different than the solar radiation incident on a horizontal surface because of differences in the angle between each surface and the incoming solar radiation. This difference also changes throughout the day and year as the position of the sun in the sky changes. Figure 2-2 shows the angles (measured in degrees) that are used to calculate the component of the solar radiation on the vertical concrete surface, where β is the angle between the direct solar radiation and the ground, φ is the angle between the horizontal component of the direct solar radiation and south, ψ is the angle between south and the vertical column normal, γ is the angle between the horizontal component of the direct solar radiation and the vertical column normal, and θ_v is the angle between the direct solar radiation and the vertical column normal (ASHRAE 1993).

Angles β and ψ are functions of the latitude L_a and longitude L_o of the column, apparent solar time expressed as an angle H (degrees), and the solar declination δ (degrees). Equation 2-3 and Equation 2-4 may be used to determine β and ψ (ASHRAE 1993):

$$\beta = \arcsin(\cos L_a \cos\delta \cos H + \sin L_a \sin\delta) \qquad \textbf{Equation 2-3}$$

$$\psi = \arccos\left[\frac{(\sin\beta \sin L_a - \sin\delta)}{(\cos\beta \cos L_a)}\right] \qquad \textbf{Equation 2-4}$$

Angle θ_v (degrees) for a vertical surface is shown in Equation 2-5 (ASHRAE 1993):

$$\theta_v = \arccos(\cos\beta \cos\gamma) \qquad \textbf{Equation 2-5}$$

The apparent solar time (AST) (minutes) may be calculated according to Equation 2-6 (ASHRAE 1993):

$$AST = LST + ET + 4(LSM - L_o) \qquad \textbf{Equation 2-6}$$

where LST is the local standard time (minutes from midnight), ET is the equation of time (minutes) as calculated in Equation 2-7 through 1-10 (Watt Engineering, Ltd 1978), and LSM is the local standard time meridian found in the weather data files. The equation of time (Equation 2-6) takes into account the change in the difference between local standard time and solar time during the year:

For D = 1 to 106: $ET = -14.2 * \sin(\pi * (D + 7)/111)$ **Equation 2-7**

For D = 107 to 166: $ET = 4.0 * \sin(\pi * (D - 106)/59)$ **Equation 2-8**

For D = 167 to 246: $ET = -6.5 * \sin(\pi * (D - 166)/80)$ **Equation 2-9**

For D = 247 to 365: $ET = 16.4 * \sin(\pi * (D - 247)/113)$ **Equation 2-10**

where D is the day of the year (Julian days). The apparent solar time is converted to H using Equation 2-11 (ASHRAE 1993):

$$H = \frac{AST}{4} \qquad \textbf{Equation 2-11}$$

The normal solar radiation E_N (W/m^2) may be calculated from E_H using Equation 2-12 (ASHRAE 1993):

$$E_N = \frac{E_H}{\sin\beta}$$ **Equation 2-12**

The component of the normal solar radiation on a vertical column is shown by Equation 2-13 (ASHRAE 1993):

$$E_v = E_N \cos\theta_v$$ **Equation 2-13**

The solar radiation seen on a vertical column E_v (W/m^2), expressed in terms of the horizontal solar radiation, can be derived from Equation 2-4, Equation 2-11, and Equation 2-12, and is expressed in Equation 2-14:

$$E_v = E_H \frac{\cos\gamma}{\tan\beta}$$ **Equation 2-14**

E_v must account for the effects of shading. If γ is between 90° and 270°, the vertical surface will be shaded from the sun. If steel forms with horizontal bracing (such as stiffeners or whalers) are used, E_v must be adjusted. Figure 2-3 shows a close-up picture of stiffeners typically used with steel formwork. Figure 2-4 shows the shading effect that stiffeners have, where Ω (degrees) is the angle between horizontal and the shaded region, where P_h is the width of the stiffener (m), B_h is the height of the stiffener (m), S_h is the height of shading below the stiffener (m), and C_h is the distance between each stiffener (m). The temperature prediction model assumes that the stiffeners are facing downwards, as shown in Figure 2-3 and Figure 2-4. Equation 2-15 shows the relationship between the percent of the forms that are sunny, S_u, and the position of the sun.

$$S_u = \frac{C_h - B_h - P_h \dfrac{\tan\beta}{\tan\gamma}}{C_h} \times 100\%$$ **Equation 2-15**

The temperature prediction model assumes that the shading effect produces no local temperature extremes. Note that E_H is a measured value, and the derivation to convert to E_v is theoretical. As a result, some stability problems can occur in the model. For example, in a case where the calculated sunset occurs before the measured sunset, E_N approaches infinity. This problem is corrected by limiting E_N to the maximum solar radiation.

2.4.2.2 Radiation Exchange between Vertical Form Surface and Form Cross-Bracing

The radiation emitted from surfaces 2 and 3 to surface 1 in Figure 2-4 is expressed in Equation 2-16 (Incropera and Dewitt 2002):

$$q_{ij}'' = A_i F_{ij} \alpha_j \varepsilon_i \sigma (T_i^4 - T_j^4)$$ **Equation 2-16**

where i is surface 2 or 3, j is surface 1, q_{ij}" is the net rate radiation that leaves surface *i* and gained by surface *j* (W/m^2), A_i is the area of surface *i* (m^2), F_{ij} is the view factor from surface *i* to surface *j*, α_j is the absorptivity of surface *j*, ε_i is the emissivity of surface *i*, σ is the Stefan-Boltzmann constant (=5.67*10^{-8} W/m^2*K^4), T_i is the temperature of surface *i* (K), and T_j is the temperature of surface *j* (K). The view factor "is defined as the fraction of the radiation leaving surface I that is intercepted by surface J (Incropera and Dewitt 2002)." The view factor for steel formwork may be calculated by considering the horizontal and vertical parts of the stiffeners separately. The view factor for the horizontal part of the stiffeners (surface 2 to surface 1) may be calculated using Equation 2-17 (Incropera and Dewitt 2002):

$$F_{ij} = \frac{1 + \frac{P_h}{C_h} - \left[1 + (\frac{P_h}{C_h})^2\right]^{\frac{1}{2}}}{2}$$ **Equation 2-17**

The view factor for the vertical portion of the form stiffeners (surface 3 to surface 1) may be calculated using Hottel's crossed string method to obtain Equation 2-18 (Siegel and Howell 1992):

$$F_{ij} = \left[\frac{\sqrt{P_h^2 + B_h^2} + \sqrt{(C_h^2 + P_h^2} - P_h - \sqrt{(C_h - B_h)^2 + P_h^2}}{2 * B_h}\right]$$ **Equation 2-18**

2.4.2.3 Atmospheric Radiation

Radiation is emitted from matter at a temperature above zero degrees Kelvin. Gas in the atmosphere emits radiation like all other matter. These gas particles follow the Stefan-Boltzmann law shown in Equation 2-19:

$$q_a'' = \sigma \varepsilon_a (T_a)^4$$ **Equation 2-19**

where q_a'' is the heat flux from the air (W/m^2), ε_a is the emissivity of the air, and T_a is the temperature of the air (K). The emissivity is dependent on the atmospheric water vapor pressure e_a (millibars), temperature, and cloud cover fraction as shown in Equation 2-20 (Wojcik 2004, Brutsaert 1975):

$$\varepsilon_a = C + 1.24(1 - C) * (\frac{e_a}{T_a})^{\frac{1}{7}}$$ **Equation 2-20**

The saturated water vapor pressure P_{ws} (kPa) is calculated using Equation 2-21 for a temperature range of -100°C to 0° C (-148°F to 32°F) and Equation 2-22 for a temperature range of 0° C to 200° C (32°F to 392°F) (ASHRAE 1993):

$$P_{ws} = \exp\left[\frac{C_1}{T_a} + C_2 + C_3 T_a + C_4 T_a^2 + C_5 T_a^3 + C_6 T_a^4 + C_7 \ln(T_a)\right]$$ **Equation 2-21**

where $C_1 = -5.6745359x10^3$, $C_2 = -5.1523058x10^{-1}$, $C_3 = -9.677843x10^{-3}$, $C_4 = 6.2215701x10^{-7}$, $C_5 = 2.0747825x10^{-9}$, $C_6 = -9.484024x10^{-13}$, and $C_7 = 4.1635019$.

$$P_{ws} = \exp\left[\frac{C_8}{T_a} + C_9 + C_{10} T_a + C_{11} T_a^2 + C_{12} T_a^3 + C_{13} \ln(T_a)\right]$$ **Equation 2-22**

where, $C_8 = -5.8002206x10^3$, $C_9 = -5.516256$, $C_{10} = -4.8640239x10^{-2}$, $C_{11} = 4.1764768x10^{-5}$, $C_{12} = -1.4452093x10^{-8}$, and $C_{13} = 6.5459673$.

The partial water vapor pressure e_a (kPa) is calculated using Equation 2-23 (ASHRAE 1993):

$$e_a = R_h * P_{ws} * (\frac{10 millibar}{kPa})$$ **Equation 2-23**

where R_h is the air relative humidity (%).

2.4.2.4 Radiation from the Ground Surface

Radiation from the ground surface can interact with the column surface. This radiation follows the Stefan-Boltzmann law for radiation (Incropera and Dewitt 2002). Equation 2-24 shows the Stefan-Boltzmann law for the ground surface radiation that contacts the column (Incropera and Dewitt 2002).

$$q_g'' = \varepsilon_g \sigma T_g^4 \qquad \textbf{Equation 2-24}$$

where q_g'' is the radiation seen by the column (W/m^2), ε_g is the emissivity of the ground, and T_g is the temperature of the ground (K). The calculation of the ground surface temperature would require a separate heat transfer analysis, would vary greatly from one location to another, and would be very dependent on the individual location, shading conditions, plant locations, etc. To make the concrete surface calculations faster and less complex, several assumptions are made. First, the temperature prediction model assumes that T_g is equal to the ambient temperature. The model also assumes that the area around the concrete is open (the concrete is not placed directly next to a wall or other vertical surface that emits radiation). Also, the stiffeners on the steel forms shade the column from radiation from the ground which may be accounted for in the same manner as with solar radiation.

2.4.2.5 Column Irradiation

The column emits radiation as part of the heat transfer process. The radiation emitted from the column is governed by the Stefan-Boltzmann law as shown in Equation 2-25:

$$q_c'' = \varepsilon_c \sigma T_c^4$$ **Equation 2-25**

where q_c'' is the heat lost from the column (W/m^2), ε_c is the emissivity of the concrete surface (concrete or formwork, whichever is exposed), and T_c (K) is the temperature of the concrete surface. When steel forms are used, the concrete surface temperature is used for the surface temperature because the steel forms "offer little resistance to heat dissipation from the concrete (ACI 207 1995)." When wood forms or insulating blankets are used, a separate temperature node is used for T_c, because the difference between the concrete surface temperature and form/blanket surface temperature. This is necessary to model the increased insulating properties of the form/blanket

2.4.2.6 Material Properties to Model Radiation

The emissivity term in the Stefan-Boltzmann law accounts for the efficiency of the surface in emitting radiation. Emissivity values range from 0 to 1, with 1 being an ideal radiator called a blackbody (Incropera and Dewitt 2002). The emissivity for each material depends on the material temperature, material color, oxidation level, and amount of polishing (Incropera and Dewitt 2002). Common materials also do not absorb 100% of the radiation that contacts the surface. All incoming radiation heat fluxes are multiplied by the material radiation absorptivity, α, to account for this inefficiency. Table 2-4 shows the emissivity and absorptivity of common relevant materials found in literature and those used in the temperature prediction model. The solar absorptivity of concrete is dependent on the color of the cementitious materials, aggregate type, concrete age, and state of weathering (Levinson and Akbari 2002).

2.4.2.7 Convection Model

Heat is transferred from the concrete surface to the surrounding fluid (usually air or water) by convection. Convection is the energy transport from a surface to a surrounding fluid by diffusion (random fluid particle motion contacting the surface) and bulk motion of the fluid. Convection is governed by Newton’s law of cooling, shown in Equation 2-26 (Incropera and Dewitt 2002):

$$q_{cv}'' = h(T_s - T_\infty) \qquad \textbf{Equation 2-26}$$

where q_{cv}'' is the convection heat flux (W/m^2), h is the convection coefficient (W/m^2*K), T_s is the surface temperature (K), and T_∞ is the fluid temperature (K). In the case of the column, the fluid temperature may be approximated as T_a, the ambient temperature (K).

Convection heat transfer can be divided up into two categories, free convection and forced convection. The bulk fluid motion in free convection is caused by buoyancy forces from differences in local fluid density. The local fluid density gradients are caused by local heating or cooling of the fluid in contact with the surface. In forced convection, the fluid motion is caused by an external source of fluid motion. In the case of concrete columns, the convection is a combination of free and forced convection. If the boundary layer air is heated by the column, the air’s density will be lowered and the air will travel up the column. This is a result of free convection. The wind will also move the air around the column, creating forced convection. Equation 2-27 shows the relation used to calculate the convection coefficient due to forced and free convection (ASHRAE 1993):

$$h = C * 0.2782 * \left[\frac{1}{T_{avg} + 17.8} \right]^{0.181} * \left| T_s - T_a \right|^{0.266} * \sqrt{1 + 2.8566 * w}$$ **Equation 2-27**

where C is a heat flow constant, T_{avg} is the average air film temperature (°C), and w is the wind speed (m/s). T_{avg} can be approximated by the average of T_a and T_s. C= 10.15 for bottom horizontal surface hotter than ambient or top horizontal surface cooler than ambient, C= 15.89 for vertical surfaces, and C= 20.4 for bottom horizontal surface cooler than ambient or top horizontal surface hotter than ambient.

The convection equation shown in Equation 2-27 is for pipes and flat surfaces. Equation 2-27 was formulated for relatively smooth surfaces tested in wind tunnels (ASHRAE 1993, ASTM C 680 2004). To correct for surface roughness, the convection coefficient h may be multiplied by a roughness multiplier R_f. Concrete has been shown to have a roughness multiplier of 1.52 and is used after the forms are removed (Clear et al. 2003). The steel form's multiplier is used before the formwork is removed, which is assumed to be smooth with a roughness multiplier of 1. The wind speed used in Equation 2-27 is for the average main wind stream speed. Local variations in wind speed from turbulence or obstructions may cause some errors in the calculations (ASTM C 680 2004).

2.4.3 CONCRETE MEMBER TEMPERATURE PREDICTION

Concrete temperatures for the structural elements listed in Table 2-1 were predicted using the model described in this paper. The measured minimum and maximum weather data were used in calculating the predicted concrete temperatures. If the minimum and maximum weather data were not used, the comparison between the predicted and measured concrete temperatures would reflect the variation in the weather from the 30-year average weather values. The shape of the measured weather data only deviated significantly from the average weather data during extreme weather events (such as thunderstorms, etc.). The measured concrete hydration parameters obtained from semi-adiabatic calorimetry were also used in the analysis.

2.5 Results and Discussion

The concrete temperatures predicted by the model described in this paper were compared to the measured values. The value for each temperature sensor was compared to the temperature predicted. Table 2-5 shows the average coefficient of determination (r^2) value for all of the temperature sensors (group 1) in the twelve concrete members. The average coefficient of determination (r^2) value for temperature sensors within 0.31 m (1 ft) of the concrete surface (group 2) for each concrete member is also shown in Table 2-5. The analysis was performed comparing the hourly temperatures for each temperature sensor for the length of time indicated in Table 2-5. The high average r^2 (above 0.8) values calculated for most members indicate that the model accurately simulated the overall concrete temperature development. Footings 1, 3, and column 1 however, showed lower average r^2 values. Column 1 showed a lower r^2 value because one of the exterior points did not capture correctly the magnitude of daily temperature fluctuations after the forms were removed. It is not known why footings 1 and 2 showed lower r^2 values. The heat of hydration for the concrete used in footings 1 and 3 was not measured. The heat of hydration from tests performed a few months earlier on the same mixture proportions were used in the analysis, and could be the cause of the associated error. The average of the average absolute error between the predicted and measured temperature for each member and the range for individual sensors is shown in Table 2-6. The average absolute error is calculated using Equation 2-28 (Carino and Tank 1992):

$$AAE = \frac{\sum\left(\left|\hat{y} - y\right|\right)}{n}$$ **Equation 2-28**

where AAE is the average absolute error, ŷ is the predicted temperature (°C), y is the measured temperature, and n is the number of data points used in the analysis. The average absolute error for the members ranged from 0.5 to 4.6°C (1.0 – 8.4°F), indicating that the magnitude of the predicted temperatures matches well with the measured values.

The maximum temperature and maximum temperature difference (the maximum difference between the maximum temperature and the minimum temperature anywhere in the concrete member) measured for each concrete member was compared to the predicted values, as shown in Table 2-7 and Table 2-8. The maximum predicted temperature and temperature difference for each member were calculated from the predicted temperatures at the temperature sensor locations. It is expected that the actual maximum temperature differences will be greater than those measured because the minimum temperature in the concrete member could not always be measured because of restrictions on temperature sensor locations. The boundary condition models described in this paper predicts well the concrete surface temperature for the concrete members. Figure 2-5 shows the predicted versus measured temperature for a temperature sensor placed near the steel formwork on Column 2. The model also provides a good estimate of the maximum temperature in the concrete, with a maximum error of 4.9%. The model output differed by as much as 17.6% in predicting the maximum temperature difference in the concrete.

Local temperature effects due to formwork shading, as shown in Figure 2-3 were investigated by installing additional temperature sensors vertically close to the formwork on Column 2. Five temperature sensors were placed 25mm (1 in.) from the surface vertically over a length of 0.4m (16 in.). Five additional temperature sensors were placed 50mm (2 in.) from the surface vertically over a length of 0.46m (18 in.) on an adjacent side where a thick polyurethane form-liner was used for aesthetic reasons. The temperature sensors placed on the side without the form-liner differed by a maximum of 3.5°C (6.3°F) over a period of two weeks. The sensors placed on the side with the form-liner differed by a maximum of 2°C (3.6°F) over the same period of time. The surface temperature data show that an average shaded surface value may be used with only a minor loss in accuracy of the model, because of the averaging effect of the heat transfer in the vertical direction.

Some variation between measured and predicted temperature data is to be expected. Rapid and short-lived temperature variations occur in the microclimate surrounding the instrumented concrete members. The data analysis showed that the boundary conditions model, using average temperature data scaled for actual maximum and minimum values, did provide an acceptable result when predicting the concrete temperature. When the assumptions associated with the boundary condition models are not met, the r^2 value decreases dramatically. Rain events, snow events, and concrete freezing were not considered in the heat transfer analysis. When precipitation events occurred, the model accuracy was reduced. The reduction in accuracy will be highly variable and will depend on the magnitude and duration of the event. For this reason, these extreme events are not modeled.

2.6 Conclusion

A model was presented to characterize the heat transfer at the top and side surfaces of concrete members. The model includes components for calculating the radiation heat transfer components due to solar radiation, atmospheric radiation, ground surface radiation, radiation exchange with formwork bracing, and irradiation. The model also includes a method to characterize the effects of free convection, forced convection, and surface roughness. The finite difference heat transfer model was compared to concrete temperature data collected from 12 concrete members of varying geometry, formwork, location, construction methods, and materials. The accuracy of the model may be reduced when model assumptions (location of walls, rain events, etc.) are violated.

2.7 Acknowledgements

The authors wish to express their gratitude to the Texas Department of Transportation through Project 0-4563 for funding this research and providing access to concrete construction sites. The advice and support of Ralph Browne and Tom Yarbrough of the Texas Department of Transportation and Rob Crowson of the Central Texas Turnpike Authority is greatly appreciated.

Table 2-1- Concrete Member Summary

Member	Placement Date (M/D/Y)	Length m (ft)	Width (m)	Height (m)	Placement Time	Formwork Removed (days)
Pedestal	6/11/04	2.9 (9.5)	3.2 (10.5)	1.7 (5.5)	10:00 AM	>7
T-shaped bent cap	6/05/04	-	2.2 (7.2)	2.5 (8)	8:00 AM	2.25
Rectangular Bent Cap	3/31/04	-	1.0 (3.2)	1.0 (3.2)	8:00 AM	5
Dolphin 1	2/05/04	4.9 (16)	4.9 (16)	2.7 (9)	11:30 AM	5
Dolphin 2	9/10/04	4.9 (16)	4.9 (16)	2.7 (9)	4:15 AM	4
Footing 1	8/06/03	2.4 (7.9)	1.8 (6)	2.0 (6.5)	10:00 AM	4
Footing 2	8/01/03	3.1 (10)	3.1 (10)	1.9 (6)	8:00 AM	-
Footing 3	8/06/03	2.4 (7.9)	1.8 (6)	2.0 (6.5)	8:00 AM	4
Footing 4	8/09/04	18.3 (60)	4.1 (13.5)	2.0 (6.5)	5:00 AM	>14
Column 1	7/10/04	1.8 (6)	3.1 (10)	20.4 (67)	8:00 AM	5
Column 2	6/11/04	2.6 (8.5)	3.1 (10)	12.2 (40)	8:30 AM	>7
Pilaster	2/22/05	2.7 (9)	1.8 (6)	1.7 (5.5)	9:00 AM	13.2

Table 2-2 - Concrete Member Mixture Proportions

Member	**Cement kg/m^3 (pcy)**	**SCM kg/m^3 (pcy)**	**Water kg/m^3 (pcy)**	**Coarse Aggregate kg/m^3 (pcy)**	**Fine Aggregate kg/m^3 (pcy)**	**SCM Type**	**Coarse Aggregate Type**	**Fine Aggregate Type**	**Chemical Admixtures**
Pedestal	295 (497)	106 (179)	164 (279)	1035 (1745)	681 (1147)	F	CL	SNS	LRWR
T-shaped Bent Cap	241 (409)	86 (143)	154 (259)	1034 (1743)	799 (1347)	F	CL	SNS	LRWR
Rectangular Bent Cap	251 (423)	64 (107)	126 (212)	1108 (1867)	727 (1225)	C	CG	CG	LRWR
Dolphin 1	253 (426)	100 (168)	123 (207)	1112 (1874)	687 (1157)	F	SRG	SNS	LRWR MRWR
Dolphin 2	244 (411)	109 (189)	123 (207)	1084 (1827)	670 (1129)	F	SRG	SNS	LRWR MRWR
Footing 1	253 (426)	64 (107)	135 (228)	1041 (1754)	845 (1424)	F	CL	SNS	LRWR
Footing 2	253 (426)	64 (107)	135 (228)	1041 (1754)	845 (1424)	F	CL	SNS	LRWR
Footing 3	253 (426)	64 (107)	135 (228)	1041 (1754)	845 (1424)	F	CL	SNS	LRWR
Footing 4	167 (282)	133 (224)	104 (175)	1109 (1869)	793 (1337)	F	SRG	SNS	LRWR HRWR
Column 1	251 (423)	64 (107)	131 (223)	1035 (1745)	847 (1427)	F	CL	SNS	LRWR
Column 2	295 (497)	106 (179)	164 (279)	1035 (1745)	681 (1147)	F	CL	SNS	LRWR
Pilaster	181 (305)	165 (278)	149 (250)	997 (1680)	746 (1258)	GGBFS	SRG	SRG	MRWR

GGBFS = Ground Granulated Blast Furnace Slag

F = ASTM C 618 Class F Fly Ash (2003)

C = ASTM C 618 Class C Fly Ash (2003)

MRWR= Mid Range Water Reducer

LRWR = ASTM C 494 Type A Water-Reducing Admixture (1999)

HRWR = ASTM C 494 Type F High Range Water-Reducing Admixture (1999)

SRG = Siliceous River Gravel

SNS = Siliceous Natural Sand

CG = Crushed Granite

CL = Crushed Limestone

Table 2-3 - Hydration Parameters as Measured by Semi-Adiabatic Calorimetry

Member	α_u	β	τ (hrs)	E (J/mol)	H_u (J/kg)
Pedestal	0.920	0.704	30.9	38,100	456,500
T-shaped bent cap	0.983	0.672	32.4	38,200	456,500
Rectangular Bent Cap	0.860	0.655	21.8	39,600	492,000
Dolphin 1	0.714	0.993	16.9	29,400	456,000
Dolphin 2	0.724	0.782	23.6	29,400	451,500
Footing 1	0.806	0.652	23.3	39,600	465,500
Footing 2	0.806	0.652	23.3	39,600	465,500
Footing 3	0.806	0.652	23.3	39,600	465,500
Footing 4	0.755	0.520	37.6	40,000	445,500
Column 1	0.720	0.616	25.9	41,300	493,500
Column 2	0.920	0.704	30.9	38,100	456,500
Pilaster	1.000	0.444	59.0	41,200	536,900

Table 2-4 - Emissivity and Absorptivity Values for Common Materials

Material	Emissivity Values in Literature	Emissivity Value Used in this Model	Absorptivity Values in Literature	Absorptivity Values Used in this Model
Concrete	0.88 - 0.93 (Incropera and Dewitt 2002)	0.92	0.23-0.59 (Levinson Akbari 2002)	0.55
Soil	0.93 - 0.96 (Incropera and Dewitt 2002)	0.92	-	-
Vegetation	0.92 - 0.96 (Incropera and Dewitt 2002)	0.92	-	-
Rocks	0.88 - 0.95 (Incropera and Dewitt 2002)	0.92	-	-
Paint on Metallic Substrate	0.97 - 0.96 (Incropera and Dewitt 2002)	0.95 (red), 0.92 (yellow)	0.97 - 0.21 (Incropera and Dewitt 2002)	0.75 (red), 0.72 (yellow)
Wood	0.82 – 0.92 (Incropera and Dewitt 2002)	0.92	-	0.6

Table 2-5 - r^2 values for Concrete Members

Name of Member	Total number of temperature sensors (Group 1)	Number of temperature sensors within 0.31 m of form or finished surface (Group 2)	Number of hours for each temperature sensor	Average r^2 for Group 1 temperature sensors (range)	Average r^2 for Group 2 temperature sensors (range)
Pedestal	9	5	119	0.94 (0.83 - 0.98)	0.96 (0.95 – 0.98)
T-Shaped Cap	16	10	120	0.88 (0.52 – 0.99)	0.83 (0.52 – 0.99)
Rectangular Bent Cap	19	15	286	0.97 (0.88 – 0.98)	0.96 (0.88 – 0.98)
Dolphin 1	18	7	262	0.89 (0.71 – 0.99)	0.87 (0.71 – 0.97)
Dolphin 2	27	8	316	0.86 (0.50 – 0.99)	0.75 (0.50 – 0.95)
Footing 1	2	1	51	0.68 (0.67 - 0.69)	0.69
Footing 2	7	1	168	0.97 (0.89 - 0.99)	0.89
Footing 3	2	1	49	0.73 (0.69 - 0.78)	0.69
Footing 4	13	7	221	0.90 (0.83 - 0.95)	0.89 (0.88 – 0.95)
Column 1	3	2	336	0.78 (0.61 - 0.88)	0.74 (0.61 – 0.88)
Column 2	3	2	336	0.93 (0.85 - 0.98)	0.90 (0.85 – 0.95)
Pilaster	18	7	316	0.89 (0.54 - 0.99)	0.77 (0.54 – 0.99)

Table 2-6 – Member Predicted to Measured Temperature Average Absolute Error

Name of Member	Average Absolute Error °C (°F)	Average Absolute Error Range °C (°F)
Pedestal	2.0 (3.6)	1.0 - 4.5 (1.8 - 8.1)
T-Shaped Cap	2.6 (4.7)	1.0 - 6.0 (1.8 - 10.9)
Rectangular Bent Cap	1.6 (2.9)	1.2 - 2.8 (2.1 - 5.0)
Dolphin 1	0.5 (1.0)	0.1 - 3.7 (0.2 - 6.7)
Dolphin 2	2.3 (4.1)	0.6 - 3.8 (1.1 - 6.9)
Footing 1	4.6 (8.4)	3.5 - 5.8 (6.4 - 10.4)
Footing 2	0.8 (1.4)	0.5 - 1.6 (1.0 - 3.0)
Footing 3	4.3 (7.8)	2.7 - 5.9 (4.9 - 10.7)
Footing 4	1.3 (2.3)	0.7 - 1.6 (1.3 - 2.9)
Column 1	2.6 (4.7)	2.0 - 3.5 (3.5 - 6.3)
Column 2	1.6 (2.8)	1.4 - 1.8 (2.6 - 3.2)
Pilaster	1.6 (2.9)	0.8 - 2.9 (1.5 - 5.1)

Table 2-7 - Comparison of Predicted to Measured Maximum Concrete Member Temperature

Name of Member	Max. Temp Measured °C (°F)	Max. Temp Predicted °C (°F)	Difference in Max Temp °C (°F)
Pedestal	74.0 (165.2)	71.7 (161.0)	-2.3 (-4.1)
T-Shaped Cap	67.5 (153.5)	67.2 (153.0)	-0.3 (-0.5)
Rectangular Bent Cap	53.5 (128.3)	52.8 (127.0)	-0.7 (-1.3)
Dolphin 1	63.0 (145.4)	65.1 (149.2)	2.1 (3.8)
Dolphin 2	65.5 (149.9)	65.5 (149.9)	0.0 (0.0)
Footing 1	63.0 (145.4)	61.1 (142.0)	-1.9 (-3.4)
Footing 2	56.1 (133.0)	57.3 (135.2)	1.2 (2.2)
Footing 3	64.0 (147.2)	60.6 (141.1)	-3.4 (-6.1))
Footing 4	57.2 (135.0)	57.2 (135.0)	0.0 (0.0)
Column 1	57.8 (136.0)	55.9 (132.6)	-1.9 (-3.4)
Column 2	73.0 (163.4)	76.6 (169.9)	3.6 (6.5)
Pilaster	54.5 (130.1)	52.1 (125.8)	-2.4 (-4.3)

Table 2-8 – Comparison of Predicted to Measured Maximum Concrete Temperature Difference

Name of Member	Max. T Measured °C (°F)	Max. T Predicted °C (°F)	Difference in Max. T °C (°F)
Pedestal	24.0 (43.2)	20.3 (36.5)	3.7 (6.7)
T-Shaped Cap	36.5 (65.7)	30.1 (54.2)	6.4 (11.5)
Rectangular Bent Cap	15.5 (27.9)	16.7 (30.1)	1.1 (2.2)
Dolphin 1	40.0 (72.0)	40.3 (72.5)	0.3 (0.5)
Dolphin 2	31.0 (55.8)	31.8 (57.2)	0.8 (1.4)
Footing 1	21.5 (38.7)	18.9 (34.0)	2.6 (4.7)
Footing 2	13 (23.4)	12.3 (22.1)	0.7 (1.3)
Footing 3	23.0 (41.4)	20.1 (36.2)	2.9 (5.2)
Footing 4	23.0 (41.4)	20.8 (37.4)	2.2 (4.0)
Column 1	22.2 (40.0)	19.3 (34.7)	2.9 (5.3)
Column 2	33.5 (60.3)	30.2 (54.4)	3.3 (5.9)
Pilaster	36.5 (65.7)	33.2 (59.8)	3.3 (5.9)

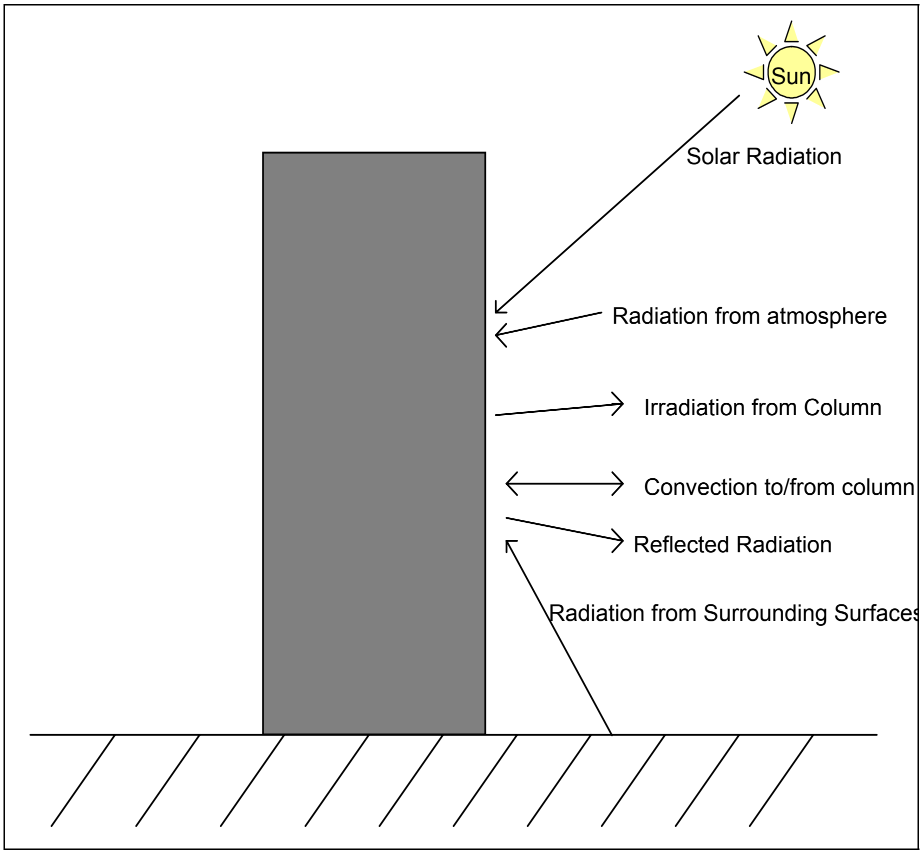

Figure 2-1 - Summary of Column Boundary Conditions

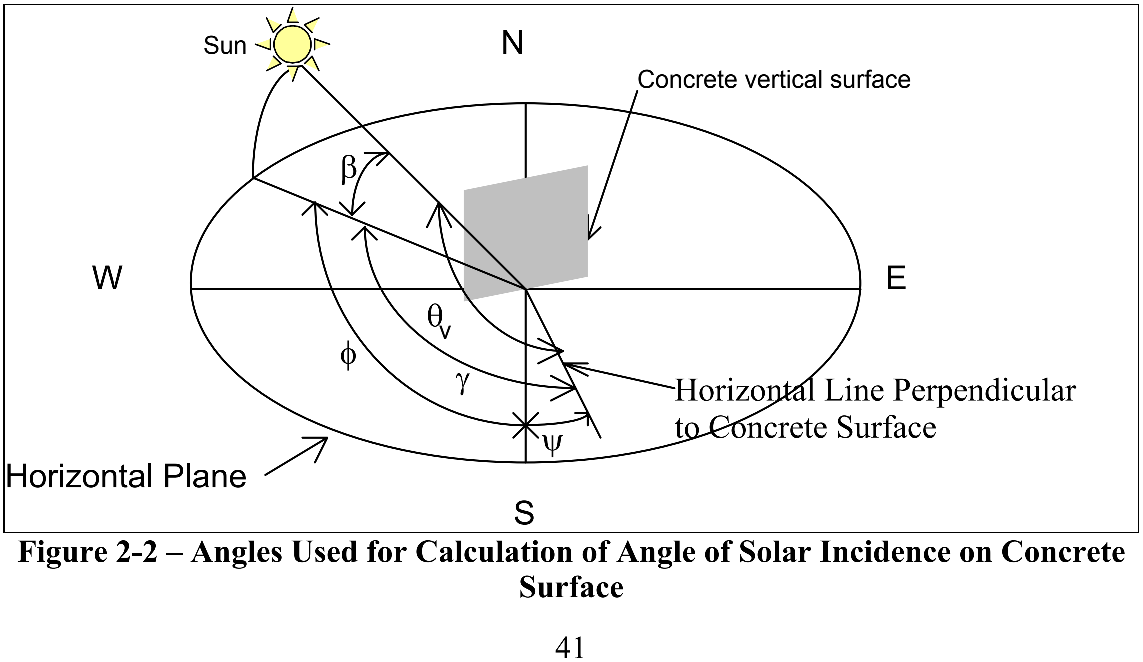

Figure 2-2 – Angles Used for Calculation of Angle of Solar Incidence on Concrete Surface

Figure 2-3 - Formwork Stiffeners

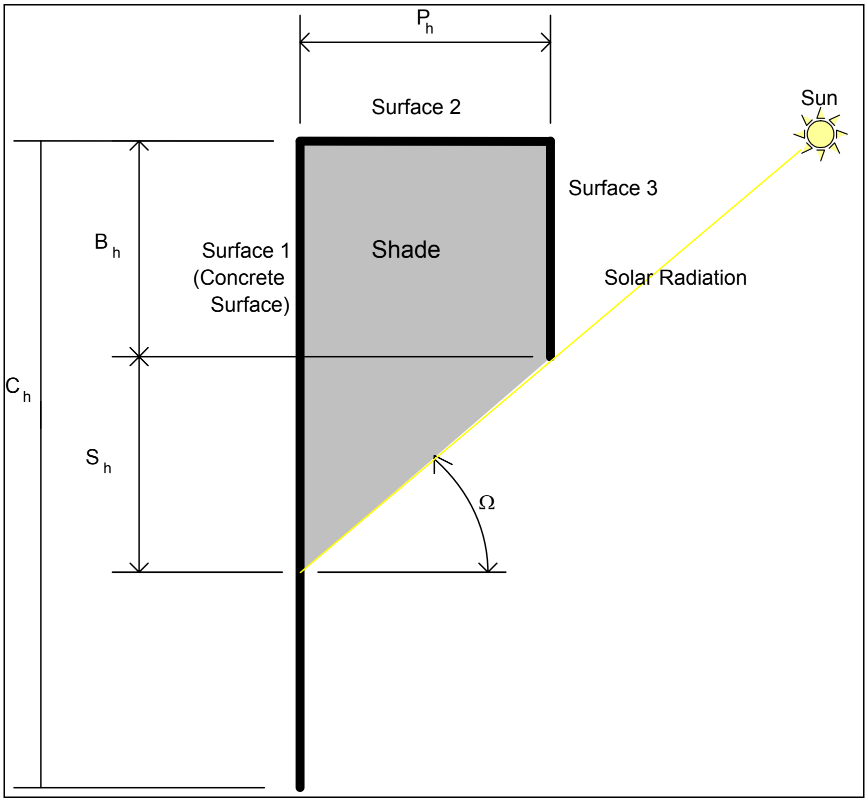

Figure 2-4 - Effect of Stiffener on Form Shade

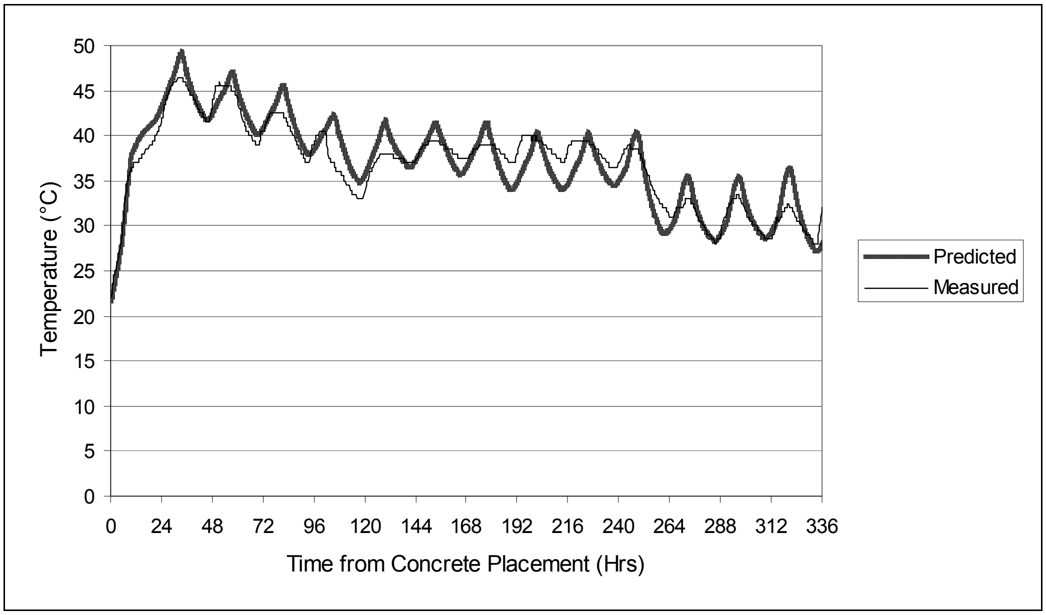

Figure 2-5 - Measured vs. Predicted Temperature for Surface Temperature Sensor on Column 2

CHAPTER 3 CALORIMETRY PERFORMED ON-SITE: METHODS AND USES

An accurate and practical method of determining the heat development of concrete mixtures under real mixing, cooling, hauling, placement, and curing conditions would greatly benefit contractors and engineers in helping predict in-place concrete member temperatures. Semi-adiabatic calorimetry was performed at several construction sites in temperature controlled rooms using concrete sampled from concrete placements. Semi-adiabatic calorimetry was also performed for comparison with concrete made under laboratory conditions from materials sampled at the respective batch plants. An energy balance-based finite difference method is presented for calculating the concrete non-linear heat generation using the measured heat of hydration determined from semi-adiabatic calorimetry. This method was used in a program which allows the direct input of values from semi-adiabatic calorimetry testing and estimates the development of in-place temperatures in mass concrete members of various geometries. Estimated concrete member temperatures are compared to the values measured on-site. Best practice suggestions are also given for performing semi-adiabatic calorimetry using concrete sampled on-site.

3.1 Introduction

Concrete temperature control has become a major issue as concrete bridge member sizes have increased. The cement content of the mixtures in these elements is often quite high in order to meet strength requirements. Also, the placement temperatures of such mixtures have often not been controlled. Finally, aggregate size is often low to meet placement requirements. These issues can lead to an increased risk of thermal cracking, and hence poor long term durability. To deal with these problems, engineers and contractors need a reliable, cost effective, and simple method to assess the thermal behavior of the concrete mixture under job-site conditions. An improved knowledge of the material behavior in-situ could help practitioners improve overall structural durability, cost, and construction sequencing.

Concrete mixing, hauling, and placing conditions can vary widely depending on the location and circumstances. Most concrete heat of hydration tests are performed in laboratories from concrete made using laboratory mixers. Ready mixed concrete can experience different amounts of agitation than laboratory made samples. The project location, such as over a large body of water, can also effect the conditions the concrete experiences before placement. Little work has been done on determining the effects of different mixing and hauling conditions on the temperature rise of concrete.

This paper presents the results of tests comparing the heat of hydration of concrete sampled at five different construction projects and performed onsite to replicate laboratory concrete mixtures performed under more controlled conditions. Semi-adiabatic calorimetry results were used to calculate the concrete adiabatic temperature rise in both cases. Also presented is an energy balance approach for determining the temperature rise of a concrete member using the heat of hydration results obtained from semi-adiabatic calorimetry. The concrete member temperatures were predicted using a finite difference control volume based concrete temperature prediction program. Actual concrete member temperatures results are compared to the predicted values.

3.2 Research Significance

Concrete temperature control is becoming increasingly important in concrete bridge construction where these issues have not been traditionally considered. Engineers and contractors need a reliable way of testing the concrete heat of hydration under job-site conditions, as well as a way of quickly predicting the concrete member performance using that concrete mixture. The work presented here is aimed at simplifying the estimation of concrete temperature by investigating the influence of mixing and testing location on test results and demonstrating the use of a free, user-friendly software package for temperature prediction.

3.3 Experimental Method

Concrete from five different construction projects in the state of Texas was tested onsite to determine their heat of hydration. The concrete placement location, concrete member type, and construction dates are shown in Table 3-1. Table 3-2 shows the mixture proportions used for each project. In some cases, tests were performed more than once onsite or in the laboratory.

The concrete heat of hydration was tested using a semi-adiabatic calorimeter. The semi-adiabatic calorimeter was placed in the nearest temperature controlled building or shed provided by the contractor. The concrete cylinders were made onsite using concrete sampled from the ready mixed truck or pump, and then transported to the nearby calorimeter. The concrete on the Galveston Causeway project differed from the rest because it was mixed and placed using a floating batch plant.

The semi-adiabatic calorimeter is an insulated steel drum with a cavity inside for a concrete cylinder. The semi-adiabatic calorimetry was performed on a 150mm by 300mm (6 in. by 12 in.) concrete cylinder. The temperature of the concrete and heat flux in the drum was recorded. The adiabatic temperature rise in the concrete was calculated from the concrete temperature and heat flux using the procedures suggested by RILEM Technical Committee 119 (1998) and a calibration procedure outlined in Poole et al (2007b). An adiabatic temperature development curve is fit to the semi-adiabatic results using Equation 3-1 (Schindler and Folliard 2005, van Breugel 1998):

$$Q_h(t) = H_u * C_c * \left(\frac{\tau}{t_e}\right)^{\beta} * \left(\frac{\beta}{t_e}\right) * \alpha_u * \exp\left(-\left[\frac{\tau}{t_e}\right]^{\beta}\right) * \exp\left(\frac{E}{R}\left(\frac{1}{273+T_r} - \frac{1}{273+T_c}\right)\right)$$ **Equation 3-1**

where Q_h is the rate of heat generation (J/hr/m^3), H_u is the total amount of heat generated at 100% hydration (J/kg), C_c is the total amount of cementitious materials (kg/m^3), τ is the hydration time parameter (hrs), t_e is the concrete equivalent age at the reference temperature (hrs), β is the hydration slope parameter, α_u is the ultimate degree of hydration (unitless), E is the apparent activation energy (J/mol), R is the universal gas constant (J/mol/K), T_r is the reference temperature (°C), and T_c is the concrete temperature (°C). H_u is calculated from the cement chemistry and supplementary cementing materials percentage (Schindler and Folliard 2005). The activation energy is based on isothermal calorimetry performed on the cement, supplementary cementing materials, and chemical admixtures sampled onsite (Ma et al. 1994). The activation energies used in the calculations for M3 and M4 were based on isothermal calorimetry conducted on similar materials, because identical materials were not available.

Concrete constituent materials were sampled at the batch plant as close as possible to the concrete placement. In most cases, this was the same day as the placement. In the case of the El Paso project, the cementitious materials were sampled the week before concrete placement. Semi-adiabatic calorimetry was performed at the laboratory using the raw materials collected and the mixture proportions used on-site.

3.4 Calorimetry Results

Results were obtained from semi-adiabatic calorimetry performed on-site and at the laboratory. The concrete heat of hydration parameters calculated from the semi-adiabatic calorimetry tests are shown in Table 3-3. Figure 3-1 through Figure 3-5 shows the results of M1 through M5. There are some results that deserve further explanation in Figure 3-1 throughFigure 3-5. The materials used in test M1-L3 were sampled close to the placement of M1-1, and the results, correspondingly, match very well. The semi-adiabatic calorimeter used for concrete mixtures M3-1 and M5-1 was placed in rooms with rather poor temperature control. The room temperature in the job trailer used to store the semi-adiabatic calorimeter for M3-1 was very hot, and caused the heat flux from the concrete to fluctuate dramatically as shown in Figure 3-6. With test M5-1, the room temperature spiked at about 28 hours after mixing, as shown in Figure 3-7, due to a power outage or air conditioning malfunction. The measured heat flux correspondingly dropped. The change in heat flux in the M3-1 and M5-1 caused a change in the calculated hydration parameters, but not necessarily a large temperature difference between the field test and the laboratory test.

Table 3-4 shows the difference between adiabatic temperature rise parameters and the maximum difference in adiabatic temperature rise development for different tests. A difference of 8% for the α_u parameter, 17% for the τ parameter, and 15% for the β parameter can be considered significant differences between tests (Poole et al. 2007b) All of the tests compared, except M4, had at least one parameter with a difference between parameters great enough to be considered significant. The only tests that had a large difference in the adiabatic temperature rise development were M1-1 compared to M1-2 and M5-1 compared to M5-L2. This indicates that the adiabatic temperature rise curves were still quite similar. M1-1 and M1-2 were tested about 6 weeks apart from concrete sampled on-site. Because mixtures M1-1 and M1-2 were placed on over 6 weeks apart, a change in the cementitious materials between the two tests may have been the cause for the difference in these tests. Mixtures M5-1 and M5-L2 have a large difference in temperature because due to a batching error, M5-L2 contained less than half of the low-range-water reducing admixture as M5-1. This large difference in water reducer decreased the dispersion of the cementing materials, decreasing the degree of hydration (Poole et al. 2007b). The mixture was then repeated, resulting in a closer adiabatic temperature rise. This indicates that semi-adiabatic calorimetry can be used as a quality control measure to detect large changes in materials or batch weights. It is recommended that the difference in hydration parameters and the difference between adiabatic temperature rise be examined for quality control testing purposes.

3.5 Hydration Parameter Use in Modeling

The hydration parameters calculated as part of semi-adiabatic calorimetry can be used as direct inputs in an energy balance-based heat transfer analysis. Although temperature prediction of concrete members has been studied for some time (Khan 1995, Khan et al. 1998), the heat transfer method used in this paper is presented for clarity and for reference as an easily implemented algorithm for calculating concrete temperature development. Equation 3-2 shows the heat diffusion equation (Incropera and Dewitt 2002):

$$\frac{d}{dx}\left(k \cdot \frac{dT}{dx}\right) + \frac{d}{dy}\left(k \cdot \frac{dT}{dy}\right) + Q_h = \rho \cdot C_p \cdot \frac{dT}{dt} \qquad \text{Equation 3-2}$$

where Q_h is the rate of heat generation (J/hr/m^3), ρ is the density (kg/m^3), C_p is the specific heat (J/kg/°C), and T is the temperature (°C). The concrete member may be idealized as a collection of control volumes, (or areas in the 1 or 2 dimensional case) (Patankar 1980). Each control volume is assumed to have different, but uniform temperature and material properties. The change in temperature over a time step can then be calculated using an energy balance, as shown in Equation 3-3 and Figure 3-8 (Incropera and Dewitt 2002):

$$\dot{E}_{in} + \dot{E}_g - \dot{E}_{out} = \dot{E}_{st} \qquad \text{Equation 3-3}$$

where $\dot{E}_{in}$ is the rate of energy entering the control volume (W/m^3), $\dot{E}_g$ is the heat generation rate (W/m^3), $\dot{E}_{out}$ is the rate of energy leaving the control volume (W/m^3) and $\dot{E}_{st}$ is the rate of energy being stored in the control volume. The temperature change in the control volume can then be calculated using Equation 3-4 (Incropera and Dewitt 2002):

$$\Delta T = \frac{\dot{E}_{st}\Delta t}{\rho c_p dxdydz} \qquad \text{Equation 3-4}$$

where ΔT is the change in temperature in the control volume (°C), Δt is the time step used in the calculation (s), dx, dy and dz are the dimensions of the control volume (m).

The heat generated may be calculated using Equation 3-1. The incremental amount of heat generated during a time step used in the heat transfer analysis may be calculated as the total heat generated up to that time step (using Equation 3-1) minus the total heat generated from the previous time step. The energy entering the control volume from conduction (in 1 dimension) to the neighbor volume may be calculated using Equation 3-5, while the energy leaving the control volume from conduction may be calculated using Equation 3-6:

$$\dot{E}_{in} = \frac{dy_i \cdot T_{i-1}}{\frac{dx_{i-1}}{2 \cdot k_{i-1}} + \frac{dx_i}{2 \cdot k_i}} + \frac{dy_i \cdot T_{i+1}}{\frac{dx_i}{2 \cdot k_i} + \frac{dx_{i+1}}{2 \cdot k_{i+1}}} \qquad \text{Equation 3-5}$$

$$\dot{E}_{out} = \frac{dy_i \cdot T_i}{\frac{dx_{i-1}}{2 \cdot k_{i-1}} + \frac{dx_i}{2 \cdot k_i}} + \frac{dy_i \cdot T_i}{\frac{dx_i}{2 \cdot k_i} + \frac{dx_{i+1}}{2 \cdot k_{i+1}}} \qquad \text{Equation 3-6}$$

where k is the thermal conductivity for the control volume (W/m/°C), and the subscript refers to the representative control volume as shown in Figure 3-8 (Patankar 1980). In the case of exterior boundary conditions that experience a radiation heat flux or convective energy exchange, the heat flux entering or leaving may be substituted for that found in Equation 3-5 and 6. The temperature distribution may then be solved using an explicit (forward) or implicit (backward) scheme. An implicit scheme will involve the simultaneous solution of the temperature values for all control volumes. In the case of the explicit scheme, a stability criterion such as the one for uniform thermal conductivity and control volume spacing shown in Equation 3-7 must be met to avoid divergence of the solution, which may require a small time step (Patankar 1980).

$$\Delta t = \frac{\rho c_p (dx)^2}{2k}$$ Equation 3-7

In the explicit case, the temperatures values used for the calculations on the left hand side of Equation 3-3 are taken as the temperatures calculated during the last time step. The temperature calculated using Equation 3-4 is the temperature for the new time step.

During the early stages of hydration, the concrete material properties and heat generation values are changing rapidly. The concrete material properties, such as the thermal conductivity and specific heat are dependent on the temperature and degree of hydration. If the implicit method is used, the solution becomes very non-linear and requires iteration. The explicit case, however, does not have this limitation and requires no iteration. When using the explicit method, the thermal properties, boundary condition heat fluxes, and degree of hydration for the present time step may be calculated using the temperatures from the previous time step. Figure 3-9 shows a flow chart of the order in which the calculations are made during a time step. As seen in the flow chart, the concrete temperature may be calculated by updating the boundary conditions, material thermal properties, and degree of hydration by direct calculations (without any of the iterations required by other methods).

3.6 Temperature Prediction Software

The procedure for calculating the temperature distribution in concrete outlined in this paper was used in a temperature prediction software package developed as part of this project. This software program can be used to quickly predict the temperature distribution for mass concrete members. When the concrete materials and mixture proportions used in the analysis do not meet the construction specifications, the inputs may be quickly adjusted and the temperatures recalculated. This software provides users the ability to rapidly perform the "what if" scenarios to help lower cost and produce more durable concrete. The software provides a summary and graph of the maximum temperature and maximum temperature difference in the member with time. Also, the software will export the temperatures calculated at the control volumes with time to a text file or spreadsheet software.

Figure 3-10 and Figure 3-11 show the measured versus predicted core and near surface temperatures for a footing placed using the concrete from M3-1 (onsite) and M3-L2 (laboratory). The measured temperatures compare quite favorably to those predicted using the hydration parameters measured for M3-1 and M3-L2 despite a difference of over 46% in the τ parameter, demonstrating that the hydration parameters measured onsite or in the laboratory may be used as direct inputs into temperature prediction software. The results shown are representative of those obtained for all mixtures, with only one being shown to conserve space.

It should be noted that temperature predictions made using adiabatic temperature development curves should be made using the most recent data available to minimize this difference. This is clear from the variations seen in the adiabatic temperature rise curves for mixtures M1-1 and M1-2, seen in Figure 3-1, which were done about 6 weeks apart. Using the data from mixture M1-1 (or M1-L3) for concrete placed using the materials from M1-2 could give inaccurate results due to differences in the materials used with time.

3.7 Conclusions and Recommendations

The temperature rise of concrete from five different construction projects was measured onsite and in the laboratory using semi-adiabatic calorimetry. The mixtures that were sampled onsite compared well to the mixtures replicated in the laboratory. This indicates that either practice is acceptable. It is recommended to test the temperature control of a room that will be used to store a semi-adiabatic calorimeter before testing, to minimize any resulting errors. As differences in the calculated hydration parameters may still give similar adiabatic temperature rise curves and consequently predicted temperatures, it is recommended that the difference in hydration parameters and the adiabatic temperature rise curve be used together to determine any differences in the material hydration behavior.

A method for easily calculating the concrete hydration using a spreadsheet or software package has also been presented. Adiabatic temperature rise parameters obtained through semi-adiabatic calorimetry may be used as direct inputs in temperature prediction calculations using the methods outlined in this paper.

3.8 Acknowledgments

The authors wish to express their gratitude to the Texas Department of Transportation for funding this work and other on-going research. The advice and support of Ralph Browne, Tom Yarbrough, and Rob Crowson are greatly appreciated.

Table 3-1 – Concrete Member Construction Information

Concrete Member Description	Member Size Length x Width x Height (m)	Mix ID	Construction Date	Location
Column & Footing	1.8 x 3.1 x 9.1	M1-1	6/16/2003	Round Rock, Texas
	3.1 x 3.1 x 1.9	M1-2	8/1/2003	Round Rock, Texas
	-	M1-L3	3/24/2004	Laboratory
Dolphin (a large concrete member used as a bumper to protect the causeway against barge impact)	4.9 x 4.9 x 2.7	M2-1	2/5/2004	South Padre Island, Texas
	4.9 x 4.9 x 2.7	M2-2	9/10/2004	South Padre Island, Texas
	-	M2-L3	3/24/2004	Laboratory
	-	M2-L4	5/10/06	Laboratory
Causeway Footing	18.3 x 4.1 x 2.0	M3-1	8/9/2004	Galveston, Texas
	-	M3-L2	11/29/2005	Laboratory
Rectangular Bent Cap	1.0 x 1.0	M4-1	3/31/2004	Wichita Falls, Texas
	-	M4-L2	5/5/2004	Laboratory
Pilaster	2.7 x 1.8 x 1.7	M5-1	2/22/2005	El Paso, Texas
		M5-L2	11/15/2005	Laboratory
		M5-L3	5/10/2006	Laboratory

Table 3-2 – Concrete Mixture Proportions

Member	M1	M2-1 & M2-L3	M2-2 & M2-L4	M3	M4	M5
Cement kg/m^3 (pcy)	253 (426)	253 (426)	244 (411)	167 (282)	251 (423)	181 (305)
SCM kg/m^3 (pcy)	64 (107)	100 (168)	109 (189)	133 (224)	64 (107)	165 (278)
Water kg/m^3 (pcy)	135 (228)	123 (207)	123 (207)	104 (175)	126 (212)	149 (250)
Coarse Aggregate kg/m^3 (pcy)	1041 (1754)	1112 (1874)	1084 (1827)	1109 (1869)	1108 (1867)	997 (1680)
Fine Aggregate kg/m^3 (pcy)	845 (1424)	687 (1157)	670 (1129)	793 (1337)	727 (1225)	746 (1258)
SCM Type	F	F	F	F	C	GGBFS
Coarse Aggregate Type	CL	SRG	SRG	SRG	CG	SRG
Fine Aggregate Type	SNS	SNS	SNS	SNS	CG	SRG
Chemical Admixtures	LRWR	LRWR MRWR	LRWR MRWR	LRWR HRWR	LRWR	MRWR

GGBFS = Ground Granulated Blast Furnace Slag

F = ASTM C 618 Class F Fly Ash (2003)

C = ASTM C 618 Class C Fly Ash (2003)

MRWR= Mid Range Water Reducer

LRWR = ASTM C 494 Type A Low Range Water Reducer (1999)

HRWR = ASTM C 494 Type F High Range Water Reducer (1999)

SRG = Siliceous River Gravel

SNS = Siliceous Natural Sand

CG = Crushed Granite

CL = Crushed Limestone

Table 3-3 – Concrete Hydration Parameters Determined by Semi-Adiabatic Calorimetry

Mix ID	H_u (J/g)	E (J/mol)	α_u	τ (hrs)	β
M1-1	465,210	29,410	0.654	14.76	0.860
M1-2	465,290	29,410	0.715	15.34	0.823
M1-L3	465,210	29,410	0.698	19.64	0.776
M2-1	455,720	21,150	0.760	12.74	0.952
M2-2	451,620	21,150	0.723	19.41	0.913
M2-L3	455,720	21,150	0.694	14.97	1.132
M2-L4	451,620	21,150	0.712	16.45	1.119
M3-1	445,260	30,500	0.748	30.88	0.565
M3-L2	445,,260	30,500	0.687	16.55	0.744
M4-1	492,190	29,620	0.789	16.75	0.828
M4-L2	492,190	29,620	0.781	16.75	0.799
M5-1	463,830	39,780	0.980	37.33	0.521
M5-L2	463,830	39,780	0.866	37.50	0.619
M5-L3	463,830	39,780	0.975	45.50	0.524

Table 3-4 – Variability of Semi-Adiabatic Calorimetry Tests

Tests Compared	Percent Difference			Temperature Difference (°C)
	α_u	τ	β	
M1-1 versus M1-2	9.3	3.9	4.3	6.2
M1-1 versus M1-L3	6.7	33.0	9.8	3.2
M2-1 versus M2-L3	8.8	17.5	19.0	3.6
M2-2 versus M2-L4	1.5	15.2	22.5	5
M3-1 versus M3-L2	8.2	46.4	31.7	3.5
M4-1 versus M4-L2	1.0	0.0	3.5	1.9
M5-1 versus M5-L2	11.6	0.4	18.8	8.1
M5-1 versus M5-L3	0.4	21.9	0.4	1.8

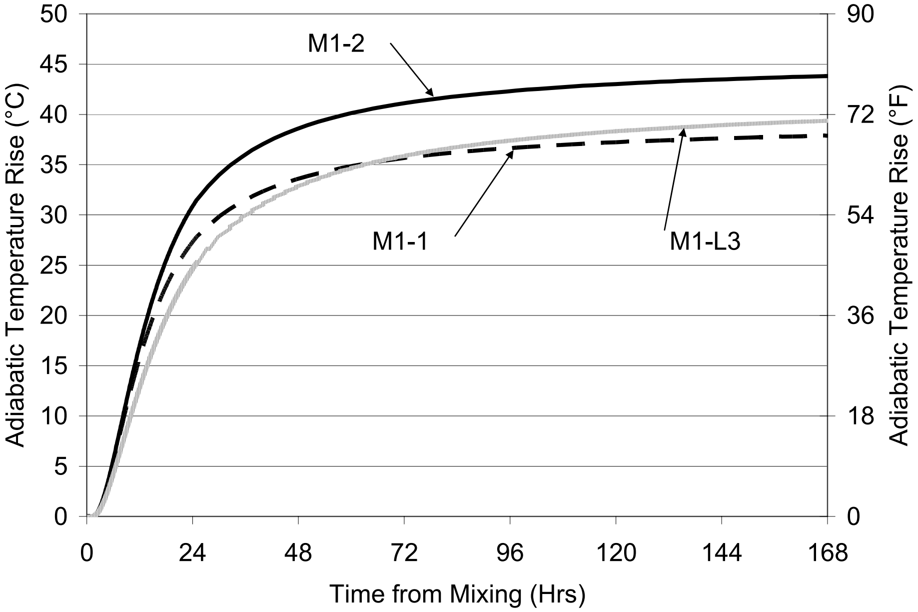

Figure 3-1 – Adiabatic Temperature Rise for M1

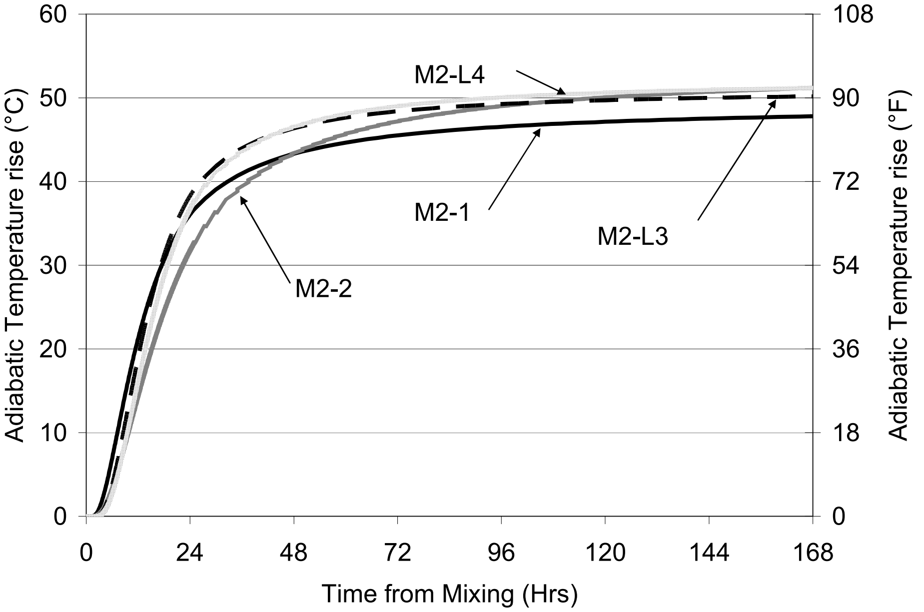

Figure 3-2 – Adiabatic Temperature Rise for M2

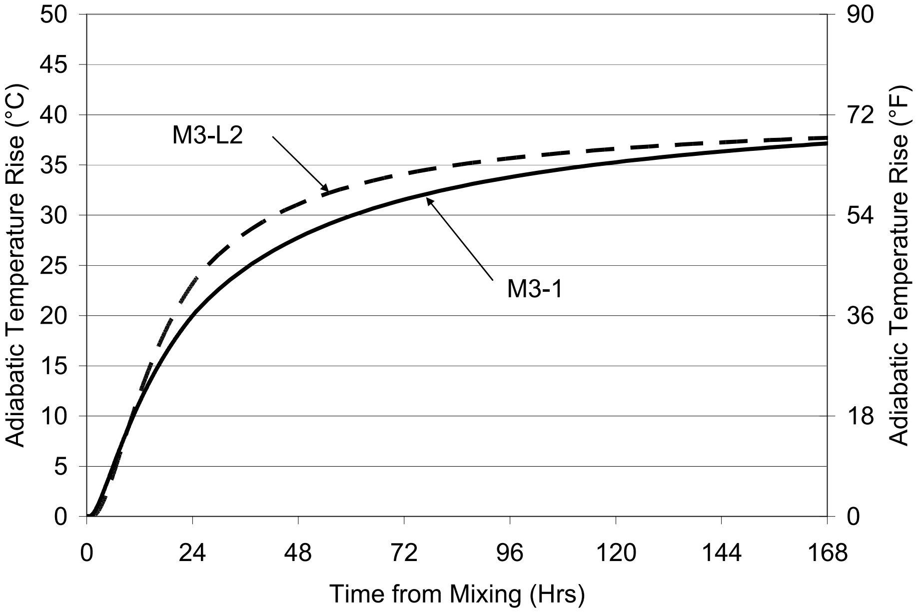

Figure 3-3 – Adiabatic Temperature Rise for M3

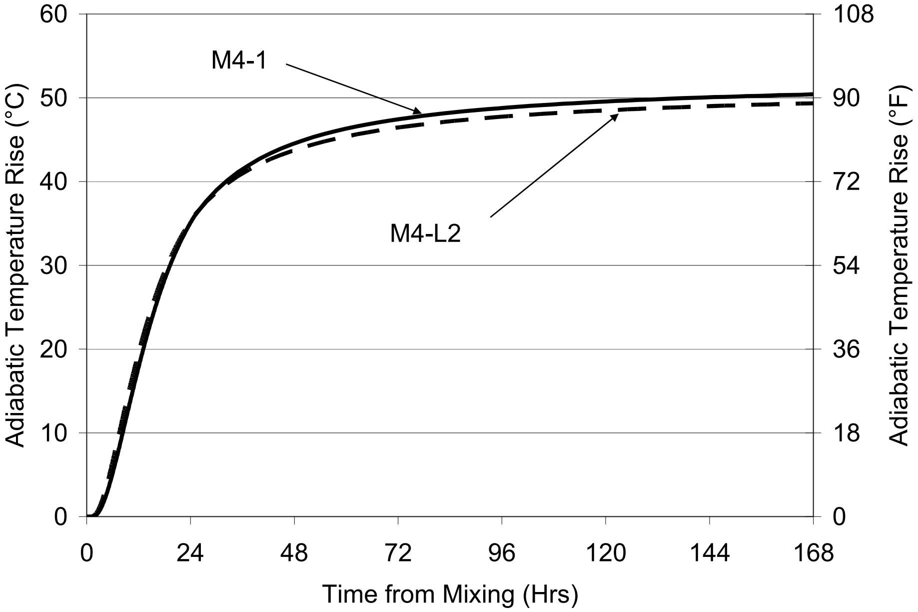

Figure 3-4 – Adiabatic Temperature Rise for M4

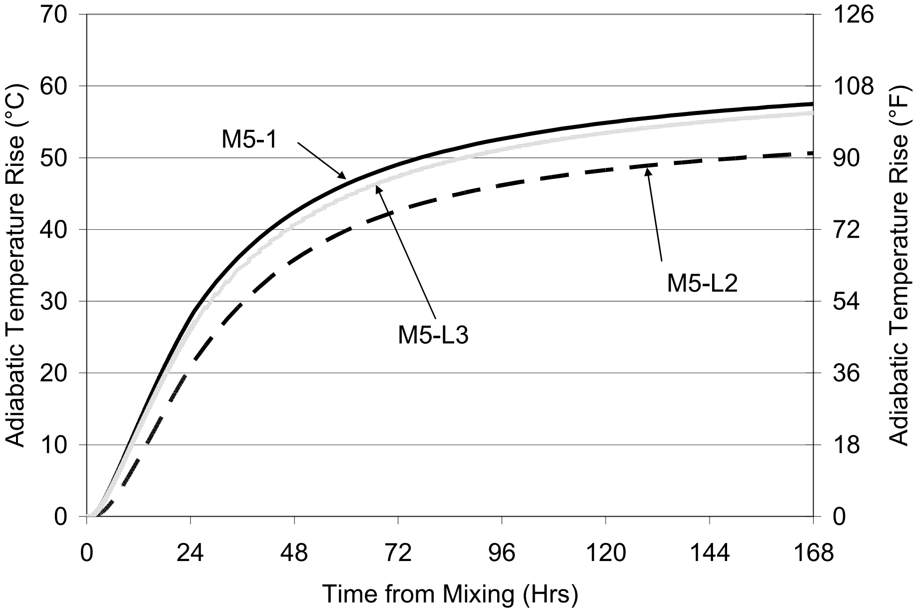

Figure 3-5 – Adiabatic Temperature Rise for M5

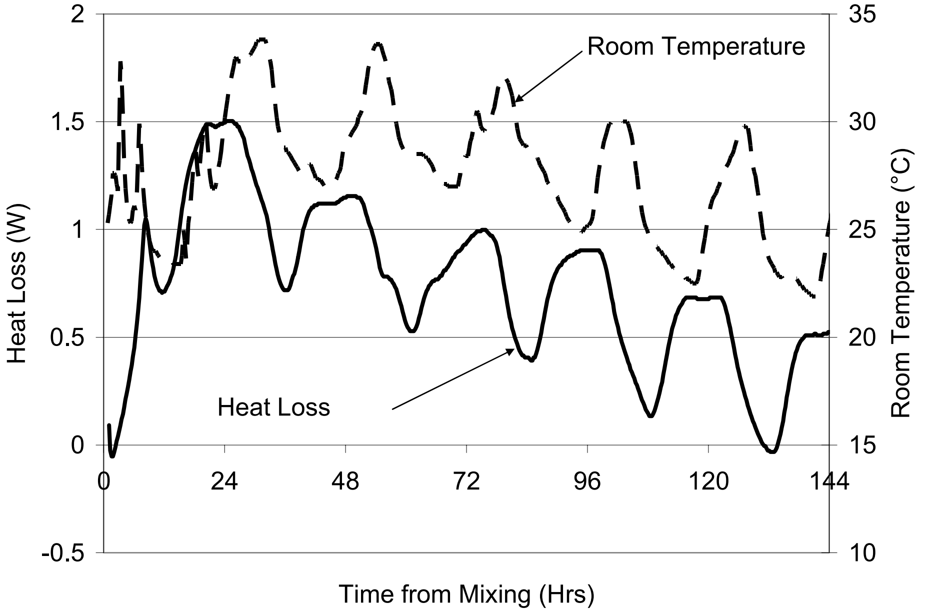

Figure 3-6 – Heat Flux and Room Temperature Measured During Test M3-1

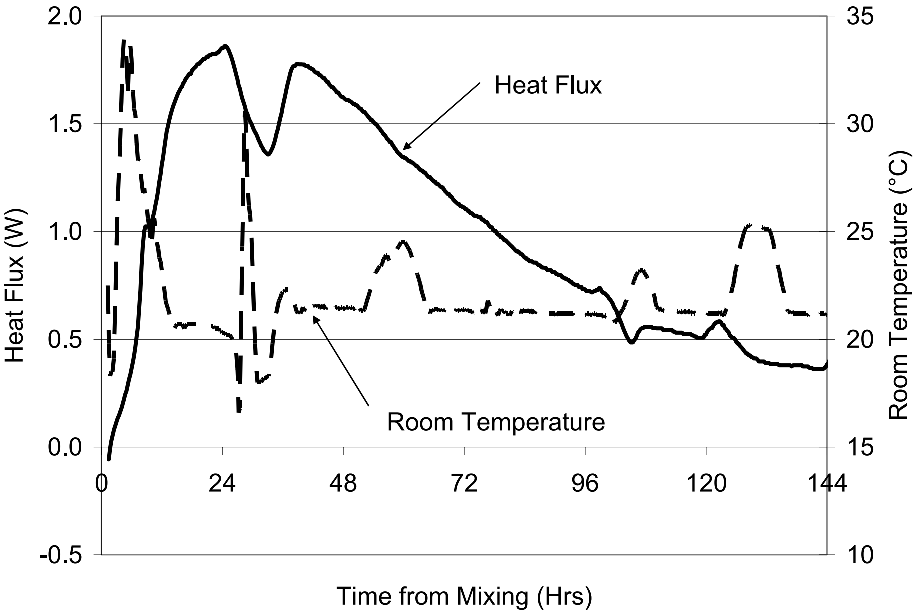

Figure 3-7 – Heat Flux and Room Temperature Measured During Test M5-1

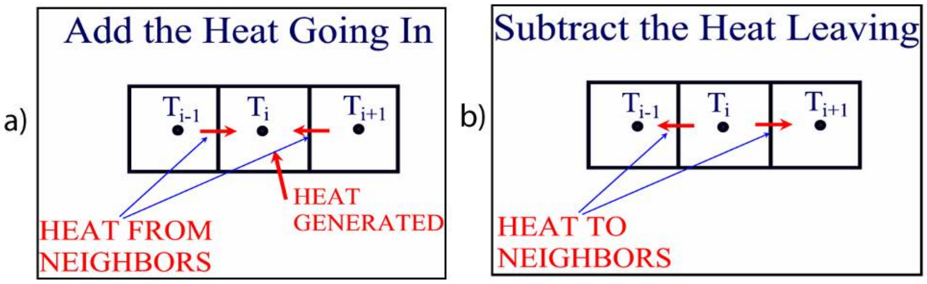

Figure 3-8 – Control Volume Method for Calculating Concrete Heat Transfer

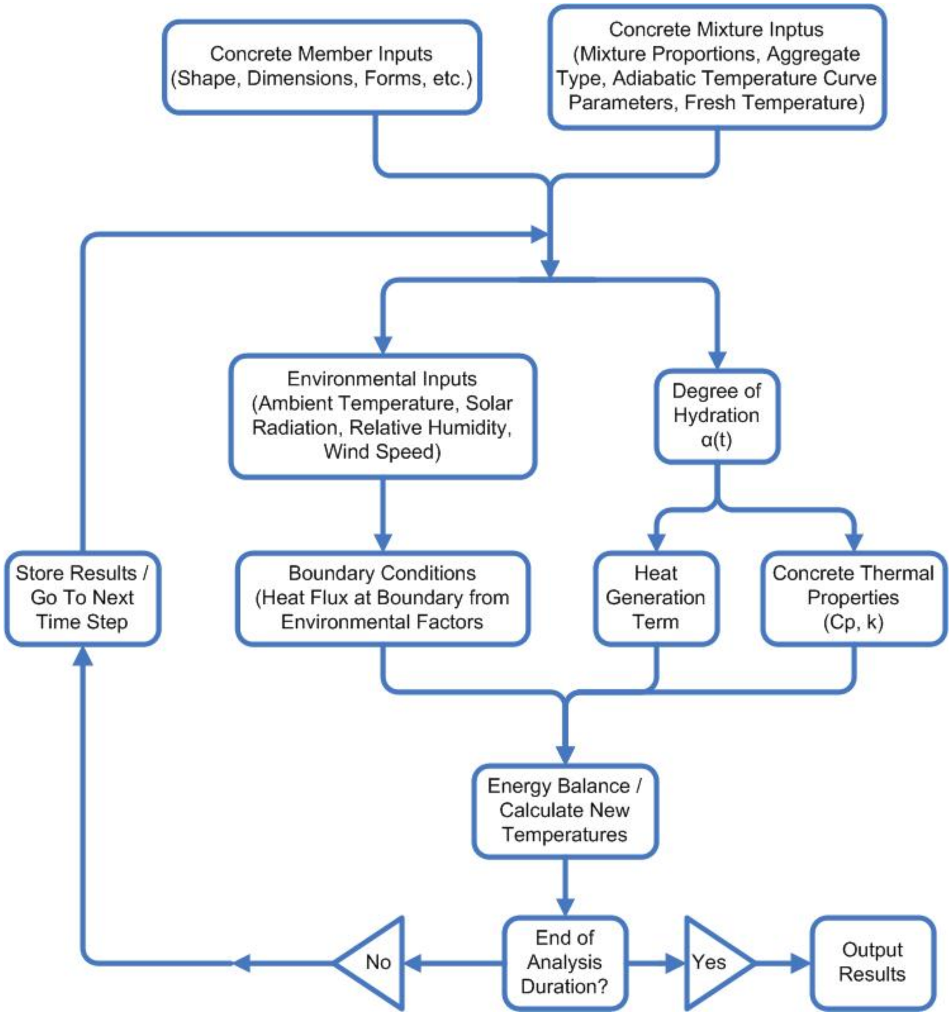

Figure 3-9 – Flow Chart of Concrete Temperature Calculations

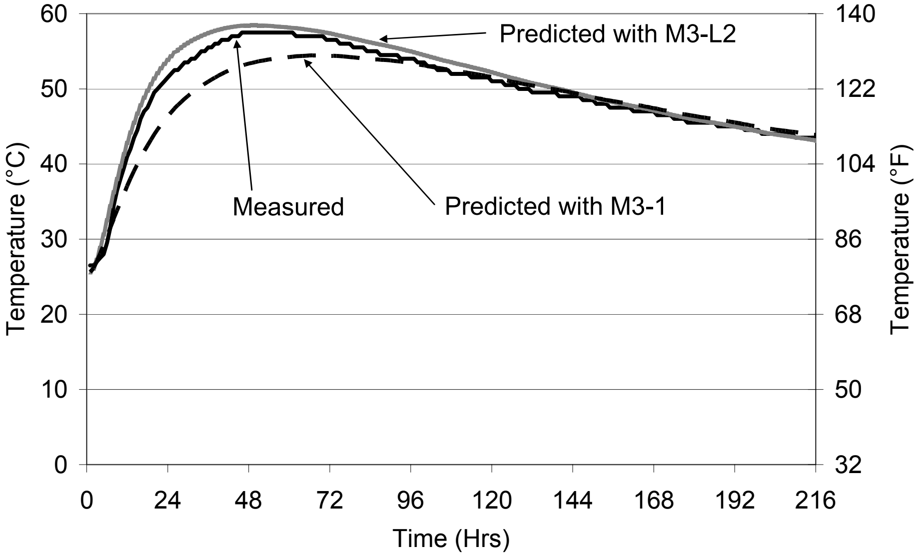

Figure 3-10 – Concrete Footing Core Measured vs. Predicted Temperature Using M3-1 and M3-L2

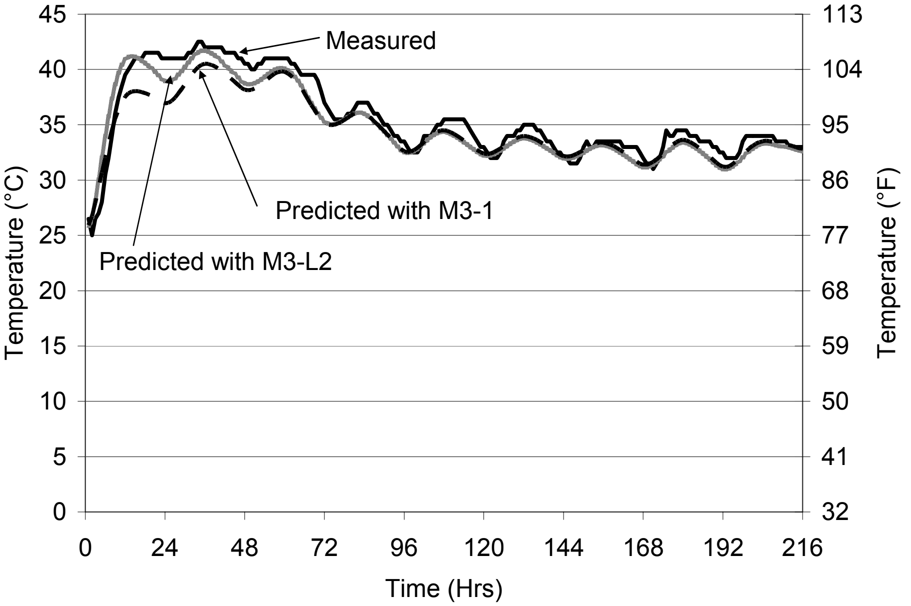

Figure 3-11 – Concrete Footing Near Surface Measured vs. Predicted Temperature Using M3-1 and M3-L2

CHAPTER 4 QUANTIFICATION OF THE EFFECTS OF FLY ASH TYPE ON CONCRETE EARLY-AGE CRACKING

The mechanisms that contribute to early age cracking are complex. Determining the relative importance of each mechanism, as well as the combined cracking potential for a given concrete material is essential to allow the concrete industry to construct structures with a long service life. A method for quantifying the cracking risk of a concrete mixture is presented. The method involves testing for the concrete heat of hydration, setting time, free thermal and autogenous movement, restrained stress, and mechanical property development. The concrete uniaxial stress under restrained conditions is measured using a rigid cracking frame. This test setup was used to quantify the effects of using fly ash on concrete cracking risk using four different fly ashes with varying calcium oxide contents. All fly ashes reduced the cracking risk, because of the decrease in the heat of hydration of the cementitious materials and to a lesser extent the increased early-age creep.

4.1 Introduction

In recent years, the drive for rapid construction and durable concrete has led to the use of very high strength concrete with lower water-to-cementing materials ratios (*w/cm*) and higher cementitious contents. At the same time, the size of many concrete bridge members has increased for structural and aesthetic reasons. The increased member size and increased cement content used, have drawn concern over the potential risk for thermal and autogenous shrinkage cracking in these members. The last thing that owners want to see is very durable concrete between the cracks, when they expect a durable structure.

The causes of restrained concrete cracking can be very complex. The cracking risk is dependent on the structural design, proper materials selection, and good construction practices. The structural design must allow for a reasonable amount of expansion and contraction. The concrete mixture proportions must then be designed to limit the heat of hydration, drying shrinkage, and autogenous shrinkage to acceptable levels for the member. The contractor must then use good construction practices, placement rates, and proper curing that are specific to the type of materials used (e.g. concrete with supplementary cementing materials (SCMs) may need extra curing time to prevent cracking).

The selection of concrete materials with a low cracking risk involves many interrelated factors. A comparison of the concrete stress development to the strength development can be used to determine the cracking risk of a mixture (Emborg 1998b). The stress development is dependent on the volume change, elastic modulus development, and rate of creep. The temperature development and hence thermal volume change of concrete, depends on the aggregate type used, fresh concrete temperature, cementitious materials used, chemical admixtures, member size and dimensions, and environmental conditions (van Breugel 1998). The autogenous shrinkage development depends on the temperature, cementitious materials used, and *w/cm* (Lura et al. 2001, Justnes 1999). The rate of elastic modulus development versus the rate of volume change and location of volume change in the member will determine how much beneficial pre-compression is developed in the concrete at early ages (Springenschmid and Breitenbücher 1998). The creep rate depends on the stress level, the concrete age, the materials, the elastic modulus, and the temperature (Bažant 1972, Bažant and Chern 1985).

This paper will focus on a battery of tests that, when performed, will allow the user to ascertain the volume change, creep behavior, and mechanical property development of different concrete mixtures. The results of these tests allow direct quantification of the cracking sensitivity of a specific mixture. The testing regime was then used to examine the effect of fly ash with varying calcium oxide (CaO) levels on concrete cracking sensitivity. The CaO level of the fly ash has been shown to be an indicator of its cementitious nature and thus the amount of heat liberated during hydration (Schindler and Folliard 2005). The following are not well understood: the relative importance of reducing the heat of hydration as compared to the reduction in early age strength, and the increase in creep and decrease in elastic modulus associated with the use of fly ash. The testing regime described in this paper presents a method of quantifying the benefits of each material property which can then be used in a varying-restraint induced stress analysis and modeling of the structure to determine the cracking risk.

4.2 Research Significance

Early-age cracking in mass concrete bridge has become a concern in recent years. Bridge member sizes have increased, increasing the risk of thermal cracking in many structures. Lower w/cm concretes have been used to produce denser, lower permeability concrete while at the same time increasing the risk of autogenous shrinkage. This paper outlines a battery of tests that together may be used to assess the early-age thermal and autogenous shrinkage cracking risk of a concrete mixture. The effects of fly ash CaO content are examined as an example of the usefulness of this method.

4.3 Experimental Procedure

The testing procedure used for this study for each concrete mixture can be divided up into two phases, the hydration characterization phase and the mechanical response phase. In the hydration characterization phase, semi-adiabatic calorimetry is performed on the concrete mixture. The adiabatic heat generation curve parameters (Schindler and Folliard 2005) obtained for the mixtures are then used to simulate the temperature development of the mixture in a specific structural element, which are imposed on the tests conducted under phase two. Other researchers have performed cracking tests by simulating various sized concrete members and boundary conditions (Westman 1999, Kanstad et al. 2001, and Schöppel et al. 1994). The center point of a simulated 1 m thick wall was chosen to allow for a large heat gain, and therefore large differentiation between material behaviors. The temperature history of concrete in the simulated wall was calculated using a constant surface temperature to keep the calculations simple and allow for the simulation of normal, hot, or cold climates. The concrete fresh temperature can also be changed in the simulation to quantify the effects of concrete pre-cooling on the mixture's cracking sensitivity. The advantage of this approach is that the configuration of the structural member and nature the cementitious materials system will dictate the concrete temperature development in each test. This approach thus allows one to test the cracking sensitivity of the concrete under realistic conditions that the concrete may be exposed to during construction. The experiments reported in this paper were conducted with a fresh temperature and simulated wall surface temperature of 23°C (73°F).

The mechanical response of the concrete mixture is tested in phase two of the testing program. The second phase of testing used in this testing regime allows for the quantification of the concrete mechanical property development, free thermal dilation, autogenous shrinkage, and early age creep response. Figure 4-1 summarizes the testing sequence used.

The concrete uniaxial stress under restrained conditions is measured using a rigid cracking frame (Mangold 1998). Figure 4-2 shows a drawing of the rigid cracking frame and a picture of the test setup. A 150 x 150 x 1250 mm (6” x 6” x 49”) concrete specimen is placed, consolidated, and cured in the rigid cracking frame. The formwork of the rigid cracking frame allows the temperature of the freshly placed concrete to be conditioned to simulate various structural elements. The temperature of the rigid cracking frame specimen is controlled using a programmable refrigerating/heating circulator that circulates a 50/50% mixture of water and ethylene glycol through copper pipes in the formwork and cracking frame crosshead. The circulator is controlled based on the temperature in the middle of cracking frame measured using a Type T thermocouple. The temperature in the concrete crossheads is also measured using Type T thermocouples. Because the temperature in the concrete is actively controlled, the difference between the temperature in the specimen middle and crosshead is generally within 0.5°C (0.9°F/hr). If the concrete specimen does not crack after 96 hours, it is cooled at a rate of 1°C/hr (1.8°F/hr) to induce cracking in the concrete and to measure the direct tensile strength. The temperature at which the concrete cracks is referred to as the “cracking temperature” (Springenschmid and Breitenbücher 1998). The lower the cracking temperature is, the better the concrete mixture’s resistance to thermal cracking (Springenschmid and Breitenbücher 1998).

The stress in the rigid cracking frame is monitored with strain gauges mounted on the 100 mm diameter Invar restraining bars. The degree of restraint provided by the Invar bars on the concrete can be calculated using Equation 4-1 (Mangold):

$$\delta = \frac{100}{1 + \left(\frac{E_c A_c}{E_s A_s} \right)} \qquad \textbf{Equation 4-1}$$

where δ is the degree of restraint (%), E_c is the concrete elastic modulus (MPa), A_c is the concrete cross sectional area (m^2), E_s is the Invar restraining bar modulus (MPa), and A_s is the invar restraining bars cross sectional area (m^2). The temperature of the Invar bars at the location of the strain gauges is measured using a resistance temperature detector (RTD) probe. The thermal movement of the Invar restraining bars also needs to be subtracted from the measured strain to calculate the actual stress induced strain in the Invar bars, as shown in Equation 4-2:

$$\varepsilon_{Tadj} = \Delta T_{ib} \cdot \alpha_{ib} \cdot \delta \qquad \textbf{Equation 4-2}$$

where ε_{Tadj} is the temperature induced strain of the invar bar, ΔT_{ib} is the temperature change of the Invar bar at the strain gauge (°C), and α_{ib} is the coefficient of thermal expansion of the invar bar (m/m/°C).

A free shrinkage frame has been developed to measure the free thermal and autogenous dilation of the concrete mixture. Figure 4-3 shows a diagram and picture of the free shrinkage frame. The free shrinkage specimen dimensions are 150 x 150 x 520 mm (6" x 6" x 20.4"). The bottom bar is made of Invar, as well as the threaded rods that are embedded in the concrete. The threaded rod is screwed onto to the linear potentiometer, which is then threaded onto a 25 x 25 mm (1" x 1") plate which is embedded in the concrete. The threaded rod is greased to allow for reuse. Two layers of plastic are used between the concrete and the formwork, with a petroleum based lubricant applied under each layer, to reduce friction between the specimen and the formwork as much as possible. The copper pipes in the free shrinkage frame's formwork are connected in series with the cracking frame and circulator to ensure that the free shrinkage frame's temperature stays within about 1°C (1.8°F) of the temperature of the concrete in the rigid cracking frame. The temperature is recorded using two thermocouples. The free shrinkage is initialized and set to zero at initial setting as determined following ASTM C 403 (2002), also using temperature controlled specimens as will be described later. Special care should be taken to make sure that the plastic extends to the end of the specimen and folds up so that mortar does not get under the plastic and increase friction. The top surface is sealed with plastic and adhesive aluminum tape. The opening on the end plate is drilled larger than the rod to reduce friction between the rod and the plate when the rod moves. Grease is used to fill the remainder of the hole left by the threaded invar rod to prevent moisture loss. The hole in the top formwork was drilled larger than the thermocouples to ensure that no restraint is provided by the thermocouple probes. Silicone is used to seal the holes in the formwork where the thermocouples are inserted.

Twenty-four 100 x 200 mm (4" x 8") concrete cylinders are match-cured to the cracking frame temperature for mechanical property testing as shown in Figure 4-4. The concrete cylinders are placed in an insulated water bath immediately after finishing. The temperature of the water bath is controlled to within about 1°C (1.8°F) of the rigid cracking frame temperature by another 28L (1 ft^3) capacity refrigerating/heating circulator. The cylinders are tested at ½, 1, 2, 3, 7, and 28 days for compressive strength, static modulus of elasticity (ASTM C 469 2002), and splitting tensile strength. When a cylinder is removed from the water bath for testing, it is replaced with a "dummy" cylinder to maintain a constant water level. A water bath is also placed in series with the concrete cylinder water bath to hold specimens for testing the time of setting of concrete mixtures by penetration resistance in accordance with ASTM C 403 (2005). When the match-cured time of setting specimens achieve initial set, the end plates in the free shrinkage rig are backed away from the concrete.

4.4 Early-Age Concrete Creep Analysis

The modulus of elasticity development, free thermal deformations, and autogenous deformation are used as inputs to predict the stress development of the concrete in the rigid cracking frame. The temperature distribution in the invar bar is also used to simulate the thermal movement of the Invar bar with time and the corresponding change in the degree of restraint of the concrete. The temperature distribution in the invar bar may be approximated by using symmetry and the temperature distribution for a fin of circular cross section with an adiabatic end tip (this is the case for symmetry in the middle of the invar restraining bar since there would be no heat exchange in the middle of a symmetrical bar). Equation 4-3 through Equation 4-6 show how the temperature distribution of a fin of uniform cross section with an adiabatic tip could be analytically simulated (Incropera and Dewitt 2002):

$$\frac{\theta}{\theta_b} = \frac{\cosh m(L-x)}{\cosh mL}$$ **Equation 4-3**

$$\theta = T - T_{\infty}$$ **Equation 4-4**

$$\theta_b = T_b - T_{\infty}$$ **Equation 4-5**

$$m = \left|\sqrt{2h / kr}\right|$$ **Equation 4-6**

where L is half the length of the invar rod (because symmetry is being exploited) (m), x is the distance along the invar rod from the cracking frame crosshead (m), T is the temperature in the invar rod at location x (°C), T_b is the temperature of the invar rod at the cracking frame crosshead (°C), T_{∞} is the ambient temperature (°C), h is the convection coefficient (W/m^2/°C), k is the invar rod thermal conductivity (W/m/°C), and r is the invar rod radius (m).

Once the elastic strain is calculated, the creep response can then be calculated using the principle of superposition (Bažant 1972). The calculated stresses after creep can then be compared to the measured stresses. A regression analysis is used to determine the creep parameters that provide the best-fit of the measured stresses. The procedure for calculating the early-age creep parameters by fitting creep constants to the measured concrete stresses in the rigid cracking frame assumes that creep in compression and tension are equal. In this paper, the Linear Logarithmic Model (LLM), as developed by Larson (2003) is used to model the creep behavior. The method models the creep compliance as two linear functions on a log scale, as shown in Figure 4-5. Equation 4-7and Equation 4-8 show the creep compliance using the Linear Logarithmic Model (Larson 2003):

$$\Delta J(\Delta t_{load}, t_0) = \begin{cases} a_1(t_0)\cdot\log\left(\dfrac{\Delta t_{load}}{\Delta t_0}\right) & \text{For } \Delta t_0 \leq \Delta t_{load} < \Delta t_1 \\ a_1(t_0)\cdot\log\left(\dfrac{\Delta t_{load}}{\Delta t_0}\right) + a_2(t_0)\cdot\log\left(\dfrac{\Delta t_{load}}{\Delta t_1}\right) & \text{For } \Delta t_{load} \geq \Delta t_1 \end{cases}$$

Equation 4-7

$$a_i(t_0) = a_i^{\min} + (a_i^{\max} - a_i^{\min})\cdot\exp\left(-\left(\frac{t_0 - t_s}{t_{ai}}\right)^{n_{ai}}\right)$$

Equation 4-8

for $i = 1,2$, where ΔJ is the increase in creep compliance (1/Pa), Δt_{load} is the time from application of the load (days), Δt_0 is the time of load application (days), Δt_1 is the time limit that transitions between short term and long term creep (days), t_s is the apparent setting time (days), a_i^{max}, a_i^{min}, t_{ai} and n_{ai} are fit parameters. Each of these parameters are defined and explained in detail elsewhere (Larson 2003).

4.5 Materials tested

A total of five different concrete mixtures were tested using the procedure outlined earlier. A Type I cement was used in all concrete mixtures tested. A No. 57 gradation (ASTM C 33 2003) siliceous river gravel coarse aggregate and natural siliceous sand were used in all mixtures. The mixture proportions used in each test are shown in Table 4-1. Four different fly ashes with varying CaO content, two ASTM C 618 Class F and two Class C fly ashes (2003), were tested at a 20% replacement level by mass. The fly ash chemical composition and Blaine fineness are shown in Table 4-2. All mixtures were tested using a *w/cm* of 0.42. All mixtures contained 4 oz/cwt of ASTM Type A low-range water reducing admixture (ASTM C 494 1999).

4.6 Results and Discussion

The semi-adiabatic test results for each mixture were used to simulate the temperature at the middle of a 1 m (39”) thick wall with a constant surface temperature of 23°C (73°F). Figure 4-6 shows the temperature measured in the middle of the cracking frame specimens and the resulting stress development. All of the concrete mixtures containing fly ash show a significant reduction in heat of hydration, with the Class F fly ashes showing the most decrease. The penetration resistance values measured from the match-cured setting test specimens are shown in Figure 4-7. All fly ashes tested show a retardation in setting, possibly due to a dilution of portland cement concentration. Both Class C fly ashes appear to retard more than the Class F fly ashes. FA3 shows more retardation than the other fly ashes tested. Previous researchers have shown that Class C fly ashes can have different setting behavior than Class F ashes, but results are highly variable (Naik and Singh 1997). The cracking behavior of mixtures with significantly delayed setting may be quite different than that of mixtures measured in this paper. More extensive testing and caution is recommended when using mixtures with very long setting times. The cracking frame results (see Figure 4-6b) show that all of the fly ashes tested lowered restraint stresses and improved cracking resistance. The Class F fly ashes lowered the cracking temperature by an average of 7.5°C (13.5°F), while the Class C fly ashes lowered the cracking temperature by an average of 4.2°C (7.6°F). Figure 4-8 shows the best-fit concrete splitting tensile strength development curves. It is significant to note that the mixtures containing Class F fly ash show the slowest strength gain rate, but the best cracking resistance. The measured modulus values for all the concrete mixtures show similar modulus developments with time, indicating that the lower heat of hydration and increased creep are more influential parameters in reducing cracking. The cracking resistance that is lost by the reduced tensile strength gain is more than made up by the lowered thermal strain (caused by the lowered heat of hydration) and increased creep. The stress-to-splitting tensile strength ratio development with time was as the quickest for the control mixture, but the fly ash mixture's development was only slightly lower, as shown in Figure 4-9. The free thermal and autogenous dilation results are shown in Figure 4-10. The fly ash mixtures showed considerable less expansion early on, probably because of the lowered heat of hydration during the first few hours of hydration during which time the coefficient of thermal expansion is higher (Yamakawa et al. 1986, Glisic 2000, Schöppel, K., and R. Springenschmid 1994).

Creep parameters were fit from the stress, free shrinkage, and modulus development data using the Linear Logarithmic Model (Larson 2003). A good fit of the stress data was achieved by adjusting only the ta_1 parameter, as shown in Table 4-3. The magnitude of a_1^{max}, a_1^{min}, and a_2^{max} are as recommended by Larson (2003). Figure 4-11 shows the decrease in the a_1 (the slope of the first linear portion or short term creep compliance) parameter with time. The creep compliance decreased faster with time in the concrete mixtures that had a higher heat of hydration. The Class F fly ashes showed higher early age creep, which helped contribute to the increased cracking resistance.

A numerical investigation into the relative importance of early age creep on the stress history was performed. Thermal stresses in a simulated cracking frame were calculated for the five mixtures using the creep parameters calculated and found in Table 4-3, the measured modulus development (using an equivalent age), and the temperature history recorded from the control mixture. The calculated stresses are shown in Figure 4-12. The higher the a_1 parameter, the lower the early-age stresses except in the case of Fly Ash 3. Fly ash 3 showed lower early-age compression stresses because of the delayed setting of the mixture. All of the mixtures were predicted to have higher tensile stresses than the control, because of less beneficial pre-compression due to the increased early age creep, but similar later age creep. Temperature effects on modulus and creep may give different actual results than that modeled. These numerical computations are not meant to imply that concrete containing fly ash increases the risk of cracking, only to illustrate the impact of the decrease in thermal strains. This simple numerical case study does show that the biggest impact on cracking resistance from the use of fly ash is the decrease in thermal movement. More research needed on concrete containing fly ash at lower *w/cm* to investigate its effect on autogenous shrinkage.

4.7 Conclusions

A method for calculating concrete early age creep parameters and determining the concrete resistance to cracking was presented. All fly ashes tested lowered the early age cracking risk of concrete. The concrete containing fly ash had a lower tensile strength development than the control mixture. This indicates that given *equal* stress development, the concrete containing fly ash should crack sooner than the control mixture. The cracking tendency for concrete containing fly ash however, was lower because the stresses were reduced by a lowered thermal strain (caused by a lowered heat of hydration) and increased early-age creep. In fact, the cracking tendency for concrete containing low calcium oxide fly ash was the lowest, even though its rate of tensile strength development was the slowest. It is the combined effect of creep, lower heat of hydration, modulus development, and tensile strength gain that defines the cracking risk. More testing needs performed on concrete containing fly ash at lower *w/cm* to investigate the effects of fly ash on autogenous shrinkage.

Further research is recommended to identify and quantify the effect of variables such as aggregate type, aggregate gradation, *w/cm*, cement type, SCM type, placement temperature, etc. on the cracking sensitivity of concrete.

4.8 Acknowledgements

The authors wish to express their gratitude to the Texas Department of Transportation through Project 0-4563 for funding this research. The advice and support of Ralph Browne and Tom Yarbrough of the Texas Department of Transportation is greatly appreciated. The guidance and assistance of Dr. Rupert Springenschmid and Mr. Erwin Gierlinger to develop the cracking frame test setup are appreciated.

Table 4-1 - Concrete Mixture Proportions (1 kg/m^3 = 1.69 lb/yd^3)

Material	**Mixture Identification**				
	Control	**FA1**	**FA2**	**FA3**	**FA4**
Cement (kg/m^3)	335	268	268	268	268
Fly Ash (kg/m^3)	0	67	67	67	67
Water (kg/m^3)	141	141	141	141	141
Coarse Aggregate (kg/m^3)	1143	1131	1133	1136	1136
Fine Aggregate (kg/m^3)	762	753	753	759	760
Air Content (%)	2.4	2	2.3	1.9	2.5

Table 4-2 - Fly Ash Chemical Composition and Blaine Fineness (1 m^2/kg = 4.9 ft^2/lb)

Item	Fly Ash Identification			
	FA1	FA2	FA3	FA4
Fly Ash Class	F	F	C	C
SiO_2 (%)	56.63	51.69	37.83	33.31
Al_2O_3 (%)	30.68	24.81	19.83	18.39
Fe_2O_3 (%)	4.94	4.22	6.17	5.4
CaO (%)	0.69	13.12	23.13	28.91
MgO (%)	0.73	2.29	4.62	5.25
Total Alkalis as Na_2O (%)	1.61	0.73	1.78	1.87
Blaine Surface Area (m^2/kg)	147.3	165.5	348.4	299.9

Table 4-3 - Calculated Concrete Creep Parameters using Linear Logarithmic Method (10^{-12}/Pa log = 6.9*10^{-9}/Psi log)

Mixture ID	Creep Parameters from Equation 4-7 and Equation 4-8							
	t_{a1} *(days)*	n_{a1}	a_1^{min} *(10^{-12}/Pa log)*	a_1^{max} *(10^{-12}/Pa log)*	t_{a2} *(days)*	n_{a2}	a_2^{min} *(10^{-12}/Pa log)*	a_2^{max} *(10^{-12}/Pa log)*
Cement	0.4	1.1	0.1	60	3	0.08	6	30
FA1	1.3	1.1	0.1	60	3	0.08	6	30
FA2	1.15	1.1	0.1	60	3	0.08	6	30
FA3	0.6	1.1	0.1	60	3	0.08	6	30
FA4	0.75	1.1	0.1	60	3	0.08	6	30

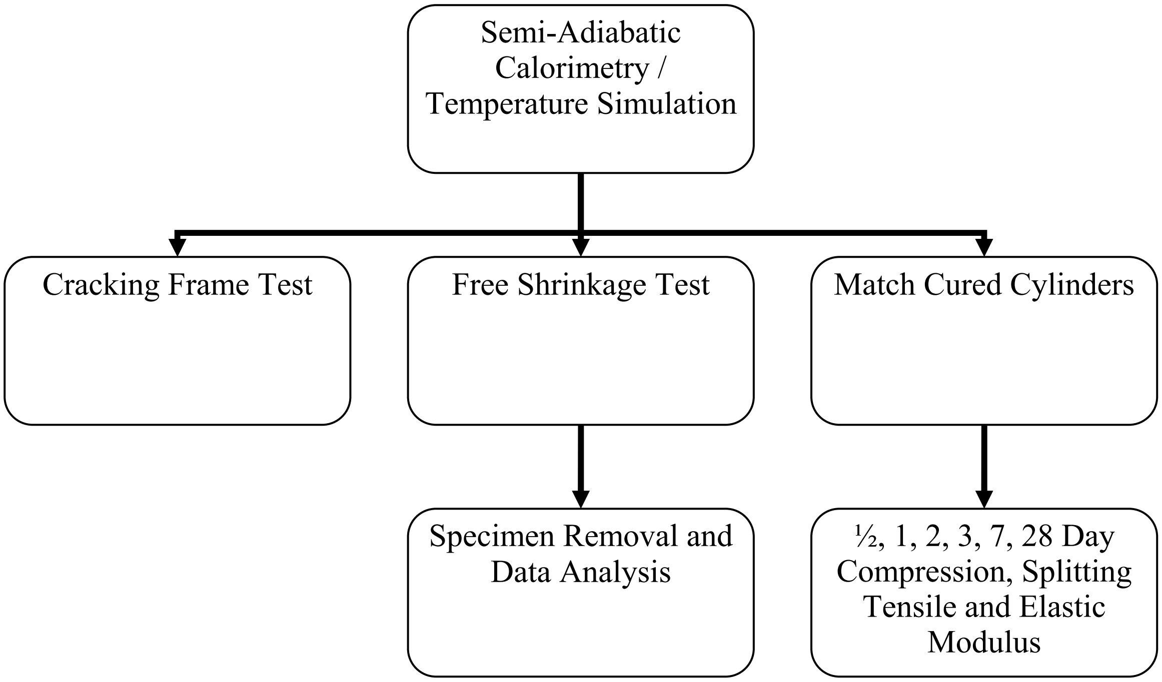

Figure 4-1 – Testing Program Summary

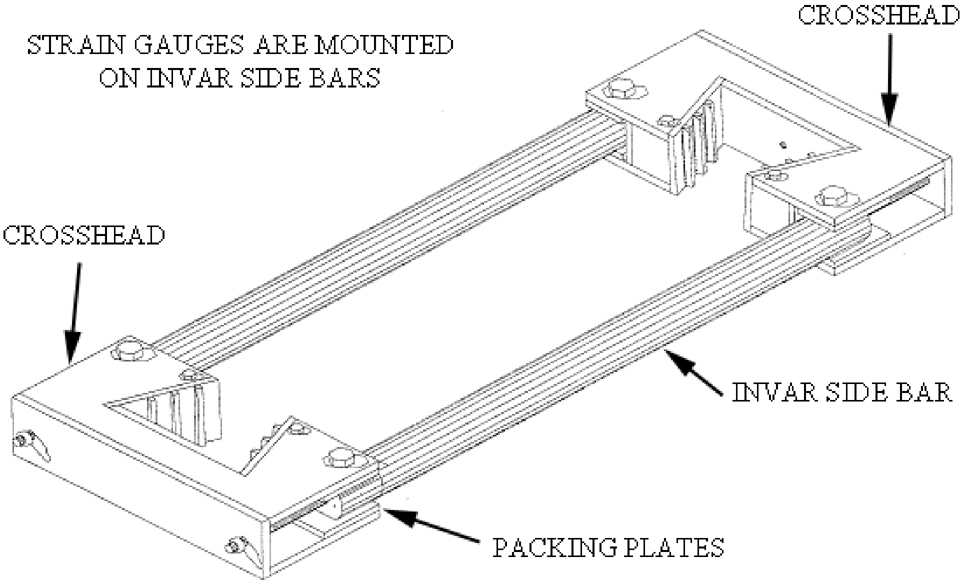

a)

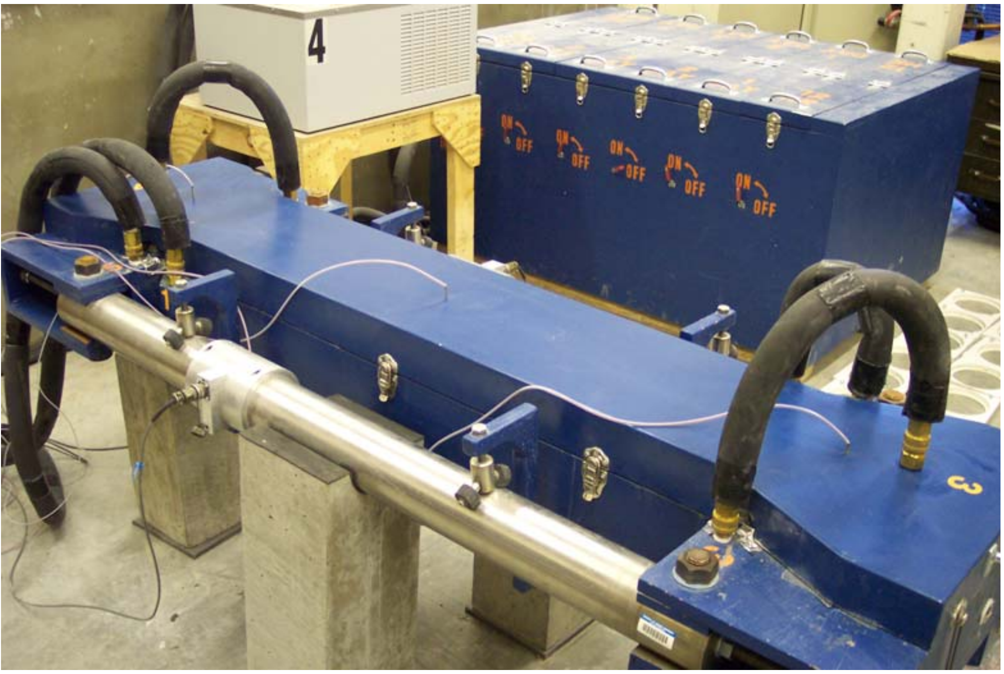

b)

Figure 4-2 –Rigid Cracking Frame a) Schematic of Frame without Crosshead Braces and Formwork b) Frame in Use (Whigham 2005)

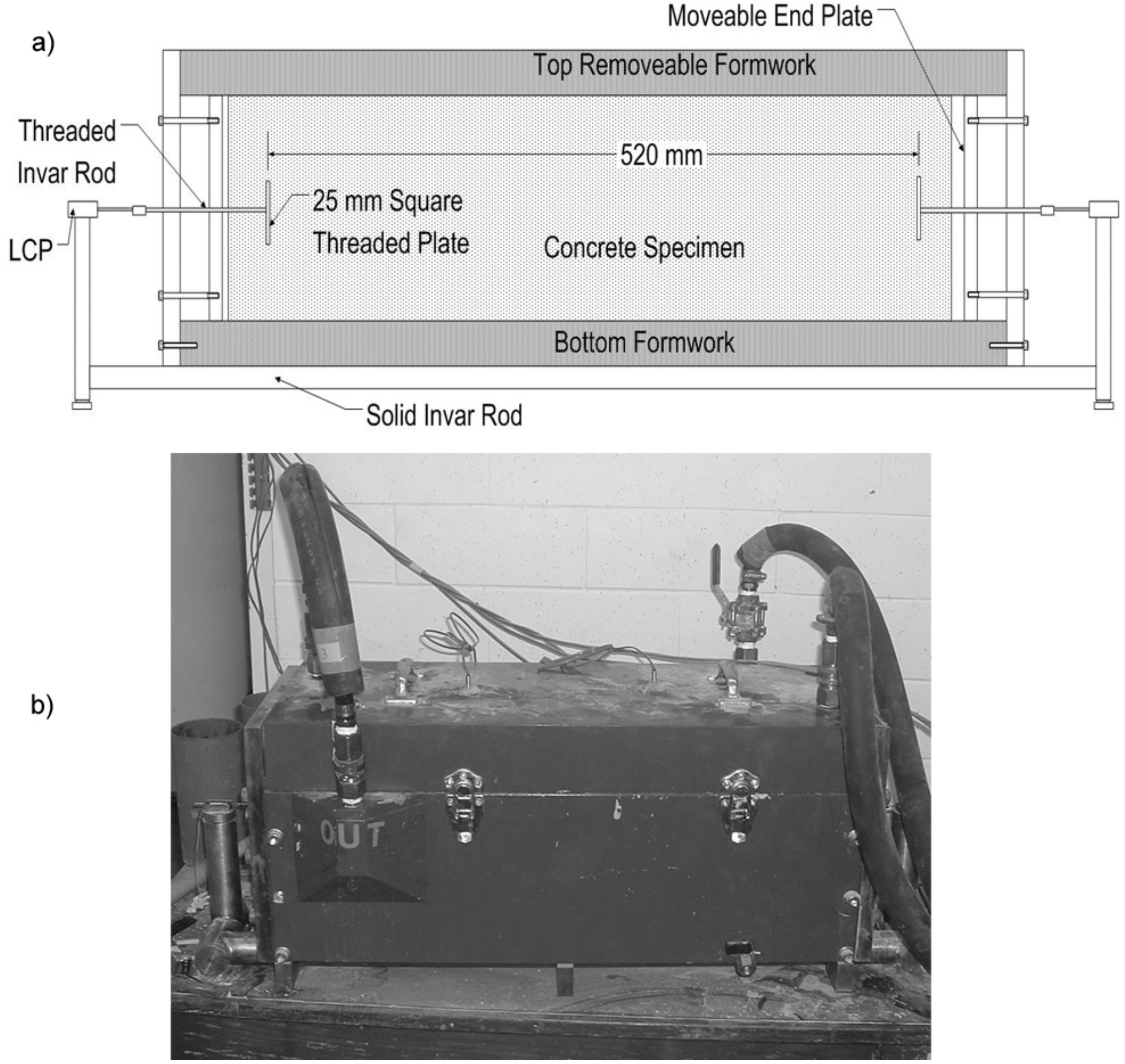

Figure 4-3 - Free Shrinkage Frame a) Diagram and b) Frame used for this Project

Figure 4-4 - Match Cured Concrete Cylinders

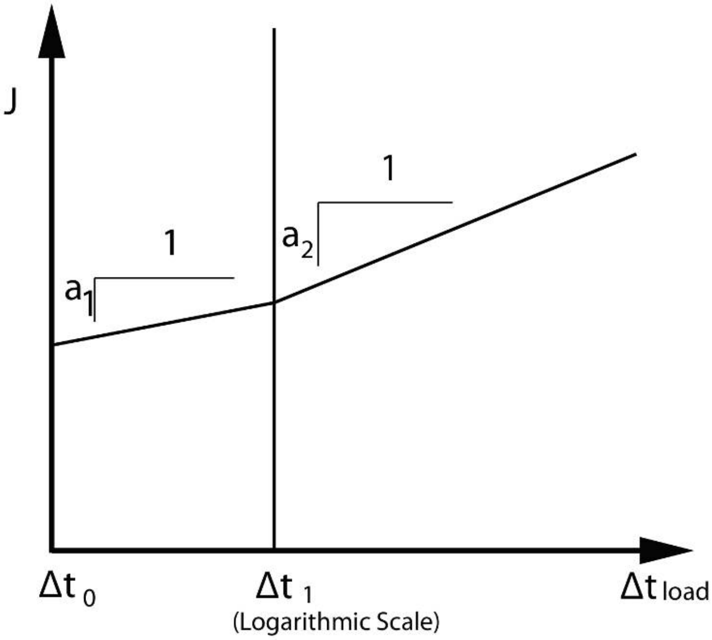

Figure 4-5 - Creep Compliance (J) Using the Linear Logarithmic Model (after Larson 2003)

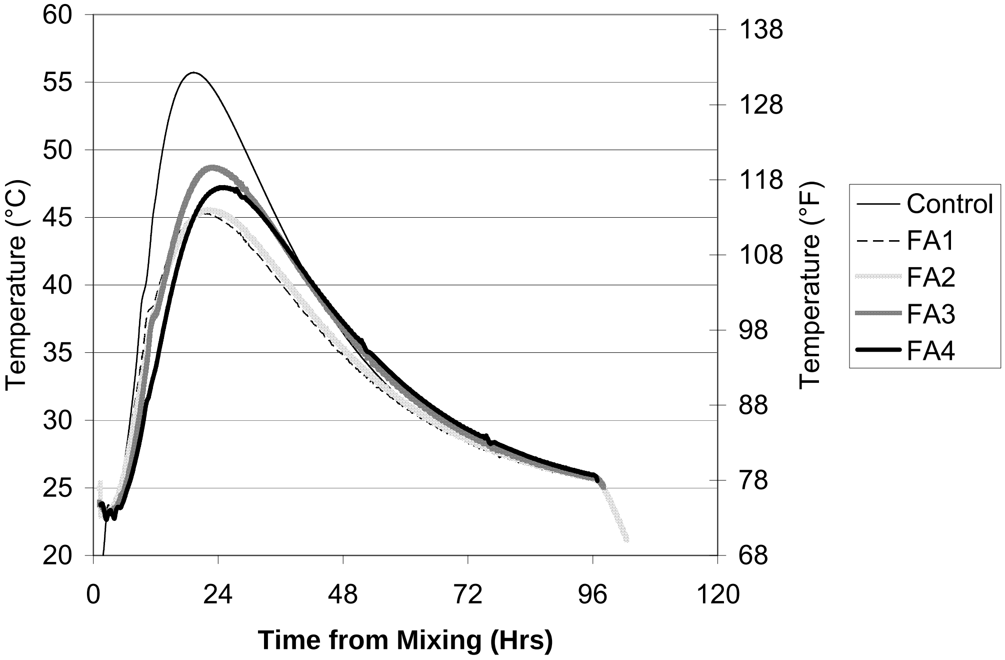

a)

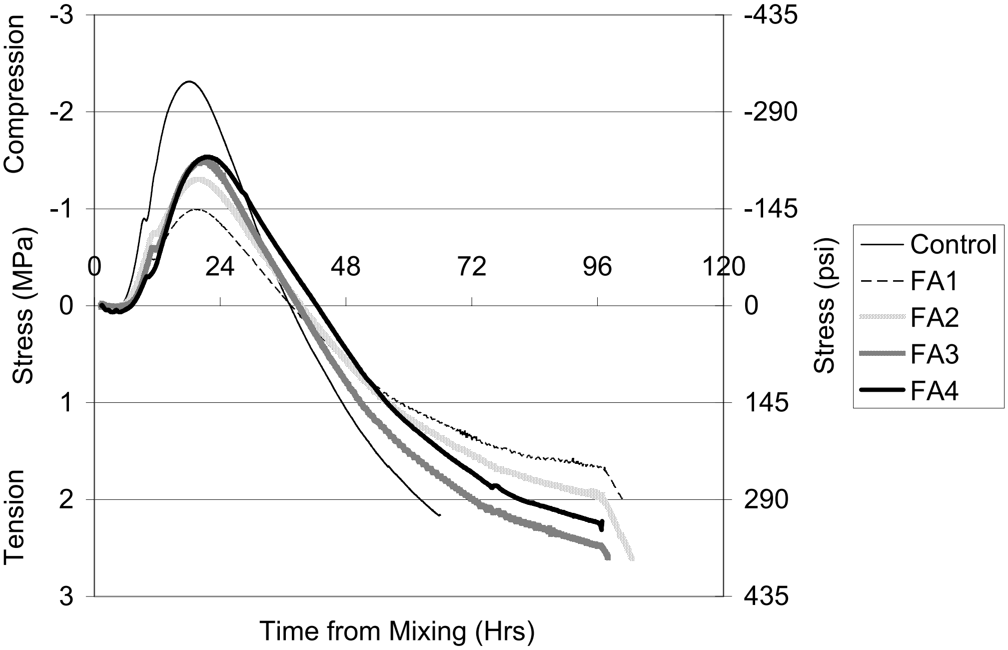

b)

Figure 4-6 - Rigid Cracking Frame a) Measured Temperatures and b) Measured Stresses

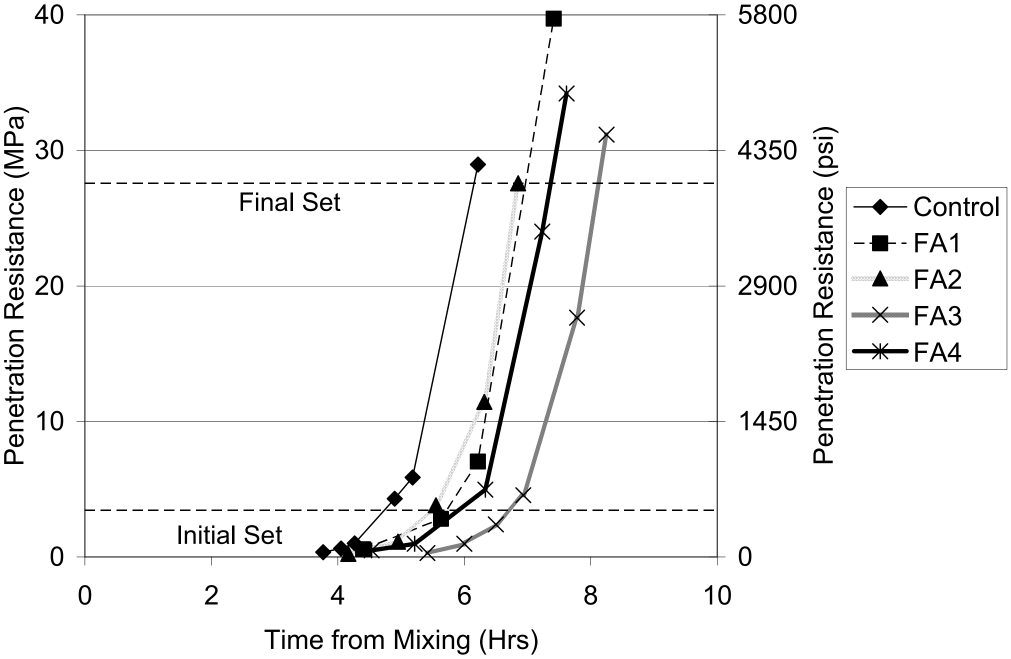

Figure 4-7 - Time of Setting of Concrete Mixtures using ASTM C 403

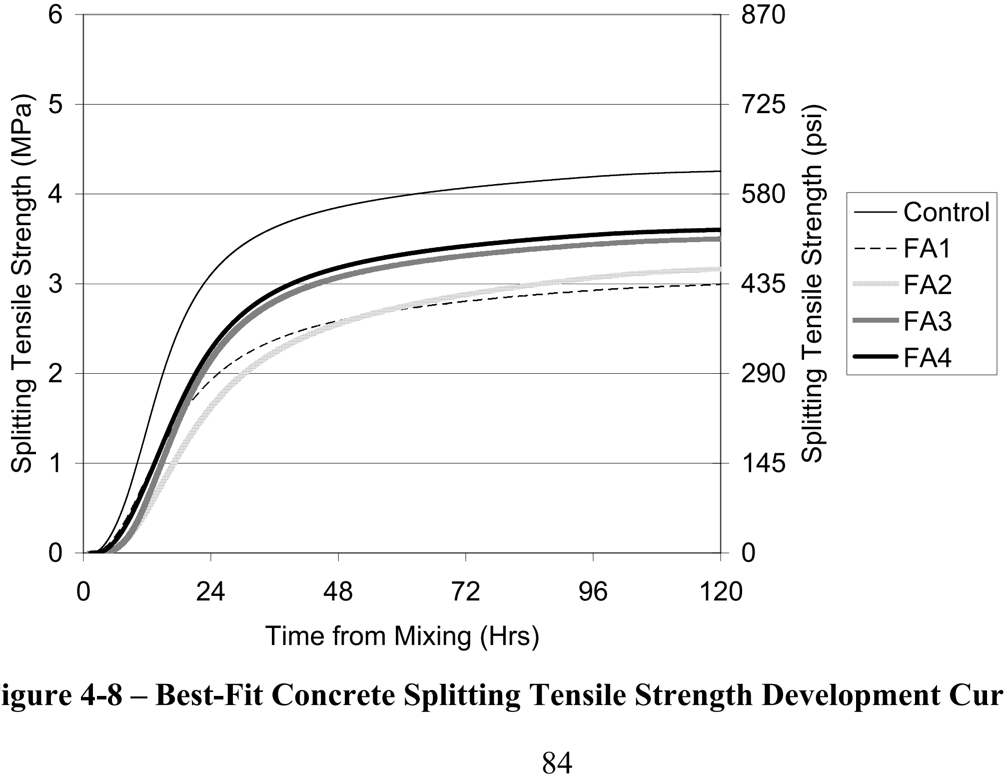

Figure 4-8 – Best-Fit Concrete Splitting Tensile Strength Development Curves

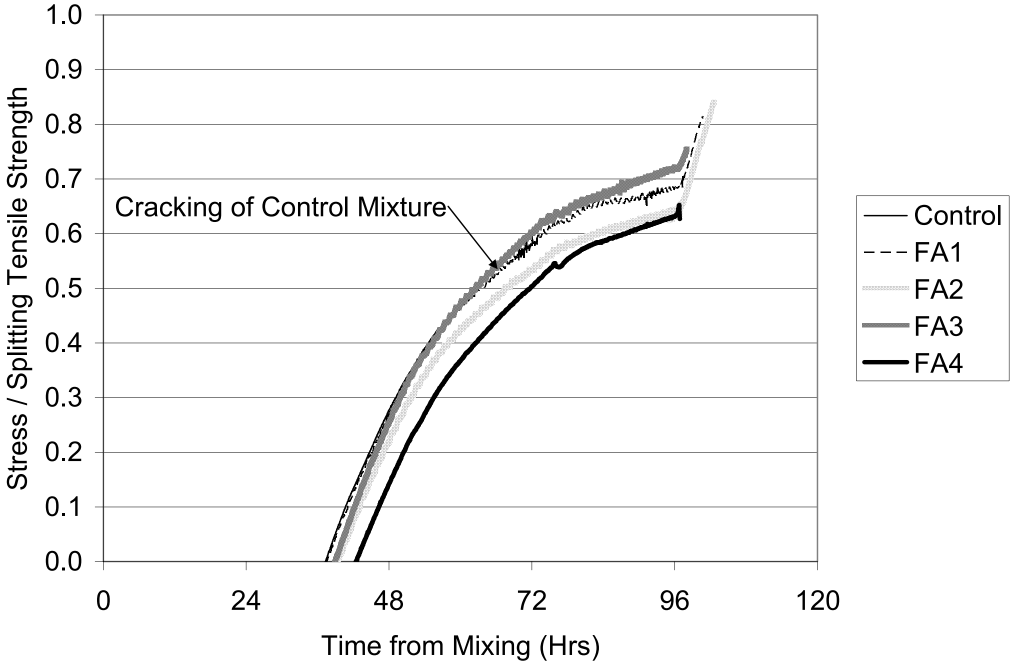

Figure 4-9 - Concrete Stress/ Splitting Tensile Strength

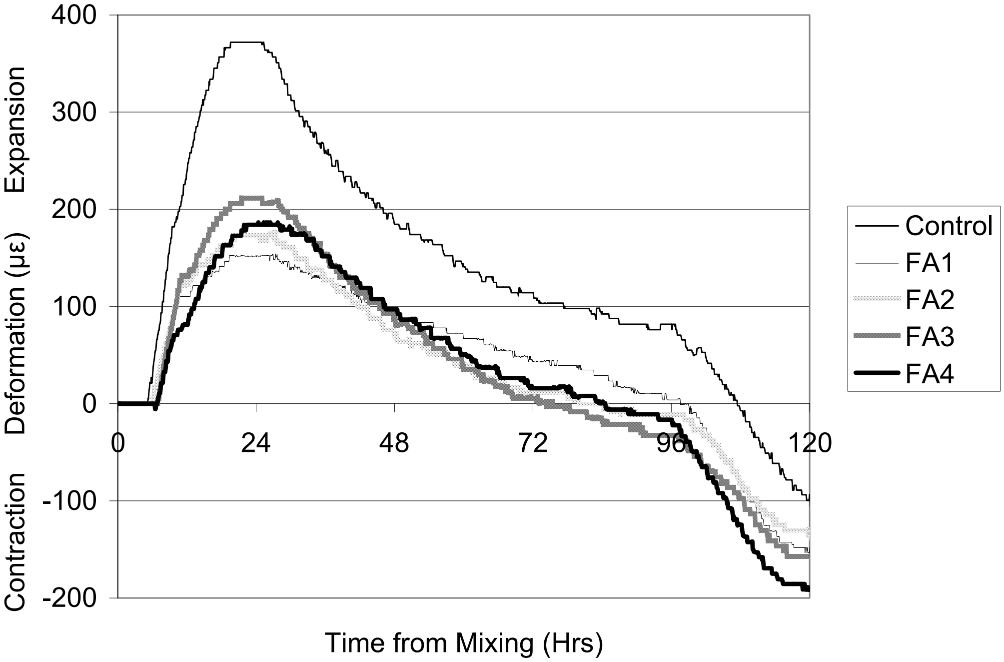

Figure 4-10 - Free Thermal and Autogenous Deformation

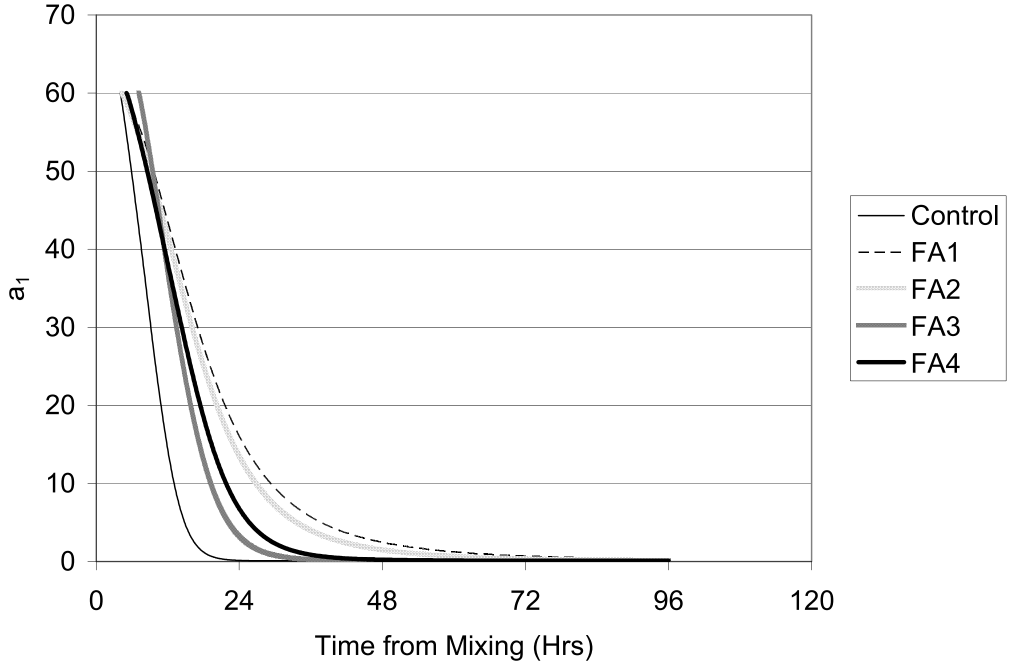

Figure 4-11 - Decrease in a_1 Parameter in Linear Logarithmic Model

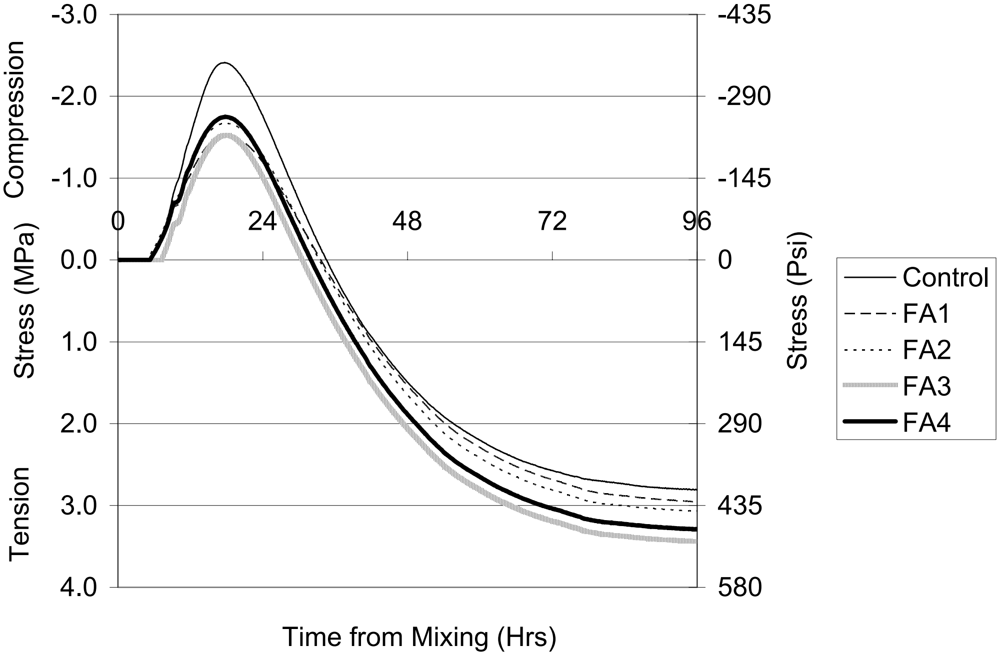

Figure 4-12 - Simulated Concrete Stress Using the Same Temperature History

CHAPTER 5 QUANTIFYING THE DEVELOPMENT OF EARLY AGE THERMAL STRESSES IN BRIDGE DECKS

Early-age bridge deck cracking is a major cause of premature bridge distress. Bridge deck temperature changes in the first few days after placement due to the concrete heat of hydration and changes in ambient conditions have long been identified as a significant contributor to early-age cracking. The goal of this project was to develop a method of examining thermal stresses in bridge decks and evaluate the effects of a few common construction practices on these thermal stresses. In this study, the ambient conditions and temperature development in a full-scale bridge deck were first measured to obtain an example bridge deck temperature profile. A series of tests on concrete mixtures, including mechanical property development and rigid cracking frame tests, were then performed to quantify the potential thermal stresses in bridge decks with different placement times and coefficients of thermal expansion. Concrete with a high coefficient of thermal expansion placed in the morning could lead to the development of thermal stresses equal to 75% of the stress at cracking. It was also found that the thermal stresses could be reduced by up to 50% by using concrete with a lower coefficient of thermal expansion and placing at night. The time of placement and the coefficient of thermal expansion of the concrete thus have a major impact on the cracking tendency of the concrete.

5.1 Introduction

Bridge decks are often exposed to large quantities of salts and deicing chemicals. In dense, un-cracked concrete, these aggressive agents penetrate into the concrete over many years and reach the reinforcing steel by capillary suction and absorption, pressure (usually hydrostatic), and diffusion (Mindess et al. 2003). In cracked concrete, the cracks provide quick access for these agents to the reinforcing steel, thus decreasing the structure's service life. The concrete early-age volume change, concrete material property development, and degree of restraint have been shown to be primary factors leading to early-age bridge deck cracking (Krauss and Rogalla 1996).

Early-age cracking can occur because of volume change that is restrained from movement. Early-age volume change in concrete occurs because of autogenous shrinkage, temperature changes, plastic and drying shrinkage. Autogenous shrinkage occurs in low water-to-cementing materials ratio (w/cm) concrete because there is not enough water available for complete hydration of the cement. As the cement hydration progresses, a water-vapor interface will form leading to a capillary underpressure in the pores. The capillary underpressure in the pores causes a hoop stress in the pore wall which consequently causes shrinkage (Mindess et al. 2003, Grasley 2006). Plastic and drying shrinkage occur because of moisture loss to the environment from concrete surfaces. Bridge decks are usually wet cured during the first several days after placement with wet blankets and plastic, which minimizes or eliminates early moisture loss to the environment. For this reason, plastic and drying shrinkage were not considered in this study.

The internal temperature profile and the period of time during which the concrete heat dissipation takes place can greatly affect the early-age stress development (Krauss and Rogalla 1996, Mangold 1995). The concrete temperature change is the driving mechanism behind thermal stress development. Furthermore, the concrete mechanical property development is dependent on the concrete temperature. The concrete mechanical properties that are relevant for early age stress development are the modulus of elasticity, the concrete coefficient of thermal expansion, Poisson's ratio, tensile strength, and creep during the first 24-36 hours after concrete placement (Springenschmid and Breitenbücher 1998). The rate of cement hydration is dependent on the temperature. The higher the temperature, the faster the cement will hydrate. Because mechanical properties are dependent on the cement hydration, they will develop faster at higher temperatures.

During the first hours after the concrete sets, any temperature rise will lead to pre-compression in restrained concrete because of the thermal expansion. After the elastic modulus increases because of the increased degree of cement hydration and microstructural formation, creep and any temperature decreases will quickly relieve the concrete pre-compression and lead to the development of tensile stresses (Springenschmid and Breitenbücher 1998). The timing of any temperature increase or decrease in relation to the modulus development is critical.

The degree of the bridge deck restraint directly affects the early-age concrete stress development. The concrete restraint is usually determined by the bridge configuration and construction sequence. The restraint can come from internal sources such as non-uniform temperature changes or drying shrinkage in the bridge deck. More importantly, the restraint can come from the girders changing volume at a different rate than the deck. This is caused by different temperature profiles, coefficients of thermal expansion, and/or different amounts of drying shrinkage in the deck and the girders. Composite construction obtained by the shear connections between the deck and girder will mean that some of the concrete bridge deck movement may cause a change in axial length of the span. Some of the differential volume change between the bridge deck and the girders will result in bending of the girders and deck. The rest of the differential volume change will be transformed into restraint. This restraint can be especially high in continuous span bridges (Krauss and Rogalla 1996). As the concrete hardens and the ratio of the bridge deck stiffness to girder stiffness decreases, the degree of restraint provided by the girders in a simple span will also decrease. Krauss and Rogalla (1996) found that bridge decks built on large girders can have a final degree of restraint of about 60%.

Rigid cracking frames have been used to quantify the relative impact of different materials, mixture proportions, and construction practices on thermal stresses (Springenschmid and Breitenbücher 1998). Figure 5-1 shows a schematic diagram and a photograph of a rigid cracking frame (RCF). A typical temperature and stress profile generated in the frame is shown in Figure 5-2, where T_{pc} is the temperature at the peak stress level, $T_{z,2}$ is the temperature at the second zero stress point, and T_c is the temperature at cracking (Springenschmid and Breitenbücher 1998). As the concrete temperature begins to increase due to the heat of hydration, the concrete will try to expand in proportion to the concrete coefficient of thermal expansion (CTE) and temperature. The concrete will not be able to expand because of the restraint provided by the cracking frame Invar steel bars, effectively converting a portion of the expansive thermal strain into compressive thermal stress. Stress relaxation and the eventual decrease in temperature will reduce the compressive stress in the concrete until it reaches zero again, or the second zero stress point $T_{z,2}$. A further decrease in the temperature will cause tensile stresses in the concrete to increase until the tensile stress exceeds the concrete tensile strength. Usually, insulation is provided in the formwork so that the temperature profile generated because of the concrete heat of hydration will simulate that of a 0.5 m thick concrete member, and if the concrete has not cracked by 96 hours, the concrete is cooled externally by 1°C/ hr (1.8°F/ hr) until it cracks, determining the cracking temperature, T_c (Mangold 1998).

The study reported in this paper focused on quantifying the development of early-age thermal stresses in bridge decks, focusing particularly on evaluating the effects of placement time and the concrete coefficient of thermal expansion. Rigid cracking frame testing combined with the examination of early age mechanical properties of the concrete were used to jointly calculate the cracking tendency of different concrete placement scenarios.

5.2 EXPERIMENTAL WORK

The experimental work performed was aimed at quantifying the potential contribution of thermal stresses to early-age bridge deck cracking. The first step in determining the potential for thermal stresses is determining the temperature history. In order to ensure that the thermal stresses measured during the restrained concrete testing would be representative of those possible in real bridge decks, a real bridge deck was instrumented and monitored for temperature development. The measured concrete bridge deck temperatures and those predicted for different placement times from the measured weather data were then used to evaluate the effects of different combinations of materials and placement times on concrete thermal stresses. A rigid cracking frame and match-cured concrete cylinders were used to quantify the thermal stress development possible in a bridge deck under these different scenarios.

5.2.1 BRIDGE DECK INSTRUMENTATION

The concrete for the bridge deck that was instrumented for temperature development was placed in Austin, Texas on August 17, 2006. The weather during the bridge deck placement and curing period was also monitored. Semi-adiabatic calorimetry testing was performed on the bridge deck concrete to obtain information on the heat produced during hydration. These data were used to predict the bridge deck temperature development with varying concrete placement times using a control-volume based finite difference method. More detailed information on the temperature development model used can be found elsewhere (Riding et al. 2007a, Riding et al. 2007b). The measured and predicted temperatures were then used as the concrete curing temperatures during the concrete thermal stress quantification testing.

A 36.6 m (120 ft) long, 7.1 m (23.3 ft) wide by 203 mm (8 inch) thick single span bridge was built next to the Ferguson Structural Engineering Laboratory at the University of Texas at Austin as part of a separate research project. The bridge was made up of 203 mm (8 in.) of cast-in-place concrete on permanent metal decking forms on two trapezoidal steel tub girders, as shown in Figure 5-3. The bridge deck was placed beginning at about 7:00 AM and finished at about 11:00 AM on August 17, 2006. Temperature sensors were installed in the concrete bridge deck as shown in Figure 5-4. The wires were attached and the temperature sensors were protected in epoxy using a previously described method (Riding et al. 2006). Some temperature sensors were placed in the vertical direction of the bridge deck as well as in the horizontal direction, over and between the steel tub girders. Table 1 shows the location of the sensors in the bridge deck. The concrete at the location of the temperature sensors above and between girders was placed at 10:00 AM. The concrete at the location of the vertical temperature sensors was placed at 8:05 AM.

A weather station for monitoring the ambient temperature, relative humidity, wind speed, and solar radiation was placed a few hundred yards from the construction site. The heat of hydration was also measured using semi-adiabatic calorimetry with concrete sampled on-site.

Table 2 shows the concrete mixture design and fresh properties. Liquid nitrogen was used to cool the concrete to comply with the Texas Department of Transportation (TxDOT) fresh concrete temperature specifications. Table 3 shows the chemistry of the cement used as calculated using both Bogue (ASTM C 150 2005) and Rietveld methods (ASTM C 1365 1998, Rietveld 1969). The fly ash used had a CaO content of 7.2%. The fresh concrete temperature at placement was 28°C (83°F). Curing blankets and black plastic were placed on top of the bridge deck and were kept in place for 10 days.

5.2.2 STRESS TESTING PROCEDURE

The actual thermal stresses in a bridge deck may be quite different than those measured in the rigid cracking frame because of differences in the degree of restraint provided by the girders, the temperature profile of the girders and bridge deck, and bending in the girders to maintain compatibility. The rigid cracking frame can, however, provide a quantitative comparison of material behavior at different temperature histories and material types that may help reduce thermal stresses in bridge decks.

The potential restrained concrete thermal stress development was tested using a rigid cracking frame (Mangold 1998). In this study, the cracking frame tests were performed using realistic bridge deck temperatures, measured and predicted, followed by cooling the concrete at 1°C/ hr (1.8°F/ hr) after 96 hours. The measured and predicted bridge deck temperature history was imposed on the cracking frame specimen through a computer-controlled water circulator that was connected to pipes in the cracking frame formwork. The stress in the rigid cracking frame is monitored with strain gauges mounted on 100 mm diameter Invar restraining bars. The degree of restraint provided by the Invar bars on the concrete can be calculated using Equation 5-1 (Mangold 1998):

$$\delta = \frac{100}{1+\left(\frac{E_c A_c}{E_s A_s}\right)}$$

Equation 5-1

where δ is the degree of restraint (%), E_c is the concrete elastic modulus (MPa), A_c is the concrete cross sectional area (m^2), E_s is the Invar restraining bar modulus (MPa), and A_s is the Invar restraining bar's cross sectional area (m^2). The temperature of the Invar bars at the location of the strain gauges is measured using a resistance temperature detector (RTD) probe. The thermal movement of the Invar restraining bars also needs to be subtracted from the measured strain to calculate the actual stress induced strain in the Invar bars, as shown in Equation 5-2:

$$\varepsilon_{Tadj} = \Delta T_{ib} \cdot \alpha_{ib} \cdot \delta$$

Equation 5-2

where ε_{Tadj} is the temperature induced strain of the Invar bar, ΔT_{ib} is the temperature change of the Invar bar at the strain gauge (°C), and α_{ib} is the coefficient of thermal expansion of the Invar bar (m/m/°C).

Twenty-four 100 x 200 mm (4” x 8”) concrete cylinders were match-cured to the cracking frame temperature for mechanical property testing. The concrete cylinders were placed in an insulated water bath immediately after finishing. The temperature of the water bath was controlled to within about 1°C (1.8°F) of the rigid cracking frame temperature by another 28L (1 ft^3) capacity refrigerating/heating circulator. The cylinders were tested at ½, 1, 2, 3, 7, and 28 days for compressive strength (ASTM C 39 2005), static modulus of elasticity (ASTM C 469 2002), and splitting tensile strength (ASTM C 496 2004). When a cylinder was removed from the water bath for testing, it was replaced with a “dummy” cylinder to maintain a constant water level. After 7 days of curing in the temperature controlled water bath, the cylinders were removed from the moulds and placed in a 100% relative humidity room. A water bath was also used to match-cure specimens for testing the time of setting of concrete mixtures by penetration resistance in accordance with ASTM C 403 (2005). An additional cylinder was made for each mixture to measure the hardened concrete coefficient of thermal expansion according to AASHTO Provisional Standard TP60-00 (2001).

Concrete constituent materials were sampled from the batch plant on August 16, 2006, the day prior to the bridge deck placement. These materials were used in all of the cracking frame tests. One set of tests was performed that used the same materials, mixture proportions, and temperature history as found in the actual bridge deck (hereafter referred to as DL – 10 AM; DL refers to the dolomitic limestone coarse aggregate). Two other sets of tests were performed using the same materials and mixture proportions, but using the bridge deck temperatures predicted for a 2:00 PM (hereafter referred to as DL – 2 PM) and a 10:00 PM placement time (hereafter referred to as DL – 10 PM). A fourth set of tests was performed using the same temperature history measured in the actual bridge deck and with the same materials, except that siliceous river gravel coarse aggregates were used (hereafter referred to as RR – 10 AM) instead of the dolomitic limestone used in the other tests. This siliceous river gravel has a much higher CTE than the limestone so it was used to investigate the effects of concrete coefficient of thermal expansion on the thermal stresses developed. To compensate for the different specific gravity of the river gravel compared to the limestone, the coarse aggregate and fine aggregate volumes of Mixture RR – 10 AM were adjusted to maintain a constant coarse aggregate to total aggregate ratio. The coarse aggregate amount was adjusted to 1082 kg/m^3 (1824 lb/yd^3) and the fine aggregate amount was adjusted to 733 kg/m^3 (1235 lb/yd^3).

5.3 RESULTS AND DISCUSSION

5.3.1 BRIDGE DECK

The weather during the bridge deck placement and curing was hot and dry. The weather monitoring station results showed that the relative humidity ranged from 25.3% to 84.7%. The peak daily solar radiation ranged from 963 to 1079 W/m^2 (305 to 342 BTU/hr/ft^2). The wind speed ranged from 0.4 to 6.9 m/s (0.9 to 15.4 mph).

Figure 5-5 shows the temperatures developed above and between the girders in the instrumented bridge deck. The temperature in the bridge deck was much higher above the girders than between them, because the girder trapped in heat that otherwise would have been lost due to convection under the deck. Figure 5-6 shows the temperature development through the deck cross-section between the girders. The top temperature is shown as Sensor 3, the middle as Sensor 2, and the bottom as Sensor 1. The difference in temperature in the vertical direction was limited to less than 8°C

(14°F), mainly because of the insulation provided by the curing blanket on the deck. The bottom of the deck tended to be cooler than the top of the deck, because of the lack of insulation underneath the deck, and the solar radiation component that influences the top more than the bottom. The temperature measured between the girders at mid-depth, as shown in Figure 5-5 was selected to be used as the target temperature history of rigid cracking frame stress tests DL – 10 AM and RR – 10 AM. The temperature between the girders was selected because the temperature prediction model used to predict the temperature history at different concrete placement times assumes that the concrete is open below the bridge deck.

Figure 5-7 shows the adiabatic temperature development curve calculated from the semi-adiabatic calorimetry data obtained from the concrete sampled at the bridge deck placement. The semi-adiabatic calorimetry data and measured weather data were used to predict the temperature of the bridge deck if the placement had started at 2 PM or 10 PM. The predicted temperatures for the 2 PM and 10 PM placement times were used as the target temperature histories for rigid cracking frame tests DL - 2 PM and DL – 10 PM.

The rigid cracking frame temperatures measured in the middle of the specimen versus the simulated time of day of the test are shown in Figure 5-8a. These temperatures start when the mixture would have been placed, and end when the concrete cracked, except in the case of DL – 10 PM, in which case the test was stopped before cracking. The corresponding cracking frame measured stresses versus the simulated time of day are shown in Figure 5-8b. The degree of restraint of the cracking frame began at 100% during the fresh plastic state, and for all tests decreased to 77% at the time of cracking.

Figure 5-9 shows the a) compressive strength development, b) elastic modulus development, and c) splitting tensile strength development of the mixtures tested. The mixtures showed very similar modulus development, but the test RR – 10AM showed slightly lower compressive and splitting tensile strengths. This is probably because of the smooth surface texture of the siliceous river gravel particles as compared to the rough texture of the crushed dolomite aggregates.

Figure 5-10 shows the rigid cracking frame measured stress history divided by the measured tensile strength development. The specimens cracked at a stress-to-splitting tensile strength ratio of between 0.61 and 0.68. The specimens cracked at a ratio less than 1.0 because of the following reasons: 1) the splitting tensile strength overestimates the direct tensile strength (Mindess et al. 2003), 2) the rapid loading rate of the splitting tensile test gives a higher measured tensile strength than the true concrete tensile strength when loaded slowly as is the case with thermal stresses (Emborg 1998a), and 3) the size effect between the 100 x 200 mm (4" x 8") concrete cylinders and the 150 x 150 mm (6" x 6") rigid cracking frame specimen cross section gives higher measured tensile strength values in the smaller splitting tensile strength specimen (Shah et al. 1995). The concrete stress at cracking as measured in the cracking frame may be more indicative of the bridge deck concrete's resistance to cracking than the splitting tensile strength because of these reasons.

The measured hardened coefficient of thermal expansion for each concrete mix is shown in Table 4. There is some variation in the results between tests DL – 10AM, DL – 2PM, and DL – 10PM, but within the 0.5 $\mu\varepsilon/°C$ (0.4 $\mu\varepsilon/°F$) tolerance of the test method. The coefficient of thermal expansion of Test RR – 10AM is 33% greater than the average of tests DL – 10AM, DL – 2PM, and DL – 10PM.

5.4 Discussion of Results

The concrete thermal stress develops as a result of the interaction between the modulus development, coefficient of thermal expansion, temperature change, high early-age creep, and restraint. As shown in Figure 5-8, Test DL – 10PM developed a large compressive stress during the first 24 hours after placement, when compared to tests DL – 10AM and DL – 2PM. This occurred because the concrete set before a significant temperature increase occurred, allowing the concrete to develop a significant amount of compressive stress. This pre-compression lowered the subsequent tensile stresses that developed, even though the mixture experienced a larger temperature decrease than the other mixtures during the second day of testing. Because the maximum tensile stress was low, the risk of thermal cracking is less than for the other conditions.

The mixture containing river gravel showed significantly higher stresses than the mixtures containing dolomitic limestone. As shown in Figure 5-8, the measured stress in test RR – 10AM was 32% larger than that in DL - 10AM, 52% larger than that measured in DL - 2PM, and 110% larger than that measured in DL-10PM. This indicates that the both the time of placement and coefficient of thermal expansion are significant parameters in avoiding thermal cracking. Also, the tensile stress at 96 hours after mixing the measured stress in test RR - 10AM was at 1.7 MPa (243 psi); this specimen cracked at a stress level of 2.2 MPa (322 psi). This means that test RR – 10AM was at 75% of the cracking stress 96 hours after mixing (or 10 AM on 8/21/06) and before the final cooling began, indicating that the river gravel mixture was quite susceptible to cracking. Just by using a coarse aggregate with a higher coefficient of thermal expansion, and placing the concrete in the daytime rather than at night, the tensile stresses significantly increased.

5.5 Conclusions

Rigid cracking frame testing performed under realistic bridge deck temperature histories was used to quantitatively compare the relative early-age behavior of different concrete materials and placement times that may help reduce early-age concrete bridge deck stresses. The thermal component of bridge deck early-age stresses can be significant. In the case of the test simulating a morning placement with a concrete with a high coefficient of thermal expansion, the early age thermal stresses were found to be as much as 75% of the cracking stress. The testing found that the early-age thermal stresses were reduced by up to 50% by using a coarse aggregate with a lower coefficient of thermal expansion and placing the concrete at night. The testing performed here does not necessarily represent the actual stresses seen in a bridge deck, but the potential stresses. Real bridge deck stresses will be affected by the degree of restraint in the deck and bending that occurs in the deck and girders due to the temperature changes. The methods in this paper may be used to further investigate the role of concrete material properties, temperature effects, and construction sequencing on bridge deck cracking. More research is also needed in modeling bridge deck cracking due to these differences between the simulated stresses and actual stresses.

5.6 Acknowledgements

The authors wish to express their gratitude to the Texas Department of Transportation through Project 0-4563 for funding this research. The assistance of Sam Slatnick in performing the cracking frame and mechanical property tests is kindly acknowledged. The guidance and assistance of Dr. Rupert Springenschmid and Mr. Erwin Gierlinger to develop the cracking frame test setup are appreciated. The authors also wish to thank Dr. Karl Frank, Timothy Barnard, and Catherine Hovell for arranging access to the bridge deck. The authors would also like to thank Karen Scrivener and Christophe Gosselin for performing the Rietveld analysis on the portland cement used.

5.7 Notation

The following Symbols are used in the paper:

δ = degree of restraint

E_c = concrete elastic modulus

A_c = concrete cross-sectional area

E_s = Invar bar modulus

A_s = Invar bar cross-sectional area

ε_{Tadj} = temperature induced strain of the Invar bar

ΔT_{ib} = temperature change of the Invar bar at the strain gauge

α_{ib} = coefficient of thermal expansion of the Invar bar

Table 5-1 - Location of Temperature Sensors in Bridge Deck

Temperature Sensor	Distance from South Side m (ft)	Distance from East Side m (ft)	Distance Vertically from Bottom Form mm (in)
Above East Girder	2.8 (9.3)	1.9 (6.3)	101 (4)
Between Girders	2.8 (9.3)	3.3 (10.8)	101 (4)
Vertical #1	9.0 (29.7)	3.5 (11.3)	0
Vertical #2	9.0 (29.7)	3.5 (11.3)	76 (3)
Vertical #3	9.0 (29.7)	3.5 (11.3)	178 (7)

Table 5-2 - Concrete Properties

Item	Content	Type
Cement kg/m^3 (lb/yd^3)	260 (439)	Type I/II
Fly Ash kg/m^3 (lb/yd^3)	88 (149)	ASTM Class F
Coarse Aggregate kg/m^3 (lb/yd^3)	1127 (1900)	1" Dolomitic Limestone
Fine Aggregate kg/m^3 (lb/yd^3)	763 (1286)	Natural Sand
Air Entraining Admixture ml/100 kg (oz/ cwt.)	19.6 (0.3)	AE 90
Water Reducer / Retarder ml/100 kg (oz/ cwt.)	189 (2.9)	ASTM Type D
Jobsite Measured Air Content	2.6%	
Jobsite Measured Slump mm (inches)	75 (3)	
Design w/cm	0.45	

Table 5-3 - Cement Chemistry

Item	Bogue Analysis Method	Rietveld Analysis Method
C_3S (Alite)	45.2	58.5
C_2S (Belite)	26.9	13.8
C_3A (Aluminate)	7.5	6.2
C_4AF (Ferrite)	10.1	10
$C\hat{S}H_2$ (Gypsum)	4.35	1.6
Hemihydrate	-	2.7
Anhydrite	-	0.5
Periclase	-	0.9
K_2SO_4	-	1.3
$CaCO_3$	-	3.2

Table 5-4 - Hardened Coefficient of Thermal Expansion Test Results

Test ID	Coefficient of Thermal Expansion με/°C (με/°F)
DL – 10AM	7.8 (4.3)
DL – 2PM	7.5 (4.1)
DL – 10PM	8.0 (4.4)
RR – 10AM	10.4 (5.8)

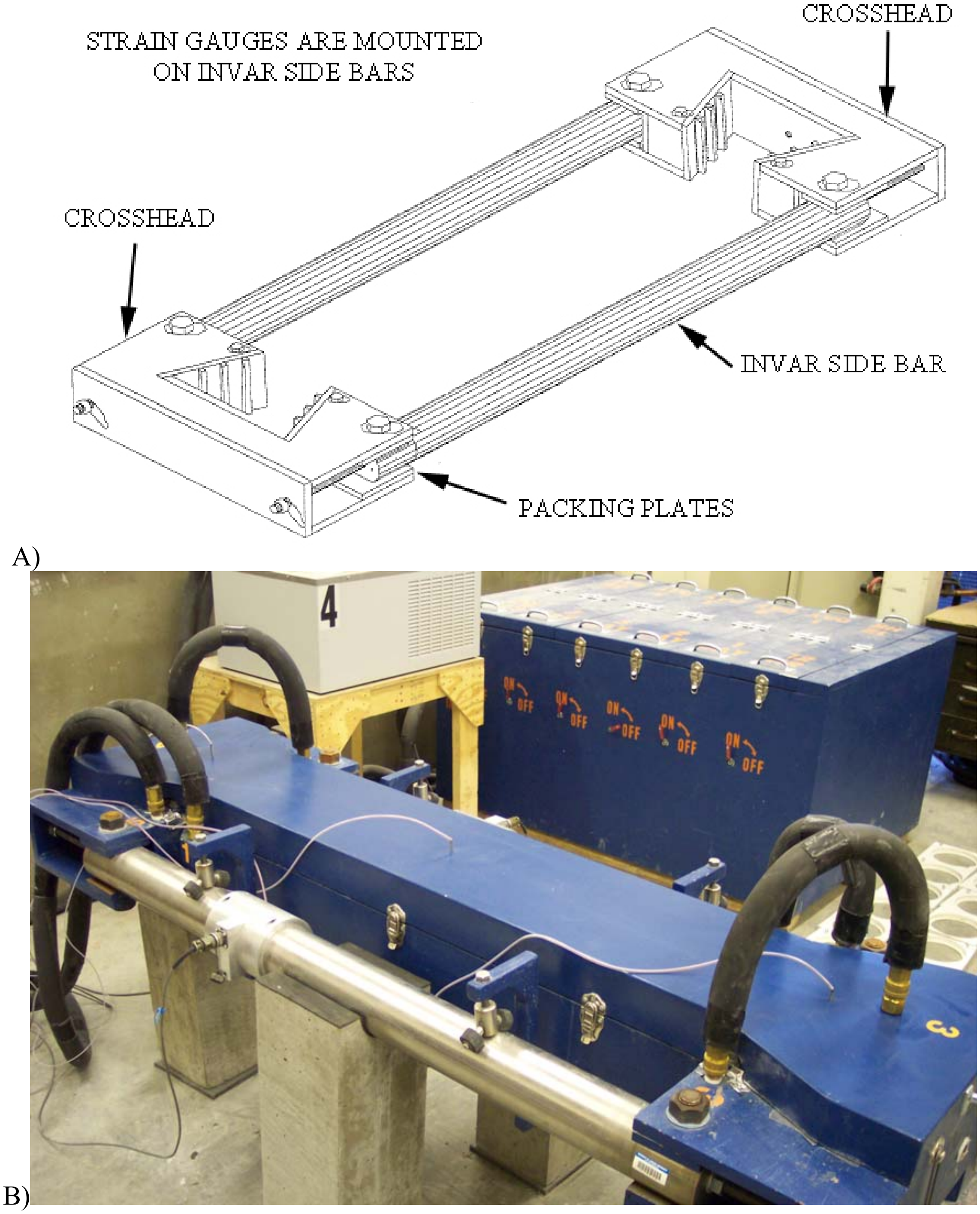

Figure 5-1 –Rigid Cracking Frame a) Schematic of Frame without Crosshead Braces and Formwork b) Frame in Use (Whigham 2005)

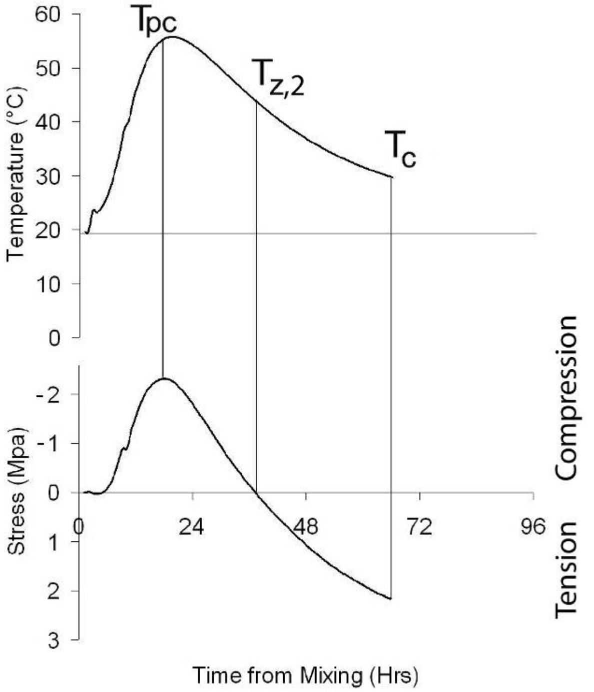

Figure 5-2 - Typical Concrete Temperature and Thermal Stress Plot During Routine Cracking Frame Testing

Figure 5-3 - Bridge during Deck Placement

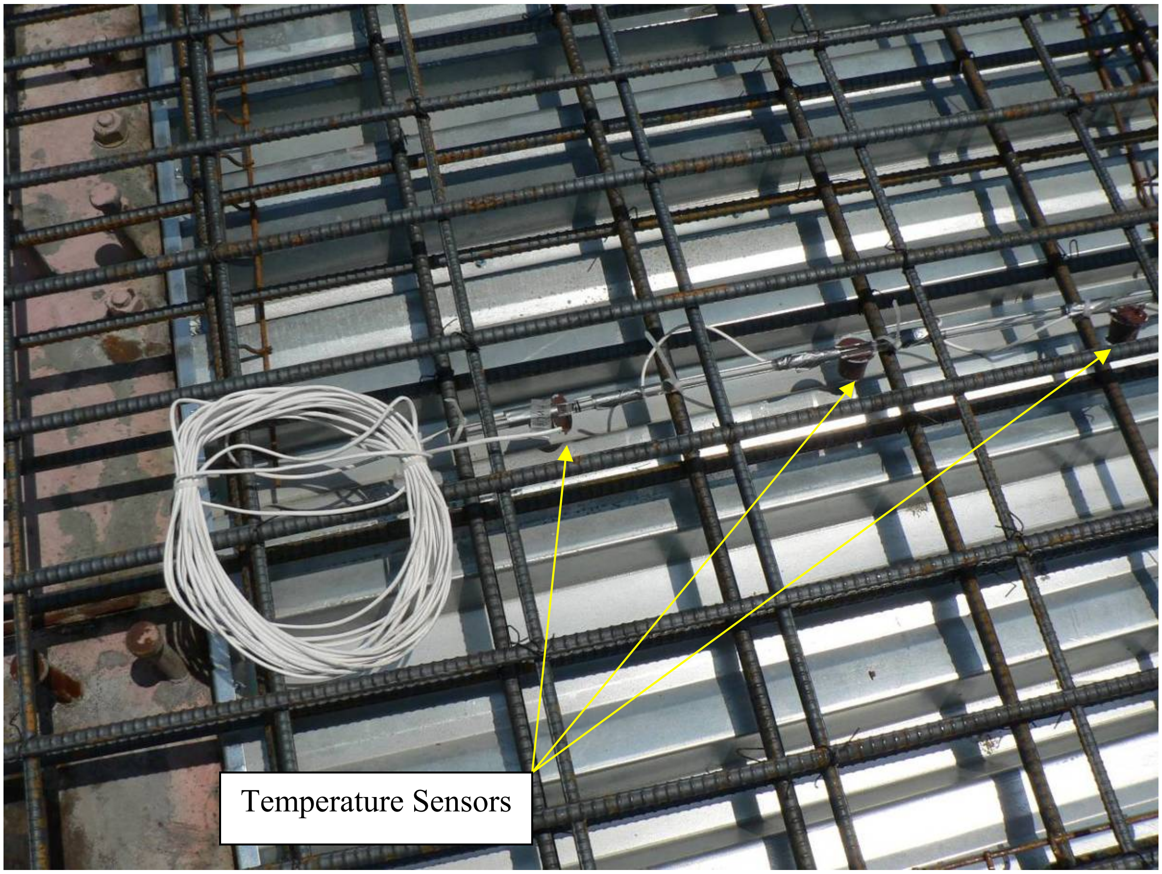

Figure 5-4 - Temperature Sensors before Concrete Placement

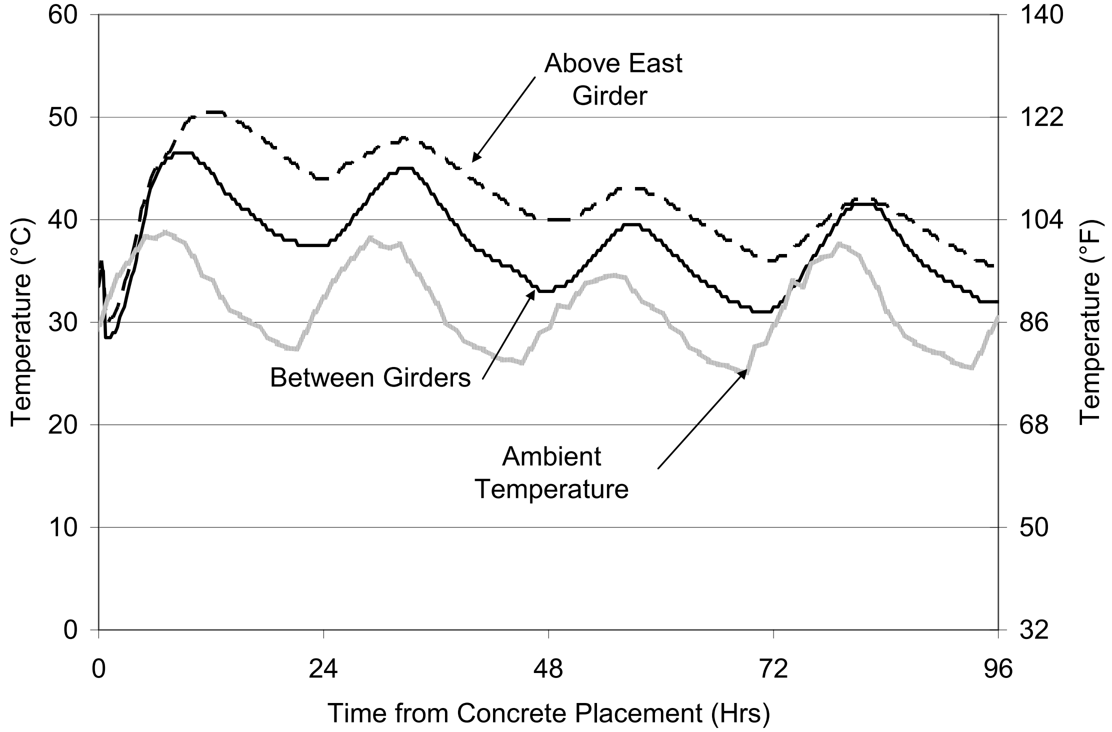

Figure 5-5 - Temperature Development in Bridge Deck at Mid Depth above and between Girders

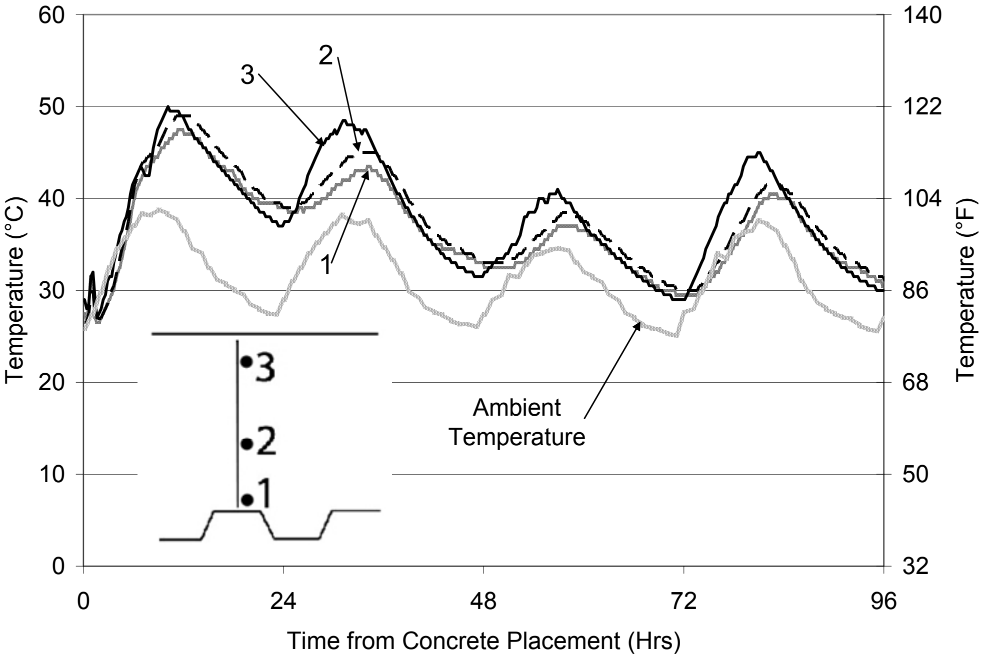

Figure 5-6 - Vertical Temperature Profile in the Bridge Deck between Girders

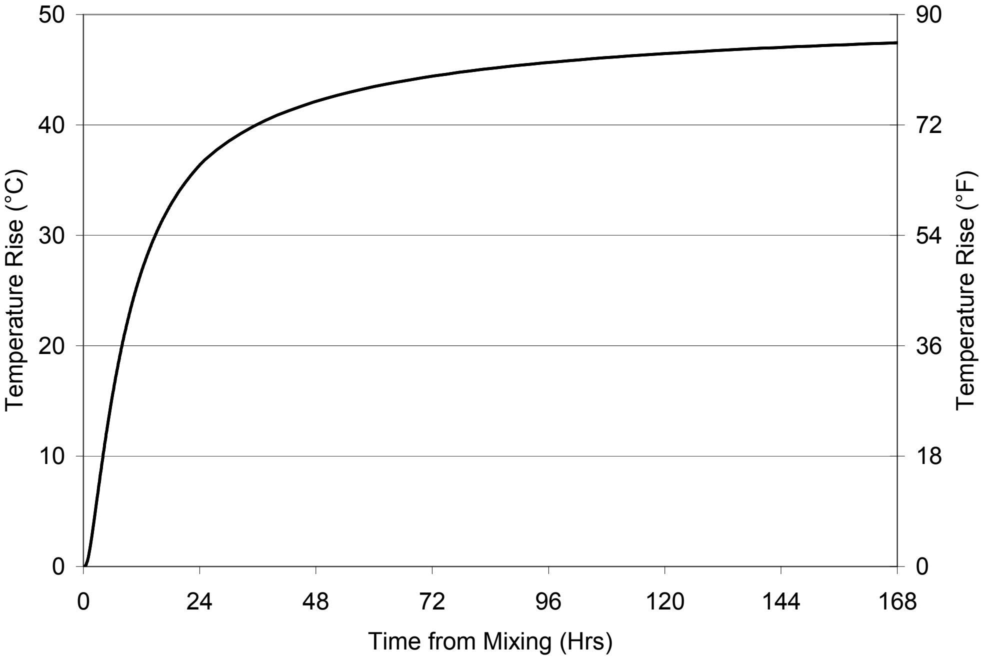

Figure 5-7 - Adiabatic Temperature Rise for Concrete Used in Bridge Deck

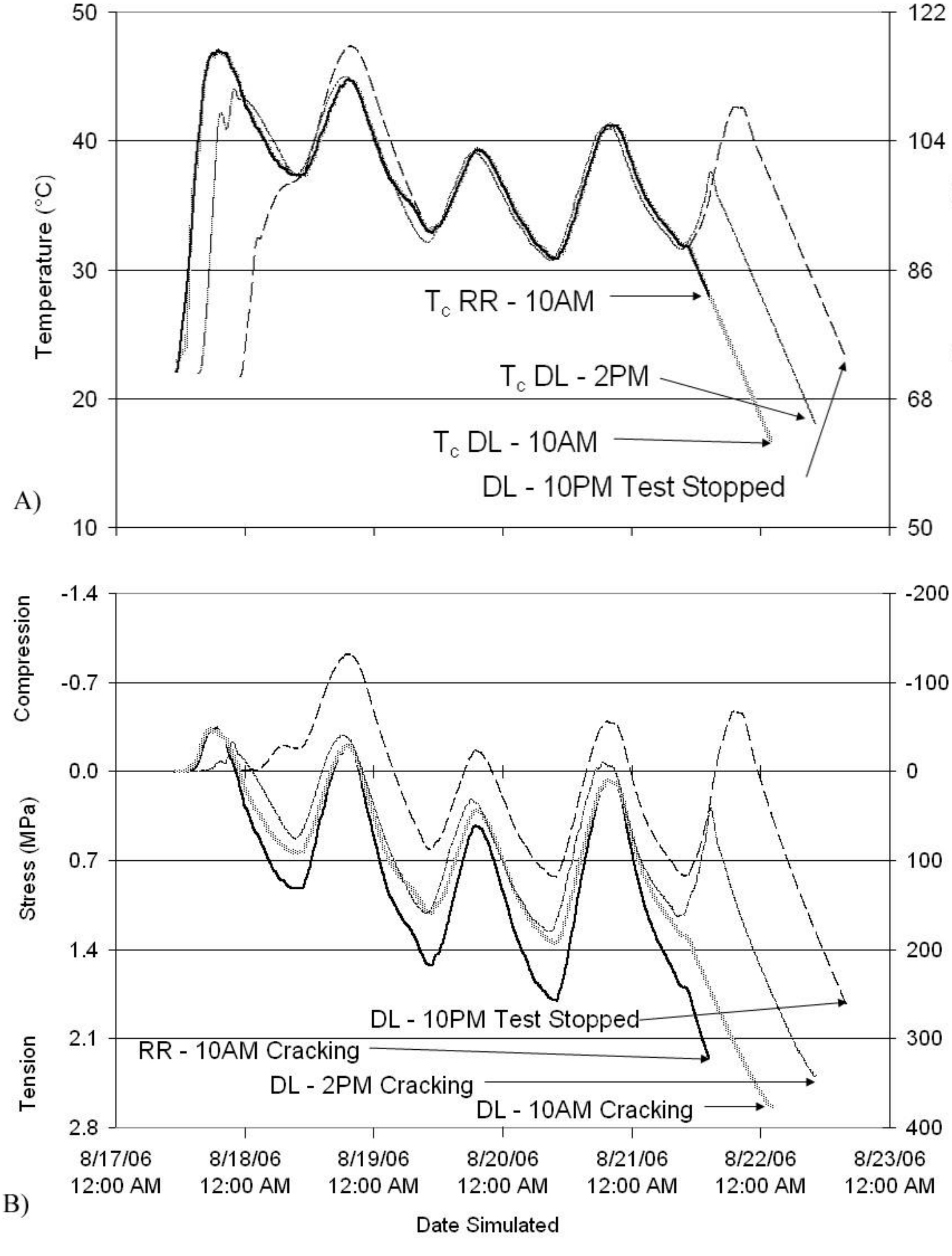

Figure 5-8 - Rigid Cracking Frame Test Data A) Middle Temperatures and B) Stress Development

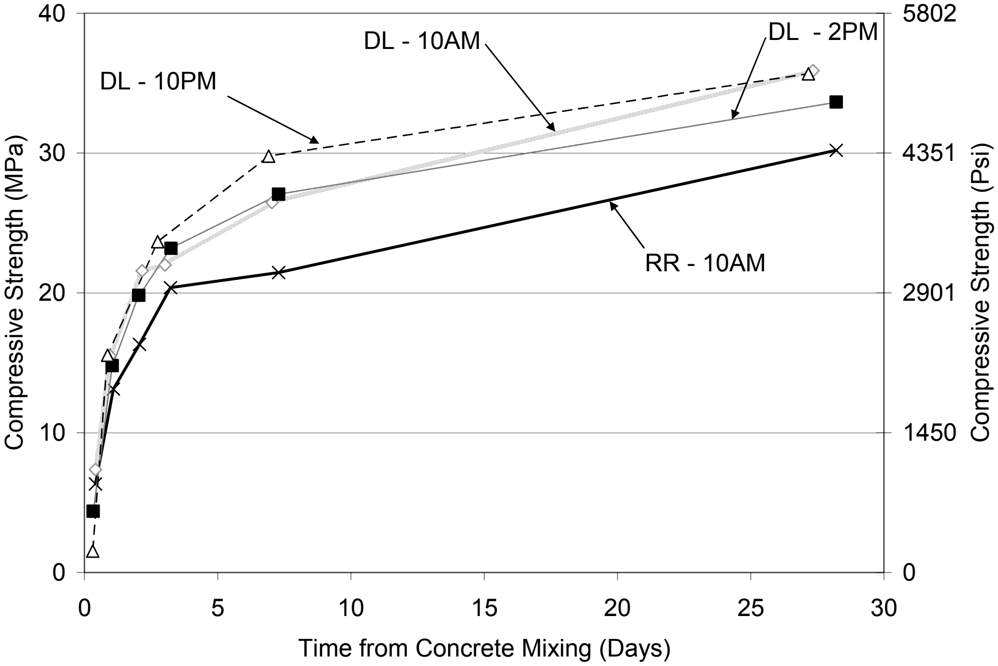

DL - 10PM
DL - 10AM
DL - 2PM
RR - 10AM
Compressive Strength (MPa)
Compressive Strength (Psi)
Time from Concrete Mixing (Days)
0
10
20
30
40
1450
2901
4351
5802
5
15
25

A)

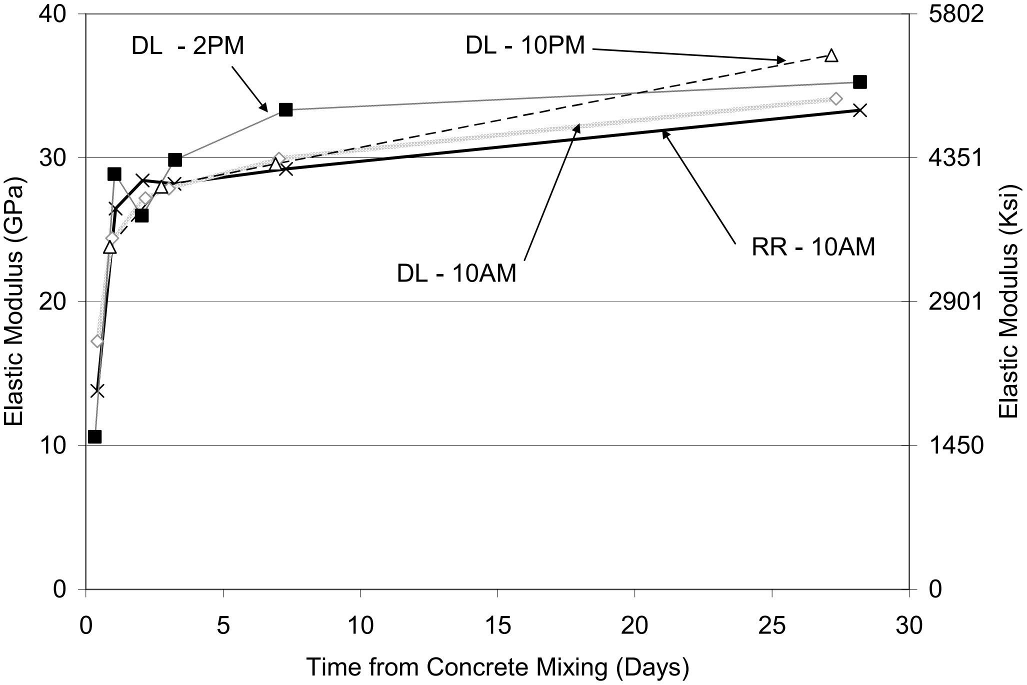

DL - 2PM
DL - 10PM
DL - 10AM
RR - 10AM
Elastic Modulus (GPa)
Elastic Modulus (Ksi)
Time from Concrete Mixing (Days)
0
10
20
30
40
1450
2901
4351
5802
5
15
25

B)

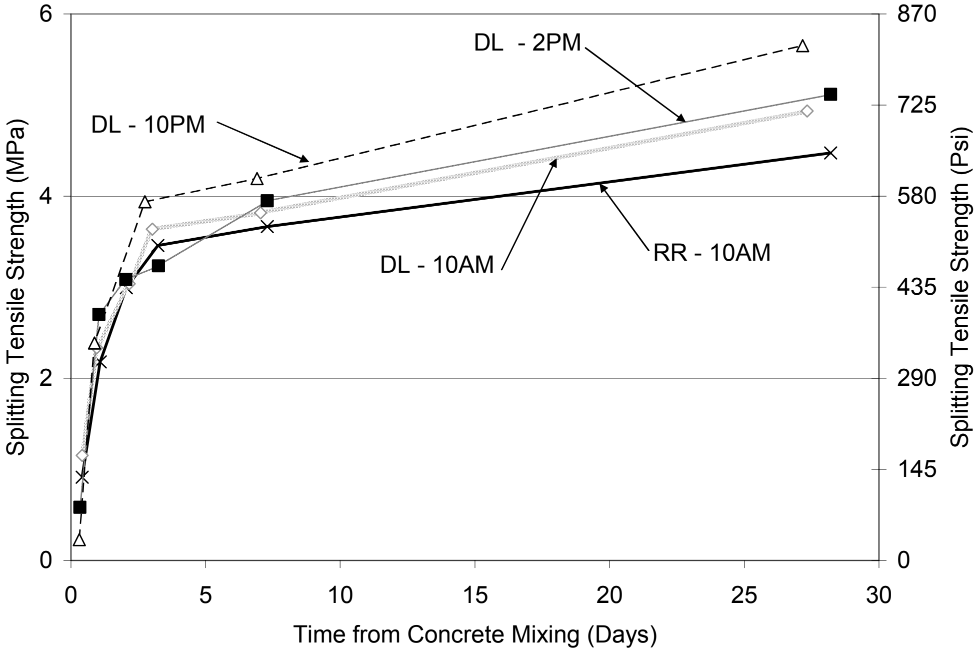

C)

Figure 5-9 –Concrete Mechanical Property Development A) Compressive Strength Development, B) Elastic Modulus Development, and C) Splitting Tensile Strength Development

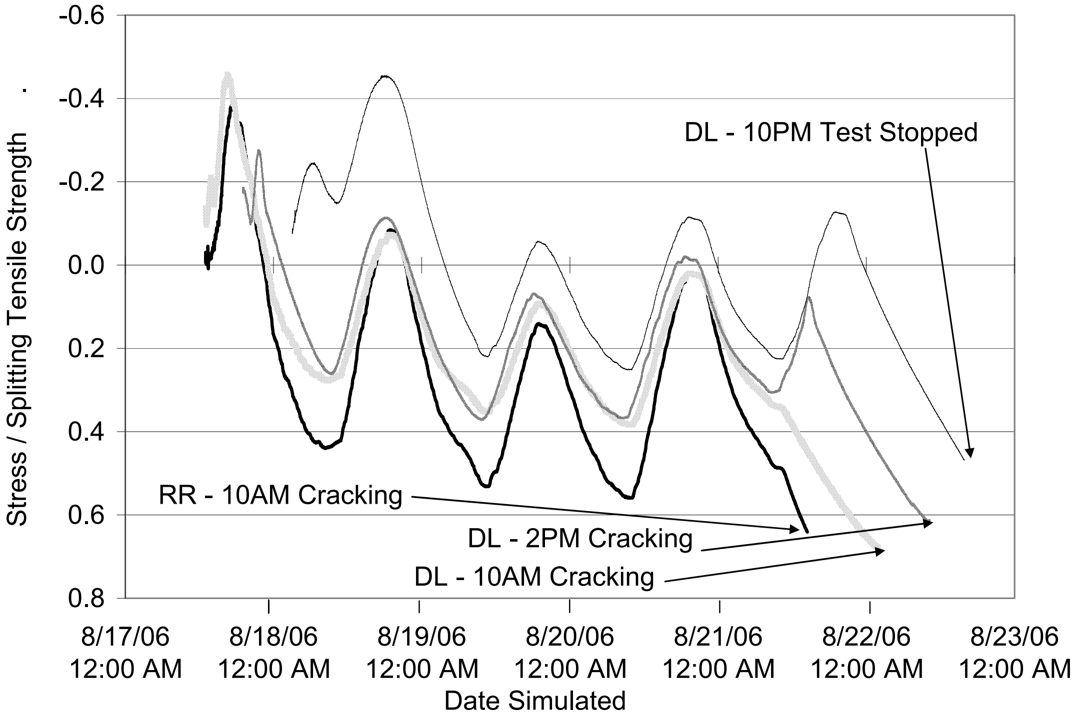

Figure 5-10 - Rigid Cracking Frame Measured Stress / Splitting Tensile Strength

CHAPTER 6 EFFECT OF CEMENTING MATERIALS ON EARLY-AGE CONCRETE STRESS RELAXATION

The restraint of early-age concrete volume change can lead to large internal stresses and consequent cracking in mass concrete members. An accurate estimate of the early-age concrete stress relaxation in concrete is necessary to perform a thermal stress analysis. To quantify the behavior of different cementitious materials, the early-age uniaxial stress development in 36 different concrete mixtures was measured using rigid cracking frames. The early-age concrete creep parameters were obtained from experimental data by comparing the measured concrete cracking frame stresses to those simulated using the measured temperature profile of the concrete in the cracking frame, the elastic modulus development, and the hardened concrete coefficient of thermal expansion. A modified version of the Linear Logarithmic Model for concrete creep—modified to account for the change in creep at different temperatures—was developed and used to simulate the concrete early-age creep behavior. A statistical model was developed to relate the concrete early-age creep parameters to the cement and supplementary cementing materials properties.

6.1 Introduction

Concrete members can develop very high internal temperatures during curing due to the heat of hydration. Early-age volume change will result from any temperature change or autogenous shrinkage in the concrete. Internal stresses in the concrete will develop when the concrete volume change is non-uniform or the concrete member is restrained externally. When the concrete internal stress exceeds its tensile strength capacity, cracking will occur.

Any concrete internal stress analysis should include viscoelastic effects, because the high early-age stress relaxation will greatly reduce the compressive stress in the concrete generated during the rapid temperature rise phase of hydration (Springenschmid and Breitenbücher 1998). This means that the concrete stress will become positive sooner than is predicted when the stress relaxation is neglected (Schindler 2002). The uniaxial constitutive equation for concrete is expressed as Equation 6-1 (Bažant 1972; Westman 1999):

$$\varepsilon(t) - \varepsilon_0(t) = \int_{t_0=0}^{t} J(t,t_0) \cdot d\sigma(t_0) \qquad \textbf{Equation 6-1}$$

where t is the concrete age, t_0 is the concrete age at load application, ε is the concrete strain, ε_0 is the concrete strain that is independent of the concrete stress state, $J(t,t_0)$ is the concrete creep compliance function, and $\sigma(t_0)$ is the concrete stress at time t_0. The concrete stress may be calculated using the numerical scheme proposed by Bažant (1972) in which the stress history is calculated from the concrete strain. The principle of superposition is used in this method, which approximates the stress and strain histories as individual stress steps and corresponding strain responses, which are then superimposed to give the total response, as shown in Figure 6-1.

Several models have been proposed for long-term concrete creep behavior (Bažant and Panula 1978; Bažant and Chern 1985; ACI 209 1992). Most concrete creep models are based on compressive concrete creep tests performed according to ASTM C 512 (2002). The test is performed by placing a concrete cylinder in a frame that applies a constant sustained load to the specimen. The concrete strain is then monitored, giving the creep response. The concrete used in a compressive creep frame would need to be hardened sufficiently to allow it to be removed from its molds and placed in a compressive stress condition. Before this concrete stiffness level is achieved, creep cannot be measured using the standard compression method. Because of this limitation, most creep models are not valid for concrete ages less than 1 or 2 days (Westman 1999). In performing a thermal stress analysis of a concrete member, the stress development during the first 2 days is not only the most difficult to measure and calculate, but also the most important. The beneficial pre-compression that may occur during the concrete temperature rise is greatly reduced by the high early relaxation. As the concrete stiffness increases and the stress relaxation is reduced, high tensile stress will develop when the concrete temperature decreases (Springenschmid and Breitenbücher 1998).

Restrained concrete tests can be used to calculate the concrete early-age creep compliance (Altoubat 2000). The creep parameters can be fit to match the measured stress in the restrained concrete test. The rigid cracking frame test is a restrained concrete test that is well-suited for measuring the stress that is generated by early-age volume change. Rigid cracking frames were originally developed to investigate transverse pavement cracking that occurred in Austria (Springenschmid, Breitenbücher, and Mangold 1994). The test is performed on a concrete specimen with flared ends that are gripped by the cracking frame as shown in Figure 6-2. Concrete is placed and consolidated in the cracking frames, which enables the determination of stress development continuously from setting through hardening. As the concrete volume changes during hydration, the early-age concrete strain is restrained by the Invar side bars which convert a portion of the volume change into stress. The sealed concrete specimen can undergo early-age volume change because of autogenous shrinkage or thermal movement from the heat of hydration. The temperature of the concrete in the cracking frame may change due to the heat of hydration that is retained by formwork insulation, or actively controlled using heated/cooled water that is circulated through copper pipes embedded in the formwork. The proportion of concrete deformation that is restrained from movement is called the degree of restraint and can be calculated using Equation 6-2:

$$\delta = \frac{100}{1+\left(\frac{E_c A_c}{E_s A_s}\right)}$$ **Equation 6-2**

where δ is the degree of concrete restraint, E_c is the concrete elastic modulus (MPa), A_c is the concrete cross sectional area (m), E_s is the Invar bar elastic modulus (MPa), and A_s is the Invar bar cross sectional area (m). Strain gauges are mounted on the Invar bars to record the strain in the Invar bars. The stress in the concrete can be obtained through a calibration process which involves correlating the frame stiffness to a known load applied with a hydraulic ram. The concrete stress is then corrected for strain in the Invar bar due to thermal movement of the Invar bar and strain gauge according to Equation 6-3:

$$\varepsilon_{Tadj} = \Delta T_{ib} \cdot \alpha_{ib} \cdot \delta$$ **Equation 6-3**

where ε_{Tadj} is the temperature induced strain of the Invar bar (m/m), ΔT_{ib} is the temperature change of the Invar bar at the strain gauge (°C), and α_{ib} is the coefficient of thermal expansion of the Invar bar (m/m/°C).

A few models have been developed to describe the concrete early-age creep and stress relaxation. The first early-age creep model was based on a modified version of the Triple Power Law by Bažant and Chern (1985). The triple power law was extended first by Emborg (1989) and then altered by Westman (1999) to include early-age behavior. A term was added to account for the change in the instantaneous deformation at early ages;

another term was added for the early-age creep. The extended triple power law does, however, allow a smooth transition from early-age creep to long term creep values. The long term creep model is already based on extensive testing (Bažant and Chern 1985), so only early-age testing is required to get the creep compliance at all ages. The extended triple power law however contains 15 parameters, making it difficult to establish trends of material behavior (Larson 2003). Rostasy et al. (1993) have also proposed an early-age creep model based on the degree of hydration and creep or stress relaxation tests. This model, however, gives no guidance on the form of the creep parameters used in calculating the creep function, other than to base them on creep or relaxation tests.

More recently, Larson (2003) developed the linear logarithmic model (LLM) as a simplified early-age creep model. The LLM idealizes the creep compliance as a bi-linear expression on a log scale as shown in Figure 6-3. The slope of each line is defined by Equation 6-4 and Equation 6-5 (Larson 2003):

$$\Delta J(\Delta t_{load}, t_0) = \begin{cases} a_1(t_0)\cdot\log\left(\dfrac{\Delta t_{load}}{\Delta t_0}\right) & \text{For } \Delta t_0 \leq \Delta t_{load} < \Delta t_1 \\ a_1(t_0)\cdot\log\left(\dfrac{\Delta t_{load}}{\Delta t_0}\right) + a_2(t_0)\cdot\log\left(\dfrac{\Delta t_{load}}{\Delta t_1}\right) & \text{For } \Delta t_{load} \geq \Delta t_1 \end{cases} \qquad \textbf{Equation 6-4}$$

$$a_i(t_0) = a_i^{\min} + (a_i^{\max} - a_i^{\min})\cdot\exp\left(-\left(\frac{t_0 - t_s}{t_{ai}}\right)^{n_{ai}}\right) \qquad \textbf{Equation 6-5}$$

where $i = 1,2$, where ΔJ is the increase in creep compliance (1/Pa), Δt_{load} is the time from application of the load (days), Δt_0 is the time of load application (days), Δt_1 is the time limit that transitions between short term and long term creep (days), t_s is the apparent setting time (days), a_i^{max} *(1/Pa)*, a_i^{min} *(1/Pa)*, t_{ai} (days) and n_{ai} are fit parameters. The LLM is much simpler to implement than other early-age creep models and has fewer fit parameters. However, the relationship for long term creep compliance according to the linear logarithmic model has not been developed. Additionally, the linear logarithmic model has no adjustment to account for the effect that curing temperature has on the creep rate.

Previous studies on early-age creep and stress relaxation or cracking sensitivity have focused on specific mixtures or qualitative cracking indices (Westman 1999; Springenschmid and Breitenbücher 1998). Currently, there are few available models that can predict the early-age concrete creep compliance function based on the materials used. This paper will focus on the development of an early-age creep model, the Modified Linear Logarithmic Model (MLLM), that has a minimum number of fit parameters, has an adjustment for the effect of temperature on early-age creep, and relates the concrete constituent material properties and mixture proportions to the early-age creep parameters.

6.2 Experimental Procedure

A combination of several tests was used in order to quantify the concrete early-age behavior. Rigid cracking frames were used to quantify the stress response for different concrete mixtures when subjected to different thermal histories. The elastic modulus was tested because it is needed in the creep compliance calculations and to quantify the degree of concrete restraint to be able to correct the measured Invar bar steel strain due to temperature changes in the Invar. The hardened concrete coefficient of thermal expansion was also measured to use in simulating the concrete volume change in the rigid cracking frame.

In the first rigid cracking frame tests performed, the concrete temperature was allowed to change due to the heat of hydration and formwork insulation. When the temperature was allowed to develop freely in these tests, the maximum concrete temperature reached was much lower than other tests on similar materials reported by Springenschmid and Breitenbücher (1998). Large cooling pipes were embedded in the forms used in this study, reducing the insulating properties of the forms and lowering the maximum temperature rise and consequent thermal stresses in the concrete. The procedure was also altered to use an active concrete temperature control method. In this method, semi-adiabatic calorimetry is performed prior to the other tests. The adiabatic temperature development is then calculated from the semi-adiabatic calorimetry using the procedure outlined by RILEM technical committee 119 (RILEM 119 1998). The calorimetry results are then used to simulate the temperature development of a one meter thick wall with a constant surface temperature. The temperature at the center of the wall, numerically simulated using a one dimensional heat transfer analysis, is used as the target concrete temperature in the rigid cracking frame testing. If the concrete in the rigid cracking frames did not crack after four days, the concrete was then cooled at 1 °C/hr (1.8 °F/hr) until cracking occurred. The temperature of the fluid circulated through the pipes in the concrete formwork is adjusted so that the temperature measured using a Type T thermocouple in the center of the rigid cracking frame will match the target concrete temperature. The fresh concrete temperature and the constant surrounding temperature can be adjusted to simulate different placement conditions. For example, a hot summer day when the fresh concrete is cooled using ice or liquid nitrogen can be simulated by using a low fresh concrete temperature and a high surrounding temperature. The concrete constituent materials were preconditioned by either cooling or heating them to the desired placement temperature before mixing.

The specimens for static modulus of elasticity tests were cured at the same temperature history as the concrete in the rigid cracking frame. The concrete static modulus of elasticity was tested according to ASTM C 469 at 12 hours, 1, 2, 3, 7 and 28 days on 100 x 200 mm (4 x 8 in.) cylindrical specimens. The concrete compressive strength was also tested at the same time as the elastic modulus using 100 x 200 mm (4 x 8 in.) cylinders also cured at the same temperature as the concrete in the rigid cracking frame. When multiple tests were conducted at different temperature histories on the same concrete, the compressive strength and modulus developments versus equivalent age were fit to best represent all of the tests performed on that mixture. The equivalent age maturity method (ASTM C 1074 2004) was used to correct for differences in curing history between tests. Recommended activation energy values from Brooks et al. (2007), shown in Table 6-1, were used in the maturity calculations. An exponential model first suggested by Freiesleben Hansen and Pedersen (1985) was used to model the concrete strength based on the concrete equivalent age maturity, as shown in Equation 6-6. The static modulus of elasticity was then modeled based on the compressive strength development using Equation 6-7 (Pauw 1960):

$$f_c(t_e) = f_{cult} \cdot \exp\left(-\left(\frac{\tau_s}{t_e}\right)^{\beta_s}\right)$$ **Equation 6-6**

$$E = E_c \cdot w_c^{1.5} \cdot (f_c)^{E_m}$$ **Equation 6-7**

where $f_c(t_e)$ *(MPa)* is the compressive strength development at equivalent age t_e (hrs), f_{cult} is the ultimate concrete compressive strength (MPa), w_c is the unit weight (kg/m^3), E is concrete elastic modulus development (MPa), and τ_s (hrs), β_s, E_c, and E_m are fit parameters.

The concrete time-of-set was measured for each concrete mixture using ASTM C 403 (2006). The sieved mortar used to measure the penetration resistance was kept in a temperature-controlled water-bath that was controlled to match the temperature of the concrete in the rigid cracking frame.

The hardened concrete coefficient of thermal expansion (CTE) was performed according to test method AASHTO TP 60-00 (2005) for each combination of aggregate types used. A fully-saturated cylinder with a length of 180 ± 2 mm (7 ± 0.1 in.) is placed in a temperature-controlled water-bath at 10°C (50°F). The water bath and specimen are then heated to 50 °C (122 °F). The concrete length at both temperatures is recorded, with the coefficient of thermal expansion calculated as the total specimen length change divided by the original length and the temperature change of 40 °C (72 °F).

6.3 Materials tested

A total of 73 rigid cracking frame tests were performed on 36 different concrete mixtures. Several of the concrete mixtures were tested at different fresh concrete placement temperatures and different temperatures surrounding the simulated 1 meter thick wall. A few of the concrete mixture and temperature combinations were also repeated for quality control. A total of nine cements (designated C1-C9), six different fly ashes (FA1-FA6), one Grade 120 ground granulated blast furnace (GGBF) slag, and one source of silica fume were evaluated in this study. Table 6-2 shows the cement physical and chemical properties as determined using Blaine specific surface area (ASTM C 204

2005), the Rietveld method of quantitative x-ray diffraction (Rietveld 1969), and the Bogue method specified in ASTM C 150 (2005) calculated from x-ray fluorescence. Cement compositions calculated using both Rietveld and Bogue methods are listed for completeness. The Rietveld method has been shown to give more accurate values for the cement composition (Walenta and Füllman 2004). However, the Bogue method is still by far the most commonly used method for determining cement composition. Table 6-3 shows the SCM compositions as determined using x-ray fluorescence. Table 6-4 shows the different material and temperature condition combinations tested. The temperatures listed in Table 6-4 show first the concrete temperature at placement and the constant temperature surrounding the simulated 1 meter thick wall used to determine the concrete target temperature history.

6.4 Analysis of Creep Behaviour

Concrete creep coefficients can be obtained by fitting simulated stress results using measured mechanical properties to the measured stress results obtained from rigid cracking frame testing. The instantaneous deformation calculated during each time step can be calculated using Equation 6-8 to Equation 6-13:

$$\varepsilon_0(t) = \delta \cdot \left(\Delta\varepsilon_{th} + \Delta\varepsilon_I + \Delta\varepsilon_{aut}\right)$$ **Equation 6-8**

$$\Delta\varepsilon_{th} = \alpha_c \cdot \Delta T_c$$ **Equation 6-9**

$$\Delta\varepsilon_I = \frac{\alpha_{ib}}{2 \cdot L} \cdot \int_0^L \Delta T_I(L)$$ **Equation 6-10**

$$\int_0^L \Delta T_I(L) = \left[2 \cdot T_\infty \cdot L + \theta \cdot (\exp(2 \cdot m \cdot L) - 1) \cdot \frac{\exp(-mL)}{m \cdot \cosh(m \cdot L)} \right]$$ **Equation 6-11**

$$m^2 = \frac{h \cdot P}{k \cdot A_c}$$ **Equation 6-12**

$$\theta = T - T_\infty$$ **Equation 6-13**

where α_c is the concrete coefficient of thermal expansion (ε/°C), ΔT_c is the change in concrete temperature (°C), $\Delta\varepsilon_{aut}$ is the change in concrete autogenous shrinkage strain, L is half of the length of the Invar bar (m), h is the convection coefficient for the Invar bar (W/m^2/°C), P is the perimeter length of the Invar bar cross section (m), k is the thermal conductivity of the Invar bar (W/m/°C), A_c is the cross sectional area of the Invar bar (m^2), T is the temperature of the Invar bar where the bar meets the cracking frame crosshead (°C), and T_∞ is the ambient temperature (°C). Equation 6-11 is the closed-form solution for calculating the integral of the temperature change along the length of a symmetrical bar (Incropera and DeWitt 2002).

The autogenous shrinkage strain is calculated in this paper using the autogenous shrinkage model proposed by Hedlund (2000). The autogenous shrinkage model used is shown in Equation 6-14 and Equation 6-15:

$$\varepsilon_{aut} = \varepsilon_{ault} \cdot \exp\left(-\left(\frac{t_{s1}}{t - t_{s0}} \right)^{\eta_{SH}} \right)$$ **Equation 6-14**

$$\varepsilon_{ault} = \left(-0.94 + 2.238 \cdot w/cm \right) \cdot 10^{-3}$$ **Equation 6-15**

where the time parameter t_{s1} is set equal to 5 days, the curvature parameter η_{SH} is set equal to 0.3, and t_{s0} is set equal to the time of concrete set. Hedlund (2002) defined t_{s0} as the time-of-set and recommended it be set to 1 day. Since the final setting time was measured in this study, t_{s0} was set equal to the measured value. Final set is defined in the simulation as the point in time when the compressive strength equals 80 psi (Tuthill and Cordon 1955). The concrete stress before final set is assumed to be zero because of its plastic state and its low elastic modulus of elasticity. The water-to-cementing materials ratio (w/cm) at which no autogenous shrinkage occurs was set at 0.42, corresponding with the theoretical limit for complete hydration proposed by T.C. Powers (Jensen and Hansen 2001) instead of at 0.5 as proposed by Hedlund (2000). Additionally, the temperature adjustment proposed by Hedlund was not used as the measured data revealed that this correction was not necessary. Sellevold and Bjøntjegaard (2006) concluded that the affect of temperature on autogenous shrinkage development cannot be corrected by simple increases in shrinkage based on the curing temperature.

As discussed earlier in this paper, the LLM does not include an adjustment for the effect that curing temperature has on early-age creep. It is well known that concrete will exhibit higher creep at higher temperatures (Bažant and Panula 1978; Emborg 1998a). In this study, the temperature correction method first proposed by Bažant and Panula (1978) was modified by a temperature modification factor, C_{TMF}, calibrated to adjust the creep compliance function calculated by the LLM as shown in Equation 6-16 to Equation 6-21:

$$\Delta J_{MLLM} = \Delta J_{LLM} \cdot C_{TMM}$$ **Equation 6-16**

$$C_{TMM} = 1 + \frac{C_T}{C_{TMF}}$$ **Equation 6-17**

$$C_T = c_T \cdot \tau_T \cdot c_0$$ **Equation 6-18**

$$c_T = \frac{19.4}{1+\left(\frac{100}{T-253.2}\right)^{3.5}} - 1$$ **Equation 6-19**

$$\tau_T = \frac{1}{1+\left(\frac{60}{\left(t_T^{'}\right)^{0.69}}\right)} + 0.78$$ **Equation 6-20**

$$c_0 = \left(\frac{1}{8}\right)\left(\frac{w}{cm}\right)\left(\frac{a}{cm}\right)\cdot a_1$$ **Equation 6-21**

where C_{TMF} can be set equal to 2.5, T is the concrete temperature (K), t_T' is the concrete age when the temperature is applied (days), w is the concrete water content (kg/m^3), cm is the concrete cementitious content (kg/m^3), a is the concrete aggregate content (kg/m^3), and a_1 is a cement type factor equal to 1 for ASTM Type I cement, 0.93 for ASTM Type III cement, and 1.03 for ASTM Type IV cement. Other than the inclusion of the temperature modification C_{TMF}, the temperature adjustment model used in this paper is identical to that proposed by Bažant and Panula (1978). The temperature modification multiplier C_{TMM} is dependent on the w/cm as shown in Figure 6-4.

The Modified Linear Logarithmic Model (MLLM) developed in this study contains 11 fit parameters. Constant values can be used for most of these parameters, however. By changing only the t_{a1}, t_{a2}, and n_{a2} parameters, a good fit can be achieved to the measured data while keeping the analysis simple enough to allow trends to be found. In this study, the Δt_0 value has been fixed at 0.001 days, the Δt_1 value at 0.1 days, the a_1^{min} value at 0.1 x 10^{-12} 1/Pa, the a_1^{max} value at 60 x 10^{-12} 1/Pa, and the a_2^{max} value at 30 x 10^{-12} 1/Pa as suggested by Larson (2003). Additionally, the n_{a1} parameter has been fixed at 1.19, the the a_2^{min} value at 5 x 10^{-12} 1/Pa, and the C_{TMF} parameter at 2.5. The effect of changing the t_{a1} parameter is shown in Figure 6-5, the t_{a2} parameter in Figure 6-6, and the n_{a2} parameter in Figure 6-7.

The stress in the cracking frame was simulated using the measured modulus and strength values fit according to Equation 6-6 and Equation 6-7 and calculated thermal and autogenous deformations for each of the rigid cracking frame tests performed. The simulation was performed for a period of 96 hours or until the concrete in the rigid cracking frame cracked, whichever came first. The creep parameters t_{a1}, t_{a2}, n_{a2} were iteratively changed until a good fit as measured by the coefficient of determination (r^2) value was achieved. Tests at different temperatures were performed on the same concrete mixtures as indicated in Table 6-4 to investigate the effects of temperature on early-age concrete creep. When a concrete mixture was evaluated at several different temperatures, the same modified linear logarithmic model (MLLM) creep parameters were used to simulate that concrete mixture at all temperatures. This was done to facilitate early-age restrained stress modeling of structural members, in which the same creep parameters must be used to model the concrete stress development in all parts of the member, irrespective of the temperature history.

6.5 Multivariate Statistical analysis procedure

A statistical analysis was performed to relate the creep parameters t_{a1}, t_{a2}, and n_{a2} found for each of the 36 different concrete mixtures with the constituent material properties shown in Table 6-4. The analysis was performed by first determining the correlation coefficient for different combinations of concrete constituent material parameters. Variable combinations, with the correlation coefficient between these individual variables less than 0.65, are considered for use in the model. An analysis of variance test for Type I and Type III errors was then performed on different combinations of variables. A Type I error occurs when a variable is used in the model when there is in fact no real relationship. A Type III error occurs when the model shows the dependence of a variable in the wrong direction (Devore 1995). The combination of variables with both Type I and Type III errors less than 5% and with the highest r^2 value is selected for use in the MLLM. A model based on the Bogue method for determining the cement composition was created, as well as a separate model based on the Rietveld method.

Different combinations of both linear and non-linear models and variables were tried during the analysis. Non-linear variations included an exponential dependence of the dependent creep parameter on all independent variables, and logarithmic variations in individual parameters, both of which are seen in Equation 6-22 (Poole 2007):

$$p_d = \exp(p_{i1} + \ln(p_{i2})) \qquad \textbf{Equation 6-22}$$

where p_d is the dependent variable, p_{i1} is an independent linear variable, and p_{i2} is an independent non-linear variable.

6.6 Results

The Modified Linear Logarithmic Model creep parameters t_{a1}, t_{a2}, and n_{a2} obtained from iteratively fitting the rigid cracking frame stress simulated for the 36 concrete mixtures to the measured rigid cracking frame stress results are shown in Table 6-5. The simulated rigid cracking frame results were calculated from the strength and modulus of elasticity fit according to Equation 6-6 and Equation 6-7, and the hardened concrete coefficient of thermal expansion. Figure 6-8 shows an example of the test results for concrete Mixture 10 for: a) compressive strength, b) modulus of elasticity, c) concrete temperature in the rigid cracking frame, and d) measured concrete stress in the rigid cracking frame.

A non-linear multivariate model was created that estimates the MLLM parameters for a concrete mixture based on the concrete constituent material properties and mixture proportions. Equation 6-23 to Equation 6-25 can be used to estimate the t_{a1}, t_{a2}, and n_{a2} MLLM creep parameters based on the Rietveld method:

$$t_{a1} = 0.680 + 0.0064 \cdot FA + 0.429 \cdot \ln(w/cm) - 0.00965 \cdot Ferrite$$

Equation 6-23

$$\begin{aligned} t_{a2} = \exp(&3.671 - 0.0192 \cdot (FA + GGBFS) - 3.7169 \cdot w/cm - \\ &0.10078 \cdot (Gypsum + Hemihydrate + Anhydrite + Arcanite) - \\ &0.0556 \cdot Ferrite) \end{aligned}$$

Equation 6-24

$$\begin{aligned} n_{a2} = \exp(&-26.735 + 0.0705 \cdot FA + 0.072 \cdot GGBFS + \\ &6.586 \cdot \ln(Alite) - 0.177 \cdot Ferrite - 0.253 \cdot Alum + 5.194 \cdot w/cm) \end{aligned}$$

Equation 6-25

where *FA* is the percent fly ash replacement of cement by mass, *w/cm* is the water-to-cementing materials ratio, *Ferrite* is the percent ferrite of the cement, as determined by Rietveld analysis, *GGBFS* is the percent Grade 120 GGBF slag replacement of cement by mass, *Gypsum* is the percent gypsum of the cement, as determined by Rietveld analysis, *Hemihydrate* is the percent hemihydrate in the cement, as determined by Rietveld analysis, *Anhydrite* is the percent anhydrite in the cement, as determined by Rietveld analysis, *Alite* is the percent alite in the cement, as determined by Rietveld analysis, and

Alum in the percent aluminate in the cement as determined by Rietveld analysis. When a supplementary cementing material is used, the percent values used for the cement chemistry are the percent of the material in the cement multiplied by the cement content expressed as a ratio of the total cementing materials. For example, the *Ferrite* value used in the model of a concrete containing 30% SCMs and a portland cement containing 10% Ferrite would be 7%. The r^2 value for the Rietveld model for the t_{a1}, t_{a2}, and n_{a2} parameters are 0.70, 0.70, and 0.75, respectively.

A comparison was made of the measured cracking frame stress values at 2 hour increments to those predicted using the MLLM creep model using the Rietveld parameters as defined in Equation 6-24 to Equation 6-26. These results are summarized in Figure 6-9. It is clear from Figure 6-9 that most of the measured data are accurately modeled by the proposed MLLM. The average absolute error comparing the Rietveld MLLM-simulated rigid cracking frame stresses at 2 hour intervals to the measured rigid cracking frame stress from the 73 tests performed is 0.19 MPa (28 psi). 95% of the measured rigid cracking frame stress values were within ±0.49 MPa (71psi) of the calculated rigid cracking frame stress values when using the Rietveld MLLM. The ability of the Rietveld MLLM to predict the measured cracking frame stress can be seen for different materials, such as fly ash replacement with Fly Ash 2 in Figure 6-10 and with GGBF Slag in Figure 6-11.

A sensitivity analysis was performed on the MLLM model parameters based on the Rietveld method to investigate each parameter's effect on the calculated early-age stress development. Each parameter was changed one at a time, while holding all other parameters the same. The heat of hydration and modulus of elasticity were not changed during this sensitivity analysis in order to investigate only the effect of a change in the stress relaxation parameters on the early-age stress relaxation. Additionally, when one value in the cement composition was changed, the remainder of the cement composition parameters were not changed. This is not realistic, and will not completely reflect the true behavior of the cement, but it allows for the investigation of the sensitivity of the model. The amount of autogenous shrinkage was, however, allowed to change based on the w/cm.

Table 6-6 summarizes the effect of a change in each MLLM parameter when using the Rietveld method of determining the cement composition on the concrete stress relaxation during the first 1-2 days of the simulations, and on the stress relaxation during days 2-4. Both the direction of the change on the early age stress relaxation and the relative sensitivity of a change in each parameter are given in the table. The up arrow indicates an increase in the stress relaxation, while a decrease indicates a decrease in the stress relaxation. The numbers of arrows indicates the relative affect on the stress relaxation, where one arrow indicates a very minor change, and 4 arrows indicates a substantial change in the stress relaxation. The use of GGBF slag during the first day slightly increased the early age stress relaxation, but at later ages of between 1 and 4 days, decreased the stress relaxation as shown in Figure 6-12a. The use of fly ash has a similar effect as GGBF slag on the concrete early-age stress relaxation, with an increased amount of stress relaxation before about 1-2 days which transitions to a decreased amount of stress relaxation after about 2 days as shown in Figure 6-12b. Grasley (2006) also found that fly ash increased the concrete early age creep, and decreased the later age creep, with the transition occurring between 1 and 28 days. The similar early-age stress relaxation trends of fly ash and GGBF slag suggest that the same mechanism may be at work for both materials in reducing the later age creep. The increase in stress relaxation from the use of fly ash and GGBF slag can be attributed to the mainly slower rate of reaction of these materials. The decrease at later ages, however, can be attributed to a change in the structure and number of creep sites available, differences in C-S-H stochastic ratios, and a different porosity of the C-S-H that results from the pozzolanic reaction (Thomas and Jennings, 2006).

A separate non-linear multivariate model for calculating the MLLM creep parameters based on the Bogue method has been created and is shown in Equation 6-26 to Equation 6-28:

$$t_{a1} = 0.728 + 0.0061 \cdot FA + 0.448 \cdot \ln(wcm) - 0.0111 \cdot C_4AF$$ **Equation 6-26**

$$\begin{aligned} t_{a2} = \exp(3.436 - 0.0179 \cdot (FA + GGBFS) - 3.404 \cdot wcm \\ - 0.0186 \cdot C_2S - 0.0566 \cdot C_4AF) \end{aligned}$$ **Equation 6-27**

$$\begin{aligned} n_{a2} = \exp(6.165 - 0.0541 \cdot FA - 0.0619 \cdot GGBFS - 0.00869 \cdot cement \\ - 0.425 \cdot C_3A - 0.572 \cdot C_4AF + 0.0107 \cdot CemBlaine) \end{aligned}$$ **Equation 6-28**

where C_4AF is the percent C_4AF of the cement, as calculated using the Bogue method, C_2S is the percent C_2S of the cement, as calculated using the Bogue method, C_3A is the percent C_3A of the cement, as calculated using the Bogue method, *cement* is the total amount of cementing materials used (kg/m^3), and *CemBlaine* is the cement Blaine fineness (m^2/kg). When a supplementary cementing material is used, the percent values used of the cement chemistry are the percent of the material in the cement multiplied by the percent cement of the total cementing materials. For example, the C_4AF value used in the model of a concrete containing 30% SCMs and a portland cement containing 10%

C_4AF would be 7%. The r^2 values for the Bogue model for the t_{a1}, t_{a2}, and n_{a2} parameters are 0.70, 0.69, and 0.77, respectively.

A comparison was made of the measured cracking frame stress values at 2 hour increments to those predicted using the MLLM creep parameters modeled using the Bogue model and Equation 6-26 to Equation 6-28 as shown in Figure 6-13. The average absolute error comparing the Bogue MLLM simulated rigid cracking frame stresses at 2 hour intervals to the measured rigid cracking frame stress from the 73 tests performed is 0. 19 MPa (28 psi). 95% of the measured rigid cracking frame stress values were within ±0.51 MPa (74psi) of the calculated rigid cracking frame stress values when using the Bogue MLLM compared to the simulated rigid cracking frame values. The ability of the Bogue MLLM to predict the measured cracking frame stress can be seen for different materials, such as fly ash replacement with fly ash 2 in Figure 6-14 and with GGBF slag in Figure 6-15. Figure 6-14 and Figure 6-15 also show the combined benefit of SCMs in reducing early age stresses in concrete by reducing the early-age modulus of elasticity, increasing early-age stress relaxation, and reducing the heat of hydration.

6.7 Discussion

The MLLM developed based on the cracking frame creep analysis can predict well the early-age concrete creep behavior for the concrete mixtures tested. This study tested several concrete mixtures under widely varying temperature histories, allowing the model to be used as part of an early-age stress cracking probability analysis of members with non-uniform temperature developments. A large number of cement types was used, albeit with a limited range of alkali contents. It should be noted, however, that there are several limitations to this model. The data set is limited to only 36 different concrete mixtures. The model is also limited by the range of cement replacement levels with supplementary cementing materials. Larger cement replacements with SCM may affect the early-age hydration and consequently creep in unexpected ways. Additionally, the effects of admixtures such as shrinkage reducing admixtures have not been quantified as part of this study.

The next obvious limitation of the model is that the rigid cracking frame simulations were only performed for a maximum of 96 hours. Any creep response beyond 96 hours calculated using this model may be inaccurate. Additionally, the principle of superposition was used in the creep analysis, which may lead to errors when the stress level is above 40% of the cracking stress (Westman 1999; Emborg 1998b). This may be because of strain softening at higher compressive stress levels due to micro-cracking. Additionally, at higher stress levels, the concrete may experience tertiary creep that can be very non-linear, which violates one of the assumptions of the principle of superposition (Emborg 1998b).

Even with the limitations discussed, the creep models outlined in this paper still provide a good estimate of the concrete early-age stress development. 95% of the measured concrete stress results were within ±0.49 MPa (71 psi) of the calculated rigid cracking frame concrete stresses when using the Rietveld MLLM, and ±0.51 MPa (74psi) when using the Bogue MLLM. This implies that both the Rietveld and Bogue MLLM models may be used with good expected results. The Rietveld MLLM is based on the Rietveld method which more accurately quantifies the cement phase composition than the Bogue method and is thus the preferred method when available (Walenta and Füllmann 2004). The Bogue MLLM, however is presented in this paper because it is still more commonly used and available to practitioners than the Rietveld method.

6.8 Conclusions

A new early-age creep model has been presented based on the Linear Logarithmic Model (LLM) originally developed by Larson (2003). The LLM has been modified to account for the effect of temperature on early-age creep. The Modified Linear Logarithmic Model (MLLM) has been used to quantify the early-age creep development of 36 different concrete mixtures from rigid cracking frame testing, compressive strength and the elastic modulus development. A statistical model relating the concrete mixture constituent materials to the creep parameters of the MLLM has also been developed. Two different statistical models have been developed, one based on the Rietveld type analysis of the cement composition and the other based on the Bogue type analysis of the cement composition. Either model developed may be used and is suitable for early-age concrete stress analysis.

6.9 Acknowledgements

The authors wish to express their gratitude to the Texas Department of Transportation through Project 0-4563 for funding this research. The guidance and assistance of Dr. Rupert Springenschmid and Mr. Erwin Gierlinger to develop the cracking frame test setup are appreciated. The authors would also like to thank Karen Scrivener, Christophe Gosselin and Ryan Chancey for performing the Rietveld analysis on the cement used.

Table 6-1 - Activation energy values used in maturity strength calculations

Material	Activation Energy (J/mol)
No SCM replacement	40,700
Class F Fly Ash	44,000
Class C Fly Ash	45,000
GGBF Slag	41,000

Table 6-2 - Cement physical and chemical properties

		Cement #								
		C1	C2	C3	C4	C5	C6	C7	C8	C9
	Blaine Fineness (m^2/kg)	391	365	409	381	353	337	317	367	563
Rietveld Method	Alite (%)	61.0	55.7	49.0	62.9	64.5	61.2	58.8	55.7	55.2
	Belite (%)	15.6	21.1	26.4	11.0	15.3	16.0	19.2	18.0	14.5
	Ferrite (%)	6.0	10.7	12.1	10.1	10.8	3.5	2.2	10.5	12.1
	Aluminate (%)	9.6	4.0	4.4	6.7	4.4	13.1	11.4	5.0	2.7
	Periclase (%)	0	0	0	0.6	0	0	0.8	1.1	0.02
	Gypsum (%)	0.4	0	2.3	2.2	1.5	1.4	2.6	2.3	0.2
	Hemihydrate (%)	1.2	2.5	2	1.8	0.5	1.5	1.9	0.9	4.3
	Anhydrite (%)	0.7	0.7	0.4	0.6	0.6	0.6	0.8	0.6	3.8
	Quartz (%)	0	0	0	0	0	0	0	0	0.5
	Portlandite (%)	0.7	0.9	0	0	0	0.5	0	0	0.0
	Calcite (%)	3.6	3.2	2.5	2.8	1.2	0.8	0	4.1	6.3
	Arcanite (%)	1	0.7	0.9	0	0.4	1.5	2	0.7	0.3
Bogue Method	C_3S (%)	63.1	66.5	49.9	60.7	64.9	58.3	49.0	60.8	48.8
	C_2S (%)	7.4	9.3	24.4	12.9	9.4	14.7	24.0	13.5	21.1
	C_3A (%)	10.3	4.0	1.8	7.5	6.8	11.0	10.9	7.0	7.0
	C_4AF (%)	7.0	11.4	16.1	10.0	10.3	6.1	5.7	9.7	11.4
	Gypsum (%)	5.4	4.0	4.7	4.7	4.5	5.7	6.1	4.5	7.9

Table 6-3 - Supplementary cementing materials oxide analysis

	FA1	FA2	FA3	FA4	FA5	FA6	GGBFS	Silica Fume
SiO_2 (%)	56.6	51.7	46.7	47.8	37.8	33.3	34.5	93.6
Al_2O_3 (%)	30.7	24.8	19.7	18.1	19.8	18.4	11.4	0.3
Fe_2O_3 (%)	4.9	4.2	5.1	5.0	6.2	5.4	0.7	0.1
CaO (%)	0.7	13.1	18.4	19.9	23.1	28.9	41.7	0.6
MgO (%)	0.7	2.3	3.0	3.3	4.6	5.3	7.3	0.6
Na_2O (%)	0.1	0.2	1.8	0.8	1.7	1.6	0.1	0.2
K_2O (%)	2.3	0.8	0.9	0.9	0.1	0.4	0.4	1.0

Table 6-4 - Rigid cracking frame tests performed

					Concrete Placement Temperature / Temperature Surrounding Simulated Wall				
Mix #	Cement #	w/cm	SCM Replacement	Chemical Admixtures	23°C /23°C	10°C /10°C	35°C /35°C	23°C /35°C	10°C /35°C
1	C1	0.42	-	MRWR	X				
2	C1	0.42	-	LRWR	X				
3	C2	0.42	-	LRWR	X		X		
4	C2	0.42	-	LRWR, AEA	X				
5	C3	0.44	-	MRWR	X				
6	C4	0.35	31% FA3	MRWR, B	X				
7	C5	0.35	44% FA4	LRWR, HRWR	X				
8	C6	0.42	-	HRWR	X		X		X
9	C6	0.42	-	LRWR	X	X	X	X	X
10	C6	0.42	20% FA2	LRWR	X				
11	C6	0.42	30% FA2	LRWR	X	X	X	X	X
12	C6	0.42	20% FA1	LRWR	X				
13	C6	0.42	30% FA1	LRWR	X				
14	C6	0.42	20% FA5	LRWR	X				
15	C6	0.42	30% FA5	LRWR	X		X	X	X
16	C6	0.42	20% FA6	LRWR	X				
17	C6	0.32	-	HRWR	X				
18	C3	0.44	-	MRWR			X	X	X
19	C7	0.42	-	HRWR	X				
20	C8	0.42	-	LRWR	X	X	X		
21	C7	0.42	30% FA6	LRWR	X				
22	C7	0.42	20% FA6	LRWR	X				
23	C7	0.42	30% GGBFS	LRWR	X			X	X
24	C6	0.42	30% GGBFS	LRWR			X		
25	C6	0.42	50% GGBFS	LRWR	X		X		
26	C7	0.42	50% GGBFS	LRWR		X		X	X
27	C7	0.42	25% FA5, 6% SF	LRWR	X				
28	C7	0.42	25% FA2, 6% SF	LRWR	X				
29	C7	0.42	30% FA2, 30% GGBFS	LRWR	X				
30	C6	0.32	-	LRWR, MRWR	X				

31	C6	0.38	-	LRWR, MRWR	X				
32	C7	0.38	-	LRWR, MRWR		X	X	X	X
33	C6	0.48	-		X				
34	C6	0.53	-		X				
35	C9	0.42	-	LRWR	X	X	X	X	X
36	C7	0.42	-	AEA	X				

Note: SF = Silica Fume, LRWR = Type A Low Range Water Reducer, MRWR= Mid Range Water Reducer, HRWR = High Range Water Reducer, AEA = Air Entraining Admixture, B = Type B Retarder

Table 6-5 - Modified Linear Logarithmic Model Creep Parameters obtained for all mixtures

Mix #	t_{a1} (days)	t_{a2} (days)	n_{a2}
1	0.24	6.00	0.50
2	0.26	6.00	0.50
3	0.20	3.50	0.45
4	0.35	3.50	0.40
5	0.18	2.00	0.10
6	0.50	3.00	0.90
7	0.30	2.00	0.99
8	0.30	3.83	0.30
9	0.30	3.83	0.30
10	0.48	3.70	0.33
11	0.50	2.50	0.85
12	0.48	3.41	0.35
13	0.40	2.50	0.75
14	0.43	3.30	0.40
15	0.53	3.00	0.70
16	0.40	3.60	0.32
17	0.20	7.00	0.20
18	0.18	2.00	0.10
19	0.22	4.00	0.25
20	0.15	2.50	0.15
21	0.50	2.00	0.99
22	0.49	3.30	0.40
23	0.25	3.00	0.55
24	0.20	2.50	0.70
25	0.40	2.00	0.75
26	0.35	2.00	0.75
27	0.40	2.50	0.70
28	0.40	2.50	0.70
29	0.43	3.00	0.50
30	0.12	5.00	0.10
31	0.20	3.83	0.31
32	0.10	3.83	0.31
33	0.30	2.75	0.45
34	0.35	2.25	0.46
35	0.10	2.00	0.70
36	0.40	3.83	0.30

Table 6-6 - Effect of a change in Rietveld MLLM parameter on early-age concrete stress relaxation

MLLM parameter	Effect of an increase in MLLM parameter on the early age concrete stress relaxation during: The first 1-2 days	After the first 1-2 days
GGBFS	↑↑	↓↓↓↓
Fly Ash	↑↑↑	↓↓↓↓
w/cm	↑↑↑	↓↓↓
Total Sulfates	↓	↓↓
Ferrite	↓↓	↓↑
Aluminate	↓↓	↑↑↑
Alite	↑↑	↓↓

↑ = Increase in stress relaxation

↓ = Decrease in stress relaxation

4 arrows indicates a substantial change in the early age stress relaxation, while 1 arrow indicates a minor change in the early age stress relaxation

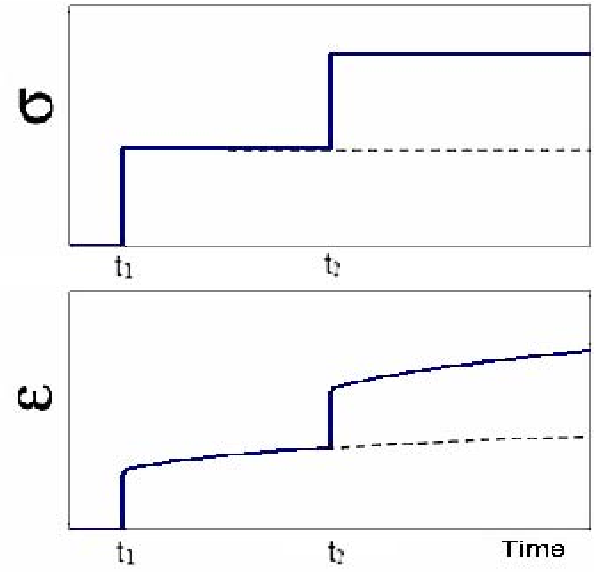

Figure 6-1 – The principle of superposition is used to calculate the viscoelastic concrete behavior for time steps t_1 and t_2 (After Emborg 1998b)

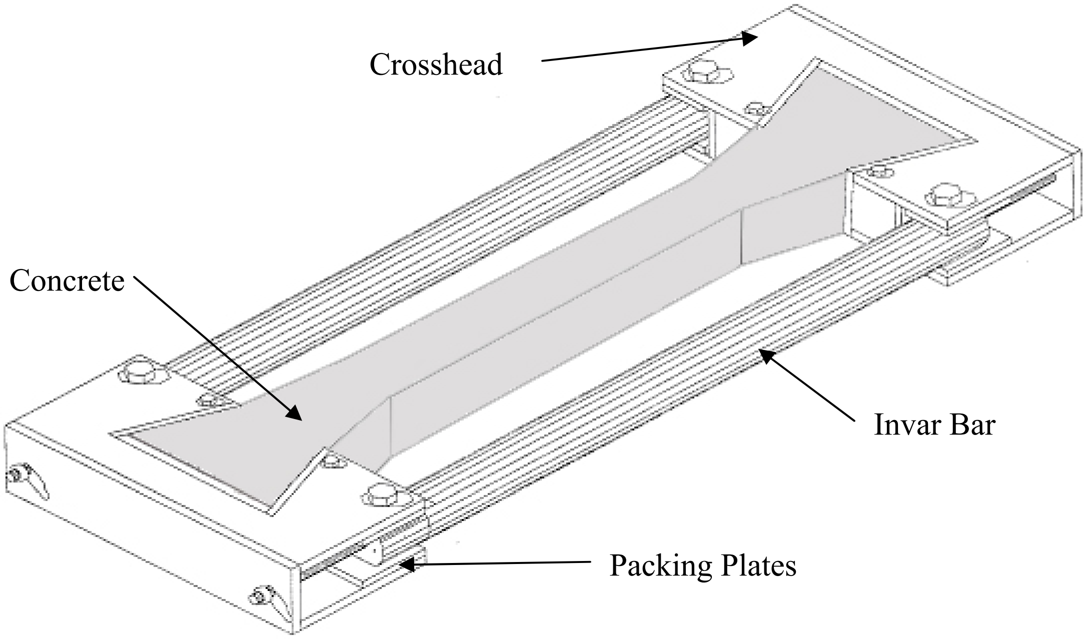

Figure 6-2 – Rigid Cracking Frame Schematic

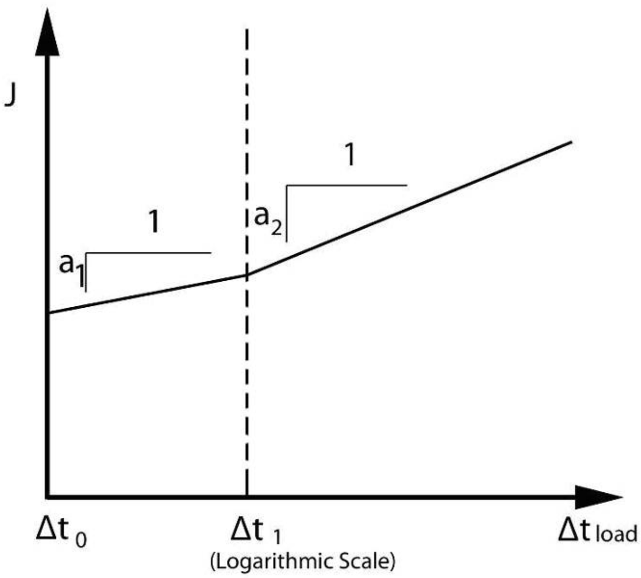

Figure 6-3 - Linear Logarithmic Model Creep Compliance (After Larson 2003)

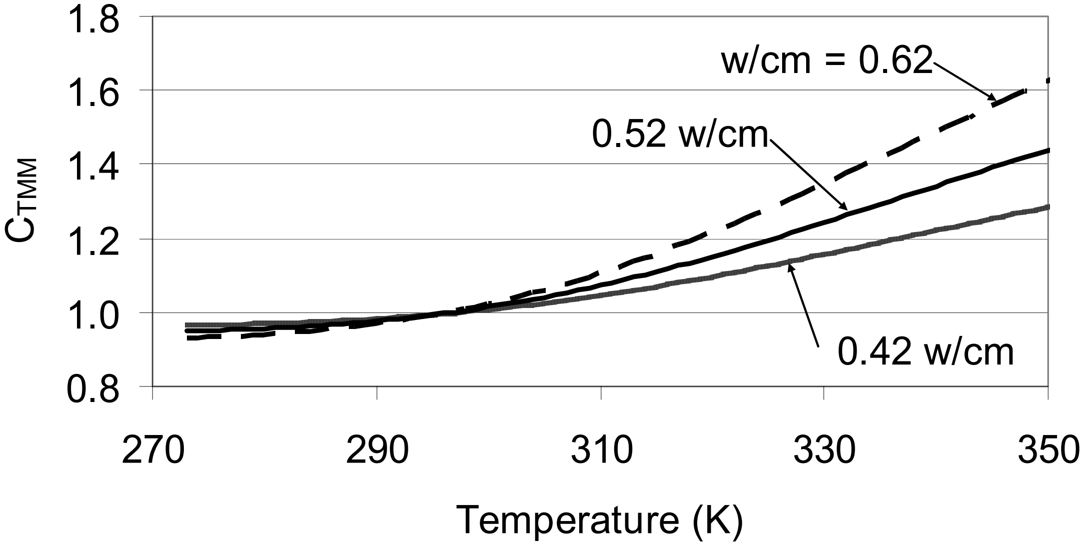

Figure 6-4 - Concrete temperature modification multiplier variation with temperature

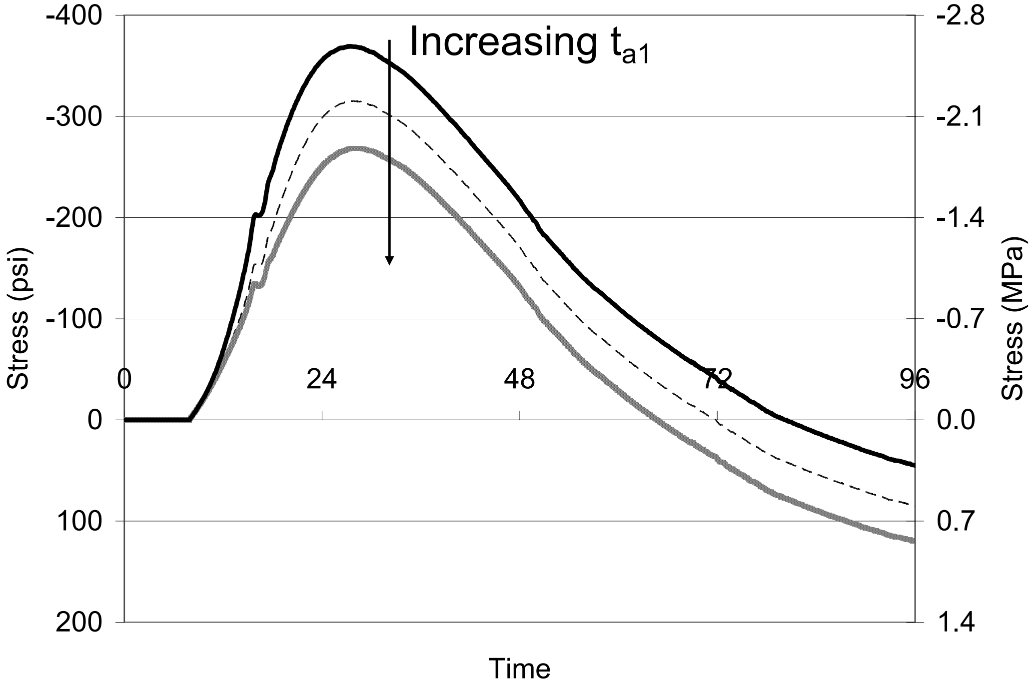

Figure 6-5 - Effect of increasing the t_{a1} parameter on simulated rigid cracking frame stress development

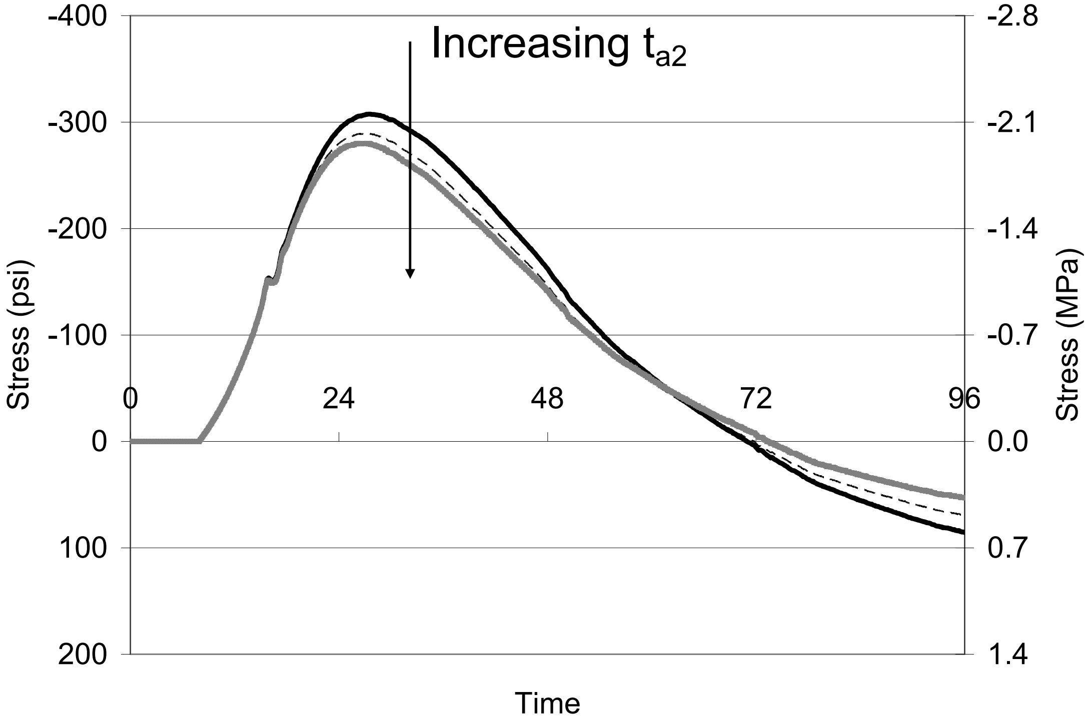

Figure 6-6 - Effect of increasing the t_{a2} paramater on simulated cracking frame stress development

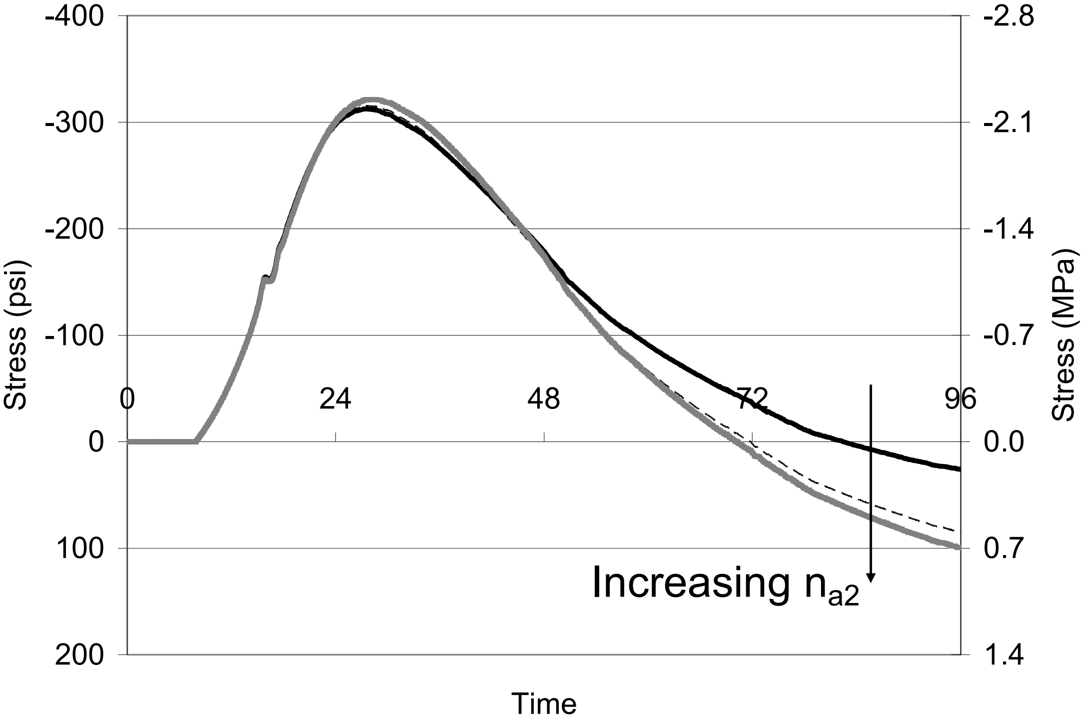

Figure 6-7 - Effect of Increasing the n_{a2} parameter on simulated rigid cracking frame stress development

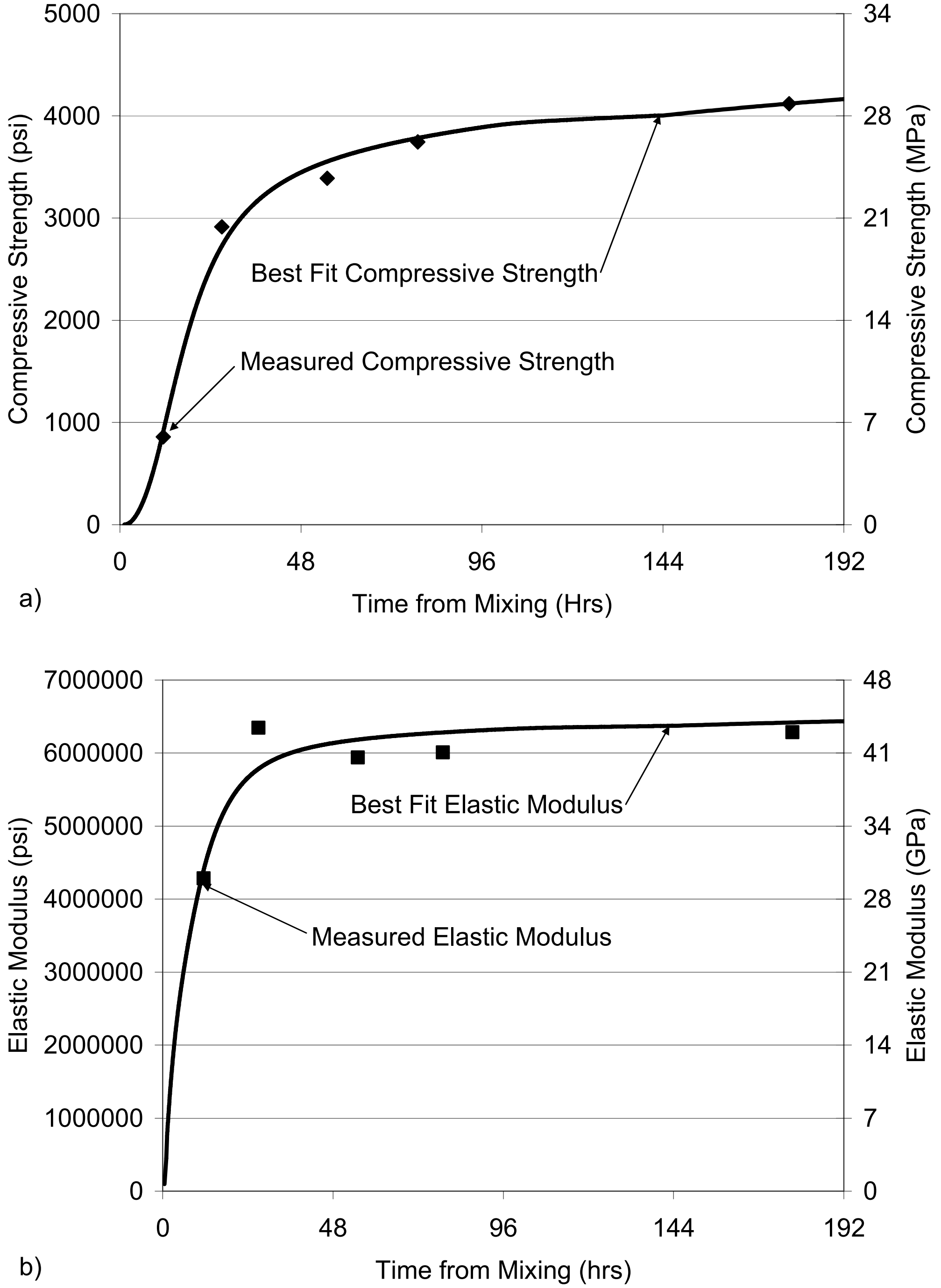
5000
4000
3000
2000
1000
0
Compressive Strength (psi)
34
28
21
14
7
0
Compressive Strength (MPa)
Best Fit Compressive Strength
Measured Compressive Strength
0
48
96
144
192
a)
Time from Mixing (Hrs)
7000000
6000000
5000000
4000000
3000000
2000000
1000000
0
Elastic Modulus (psi)
48
41
34
28
21
14
7
0
Elastic Modulus (GPa)
Best Fit Elastic Modulus
Measured Elastic Modulus
0
48
96
144
192
b)
Time from Mixing (hrs)

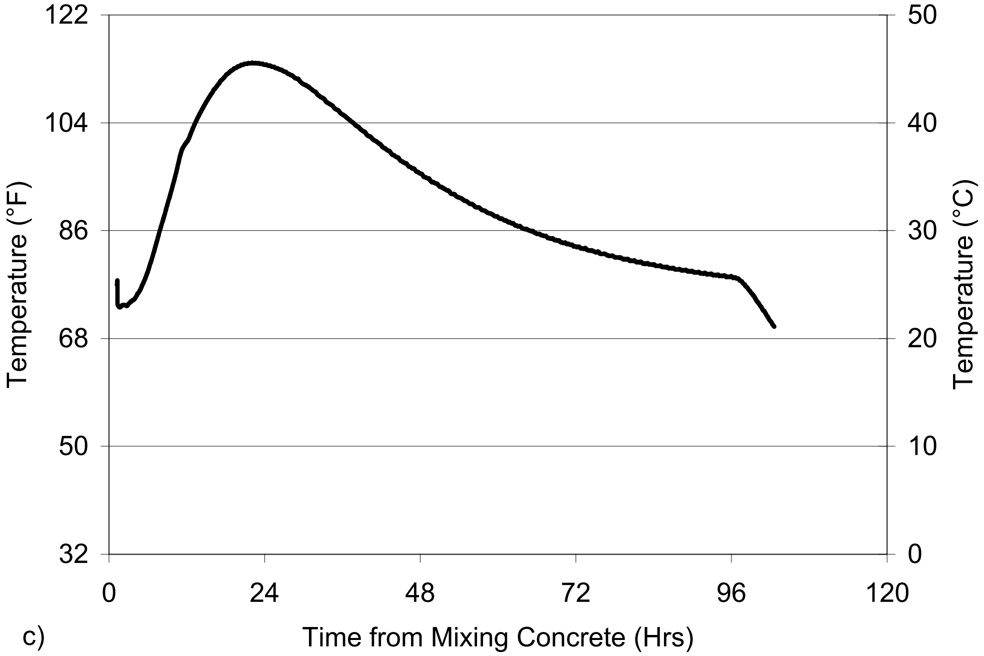

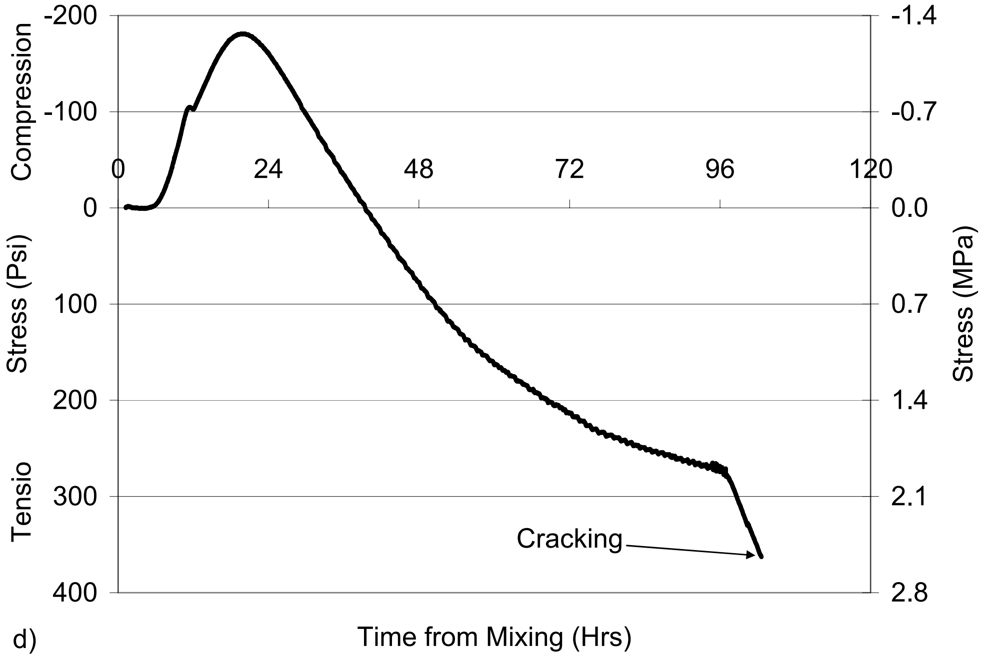

Figure 6-8 - Concrete Mixture 10 Cured Using a 23°C (73°F) Placement Temperature and 23°C (73°F) Constant Surface Temperature in Temperature Simulation a) Compressive strength Development b) Elastic Modulus Development c) Temperature and d) Measured Stress in the Rigid Cracking Frame

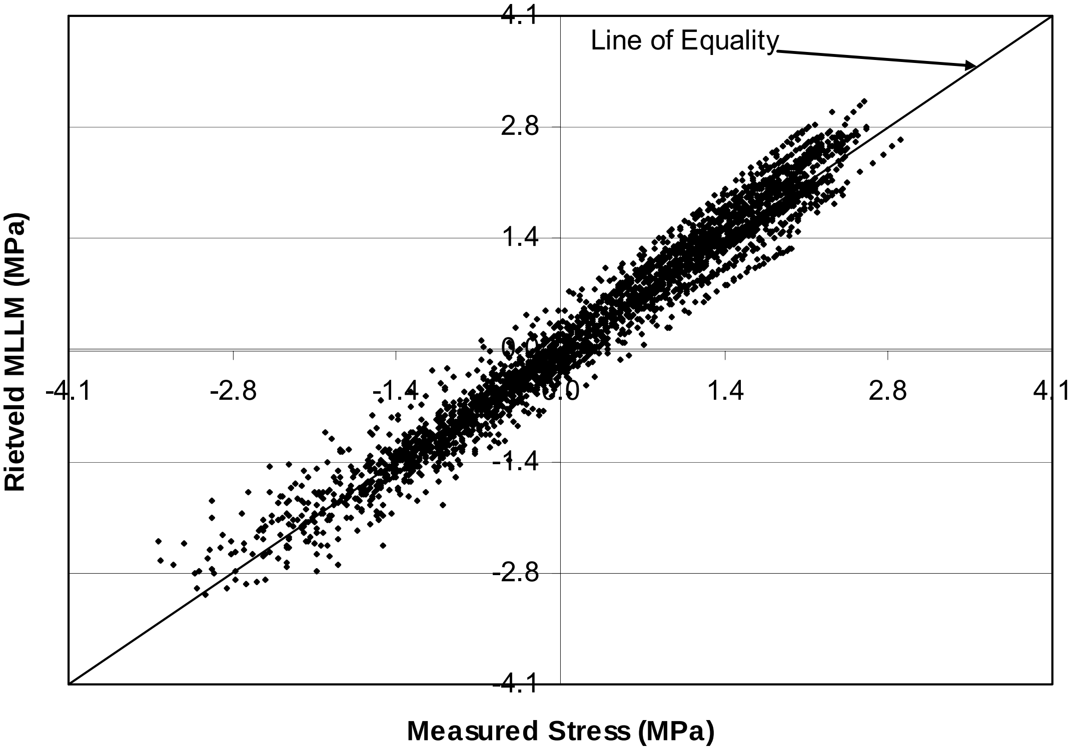

Figure 6-9 - Comparison of Cracking Frame Stress Simulated Using the Rietveld MLLM versus the Measured Cracking Frame Stress

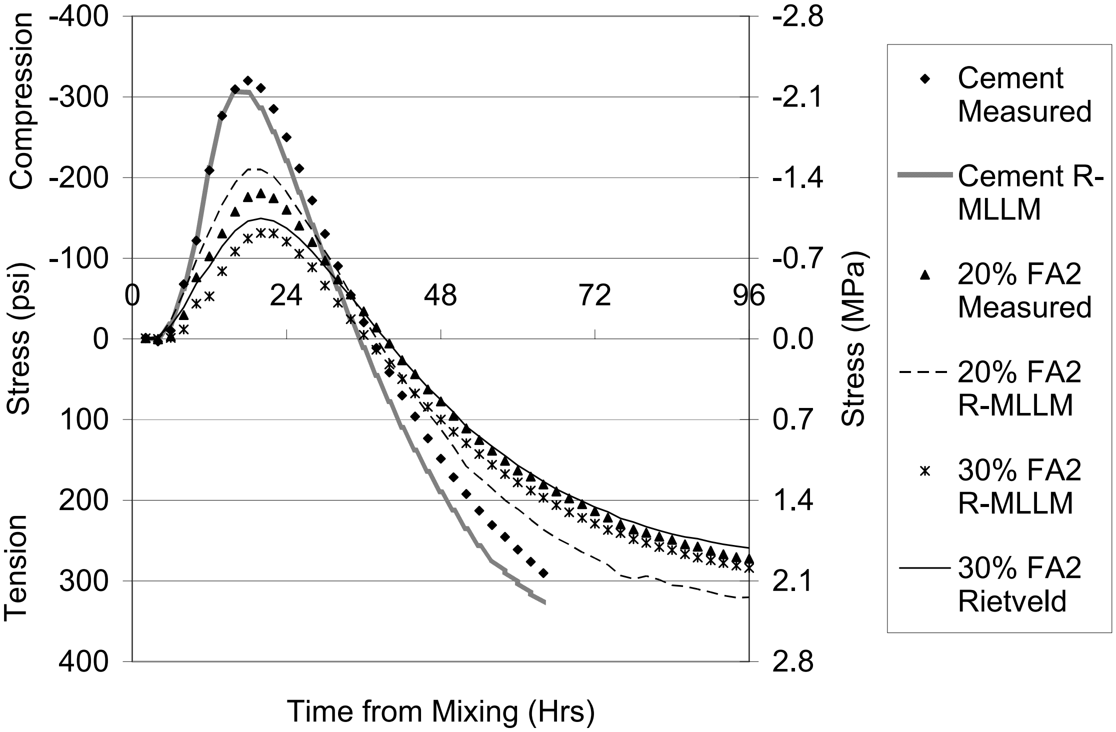

Figure 6-10 - Rigid Cracking Frame Measured Stress and Simulated Stress Using Rietveld MLLM (R-MLLM) for Fly Ash 2

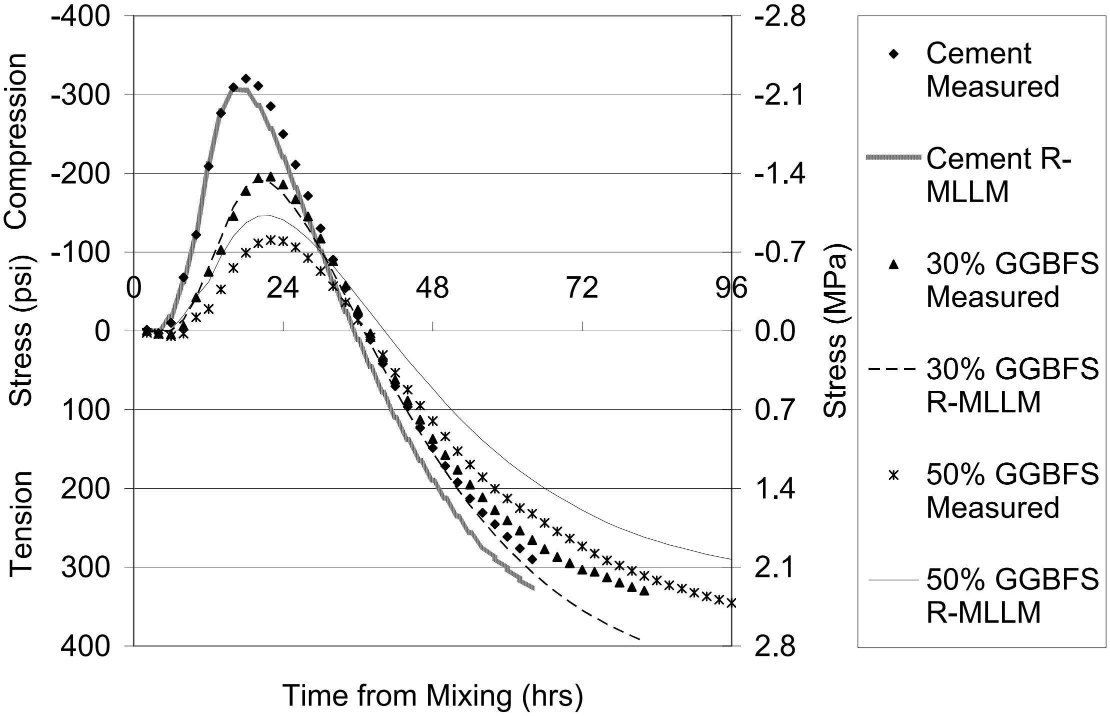

Figure 6-11 - Rigid Cracking Frame Measured Stress and Simulated Stress Using Rietveld MLLM (R-MLLM) for GGBFS

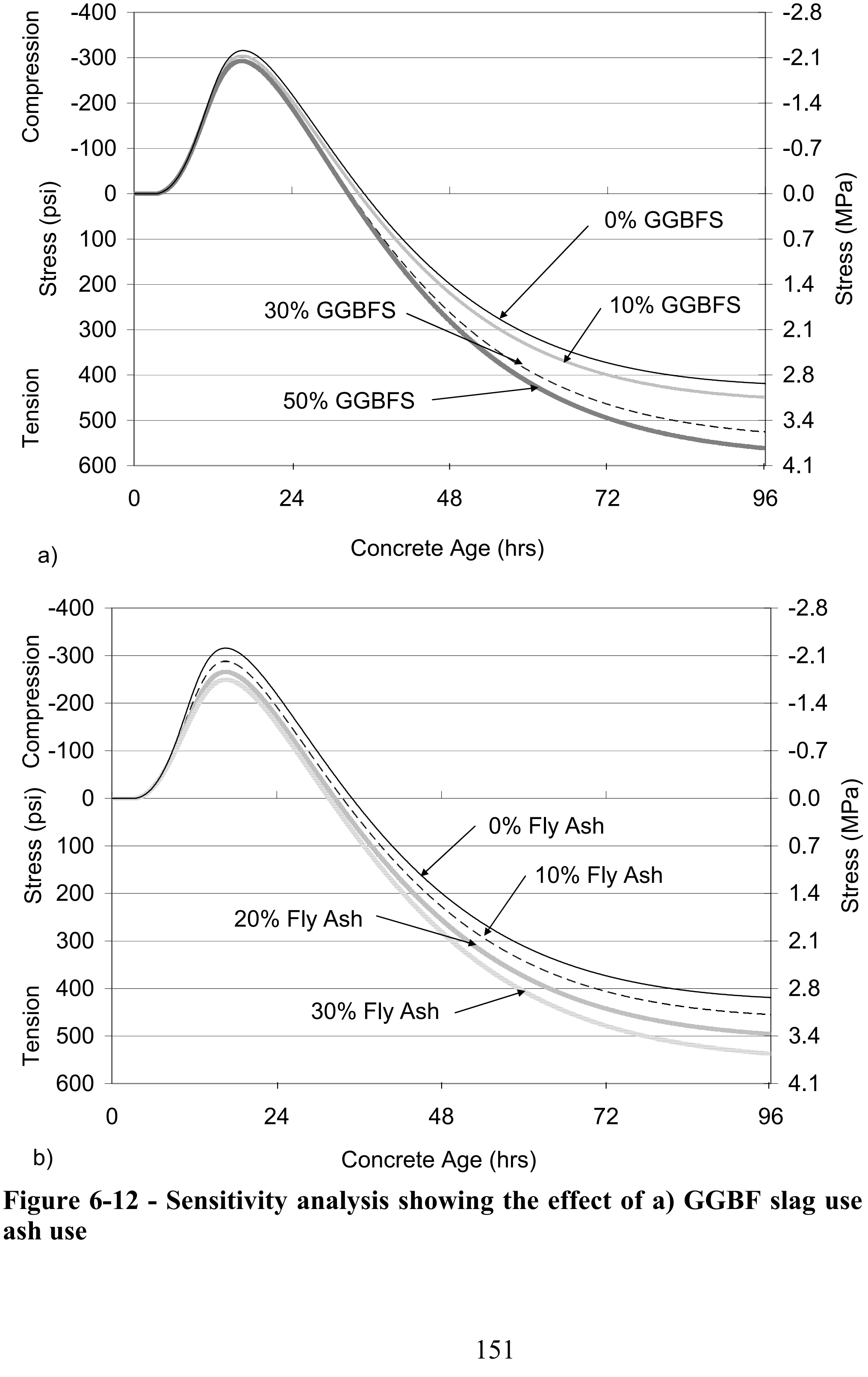

Figure 6-12 - Sensitivity analysis showing the effect of a) GGBF slag use and b) fly ash use

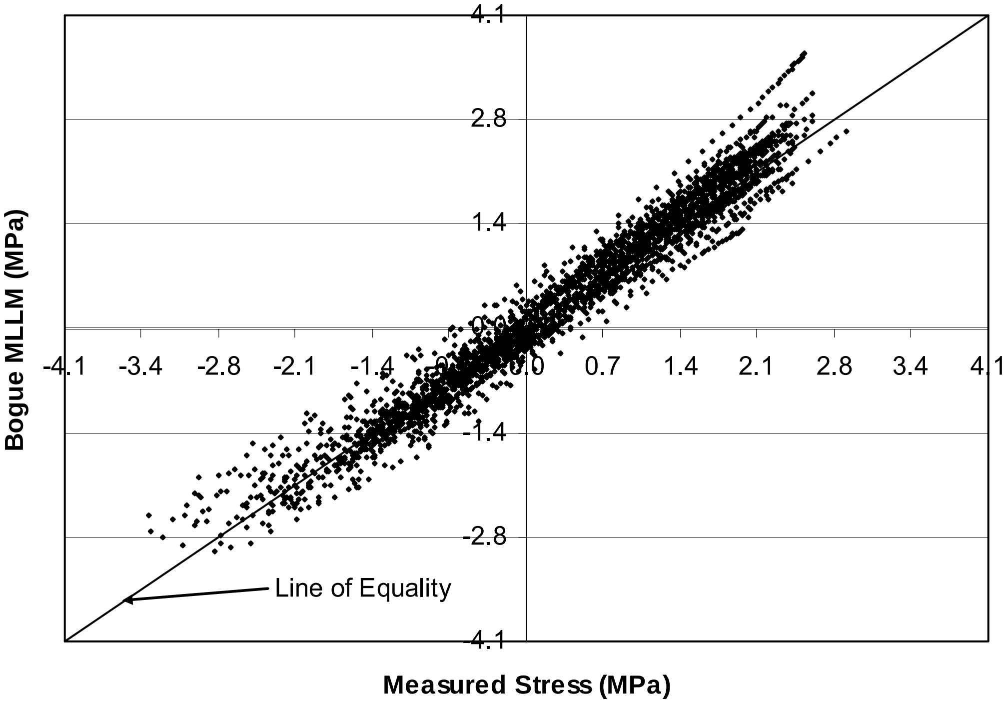

Figure 6-13 - Comparison of Cracking Frame Stress Simulated Using the Bogue MLLM versus the Measured Cracking Frame Stress

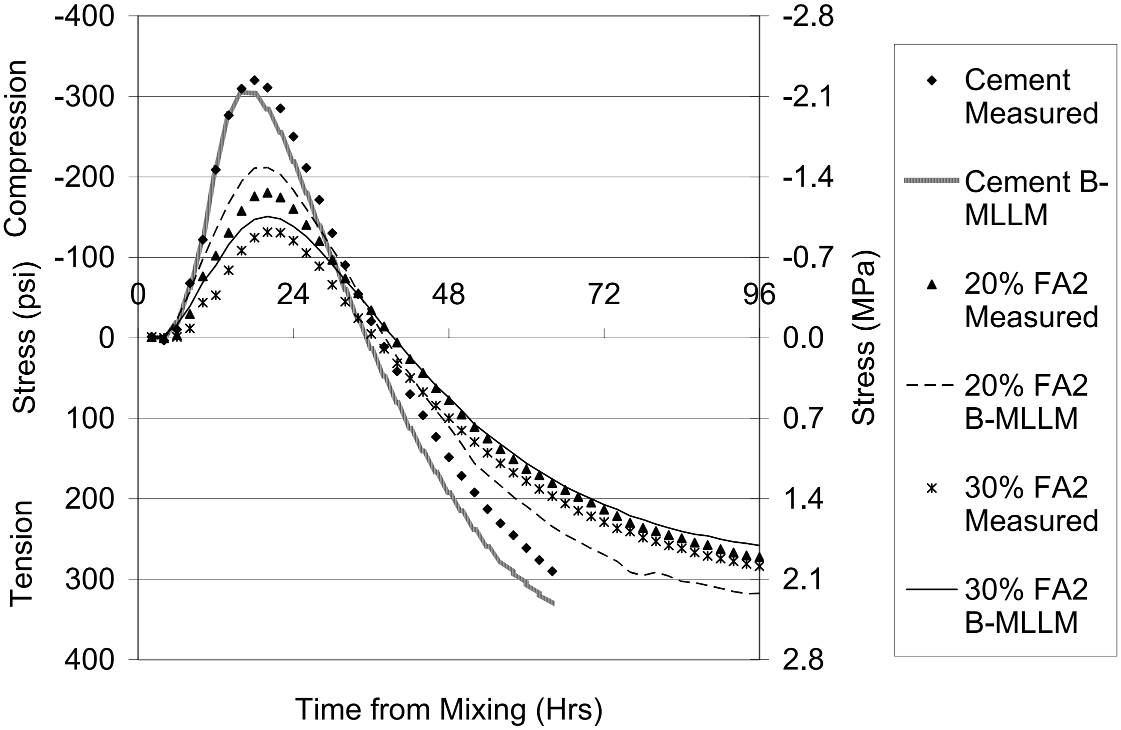

Figure 6-14 - Rigid Cracking Frame Measured Stress and Simulated Stress Using Bogue MLLM (B-MLLM) for Fly Ash 2

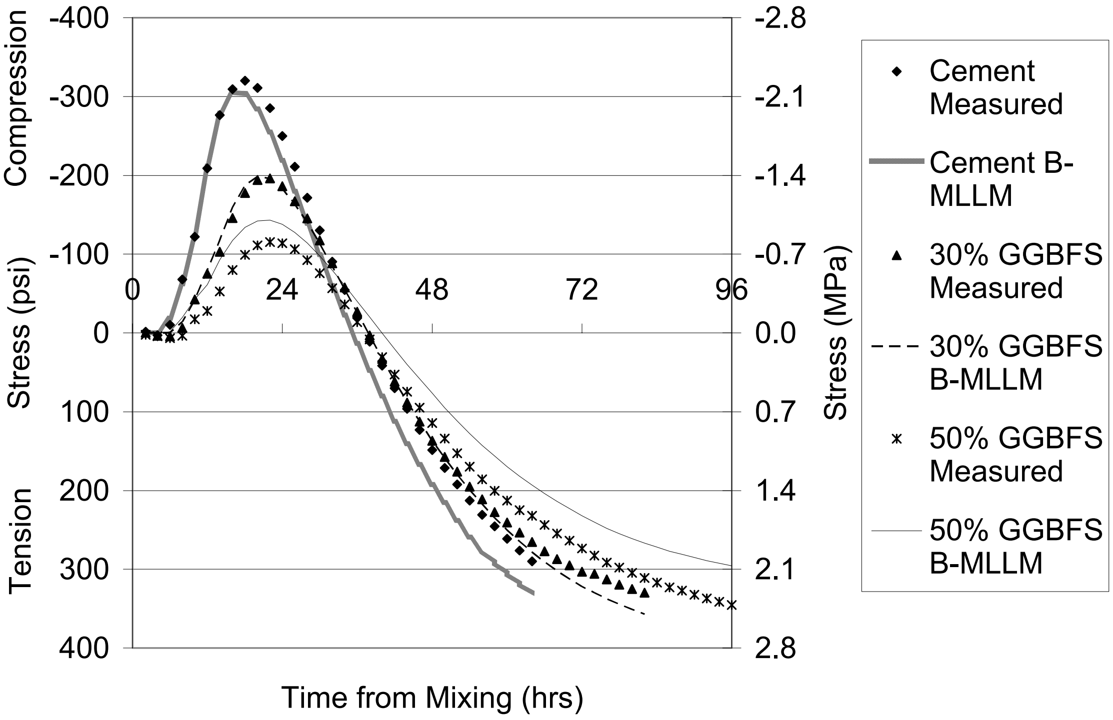

Figure 6-15 - Rigid Cracking Frame Measured Stress and Simulated Stress Using Bogue MLLM Model for GGBFS

CHAPTER 7 ALLOWABLE STRESS DESIGN METHOD FOR THERMAL CRACKING OF CONCRETE

Mass concrete members are especially vulnerable to early-age cracking as large thermal gradients may develop due to the uneven dissipation of heat released during hydration. Thermal stress analyses are increasingly being used in the design of concrete mixture proportions and selection of "best placement practices" to help limit this risk of cracking. An important part of any concrete thermal stress analysis is the failure criterion used. This study presents the results of 64 restrained cracking frame tests and accompanying match-cured concrete cylinders used to determine the ratio of stress-to-splitting tensile strength at cracking. The splitting tensile strength was compared to the measured compressive strength from 743 tests to help determine an appropriate way to use the more commonly known compressive strength during the thermal stress analysis. A stress-to-splitting tensile strength ratio of 0.57 was found give a 50% probability of cracking when 100 mm by 20 0mm (4" by 8") concrete cylinders were used for the splitting tensile tests. A lognormal distribution was found to adequately characterize the distribution of the measured stress-to-splitting tensile strength ratios at failure. Lognormal probability distributions were developed that may be used to calculate the probability of early-age concrete cracking for different splitting tensile strength models.

7.1 Introduction

Cementitious materials can release a large amount of heat during the early stages of the hydration reaction. As a result, concrete members can develop very high interior temperatures during curing, while the exterior can be closer to ambient temperatures. The non-uniform temperature, modulus of elasticity development and restraint of the concrete member can create large internal stresses (ACI 207 1995). These internal stresses, when high enough relative to the tensile strength capacity at this age, can cause cracking in the concrete member, which may reduce the structure's intended service life.

In recent years, specifications have begun to require contractors and material suppliers to consider thermal cracking when engineering mixture proportions, designing formwork, and planning construction sequences. Several methods have been proposed for estimating the cracking risk of concrete members. These methods range in complexity from simple temperature difference requirements to non-linear time-dependent finite element thermal stress or fracture mechanics models (ACI 207 1995; Gajda and VanGeem 2002; Rostásy, Tanabe and Laube 1998; Emborg 1998b) Both stress and strain based failure criteria have been proposed (Emborg 1998b). The level of cracking is often defined as the ratio between the stress and strength (or, alternatively, the actual strain and failure strain at time t), as shown in Equation 7-1 (Emborg 1998b):

$$\eta^{\max} = \left[\frac{\sigma_t(t)}{f_{ct}^*(t)} \right]^{\max}$$ **Equation 7-1**

where η^{max} is the maximum cracking risk in the member during the analysis period, σ_t is the tensile stress (MPa) in the member at a time t (hrs), and f_{ct}^* is the tensile strength of the member at time t (MPa). There is an inherent variability to the stress and strength as measured or calculated. Normal distributions of stress and strength are usually assumed in probabilistic models of concrete, as shown in Figure 7-1. The overlap between the stress probability density function and the strength probability density function defines the probability of cracking. Several researchers have explored the probability of cracking due to thermal stresses using assumed mean and standard deviations of the concrete strength and stress (Eberhardt, Lokhorst, and van Breugel 1994; van Breugel and Lockhorst, 2001).

The stress at failure may not always be equal to the concrete tensile strength measured in different ways. One commonly used method to assess the tensile strength of concrete is the modulus of rupture (ASTM C 78 2002). This test is most commonly used as a quality control test for concrete pavements. The modulus of rupture can overestimate the true tensile strength of concrete by even more than the splitting tensile test (Mindess, Young and Darwin 2003).

The concrete splitting tensile test (ASTM C 496 2004) is the most common practical means to measure the tensile strength of concrete. This test, however, does not measure the true direct tensile strength of the concrete. Small regions of compression are developed on the top and bottom of the specimen, leading to an overestimation of the true concrete tensile strength (ASTM C 496 2004; Mindess, Young and Darwin 2003). Even though the splitting tensile test is the most widely performed concrete tensile strength test, it is still not commonly performed for actual construction projects. In most cases, the concrete tensile strength is estimated from its compressive strength. Methods of calculating the splitting tensile strength from compressive strength have been studied by numerous researchers. Most of these models assume a power type function based on the compressive strength, as shown in Equation 7-2 (Raphael 1984; Oluokun, Burdette, and Deatherage 1991; Arıoglu, Girgin, and Arıoglu 2006; Carino and Lew 1982; ACI Committee 318 2005):

$$f_{ct} = a \cdot \left(f_c\right)^b$$

Equation 7-2

where f_{ct} is the concrete splitting tensile strength, a and b are fit parameters, and f_c is the concrete compressive strength.

The specimen size will also affect the measured tensile strength of the concrete (Shah, Swartz, and Ouyang 1995; Kadlečeck Sr., Modrý, and Kadlečeck Jr. 2002). For instance, the splitting tensile measured in a 100 by 200 mm (4 by 8 in.) cylindrical specimen would be expected to be 10% larger than that of a 150 by 300 mm (6 by 12 in.) specimen (Kadlečeck Sr., Modrý, and Kadlečeck Jr. 2002). Finally, the measured tensile strength of concrete is strongly influenced by the loading rate. Slower loading rates usually associated with thermal stresses may lead to a reduction in tensile strength of up to 30% (Emborg 1998a). One explanation for this may be that the concrete under slow loading rates goes into tertiary creep and experiences a creep failure (Emborg 1998a). The formation of microcracks in the concrete, which have additional time to propagate, may also be a cause for the reduction in strength under slow loading rates (Emborg 1998a).

Several investigations have been performed that have developed relationships for calculating the probability of cracking based on assumed strength and stress distributions. The current study focused on establishing lognormal distributions of the probability of early-age concrete cracking based on measured stress from early age restrained concrete tests and the measured concrete splitting tensile strength. Additionally, this study investigated the applicability of different models available for calculating the splitting tensile strength development from the measured compressive strength for use in calculating the probability of early-age restrained concrete cracking. The work reported in this paper will enable designers to use the more commonly available compressive strength development in thermal stress calculations.

7.2 Research Significance

Concrete material designs and construction plans to prevent thermal cracking in mass concrete have become increasingly common in recent years. An important part of any early-age stress analysis is the failure criterion used. Restrained concrete stress tests and splitting tensile tests were performed on various types of concrete to quantify the risk of concrete thermal cracking based on the stress-to-splitting tensile strength of the concrete. This paper presents a method of calculating the allowable stress for an acceptable probability of cracking for use in early-age stress analysis.

7.3 Experimental Methods

The stress level at cracking due to thermal and autogenous shrinkage were investigated using a rigid cracking frame (RCF) (Mangold 1998). The rigid cracking frame uses a passive restraint system, as shown in Figure 7-2. When the concrete temperature changes and the concrete experiences autogenous shrinkage, the concrete deformations are restrained by the two large Invar steel bars. When the temperature increases, the concrete expansion is converted into compressive stresses as shown in Figure 7-3. At the same time that a compressive stress develops in the rigid cracking frame concrete, a tensile stress develops in the Invar side bars to maintain equilibrium. The concrete compressive stress is then reduced by stress relaxation and the eventual concrete temperature decrease. As the concrete temperature continues to decrease, tensile stresses develop in the concrete and the stress state in the Invar side bars becomes compressive. The concrete stresses may be obtained by strain gauges that are mounted on the Invar steel bars because the rigid cracking frame is a statically determinant structure. The restraint provided by the cracking frame is 100% at the time of placement (because the stiffness of the Invar steel bars is infinitely greater than the plastic concrete) and decreases as the concrete modulus increases according to Equation 7-3 (Mangold 1998):

$$\delta = \frac{100}{1 + \left(\frac{E_c A_c}{E_s A_s} \right)} \qquad \textbf{Equation 7-3}$$

where δ is the degree of restraint (%), E_c is the concrete elastic modulus (MPa), A_c is the concrete cross sectional area (m^2), E_s is the Invar restraining bar modulus (MPa), and A_s is the Invar restraining bar's cross sectional area (m^2). Invar steel is used because of the material's low coefficient of thermal expansion, which reduces the measurement errors caused by the thermal movement of the side bars. The thermal movement of the Invar side bars can be calculated using Equation 7-4:

$$\varepsilon_{Tadj} = \Delta T_{ib} \cdot \alpha_{ib} \cdot \delta \qquad \textbf{Equation 7-4}$$

where ε_{Tadj} is the temperature induced strain of the invar bar, ΔT_{ib} is the temperature change of the Invar bar at the strain gauge (°C), and α_{ib} is the coefficient of thermal expansion of the invar bar (m/m/°C).

The temperature in the concrete was controlled by circulating tempered water through copper pipes embedded in the RCF formwork. In all tests, if the concrete did not crack within 96 hours after mixing, the concrete was cooled at 1°C/hr (1.8°F/hr) until cracking occurred. In 58 of the tests, the concrete temperature was adjusted to match that of a simulated 1 m (39.4") wall, with a constant temperature surrounding the wall. The concrete placement temperature and constant temperature surrounding the simulated wall were also varied. In one test, the temperature of a 0.75 m thick wall was imposed on the concrete. In four of the tests, bridge deck temperature histories were imposed on the concrete, simulating the daily rise and fall of the temperature in the bridge deck during the diurnal temperature cycles. Figure 7-4 shows the temperature history and corresponding measured stress development as measured in the rigid cracking frame in one of the tests performed using the bridge deck temperature history. In one test, the concrete was allowed to cure due to the internal heat of hydration, meaning that there was no active temperature control used and that any temperature rise in this test occurred because the sample formwork was insulated during curing. Figure 7-5 shows the temperature development and corresponding stress development as measured in the rigid cracking frame in the same concrete mixture that was cured with no active temperature control, and with the temperature adjusted to that of simulated 0.75 m and 1 m thick walls. Figure 7-6 shows the temperature development and corresponding stress development as measured in the rigid cracking frame in three different rigid cracking frame tests performed using the same concrete mixture proportions and different concrete placement temperatures and simulated 1-m thick wall constant surface temperatures.

Twenty-four 100-mm by 200-mm (4” by 8”) concrete cylinders were match-cured to the concrete temperatures measured in the middle of the cracking frame. Two compression and two splitting tensile tests were performed on the cylinders at 0.5, 1, 2, 3, 7, and 28 days to obtain the strength development of the concrete. In addition, 405 compression and splitting tensile tests were performed on various concrete mixtures cast and cured at room temperature and 100% relative humidity, and were used to further examine the relationship between compressive strength splitting tensile strength development.

Various concrete mixtures were tested as part of this study. The base concrete mixture used in the rigid cracking frame portion of this study consisted of 335 kg/m^3 (564 lb/yd^3) of total cementing materials and a coarse aggregate-to-total aggregate ratio of 0.6. Concrete water-to-cementing materials ratio (w/cm) ranged between 0.32 and 0.53 with a majority of the test conducted at a w/cm of 0.42. The total amount of cementing materials was changed to 279 kg/m^3 (470 lb/yd^3) on one test conducted at a 0.53 w/cm, 307 kg/m^3 (517 lb/yd^3) on one test conducted at a 0.48 w/cm, 362 kg/m^3 (611 lb/yd^3) on five tests conducted at a 0.38 w/cm, and 390 kg/m^3 (658 lb/yd^3) on one test conducted at a 0.32 w/cm. Seven different fly ashes (five ASTM C 618 (2003) Class F and two Class C fly ashes) were used in this study with replacement percentages varying from 20-40%. Grade 120 ground-granulated blast furnace (GGBF) slag was also used, with replacement levels ranging from 30-50%. Two ternary blends of fly ash and silica fume (25% fly ash and 6% silica fume) were tested, along with one of fly ash and GGBF Slag ternary blend (30% fly ash and 30% GGBF Slag). Five Type I cements, three Type I/II cements, one Type III cement, and one Type V cement were used in the testing. River gravel, limestone, and dolomitic limestone coarse aggregate were used in the testing. Dolomitic limestone sand was used in one mixture, while natural river sand was used in all other tests.

7.4 Results

A total of 743 tests of compressive and splitting tensile strength were performed. The power-law relationship between the measured splitting tensile strength and the compressive strength shown in Equation 7-2 fit the data reasonably well, as shown in Figure 7-7. Fit parameters *a* and *b* were found to be 0.266 and 0.907, respectively, with

R^2 equal to 0.95. For a fixed *a*-value, any formulation with a power lower than 0.907 overestimates the splitting tensile strength of the concrete at lower compressive strengths, and underestimates the splitting tensile strength at the higher compressive strengths, as shown in Figure 7-8 using a fit equation of a= 1.7 and b = 2/3 as suggested by Raphael (1984) and referred to in this paper as the Raphael model. The splitting tensile tests performed as part of this study were performed on smaller cylinders than those used in the Raphael study, leading to higher measured values because of the size effect.

Sixty-four rigid cracking frame tests were performed with accompanying splitting tensile tests. In some tests, micro-cracking occurred before a final through-crack, as shown in Figure 7-9. The cracking stress used in the comparison with the concrete splitting tensile strength was the first significant crack measured during the test, whether it was a micro-crack or a through-crack. Ratios of the measured concrete stress at cracking to the measured splitting tensile strength ranged between 0.37 and 0.79. The distribution was fit well by a lognormal-type distribution, as shown in Figure 7-10, with a 50% probability of cracking occurring at a stress-to-strength ratio of 0.57, and a standard deviation of 0.16. The mean concrete cracking stress to splitting tensile strength value compares well to the expected value of 1.0 when reductions of 30% for loading rate and 10% for specimen size are considered. Starting at a ratio of 1.0 and applying these corrections, this gives an expected mean cracking stress to splitting tensile strength of 1.0 x 0.70 x 0.90 = 0.63, which corresponds well to the measured value of 0.57.

The measured concrete stress at cracking was also compared to the estimated concrete splitting tensile strength. The splitting tensile strengths were estimated using several different models (based on Equation 7-2) that have been developed to predict the concrete splitting tensile strength from the compressive strength. The first model used for predicting the splitting tensile strength based on the splitting tensile and compressive strength tests performed in this study, hereafter call the current study model. The Raphael model was also examined in this study. The model suggested in the ACI 318 building code (2005) for calculating the splitting tensile strength from compressive strength tests is also shown and is hereafter referred to as the ACI 318-05 model. Finally, a model developed by Carino and Lew (1982) was examined in this study, hereafter referred to as the Carino and Lew model. Table 7-1 shows the fit parameters for each model according to Equation 7-2 and the maximum and minimum stress-to-strength values at cracking of the 64 tests. Table 7-1 also shows the mean and standard deviation of a lognormal distribution of the probability of cracking fit to the stress-to-strength ratio at cracking, as well as three commonly used tests for gauging the goodness of fit of the lognormal distribution to the data. The Kolmogorov – Smirnov test allows the user to reject a type of probability distribution for the data if the calculated D-value is greater than a threshold value for a given probability of the fit being valid and the number of sample data points. For 64 tests and a 5% level of significance is 0.17. The Anderson-Darling test is a modified version of the Kolmogorov-Smirnov test that gives more weight to the distribution tails, which can be rejected at the 5% point for values above 2.492 (Johnson 2000). The Chi-Squared test is another goodness of fit test that can be used to reject a type of fit distribution if the value is greater than a threshold value and may be used on discrete distributions (Johnson 2000). The results from these three goodness of fit tests are all below their threshold values, indicating that the log-normal distribution cannot be rejected as an appropriate statistical distribution. Overall, all of the models have similar standard deviations and can be represented well by a lognormal distribution. This means that any of the models examined in this study could work well in a thermal stress cracking risk analysis, as long as the lognormal distribution used to calculate the probability of cracking corresponds to the splitting tensile strength model used.

A previous study using a Temperature Stress Testing Machine (TSTM) (van Breugel 2001) and 32 tests showed a mean cracking stress to splitting tensile strength of 0.75, significantly higher than the 0.57 value found in the current study. The value of 0.75 is close to the 50% probability of cracking obtained when either the Raphael (1984) or Carino and Lew (1982) models are used. The splitting tensile specimen size was not given in the van Breugel (2001) study, making it difficult to compare results to this study exactly. Another factor that may influence the stress-to-strength ratio at cracking may be the loading rate. The TSTM is an active restraint system and imposes 100% restraint on the concrete. This may lead to some differences in the specimen loading rate. The degree of restraint in the rigid cracking frame may be closer to that of a concrete column or footing, while the TSTM may simulate better the cracking in a continuously reinforced concrete pavement or some other structure subjected to 100% restraint.

For each lognormal distribution described in Table 7-1, a probability of failure may be calculated for different stress/ tensile strength levels. Table 7-2 shows the cracking stress-to-tensile strength ratios for different probabilities of failure. The level of risk that is acceptable is very subjective. Different levels of cracking risk may be determined based on the calculated stress to tensile strength ratio in design, with a low, medium, high, or very high cracking risk being acceptable in different circumstances. A low cracking risk may be one with a cracking probability of 25% and may be needed for projects in corrosive environments or where thermal cracking may be intolerable. A moderate or general cracking risk may be associated with a probability of cracking between 25% and 50%. Between 50% and 75% probability may be classified as a high probability of cracking. A very high cracking risk would be anything over 75% chance of cracking. Figure 7-11 shows the probability of cracking for the different cracking probability categories versus the stress to splitting tensile strength ratio using Raphael's correlation between tensile and compressive strength. The thermal stress cracking probability categories based on the Raphael model is particularly suited for use in thermals stress control plans. The Raphael model allows the use of the more commonly performed compressive strength testing in lieu of splitting tensile strength testing to be used in the analysis. The model is also easily implemented in thermal stress analysis. Additionally, the 50% cracking probability level based on the Raphael model corresponds to commonly used stress-to-splitting tensile strength limits already in use. Finally, the proposed cracking probability categories do not suggest an overly precise level of significance in the thermal stress analysis.

7.5 Conclusions

A new relationship for predicting the concrete splitting tensile strength from the compressive strength for the concrete mixtures tested was developed. It was also found that the model developed by Raphael (1984) for predicting the concrete splitting tensile strength development under-predicted the concrete splitting tensile strength as measured 100-mm by 200-mm (4" by 8") concrete cylinders. The concrete risk of cracking was also determined by comparing the tensile stress at cracking in a rigid cracking frame test to the splitting tensile strength of match-cured concrete cylinders. A measured stress-to-splitting tensile strength of 0.57 corresponded to a 50% probability of cracking. This value agrees well with expected ratio when reductions in strength for loading rate and specimen size are considered. A lognormal distribution fit the cracking frame to splitting tensile strength ratios well. When the concrete stress at cracking was compared to the splitting tensile strength calculated from the compressive strength—using several published models—the standard deviation using a lognormal distribution only changed slightly. This implies that for design purposes, the concrete tensile strength used to determine the concrete cracking probability may be obtained without much loss in accuracy from the compressive strength, a much more commonly known quantity. When the compressive strength is used to estimate the splitting tensile strength for use in determining the probability of cracking, any of the splitting tensile strength models examined in this paper may be used, as long as the cracking probability lognormal distribution used corresponds to the splitting tensile strength model used in calculating the stress-to-splitting tensile strength ratio.

7.6 ACKNOWLEDGEMENTS

The authors wish to express their gratitude to the Texas Department of Transportation through Project 0-4563 for funding this research. The work of Jason Meadows in performing some of the rigid cracking frame and concrete mechanical property tests is also gratefully acknowledged. The guidance and assistance of Dr. Rupert Springenschmid and Mr. Erwin Gierlinger to develop the cracking frame test setup are appreciated.

Table 7-1 - Comparison of lognormal distributions of concrete cracking stress to tensile strength as calculated from the compressive strength

Equation Source	Test Results of this Study	Current Study Model	Raphael model 1984	ACI 318-05 model	Carino and Lew model 1982
fit parameter a	-	0.266	1.7	6	1.15
fit parameter b	-	0.907	0.666	0.5	0.71
Maximum stress-to-splitting tensile strength at cracking	0.79	0.81	0.90	0.99	0.93
Minimum stress-to-splitting tensile strength at cracking	0.37	0.40	0.49	0.57	0.5
Mean, μ	-0.57	-0.57	-0.40	-0.25	-0.37
Standard Deviation, σ	0.16	0.16	0.14	0.13	0.14
Kolmogorow - Smirnov GOF D-value	0.087	0.058	0.068	0.067	0.063
Anderson - Darling GOF test value	0.59	0.31	0.30	0.45	0.26
Chi - Squared GOF test	4.0	3.56	1.95	2.04	1.73

*GOF = Goodness of Fit

Table 7-2 - Concrete cracking probability versus cracking stress to tensile strength ratios for different splitting tensile strength models

Failure Probability	Test Results of this Study	Relationship Developed in This Study	Raphael 1983	ACI 318-05, Chapter 18	Carino and Lew 1982
75%	0.64	0.63	0.74	0.85	0.76
50%	0.57	0.56	0.67	0.78	0.69
25%	0.51	0.51	0.61	0.72	0.63
10%	0.46	0.46	0.56	0.66	0.57
5%	0.44	0.43	0.54	0.64	0.55
1%	0.39	0.38	0.49	0.58	0.50

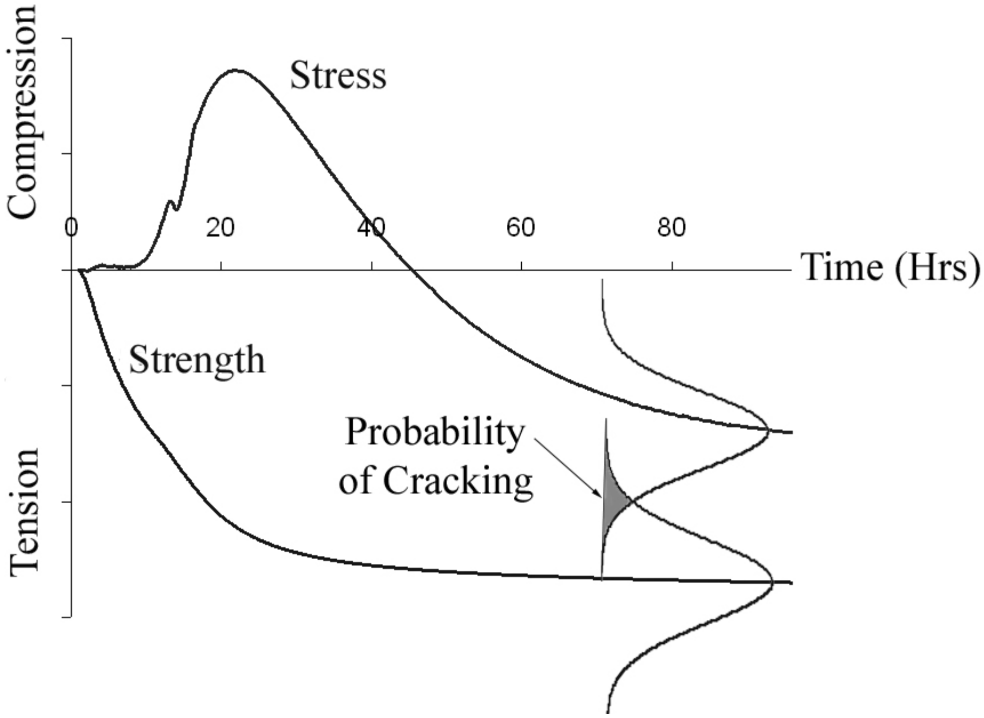

Figure 7-1 - Graphical Representation of Probability of Concrete Cracking (Adapted from Eberhardt, Lokhorst, and van Breugel 1994)

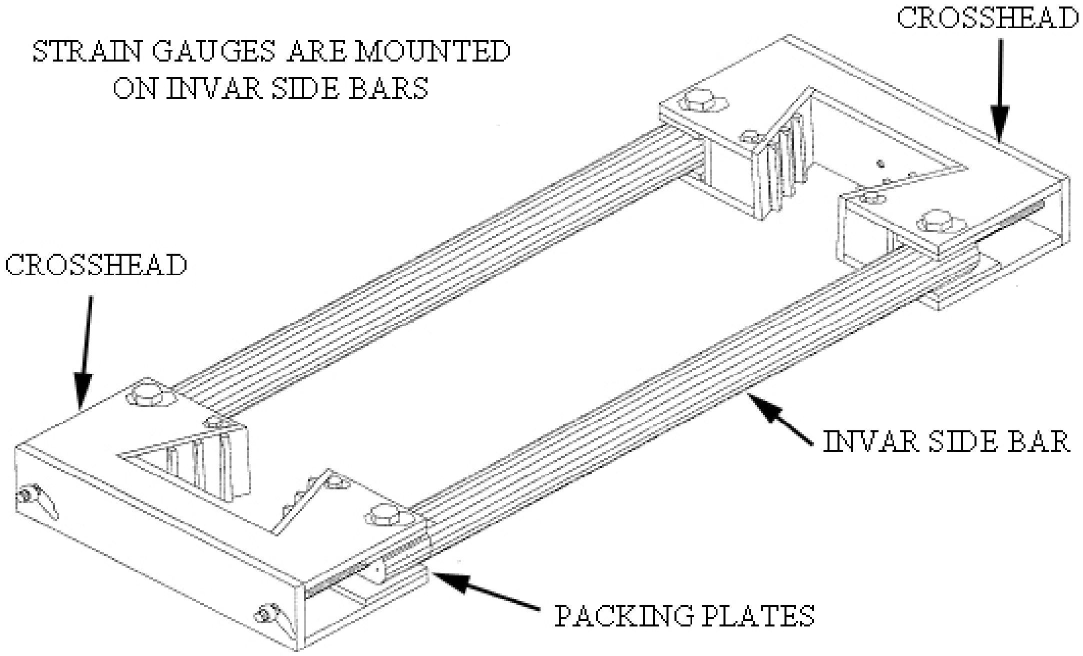

Figure 7-2 - Rigid Cracking Frame Schematic (Whigham 2005)

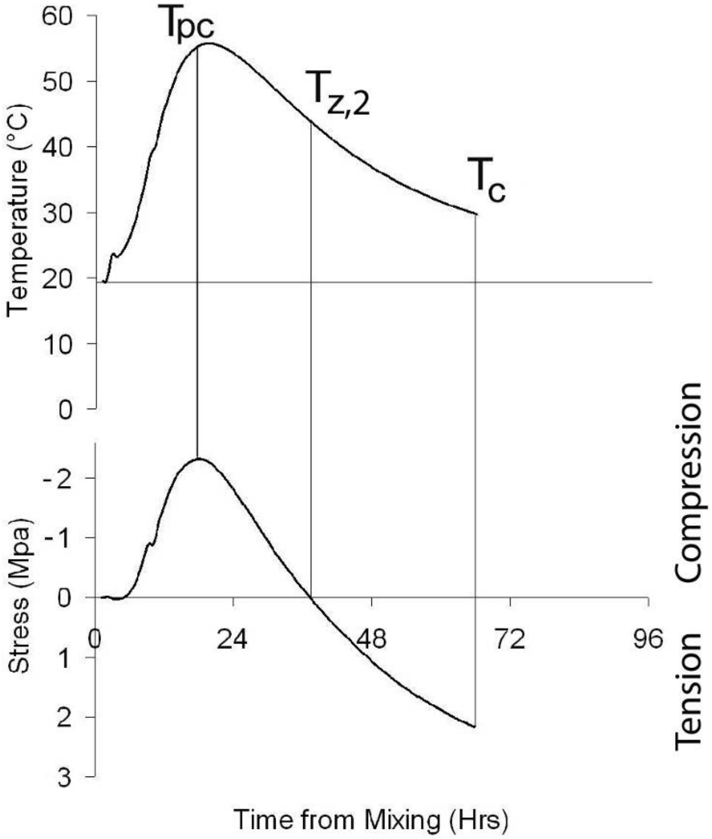

Figure 7-3 - Rigid Cracking Frame Temperature Development and Corresponding Early-Age Concrete Stress Development (After Springenschmid, R. and R. Breitenbücher, 1998)

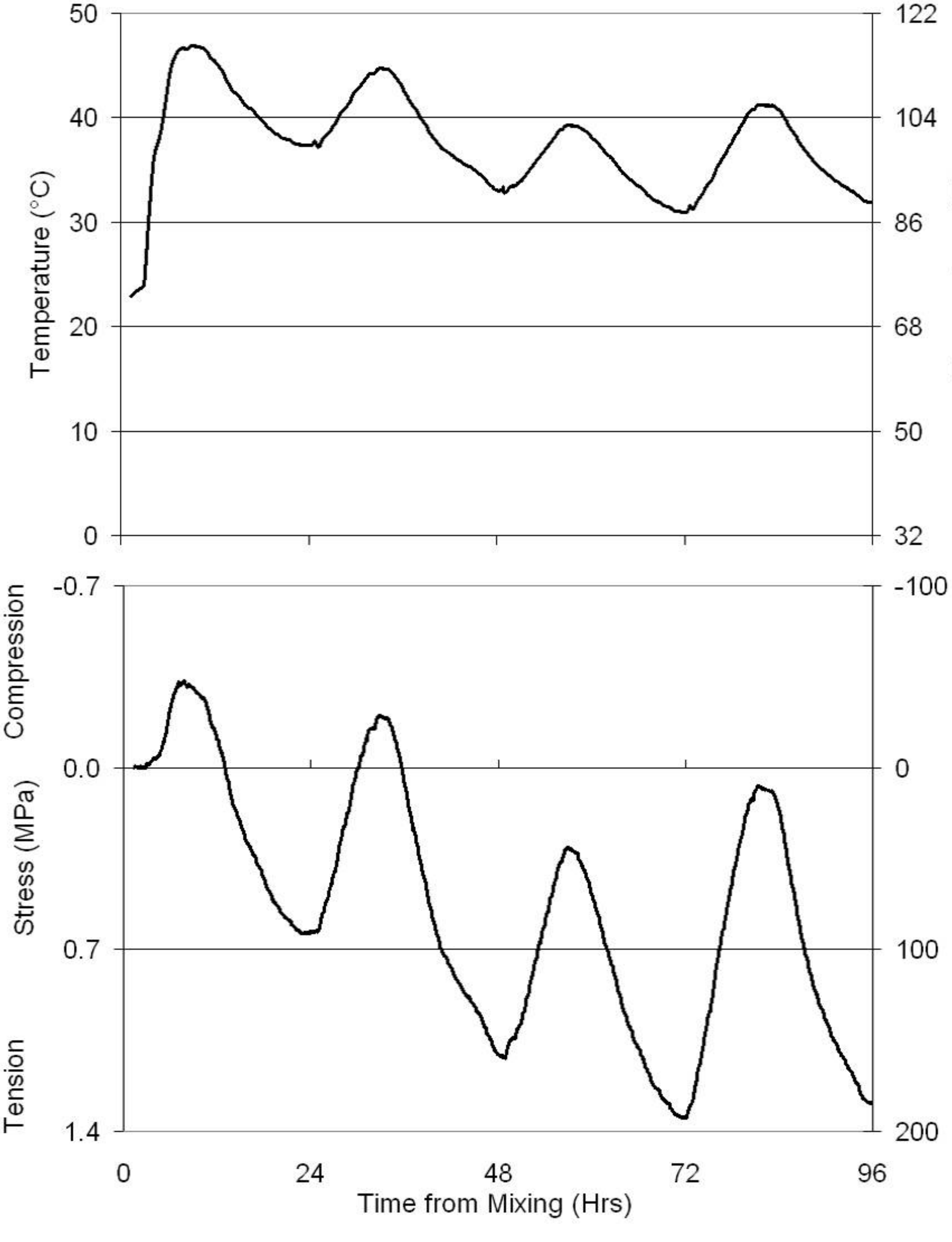

Figure 7-4 - Temperature Development Enforced on a Rigid Cracking Frame Test Simulating a Bridge Deck Temperature Profile

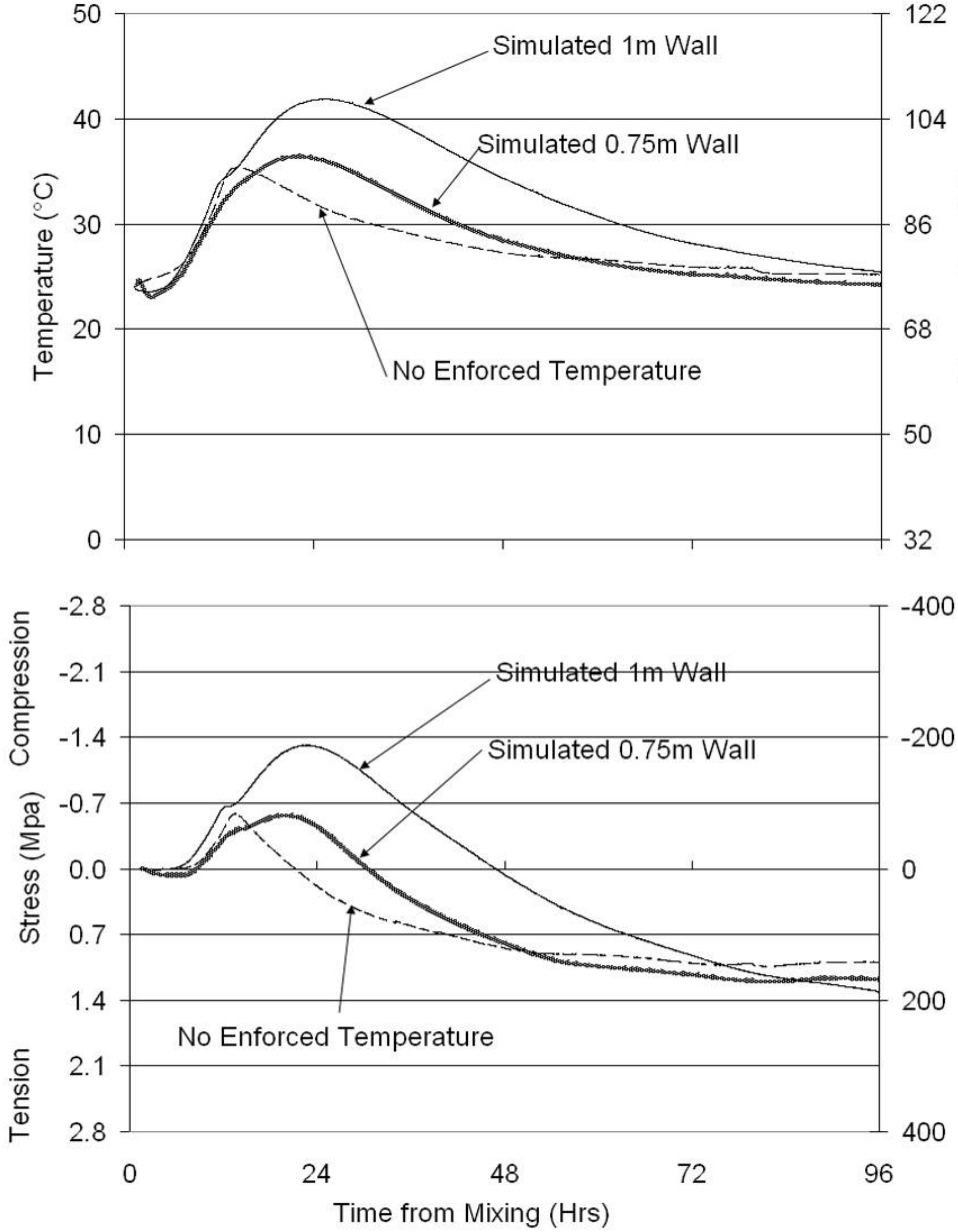

Figure 7-5 - Temperature Development for the Same Concrete Mixture Proportions under three temperature scenarios: no enforced temperature, simulated 0.75 m thick wall, and simulated 1 m thick wall

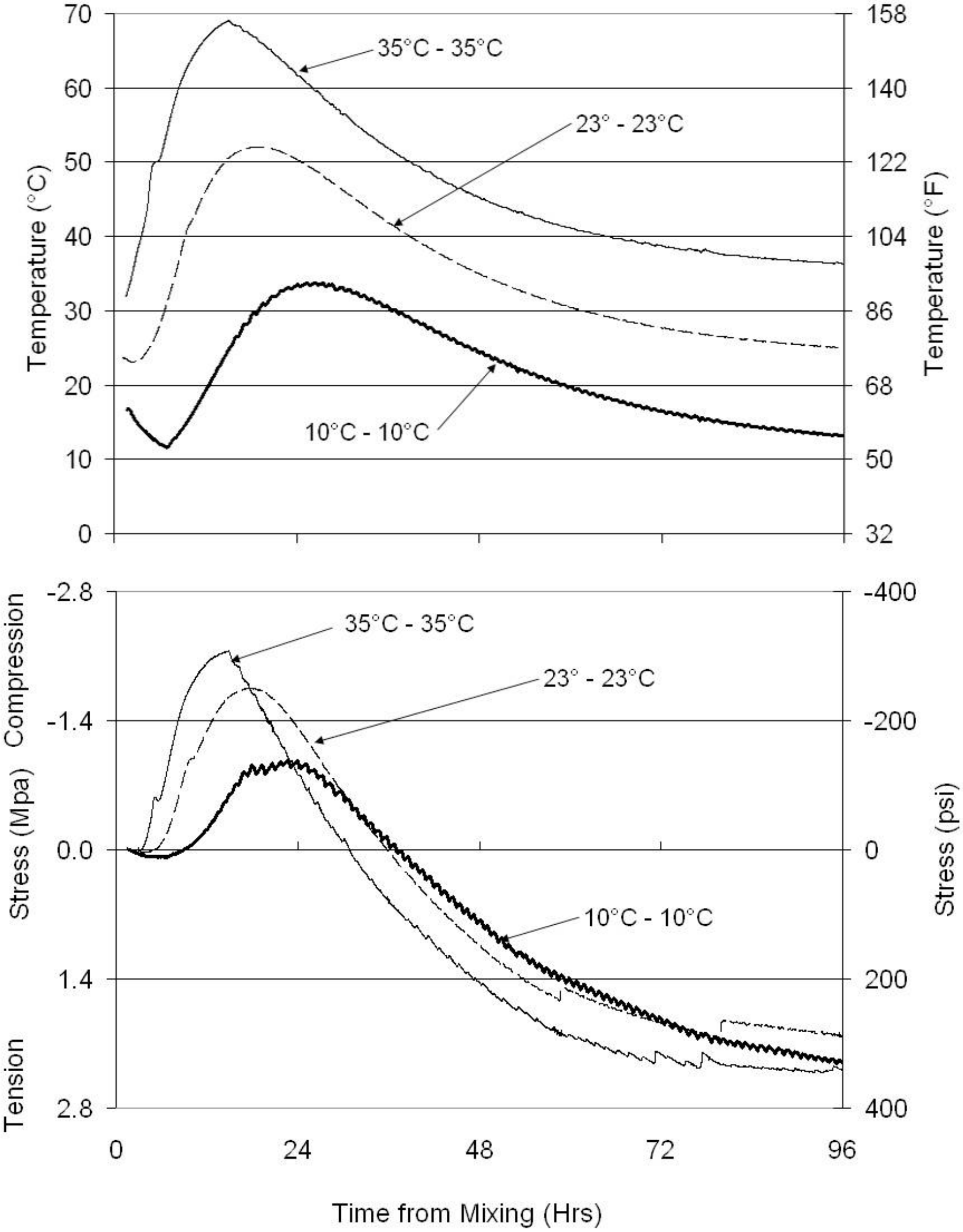

Figure 7-6 – Measured Temperature Profile for the Same Concrete Mixture Tested Simulating Different Concrete Placement Temperatures and Curing Conditions. The First Number Listed is the Placement Temperature; the Second Number is the Constant Surface Temperature Used in 1m Thick Wall Temperature Simulation

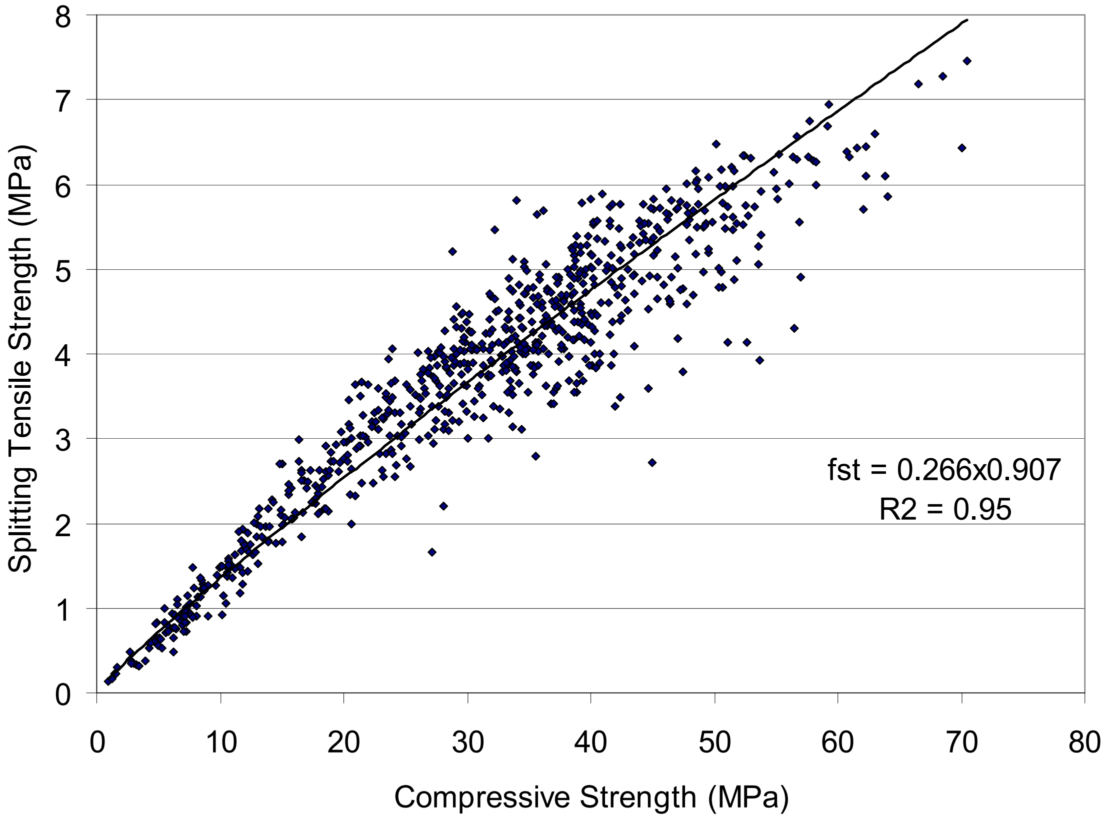

Figure 7-7 – Relationship between measured compressive strength and splitting tensile strength

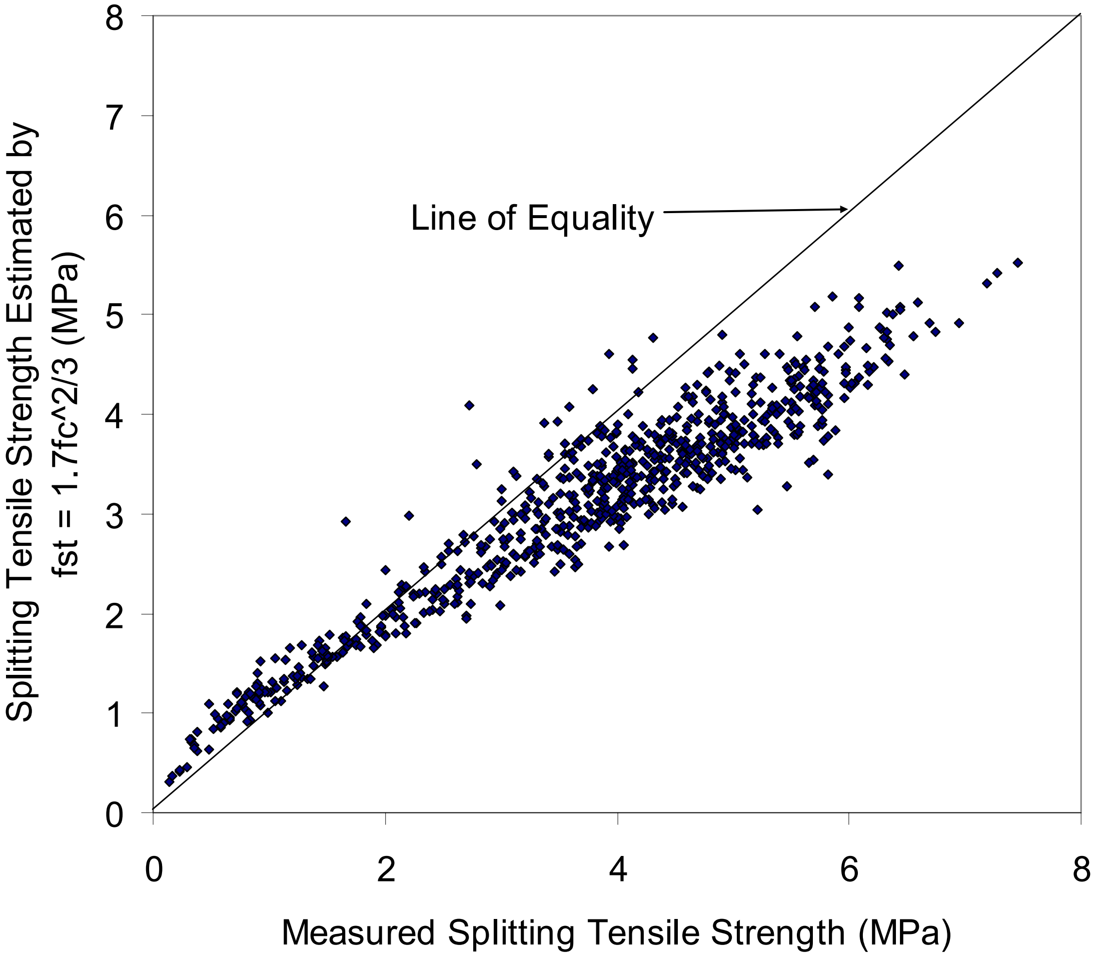

Figure 7-8 - Comparison of measured splitting tensile strength values and calculated values using a = 1.7 and b = 2/3

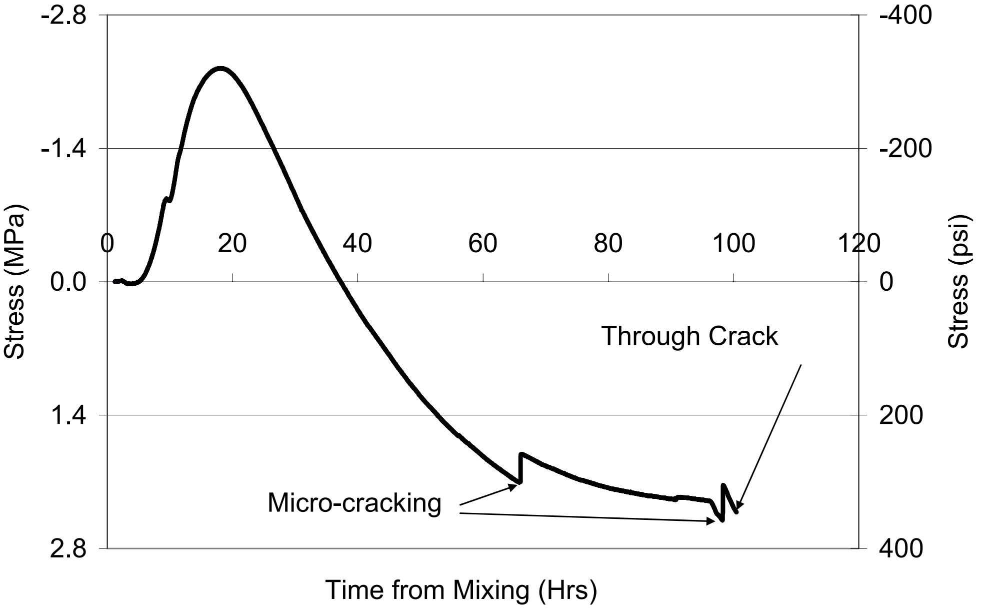

Figure 7-9 - Types of cracking types observed in rigid cracking frame specimens

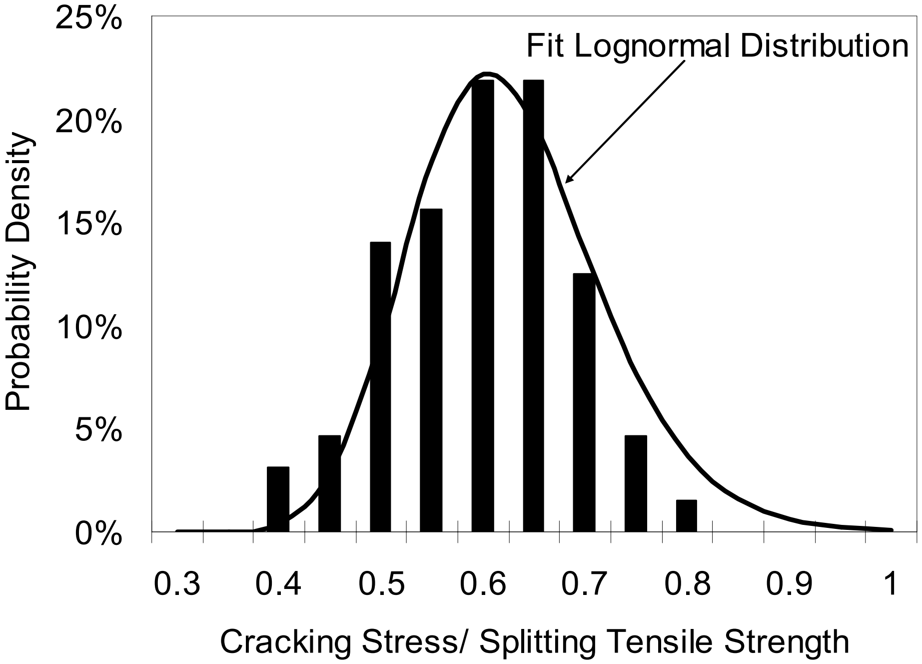

Figure 7-10 - Measured cracking stress to splitting tensile strength ratio distribution

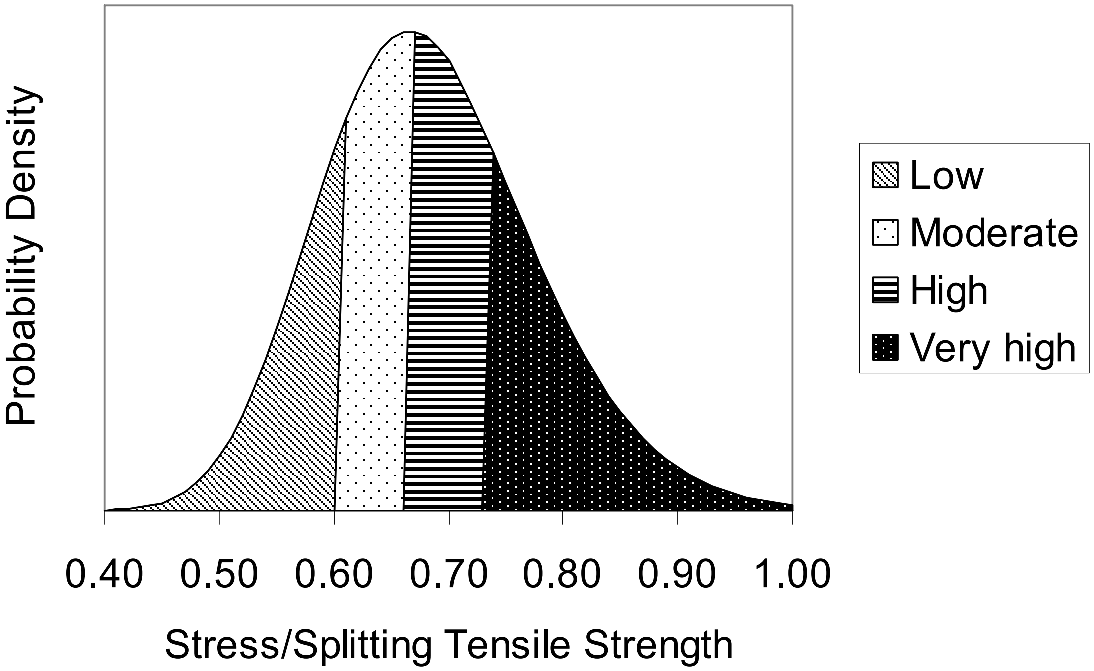

Figure 7-11 - Cracking probability categories for versus stress to splitting tensile strength ratios using the Raphael (1984) model

CHAPTER 8 SIMPLIFIED CONCRETE RESISTIVITY AND RAPID CHLORIDE PERMEABILITY TEST METHOD

A simplified method of measuring concrete resistivity, as an index of permeability, has been developed that is similar to ASTM C 1202 or the Rapid Chloride Permeability Test, but is significantly faster and easier to perform. In this test, 100-mm by 200-mm (4 inch by 8 inch) cylinders that have been cured in 100% relative humidity are tested using the same solutions, test cells and rubber gaskets as specified in ASTM C 1202. To eliminate the problem of the temperature rise of the sample during the test, only one current reading is taken (after five minutes) that may be used to calculate the concrete resistivity. Testing was conducted on various different concrete mixtures after 91 days of moist curing using both the new quicker method and the standard ASTM C 1202 method. An empirical correlation between the new method and the standard method demonstrates the validity and promise of the new method.

8.1 Introduction

First developed by Whiting (1981), ASTM C 1202 or the Rapid Chloride Permeability Test (RCPT) (ASTM C 1202 2005) has become a common test to assess concrete's ability to resist chloride intrusion. The test method is commonly used because it is relatively quick (approximately twenty-four hours for sample preparation plus six additional hours for testing) and inexpensive as opposed to the alternative AASHTO T 259 salt ponding test, which takes at least 119 days to perform after concrete curing (AASHTO 2002).

ASTM C 1202 measures the electrical conductivity of a 50-mm (2 inch) thick concrete disk over a 6-hour time period. The current readings taken are then integrated over the six hour period to obtain the final charge passed (ASTM C 1202 2005). Because it is the electrical conductivity (or resistance) that is measured, the test is really a long duration resistivity test. It is assumed that the resistivity is directly related to the tortuosity of the pore network or concrete permeability, although the relation is not perfect (Mindess et al. 2003).

One problem with ASTM C 1202 is that the current tends to increase during the test, especially with low quality/high permeability concrete, because the specimens heat up, thus increasing the conductivity. Furthermore, chloride ions may migrate in while hydroxyl ions migrate out, changing the concrete conductivity (Beaudoin and Liu 2000, Arup et al. 1993). Another problem with ASTM C 1202 is the amount of sample preparation needed. Sample cutting, vacuum saturation, and testing take at least 24 hours to complete. Additionally, sample cutting can introduce a significant amount of variation in the test method. Two samples both cut according to ASTM C 1202 could have a difference in length between the two of 6 mm (1/4 inch) or over 12%. The samples may also not be reused because of concerns over leaching in a moist environment and the exposure to chlorides during the test, which may change the pore solution conductivity.

It is well known that ASTM C 1202 may give a false estimate of the concrete chloride diffusion when some supplementary cementing materials are used, especially silica fume (Arup et al. 1993, Feldman et al. 1999), when some chemical admixtures such as calcium nitrite are used, or when steel fibers or reinforcing steel bars are present (ASTM C 1202 2005). Some supplementary cementing materials (SCMs) and chemical admixtures change the pore solution hydroxyl or other ionic species concentration. This can change the electrical conductivity of the concrete, without necessarily changing the tortuosity of the pore structure (Beaudoin 2000). Because of their high electrical conductivity, the presence of steel fibers or reinforcing bars cause very high resistance values in ASTM C 1202, even though they do not fundamentally change the concrete pore structure (ASTM C 1202 2005).

In spite of its flaws, ASTM C 1202 or any other electrical resistivity based test may still useful for quality control to detect radical changes in water-to-cementing materials ratio (w/cm) or material properties. It is also useful to know the concrete electrical resistivity for modeling the galvanic cell that is formed after corrosion has initiated (ASTM C 1202 2005, Stanish et al. 2000).

Previous research has suggested that the current rapid chloride permeability test may be greatly simplified. Scali, Chin and Berke (1987) first suggested that the permeability test could be simplified into just a resistivity test; conversion factors are used to achieve the same results as ASTM C 1202. In other studies, good correlations were shown between the initial current readings, or conductance, and the total charge passed for a limited number of concrete samples. These tests were conducted on a limited variety of blended cements and chemical admixtures (Arup et al. 1993, Feldman et al. 1999, Feldman et al. 1993, Zhao et al. 1998).

Several other methods have been developed for measuring the chloride permeability of concrete. Electrical methods include the electrical migration technique, the rapid migration test, concrete resistivity (Stanish et al. 2000), and A.C. impedance techniques (Beaudoin and Liu 2000, Feldman et al. 1993). The electrical migration technique is similar to ASTM C 1202, but the chloride ion concentration is measured in the anode solution instead of simply measuring the total charge passed through the concrete during a 6 hour period of time. In the rapid migration tests an electrical charge is applied to the sample, after which the sample is split and the depth of chloride penetration is determined using chemical indicators. Concrete resistivity tests are simple measures of the concrete's electrical resistance per unit cross section and length (Stanish et al. 2000). A.C. Impedance measurements are similar to resistivity measurements, except that an alternating current is used instead of a direct current. Pressure and temperature have also been used as driving forces to speed up chloride diffusion in concrete for direct measurement. ASTM C 1556, the concrete bulk diffusion test, uses high temperatures to speed up the diffusion of chloride ions into concrete (ASTM C 1556 2004).

A new, simplified method of performing ASTM C 1202 has been developed and is reported herein. The method greatly simplifies the sample preparation needed on lab-cured samples to measure the rapid chloride permeability of concrete. The new test uses the same setup as ASTM C 1202, except that specimen is cured at 100% relative humidity instead of vacuum saturation, the specimen is 200 mm (8 inches) in length and uncut, and the specimen is only tested for 5 minutes. The total test may now take less than a half hour from sample setup to finish. The new test method also can be run with only minor modifications to existing ASTM C 1202 testing equipment, and the same test cylinder can be tested at a given age, returned to moist-curing conditions, and re-tested at subsequent ages. Additionally, because the test is run for such a short duration, the sample temperature increase should be negligible. Because this new test method is so similar to ASTM C 1202 and can use the same equipment, practitioners can easily implement this new test method.

8.2 Research Significance

Corrosion of reinforcing steel is the largest durability problem worldwide in concrete structures. Engineers have been specifying high performance concrete (high strength/low permeability) in recent years in an effort to reduce concrete chloride diffusion and increase the service life of structures. In this paper, a simplified procedure for measuring electrical resistivity of concrete containing different types of cements and supplementary cementing materials is described. The test method may serve as a quick and inexpensive quality control test for concrete construction.

8.3 Experimental Methods

ASTM C 1202 (2005), the Rapid Chloride Permeability Test, was used to evaluate 117 concrete mixtures. After 91 days of moist curing, two 50-mm (2 inch) specimens were cut from the same 100-mm by 200-mm (4 inch by 8 inch) cylinder for each mixture. Both specimens for each batch were tested according to ASTM C 1202. Specimens were tested using rubber gaskets instead of silicone rubber caulking to prevent leakage of the solution, as allowed by ASTM C 1202. The total charge passed during the six hour test, as well as the initial voltage drop across the sample were recorded.

Fifty-five of the concrete mixtures tested according to ASTM C 1202 were also tested at 91 days using a simplified version of the RCPT method, hereafter called the "simplified RCPT." The test was conducted using the same electronic equipment, ionic solutions, and voltage cells as used in the ASTM C 1202. The differences were as follows. The simplified RCPT test was conducted on a full 100-mm by 200-mm (4 inch by 8 inch) cylinder, using a 188-mm (7.4 inch) long acrylic sleeve as shown in Figure

8-1, instead of the shorter 50-mm (2 inch) specimen and 36-mm (1.4 inch) sleeve prescribed by the ASTM C 1202 test. In the simplified RCPT test, the sample was taken directly out of the curing room (100% relative humidity) and tested; no vacuum desiccation was performed. In the simplified RCPT test, only the initial voltage drop across the sample was recorded; the total charge passed through the sample was not recorded.

To illustrate the effect of temperature on the resistivity of concrete, cylinders from three different concrete mixtures were placed overnight in water at 60 °C (140°F) and 38 °C (100 °F), and in the 23 °C (73 °F), 100% relative humidity chamber. The three concrete mixtures were over a year old to reduce the effects of the temporary high temperature on hydration and leaching. The samples were tested for resistivity using the simplified RCPT method.

8.4 Concrete Materials

A wide variety of materials were tested using ASTM C 1202 (2005). Several types and brands of ASTM C 494 (1999)Type A water reducer , mid-range water reducer, and ASTM C 494 (1999) high-range water reducer were used. One type of calcium nitrate-based accelerator was used in four mixtures, and a calcium nitrite corrosion inhibiting admixture was used in one mixture. Water-to-cementitious material ratios ranged from 0.32-0.53 for the ASTM C 1202 tests and 0.32-0.50 for the simplified tests, with the majority being between 0.40-0.44. Three types of ASTM C 618 (2003) Class C fly ash were used, while five types of ASTM C 618 (2003) Class F fly ash were used. One type each of silica fume, ultra fine fly ash, and Grade 120 ground granulated blast furnace slag (GGBFS) (ASTM C 989 2005) were used in the study. Table 8-1 summarizes the number of material sources and the number of mixtures that contained each type of material for the tests performed according to ASTM C 1202 and the simplified RCPT test. As seen in Table 8-1, not all mixtures were tested using the simplified RCPT test. Table 8-2 summarizes the range of material quantities used in the study. When comparisons between tests were made, concrete cylinders from the same concrete batches were tested using each test.

8.5 Results

The initial readings taken during the testing for the ASTM C 1202 test and the simplified RCPT test were converted to resistivity values using Equation 8-1:

$$\rho_c = \left(\frac{(E_s - 2) * R}{E_m} \right) * \left(\frac{A}{L} \right) \qquad \textbf{Equation 8-1}$$

where ρ_c is the concrete resistivity (Ω-m), E_s is the supplied DC voltage (60 V), R is the resistance provided by the shunt resistor (0.01 Ω), E_m is the voltage drop measured, A is the cross sectional area of the cylinder (m^2), and L is the length of the specimen (m). Following the method suggested by Arup et al. (1993), two volts are subtracted from the supplied voltage to account for "the voltage loss due to polarization of the electrodes (or the voltage loss in electrolyzing water and forming hydrogen and oxygen)." Figure 8-2 shows a comparison of the average calculated resistivity values for the two samples tested for each mixture using ASTM C 1202 versus the simplified RCPT method. Figure 8-3 shows the resistivity values measured for the first ASTM C 1202 sample versus the values measured for the second ASTM C 1202 sample from the same concrete batch to illustrate the inherent scatter in the ASTM C 1202 test method itself.

The r^2 value of 0.97 shown in Figure 8-3 is an indicator how well the two tests relate. A perfect match between the two tests would give an r^2 value of 1. As shown in Figure 8-2 and Figure 8-3, the scatter from the resistivity tests obtained from the simplified test method is higher at the higher resistivity values. This increased scatter may be because of the 200-mm (8 inch) sample length in the simplified RCPT test, which results in more resistance and hence a lower voltage drop. The voltmeter used in this study is not sensitive enough to distinguish between very dense concrete with very low voltage drops. This leads to an increase in scatter in the data with concrete with a high electrical resistivity. A higher precision voltmeter or measurement of the sample current instead of voltage drop would reduce this scatter in the higher resistivity values.

Another way to compare the two tests is using a method suggested by Arup et al. (1993), who calculated equivalent coulomb values from the initial readings assuming a constant voltage drop during a six hour period. These calculated values for the simplified RCPT test are compared to the measured values of total charge passed from the ASTM C 1202 test. The coulomb values from the simplified test are multiplied by four to compensate for the length of the specimen. The data from the simplified test were extrapolated to an equivalent six hour charge passed in order to facilitate a direct comparison of the two test methods. Figure 8-4 shows a comparison of the coulomb readings for the simplified RCPT test assuming a constant voltage drop during six hours versus the average of the two coulomb values for a full six hour ASTM C 1202 test. Figure 4 clearly shows that the differences between the two test methods examined in this study are very predictable.

The data presented in Figure 8-4 from the ASTM C 1202 and the simplified RCPT tests were combined with similar data from previous studies where dc resistivity values were collected at the same time as ASTM C 1202 values. This joint dataset was used to develop an empirical model to relate the increase in charge passed during a six hour time period to that extrapolated from initial values. This relationship is also shown in Figure 8-5. The values for concrete at early ages from Feldman, Prudencio, and Chan (1999) were not included in the data set because heating during the 6 hour test can increase the hydration reaction, changing the results expected. A quadratic trend worked well to describe the increase in charge passed during the six hour time as shown in Equation 8-2:

$$Q_{6h} = -0.0000205 \cdot Q_i^2 + 0.8758 \cdot Q_i \qquad \textbf{Equation 8-2}$$

where Q_{6h} is the charge passed during a full ASTM C 1202 test (Coulombs), and Q_i is the charge for a six-hour period extrapolated from one initial current reading normalized to a 50-mm (2-inch) length (Coulombs). Equation 8-2 is non-linear because of heating that occurs in the samples, especially in more porous concrete. Equation 8-2 may be used to develop a concrete rating system similar to that used in ASTM C 1202 based on the simplified RCPT test extrapolated to 6 hours of charge passed. The new concrete classification guidelines recommended for use with the new simplified RCPT test are shown in Table 8-3.

8.5.1 EFFECTS OF TEMPERATURE

The three concrete mixtures tested at different temperature using the simplified method decrease in resistivity with increasing temperature, as expected. As shown in Figure 8-6, the temperature dependence of concrete resistivity follows Equation 8-3 (Beaudoin and Liu 2000):

$$\rho_c(T) = \frac{1}{A\exp(\frac{-\Delta E}{k_b T})}$$

Equation 8-3

where *A* and *ΔE* are empirical constants determined for each mixture, k_b is Boltzmann's constant, and *T* is the absolute temperature (K). The concrete resistivity increased by 92%, 71%, and 65% for the three concrete mixtures when the temperature was increased from 23°C (73°F) to 60°C (140°F). As the data in Figure 8-6 shows, the simplified RCPT test can be used to measure the temperature dependence of the concrete mixtures. These data can be useful for modeling the galvanic current present once reinforcing steel corrosion has initiated which is dependent on the concrete resistivity. The modeling of the galvanic current may prove useful in service life models to determing both the rate of corrosion and the possible extent of damage from corrosion.

8.5.2 ADVANTAGES AND DISADVANTAGES OF SIMPLIFIED RCPT

The simplified RCPT greatly simplifies the test procedure found in ASTM C 1202 for determining the electrical resisitivity of concrete. The simplified RCPT test gives results that are comparable to those obtained from ASTM C 1202 as shown in Figure 8-2, Figure 8-4, and Figure 8-5. The procedure eliminates saw cutting, and the inherent problems and variability associated with it. The simplified RCPT can be run very quickly; consequently the specimen temperature does not increase during the test and change the charge passed. The test method also may be used as a simple indicator of the concrete permeability based on revised guidelines for interpreting the data shown in Table 8-3. The simplified test method for concrete resistivity may serve as an important method for characterizing the temperature dependence of concrete resistivity on temperature for modeling the corrosion rate in service life models. Additionally, the specimens may be reused at a later age to track the change of the concrete resistivity with time.

The simplified RCPT test does not solve all of the problems associated with the RCPT test. Because the new test is still an electrical test, changes in pore solution chemistry will still register a change in the measured values which may not be indicative of a change in porosity and pore structure tortuosity. The test method also may produce a large amount of scatter when the voltage is measured instead of current at higher concrete resistivity values. However, using a more sensitive voltmeter may eliminate this problem.

8.6 Conclusion

A simplified method for quickly measuring the concrete resistivity and corresponding Rapid Chloride Permeability value has been developed. The test is based on the procedures outlined in ASTM C 1202, simplified to avoid cutting samples, desiccation, test duration, and sample heating. Specimens containing various cement types, supplementary cementing materials, water-to-cementitous materials ratios, and chemical admixtures were tested using the new simplified test and ASTM C 1202 for comparison. The correlation between the simplified RCPT and the ASTM C 1202 worked well for all materials tested. The difference in values obtained from the two different tests was due mainly to concrete heating that occurred during the ASTM C 1202 test and was found to be very predictable. A correlation between the two tests and implementation guidelines were also developed. The simplified procedure is advantageous in that existing RCPT equipment may be used, the only modification being a longer acrylic sleeve around the concrete and longer bolts to provide compression to the rubber gaskets. The test method may also be used to determine the temperature dependence of concrete resistivity for a particular concrete mixture. The test method, like other electrical methods, does not directly measure the chloride diffusion of a concrete sample. The method has only been performed on laboratory cured samples, and its suitability for cored field samples has not yet been determined.

8.7 Acknowledgements

The authors wish to express their gratitude to the Texas Department of Transportation through Project 0-4563 for funding this research. The advice and support of Ralph Browne of the Texas Department of Transportation is greatly appreciated.

8.8 Notations:

GGBFS = Ground Granulated Blast Furnace Slag

F = ASTM C 618 Class F Fly Ash

C = ASTM C 618 Class C Fly Ash

MRWR= Mid Range Water Reducer

LRWR = ASTM C 494 Type A Water-Reducing Admixture

HRWR = ASTM C 494 Type F High Range Water-Reducing Admixture

Table 8-1- Number of sources and mixtures for different mixtures used in testing

	ASTM C 1202		Simplified Method	
Material	# Sources	# Mixes	# Sources	# Mixes
Type I Cement	3	47	2	14
Type I/II Cement	6	58	5	28
Type V Cement	1	12	1	12
Class F Fly Ash	5	34	5	13
Class C Fly Ash	3	28	3	12
GGBFS	1	12	1	6
Ultra Fine Fly Ash (UFFA)	1	7	1	4
Silica Fume	1	7	1	2

Table 8-2 - Material amount ranges used

	ASTM C 1202		Simplified Method	
	minimum	maximum	minimum	maximum
Calcium Nitrite based corrosion inhibitor L/100 kg of total cementing materials (gal/100 lb of total cementing materials)	0	8.3 (1)	0	8.3 (1)
Calcium Nitrate based accelerator L/100 kg of total cementing materials (gal/100 lb of total cementing materials)	0	2.2 (0.26)	0	2.2 (0.26)
w/cm	0.32	0.53	0.32	0.5
Class F Fly Ash (% Replacement)	0	55	0	31
Class C Fly Ash (% Replacement)	0	40	0	40
GGBFS (% Replacement)	0	70	0	70
Ultra Fine Fly Ash (% Replacement)	0	9	0	8
Silica Fume (% Replacement)	0	10	0	10

Table 8-3 - Recommended guidelines for equivalent concrete classification based on initial current reading

Concrete Permeability	Charge Passed During Full 6 Hour Test (Coulombs)	Extrapolated Charge from Initial Reading Normalized to a 2” Length for simplified RCPT (Coulombs)
Very Low	<1000	<900
Low	1000-2000	900-1600
Moderate	2000-4000	1600-3000
High	>4000	>3000

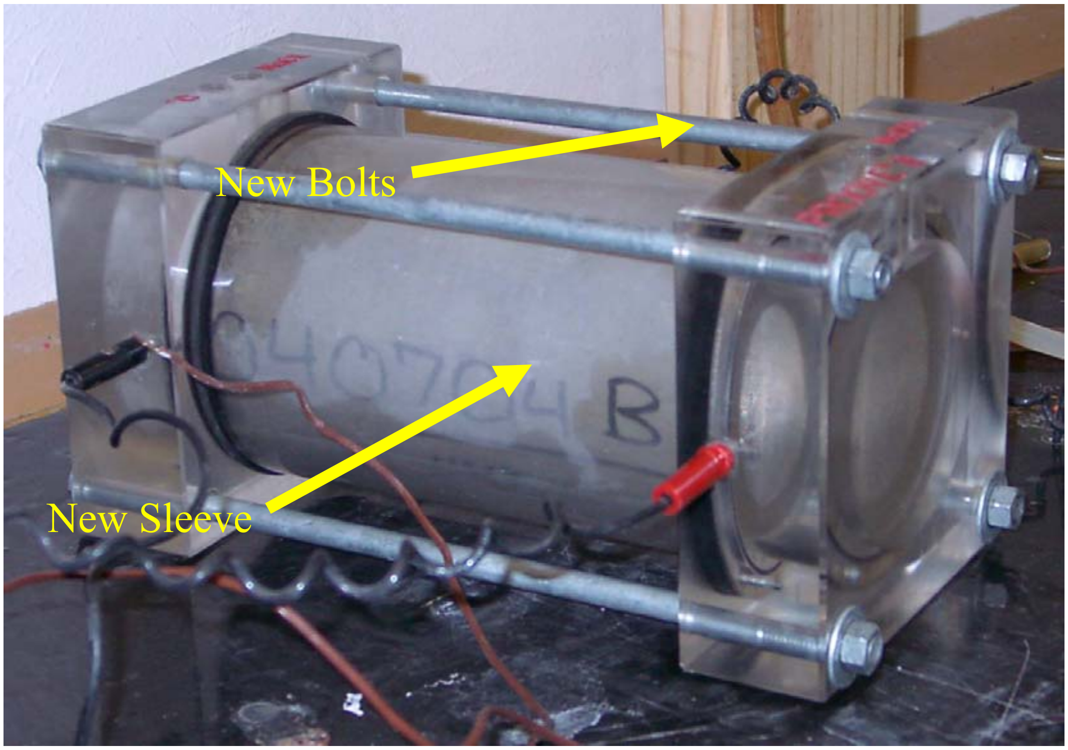

Figure 8-1 - Simplified RCPT Test Setup

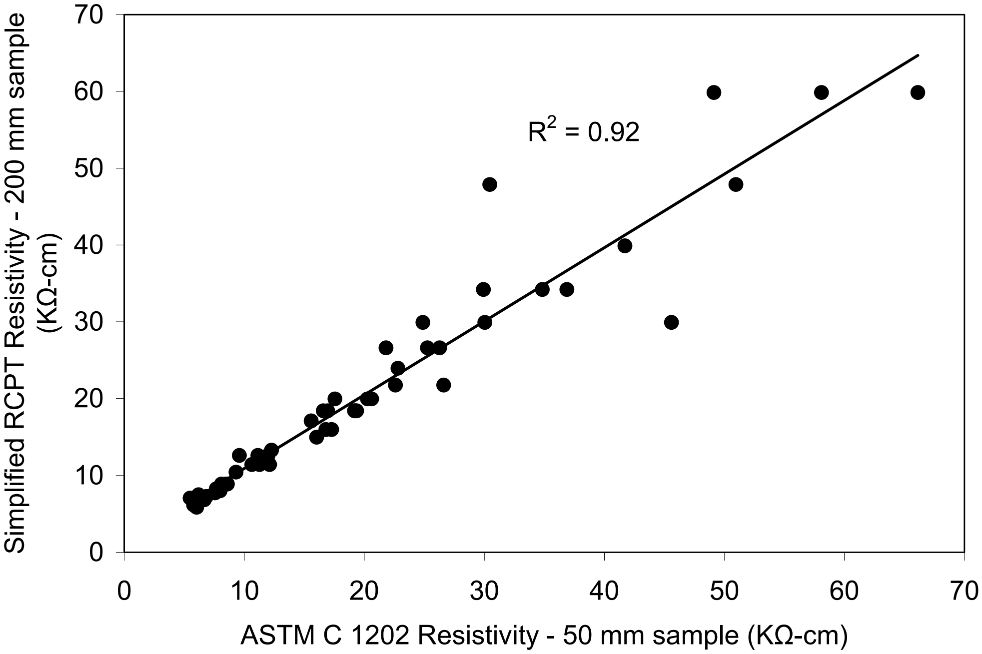

Figure 8-2 - Resistivity values for ASTM C 1202 method versus the simplified RCPT method

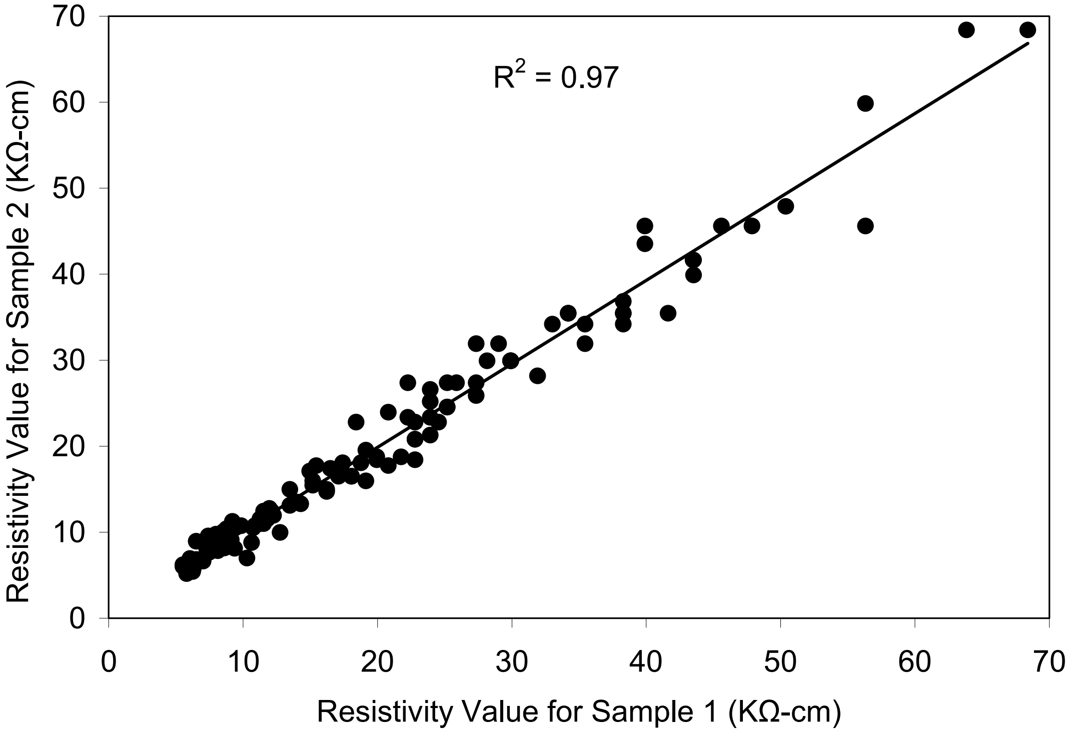

Figure 8-3 – Comparison of resistivity values from two samples tested from the same concrete batches using ASTM C 1202

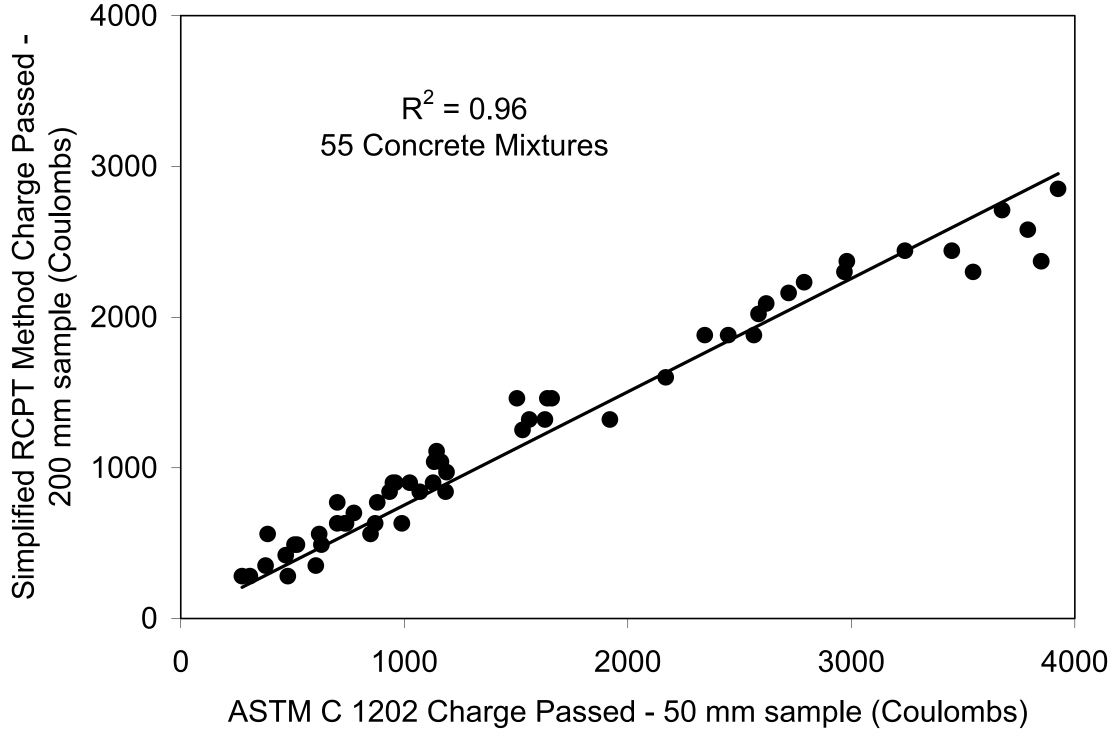

Figure 8-4 - Comparison of ASTM C1202 test to simplified RCPT method assuming constant current

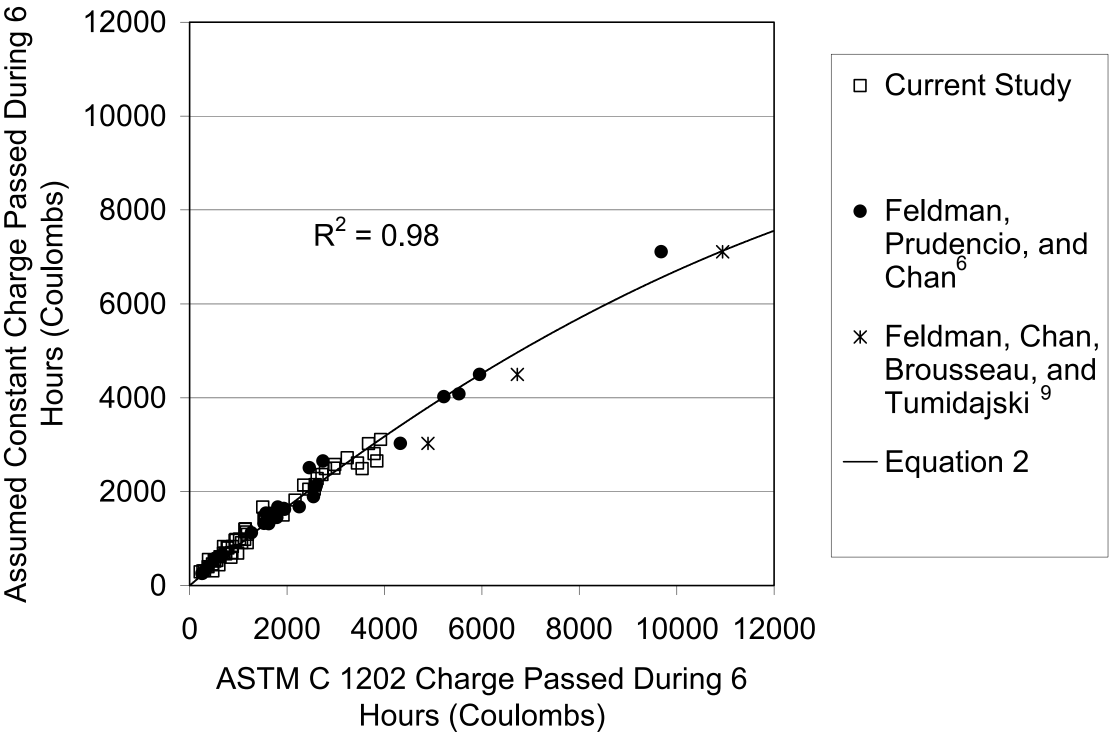

Figure 8-5 - Comparison of Colulomb Values Extrapolated from Initial Resistivity Reading in the simplified RCPT test to the total charge passed in the 6 hour ASTM C 1202 Test

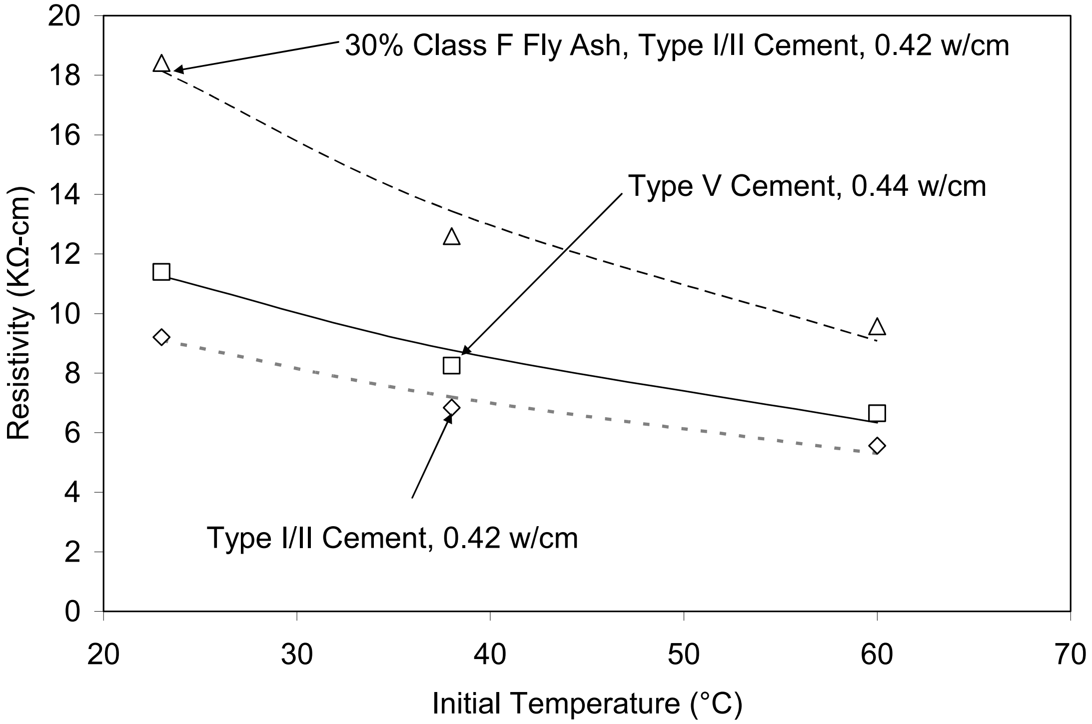

Figure 8-6 - Concrete resistivity versus concrete temperature at testing using the simplified RCPT method

CHAPTER 9 CONCRETEWORKS USER MANUAL

9.1 Introduction

ConcreteWorks is designed to be a user-friendly software package that can help concrete professionals optimize concrete mixture proportioning, perform a concrete thermal analysis, and increase the chloride diffusion service life. The software package contains design modules for several structural concrete applications including mass concrete shapes, bridge deck types, precast concrete beams, and concrete pavements. Table 9-1 shows the ConcreteWorks analysis modules available for each member type.

In order to obtain accurate temperature, thermal stress, and corrosion risk calculations, the user should be familiar with the fundamental principles and mechanics of concrete proportioning, temperature concerns in concrete members, concrete maturity, and diffusion theory for concrete employed in the software inputs and calculations explained in this user manual. It is assumed that users will have a good knowledge of fundamental concrete materials principles and practices. The purpose of this manual is not to exhaustively compile all concrete thermal, durability and corrosion research in the literature. Instead, this manual is designed assist the user with the specific knowledge of concrete behavior needed to successfully use ConcreteWorks, built upon an already existing knowledge of fundamental concrete behavior. It is recommended that users carefully read this user manual as well as cited references as needed before using the software.

This manual is divided in several sections. The first section is the information on the ConcreteWorks mixture proportioning guide. The second section describes how the heat transfer calculations in the program are performed. Section three explains how the program's thermal stress analysis and consequent cracking probability assessment is done. The fourth section discusses the chloride service life model built into ConcreteWorks. Finally, a ConcreteWorks operator's manual is provided in Appendix C.

9.2 Concrete Mixture Proportioning Guide

9.2.1 BASIC MIXTURE PROPORTIONING

The backbone for the mixture proportioning guide found in ConcreteWorks is the procedure outlined in the ACI 211 document "Standard Practice for Selecting Proportions for Normal, Heavyweight, and Mass Concrete" (ACI 211, 1991). For a detailed explanation of this mixture proportioning method, users are encouraged to read the ACI 211.1-91 document.

The basic steps of the concrete mixture proportioning procedure can be summarized as the following:

1. Determine the amount of water needed to achieve a given slump for the selected maximum aggregate size. Make adjustments to the required water amount based on material conditions, chemical admixtures, air entrainment, etc. (covered in section 9.2.2).

2. Determine the water to cementitious materials ratio (w/cm) needed for a given air content to achieve the selected target strength. The use of supplementary materials is assumed to not affect the w/cm needed to achieve the target strength (which may or may not be true depending on the reactivity of the material and the replacement rate). Supplementary

cementing materials replacement percentages are only used in calculating the volume of cementitious materials.

3. Make adjustments to the w/cm to account for maximum w/cm allowed for given exposure conditions (chloride and sulfate exposure levels).

4. Calculate the coarse aggregate fraction based on the maximum size aggregate, the sand fineness modulus, and the coarse aggregate dry-rodded unit weight.

5. Calculate the amount of sand needed to fill the remaining concrete volume (that volume not already accounted for by the cementitious materials, water, coarse aggregate, or air). The sand weight is then calculated for this volume using the sand specific gravity.

The required water amount is calculated using Equation 9-1 and the coefficients found in Table 9-1 are based on ACI 211.1-91 Table 6.3.3. The required water amount is then reduced by the percentages specified using the water adjustment factors discussed in section 2.2 and calculated using Equation 9-1

$$W = (a_w \cdot \ln(sl) + b_w) \cdot (1 - WA) \quad \textbf{Equation 9-1}$$

where *W* is the required water (lb/yd³), aw and bw are constants determined from Table 9-2 (lb/yd³), sl is the desired concrete slump (in), and *WA* is the water reduction factor. The amount of water needed to obtain the required slump increases as the maximum aggregate size decreases and consequently the total aggregate surface area increases.

The connection between compressive strength and w/cm was first published in 1918 by Duff Abrams (Abrams 1918). W/cm is one of the major factors in determining the concrete porosity and consequently compressive strength (Mindess, Young, and Darwin, 2003). Air entrainment will increase the amount of voids in concrete, and consequently reduce the strength. The required w/cm is calculated using Equation 9-2 to Equation 9-4:

$$w/cm = (a_a \cdot \ln(f_{ct}^{'}) + b_a)$$ **Equation 9-2**

$$a_a = 0.00065 * air - 0.3762$$ **Equation 9-3**

$$b_a = -0.0263 * air - 3.7275$$ **Equation 9-4**

where *air* is the target percent air in the concrete, and f_{ct}' is the concrete target strength. Equations 3 and 4 were calculated using a regression analysis from the data found in ACI 211.1-91 table 6.3.4 assuming the quoted values of 2% entrapped air for the non-air entrained concrete and 6% for the air entrained concrete.

The coarse aggregate weight is calculated using Equation 9-5:

$$CAW = (a_{ca} + \frac{(2.4 - FM)}{10}) \cdot DRUW$$ **Equation 9-5**

where *CAW* is the coarse aggregate weight (lb/yd^3), a_{ca} is a fit parameter found in

Table 9-2, *FM* is the fineness modulus, and *DRUW* is the coarse aggregate dry rodded unit weight (lb/yd^3). The coefficient a_{ca} was derived by fitting the data found in ACI 211.1-91 Table 6.3.6.

9.2.2 WATER ADJUSTMENTS

The required water adjustments procedures and magnitudes are based on the National Highway Institute (NHI) Course 15123 Participant Workbook (Hover, 2003). The amount of water adjustment needed for each material used is highly material dependent. Concrete mixture proportioning knowledge and experience with the local materials used is critical to accurately estimate the influence of each material on the concrete mixture. A trial batch is normally required to confirm the validity of the concrete mixture designed, and to make any necessary adjustments to the concrete workability.

The range of water adjustment permitted for different materials in ConcreteWorks is that suggested by the NHI course 15123 Participant Workbook (2003) and shown in Table 9-3. Water reducing chemical admixtures will reduce the required water content in the concrete mixture by different amounts depending on the chemical admixture chemistry and dose used. Values selected for water reducers should be based on experience or recommendations from the chemical admixture supplier. Air entrainment will also increase the concrete workability by both chemical and physical means (Mindess, Darwin, and Young, 2003). The effect of supplementary cementing materials will depend on the particle size and shape. Silica fume will greatly increase the water demand and should not be used without a high range water reducer that will aid in the dispersion. Fly ash can however increase the workability, although the amount is very material dependent. Aggregates will also have a large effect on the concrete workability. Poorly shaped and graded aggregates will have a very high water demand. Round, smooth and well-graded aggregates will however decrease the concrete water demand. Experience with the use of local aggregates is especially important when gauging the amount of water adjustment needed in the mixture proportioning.

9.2.3 AGGREGATE GRADATIONS

There are three commonly used simple methods of optimizing aggregate gradations to decrease the amount of water needed in the concrete. Two of the methods, the 0.45 power curve method and the percent retained method, are based on the combined aggregate gradation. The third method, the Shilstone Coarseness Factor –Workability Factor method (Shilstone, 2002) uses an empirical relationship between the percent retained on the No. 8 sieve, the percent retained on the 3/8” sieve, and the cementitious content to determine if a mixture is acceptable.

The 0.45 power curve method is commonly used in asphalt aggregate gradations. The aggregate percent passing is plotted versus the sieve size to the 0.45 power on a log scale. The aggregate maximum density line is plotted on the same graph; with the percent passing (PP) calculated using Equation 9-6:

$$PP = \left(\frac{d}{D}\right)^{0.45}$$

Equation 9-6

where d is the sieve size (in), and D is the maximum aggregate size (in).

The Shilstone Coarseness Factor-Workability Factor method uses an empirically derived, graphical relationship between aggregate gradation and cementitious content to classify a mixture as acceptable or not. The coarseness factor is plotted on the x-axis while the workability factor is plotted on the y-axis. The coarseness factor is the cumulative percent retained on the 3/8” sieve divided by the cumulative percent retained on the No. 8 sieve times 100 (%). The workability factor is the “percent of the combined aggregate that passes the No. 8 sieve (Shilstone, 2002).” The workability factor is then adjusted for the cementitious content by Equation 9-7:

$$WF = CA8 \cdot \frac{cm - 564}{94} * 2.5 \qquad \textbf{Equation 9-7}$$

where *WF* is the workability factor, *CA8* is the combined aggregate that passes the No. 8 sieve (%), and *cm* is the concrete cementitious material content (lb/yd^3). If the coarseness factor and workability factor for the mixture plots inside of an empirically derived box, defined below, then the mixture is deemed acceptable (Shilstone, 2002). The concrete mixture proportions acceptability box whose corners are shown in Table 9-4.

The percent retained method involves plotting the percent retained on each sieve, and eliminating large valleys and peaks in the gradation. This method is very subjective, but may help avoid having a very gap-graded mixture.

9.3 Temperature Prediction

9.3.1 HEAT TRANSFER MODELING

9.3.1.1 Fundamentals and Numerical Scheme

Heat transfer is governed by the second order differential equation known as the *heat diffusion equation*, as shown in Equation 9-8:

$$\frac{\partial}{\partial x}\left(k\frac{\partial T}{\partial x}\right)+\frac{\partial}{\partial y}\left(k\frac{\partial T}{\partial y}\right)+\frac{\partial}{\partial z}\left(k\frac{\partial T}{\partial z}\right)+q'=\rho c_p\frac{\partial T}{\partial t}$$ **Equation 9-8**

where k is the material thermal conductivity (W/m/K), $T(x,y,z)$ is the scalar temperature field (°C), q' is the heat generation term (W), ρ is the material density (kg/m^3), c_p is the material specific heat (kJ/kg/°K), and t is the time (s) (Incropera and Dewitt, 2002).

Closed form solutions for the heat diffusion equation are only available for very simple geometries and conditions. The heat transfer in real concrete members is much too complex for direct solutions. Numerical approximations can however be used to estimate the concrete temperature development. One such method is the finite difference method. An energy balance on an assumed differential control volume can be used to account for all thermal energy changes inside the control volume, as shown in Equation 9-9:

$$E_{in}-E_{out}+E_{gen}=\Delta E_{st}$$ **Equation 9-9**

where E_{in} is the thermal energy entering the control volume (W), E_{out} is the thermal energy leaving the control volume (W), E_{gen} is the thermal energy being generated in the control volume (in the case of concrete, the heat generated by hydration) (W), and ΔE_{st} is the change in thermal energy stored in the control volume (W). The energy entering and leaving the control volume by conduction is equivalent to the first three terms in the heat diffusion equation. The heat generation term is the chemical energy being released in the control volume. The change in heat energy being stored in the control volume is equal to the change in temperature in the control volume times the specific heat and density. The temperature and material properties are assumed to be constant for each control volume. Sufficiently small control volumes must then be used to adequately approximate the heat transfer for each volume.

Figure 9-1 shows three neighboring control volumes with insulated sides. An explicit time discretization has been used in formulating these equations, which is explained in the section 3.1.2. The change in energy entering and leaving the control volume 2 can be calculated using Equation 9-10 and Equation 9-11.

$$E_{in} = T_1 \cdot a_{1-2} + T_3 \cdot a_{2-3}$$ **Equation 9-10**

$$E_{out} = T_2 \cdot a_{1-2} + T_2 \cdot a_{2-3}$$ **Equation 9-11**

where T_1, T_2, and T_3 are the temperatures at the respective nodes shown in Figure 9-1 for the current time step (°C), a_{1-2} and a_{2-3} are heat transfer coefficients between control volumes 1 – 2 and 3 – 4 and are defined by Equation 9-12 and Equation 9-13 (Patankar, 1980).

$$a_{1-2} = \left[\frac{dx_1}{k_1} + \frac{dx_2}{k_2} \right]^{-1} \cdot \Delta y$$ **Equation 9-12**

$$a_{2-3} = \left[\frac{dx_2}{k_2} + \frac{dx_3}{k3} \right]^{-1} \cdot \Delta y \qquad \textbf{Equation 9-13}$$

where dx_1, dx_2, dx_3, and Δy are as shown in Figure 9-1 (m); k_1, k_2, and k_3 are the thermal conductivity for the material in the respective control volume (W/m/K). The energy generated in control volume 2 is equal to the heat generated by hydration per unit mass of cementitious materials times the mass of cementitious materials in the control volume as shown in Equation 9-14.

$$E_{gen} = Q \cdot \Delta x_2 \cdot \Delta y \qquad \textbf{Equation 9-14}$$

where Q is the heat generated per unit mass of cementitious materials (W); Δx_2 and Δy are as shown in Figure 9-1 (m). For control volume 2, Q may be calculated based on the Arrhenius equation as shown in Equation 9-15 (Schindler, 2004):

$$Q(t_e) = H_u \cdot C_c \cdot \left(\frac{\tau}{t_e} \right)^{\beta} \cdot \left(\frac{\beta}{t_e} \right) * \alpha_u \cdot \exp\left(-\left[\frac{\tau}{t_e} \right]^{\beta} \right) \cdot \exp\left(\frac{E_a}{R} \left(\frac{1}{273+T_r} - \frac{1}{273+T_2} \right) \right) \cdot \left(\frac{1}{3600} \right) \qquad \textbf{Equation 9-15}$$

where t_e is the concrete equivalent age at the reference temperature as shown in Equation 9-16 (hrs), H_u is the total amount of heat generated at 100% hydration (J/kg), C_c is the total amount of cementitious materials (kg/m^3), τ is the hydration time parameter (hrs), β is the hydration slope parameter, α_u is the ultimate degree of hydration, E_a is the activation energy (J/mol), R is the universal gas constant (J/mol/K), and T_r is the reference temperature (°C). The degree of hydration is calculated as shown in Equation 9-17.

$$t_e(T_2) = \int_0^t \exp\left(\frac{AE}{R} \cdot \left(\frac{1}{273+T_r} - \frac{1}{273+T_2} \right) \right) \cdot dt$$ **Equation 9-16**

$$\alpha(t_e) = \alpha_u \cdot \exp\left(-\left[\frac{\tau}{t_e} \right]^{\beta} \right)$$ **Equation 9-17**

The change in energy stored in the control volume is shown in Equation 9-18:

$$\Delta E_{st} = \frac{\rho_2 \cdot c_{p2} \cdot \Delta x_2 \cdot \Delta y \ \cdot (T_2^{+1} - T_2)}{\Delta t}$$ **Equation 9-18**

where ρ_2 is the material density in control volume 2 (kg/m^3), c_{p2} is the material specific heat in control volume 2 (J/kg/K), T_2^{+1} is the temperature at node 2 for the next time step (°C), T_2 is the temperature at node 2 for the current time step (°C), and Δt is the time step (seconds).

Boundary conditions are easily handled using the energy balance approach. A control volume with a side exposed to convection is shown in Figure 9-2.

A "half control volume" is used for control volumes located on an external boundary (Patankar, 1980). The conduction energy entering or leaving that side of the control volume can be replaced with the convection energy entering or leaving the control volume, as shown in Equation 9-19 and Equation 9-20:

$$E_{in} = T_1 \cdot a_{1-2} + T_\infty \cdot h \cdot \Delta y$$ **Equation 9-19**

$$E_{out} = T_2 \cdot a_{1-2} + T_2 \cdot h \cdot \Delta y$$ **Equation 9-20**

where h is the convection heat transfer coefficient (W/m^2/K). Radiation and irradiation terms may be similarly added to E_{in} and E_{out}. Constant temperatures, such as those found at the concrete exterior of a submerged concrete member may be enforced by setting the next time step for the control volume equal to the prescribed temperature.

9.3.1.2 Time Discretization

To calculate the temperature in a node, the temperature variation with time needs to be assumed. A common assumption is to assume that the integral with respect to time and temperature is a linear combination of the temperature at the beginning and end of the time step as shown in Equation 9-21 (Patankar, 1980).

$$\int_t^{t+\Delta t} T_p dt = \left[f \cdot T_2^{+1} + (1-f) \cdot T_2\right] \cdot \Delta t$$ **Equation 9-21**

where t is the beginning of the time step being evaluated (s), $t + \Delta t$ is the end of the time step in question (s), f is a constant between 0 and 1, T_2^{+1} is the temperature at node 2 at the end of the time step (°C), and T_2 is the temperature at node 2 at the beginning of the time step (°C). When f is chosen to be 0, the time discretization is said to be fully explicit and the temperature during the time step is assumed to be equal to the beginning temperature during the time step. If f is greater than 0, the method is called implicit. If f is assumed to be 1, the method is called fully implicit. The temperature during the time step is then assumed to be equal to the ending temperature during the time step. Explicit methods allow for temperature calculations directly from previous time step temperatures. Implicit methods however, are dependent on unknown temperatures. A system of unknown temperatures must be solved for simultaneously (Patankar, 1980). When the explicit method is used, the temperature at a node for the next time step is completely dependent on the current time step. This means that the unknown temperatures for the next time step do not have to be solved simultaneously.

If care is not taken when fully explicit methods are used, unstable results may be calculated. The stability criterion is shown in Equation 9-22:

$$E_{out} < \frac{\rho_2 \cdot c_{p2} \cdot \Delta x_2 \cdot \Delta y \cdot T_2}{\Delta t}$$ **Equation 9-22**

where E_{out}, ρ_2, c_{p2}, Δx_2, Δy, T_2, and Δt are as defined above. Equation 9 means that the amount of energy leaving the control volume has to be less than the amount of the energy stored in the control volume to give physically possible results. As seen in Equation 9-22, as the control volume decreases, the time step must also decrease. As a result, explicit finite difference methods can be computationally expensive.

9.3.1.3 Symmetry

The use of symmetry can significantly decrease the amount of computations needed. At a line of symmetry, the derivative of the temperature profile is zero. This implies that there is no heat exchanged across the line of symmetry. The energy leaving and entering the face of the control volume on the line of symmetry is set equal to zero. The assumption of symmetry may lead to some inaccuracies when modeling boundary conditions, such as when one side of a concrete member is shaded and the other is not. If symmetry were not assumed, longer run times would occur and more complex program inputs (including inputs that may not be available to the engineer) would be required.

9.3.1.4 Concrete Thermal Properties

Because of the constantly changing early age properties of concrete, the concrete thermal properties must be updated at every time step. The thermal conductivity is known to be a function of "the moisture content, content and type of aggregate, porosity, density and temperature" (Van Breugel, 1998). The concrete thermal conductivity increases with increasing moisture content. There is conflict in the literature about the change in thermal conductivity with increasing hydration. Some suggest that the thermal conductivity increases with the degree of hydration, while others report that it decreases up to 30% (Van Breugel, 1998; Schindler, 2002). Based on the recommendation of Schindler (2002), ConcreteWorks assumes a linear decrease of the thermal conductivity with the degree of hydration from 1.33 times the ultimate thermal conductivity to the ultimate thermal conductivity as shown in Equation 9-23:

$$k_c(\alpha) = k_{uc} \cdot (1.33 - 0.33 \cdot \alpha)$$ **Equation 9-23**

where k_c is the concrete thermal conductivity (W/m/K), α is the degree of hydration, and k_{uc} is the ultimate hardened concrete thermal conductivity. The thermal conductivity of the concrete is not adjusted for moisture content in ConcreteWorks because the moisture content in mass concrete does not change significantly during early ages. The thermal conductivity is also not adjusted for temperature because of the differing responses of different aggregates.

The specific heat of concrete is also dependent on the mixture proportions, degree of hydration, temperature and moisture level (Van Breugel, 1998; Schindler, 2002). A model proposed by Van Breugel accounts for changes in the specific heat based on degree of hydration, mixture proportions, and temperature as shown in Equation 9-24:

$$c_{pconc} = \frac{1}{\rho_{conc}} \cdot (W_c \cdot \alpha \cdot c_{cef} + W_c \cdot (1-\alpha) \cdot c_c + W_a \cdot c_a + W_w \cdot c_w) \qquad \textbf{Equation 9-24}$$

where c_{pconc} is the specific heat of the concrete (J/kg/K), ρ_{conc} is the concrete density (kg/m^3), W_c is the weight of cement (kg/m^3), W_a is the weight of aggregate (kg/m^3), W_w is the weight of water (kg/m^3), C_c is the cement specific heat (J/kg/K), C_a is the aggregate specific heat (J/kg/K), C_w is the water specific heat (J/kg/k), and C_{cef} is a fictitious specific heat of the hydrating cement as shown in Equation 9-25:

$$c_{ref} = 8.4 \cdot T_c + 339 \qquad \textbf{Equation 9-25}$$

where T_c is the concrete temperature (°C).

9.3.1.5 Concrete Heat of Hydration

The concrete heat of hydration parameters H_u, τ, β, α_u, and E_a can be calculated based on the concrete mixture proportions and constituent material properties. The τ, β, α_u parameters are calculated from a statistical analysis based on over 300 semi-adiabatic calorimetry tests performed according to recommendations from the RILEM technical committee 119 (1998) and validated by 18 tests conducted on concrete sampled from concrete construction sites and 44 tests conducted independently by Schindler and Folliard (2005) and Ge (2006). The dataset used includes concrete containing various chemical admixtures, cement fineness and chemical compositions, and supplementary cementing materials. The apparent activation energy, E_a, can also be calculated based on the cementing material properties and the chemical admixtures used. A statistical analysis of 117 apparent activation energies calculated from isothermal calorimetry was developed by Poole (2007). The H_u parameter can also be calculated from the cement chemical composition using a model developed by Schindler and later altered to better characterize the influence of grade 120 ground granulated blast furnace slag by Poole (2007). The cement composition can be defined in ConcreteWorks using either the Rietveld method (Rietveld, 1969) determined from quantitative x-ray diffraction or the Bogue method calculated according to ASTM C 150 (2005). When the Rietveld method is used to determine the cement chemical composition, Equation 9-26 to Equation 9-31 are used in ConcreteWorks to calculate the concrete heat of hydration parameters:

$$\alpha_u = \frac{1.031 \cdot w/cm}{0.194 + w/cm} + \exp\begin{pmatrix} -0.297 - 9.73 \cdot p_{Ferrite} \cdot p_{cem} \\ -325 \cdot p_{Na_2Oeq} \cdot p_{cem} \\ -8.90 \cdot p_{FA} \cdot p_{FA-CaO} \\ -331 \cdot WRRET - 93.8 \cdot PCHRWR \end{pmatrix}$$

Equation 9-26

$$\tau = \exp\begin{pmatrix} 2.95 - 0.972 \cdot p_{Alite} \cdot p_{cem} + 152 \cdot p_{Na_2O} \cdot p_{cem} + 1.75 \cdot p_{GGBF} \\ -4.00 \cdot p_{FA} \cdot p_{FA-CaO} - 11.8 \cdot ACCL + 95.1 \cdot WRRET \end{pmatrix}$$

Equation 9-27

$$\beta = \exp\begin{pmatrix} -0.418 - 2.66 \cdot p_{Alu\min ate} \cdot p_{cem} - 0.864 \cdot p_{GGBF} \\ +108 \cdot WRRET + 32.0 \cdot LRWR + 13.3 \cdot MRWR \\ +42.5 \cdot PCHRWR + 11.0 \cdot NHRWR \end{pmatrix}$$

Equation 9-28

$$\begin{aligned} H_u &= H_{cem} \cdot p_{cem} + 461 \cdot p_{GGBF-100} + 550 \cdot p_{GGBF-120} \\ &+ 1800 \cdot p_{FA-CaO} \cdot p_{FA} + 330 \cdot p_{S.F.} \end{aligned}$$

Equation 9-29

$$\begin{aligned} H_{cem} &= 500 \cdot p_{Alite} + 260 \cdot p_{Belite} + 866 \cdot p_{Alu\min ate} + 420 \cdot p_{Ferrite} \\ &+ 624 \cdot p_{sulfate} + 1186 \cdot p_{Lime} + 850 \cdot p_{Periclase} \end{aligned}$$

Equation 9-30

$$\begin{aligned}E_a &= 39{,}200 + 107 \cdot \left\lfloor \left(P_{Aluminate}\right) \cdot p_{Cement} \cdot \left(P_{CaSO_4 \cdot xH_2O} + p_{Arcanite}\right) \cdot p_{Cement} \right\rfloor \\ &- 12.2 \cdot Blaine + 1.24 \cdot p_{FlyAsh} \cdot p_{CaO-FlyAsh} + 120 \cdot p_{GGBFS} - 533 \cdot p_{SF} \\ &- 30{,}100 \cdot WRRET - 1{,}440 \cdot ACCL\end{aligned}$$

Equation 9-31

where p_{alite} is the percent alite content in the portland cement, p_{cem} is the percent portland cement of total cementing materials, p_{Na2Oeq} is the percent sodium equivalent alkalis in the portland cement, p_{Na2O} is the percent Na_2O in the portland cement, $p_{Aluminate}$ is the percent aluminate in the portland cement, p_{Belite} is the percent belite in the portland cement, $p_{Ferrite}$ is the percent ferrite in the portland cement, $p_{sulfate}$ is the percent total sulfate in the portland cement, p_{Lime} is the percent lime in portland cement, $p_{Periclase}$ is the percent periclase in the portland cement, $p_{CaSO4*xH2O}$ is the percent total gypsum in the portland cement, p_{FA} is the percent fly ash of the total cementing materials, $p_{FA\text{-}CaO}$ is the percent CaO content of the portland cement, p_{GGBFS} is the percent ground granulated blast furnace slag of the total cementing materials, p_{SF} is the percent silica fume of the total cementing materials, *WRRET* is the ASTM Type B & D water reducer/ retarder dose, *PCHRWR* is an ASTM Type F polycarboxylate based high range water reducer dose, *LRWR* is the ASTM Type A water reducer dose, MRWR is the mid-range water reducer dose, *NHRWR* is the Type F naphthalene high range water reducer dose, and *ACCL* is the ASTM type C accelerator. The chemical admixture dosages are in percent solids by weight of cementing materials.

When the Bogue method is used however, ConcreteWorks uses Equation 9-32 to Equation 9-37 to calculate the concrete heat of hydration parameters:

$$\alpha_u = \frac{1.031 \cdot w/cm}{0.194 + w/cm} + \exp\left(\begin{array}{l} -0.885 - 13.7 \cdot p_{C_4AF} \cdot p_{cem} \\ -283 \cdot p_{Na_2Oeq} \cdot p_{cem} \\ -9.90 \cdot p_{FA} \cdot p_{FA-CaO} \\ -339 \cdot WRRET - 95.4 \cdot PCHRWR \end{array} \right)$$

Equation 9-32

$$\tau = \exp\left(\begin{array}{l} 2.68 - 0.386 \cdot p_{C_3S} \cdot p_{cem} + 105 \cdot p_{Na_2O} \cdot p_{cem} + 1.75 \cdot p_{GGBF} \\ -5.33 \cdot p_{FA} \cdot p_{FA-CaO} - 12.6 \cdot ACCL + 97.3 \cdot WRRET \end{array} \right)$$

Equation 9-33

$$\beta = \exp\left(\begin{array}{l} -0.494 - 3.80 \cdot p_{C_3A} \cdot p_{cem} - 0.594 \cdot p_{GGBF} \\ +96.8 \cdot WRRET + 39.4 \cdot LRWR + 23.2 \cdot MRWR \\ +38.3 \cdot PCHRWR + 9.07 \cdot NHRWR \end{array} \right)$$

Equation 9-34

$$\begin{array}{l} H_u = H_{cem} \cdot p_{cem} + 461 \cdot p_{GGBF-100} + 550 \cdot p_{GGBF-120} \\ +1800 \cdot p_{FA-CaO} \cdot p_{FA} + 330 \cdot p_{S.F.} \end{array}$$

Equation 9-35

$$\begin{array}{l} H_{cem} = 500 \cdot p_{C_3S} + 260 \cdot p_{C_2S} + 866 \cdot p_{C_3A} + 420 \cdot p_{C_4AF} \\ +624 \cdot p_{SO_3} + 1186 \cdot p_{FreeCa} + 850 \cdot p_{MgO} \end{array}$$

Equation 9-36

$$\begin{array}{l} E_a = 41{,}230 + 8{,}330 \cdot \left[\left(C_3A + C_4AF \right) \cdot p_{Cement} \cdot Gypsum \cdot p_{Cement} \right] \\ -3{,}470 \cdot Na_2O_{eq} - 19.8 \cdot Blaine \\ +2.96 \cdot p_{FlyAsh} \cdot p_{CaO-FlyAsh} + 162 \cdot p_{GGBFS} - 516 \cdot p_{SF} \\ -30{,}900 \cdot WRRET - 1{,}450 \cdot ACCL \end{array}$$

Equation 9-37

where p_{C3S} is the percent alite content in the portland cement, p_{C3A} is the percent aluminate in the portland cement, p_{C2S} is the percent belite in the portland cement, p_{C4AF} is the percent ferrite in the portland cement, p_{SO3} is the percent total sulfate in the portland cement, p_{MgO} is the percent MgO in the portland cement and p_{freeCa} is the percent CaO in the portland cement. To simplify the inputs needed, ConcreteWorks uses average assumed chemical admixture dosages as shown in Table 9-5.

9.3.1.6 Boundary Conditions

In calculating the heat transfer of concrete members, the boundary conditions are usually the most difficult parameters to quantify. ConcreteWorks makes numerous assumptions about the heat sources and sinks that are external to the concrete, depending on the member type chosen. The heat sources and sinks modeled in ConcreteWorks may include: irradiation from the member, radiation from the ground, radiation from the air, solar radiation, radiation from the formwork, convection to/from the member, evaporative cooling, conduction to the soil/subgrade, and exposure to water. The amount of each heat source or sink that is included in ConcreteWorks depends on the member type, shading effects, and other user inputs. More details on the assumptions made for each member type are discussed in section 9.3.2.

There are numerous equations needed to model each type of heat source or sink in ConcreteWorks. Details about many of the boundary conditions equations used in ConcreteWorks, especially for vertical members may be found in the paper "Temperature Boundary Condition Models for Concrete Bridge Members (Riding et al., 2007b)." The evaporative cooling model is from Schindler (2002). It combines models from the ASHRAE handbook (1993) and Al-Fadhala and Hover (2001) to predict the evaporation and consequently the cooling rate for concrete surfaces. The model uses water evaporation rate equations that are applied to concrete. The evaporation rate follows Dalton's law, which relates the water-vapor pressure of the air, at the water surface, and the wind speed (which helps speed up evaporation) to the evaporation rate (Hover, 2006). Menzel's equation is shown as Equation 9-38 (Al-Fadhala and Hover, 2001):

$$E_w = 0.315(e_0 - RH \cdot e_a)(0.253 + 0.060w)$$ **Equation 9-38**

where E_w is the water evaporation rate (kg/m^2/hr), e_0 is the water surface saturated water vapor pressure (mmHg), e_a is the air water vapor pressure (mmHg), RH is the relative humidity (as a decimal), and w is the wind speed (m/s). The terms e_0 and e_a are dependent on the water surface and air temperatures. Concrete follows Dalton's law pretty well when bleed water is on the surface, and decreases rapidly during setting. The amount of evaporation from concrete may be related to the amount of evaporation from a water surface by Equation 9-39 (Al-Fadhala and Hover, 2001):

$$\frac{E_c}{E_w} = \exp\left[-\left[\frac{t}{a_{evap}}\right]^{1.5}\right]$$ **Equation 9-39**

where Ec is the evaporation rate from concrete (kg/m^2/hr), t is the time from mixing (hrs), and a_{evap} is mixture dependent time constant (hrs). ConcreteWorks assumes that $\mathrm{a}_{\mathrm{evap}}$ is equal to 3.75 hrs. The evaporative cooling model is applied until either a cure method is applied or 24 hours after placing.

9.3.2 CONCRETE MEMBER MODELS

Each type of concrete member modeled in ConcreteWorks has different formwork, boundary conditions, geometry, and opportunities to use symmetry. Different nodal arrangements are also required to keep nodes in a regular pattern and in line.

9.3.2.1 Rectangular Column

ConcreteWorks models a 2D horizontal cross section for rectangular columns, as shown in Figure 9-3. The column heat transfer in the vertical direction is assumed to be zero, which is a reasonable assumption except near the top and bottom ends of the column. Rectangular columns are modeled using symmetry in both directions as shown in Figure 9-4. The formwork is handled by using half control volumes around the concrete, as shown in Figure 9-5. ConcreteWorks allows the user to select up to three construction stages to model for rectangular columns by selecting different formwork removal times and curing techniques.

The first construction stage is during concrete placement and curing before form removal. When steel formwork is selected and form-liners are not selected, ConcreteWorks assumes that the steel provides no insulation because of the "little resistance to heat dissipation from the concrete (ACI 207, 1995)." The steel emissivity, absorptivity, and shading values are then assigned to the concrete surface node, so that the surface of the column will still see the same heating from the environment. Eliminating the form control volumes for steel formwork greatly increases the runtime because of the small time step needed to maintain stability with such a thin control volume needed to model a steel form. When form-liners are used, ConcreteWorks calculates an equivalent form thermal conductivity, density and specific heat for the selected combination of form and form-liner. The thermal conductivity, density, and specific heat of the equivalent form are calculated using Equation 9-40 to Equation 9-42:

$$k_{ef} = \left[\frac{w_f}{k_f} + \frac{w_{fl}}{k_{fl}} \right]^{-1}$$ **Equation 9-40**

$$\rho_{ef} = \frac{\rho_f \cdot w_f + \rho_{fl} \cdot w_{fl}}{w_f + w_{fl}}$$ **Equation 9-41**

$$cp_{ef} = \frac{cp_f \cdot w_f + cp_{fl} \cdot w_{fl}}{cp_f + cp_{fl}}$$ **Equation 9-42**

where k_{ef} is the effective form thermal conductivity (W/m/K), w_f is the width of the form (m), w_{fl} is the width of the form-liner (m), k_f is the form thermal conductivity (W/m/K), k_{fl} is the form-liner thermal conductivity (W/m/K), ρ_{ef} is the effective form density (kg/m^3), ρ_f is the form density (kg/m^3), ρ_{fl} is the form-liner density (kg/m^3), cp_{ef} is the effective form specific heat (J/kg/K), cp_f is the form specific heat (J/kg/K), and cp_{ef} is the form-liner specific heat (J/kg/K). In ConcreteWorks, formliners are assumed to have a thickness of 0.036 m (1.4 in), a thermal conductivity of 0.7437 W/m/°C, a specific heat of 1549.1 J/kg/K, and a density of 1121 kg/m^3.

The second construction stage modeled is after form-removal and before curing techniques such as plastic, cure blankets, or cure compounds are applied. An example of a structure during the beginning of the second construction stage is shown in Figure 9-6. The formwork is virtually removed in ConcreteWorks by eliminating the formwork control volume, and applying boundary conditions such as convection and radiation directly to the surface concrete control volumes. Concrete emissivity, absorptivity and surface roughness values are assigned at this point to the surface concrete control volumes.

Construction stage three is during the time period of concrete curing using blankets, curing compounds or plastic. When only curing compounds or only plastic are used, ConcreteWorks assigns the curing compound or plastic emissivity, absorptivity and roughness values to the concrete surface control volumes. When curing compounds are used in conjunction with plastic or blankets, the effect of curing compounds is assumed to be negligible. When blankets are used but no plastic is used for curing, half control volumes (similar to those used for modeling the formwork) are applied to the exterior of the concrete control volumes. Blanket thermal and roughness properties are assigned to the exterior half control volumes. When plastic and blankets are used to cure the concrete, blanket insulation properties (thermal conductivity, specific heat, density, and thickness) are assigned to the exterior half control volumes while the plastic emissivity, absorptivity and roughness values are used.

Blanket insulation properties are calculated from the blanket R-value entered by the user. The R-value is equivalent to the thickness divided by the thermal conductivity. ConcreteWorks assumes a blanket thickness of 0.02 m and then solves for the blanket thermal conductivity k_{bl} (W/m/K) as shown in Equation 9-43:

$$k_{bl} = \frac{0.02}{R_{bl}}$$

Equation 9-43

where R_{bl} is the blanket R-value (m^2K/W). The specific heat of the wet blanket is assumed to be 320 kg/m^3 while the specific heat is assumed to be 2000 J/kg/K.

9.3.2.2 Rectangular Footing

Footings have some unique features that require special cases for modeling. When footings are modeled in 2-D, ConcreteWorks assumes a vertical cross-section of the footing as shown in Figure 9-7 with no heat transfer perpendicular to the cross-section. The heat exchange between the footing and the environment is dependent on: the formwork, cure blankets and plastic used, soil conditions, weather, orientation of the footing, shading from scaffolding and embankments, and heat conduction from the concrete interior. Figure 9-8 summarizes the footing surface boundary conditions.

9.3.2.2.1 Radiation

Solar radiation, atmospheric radiation, irradiation from the footing, and the radiation exchange between the vertical surface and form horizontal cross bracing models are used in the side and top boundary condition calculations. Radiation emitted by the ground surface is assumed to be incident on the side surface only. If the user chooses to shade the sides of the footing because of scaffolding or the embankment, then the solar radiation is set to zero.

9.3.2.2.2 Conduction to/from Soil

Conduction to or from the soil underneath the footing is modeled by assuming a constant depth of soil. The initial temperature of the soil is set to the user-defined average soil temperature. The temperature at the bottom of the modeled soil is set also set to the user-defined average soil temperature. Table 9-6 lists the thermal properties of the different soil and rock types modeled by ConcreteWorks. Figure 9-9 shows how the rectangular footing is modeled, and Figure 9-10 illustrates the node and control volume boundaries assumed. Symmetry is assumed in the model in the width and length (when calculated in three dimensions) direction as shown in Figure 9-10.

9.3.2.2.3 Construction Stages

Rectangular footings can modeled with up to four potential construction stages. The first stage is before the blanket or any cure method is applied to the top surface. The second stage is when the cure method is applied to the top surface. ConcreteWorks assumes that a cure blanket is placed on the top surface when the cure method is applied. Any other cure methods such as plastic will also be placed and will affect the absorptivity and emissivity of the top cure surface. The third stage is after form and cure method removal. The fourth construction stage represents the time period when a cure method on the top and sides is used after the forms and initial top surface curing methods are removed. If a cure blanket is selected for this stage, it is applied uniformly over the top and side surfaces.

9.3.2.3 Rectangular Footing with Soil on the Sides

ConcreteWorks contains an option for soil to be used as the formwork, as shown in Figure 9-11. Symmetry is assumed in the middle of the member as shown. Conduction to or from the soil on the sides is treated in a similar manner to the soil underneath the footing. A constant thickness of soil is modeled on the sides of the footing. The average soil temperature is enforced on the sides at the edge of the soil, as shown in Figure 9-12. The node and control volume layout for the rectangular footing with soil on the sides is shown in Figure 9-13.

9.3.2.3.1 Construction Stages

Rectangular footings surrounded by soil can contain up to two construction stages. The first is before any cure methods are placed on the top surface. The second is after cure methods are placed on the top surface. It is assumed that a cure blanket is used in addition to any other cure methods applied.

9.3.2.4 Bent Caps

The heat transfer at the exterior of the bent caps is handled using many of the same equations as that of the other concrete members. There are a few types of bent caps, each with unique boundary conditions. Symmetry is assumed in all bent cap members.

9.3.2.4.1 Rectangular Bent Cap

Figure 9-14 shows the vertical cross section assumed in the 2-dimensional heat transfer analysis performed for rectangular bent caps. Figure 9-15 summarizes how ConcreteWorks models radiation for a rectangular bent cap. Solar radiation is assumed to be incident on the top and side surfaces only. Radiation from the ground surface is assumed to be incident on the bottom and side surfaces only. Radiation from the atmosphere is assumed to be incident on all surfaces of the rectangular bent cap. ConcreteWorks assumes that the rectangular bent cap emits radiation from all surfaces. ConcreteWorks assumes that the wind creates convection on all of the rectangular bent cap surfaces, as shown in Figure 9-16. ConcreteWorks allows the user to select different types of bottom and side formwork, as shown in Figure 9-17. A summary of the node and control volume layout for rectangular bent caps is shown in Figure 9-18.

9.3.2.4.1.1 Construction Stages

Rectangular bent caps have a total of four possible construction stages. The first stage is before a curing blanket is placed on the bent cap top surface. The second stage is after the curing blanket is placed on the top surface and before the formwork is removed. The third possible construction stage is after the formwork and curing blanket is removed. The last possible construction stage is after a curing blanket is wrapped around the bent cap.

9.3.2.4.2 Dolphin

ConcreteWorks allows the user to select pre-cast concrete as the bottom formwork material. Pre-cast concrete is assumed to have the same material thermal properties as the concrete mixture used for the bent cap with a degree of hydration equal to 0.6. When the user inputs that the bent cap is a dolphin, the temperature of the bottom of the bent cap is set equal to the average water temperature. Figure 9-19 shows a summary of a dolphin with a pre-cast concrete bottom.

9.3.2.5 T-Shaped Bent Cap

The T-shaped bent cap modeled in ConcreteWorks assumes the same type of vertical cross section as the rectangular bent cap. Figure 9-20 shows a summary of how ConcreteWorks models radiation boundary conditions in T-shaped bent caps. Radiation from the ground surface is assumed to be incident on the cap bottom and sides. Solar radiation is assumed to be incident on all the top of the cap, the top of the corbel, and the sides. Radiation from the atmosphere is assumed to be incident on all sides. The cap is assumed to emit radiation from all surfaces. ConcreteWorks assumes that the wind creates convection on all of the T-shaped bent cap surfaces, as shown in Figure 9-21. ConcreteWorks allows the user to select different types of bottom and side formwork, as shown in Figure 9-22. The node and control volume layout for the T-shaped bent cap is shown in Figure 9-23.

9.3.2.5.1 Construction Stages

T-shaped bent caps use the same construction stages as rectangular bent caps.

9.3.2.6 Circular Columns

ConcreteWorks models a horizontal cross section of the circular column, just like that of a rectangular column. The boundary conditions for both rectangular and circular columns are handled in a similar manner. Circular columns are modeled in ConcreteWorks using the same radiation and convection boundary conditions as rectangular columns. Figure 9-24 shows a summary of the construction model used for a circular column in ConcreteWorks. Symmetry is assumed in the circumferential direction. Figure 9-25 shows the node and control volume layout for a circular column. Figure 9-26 shows the boundary conditions modeled for circular columns. ConcreteWorks applies convection on the outer surface of the model of the circular column. Radiation from ground surfaces, atmospheric radiation, solar radiation, and irradiation are also modeled on the outer surface of the column.

9.3.2.6.1 Construction Stages

Circular columns use the same construction stages as rectangular columns.

9.3.2.7 Bridge Decks

The fundamental heat transfer calculations performed for all four types of bridge decks modeled in ConcreteWorks are the same. Figure 9-27 shows the basic layout of the bridge deck modeled. In the case of a bridge deck with a precast panel, there is no bottom form modeled. The precast panel thermal conductivity and specific heat properties are calculated using Equation 9-23 and Equation 9-24, with a degree of hydration equal to 0.6. The precast panel is assumed to generate no heat. The bottom formwork is also not modeled when a galvanized panel is used. The calculations are performed assuming one-dimensional heat transfer, and control volumes as shown in Figure 9-28. The portion modeled is assumed to be open underneath the bottom form (i.e. not directly over a beam). Figure 9-29 shows the bridge deck temperature boundary conditions modeled in ConcreteWorks.

9.3.2.7.1 Construction Stages

Bridge decks have up to four possible construction stages. The first is before the cure method is applied to the top surface. A cure blanket is assumed to be used along with any additional curing methods selected by the user. The second stage is after the cure blanket is placed on the top surface, but before form removal and cure method removal. There are two possible final construction stages. An optional third construction stage is when the formwork still remains on, but the cure method is removed from the top surface. The fourth construction stage in this option is when the form has been removed following the blanket removal. In the second option, the third construction stage is when the formwork is removed before the cure method is removed from top. Option two's fourth construction stage is when the cure method is removed after the bottom formwork removal.

9.3.2.8 Precast Rectangular and U-Shaped Beams

Precast rectangular and U-shaped beams are handled in the same way in ConcreteWorks. Only the dimensions and number of nodes are changed, depending on which member is selected. ConcreteWorks only models a vertical cross section of the solid beam end block, as shown in Figure 9-30. Only the end block is modeled to greatly simplify the analysis, and to capture the maximum temperature in the beam, which occurs in the solid end region. Figure 9-31 shows how the end region concrete, formwork and soil underneath are modeled in ConcreteWorks. Figure 9-32 shows the node and control volume layout for the rectangular and U-shaped precast beams.

9.3.2.8.1 Boundary Conditions

The rectangular and U-shaped beam model uses boundary conditions similar to the rectangular footing.

9.3.2.8.2 Construction Stages

The rectangular and U-shaped beam model can have up to three construction stages. The first is before the cure methods are applied. The second is after the cure methods are applied. It is assumed that a cure blanket is placed on top of the precast beam at this stage along with any other selected cure methods. The third stage occurs after the formwork is removed. It is assumed that no further curing is performed on precast concrete members after the formwork is removed.

9.3.2.9 Precast Type IV Beams

The precast type IV beam model in ConcreteWorks models a vertical cross-section through the middle of the beam. The model assumptions are shown in Figure 9-33. The type IV beam node and control volume boundaries assumed in the model are shown in Figure 9-34.

9.3.2.9.1 Boundary Conditions

The precast type IV beam top and side boundary conditions include solar radiation, irradiation, radiation from the air, and convection. Convection and irradiation occur under the bottom of the precast concrete member because of a gap that exists between the bottom formwork and the soil. Because the gap is not sealed, convection may occur, resulting in cooling.

9.3.2.9.2 Construction Stages

The precast type IV beam utilizes the same construction stages as the rectangular precast beam.

9.3.2.10 Pavements

Pavements are modeled assuming one dimensional heat transfer in the vertical direction. Figure 9-35 shows the pavement layers modeled in ConcreteWorks. The thermal conductivities, specific heat, and density values used for the pavement subgrade depend on the user inputs, according to Table 9-6.

9.3.2.10.1 Boundary Conditions

The top surface of the pavement is exposed to the same boundary conditions as the bridge deck top surface. The pavement may be cured with a monomolecular compound, a single coat of curing compound, a double coat of curing compound, a clear or black plastic sheet, or a cure blanket. If a monomolecular compound or a curing compound is used, then the user may enter the concrete color after the cure method application. The cure method color will change the concrete surface emissivity and absorptivity. Darker colors (like black and dark gray) have higher solar absorptivity and emissivity values than lighter colors (like white or light gray).

The pavement layered system provides conduction to the supporting subbase layers and to the subgrade. ConcreteWorks models 49.2 ft (15 meter) of subbase. The temperature of the bottom of the subbase is modeled using the deep ground water temperature calculated using Equation 9-44 (Yoshitake, Nagai, Tanimoto, and Hamada 2002):

$$T_{gw} = 0.83 \cdot T_{aat} + 3.7$$ **Equation 9-44**

where T_{gw} is the deep ground water temperature (°C), and T_{aat} is the average annual temperature (°C). The average annual temperature in ConcreteWorks is calculated from the weather data entered for the city selected. The soil about 0.6 m below the ground surface remains at a fairly constant temperature throughout the year (Yoshitake, Nagai, Tanimoto, and Hamada 2002).

The initial subbgrade and subbase temperature profile used in the analysis is then calculated using the Barber model. The Barber model can estimate the subbase and subgrade temperature profile based on the weather data selected in ConcreteWorks, as shown in Equation 9-45 to Equation 9-49 (Barber 1957, Schindler 2002):

$$T(z) = T_M + T_V \cdot \left(\frac{H \cdot \exp(-z \cdot C)}{\sqrt{(H+C)^2 + C^2}} \right) \cdot \sin\left(0.262 \cdot t - z \cdot C - \arctan \frac{C}{H+C} \right)$$ **Equation 9-45**

$$T_M = 0.5 \cdot T_A + (0.0498 \cdot \mathrm{L}) \qquad \text{for } T \geq T_A$$ **Equation 9-46**

$$T_m = 0.5 \cdot T_A + 0.278 \cdot (0.0498 \cdot \mathrm{L}) \quad \text{for } T<T_A$$

$$T_V = 0.5 \cdot T_R + 1.67 \cdot (0.0498 \cdot \mathrm{L}) \quad \text{for } T \geq T_A$$

Equation 9-47

$$T_V = 0.5 \cdot T_R \quad \text{for } T<T_A$$

$$H = \left(\frac{4.1 + 1.13 \cdot w^{0.75}}{k} \right)$$

Equation 9-48

$$C = \left(\frac{k}{c_p \cdot \rho} \right)$$

Equation 9-49

where *T(z)* is the soil temperature (°C) at depth *z* (m), T_M is the mean effective air temperature (°C) as calculated in Equation 9-46, T_A is the mean air temperature (°C), *L* is the solar radiation (W/m^2), T_V is the maximum variation in temperature from the mean (°C) calculated using Equation 9-47, T_R is the maximum daily temperature minus the minimum daily temperature (°C), *H* is calculated using Equation 9-48, *w* is the wind speed (m/s), *k* is the soil thermal conductivity (W/m^2), *C* is the soil thermal diffusivity calculated using Equation 9-49 (m^2/s), c_p is the soil specific heat (J/kg/°C), ρ is the soil density (kg/m^3), and *t* is the time from the beginning of the temperature cycle (hours). The finite difference model excluding the concrete is then run from midnight of the placement date to the placement time to further improve the initial soil temperature profile. The thermal conductivity, specific heat, density, solar absorptivity, and emissivity values assumed for different subbase materials are shown in Table 9-7.

9.3.2.10.2 Construction Stages

The pavement temperature analysis module contains three possible construction stages: before the cure method is applied, after the cure method is applied, and after the cure method is removed. If a monomolecular compound or a curing compound is chosen, then it is assumed to stay on during the length of the analysis.

9.4 Thermal Stress Analysis

9.4.1 OVERVIEW

Thermal stress modeling in concrete members is non-linear because of changing early age material properties (elastic modulus, strength, Poisson's ratio, and coefficient of thermal expansion), differential temperature development, and creep. Figure 9-37 shows how the non-linear concrete property and restrained stress development are calculated in ConcreteWorks.

In order to calculate the thermal stresses, the concrete member degree of hydration and temperature development must first be calculated as described in section 9.3. Next, the degree of hydration and temperature development are used to calculate the member mechanical properties, including the strains the concrete would undergo if there were restraint, the elastic modulus development, Poisson's ratio, the tensile strength development, the coefficient of thermal expansion, and autogenous and drying shrinkage. Next, the concrete elastic stress must be calculated from the free shrinkage strains and mechanical properties by performing a structural analysis. Stress relaxation may then be applied to the concrete elastic stress. Finally, a failure criterion such as the stress-to-tensile strength ratio may be used to determine the cracking probability.

9.4.2 FREE SHRINKAGE AND MECHANICAL PROPERTIES

Both the concrete the mechanical property development and the early-age free shrinkage strains are dependent on the concrete degree of hydration and temperature development. The mechanical property development is calculated using the equivalent age maturity method (ASTM C 1074, 2004). Several different equations have been developed to relate the maturity to strength development and are discussed in section 9.4.2.1. Section 9.4.2.2 discusses the development of Poisson's ratio. The free shrinkage strain is composed of the concrete thermal strains, the autogenous strains, the drying shrinkage strains, and the plastic shrinkage strains. In mass concrete, the drying shrinkage may be assumed equal to zero for early-age analysis because of the small surface-to-volume ratio. Free thermal deformation calculation methods are discussed in section 9.4.2.3 and autogenous shrinkage calculation methods are discussed in section 9.4.2.4.

9.4.2.1 Concrete Maturity and Strength Development

The rate of cement hydration is dependent on the temperature and the time since mixing (Mindess, Young and Darwin, 2003). Maturity is a method of comparing the cement hydration progress made at different temperatures. There are two maturity methods commonly used, both of which are described in ASTM C 1074 (2004). They are the Nurse-Saul method and the Equivalent Age method. The Nurse-Saul method concept was developed first in the 1950's and uses a temperature-time factor to define maturity. The temperature-time factor may be defined as the integral of the temperature history and may be calculated using Equation 9-50 (ASTM C 1074, 2004):

$$M(t) = \sum (T_a - T_0) \cdot \Delta t$$ **Equation 9-50**

where $M(t)$ is the maturity (°C-hrs) at time t (hrs), T_a is the average temperature (°C) during time interval Δt (hrs), and T_0 is the datum or baseline temperature used (°C). The equivalent age maturity is the age a concrete sample would have to be cured isothermally at some reference temperature T_r (°C) to have the same degree of reaction or properties as the sample cured at a different temperature. The equivalent age maturity may be calculated using Equation 9-51 (ASTM C 1074, 2004):

$$t_e = \sum e^{-Q\left(\frac{1}{(T_a+273)} - \frac{1}{(T_r+273)}\right)} \Delta t$$ **Equation 9-51**

where t_e is the equivalent age maturity (hrs), and Q is the activation energy divided by the gas constant (°K). ConcreteWorks uses the equivalent age maturity method because it does a better job of predicting the concrete strength development than the Nurse-Saul method (Emborg 1998a, Mindess, Young and Darwin 2003). One of the problems with the maturity method, termed the cross-over effect, is that curing at higher temperatures can result in lower long-term concrete strengths than concrete cured at lower temperatures (Emborg 1998a). This effect does not usually occur until later ages, meaning that the maturity method may still be used at early-ages with little expected loss of accuracy. For this reason, ConcreteWorks does not take the cross-over effect into account in calculating the strength from the maturity.

9.4.2.1.1 Compressive Strength Development

A good model that describes the compressive strength development is essential in ConcreteWorks because it is used to calculate the elastic modulus development and the splitting tensile strength development. The compressive strength is the most widely used strength quality control test. Many engineers and contractors have already gained experience in developing compressive strength-maturity relationships, making it a much easier parameter for ConcreteWorks users to input than the modulus or splitting tensile strength to maturity relationship.

Many equations of different forms have been developed to relate the compressive strength to the maturity development. Two very common equations used are shown in Equation 9-52 and Equation 9-53 (Viviani, 2005):

$$f_c(t) = a + b \cdot \log(\log(M(t))), f_c \geq 0$$ **Equation 9-52**

$$f_c(t_e) = f_{cult} \cdot \exp\left(-\left(\frac{\tau_s}{t_e} \right)^{\beta_s} \right)$$ **Equation 9-53**

where f_c is the compressive strength development (MPa), a is a fit parameter which is usually negative (MPa), b is a fit parameter (MPa/°C/hr), f_{cult} is the ultimate compressive strength parameter fit from the compressive strength tests (MPa), τ_s is a fit parameter (hrs), and β_s is a fit parameter. Any modulus value equal to zero calculated from the compressive strength will result a singular matrix in the structural analysis. The thermal stress analysis is started when all of the concrete in the member has reached initial set, to prevent singular matrices. Equation 9-53 is only allowed to be used in ConcreteWorks when the equivalent age maturity method is used, while Equation 9-52 is only allowed to be used when the Nurse-Saule maturity method is used.

9.4.2.1.2 Elastic Modulus Development

The elastic modulus provides the link between restrained strains and stresses. The elastic modulus is known to be dependent on the mixture proportions, unit weight, maturity, aggregate modulus, strength, and moisture condition. The elastic modulus is known to develop faster than the tensile and compressive strength. Several models for the elastic modulus development with time are based on a form of Equation 9-54:

$$E(t) = E_{ref} * \beta(t)$$ **Equation 9-54**

where E_{ref} is the reference modulus (MPa), E is the elastic modulus at time t, and β is a modification factor that accounts for the modulus development with time. Equation 9-55 to Equation 9-57 show different equations used to model β (Larson, 2003):

$$\beta(t) = \begin{cases} 0 & for \quad t < t_s \\ b_1 * \log(t/t_s) & for \quad t_s \le t_0 < t_B \\ b_1 * \log(t_B/t_s) + b_2 * \log(t/t_s) & for \quad t_B \le t < 28day \\ 1 & for \quad t \ge 28day \end{cases}$$ **Equation 9-55**

$$\beta(t) = \left(\exp\left(s \cdot \left(1 - 1/\sqrt{\frac{t - t_s}{28 - t_s}} \right) \right) \right)^{0.5}$$ **Equation 9-56**

$$\beta(t) = \frac{E_\infty}{E_{ref}} \cdot \exp\left(-\left(\frac{\tau}{t}\right)^{\alpha}\right)$$ **Equation 9-57**

where t_s is the apparent setting time (hours); b_1, b_2, α, τ, and s are model parameters; t_B is a constant that represents the time of change in slope of the elastic modulus (hours); and E_∞ is the ultimate elastic modulus (MPa). Larson (2003) found that all three models gave satisfactory results when elastic modulus data from concrete less than one day old was used in the model parameter regression analysis.

Rostasy, Gutsch and Laube (1993) have proposed a model for the normalized modulus development based on degree of hydration as shown in Equation 9-58:

$$\hat{E} = \left[\frac{\alpha - \alpha_0}{1 - \alpha_0}\right]^{\frac{2}{3}}$$ **Equation 9-58**

where $\hat{E}$ is the normalized elastic modulus, α is the degree of hydration, and α_0 is the degree of hydration at time of initial setting. Bernard, Ulm, and Lemarchand (2003) found that the elastic modulus of cement paste increases almost linearly with the degree of hydration. This is because the modulus development is highly dependent on the porosity of the cement paste. They found that when aggregates are added, the relationship between elastic modulus and degree of hydration stops being linear.

The elastic modulus is also commonly calculated from the compressive strength of the concrete. Most models of this type follow a form of Equation 9-59:

$$E = k \cdot (f_c)^n$$ **Equation 9-59**

where f_c is the compressive strength (MPa), and k and n are model parameters. ACI 318 (2005) uses a form of this equation where n is equal to 0.5 and k is as shown in Equation 9-60:

$$k = 0.043 \cdot w_c^{1.5}$$ **Equation 9-60**

where w_c is the unit weight of the concrete (kg/m^3). ConcreteWorks uses Equation 9-59 and Equation 9-60 in calculating the elastic modulus from the compressive strength development. The default values set in ConcreteWorks are equal to those used in the ACI 318 building code. This equation was chosen because most engineers are familiar with this equation from prior experience in structural design, and readily accept its use. Most ConcreteWorks users will also not have test data available to model the elastic modulus development, making the use of readily accepted default equations necessary.

9.4.2.1.3 Tensile Strength Development

Concrete failure in early age concrete stress models is usually considered to occur when the stress exceeds the concrete strength. An accurate knowledge of the tensile strength development of concrete is just as crucial in determining the concrete cracking probability as knowing the stress. The tensile strength development of concrete is known to be affected by aggregate strength, smoothness and size, saturation level, and cementitious materials.

The tensile strength has been found to develop faster than compressive strength, but slower than the elastic modulus. The elastic modulus is often related to the compressive strength by Equation 9-61 (Raphael, 1984):

$$f_t = l \cdot (f_c)^m$$ **Equation 9-61**

where f_t is the tensile strength (MPa), and l and m are fit parameters.

The tensile strength of concrete can be determined by uniaxial tensile tests, the splitting tensile test, or the flexural tensile test. The uniaxial tensile test is difficult to perform, especially at early ages. The uniaxial tensile strength, splitting tensile strength, and flexural tensile strength of concrete have been found to develop at the same rate, allowing conversion from the splitting tensile and flexural tensile strength to the uniaxial tensile strength (De Schutter and Taerwe, 1996). Rostasy, Gutsch, and Laube (1993) have shown that the tensile strength development is independent of the load history, allowing for independent calculation of the strength and stress. ConcreteWorks assumes that the splitting tensile strength is used, and uses the parameters developed by Raphael (1984) of l equal to 1.7 and m equal to 2/3 for the default values.

9.4.2.2 Poisson Ratio

Stress modeling in two or three dimensional elements requires the knowledge of Poisson's ratio. Poisson's ratio is a measure of the deformation in one direction due to a load in the transverse direction. There is debate as to whether Poisson's ratio is constant or changing in young concrete. Oluokun, Burdette, and Deatherage (1991) have concluded that Poisson's ratio is independent of the age of the concrete. This conclusion is not supported by their data, which shows the Poisson's ratio at 6 hours to be less than that at later ages. To illustrate why the Poisson's ratio of concrete must not be a constant value, consider the concrete fresh plastic state. The Poisson's ratio of concrete while the concrete is in its liquid state must be equal or close to that of water, 0.5. After setting, the cementitious system stiffens and transforms from a suspended liquid to a rigid skeleton. The long-term Poisson ratio of concrete varies between 0.15 and 0.2 (Mindess, Young, and Darwin, 2003). A transition from a Poisson ratio of 0.5 to around 0.2 must occur during hardening.

There are three models that describe how Poisson's ratio changes with time. The first model assumes a linear decrease in Poisson's ratio with time. Experimental data has shown that with concrete the Poisson ratio decreases to a minimum value before rising slightly to its final long term value (De Schutter and Taerwe, 1996). This is the second model. Byfors suggests that the Poisson ratio changes from 0.48 during the plastic state to 0.13 at a strength 1 to 2 MPa, to a final long term value of around 0.28 (De Schutter and Taerwe, 1996; Byfors, 1980). Bernard, Ulm and Lemarchand (1994) suggest that during the plastic state, the continuous water structure dominates the Poisson ratio. As the concrete begins to set, the water structure becomes discontinuous, decreasing the component of Poisson's ratio supplied by the water structure. During setting, the concrete microstructure begins to form, increasing the component of the Poisson ratio supplied by the solid skeleton. The sum of the components of the Poisson ratio results in a minimum value during setting which increases to a stable long term value as shown in Figure 9-38. (Bernard, Ulm, and Lemarchand, 2003). De Schutter and Taerwe (1996) proposed a model for the Poisson ratio, υ, based on the degree of hydration, as shown in Equation 62:

$$\upsilon(r) = 0.18\sin\frac{\pi \cdot r}{2} + 0.5e^{-10r}$$ **Equation 9-62**

where r is the degree of hydration. ConcreteWorks uses this model because the model captures the shape of Poisson's ratio development and because of the model's simplicity.

The third model is based on the composite sphere model. Poisson's ratio is calculated form the bulk modulus K (GPa) and the shear modulus G (GPa) of the concrete as shown in Equation 9-63. Paulini and Gratl (1994) conclude from this model that Poisson's ratio does not reach a minimum value and then increase, but steadily decreases to an asymptotic value. Bernard, Ulm and Lemarchand (2003), on the other hand, use Equation 9-63 to support the second model by suggesting that the bulk modulus and shear modulus change at different rates. The ratio of the shear modulus to bulk modulus increases to a maximum value and then declines.

$$\upsilon = \frac{3K - 2G}{6K + 2G}$$ **Equation 9-63**

Poisson's ratio has been found to be equivalent in tension and compression (Lydon and Balendran, 1986). This is a very important point for use in computer models of thermal stresses. ConcreteWorks assumes that the Poisson's ratio is equal in compression and tension.

The dynamic Poisson ratio is about 25-40% higher than the static Poisson ratio (Byfors, 1980). The dynamic Poisson ratio is thought to be more representative of the actual elastic behavior of concrete (Mindess, Young, and Darwin, 2003). The static Poisson's ratio has been found to be principally a function of the percent volume of aggregates in the mixture, while the dynamic Poisson's ratio has been found to be a function of the age, w/cm, and percent volume of aggregates.

Poisson’s ratio has been shown to be constant up to a stress of 50 – 60% of the compressive strength. Micro-cracking at higher stress levels can change the Poisson’s ratio. Poisson’s ratio may also be different under biaxial or triaxial states of stress (Anson and Newman, 1966). ConcreteWorks assumes that the Poisson’s ratio is independent of the stress level and the state of stress.

9.4.2.3 Coefficient of Thermal Expansion

The coefficient of thermal expansion (CTE) of concrete is an indicator of the concrete member length change due to temperature changes in the concrete. It is one of the most important parameters in predicting stress distributions in concrete members. Knowledge of the CTE allows researchers to separate the effects of temperature induced deformations from autogenous shrinkage in laboratory tests. Separate models for thermal and autogenous deformations can then be made, allowing for their superposition in computer-based stress models. There are several factors which can affect the CTE including mixture proportions, aggregate type, degree of saturation, and age.

The hardened concrete CTE is primarily a function of the coefficient of thermal expansion of the concrete mixture’s constituent materials (Mitchell, 1953; Emanuel and Hulsey, 1977). Because of the volume of aggregates in concrete mixtures, the hardened concrete CTE is dominated by the CTE of the aggregate. Some common values of the CTE for concrete containing different types of aggregates are shown in Table 9-8. A change in the cementitious material properties such as fineness, type, and composition will also affect the CTE (Mitchell, 1953).

Materials change volume as the temperature changes because the temperature changes the attractive forces in molecular and atomic structures, as well as capillary stresses. It has been observed that concrete has a higher CTE when partially saturated than when oven-dry or saturated. The CTE reaches a maximum value between 60% and 80% relative humidity (Meyers, 1950; Mitchell, 1953; Emanuel and Hulsey, 1977; Walker, Bloem, and Mullen, 1952). As the water in capillary pores expands with temperature, the surface curvature and hence surface tension and capillary under pressure in the pores decrease. This surface tension induced volume change does not occur at oven-dry conditions or at saturated conditions because the pore has no air-water meniscus in these states (Bjøntegaard, 1999). When autogenous shrinkage occurs in concrete, the relative humidity will drop in the capillary pores to a limiting value of about 75% (Jensen and Hansen, 2001). The CTE will then rise because of the change in relative humidity (Hedlund, 2000), further increasing the development of thermal stresses.

Some researchers have found different coefficients for thermal expansion and contraction (Byfors, 1980; Emborg, 1989). The difference in measured coefficients may be explained by the changing mechanical properties of concrete at young ages, so that the concrete that is measured during the heating phase is different mechanically than that measured during cooling a short time later (Emborg, 1989). Differences between measured coefficients of thermal expansion and contraction may also be due to non-linear effects from differences in the CTE between the concrete and embedded strain gauges (Yamakawa, Nakauchi, Kita, and Onuma, 1986).

As the concrete hydrates, the coefficient of thermal expansion will change. The fresh concrete CTE is estimated to be 8-10 times greater than the hardened CTE (Schöppel and Springenschmid, 1994). There is debate about how the CTE changes during hydration. Kada et. al. (2002) measured a decrease in the CTE for a low w/cm mixture (0.30) during the first few hours after setting. The CTE then increased to a stable long term value. Mixtures with a w/cm of 0.35 and 0.4 both showed the CTE decreasing to assume a stable value at around 10 hours. The drop in the CTE and subsequent rise can be attributed to the reduction of relative humidity in the sample because of self-desiccation, which increases the CTE. Other researchers have found that the CTE decreases to an asymptotic long-term value (Byfors, 1980; Glisic, 2000). Hashida and Yamaziki (2002) have developed an equation to relate the time of final set to the coefficient of thermal expansion, as shown in Equation 9-64:

$$\alpha_{cte}(t) = a_1 \cdot \ln\left(\frac{t}{t_{fs}}\right) + b$$

Equation 9-64

where α_{cte} is the concrete coefficient of thermal expansion (με/°C), a_1 and b are fit parameters (με/°C), t is the time, and t_{fs} is the time of final set. The parameters a_1 and b are dependent on the w/cm, supplementary cementitious materials, cement type, and aggregates used.

ConcreteWorks uses a constant CTE, because of the lack of a data to model how the mixture proportions relate to CTE development. Because the CTE decreases very rapidly before the time of set, little loss in accuracy is expected from using a constant value except in the case of low w/cm where the CTE may increase after set and during curing. The constant coefficient of thermal expansion used in ConcreteWorks is calculated from the mixture proportions and the aggregate type using the method proposed by Emanual and Hulsey (1977) shown in Equation 9-65.

$$\alpha_{cteh} = \frac{\alpha_{ca} \cdot V_{ca} + \alpha_{fa} \cdot V_{fa} + \alpha_{p} \cdot V_{p}}{V_{ca} + V_{fa} + V_{p}}$$ **Equation 9-65**

where α_{cteh} is the hardened concrete CTE, α_{ca} is the coarse aggregate CTE (με/°C), V_{ca} is the coarse aggregate volume (kg/m^3), α_{fa} is the fine aggregate CTE (με/°C), V_{fa} is the fine aggregate volume (kg/m^3), α_p is the paste CTE (με/°C), and V_p is the paste volume (kg/m^3). In order to simplify the inputs, ConcreteWorks uses the assumed material specific gravity values for constituent materials shown in Table 9-9 in calculating the hardened concrete CTE. The assumed constituent material CTE values are shown in Table 9-10. Material coefficient of thermal expansion and specific gravity values can vary substantially, and may affect the calculated coefficient of thermal expansion value substantially. The values selected for use in ConcreteWorks were selected to represent typical, commonly used Texas materials. For more accurate results, it is suggested that the user test and input into ConcreteWorks the hardened concrete CTE of the specific materials used.

9.4.2.4 Autogenous Shrinkage Model

The volume of the cement hydration products is less than the volume of the cement and water before hydration. In low w/cm concrete, all of the water will be used to react with the cement. The unhydrated cement will then react with the water in the concrete pores, drying the pores and causing shrinkage. ConcreteWorks uses a modified version of the autogenous shrinkage model developed by Hedlund (2000). Hedlund developed a model based on his testing and that found in the literature for autogenous shrinkage starting at 24 equivalent age hours. The model is based on an ultimate autogenous shrinkage calculated from the w/cm which is altered to account for temperature effects. Equation 9-66 to Equation 9-69 show the equations proposed by Hedlund for calculating the autogenous shrinkage with the concrete equivalent age:

$$\varepsilon_{SH} = \varepsilon_{su} \cdot \beta_{s0}(t_e) \cdot \beta_{ST}(T)$$ **Equation 9-66**

$$\varepsilon_{su} = (-0.65 + 1.3 \cdot \frac{w}{cm}) \cdot 10^{-3}$$ **Equation 9-67**

$$\beta_{s0}(t_e) = \exp\left(-\left[\frac{t_{s1}}{t - t_{s0}}\right]^{\eta_{SH}}\right)$$ **Equation 9-68**

$$\beta_{ST}(T) = a_0 + a_1 \cdot \left[1 - \exp\left(-\left(\frac{T}{T_1}\right)^{b_1}\right)\right] + a_2 \cdot \left[1 - \exp\left(-\left(\frac{T}{T_2}\right)^{b_2}\right)\right]$$ **Equation 9-69**

where t_{s0} (days), t_{s1} (days), η_{SH}, a_0, a_1, a_2, b_1, b_2, T_1 (°C), and T_2 (°C) are fit parameters. Hedlund recommends setting the parameters t_{s1}, η_{SH}, a_0, a_1, b_1, b_2, T_1 (°C), and T_2 (°C) equal to 5 days, 0.3, 0.4, 0.6, 9 °C, 2.9, 55 °C, and 7, respectively. Additionally, he recommends setting the parameter a_2 equal to 1.3 for normal strength concrete and 0.1 for high performance concrete. The parameter t_{s0} is the time at which the concrete shrinkage begins. Before this time, the concrete autogenous shrinkage is set equal to zero (Hedlund, 2000).

The autogenous shrinkage model used in ConcreteWorks modifies the model developed by Hedlund to reduce the w/cm at which autogenous shrinkage develops, the time at which autogenous shrinkage begins, and does not include the temperature modification term. The ultimate concrete shrinkage value used in ConcreteWorks is calculated using Equation 9-70:

$$\varepsilon_{ault} = \left(-0.94 + 2.238 \cdot w / cm\right) \cdot 10^{-3}$$ **Equation 9-70**

The w/cm at which autogenous shrinkage develops in ConcreteWorks is 0.42, which corresponds to the theoretical w/cm at which complete hydration is possible (Mindess, Young and Darwin, 2003). Additionally, autogenous shrinkage begins at the virtual time-of-set, not at 24 equivalent age hours as in the Hedlund model. The autogenous shrinkage model will be improved in future versions of ConcreteWorks as more data and models become available.

9.4.3 ELASTIC STRESS AND DEGREE OF RESTRAINT

The restraint is needed at each point in the concrete member at each time step to be able to accurately model the stresses in the concrete. The restraint can be obtained by performing a structural analysis of the concrete member with non-uniform material properties across the cross-section. ConcreteWorks uses a plane strain finite-difference scheme to calculate the elastic stress in the member. The software considers the non-homogenous material development of the member by assuming a constant modulus and Poisson ratio for each control volume. The elastic modulus and Poisson ratio for each control volume is different, and are based on the maturity for the case of the elastic modulus and the degree of hydration for the Poisson ratio. The restraint case modeled for the rectangular column is the same as that shown in Figure 9-4, a two-dimensional horizontal cross section of the column. The restraint case modeled for the rectangular bent cap is the same as that shown in Figure 9-14, a two-dimensional vertical cross section of the cap. Footings are modeled assuming a two-dimensional cross section as shown in Figure 9-7, assuming a fixed base condition. The state of stress in the rectangular column and bent cap can be adequately represented using the two-dimensional models assumed because the stress in the third direction should be relatively small compared to the other two dimensions. The footing model however may deviate from the actual member stresses because the stress in the third dimension may not be small relative to the other two dimensions. Care should be taken in interpreting results from the footing model in ConcreteWorks. Improvements in the footing elastic stress calculation module are being considered for future versions of ConcreteWorks.

After the elastic stress is calculated, the elastic strain is then calculated using Hooke's law for plane strain cases, as shown in Equation 9-71 to Equation 9-73.

$$\varepsilon_x = \frac{\lfloor \sigma_x - \upsilon \cdot \sigma_y - \upsilon^2 \cdot (\sigma_x + \sigma_y) \rfloor}{E}$$ **Equation 9-71**

$$\varepsilon_y = \frac{\lfloor \sigma_y - \upsilon \cdot \sigma_x - \upsilon^2 \cdot (\sigma_x + \sigma_y) \rfloor}{E}$$ **Equation 9-72**

$$\varepsilon_{xy} = \frac{\sigma_{xy} \cdot 2 \cdot (1 + \upsilon)}{E}$$ **Equation 9-73**

where ε_x is the strain in the x direction, σ_x is the stress in the x direction (MPa), ν is the Poisson ratio, σ_y is the stress in the y direction (MPa), ε_y is the strain in the y direction, ε_{xy}

is the shear strain in the *xy* direction, σ_{xy} is the shear stress in the *xy* direction, and *E* is the elastic modulus (MPa).

9.4.4 EARLY-AGE CONCRETE CREEP MODEL

Creep may be defined as a time-dependent deformation during a constant stress. Stress relaxation may be defined as a time-dependent decrease in stress during a constant strain. Creep is applied to the stresses in the x, y and xy directions independently. The uniaxial constitutive equation for concrete creep is shown in Equation 9-74.

$$\varepsilon(t) = \int_0^t J(t,t_0) \cdot d\sigma(t_0) + \varepsilon_0(t)$$ **Equation 9-74**

where ε is the total strain, *t* is the time, t_0 is the time of the load application, $J(t,t_0)$ is the creep compliance, $d\sigma(t_0)$ is the stress imposed at time t_0, and ε_0 is the instantaneous or elastic response to the stress application.

Creep is applied to the elastic strains using the principle of superposition. The principle of superposition assumes that a step stress function is applied, with a corresponding strain response. The strain responses are then superimposed using the assumption of linearity as shown in Figure 9-39. The assumption of linearity is probably a valid assumption up to stress levels of about 40% (Emborg, 1998b). The two obvious problems with the approach used in ConcreteWorks are 1) the thermal stresses calculated in the model can exceed 40% of the tensile strength and 2) the model assumes linearity. The second assumption is a simplification necessary for simplicity and to reduce the runtime of the analysis. This assumption is definitely not true. Because the stresses in the member are relieved non-linearly by stress relaxation, the thermal stresses would redistribute in the member. These assumptions however do not preclude ConcreteWorks from being used in design. High tensile stresses should be avoided during the design stage to prevent damage from micro-cracking and potential through-cracks.

ConcreteWorks uses a modified version of the Linear Logarithmic Model for calculating the early-age concrete stress relaxation. The Linear Logarithmic Model was developed in Sweden by Larson (2003) to model early-age concrete creep. The method models the early-age concrete creep compliance function as a series or lines in log scale, as shown in Figure 9-40. The slope of the lines can be calculated using Equation 9-75 to Equation 9-78.

$$J(\Delta t_{load}, t_0) = \frac{1}{E(t_0)} + \Delta J(\Delta t_{load}, t_0)$$

Equation 9-75

$$\Delta J(\Delta t_{load}, t_0) = a_1 \cdot \log\left(\frac{\Delta t_{load}}{\Delta t_0}\right)$$

Equation 9-76

For $\Delta t_0 \leq \Delta t_{load} < \Delta t_1$

$$\Delta J(\Delta t_{load}, t_0) = a_1 \cdot \log\left(\frac{\Delta t_{load}}{\Delta t_0}\right) + a_2 \cdot \log\left(\frac{\Delta t_{load}}{\Delta t_0}\right)$$

Equation 9-77

For $\Delta t_{load} \geq \Delta t_1$

$$a_i(t_0) = a_i^{\min} + (a_i^{\max} - a_i^{\min}) \cdot \exp\left(-\left(\frac{t_0 - t_s}{t_{ai}} \right)^{n_{ai}} \right)$$ **Equation 9-78**

For i=1,2

where $J(\Delta t_{load}, t_0)$ is the creep compliance (1/Pa), $E(t_0)$ is the concrete elastic modulus at the time of load application, $\Delta J(\Delta t_{load}, t_0)$ is the change in creep compliance (1/Pa), Δt_{load} is the time since load application (days), t_0 is the time of load application (days), Δt_1 is the time of the change in creep compliance slope (days), t_s is the concrete time of set, a_i^{min}, a_i^{max}, t_{ai}, and n_{ai} are fit parameters. ConcreteWorks assumes that the time-of-set occurs when the concrete reaches a compressive strength of 80 psi (Tuthill and Cordon, 1955).

The Linear Logarithmic Model contains no creep compliance adjustment for changes in temperature. It is well known that the creep rate increases at elevated temperatures (Emborg, 1998a). The creep compliance can be modified by a temperature modification factor, as shown in Equation 9-79 (Emborg, 1998a):

$$J(t, t_0, T) = \Phi_c(T) \cdot J(t, t_0)$$ **Equation 9-79**

where $J(t,t_0,T)$ is the temperature adjusted creep (1/Pa), T is the absolute temperature (K), and $\Phi_c(T)$ is the creep modification adjustment factor. ConcreteWorks uses a temperature modification factor based on the empirical temperature adjustment parameter suggested by Bažant and Panula (1978) as shown in Equation 9-80 through Equation 9-84, where Equation 9-81 to Equation 9-84 come from Bažant and Panula:

$$\Phi_c(T) = 1 + \frac{C_T}{C_{TMF}}$$ **Equation 9-80**

$$C_T = c_T \cdot \tau_T \cdot c_0$$ **Equation 9-81**

$$c_T = \frac{19.4}{1 + \left(\frac{100}{T - 253.2}\right)^{3.5}} - 1$$ **Equation 9-82**

$$\tau_T = \frac{1}{1 + \left(\frac{60}{(t_T)^{0.69}}\right)} + 0.78$$ **Equation 9-83**

$$c_0 = \left(\frac{1}{8}\right) \cdot \left(\frac{w}{cm}\right)^2 \cdot \left(\frac{a}{cm}\right) \cdot a_1$$ **Equation 9-84**

where C_{TMF} is a fit parameter equal to 2.5, t_T is the concrete age at the time the temperature is applied, w is the water content (kg/m^3), cm is the cementing materials content (kg/m^3), a is the aggregate content (kg/m^3), a_1 is a constant that accounts for the type of cement used.

9.4.4.1 Creep Parameter Estimates

The creep parameters used in ConcreteWorks are based on a statistical model developed from early-age rigid cracking frame tests on 36 different concrete mixtures. A few of these mixtures were tested under several different temperature histories, in order to quantify the effects of temperature on concrete early-age creep. The creep parameters t_{a1}, t_{a2}, and n_{a2} are calculated from the concrete mixture proportions and constituent material properties according to Equation 9-85 to Equation 9-87 when the Rietveld method (Rietveld, 1969) of determining the cement composition is used as already described in Chapter 6:

$$t_{a1} = 0.680 + 0.0064 \cdot FA + 0.429 \cdot \ln(w/cm) - 0.00965 \cdot Ferrite \qquad \textbf{Equation 9-85}$$

$$t_{a2} = \exp(3.671 - 0.0192 \cdot (FA + GGBFS) - 3.7169 \cdot w/cm - \\ 0.10078 \cdot (Gypsum + Hemihydrate + Anhydrite + Arcanite) - \\ 0.0556 \cdot Ferrite) \qquad \textbf{Equation 9-86}$$

$$n_{a2} = \exp(-26.735 + 0.0705 \cdot FA + 0.072 \cdot GGBFS + \\ 6.586 \cdot \ln(Alite) - 0.177 \cdot Ferrite - 0.253 \cdot Alum + 5.194 \cdot w/cm) \qquad \textbf{Equation 9-87}$$

where *FA* is the percent fly ash replacement of cement by mass, *w/cm* is the water to cementing materials ratio, *Ferrite* is the percent ferrite of the cement, as determined by Rietveld analysis, *GGBFS* is the percent grade 120 ground granulated blast furnace slag replacement of cement by mass, *Gypsum* is the percent gypsum of the cement, as determined by Rietveld analysis, *Hemihydrate* is the percent hemihydrate in the cement, as determined by Rietveld analysis, *Anhydrite* is the percent anhydrite in the cement, as determined by Rietveld analysis, *Alite* is the percent alite in the cement, as determined by Rietveld analysis, and *Alum* in the percent aluminate in the cement as determined by Rietveld analysis. When a supplementary cementing material is used, the percent values used of the cement chemistry are the percent of the material in the cement times the percent cement of the total cementing materials.

When the Bogue method (ASTM C 150) of determining the cement composition is used, Equation 9-88 to Equation 9-90 are used to relate the mixture proportions and constituent material properties to the early age MLLM creep parameters t_{a1}, t_{a2}, n_{a2} as already described in section 9.6:

$$t_{a1} = 0.728 + 0.0061 \cdot FA + 0.448 \cdot \ln(wcm) - 0.0111 \cdot C_4AF$$ **Equation 9-88**

$$t_{a2} = \exp(3.436 - 0.0179 \cdot (FA + GGBFS) - 3.404 \cdot wcm \\ - 0.0186 \cdot C_2S - 0.0566 \cdot C_4AF)$$ **Equation 9-89**

$$n_{a2} = \exp(6.165 - 0.0541 \cdot FA - 0.0619 \cdot GGBFS - 0.00869 \cdot cement \\ - 0.425 \cdot C_3A - 0.572 \cdot C_4AF + 0.0107 \cdot CemBlaine)$$ **Equation 9-90**

where C_4AF is the percent C_4AF of the cement, as calculated using the Bogue method, C_2S is the percent C_2S of the cement, as calculated using the Bogue method, C_3A is the percent C_3A of the cement, as calculated using the Bogue method, *cement* is the total amount of cementing materials used in lb/yd^3, and *CemBlaine* is the cement Blaine fineness (m^2/kg). When a supplementary cementing material is used, the percent values used of the cement chemistry are the percent of the material in the cement times the percent cement of the total cementing materials. The remainders of the MLLM creep parameters are kept constant, according to Table 9-11.

9.4.5 CRACKING POTENTIAL

In ConcreteWorks, the cracking potential classification of a concrete member is based on the calculated tensile stress-to-tensile strength ratio. The concrete tensile stress-to-tensile strength ratio calculated in the software is assigned a cracking probability classification using the probability density shown in Figure 9-41. The cracking probability density was obtained from the distribution of the tensile stress-to-splitting tensile strength at cracking in the rigid cracking frame tests performed.

A lognormal distribution is assumed to model the relationship between the stress-to-strength ratio and the probability of cracking. A 25% or lower cracking probability is assumed to be low, a 25 to 50% cracking probability is assumed to be moderate, a 50 to 75% is assumed to be high, and higher than a 75% cracking probability is assumed to be a very high cracking probability. A lognormal distribution is used instead of a normal distribution because the tensile stress and splitting tensile strength are both positive quantities.

9.5 Chloride Service-Life Modeling

ConcreteWorks contains a chloride diffusion service life model for mass concrete and bridge decks. The model is based on Fick's second law of diffusion, as shown in Equation 9-91 (Incropera and Dewitt, 2002):

$$\frac{\partial}{\partial x}\left(D_c\frac{\partial c}{\partial x}\right)+\frac{\partial}{\partial y}\left(D_c\frac{\partial c}{\partial y}\right)+\frac{\partial}{\partial z}\left(D_c\frac{\partial c}{\partial z}\right)=\frac{\partial c}{\partial t}$$ **Equation 9-91**

where D_c is the concrete diffusion coefficient (m^2/s), and c is the chloride concentration (%). Equation 9-91 assumes that the concrete is uncracked, saturated, the density is constant, and that diffusion is the only mass transport mechanism (the mass transport from any temperature gradient or pressure gradient is negligible). A comparison of Equation 9-8 and Equation 9-91 shows that the mechanisms for heat transport and mass transport are similar and may be calculated using the same numerical scheme.

The concrete service life can be modeled using a simplified corrosion damage model proposed by Tuutti (1982), as shown in Figure 9-42. The concrete is assumed to be undamaged during a corrosion initiation period. The corrosion initiation period ends when a threshold chloride concentration is reached, indicating that the protective steel passive layer has been broken down and corrosion has initiated. After the corrosion has initiated, damage in reinforcing bars is assumed to occur linearly with time. The propagation period for reinforcing bars is assumed to occur over a period of 6 years. Prestressed strand service life is assumed to end when the chloride threshold is reached because of the increased consequences of strand failure and higher rates of corrosion in the highly stressed strands.

The service life model used in ConcreteWorks assumes that the concrete is uncracked, and that the chloride ingress occurs only through diffusion. The concrete structure's service life will be lower than that predicted if joints are not properly sealed, cracks occur and are not sealed properly, if the service conditions or materials used differ significantly from those used in the software inputs, or if the concrete is not cured properly. Significant engineering judgement is needed in ensuring that the software results, including the software limitations, are applied properly.

9.5.1 DIFFUSION COEFFICIENT

The diffusion coefficient for concrete changes as the concrete hydration progresses and the porosity decreases. Both the total amount of porosity and the interconnectedness of the porosity play a significant role in concrete mass transport. Concrete diffusivity will decrease as hydration progresses and the pore size distribution changes and the network of pores becomes more discontinuous. This decrease in porosity and consequent diffusivity should decrease indefinitely; there is a limit to how much the concrete diffusivity can decrease. ConcreteWorks assumes that the concrete diffusion coefficient decays asymptotically to an ultimate value as shown in Equation 9-92 to Equation 9-94 (Michael D.A. Thomas, personal communication, Feb. 11, 2007). The ultimate diffusion coefficient value is shown in Equation 9-93. Elevated temperatures will increase the chloride diffusion, and may be approximated using an Arrhenius-type relationship. The concrete diffusion coefficient is multiplied by an Arrhenius temperature adjustment term as shown in Equation 9-94 (Bentz and Thomas, 2001).

$$D_t(t) = D_{28} \cdot \left(\frac{28}{t}\right)^m + D_{ult} \cdot \left(1 - \left(\frac{28}{t}\right)^m\right) \qquad \textbf{Equation 9-92}$$

$$D_{ult} = D_{28} \cdot \left(\frac{28}{36500} \right)^{m}$$ **Equation 9-93**

$$D_{tT}(t,T) = D_{t}(t) \cdot \exp\left[\frac{U}{R} \cdot \left(\frac{1}{T_{ref}} - \frac{1}{T} \right) \right]$$ **Equation 9-94**

where $D_t(t)$ is the concrete diffusion coefficient (m^2/s) at time t (days), D_{28} is the 28 day concrete diffusion coefficient (m^2/s), m is the concrete diffusion decay constant, U is the diffusion process activation energy which can be assumed to 35000 J/mol, R is the universal gas constant (8.314 J/K/mol), T_{ref} is the concrete diffusion coefficient reference temperature (293 K), and T is the temperature of the concrete (K). Figure 9-43 and Figure 9-44 show the effect of a change in the 28 day concrete diffusion coefficient D_{28} and the decay constant m on the concrete apparent diffusion coefficient.

ConcreteWorks uses a yearly temperature profile in Equation 9-94; this profile is calculated from the weather data files for the city selected. The value for each temperature point used in the yearly temperature profile is calculated as the average of the 24 hourly temperature points for the day selected. When the user selects 12 temperature points per year, the 12 temperature data points are calculated using the first day of each month. When the user selects 24 points per year, the 24 temperature data points are calculated using the first and fifteenth days of each month. When the user selects 52 temperature points per year, a temperature point is calculated for every 7 days.

All concrete bulk diffusion material models used in ConcreteWorks were developed by Dr. Michael Thomas at the University of New Brunswick based on tests performed according to ASTM C 1556. There are many differences in reported chloride diffusion values in the literature because of differences in material, testing conditions, and analysis method. Because the materials used were well characterized, the testing and analysis methods are known, and for consistency, only data collected at the University of Toronto and the University of New Brunswick were used in developing the concrete diffusion coefficient material models used in ConcreteWorks (Michael D.A. Thomas, personal communication, Feb. 11, 2007).

9.5.1.1 Water to Cementitious Materials Ratio

The water-to-cementitious materials ratio (w/cm) is a major factor determining the chloride diffusion coefficient. It is well known that the concrete porosity and, consequently, permeability decrease as the w/cm decreases (Mindess, Young and Darwin, 2003). The base 28-day diffusion coefficient D_{28} used in ConcreteWorks is calculated using the w/cm as shown in Equation 9-95:

$$D_{28} = 2.17 \cdot 10^{-12} \cdot e^{\frac{w/cm}{0.279}}$$ **Equation 9-95**

Figure 9-45 shows the test results from a study performed at the University of New Brunswick (UNB) and the University of Toronto (UT) used to model the effect of w/cm on the concrete 28-day bulk diffusion value. All of the tests shown in Figure 9-45 were cast with a Type I cement with 12% C_3A, with w/cm varying between 0.2 and 0.8, and cement contents varying between 225 and 725 kg/m^3 (Michael D.A. Thomas, personal communication, Feb. 11, 2007).

9.5.1.2 Supplementary Cementing Materials

Supplementary cementing materials can reduce the diffusivity of concrete by reducing the porosity and pore size distribution of concrete (Mindess, Young, and Darwin, 2003). Ultra-fine fly ash and silica fume will reduce the 28-day diffusivity by particle packing and the pozzolanic reaction, which will occur at a faster rate because of the high surface area. The effects of ultra fine fly ash and silica fume on concrete 28 day diffusivity are calculated in ConcreteWorks using Equation 9-96 and Equation 9-97:

$$\frac{D_{UFFA}}{D_{PC}} = 0.170 + 0.829e^{(-UFFA/6.07)}$$ **Equation 9-96**

$$\frac{D_{SF}}{D_{PC}} = 0.206 + 0.794e^{(-SF/2.51)}$$ **Equation 9-97**

where D_{UFFA} is 28-day diffusivity of concrete containing ultra fine fly ash (m^2/s), D_{PC} is the 28-day diffusivity of concrete containing no supplementary cementing materials (m^2/s), $UFFA$ is the percent replacement of cement with ultra fine fly ash, D_{SF} is the 28-day diffusivity of concrete containing silica fume (m^2/s), and SF is the percent replacement of cement with silica fume. The concrete diffusivity adjustments used for silica fume replacement are based on bulk concrete diffusivity tests performed using ASTM C 1556 and an immersion period of 35 days. The concrete diffusivity adjustments used for ultra-fine fly ash are based on bulk diffusivity tests using ASTM C 1556 using an immersion period of 40 days. Both silica fume and ultra-fine fly ash testing were performed at the University of New Brunswick and the University of Toronto (Michael D.A. Thomas, personal communication, Feb. 11, 2007).

Fly ash will reduce the later age concrete diffusivity due to the pozzolanic reaction, although there is no clear trend on the effect of fly ash on the young concrete (28-day) diffusivity. No model has yet been developed that can explain why some fly ashes will increase the 28-day concrete diffusivity while other will decrease it. Because of this inconsistency, fly ash is assumed to have no effect on the 28-day concrete apparent diffusivity. Fly ash will however increase the reduction in the concrete bulk diffusivity with time, as modeled using the concrete diffusivity *m* parameter. Ground granulated blast furnace slag will also increase the reduction in the concrete bulk diffusivity. A linear increase in the *m* parameter (which consequently reduces the concrete diffusivity with time) is used in ConcreteWorks as shown in Equation 9-98:

$$m = 0.26 + 0.4\left(\frac{FA}{50} + \frac{SG}{70}\right)$$

Equation 9-98

where *FA* is the percent cement replacement with fly ash, and *SG* is the replacement with ground granulated blast furnace slag (Michael D.A. Thomas, personal communication, Feb. 11, 2007).

9.5.2 CHLORIDE SURFACE CONCENTRATION

The chloride surface concentration is a major parameter in calculating the chloride concentration profile with time. For relatively constant boundary conditions, such as marine exposure conditions, the surface concentration can be accurately modeled. For structures such as bridge decks and parking garages, the surface concentration will vary dramatically, even in the same structure. The local conditions in the member may vary because of local differences in slope, proximity to drains, location relative to wheel-paths and deicer salt application, and local variability in materials. Chloride service life analysis can still be used as a design tool to compare the relative performance of different materials.

9.5.2.1 Chloride Surface Concentration Buildup

The concrete surface concentration will also change with time. The concrete surface level will be higher during the winter when deicer salts are applied to the road, and lower in the summer and after rain storms wash away some of the salt. A smooth curve may however be used as a good approximation of the seasonal surface chloride concentration build-up, as shown in the hypothetical surface chloride buildup and approximation in Figure 9-46.

ConcreteWorks uses a smooth curve to approximate the surface chloride according to Equation 9-99:

$$C_s(t) = C_{s\max} \cdot \frac{b \cdot t}{1 + b \cdot t}$$ **Equation 9-99**

where $C_s(t)$ is the chloride surface concentration with time t (years), C_{smax} is the maximum chloride surface concentration, and b is the chloride surface concentration build-up rate constant. The time t is not equal to zero at the time the concrete is placed, but at the age of the concrete when it is exposed to chlorides.

The maximum chloride surface concentration and build-up rate constant for each city used in ConcreteWorks are stored in a data file in the application's root directory. There are three possible structural classifications used in determining the maximum chloride surface concentration, Urban Bridge, Rural Bridge and Parking Garage, similar to those used in the software Life365 (Bentz and Thomas, 2001). If the city selected is near the ocean, the user will also have the option of selecting the structure to be in a marine splash zone, spray zone, within 0.5 miles of the ocean, and within 1 mile of the ocean. The maximum chloride surface concentration and build-up rate constants used in ConcreteWorks for marine exposure are shown in Table 9-12. ConcreteWorks uses the same maximum surface concentration values as found in the software package Life365, except for Florida. The build-up rate constants used in ConcreteWorks were determined by fitting the initial slope of the smooth curve used in ConcreteWorks to the initial slope of the bilinear surface concentration build-up used in Life-365. The build-up rate constant for a few of the cities available for selection in Texas were increased, while the build-up rate constants for the Florida cities were decreased to better reflect the amount of deicer salt actually used. Figure 9-47 shows the build-up rate constants used in ConcreteWorks. In order to determine the build-up rate constant for cities in ConcreteWorks that were not available in Life365, the annual snowfall for each city was compared to that of other cities in the same state for which values were available in Life365. This is expected to give a reasonable approximation for these cities, because states usually have uniform deicer salting policies. The maximum surface concentrations used for different exposure conditions corresponding to the build-up rate constant are shown in Table 9-13.

9.5.2.2 Membranes and Sealers

Membranes are modeled in ConcreteWorks by using an equivalent time approach. The equivalent age used in calculating the chloride surface concentration in Equation 9-99 is considered zero during the warranty period. After the warranty period ends, the membrane is assumed to degrade linearly. The change in the surface chloride build-up equivalent age for a time step during the membrane degradation period is assumed to follow Equation 9-100:

$$t_{esc} = \sum_{t_{ewp}}^{t_{edp}} \frac{(t - t_{ewp}) \cdot \Delta t}{t_{edp} - t_{ewp}}$$

Equation 9-100

where t_{esc} is the equivalent time for calculating the surface concentration (years), t_{ewp} is the time when the warranty period ends (years), t_{edp} is the time when the degradation period ends which is equal to the warranty period plus the degradation period (years), t is the real time, and Δt is the time step used. After the degradation period ends, the change in equivalent time for calculating the surface concentration is equal to the change in real time.

Sealers are also modeled using an equivalent time approach. Sealers are also assumed to degrade linearly, from being 100% effective at the time of application to 0% effective at the end of the degradation period. Sealers are assumed to be 100% effective again when reapplied. Figure 9-48 shows a comparison of the chloride surface concentration build-up without a membrane or sealer, with a membrane, and with a sealer used. In this case, the membrane is assumed to have a 10-year warranty period and a 10-year degradation period. The sealer is assumed to have a 5-year degradation period and is reapplied every 5-years.

9.5.3 CHLORIDE THRESHOLD

In ConcreteWorks, corrosion is assumed to initiate after the chloride concentration at the steel reaches a threshold value. A one-size fits all corrosion threshold value is certainly not valid. There are many different chloride threshold values published in literature. However, a comprehensive model for determining the chloride threshold value from the temperature, relative humidity, mixture proportions, and steel type used does not currently exist. A single chloride threshold value that is dependent on the type of steel chosen is a reasonable assumption for design. A chloride threshold value of 0.07% chloride by mass of concrete is used for black steel and epoxy coated steel (need references). A chloride threshold value of 0.7% chloride by mass of concrete is used for grade 316 Stainless steel.

ConcreteWorks contains inputs for two types of corrosion inhibitors, calcium nitrite based corrosion inhibitors or amines and esters. ConcreteWorks uses the same chloride threshold values as Life365 when a corrosion inhibitor is used, as shown in Table 9-14. Corrosion inhibitors in ConcreteWorks are only used in the cast-in-place concrete. This means that if the user selects a precast panel to be used with a bridge deck, the chloride threshold value of the steel in the precast panel does not change when a corrosion inhibitor is used in cast-in-place concrete above it. In addition, like in Life365, the diffusion coefficient is reduced by 10% and the chloride surface concentration build-up rate constant is also reduced by 50% when “amines and esters” is selected.

9.5.4 INITIAL CHLORIDE PROFILE

ConcreteWorks contains an option to model the chloride diffusion considering an initial chloride profile. This initial chloride concentration profile may be used because of the addition of a significant amount of chlorides in the concrete mixture (such as the ill-advised use of sea water instead of fresh water or the use of a calcium-chloride based admixture in reinforced concrete). Additionally, the initial chloride profile may be used to enter the chloride profile obtained from performing chloride profile grinding of the actual structure. Considerable engineering judgment should be used in performing this type of test and the subsequent service-life analysis. Chloride profile tests can be highly variable depending on the location in the structure because of local water runoff conditions and local variability in the concrete cover quality. When an existing structure is modeled, the age of the structure is added to the time used in determining the chloride surface concentration and the concrete diffusion coefficients. The default chloride surface concentration constants should be altered to account for the actual concrete chloride surface concentration and the expected future concentrations. This type of analysis should only be performed by those intimately familiar with the service life calculation methods used in ConcreteWorks and those with considerable experience in corrosion investigations. Additionally, if corrosion has already initiated, it is not recommended to use ConcreteWorks to estimate the remaining concrete service life.

Table 9-1- Software features available for each concrete member type

Member Type		Initial Chloride Profile Input for Existing Structures	Chloride Service Life	Thermal Cracking Probability	Temperature Prediction
Mass Concrete	Rectangular Column		X	X	X
	Rectangular Footing		X	X	X
	Partially Submerged Rectangular Footing		X	X	X
	Rectangular Bent Cap		X	X	X
	T-Shaped Bent Cap		X		X
	Circular Column		X		X
	Drilled Shaft		X		X
Precast Concrete Members	Box Beam (Type 5B40)				X
	Type IV I-Beam				X
	U40 Beam				X
	U54 Beam				X
Bridge Deck Types	Pre-cast 1/2 Depth Panels	X	X		X
	Permanent Metal Decking	X	X		X
	Removable Forms	X	X		X
	User-Defined	X	X		X
Pavements	User-Selected Layers				X

Table 9-2 – Concrete water requirement and coarse aggregate volume fit parameters based on the maximum size aggregate

Maximum Aggregate Size (in)	a_w (lb/yd³)	b_w ((lb/yd³)	a_{ca}
2	27.411	249.41	0.78
1.5	27.411	264.41	0.75
1	27.411	289.41	0.71
0.75	30.618	302.31	0.66
0.5	34.176	321.45	0.59
0.375	40.941	333.49	0.5

Table 9-3 - Range of water adjustment factors used in ConcreteWorks (Hover, 2003)

Factor	Water Adjustment Range (a negative value is a water reduction)	
ASTM Type A Low Range Water Reducer	0	-10
Mid-Range Water Reducer	-8	-15
ASTM Type F High Range Water Reducer	-12	-30
Air Entrainment	0	-10
Aggregate Shape & Texture	5	-5
Aggregate Gradation	-10	10
Supplementary Cementing Materials	-10	15

Table 9-4 - Corners of box of acceptable mixtures for Shilstone Coarseness Factor-Workability Factor aggregate gradation method (TxDOT Special Provision 421)

Corner #	Coarseness Factor	Workability Factor
1	68	36
2	68	32
3	52	38
4	52	34

Table 9-5 - Chemical admixture dosages assumed in ConcreteWorks

Chemical Admixture	Dose by Mass of Cementing Materials (%)
LRWR	0.0029
WRRET	0.0035
MRWR	0.0032
NHRWR	0.0078
PCHRWR	0.0068
ACCL	0.013

Table 9-6 - Footing subbase material thermal properties

Subbase Material	Density (kg/m3)	Thermal Conductivity (W/m/K)	Specific Heat (J/kg/K)	Reference
Clay	1460	1.3	880	Incropera and Dewitt, 2002
Granite	2630	2.79	775	
Limestone	2320	2.15	810	
Marble	2680	2.8	830	
Quartzite	2640	5.38	1105	
Sandstone	2150	2.9	745	
Sand	1515	0.27	800	
Top Soil	2050	0.52	1840	
Concrete	-	-	-	

Note: Concrete is assumed to have the same thermal properties of the concrete used on the footing, with a degree of hydration equal to 0.6. This option is only available with rectangular footings without soil on the sides.

Table 9-7 - Pavement subbase material properties

Material	Thermal Conductivity (W/m^2)	Specific Heat (J/kg/°C)	Density (kg/m^3)	Solar Absorptivity	Emissivity
Asphalt Concrete	1.38	1047	2302	0.93	0.93
Cement Stabilized Base	0.985	985	2101	0.65	0.9
Asphalt Stabilized Base	0.865	1025	2002	0.9	0.9
Granular Base	1.59	1214	2066	0.8	0.9
Existing Concrete	2.7	921	2403	0.55	0.92

Table 9-8 - Coefficient of thermal expansion for concretes made with different aggregates (Bamforth and Price, 1995)

Aggregate Type in Concrete	Coefficient of Thermal Expansion (m/m/°C)	Coefficient of Thermal Expansion (in/in/°F)
Siliceous River Gravel	12.0	6.7
Granite	10.0	5.6
Limestone	8.0	4.4
Lightweight	7.0	3.9

Table 9-9 - Concrete constituent materials assumed specific gravity values

Material	Specific Gravity
Water	1
Cement	3.14
Class F Fly Ash	2.4
Class C Fly Ash	2.7
Slag	2.87
UFFA	2.57
Silica Fume	2.2
Coarse Aggregate	2.65
Fine Aggregate	2.65

Table 9-10 - Concrete constituent materials' assumed CTE

Material	Coefficient of Thermal Expansion values used in ConcreteWorks (με/°C)	Coefficient of Thermal Expansion from Emanuel and Hulsey, 1977 (με/°C)
Hardened Cement Paste	10.8	10.8
Limestone Aggregate	3.5	3.5 - 6
Siliceous River Gravel and Sand	11	11 – 12.5
Granite Aggregate	7.5	6.5 – 8.5
Dolomitic Limestone Aggregate	7	7 - 10

Table 9-11 – Modified Linear Logarithmic Model Parameters assumed to remain constant in ConcreteWorks

Modified Linear Logarithmic Model Parameter	Value	Units
Δt_0	0.001	days
Δt_1	0.1	days
a_1^{min} $(*10^{-12})$	0.1	1/Pa
a_1^{max} $(*10^{-12})$	60	1/Pa
n_{a1}	1.19	
a_2^{min} $(*10^{-12})$	5	1/Pa
a_2^{max} $(*10^{-12})$	30	1/Pa

Table 9-12 - Chloride surface concentration constants used in ConcreteWorks for marine exposure

Exposure condition	Maximum surface concentration (%)	Build-up rate constant
Splash zone	0.8	Instantaneous
Spray zone	1	0.15
Within 0.5 miles of ocean	0.6	0.06
Within 1 mile of ocean	0.6	0.03

Table 9-13 - Build-up rate constants with their corresponding maximum surface concentration values used in ConcreteWorks

Build-up Rate Constant	Parking Garage Maximum Surface Concentration, C_{smax}	Urban Road Maximum Surface Concentration, C_{smax}	Rural Road Maximum Surface Concentration, C_{smax}
0.0045	0.8	0.68	0.56
0.018	0.8	0.68	0.56
0.03	0.8	0.68	0.56
0.04	0.8	0.68	0.56
0.06	0.8	0.68	0.56
0.07	0.8	0.68	0.56
0.09	0.8	0.68	0.56
0.11	0.8	0.68	0.56
0.12	0.8	0.68	0.56
0.14	0.8	0.68	0.56
0.17	0.8	0.68	0.56
0.20	1.0	0.85	0.7
0.21	1.0	0.85	0.7
0.24	1.0	0.85	0.7

Table 9-14 - Chloride Threshold Values Assumed for Black Steel based on Corrosion Inhibitor Dose

Corrosion Inhibitor and Dosage	Chloride Threshold Value (% of Concrete)
Calcium Nitrite at 10 L/m^3	0.15
Calcium Nitrite at 15 L/m^3	0.24
Calcium Nitrite at 20 L/m^3	0.32
Calcium Nitrite at 25 L/m^3	0.37
Calcium Nitrite at 30 L/m^3	0.40
Amines and Esters at 5 L/m^3	0.12

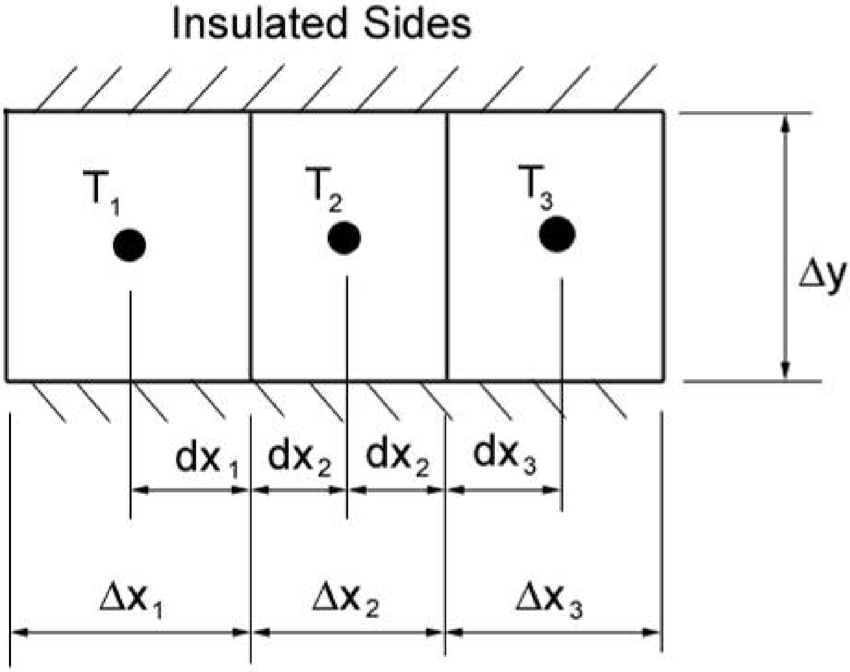

Figure 9-1- Control volume example - three neighboring nodes

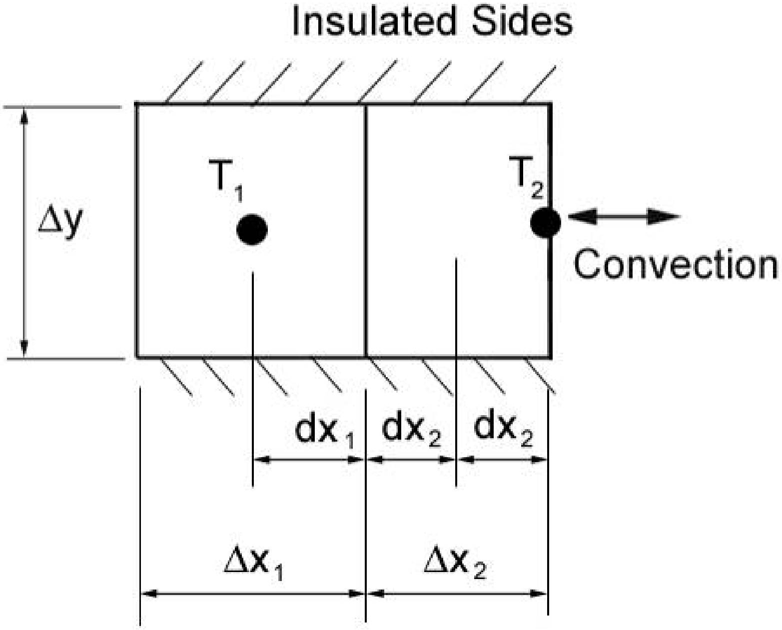

Figure 9-2 - Example of control volume with a convection boundary condition

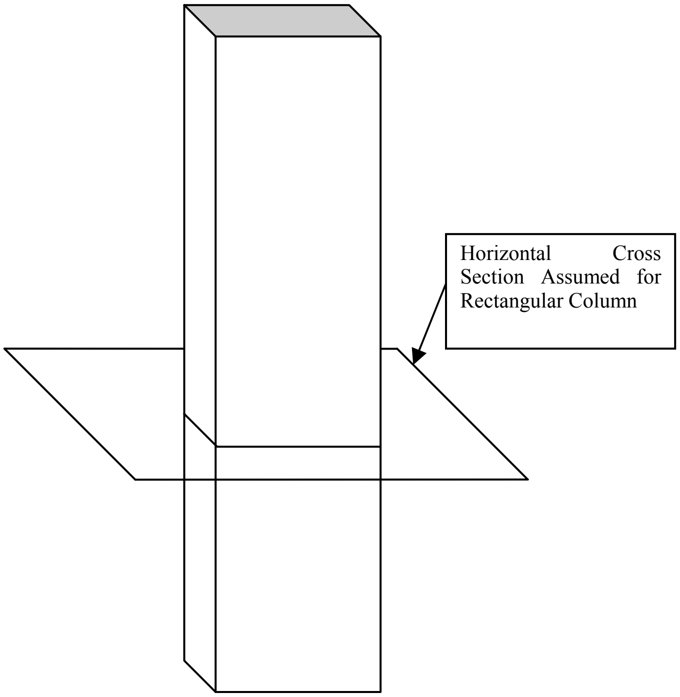

Figure 9-3 – Horizontal cross-section of rectangular column assumed in ConcreteWorks

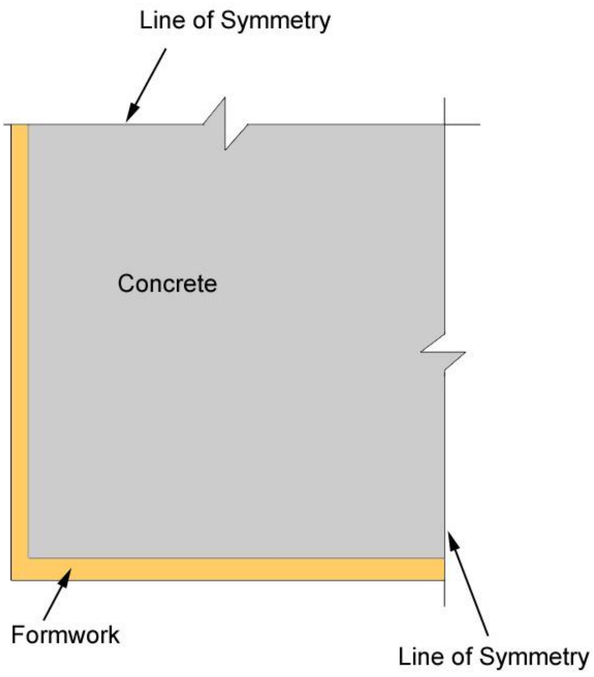

Figure 9-4 - Simplified rectangular column model used in ConcreteWorks

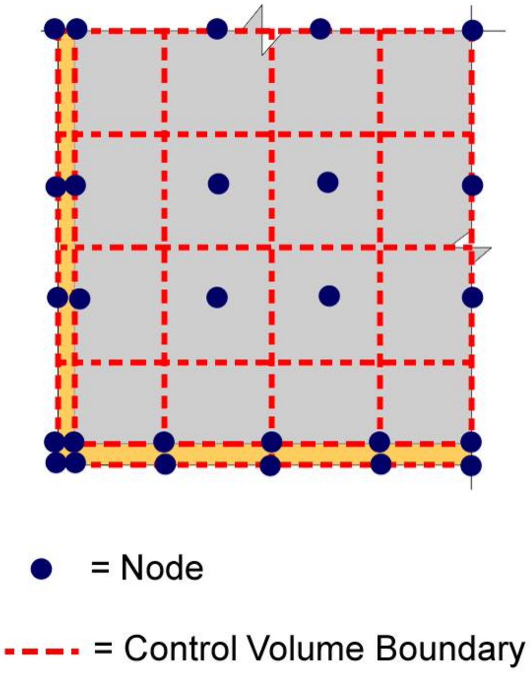

Figure 9-5 - Example rectangular column node and control volumes

Figure 9-6 - Rectangular column during form removal and the beginning of construction stage two

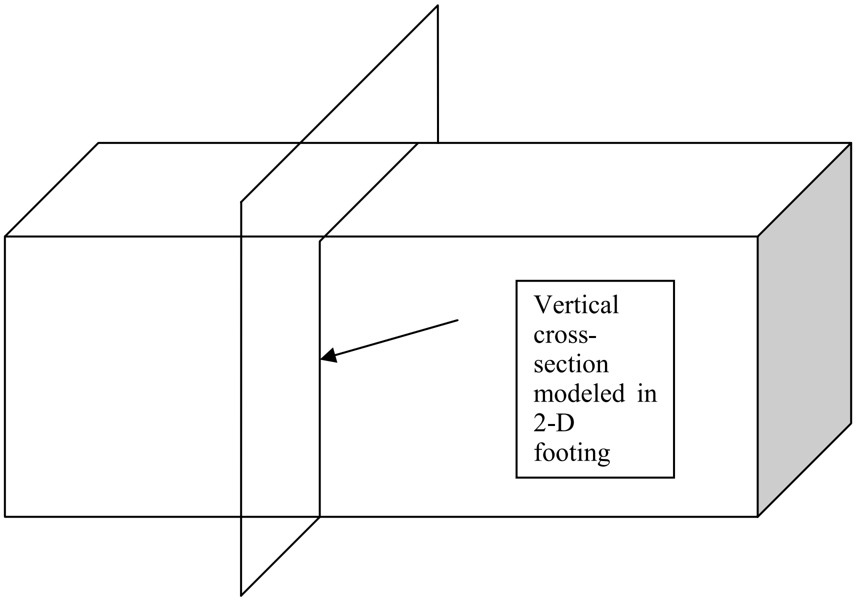

Figure 9-7 – Diagram of the vertical cross-section assumed in modeling a 2-D footing

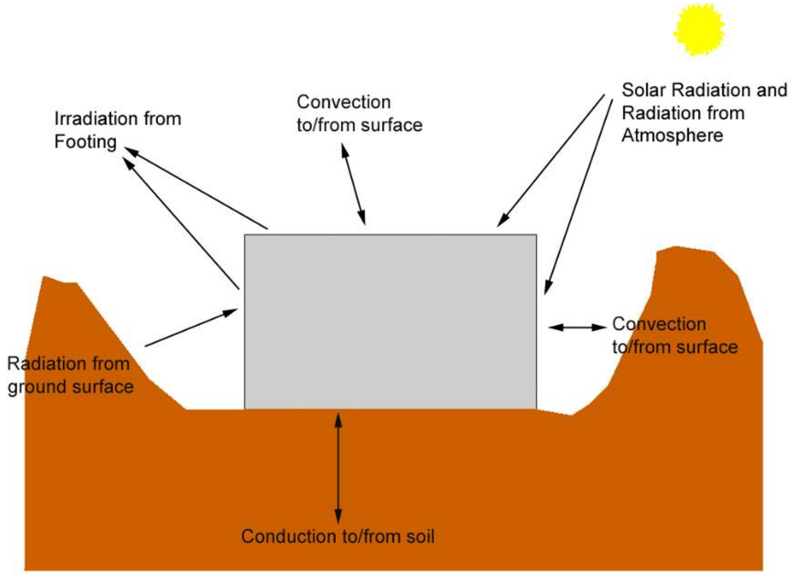

Figure 9-8 - Summary of rectangular footing boundary conditions

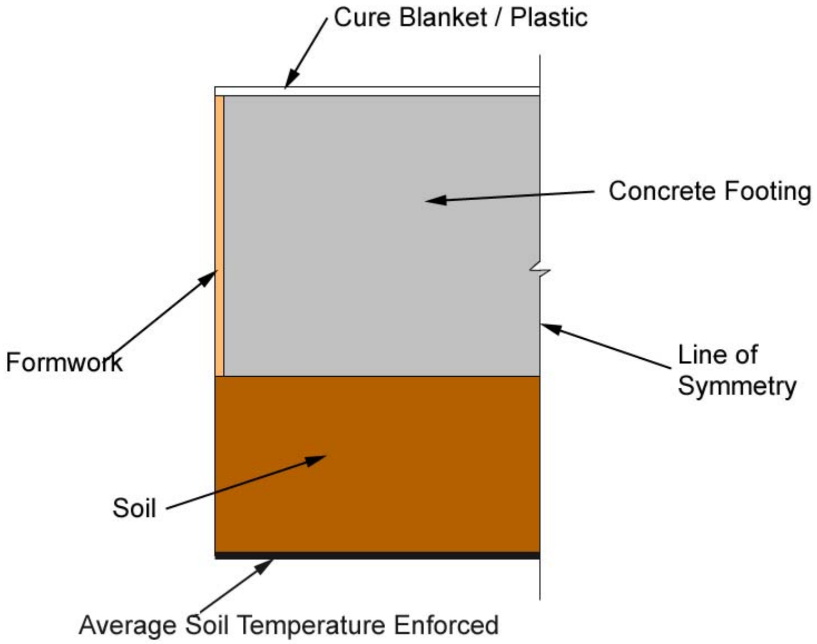

Figure 9-9 - Rectangular footing model

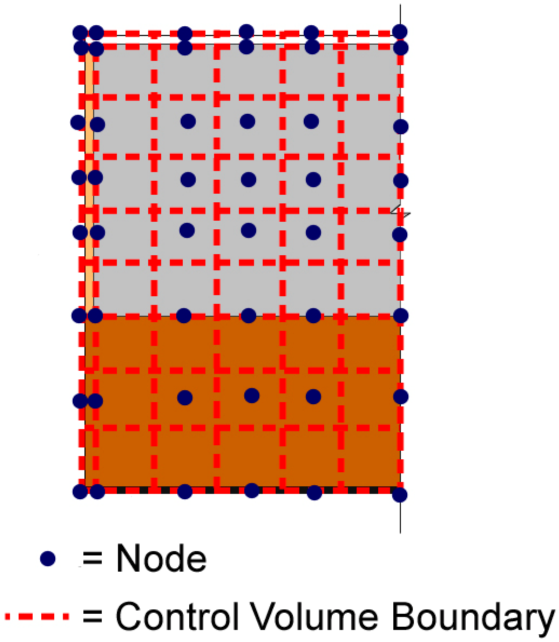

Figure 9-10 - Node layout for rectangular footing

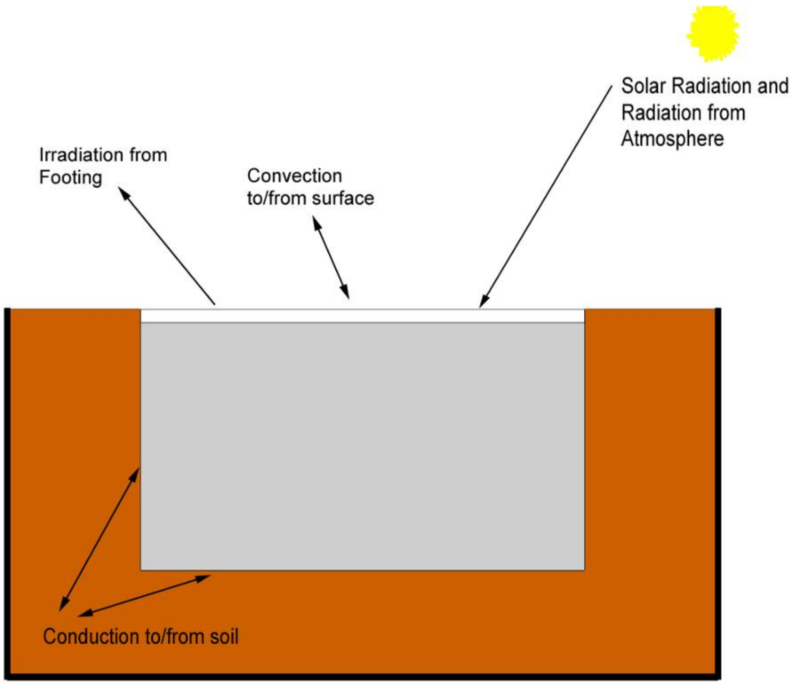

Figure 9-11 – Summary of rectangular footing with soil on the sides

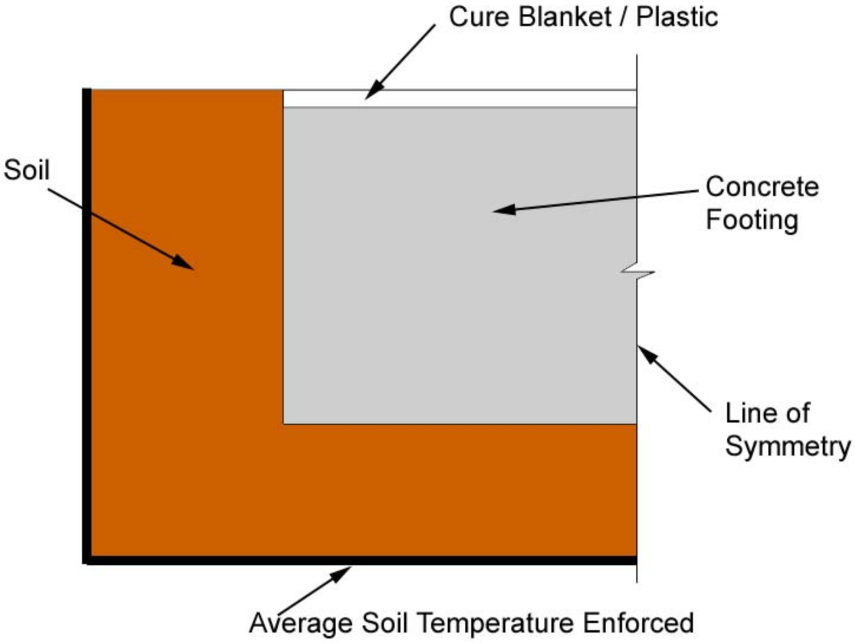

Figure 9-12 – Rectangular footing with soil on sides model

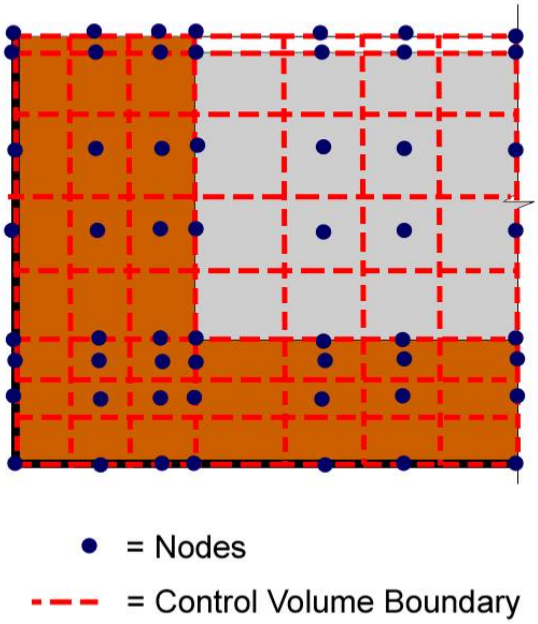

Figure 9-13 - Node and control volume layout for rectangular footing with soil on the sides

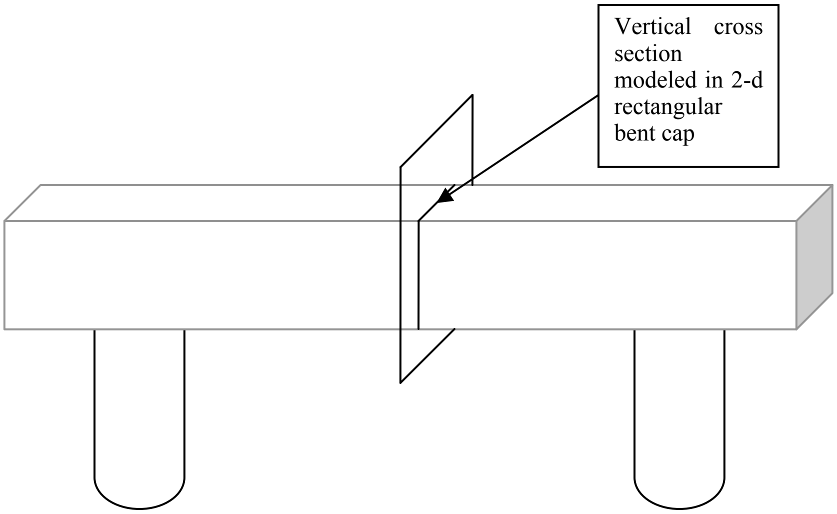

Figure 9-14 –Diagram of the vertical cross section modeled in a rectangular bent cap

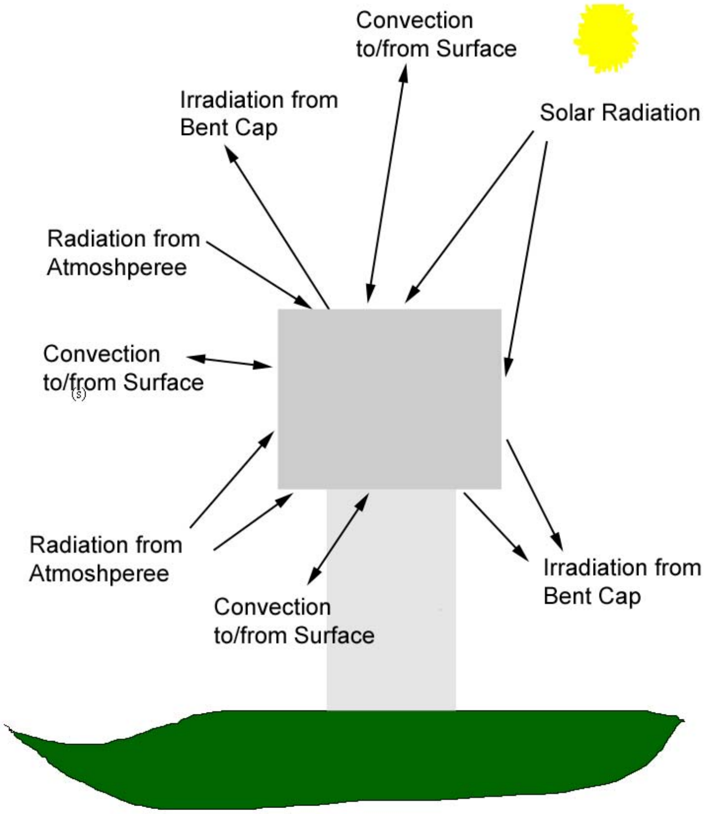

Figure 9-15 -Rectangular bent cap radiation summary

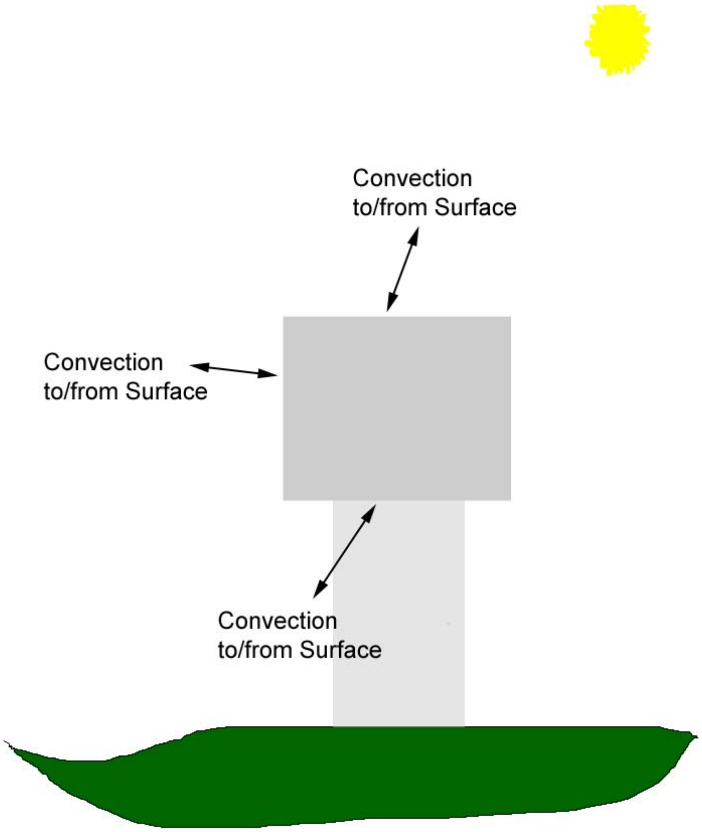

Figure 9-16 -Rectangular bent cap convection summary

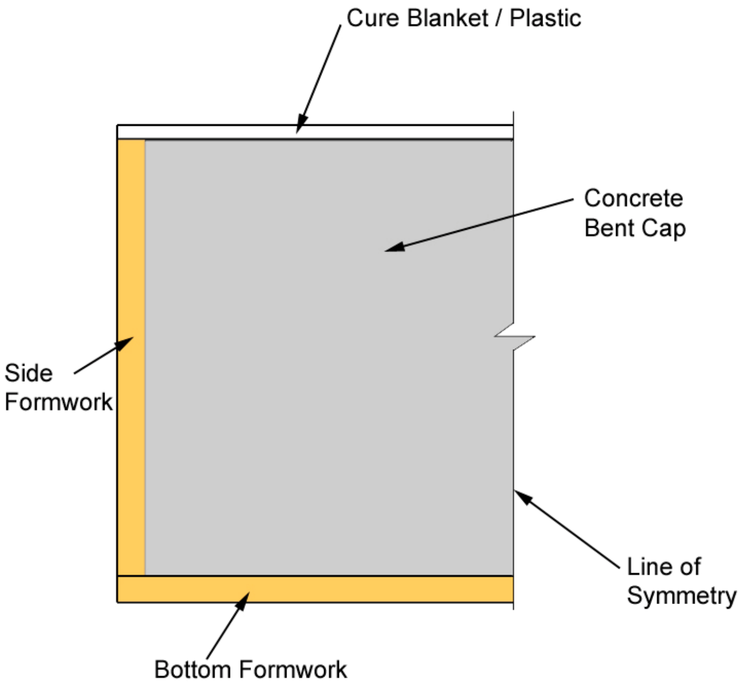

Figure 9-17 – Summary of rectangular bent cap

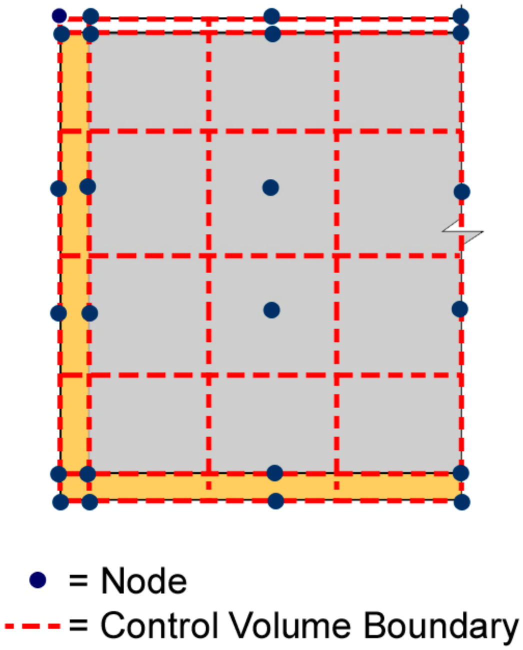

Figure 9-18 - Node and control volume layout of rectangular bent cap

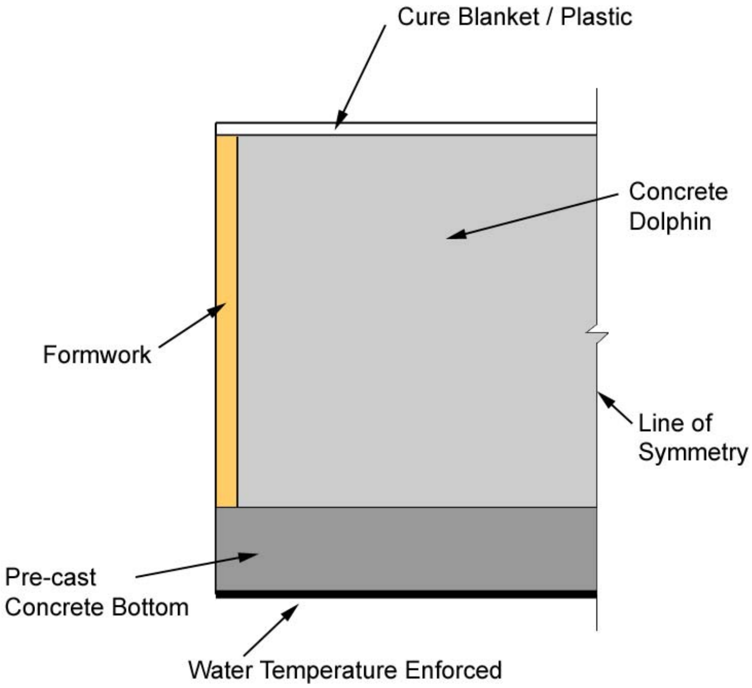

Figure 9-19 - Summary of dolphin with pre-cast concrete bottom

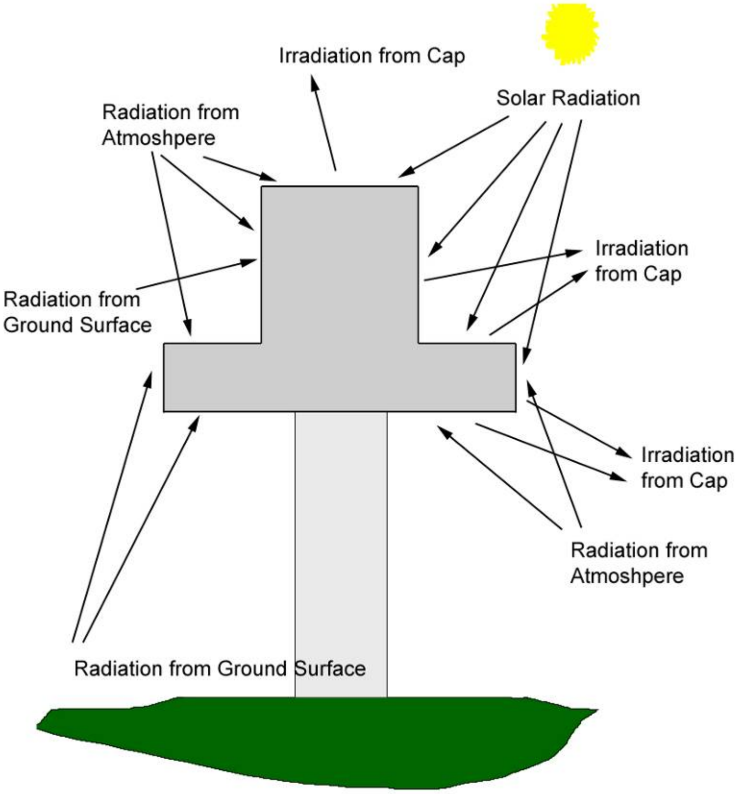

Figure 9-20 - Summary of radiation boundary conditions for T-shaped bent caps

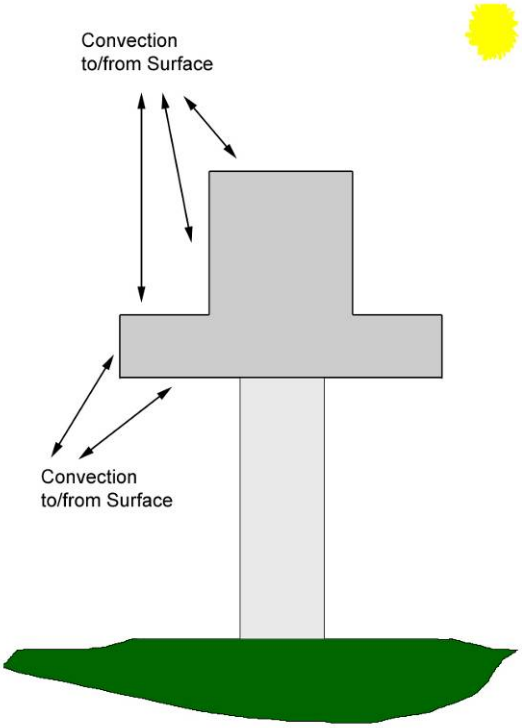

Figure 9-21 - Summary of convection boundary Conditions on T-shaped bent cap

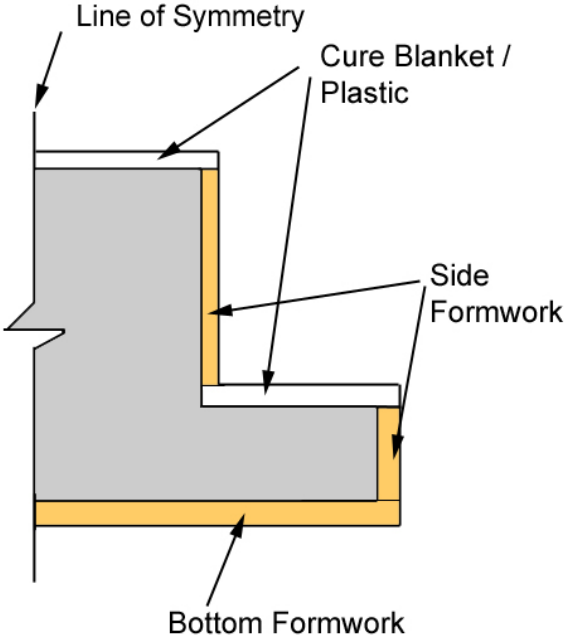

Figure 9-22 - Construction summary form T-shaped bent cap

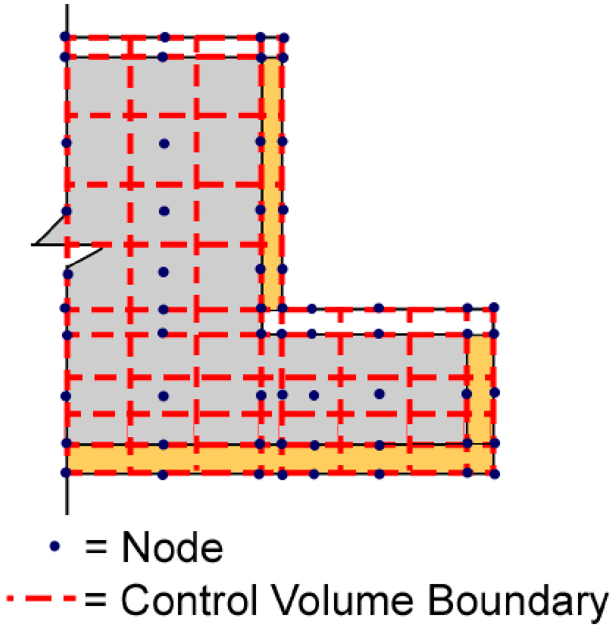

Figure 9-23 - Node and control volume layout for T-shaped bent caps

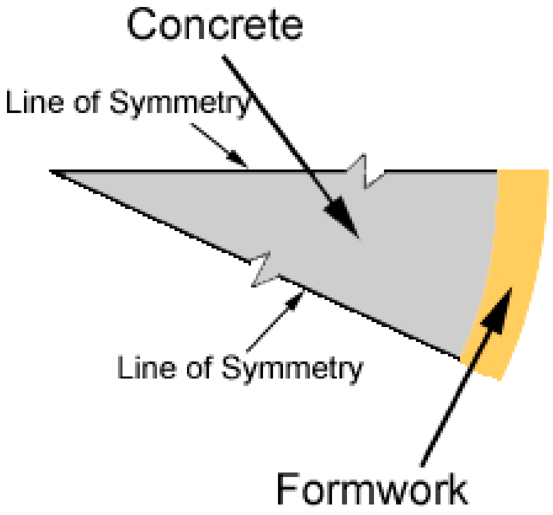

Figure 9-24 - Circular column model

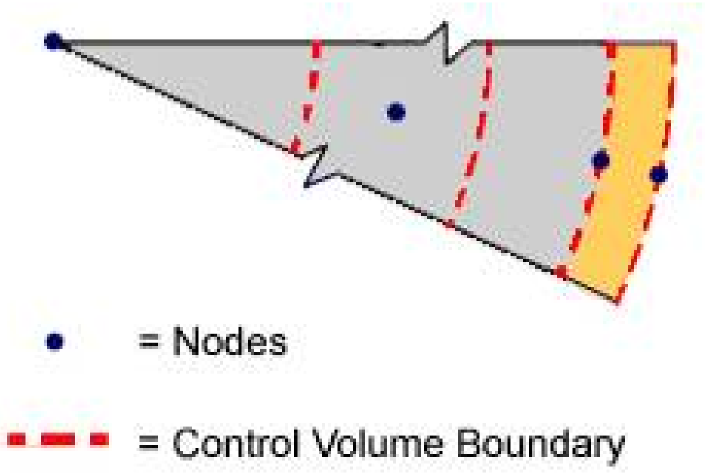

Figure 9-25 - Node and control volume layout for circular columns

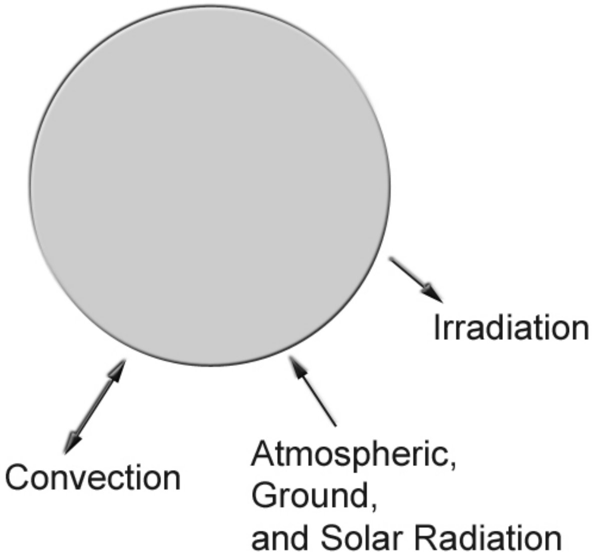

Figure 9-26 - Circular column boundary conditions

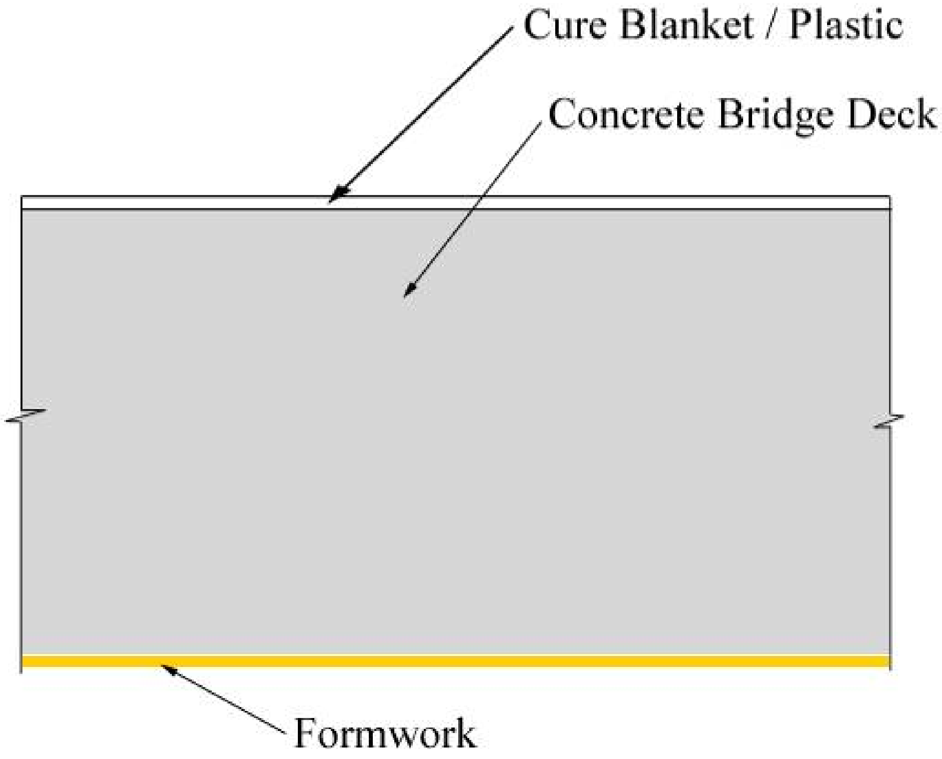

Figure 9-27 - Bridge deck layout

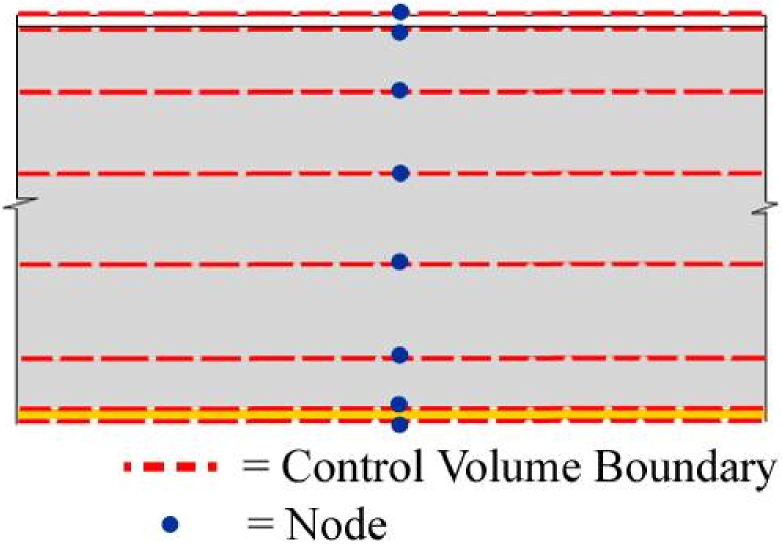

Figure 9-28 - Bridge deck node and control volume layout

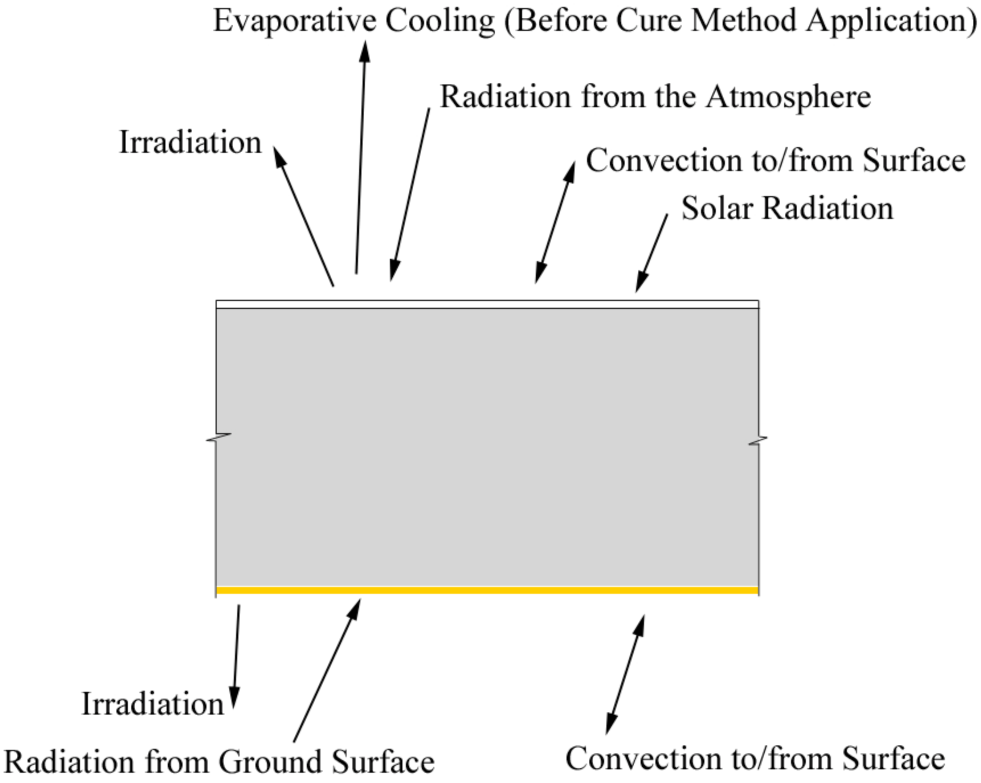

Figure 9-29 - Bridge deck temperature boundary conditions

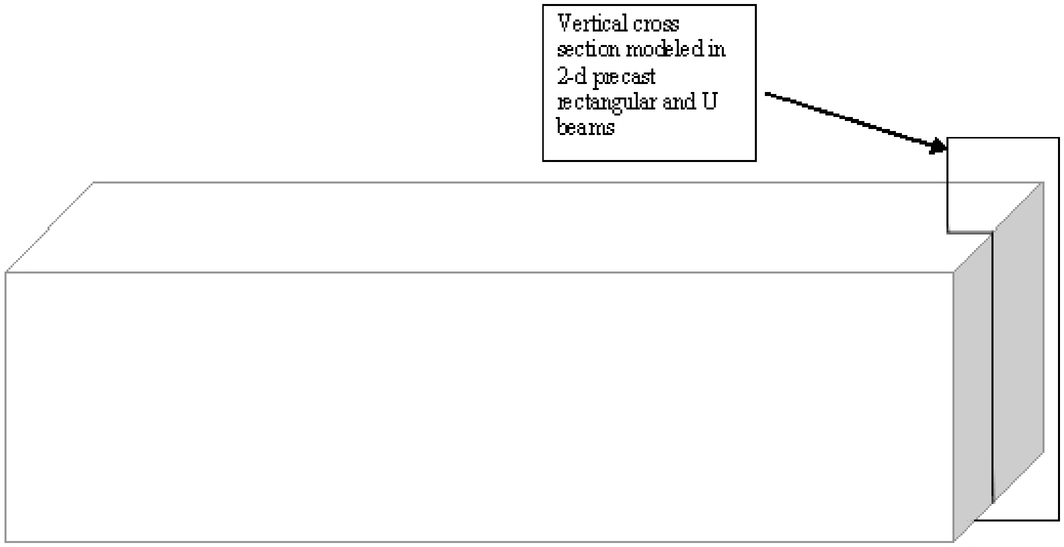

Figure 9-30 - Modeled region of rectangular and U-shaped beams

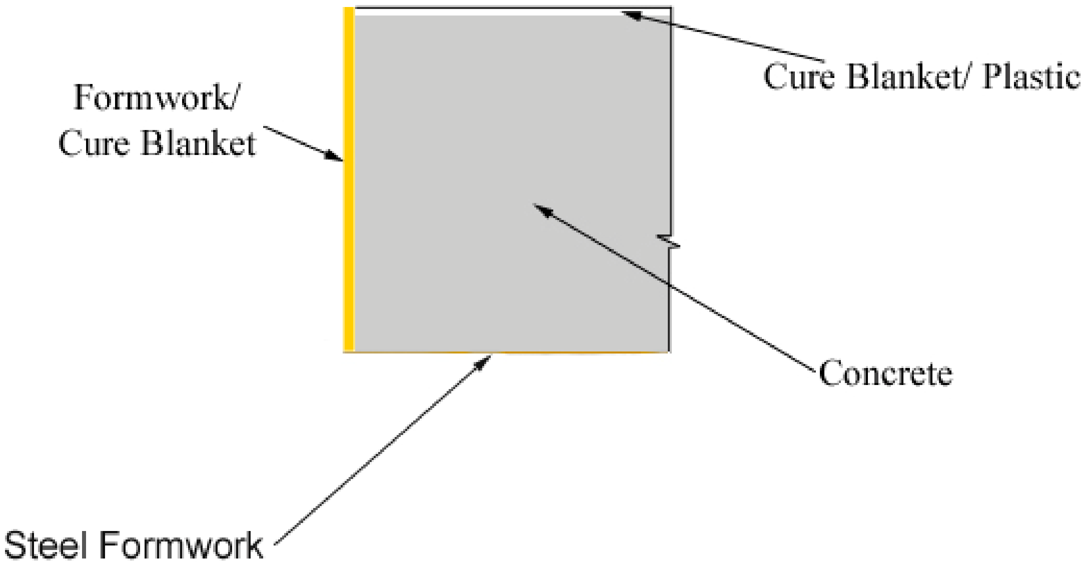

Figure 9-31 - ConcreteWorks simplified model for rectangular and U-shaped beams

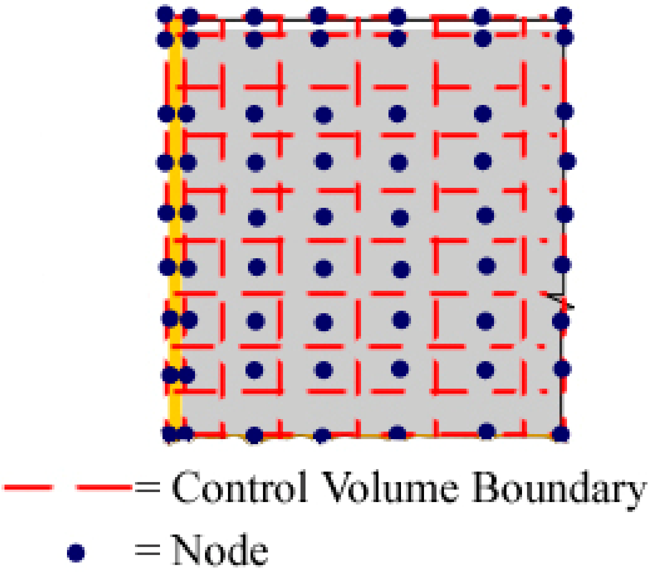

Figure 9-32 - Rectangular and U-shaped beam node and control volume layout

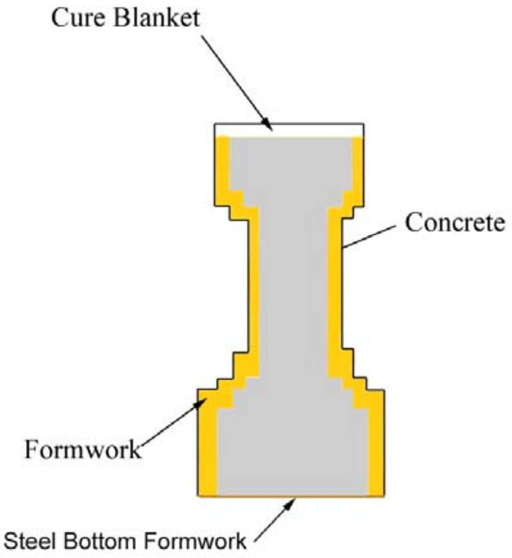

Figure 9-33 - Precast type IV beam model assumed in ConcreteWorks

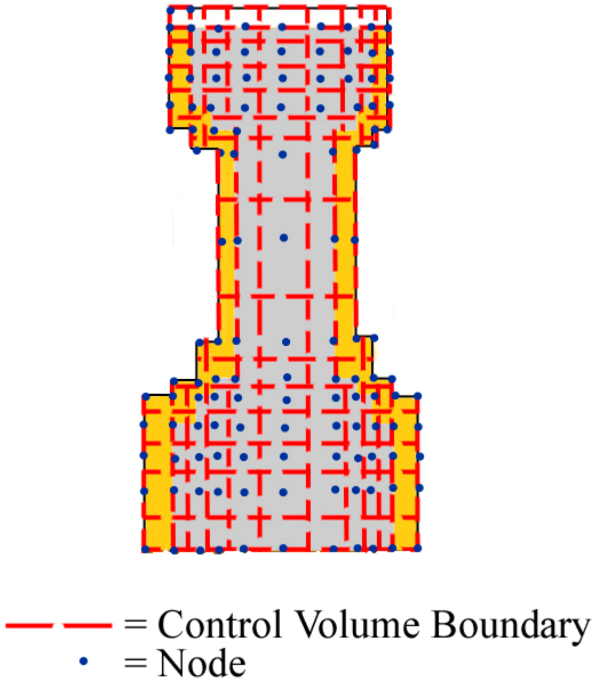

Figure 9-34 - Precast type IV beam node and control volume boundary layout

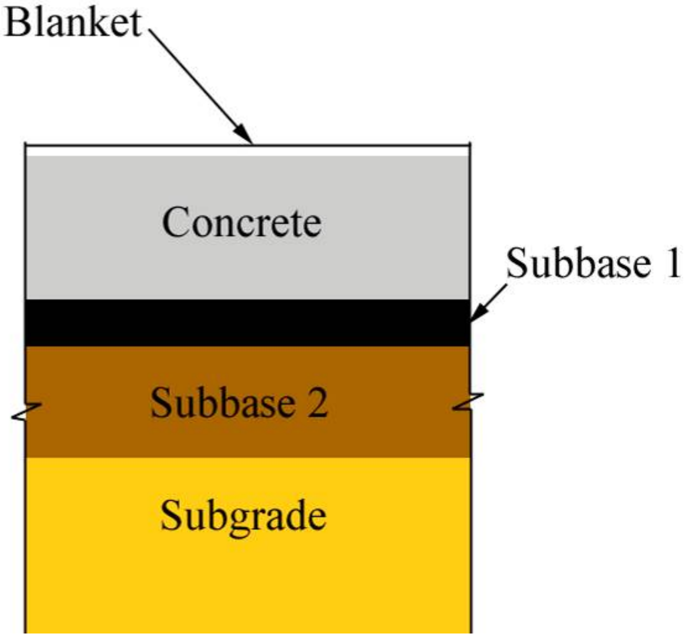

Figure 9-35 - Pavement layers modeled

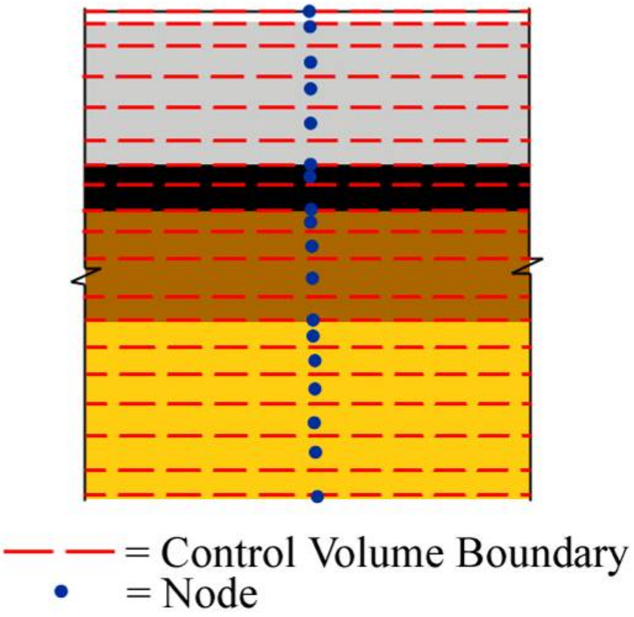

Figure 9-36 - Pavement node and control volume boundary layout

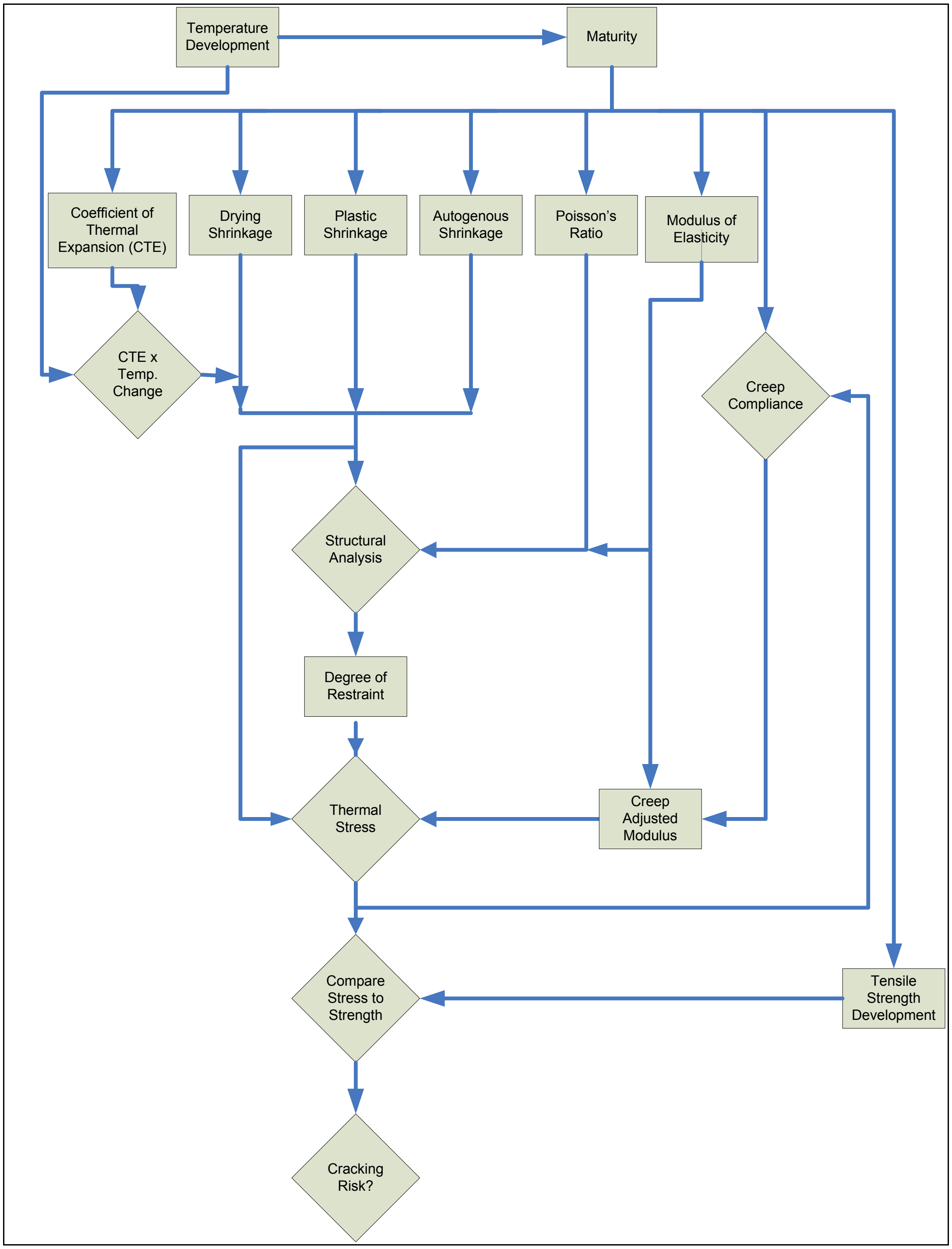

Figure 9-37 - Flow chart describing the relationship between different parameters in thermal stress modeling of concrete structures

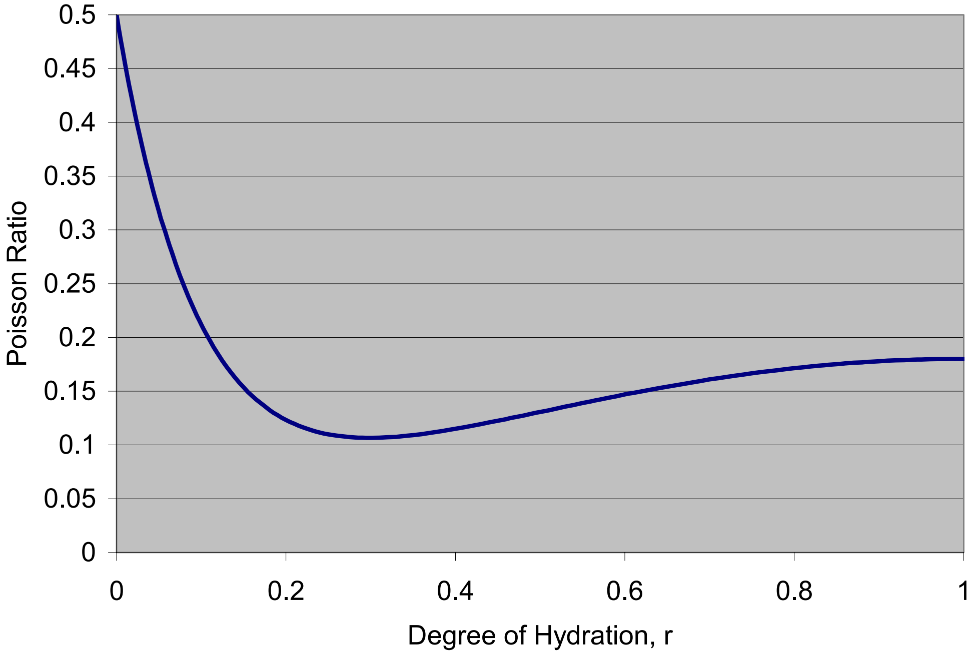

Figure 9-38 - Poisson ratio development during hydration

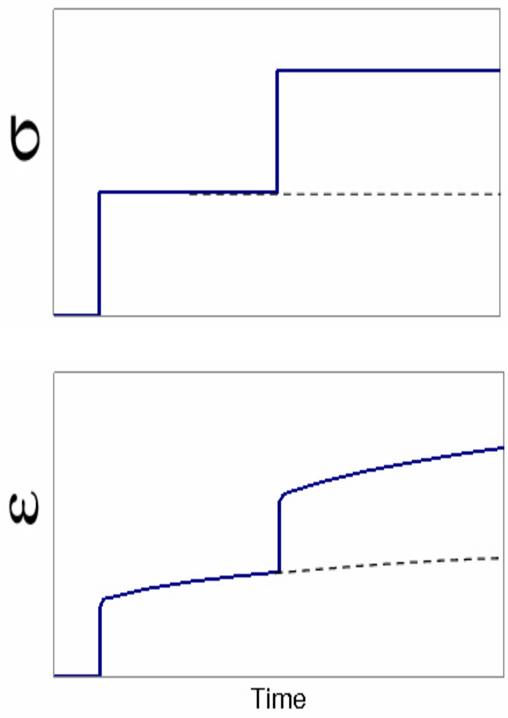

Figure 9-39 – Illustration of the principle of superposition

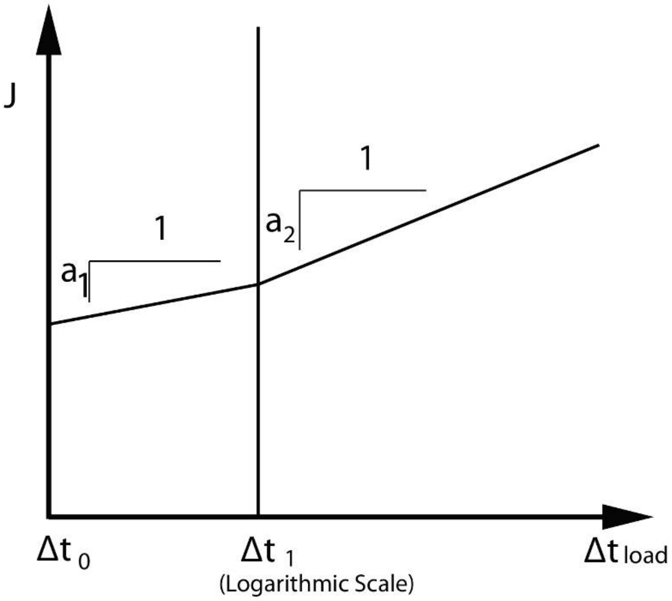

Figure 9-40 – Creep Compliance modeled using the Linear Logarithmic Model (Larson, 2003)

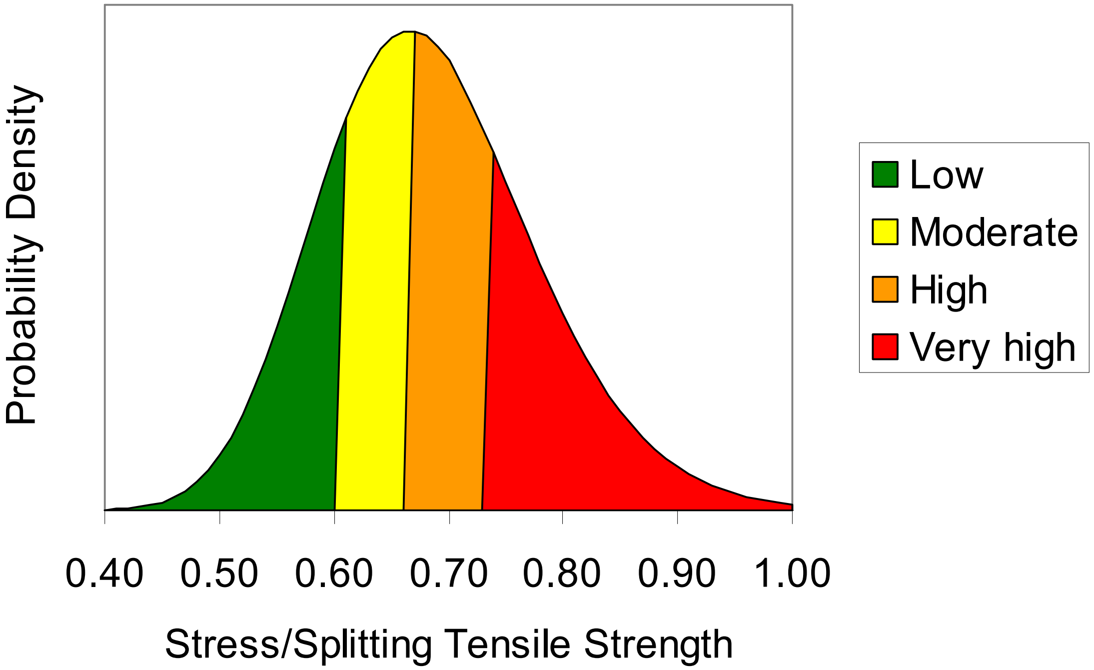

Figure 9-41 - Probability Density for Cracking Based on the Stress/Splitting Tensile Strength

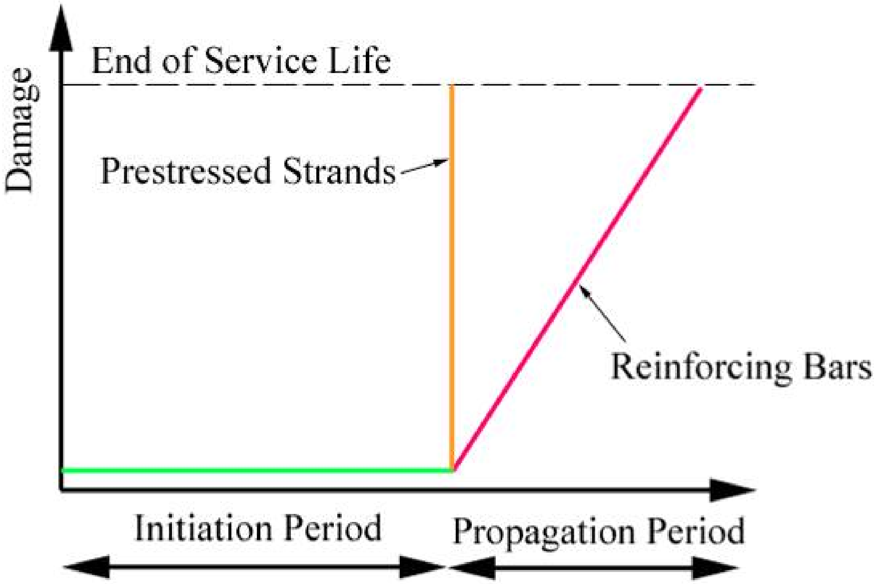

Figure 9-42 - Damage Model Used in ConcreteWorks Based on the Tuutti Model (1982)

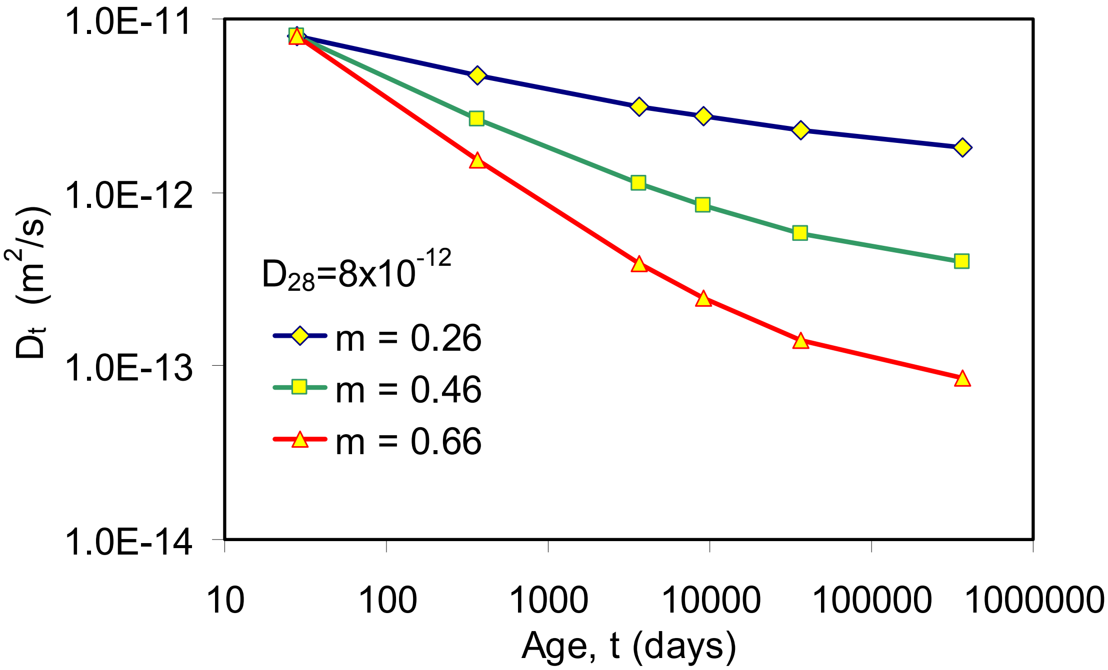

Figure 9-43 - Effect of a Change in the Decay Constant *m* on the Concrete Apparent Diffusion Coefficient, D_t

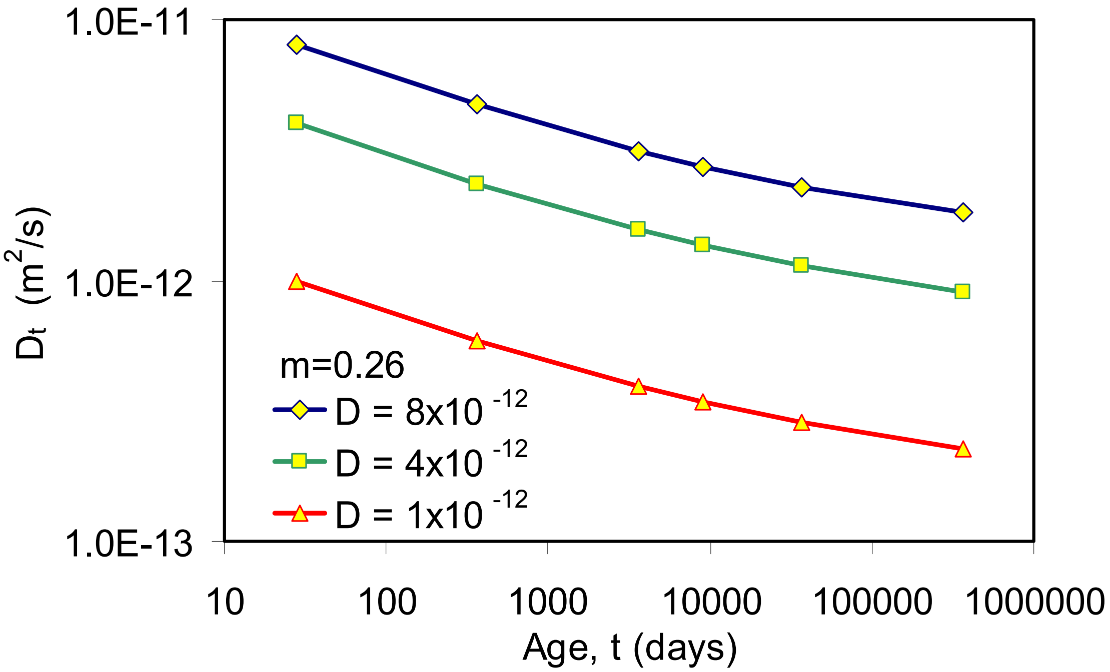

Figure 9-44 - Effect of a Change in the 28-Day Apparent Diffusion Coefficient on the Concrete Apparent Diffusion Coefficient, D_t, with Time

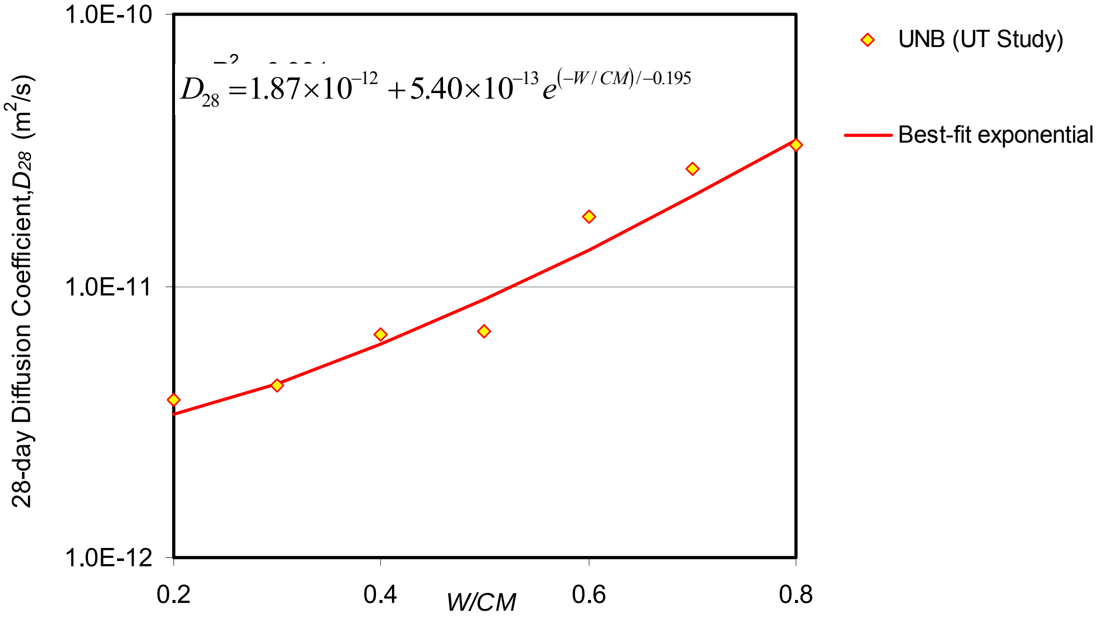

Figure 9-45 - Relationship between 28-Day Concrete Apparent Diffusion Coefficient and w/cm

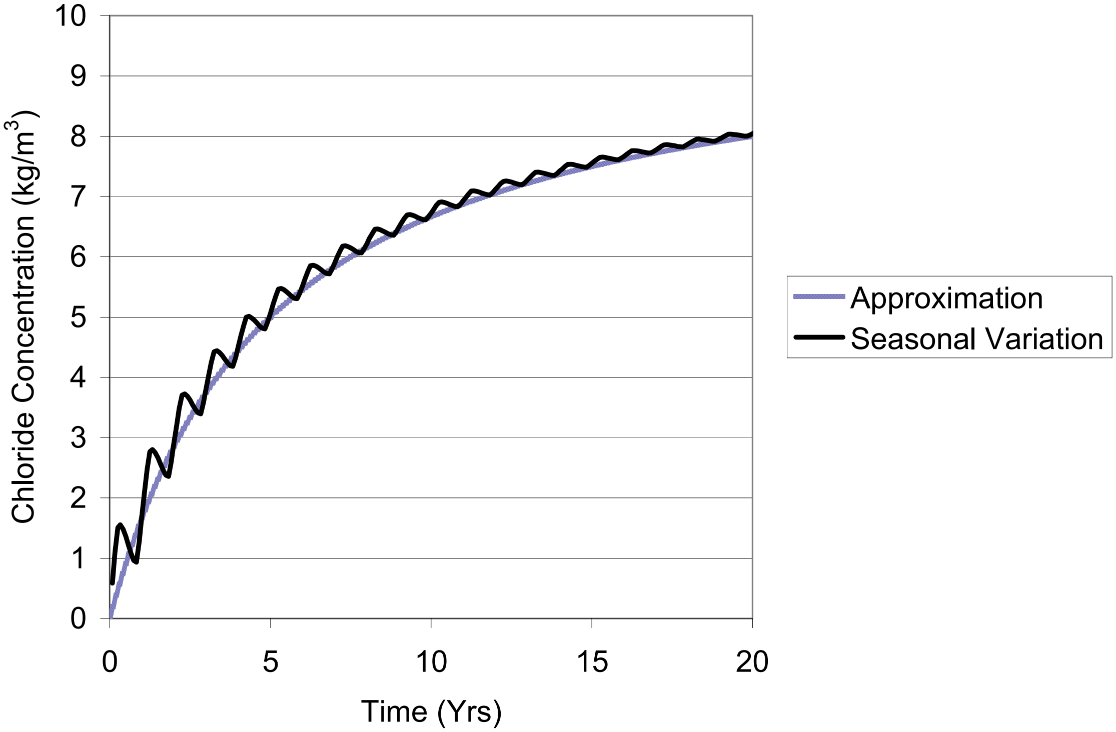

Figure 9-46 - Chloride Surface Concentration versus Time with and without Accounting for Seasonal Variations

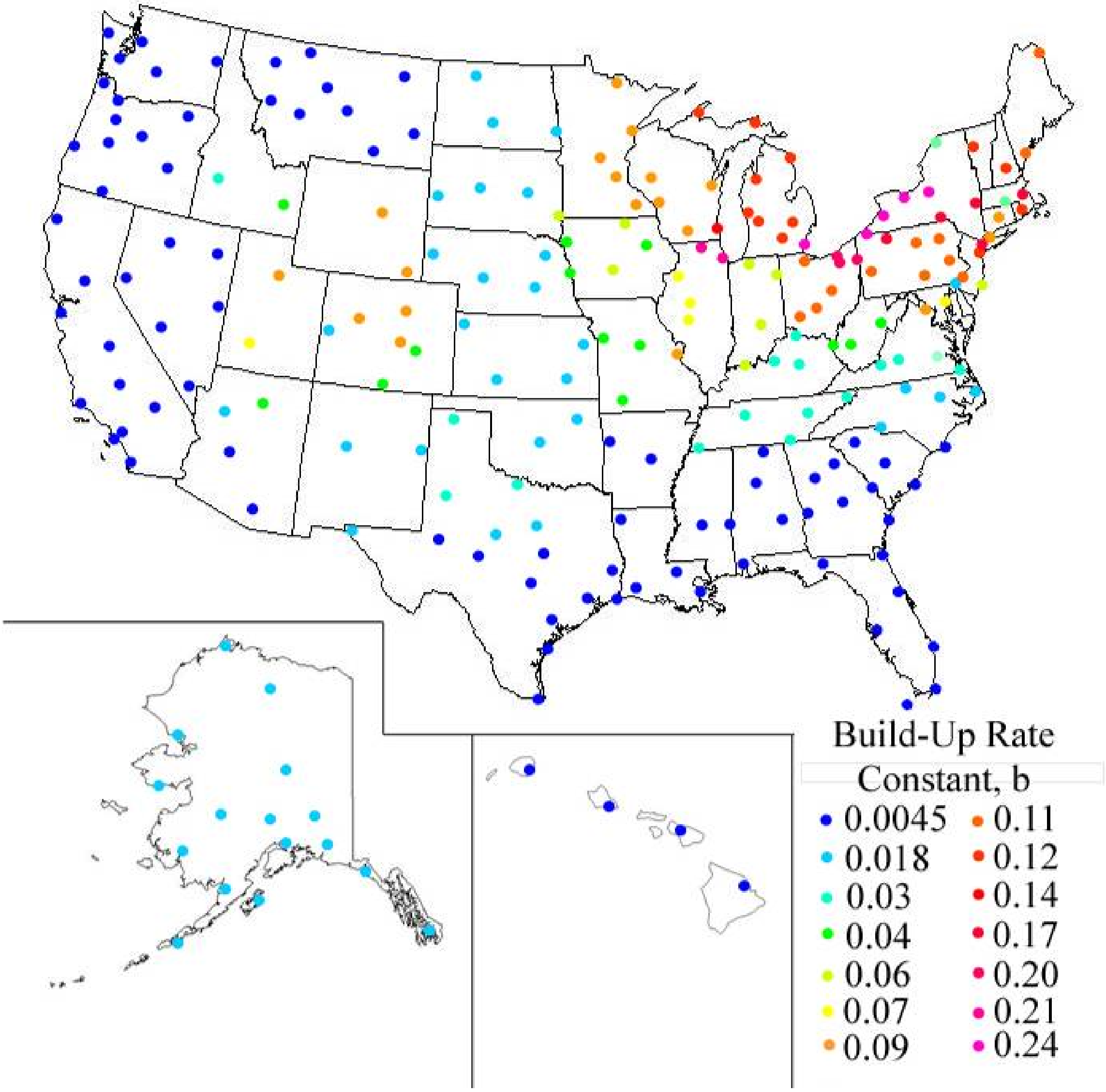

Figure 9-47- Build-up rate constants used in ConcreteWorks

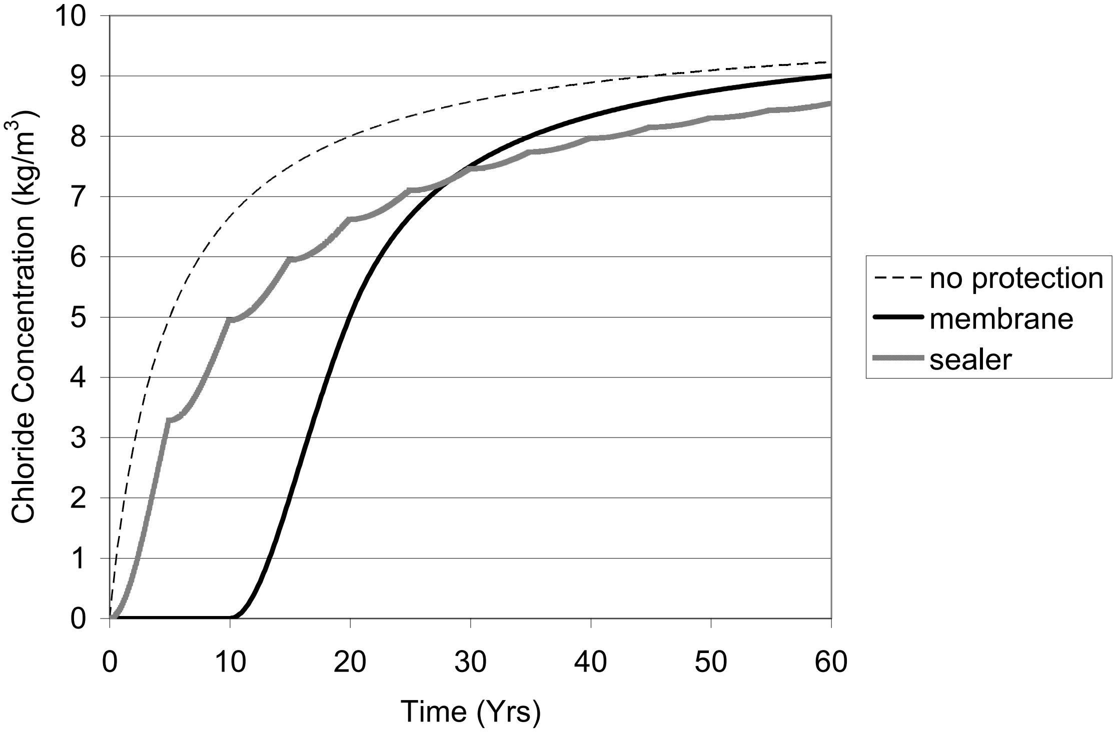

Figure 9-48 - Chloride surface concentration for cases where no barrier protection method is used, a membrane is used, and a sealer is used

CHAPTER 10 CONCLUSIONS

This chapter provides a summary of the research performed and conclusions made as part of this study, areas of work to be done to improve ConcreteWorks, and ideas for future research.

10.1 Summary

Concrete premature degradation by cracking and corrosion is a major cause of the deterioration of the United States infrastructure. In order to control the concrete temperatures during curing and prevent thermal stress cracking, materials and construction sequences need to be optimized before the concrete is placed. Concrete early age cracking is most often dealt with indirectly by limiting the concrete placement temperature and/or the in-place temperature rise and gradients. However, it is not simply the temperature development that determines the concrete cracking probability, but the interaction of the temperature development with concrete stress relaxation, modulus and tensile strength development. In order to economically reduce the probability of early age cracking in concrete, engineers and contractors need a way of quantifying the internal stresses that develop from the interaction of the materials used, the environment and the construction techniques used.

As part of this research study, a software package named ConcreteWorks was developed that will guide users through the concrete mixture proportioning procedure, calculate the temperature development for several types of concrete members, the thermal stress cracking probability for several mass concrete members, and the chloride service life for mass concrete and bridge deck members. A temperature prediction model was developed to predict the concrete temperature development, including the interaction between the concrete edges and the environment. Over 12 mass concrete members, a bridge deck, and several precast concrete beams were instrumented for temperature to calibrate the temperature prediction module in ConcreteWorks.

A method of obtaining the concrete early age creep response from restrained early age concrete tests at different temperatures was also developed. Additionally, an early age concrete creep model was developed based on a modified version of the Linear Logarithmic Model (Larson 2003), which is called the Modified Linear Logarithmic Model (MLLM). A statistical model was developed that relates the early age concrete creep MLLM parameters obtained from 73 rigid cracking frame tests performed on 36 different concrete mixtures to the concrete mixture proportions and constituent material properties. An early age stress model was integrated into ConcreteWorks using the Modified Linear Logarithmic Model. The cracking probability is calculated in the model using a lognormal cracking probability density created from the stress-to-strength ratio from the stress-to-strength ratio at cracking from 64 rigid cracking frame tests and their splitting tensile strength development.

ConcreteWorks contains a chloride service-life analysis module, allowing the engineer to optimize the concrete mixture and protective measures to ensure a long service life. The service life model developed is based on Fick's second law of diffusion, and can be highly sensitive to changes in the chloride surface concentration profile assumed. The model is, however, a good design tool that allows the user to rapidly compare different strategies to determine the most economical steel protection method.

Additionally, a simplified version of the ASTM C 1202 Rapid Chloride Permeability Test (RCPT) was developed. It was shown that the standard RCPT test can be simplified to reduce the labor involved and obtain results quicker without losing any accuracy from the standard method.

10.2 Conclusions

The development of ConcreteWorks satisfied this study's objective of developing a user-friendly concrete durability design tool. ConcreteWorks allows the user to quantify the combined effect of the materials used, environmental conditions, and construction techniques and sequencing on the durability and service of life of the concrete. Conclusions can be drawn in the three areas of research discussed in this dissertation: concrete temperature modeling, concrete early age stress measurement and modeling, and durability quality control test methods.

10.2.1 TEMPERATURE PREDICTION

A model for calculating the interaction of a concrete member with the environment was developed that focuses especially on vertical surfaces. The model incorporates the effects of solar radiation, irradiation, radiation from the atmosphere and exterior surfaces, shading from formwork, and natural and forced convection. Over 12 concrete members were instrumented for temperature development to calibrate the concrete temperature prediction model. Weather data were collected during the concrete placement and curing. Calorimetry was also performed on the concrete materials used. From the concrete member temperature data measured, it can be concluded that the concrete temperature prediction performed well. The average absolute error for the measured temperatures to the predicted member temperatures ranged from 0.5 to 4.6°C (1.0 – 8.4°F).

Calorimetry was performed on concrete sampled at the job-site and concrete made at the laboratory from constituent materials. The calorimetry results were then used to predict the concrete temperature development using ConcreteWorks, and to investigate the effect of mixing conditions and material variability on the accuracy of the temperature prediction model developed. The results showed that either field or laboratory made concrete could be used in a temperature prediction model with good expected results. It was also determined that semi-adiabatic calorimetry could be used as a quality control tool to detect large changes in materials.

10.2.2 CONCRETE EARLY AGE STRESS MEASUREMENT AND MODELING

A combination of rigid cracking frame tests, free shrinkage tests, hardened concrete coefficient of thermal expansion tests, and elastic modulus tests can be used to determine the early age concrete creep response fit parameters. These tests, along with the results from splitting tensile strength tests, can be used in a numerical model such as ConcreteWorks to estimate the cracking probability of a mass concrete member. An empirical model was developed that relates the concrete materials used to the concrete early age creep parameters, allowing ConcreteWorks to simplify the inputs needed for determining a concrete members cracking probability. The model includes the effects of:

- The concrete composition when the Rietveld method is used:
  - Alite, Aluminate, Ferrite, Gypsum, Bassanite, and Anhydrite content
  - Fly ash content

  - Grade 120 slag content
  - W/cm
- When the Bogue (ASTM C 150) is used:
  - C_4AF, C_2S, and C_3A content
  - Fly ash content
  - Grade 120 slag content
  - W/cm
  - Cement content
  - Cement Blaine fineness

10.2.3 DURABILITY QUALITY CONTROL TEST METHODS

A simplified ASTM C 1202 rapid chloride permeability test method was developed that is rapid and much easier to run than the standard test. From the results of the testing performed on both the standard and simplified rapid chloride permeability test, it can be concluded that:

- Heating significantly affected the results of the rapid chloride permeability test, but occurs in a predictable manner for all concrete specimns tested.
- Concrete vacuum saturation and saw cutting is unnecessary for laboratory prepared samples cured at 100% relative humidity.
- A correlation between the standard and simplified rapid chloride permeability test was developed to account for the heating in the standard test.

10.3 Suggestions for Future Research

Possible areas of future related research could include:

- Devloping an improved autogenous shrinkage model that:
    - Models early age expansion and later contraction based on the concrete viscoelastic behavior
    - Includes the effects of supplementary cementing materials
    - Correctly models the effect of temperature on autogenous shrinkage
- Developing a model for the concrete coefficient of thermal expansion development with the degree of hydration
- Developing a model that better describes the bleed rate and consequent evaporation rate of bleed water from freshly placed concrete
- Improving the early age creep model developed based on an increased number of concrete early age restrained shrinkage tests
- Developing a model that better predicts the concrete chloride surface concentration
- Developing a model that relates the mixture proportions to the chloride threshold level for corrosion initiation
- Validating the concrete service life estimation module
- Developing a simplified temperature specification for mass concrete members based on early age stress analysis

10.4 Suggestions for Future Improvements to ConcreteWorks

There are many areas in which ConcreteWorks can be improved. Some of these are:

- The development of a thermal stress module for circular columns.

- The development of a thermal stress module for footings based on a compensation plane.
- The use of a changing concrete coefficient of thermal expansion in the thermal stress calculations
- The development of a model that relates the concrete mixture proportions and constituent material properties to the compressive strength development

APPENDIX A

Field Site Temperature Instrumentation Technical Memorandums

APPENDIX A-1 2002-2003 FIELD SITE INSTRUMENTATIONS

A-1.1 Introduction

As part of the Texas Department of Transportation (TxDOT) project 4563, we are developing a heat prediction model for mass concrete elements. Each project presents a different variation in member dimensions, materials, construction methods, or environmental conditions. Field data are needed to calibrate the heat prediction model for as many of these variations as possible. During the fiscal year 2003, field data were acquired for three columns and two footings.

A-1.2 Columns

A-1.2.1 COLUMN 1

The first mass concrete site that we instrumented was a rectangular column in Austin, TX. The concrete was placed in two sections, totaling 98 feet in height. The column plan dimensions were 11’-10” by 7’-7”. Twenty thermocouples were placed in the column, but very little valid data were obtained. Concrete was placed starting at 11:45 a.m. on December 18th, 2002. The concrete was produced at the onsite plant by the contractor, JD Abrams. A sample of concrete was taken onsite for semi-adiabatic calorimetry.

Instrumentation

For redundancy, we placed thermocouples at two different heights in the column. Ten thermocouples were placed at a height of 8’-8” in the column. The other ten were placed at a height of 28’6”. All thermocouples were placed inside the column after the forms were erected. We attached the thermocouples to the rebar with plastic electrical ties. The wire was then brought down to the base of the column and secured in place. We then tied the wires to the rebar at about 12 inch intervals using the plastic ties. After placement, we measured the precise location of each thermocouple. Table A 1-1 shows the distance of each thermocouple from the bottom west corner of the column. Figure A 1-1 shows a close up view of the instrumentation. The yellow arrow points to the exposed thermocouple.

After stringing the wires to the bottom of the column, we pushed the thermocouples wires underneath the formwork. We then attached the wires were to a Campbell Scientific CR 10X Datalogger using a Campbell Scientific AM416 Multiplexer.

Instrumentation Problems

The first problem encountered destroyed the first 24 hours of data. The problem was pressure head. The pressure head inside the column forced pore water inside the thermocouple wire insulation. The water then traveled down the wire and trickled onto the multiplexer. The multiplexer shorted out because of the water damage.

After discovering the problem, we hooked up five thermocouples directly to the datalogger upside down. This allowed any water in the wires to trickle down the wires, instead of falling on the multiplexer. We then hung the box with the datalogger on the forms, about 10 feet off of the ground. We returned to the site the next day and downloaded the twenty-four to forty-six hour data (Figure A 1-2). The maximum temperature recorded was 154°F. The maximum temperature difference recorded in the column was 86°F. The box was restrung on the forms and left there for a week.

During the following week, it rained very hard in Austin. The dug out area around the column filled up with water and soaked the datalogger equipment once again, ruining the CR 10X and power supply.

A-1.2.2 COLUMN 2

The second column we instrumented was located in Round Rock, TX. The concrete was placed on June 16, starting at 8:00 a.m. The column was 6’ by 10’ feet by 30’ high with architectural cut outs on the corners. Symons Elasto-Tex, Custom Ashlar Stone Finish architectural form liners were used on the 10 feet sides. There was also an eight-inch drainpipe running down the middle of the column. A sample of concrete was taken onsite for semi-adiabatic calorimetry.

Concrete Properties

Transit Mix Concrete and Materials CO supplied the concrete. The concrete mix design was a class C concrete. Table A 1-2 shows the concrete design and measured characteristics.

Instrumentation

Because of instrumentation problems on the first site, we decided to try a different instrumentation method. We chose to use Thermochron iButtons®[1] made by Dallas Semiconductors (Dallas Semiconductor, 2003). The Thermochron iButtons take and log temperature data at programmable intervals. We followed procedures similar to that used in an earlier TxDot study (Ramaiah, 2002). We soldered wires onto the outside surface of the iButtons in series. Five iButtons were soldered to each wire. We then coated the iButtons with a plastic coating. The wires were used to access the data stored in the iButtons with a laptop.

---

[1] iButton® is a registered trademark of Dallas Semiconductor

To speed installation of the instruments in the columns, we mounted iButtons on precut pieces of #4 rebar (Figure A 1-3). We installed the prefabricated temperature bars before all of the forms were set as seen in Figure A 1-4. The location of surviving iButtons is shown in Figure A 1-5 and 6. Figure A 1-5 shows the location of temperature bar number two, located 9’-6” off of the footing. Figure A 1-6 shows the location of temperature bar number four, located 19’-6” off of the footing.

The temperature bars and wires were duct taped into place. All wires were strung to the bottom of the column, and exited under the formwork. All iButtons were pre-programmed to record temperature at fifteen-minute intervals.

Instrumentation Problems

When one iButton becomes corrupted, you lose access to all of the other iButtons on that series. Possible causes of uncoated iButton corruption include: immersion in water, electrical short, wire connection becoming severed, and severe impact.

Within 24 hours, we lost the iButtons on two wires. After 72 hours, only two series of iButtons could be downloaded. To test if column pressure head was the problem, we placed coated iButtons in a pressure pot. Enough water was placed in the pot to cover the iButtons. The pressure pot was sealed, and placed at a constant pressure of 60 psi. This pressure corresponds to the total static pressure corresponding to a 58 feet tall column. The pressure pot was left at 60 psi for two days. After two days the iButtons still functioned. Unlike the thermocouple wires, pressure head was not the only probable cause of our iButton failures. We suspect that a combination of problems including pressure head, impact, and poorly coated wire splices contributed to the iButton failures.

Data Acquired

Weather data were acquired using a Campbell Scientific weather station. Data collected from the weather station included: temperature, relative humidity, wind speed, wind direction, rainfall, and solar radiation. We used the same weather station without being moved for columns 2 and 3, and footings 1 and 2. Figure A 1-7 shows a picture of the weather station on site. Figure A 1-8 through Figure A 1-10 show graphs of the temperature, relative humidity and wind speed, and solar radiation values measured. Figure A 1-11 shows the temperatures measured by the iButtons in run number 2. Figure A 1-12 shows the temperatures measured by the iButtons in run number 4. There was no measured rain during the curing of the column. The maximum recorded temperature in the column was 136°F. The maximum recorded temperature difference in the column was 35°F.

For Figure A 1-8 through Figure A 1-10, values are plotted starting at 8:00 a.m. June 16th, 2003 (the start of the concrete placement in the column). The values in Figure A 1-11 and Figure A 1-12 are plotted from the estimated time that concrete came into contact with the respective iButtons. For run 2, we estimated that the concrete height reached 9'-6" at 11:30 a.m. For run 4, we estimated that the concrete height reached 19'-6" at 1:15 p.m.

The outermost iButton readings on run #4 vary a great deal with time. The outermost iButton temperatures on run #2 do not vary much because of the extra insulation provided by the form liner. The peak temperatures for both runs occur in the middle of the column and appear consistent with each other.

A-1.2.3 COLUMN 3

The third column instrumented was located in Round Rock, TX on the same project as Column 2. The column was 6' by 10' by 67' high with architectural cut-outs on the corners. Symons Elasto-Tex, Custom Ashlar Stone Finish architectural form liners were used on the 10 foot sides. This column did not have a drainpipe. Otherwise, this column was identical in plan to the column discussed in section 2.2.

Concrete properties

Transit Mix Concrete and Materials Co. supplied the concrete. Table A 1-3 shows the concrete design and characteristics. The concrete was placed on July 10th, 2003 starting at 8:00 a.m.

Instrumentation

To instrument column 3, we made four temperature bars with iButtons pre-positioned and taped in place. To solve the instrumentation problems that we experienced with column 2, we changed the method of coating the iButtons. We decided to pot the iButtons using a two-part epoxy. Plastic specimen cups were used as the mold. For ease in fabrication, the plastic cups were not removed after the epoxy cured. Figure A 1-13 shows an up-close picture of an installed temperature bar using the epoxy potting method. We were worried that the epoxy surrounding the iButtons could cause a thermal lag. To test whether the epoxy caused a thermal lag, we placed an iButton potted in epoxy next to an iButton coated in a plastic dip in a water bath. The iButtons were programmed to record the temperature every minute (a much faster interval than generally used on mass concrete elements). We set the initial temperature of the water bath to be 122 °F. We set the water bath to ramp down to 50 °F. Figure A 1-14 shows the temperatures recorded by both iButtons. The epoxy method gave results within the manufacturer's tolerance of 1.8°F (Dallas Semiconductor, 2003).

Three of the temperature bars had five iButtons each. The fourth temperature bar only had four iButtons attached. Two temperature bars were placed in the configuration shown in Figure A 1-15, one at a height of 10’-6” (hereafter called K1) off of the footing and the other at 19’-6” (hereafter called J1). IButton #4 of K1 was removed because of fabrication defect, leaving only four buttons. Two additional temperature bars were placed in the same configuration shown in Figure A 1-15, one at 10’-6” (Hereafter called K2) off of the footing and the other at 19’-6” (hereafter called J2).

Data Acquired

We used the same weather station as used in the sites discussed in sections 3.1.2 and 3.2.2 to get the environmental conditions during the column curing time period. Figure A 1-16 and Figure A 1-17 show graphs of the temperature, relative humidity and wind speed, and solar radiation values measured. There were 0.4 inches of rain measured on July 16th. Figure A 1-18 through Figure A 1-22 show graphs of the temperatures recorded by the iButtons on K1, J1, K2 and J2, respectively. The maximum temperature reached in the column was 136°F. The maximum temperature difference recorded in the column was 40°F.

The data from K1 look very similar to the data from J1, and the data from K2 look similar to the data from J2. Table A 1-4 lists the r^2 values when you compare temperatures at 10’-6” off of the footing to the temperatures at the corresponding location at 19’-6” off of the footing. The r^2 value for iButton 4 on K1 vs. J1 is missing because the iButton #4 on K1 was removed before installation.

When you compare K1 values versus J1 values, all r^2 values are above 0.97. This indicates that there is very little temperature gradient between these horizontal cross sections at these points. The r^2 values for iButtons two through 5 on K2 vs. J2 are also very good. The only low r^2 value calculated was for iButton #1 on K2 vs. J2. There are many reasons for the difference in temperature. The first is that there is no form liner and its corresponding insulation. This allows the temperature under the form to fluctuate more with environmental conditions. The exact location of the iButton also makes a difference. A change in position of even one inch can make a big difference because of the lower amount of formwork insulation. One other cause for the difference is the location in relation to a rib on the Symons form. The rib on the form can cover the form surface from solar radiation.

A-1.3 Footings

A-1.3.1 CENTRAL FOOTING 1

The first footing we instrumented was located in Round Rock, TX on the same project as columns 2 and 3. The footing had dimensions of 24’-0” by 26’-1” by 7’-4” in height. Rust colored Symons forms were used. About half of the forms had previously been sprayed with foam insulation.

Concrete Properties

Transit Mix Concrete and Materials Co. supplied the concrete again. The concrete mix design was a Class F concrete. Table A 1-5 shows the concrete design and measured characteristics. We estimated that the concrete placement started at 7:00 a.m. on June 17th, 2003.

Instrumentation

We made five iButtons in the same way as described in section 3.1.1 (except that these iButtons were not mounted on a temperature bar, they were separately mounted directly to the footing steel).

Table A 1-6 shows the location of each iButton, measured from the upper northeast corner of the footing. Figure A 1-23 shows a picture of iButton #5 taped to the northeast corner of the footing form. The yellow arrow on Figure A 1-23 points to iButton #5.

Data Acquired

We used the same weather station as shown in Figure A 1-7. Figure A 1-24 through Figure A 1-26 show graphs of the temperature, relative humidity and wind speed, and solar radiation values measured. Figure A 1-27 shows the measured temperature values for each iButton. There was no measurable amount of rain during the curing of the footing. The maximum temperature reached in the footing was 161°F. The maximum temperature difference recorded in the footing was 72°F.

A-1.3.2 FOOTING 2

The second footing instrumented was located in Round Rock, TX. Footing 2 had dimensions of 10’-0” by 10’-1” by 6’-2” in height. The footing was placed without steel forms. Wood 2’x8’ boards were used to form a 6’-0” by 8’-0” area on the surface to be finished. For the rest of the footing, concrete was placed up to the edge of the embankment (see Figure A 1-29). A sample of concrete was taken onsite for semi-adiabatic calorimetry.

Concrete Properties

Transit Mix Concrete and Materials Co. supplied the Class C concrete. Table A 1-7 gives a summary of the mix design and measured characteristics. Concrete placement was started at 8:00 a.m. on August 1st, 2003.

Instrumentation

We placed eight epoxied iButtons in the footing. The contractor placed an additional two epoxied iButtons in the footing, giving us access to ten data points. Table A 1-8 shows the location of each iButton in relation to the bottom southwest corner of the footing. IButtons 1-6 were placed placed using the temperature bar method. We placed the other two points individually in the footing next to the soil-footing interface.

Data Acquired

We decided that the jobsite for footing 2 was too dangerous to place a weather station on site, so we placed the weather station in a field about a half mile from footing 2. Figure A 1-29 through 31 show graphs of the temperature, relative humidity and wind speed, and solar radiation values measured. Figure A 1-32 shows the data for the iButtons on the temperature bar. Figure A 1-33 shows the data for the individually placed iButtons. The maximum temperature recorded in footing 2 was 133°F. The maximum temperature difference recorded in the footing was 45°F.

A-1.4 Summary

During the first year of TxDOT project 4563, temperature recording devices were installed in three columns and two footings. After some initial struggles, we developed a system for rapidly installing durable temperature recording devices in mass concrete elements. This system involves making custom pre-fabricated iButton temperature bars for each element measured, and installing them onsite the day before concrete is placed. Weather data, concrete member temperature development data, and semi-adiabatic calorimetry data were collected for use in calibrating a computerized heat development model for mass concrete members.

Table A 1-9 shows the maximum temperature reached in each concrete member and the maximum temperature difference recorded in each member. All of the concrete members instrumented had a maximum temperature difference of at least 35°F. The highest temperature difference recorded was in column 1 at 86°F.

A-1.5 Acknowledgements

The advice and assistance of the TxDOT Bridge Division and the Texas Turnpike Authority (TTA) personal are greatly appreciated. The authors wish to thank Ralph Browne, Tyler Ley, Charles Chance, Roger White and Rob Crowson for arranging access to field sites.

Table A 1-1 - Location of thermocouples in column measured from the bottom west corner of the column

Thermocouple Number	x	y	z
1	0’ – 0.5”	0’ – 0.5”	28’ – 2”
2	0’ – 2”	0’ – 5.5”	28’ – 2”
3	6’ – 2”	0’ – 0.5”	28’ – 6”
4	6’ – 2”	0’ – 3”	28’ – 6”
5	6’ – 2”	1’ – 10”	28’ – 6”
6	6’ – 2”	3’ – 5”	28’ – 6”
7	4’ – 6”	3’ – 8”	28’ – 2”
8	0’ – 0.5”	3’ – 8”	28’ – 2”
9	6' – 2”	7’ – 6.5”	28’ – 6”
10	11’ – 9.5”	3’ – 7”	28’ – 5”
11	0’ – 0.5”	0’ – 0.5”	8’ – 10”
12	0’ – 0.5”	0’ – 2”	8’ – 10”
13	5’ – 8”	0’ – 0.5”	8’ – 5”
14	5’ – 11”	0 – 2”	8’ – 10”
15	6’ – 6”	1’ – 9”	8’ – 8”
16	6’ – 6”	3’ – 11”	8’ – 8”
17	1’ – 10”	3’ – 10”	8’ – 9”
18	0’ – 0.5”	3’ – 8”	8’ – 9”
19	6’ – 0”	7’ – 6.5”	8’ – 9”
20	11’ – 9.5”	3’ – 10”	8’ – 9”

Table A 1-2 – Column #9 concrete characteristics

Item	Content	Material Description
Cement	423 lb./yd.^{3}	TXI Hunter Ty I/II
Class F Fly Ash	107 lb./yd.^{3}	Big Brown
Coarse Aggregate	1745 lb./ yd.^{3}	1" Crushed Limestone
Fine Aggregate	1420 lb./ yd.^{3}	Natural Sand
Air	2.64 oz/100 wt.	
Water Reducer/Retarder	3.58 oz/100 wt.	
Ice	120 lb./ yd.^{3}	
water	45 lb./ yd.^{3}	
Jobsite Measured Air Content	6.50%	
Jobsite Measured Slump	5.5"	
Water/cementitious materials ratio	0.42	

Table A 1-3- Bent #11 concrete design and characteristics

Item	Content	Material Description
Cement	423 lb./yd.^{3}	TXI Hunter Ty I/II

Class F Fly Ash	107 lb./yd.^{3}	Big Brown
Coarse Aggregate	1745 lb./ yd.^{3}	1" Crushed Limestone
Fine Aggregate	1427 lb./ yd.^{3}	Natural Sand
Air	3.32 oz/100 wt.	
Water Reducer/Retarder	3.58 oz/100 wt.	
Ice	160 lb./ yd.^{3}	
water	24 lb./ yd.^{3}	
Jobsite Measured Air Content	7.10%	
Jobsite Measured Slump	5.5"	
Water/cementitious materials ratio	0.42	

Table A 1-4- R2 values comparing temperature at 10'6" with the corresponding location at 19'6"

iButton #	K1 vs. J1	K2 vs J2
1	0.98	0.68
2	0.98	0.91
3	1.00	0.96
4	-	0.97
5	0.99	0.97

Table A 1-5 - Footing concrete design and measured characteristics

Item	Content	Material Description
Cement	528 lb./yd.^{3}	TXI Hunter Ty I/II
Fly Ash	135 lb./yd.^{3}	Cl F Big Brown
Coarse Aggregate	1745 lb./yd.^{3}	1" Crushed Limestone
Fine Aggregate	1084 lb./yd.^{3}	Natural Sand
Air	3.47 oz/100 wt.	
Water Reducer/Retarder	3.02 oz/100 wt.	
Ice	120 lb.	
water	70 lb.	
Water/cementitious materials ratio	0.4	

Table A 1-6 - Location of each iButton as measured from the upper northeast corner of central footing 1

iButton number	x	y	z
1	10' - 3"	6' - 4"	3' - 0"
2	10' - 3"	6' - 4"	0' - 5"
3	3' - 3"	6' - 4"	2' - 10"
4	0' - 0"	6' - 4"	0' - 4.5"
5	0' - 0"	0' - 0"	0' - 8.5"

Table A 1-7 - Footing B concrete design and measured characteristics

Item	Content	Material Description
Cement	423 lb./yd.^{3}	TXI Hunter Ty I/II
Class F Fly Ash	107 lb./yd.^{3}	Big Brown
Coarse Aggregate	1745 lb./ yd.^{3}	1" Crushed Limestone
Fine Aggregate	1420 lb./ yd.^{3}	Natural Sand
Air	2.45 oz/100 wt.	
Water Reducer/Retarder	3.58 oz/100 wt.	
Ice	160 lb./ yd.^{3}	
water	30 lb./ yd.^{3}	
Jobsite MeasuredAir Content	5.30%	
Jobsite Measured Slump	4"	
water/cementitious materials ratio	0.42	

Table A 1-8 - Location from bottom southwest corner of iButtons on footing B

iButton #	x	y	z
1	4' 7"	4' 10"	5' 11.75"
2	4' 7"	4' 10"	4' 3.75"
3	4' 7"	4' 10"	3' 0"
4	4' 7"	4' 10"	1' 8.25"
5	4' 7"	4' 10"	0' 8.5"
6	4' 7"	4' 10"	0' 1"
7	0' 0"	10' 0"	4' 4"
8	3' 0"	0' 0"	4' 4"
9[1,2]	0' 4"	0' 10"	0' 3"
10 [1]	4' 10"	5' 0"	2' 10"
[1]Denotes iButton installed by the contractor			
[2]Distances measured from top northwest corner of wood form			

Table A 1-9 - Maximum temperature and maximum temperature difference in each concrete member

Concrete Member	Maximum Temperature Recorded (°F)	Maximum Temperature Difference Recorded (°F)
Column 1	154	86
Column 2	136	35
Column 3	136	40
Footing 1	161	72
Footing 2	133	45

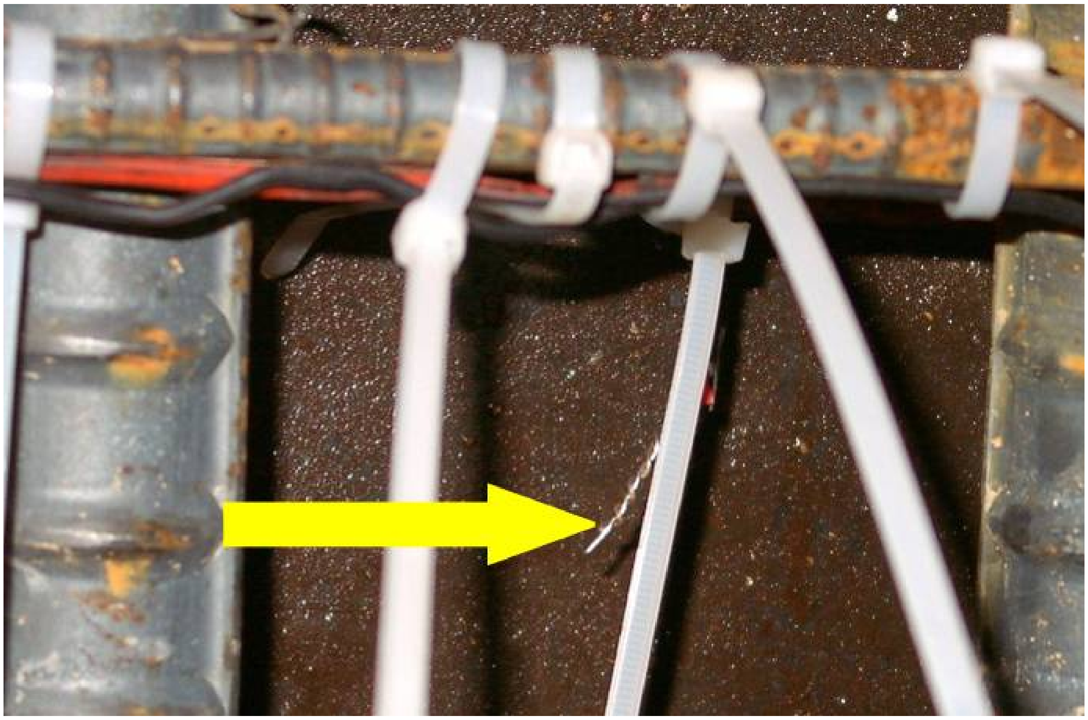

Figure A 1-1 – Close-up view of column instrumentation

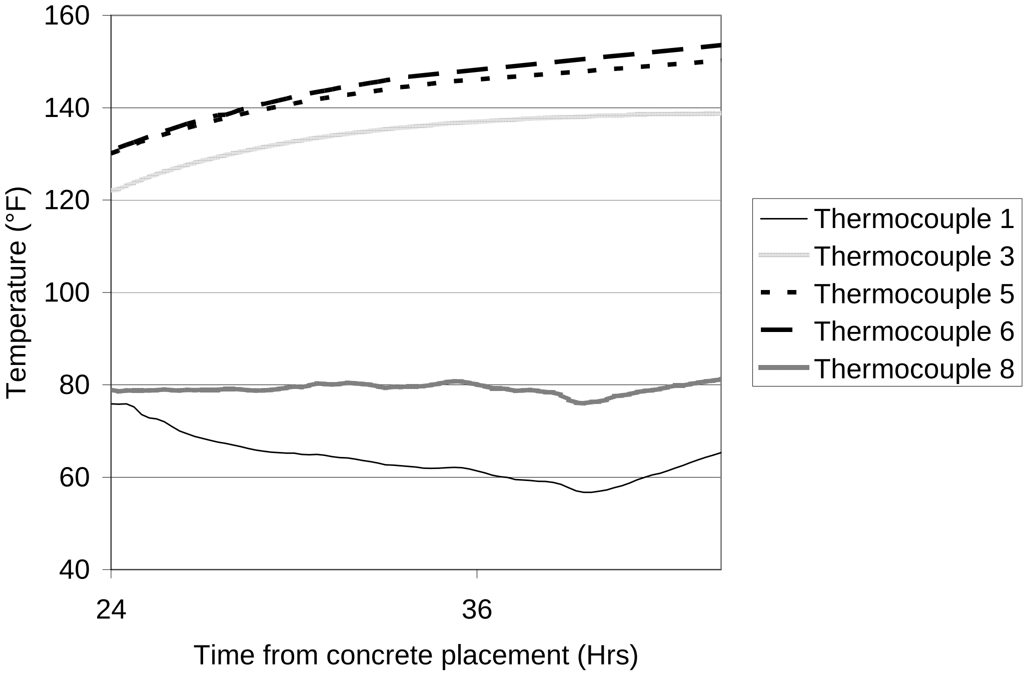

Figure A 1-2- US 290 / Texas 71 Column Data

Figure A 1-3 – Up-close view of installed temperature bar

Figure A 1-4 - Installation of iButtons

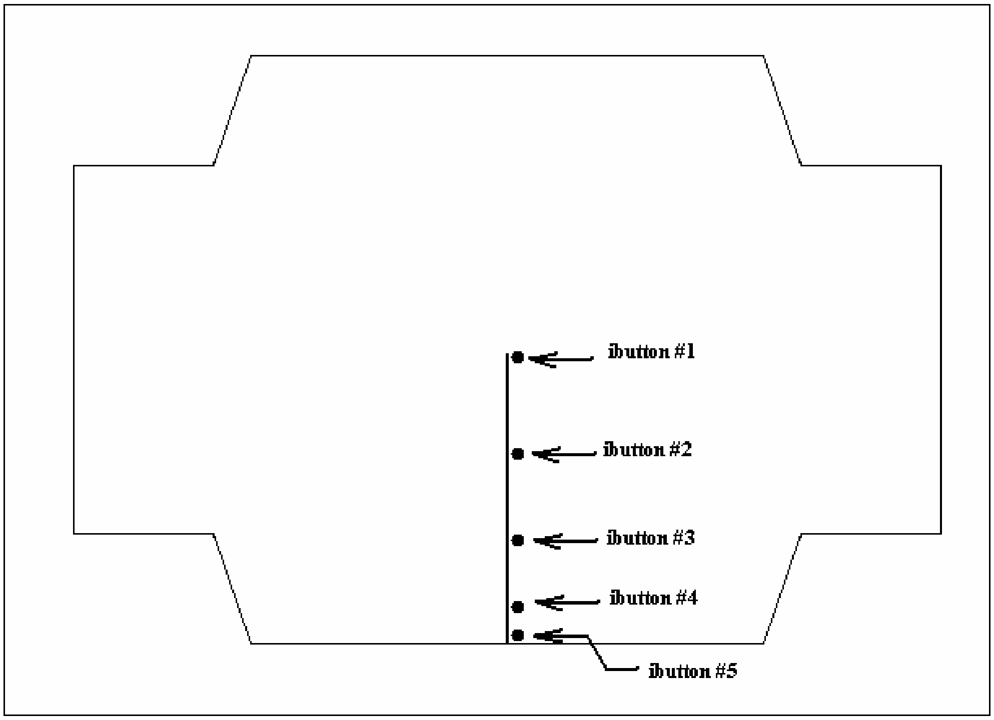

Figure A 1-5 - Plan view of column showing iButton run #2 layout (not to scale)

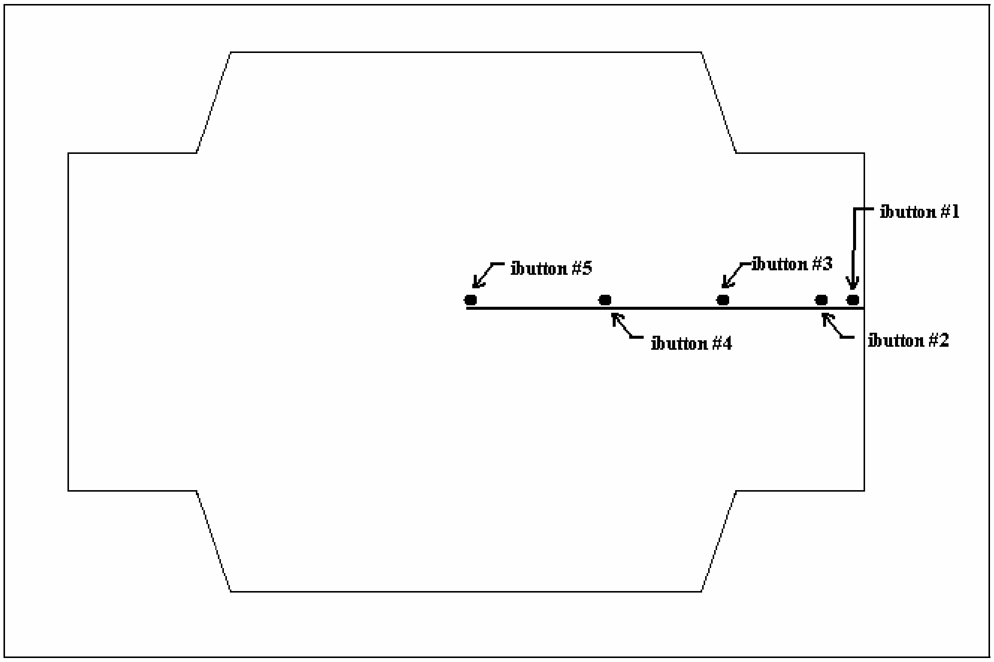

Figure A 1-6 - Plan view of column showing iButton run #4 layout (not to scale)

Figure A 1-7 - Weather Station on site

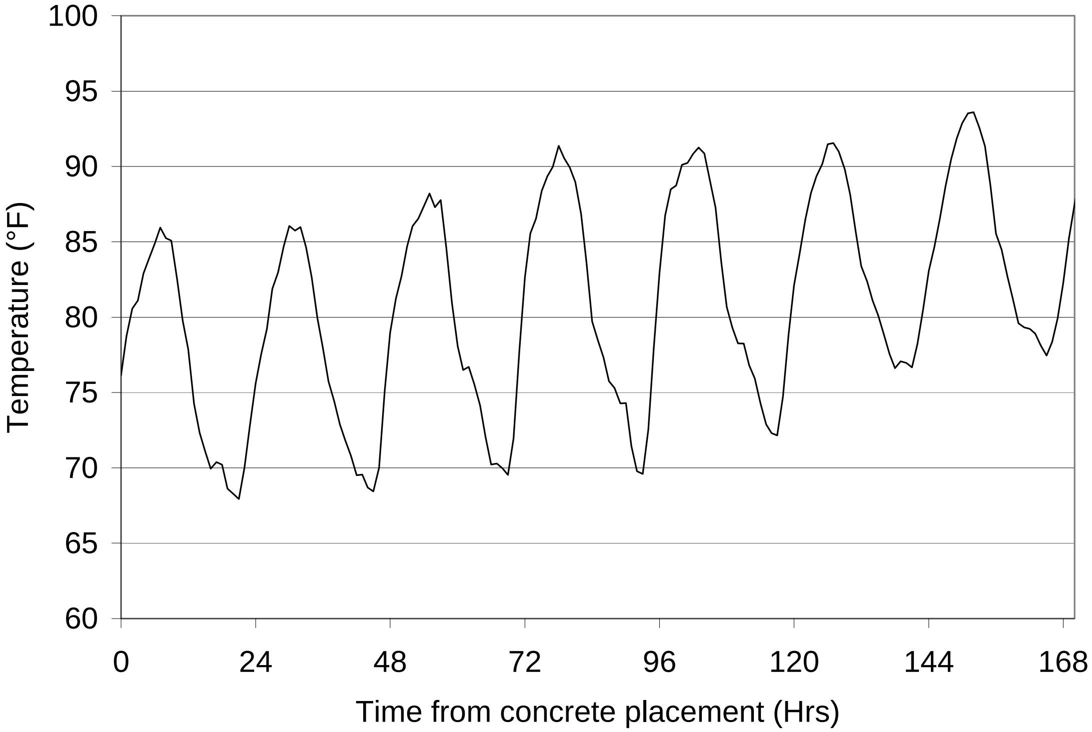

Figure A 1-8 - Temperature measured by weather station

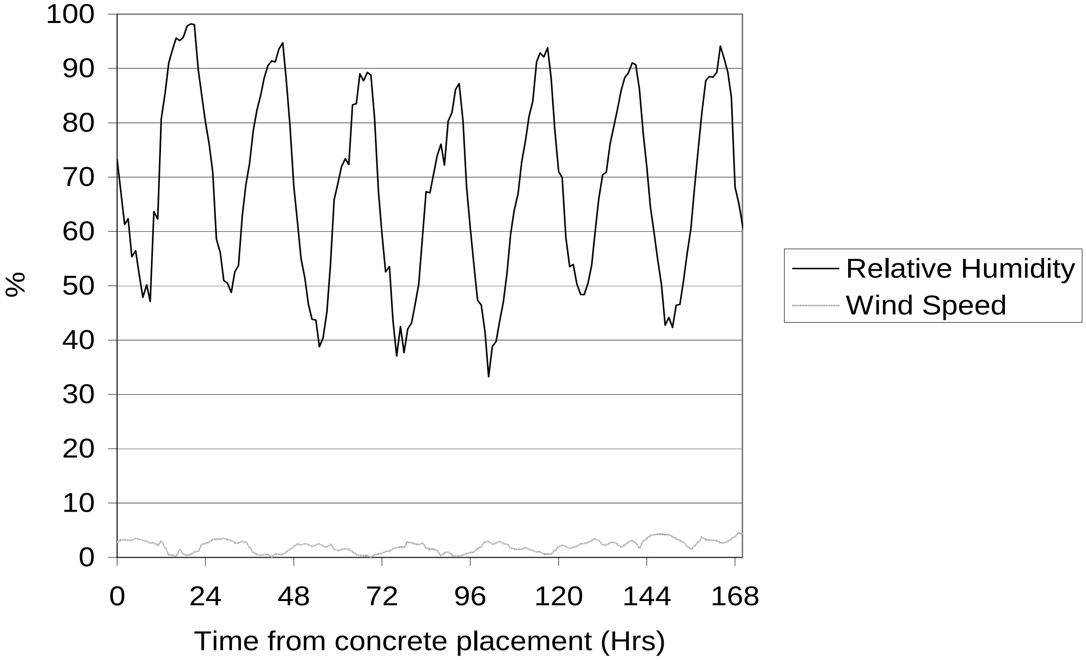

Figure A 1-9 - Relative humidity and wind speed measured by weather station

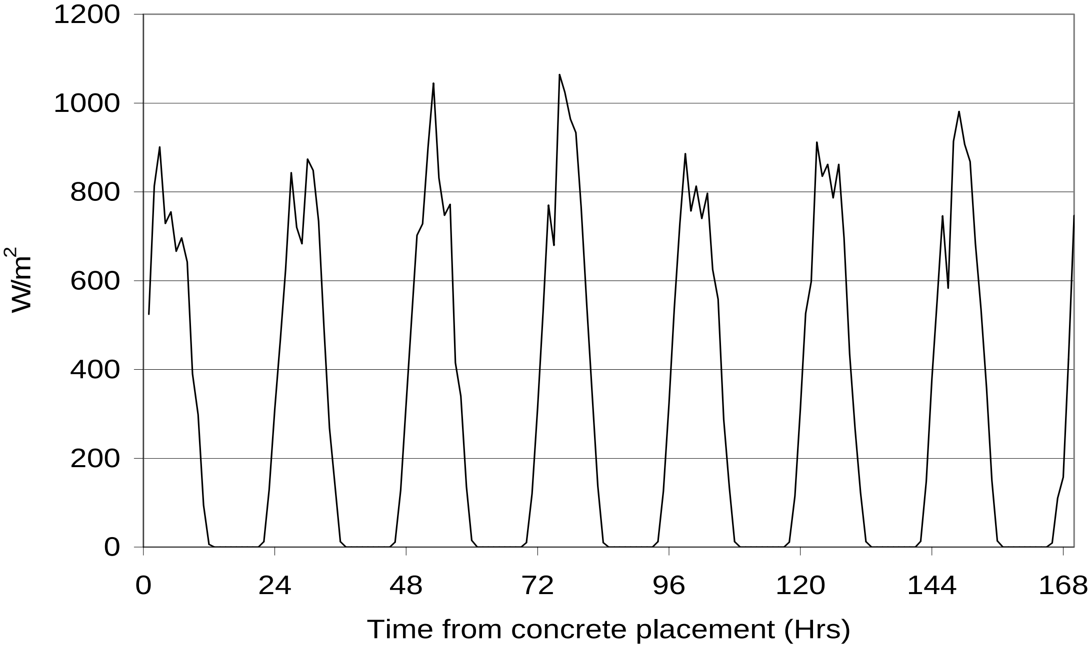

Figure A 1-10 - Solar radiation measured by weather station

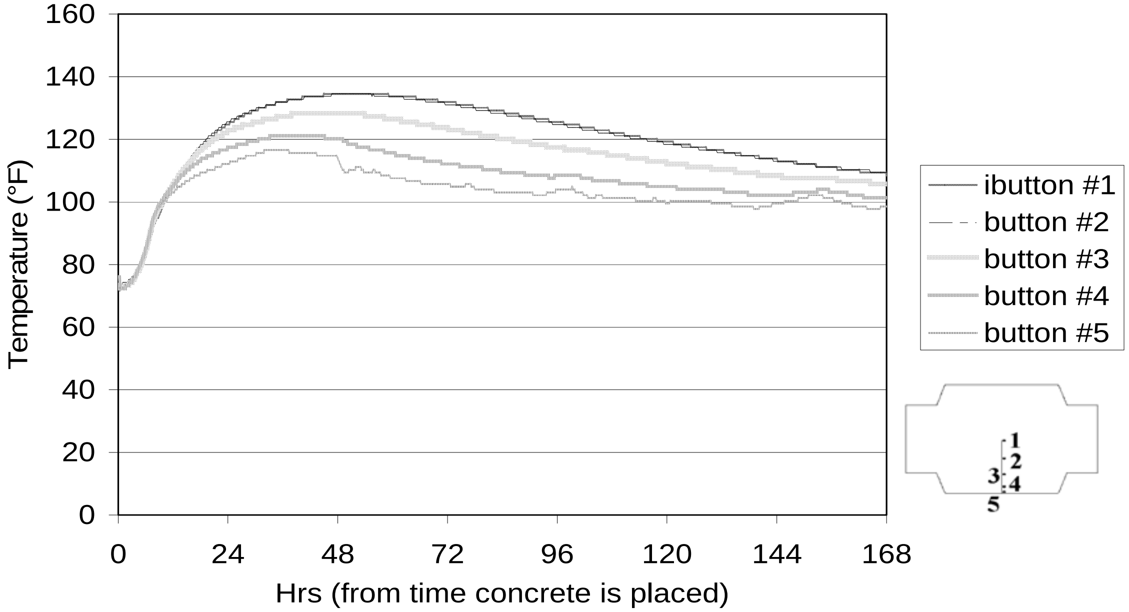

Figure A 1-11 - Temperature vs. time for temperature bar run #2

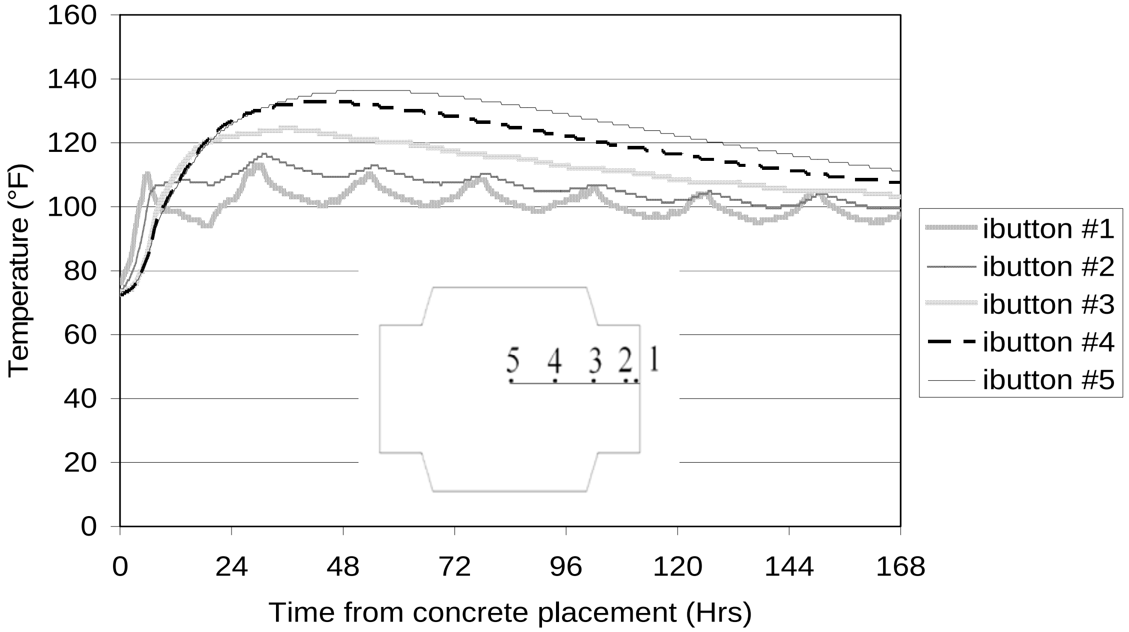

Figure A 1-12 - Temperature versus time for temperature bar run #4

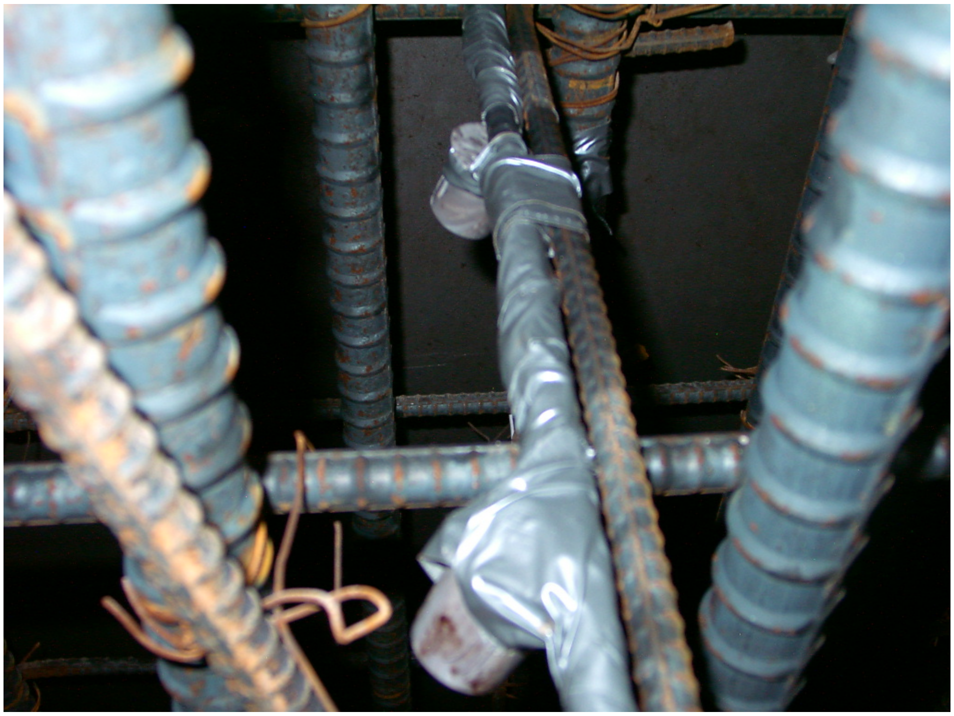

Figure A 1-13 – Up-close view of temperature bar using epoxy for iBution coating

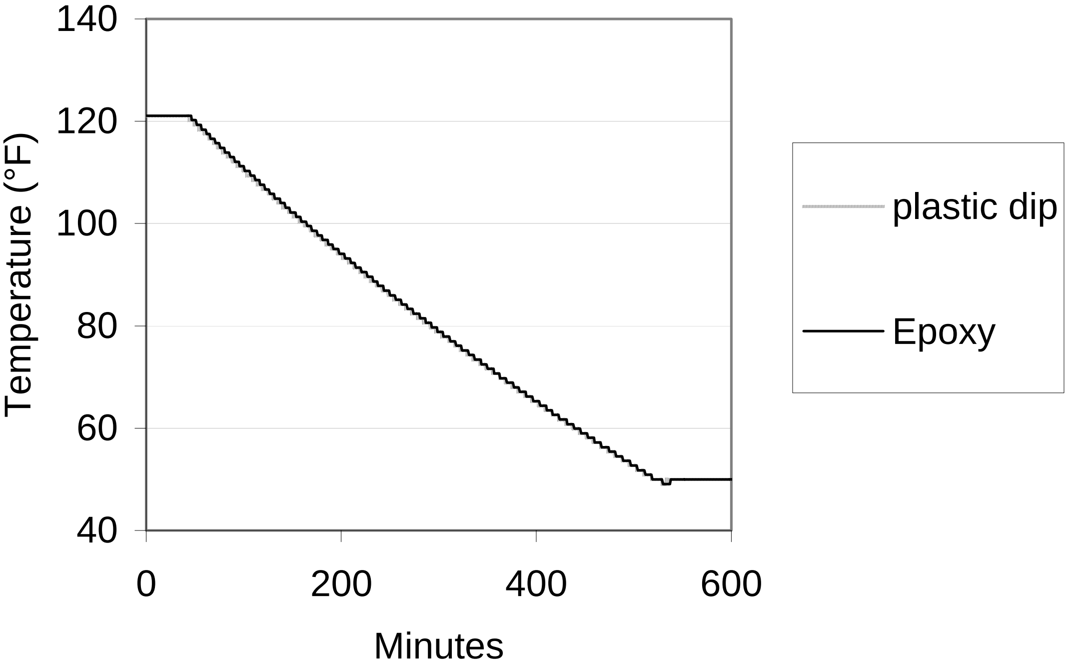

Figure A 1-14 - Water bath comparison of iButton coating methods

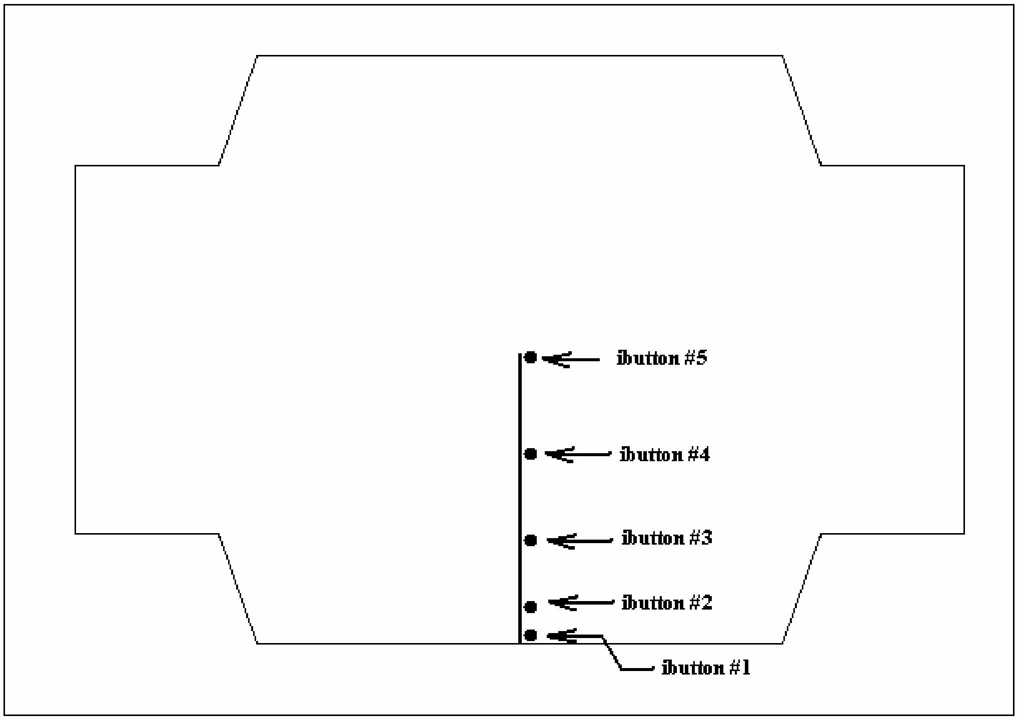

Figure A 1-15 - Plan view of column showing iButton runs K1 and J1 layout (not to scale)

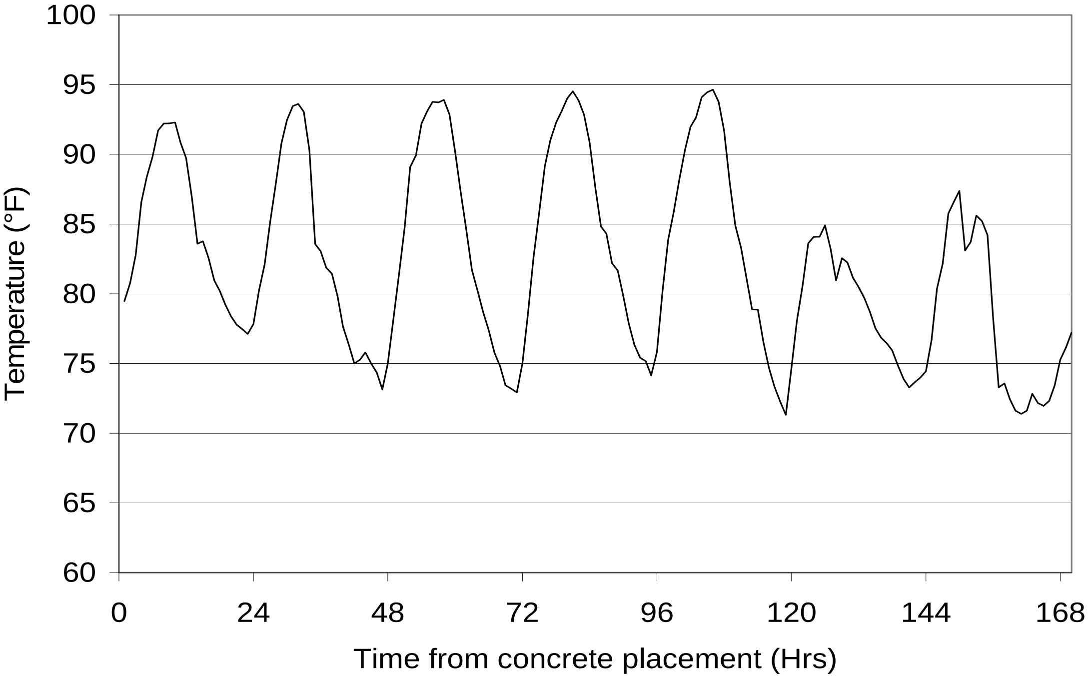

Figure A 1-16 - Temperature measured by weather station

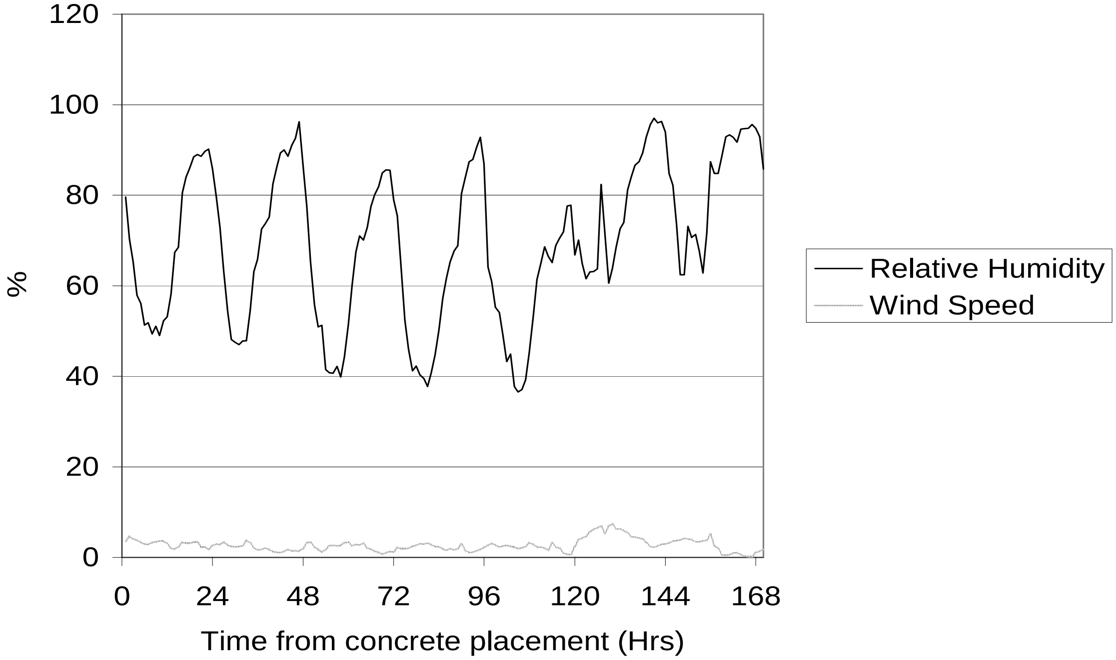

Figure A 1-17 - Relative humidity and wind speed measured by weather station

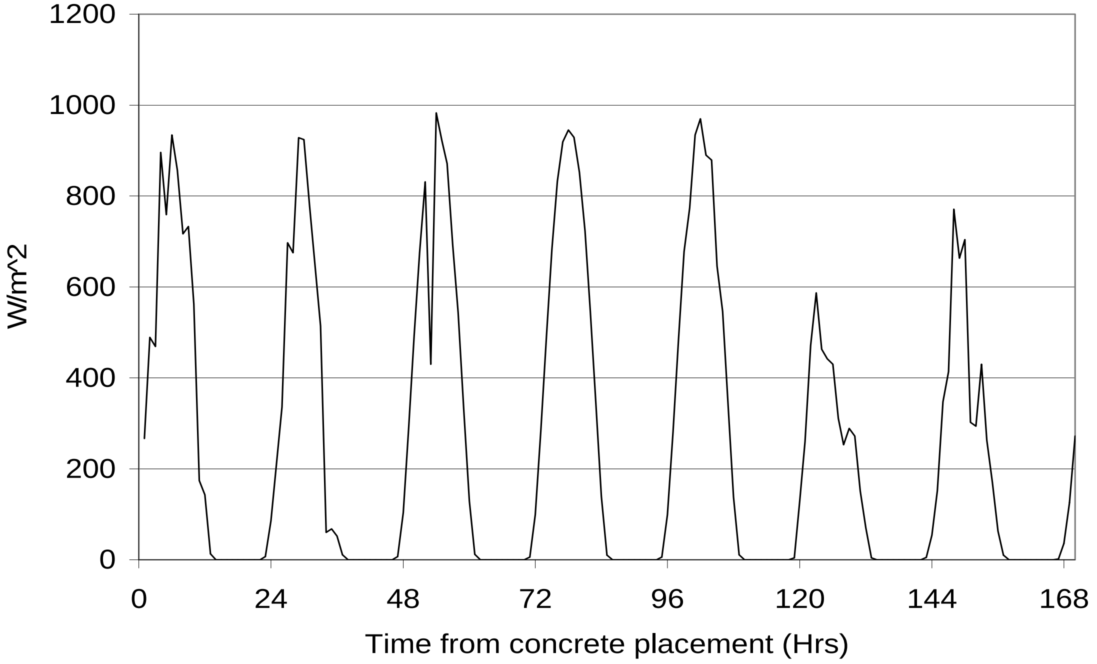

Figure A 1-18 - Solar radiation measured by weather station

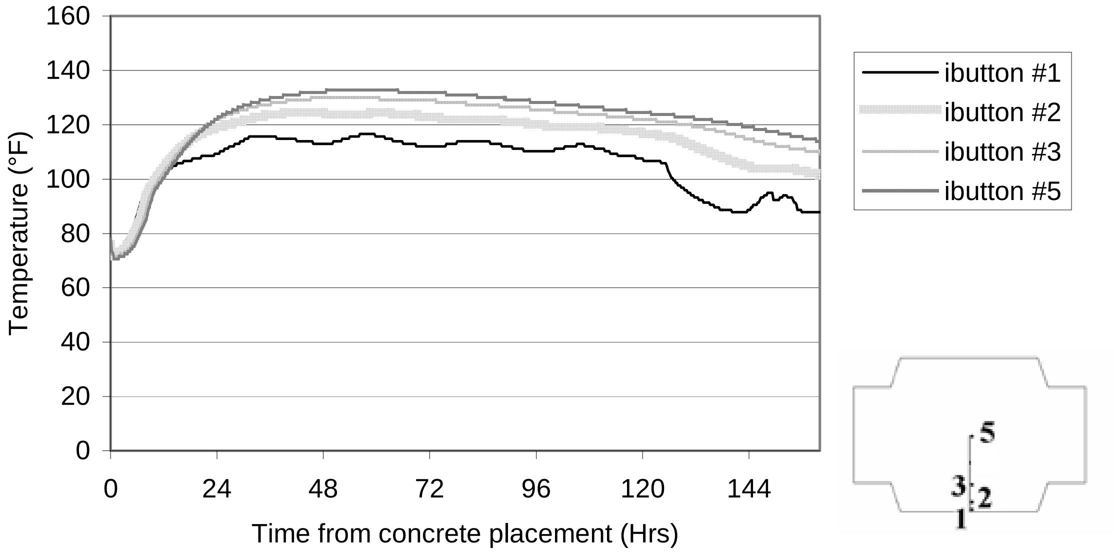

Figure A 1-19 - Temperature of iButtons from K1

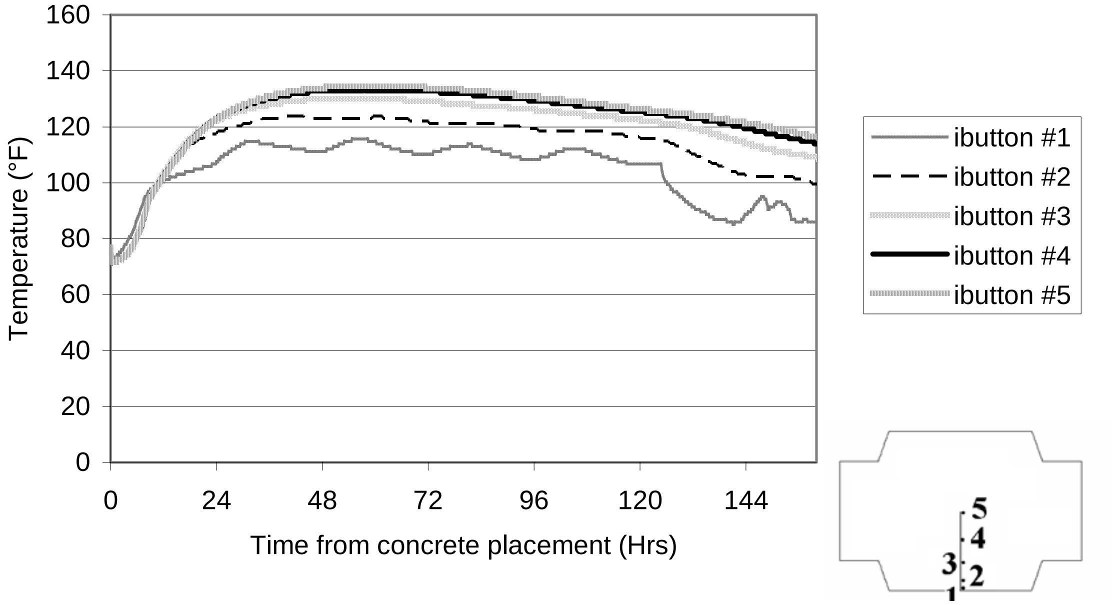

Figure A 1-20 - Temperature of iButtons from J1

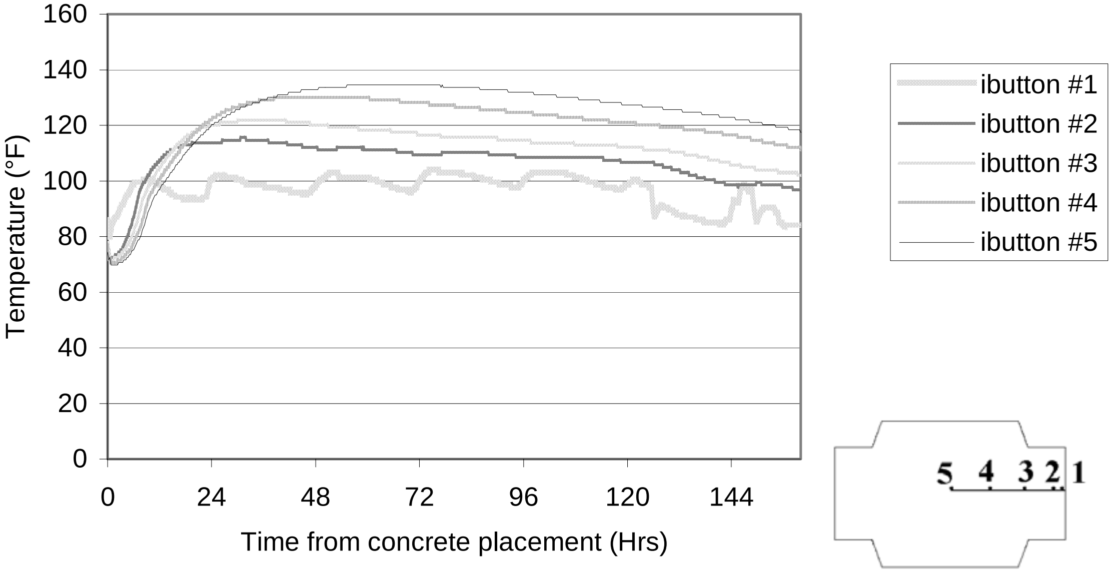

Figure A 1-21 - Temperature of iButtons from K2

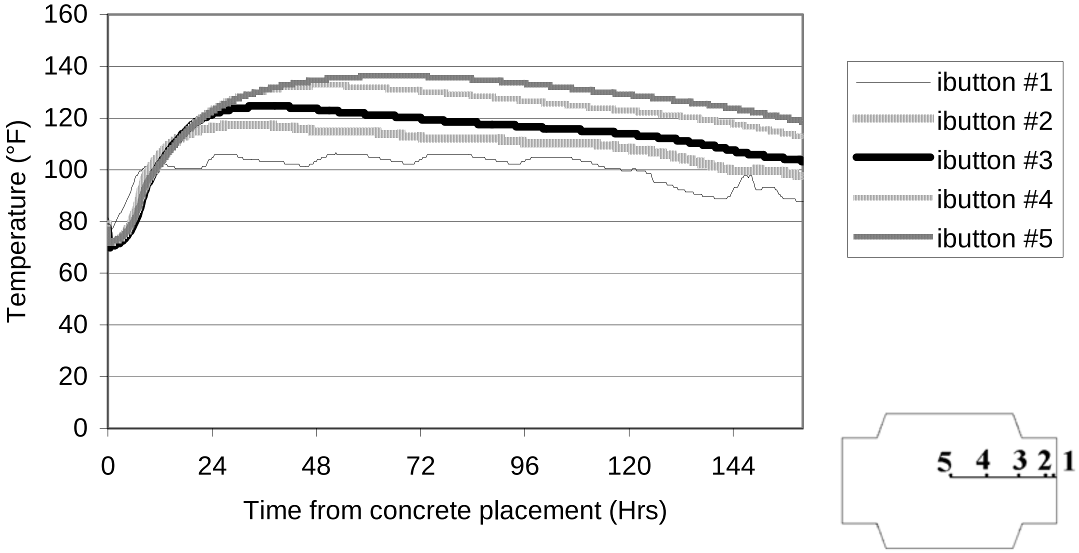

Figure A 1-22 - Temperature of iButtons from J2

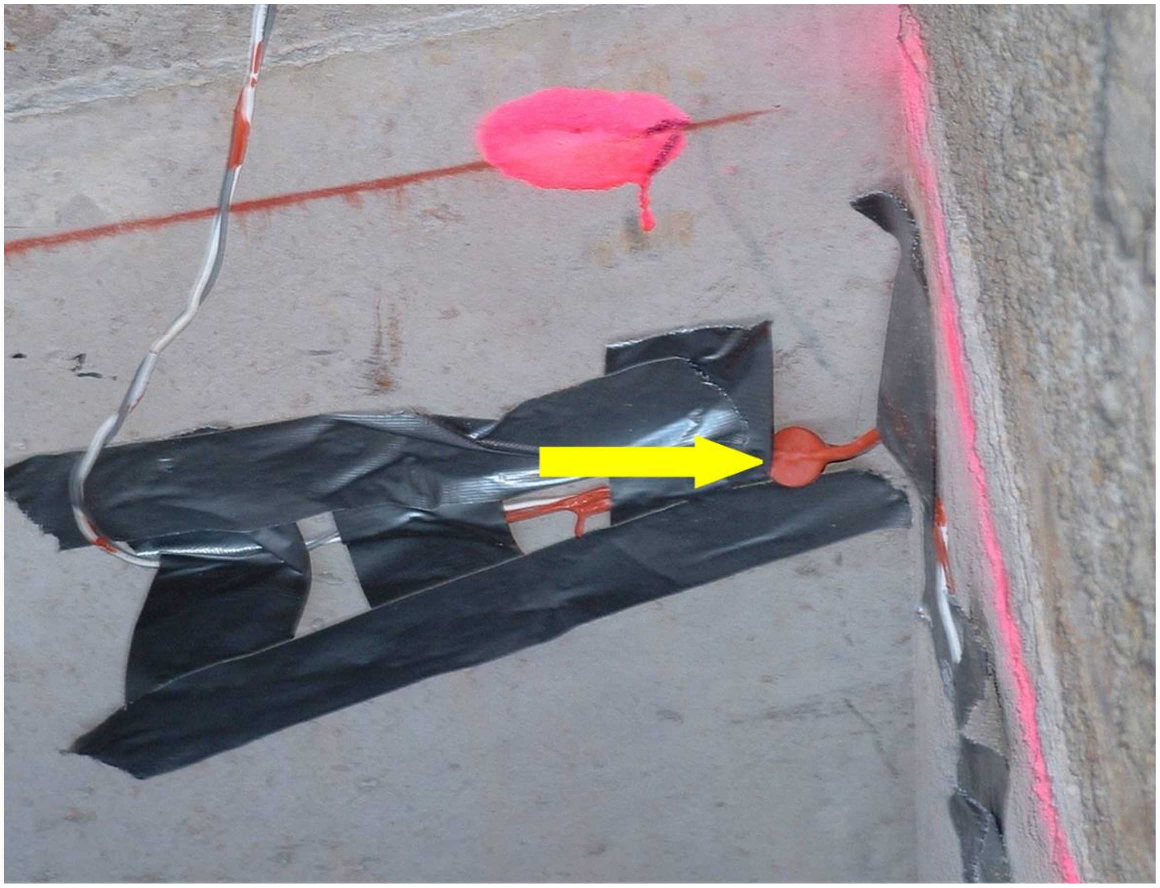

Figure A 1-23 - Picture of iButton #5 taped onto form of northeast corner

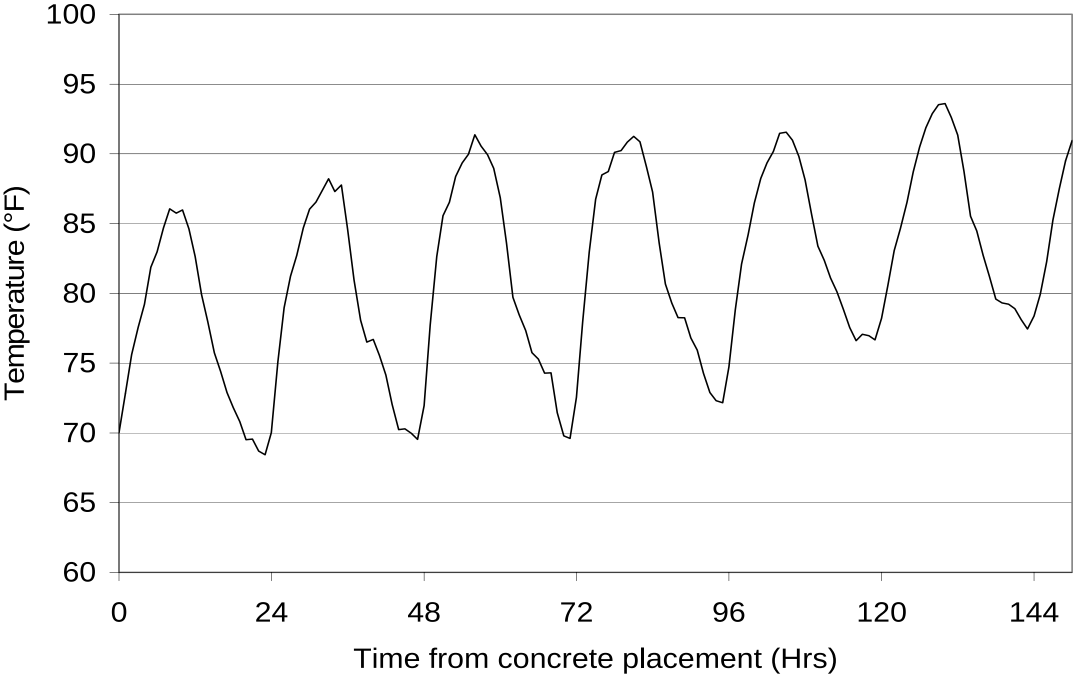

Figure A 1-24 - Temperature measured by weather station

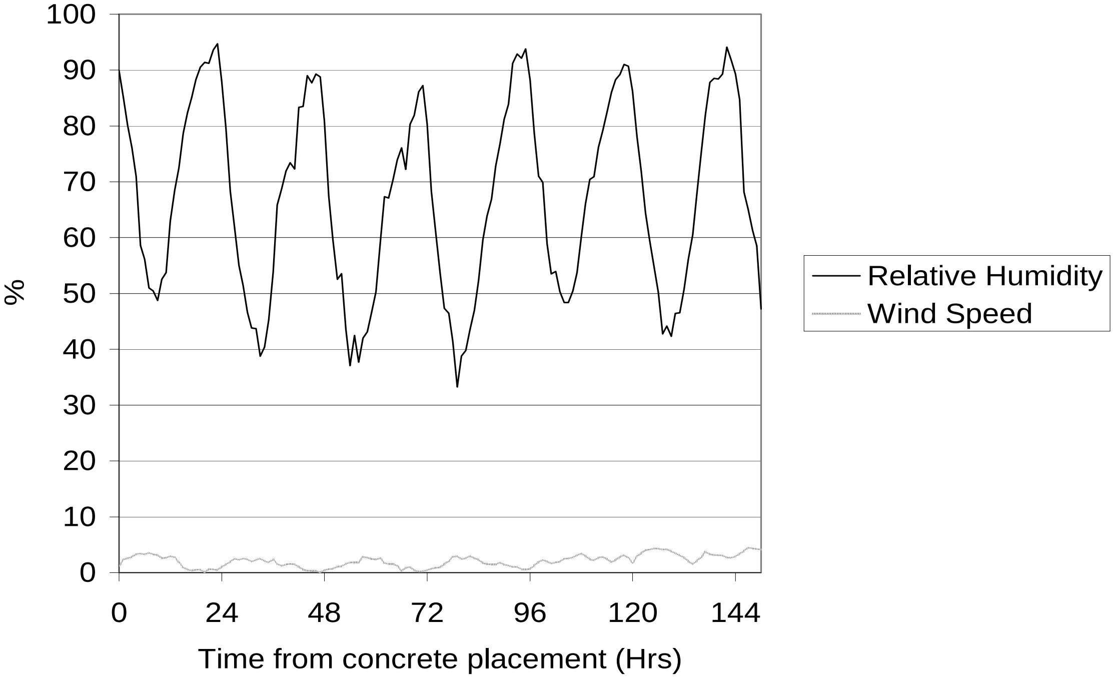

Figure A 1-25 - Relative humidity and wind speed measured by weather station

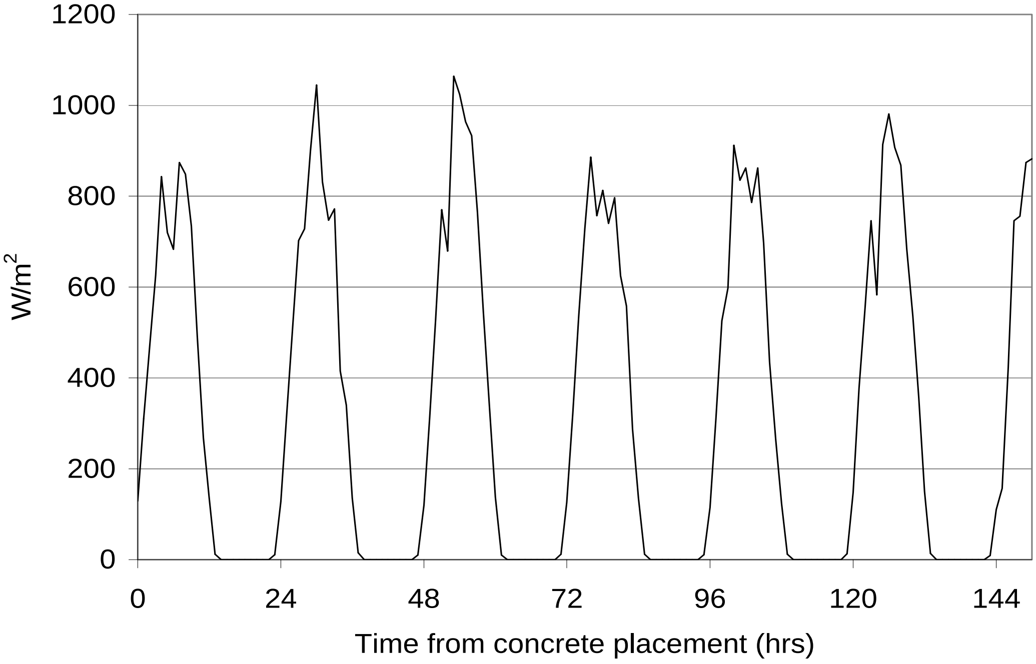

Figure A 1-26 - Solar Radiation measured by weather station

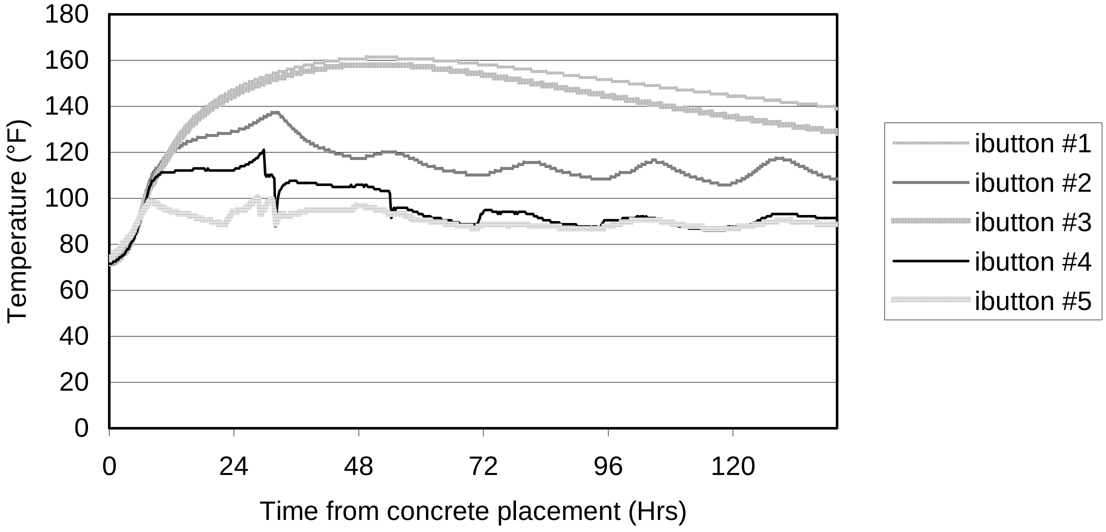

Figure A 1-27 - Measured iButton footing temperatures

Figure A 1-28 - Southward facing view of footing 2

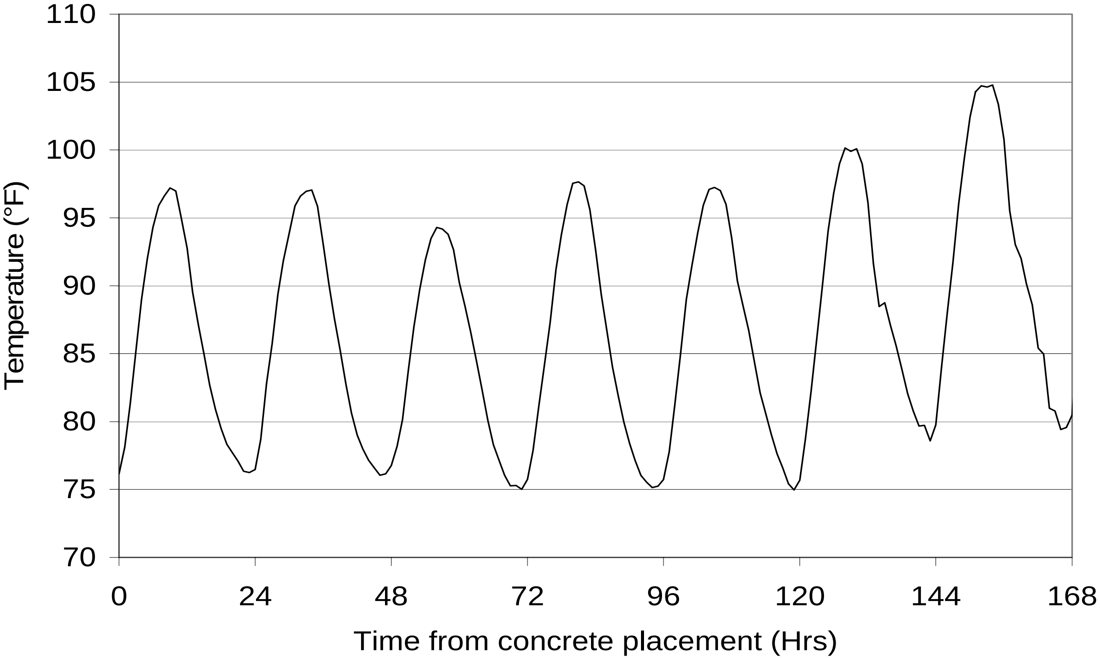

Figure A 1-29 - Temperature measured by weather station

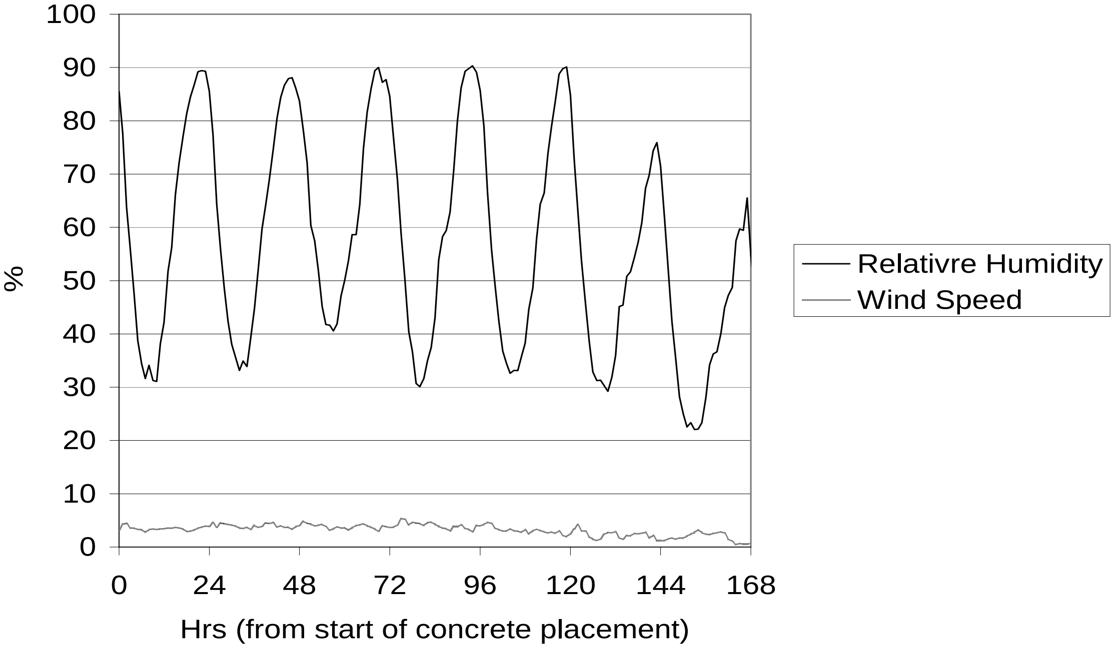

Figure A 1-30 - Relative humidity and wind speed measured by weather station

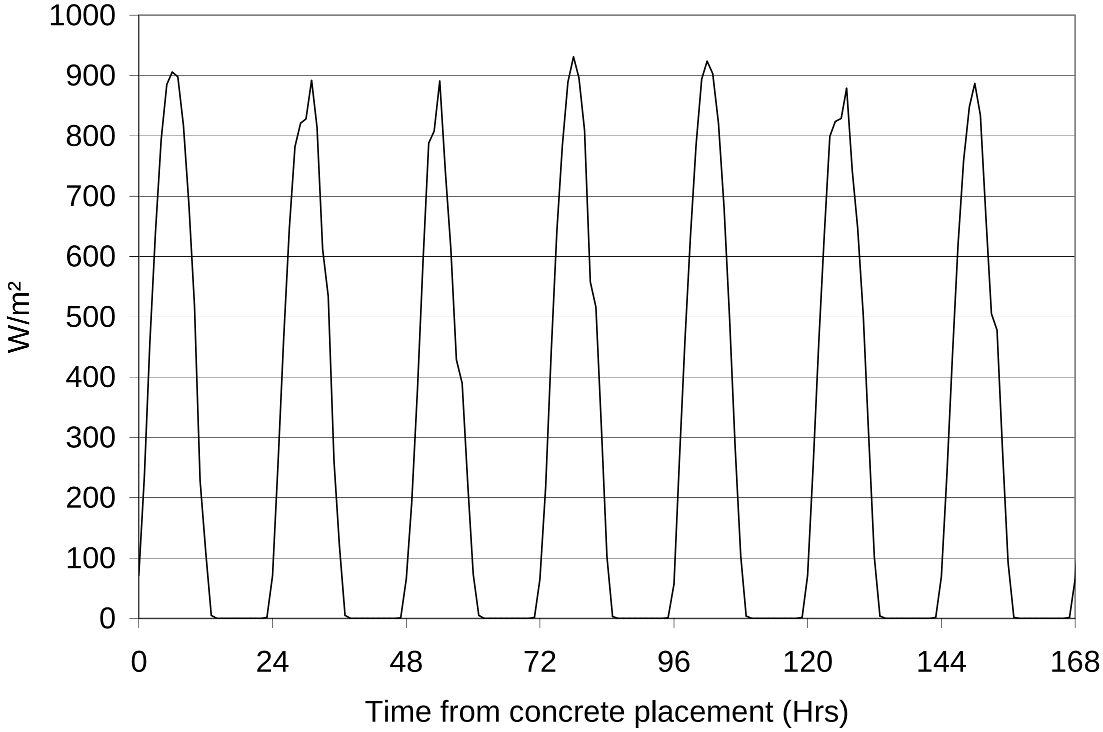

Figure A 1-31 - Solar radiation measured by weather station

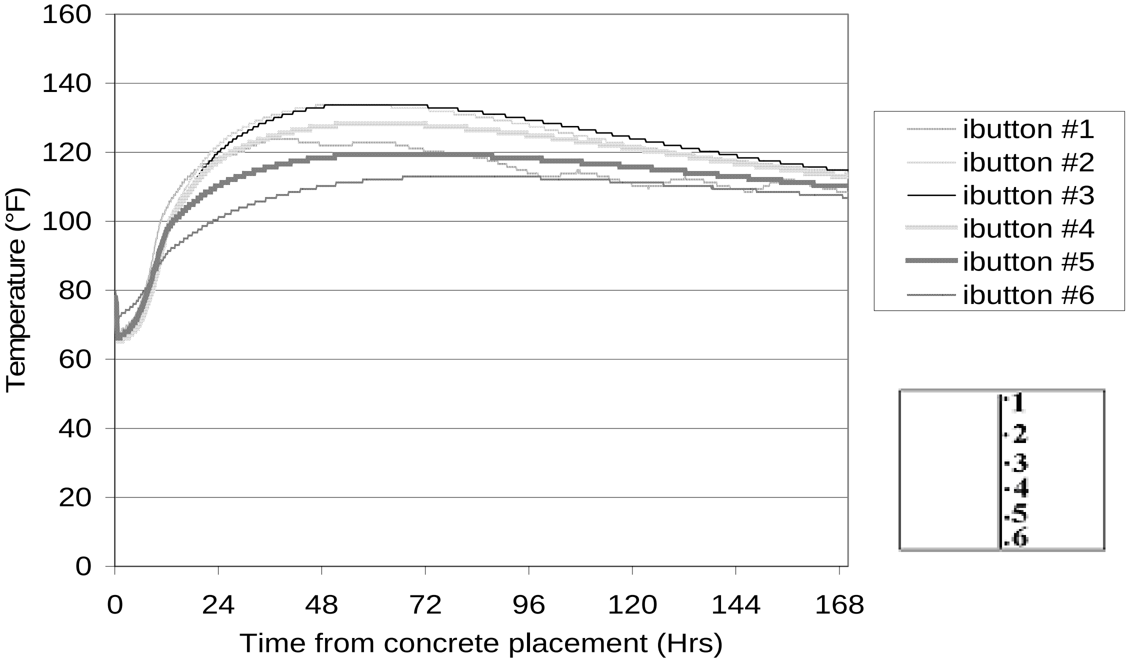

Figure A 1-32 - Temperature measured by iButtons on temperature bar

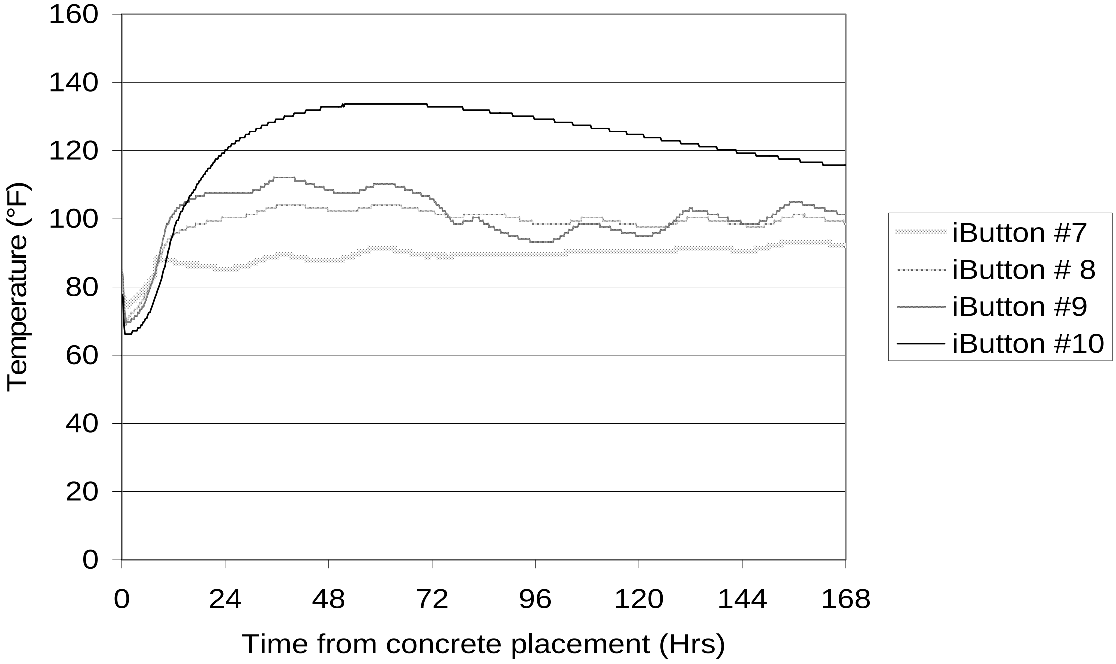

Figure A 1-33 - Temperature measured by iButtons 7-10

APPENDIX A-2 QUEEN ISABELLA CAUSEWAY FEBRUARY 2004

A-2.1 Introduction

As part of TxDOT project 4563, a graphical user-friendly computer program is being developed to predict the in-place temperature development of concrete members during curing. Each construction project uses different combinations of formwork, architectural form liners, concrete raw materials and curing techniques for concrete. In addition, environmental conditions during concrete placement and curing differ for every placement. To assure accurate results for the model, data from as many of these variations as possible must be captured and used in the model calibration.

On September 15, 2001 a barge ran into the Queen Isabella Causeway. The impact destroyed a 240 ft. section of the bridge, killing 8 people and cutting off the only road to South Padre Island. As part of a three point plan to improve bridge safety, mass concrete dolphins were built to form a “bumper” around the bridge piers (The Associated Press 2003). The dolphins at the Queen Isabella Causeway were selected for temperature instrumentation for model calibration because of the type of materials used, weather conditions expected, location, project accessibility and formwork used. The field site was instrumented on February 4-16, 2004.

A-2.2 Dolphin Construction

The dolphin’s dimensions were 16’ square by 9’ in depth. The dolphins were supported by nine piers that elevate the dolphins a few feet above the water line. A 2’ thick precast panel was used as a stay-in-place bottom formwork. Figure A 2-1 shows dolphins 8, 9 and 10 before the side formwork was placed. The remaining 7’ thick sections were placed by a pump truck from the bridge. Figure A 2-2 shows the concrete being placed in dolphin 6. Figure A 2-3 shows the steel formwork used on dolphin 6.

Orion Construction was the prime contractor and placed the concrete. Transit Mix Concrete and Materials Co. designed the concrete mix and supplied the concrete. Table A 2-1 shows the concrete mix design and fresh properties. Table A 2-2 shows the tested, hardened concrete properties. Semi-adiabatic calorimetry was also performed on a sample taken on-site; these results will be reported at a later time.

Concrete placement on dolphin 6 started at approximately 11:30 am on February 5th. Concrete placement on dolphin 7 started at about 4:00 pm on February 5th. Forms were removed on February 10th. The maximum in-place fresh concrete temperature was 75°F. No curing methods were used after forms were removed.

A-2.3 Instrumentation

Thermochron iButtons®[2] made by Dallas Semiconductor (Dallas Semiconductor, 2003) were used to measure and log the dolphin in-place temperature. Thermochron iButtons record the temperature in increments of 0.9°F and have an accuracy of ±1.8 °F (Dallas Semiconductor, 2003). The procedures for preparing the iButtons for installation were similar to those used in an earlier TxDOT study (Ramaiah, 2002). Wires were soldered onto the iButtons to allow external access to the iButton data. After the wires were attached, the iButtons were coated with epoxy to prevent water damage. To speed-up installation, series of iButtons were attached to ½" diameter acrylic dowels with duct tape. These prefabricated "temperature bars" were placed in dolphins 6 and 7 the day before concrete was placed. Temperature bars 1-3 were installed on dolphin 6 while temperature bar 4 was installed on dolphin 7. An additional iButton was taped to the chamfer on the southwest corner of dolphin 6 and for convenience will be included on all tables and charts as iButton #4 on temperature bar 3. Table A 2-3 to Table A 2-6 show

---

[2] iButton® is a registered trademark of Dallas Semiconductor

the locations of temperature bars 1-4. Figure A 2-4 and Figure A 2-5 show temperature bars 1 and 2, respectively, after installation.

A-2.4 Weather Data

Weather data were acquired using a Campbell Scientific weather station. The weather station has instrumentation to record relative humidity, temperature, solar radiation, precipitation, wind speed and wind direction. The relative humidity and temperature sensor was damaged during transport and could not collect data. Ambient temperature was instead recorded using an iButton that was taped to the bottom of the weather station data logger box. Figure A 2-6 to Figure A 2-8 show the temperature, wind speed and solar radiation measured. The time shown on the graphs is from the start of concrete placement for dolphin 6. Dolphin 7 was placed four and a half hours after dolphin 6. The weather station was placed on a sand bar next to the barge dock at the contractor's construction yard. Figure A 2-9 shows a picture of the weather station next to the sand bar.

A-2.5 Concrete Temperature Data Acquired

The Thermochron iButtons were programmed to measure and log the temperature every 15 minutes. Figure A 2-10 to Figure A 2-13 show the data acquired from temperature bars 1-4. The data from iButtons 1 and 3 on temperature bar 1 were not recorded properly because of programming errors and consequently are not shown in Figure A 2-10. Figure A 2-14 shows the maximum temperature, minimum temperature and maximum temperature difference recorded in dolphin 6. The maximum temperature and maximum temperature difference recorded in dolphin 6 were 145.4°F and 72°F respectively. The maximum temperature recorded in dolphin 6 was recorded by iButton 5 on temperature bar 2. Figure A 2-15 shows the maximum temperature, minimum temperature and maximum temperature difference recorded in dolphin 7. The maximum temperature and maximum temperature difference recorded in dolphin 7 were 123.8°F and 45.9°F respectively. The maximum temperature recorded in dolphin 7 was recorded by iButton 1 on temperature bar 4. The maximum recorded temperatures for dolphin 7 were not as high as that of dolphin 6 because iButtons were not placed vertically in dolphin 7 like they were in dolphin 6 (temperature bar 2). A visual inspection for cracking of dolphins 6 and 7 was made 11 days after concrete placement. Even though the temperature difference on both dolphins was large, no cracks were found.

A-2.6 Summary

Table A 2-7 shows the maximum temperatures and temperature differences recorded in each dolphin. Both dolphins should show similar temperature development because they are at the same location. The concrete was placed within a few hours on the same day from the same batch plant and from the same mix design. The temperature data for the dolphins is not the same because iButtons were not placed at the point of maximum temperature rise in dolphin 7 and hence this information was not recorded. Eleven days after construction, no visual signs of cracking in dolphins 6 or 7 were found. The temperature data collected will be used to calibrate the concrete temperature prediction model being developed as part of TxDot project 4563.

A-2.7 Acknowledgements

The advice and assistance of the TxDOT Bridge Division and TxDOT McAllen office is greatly appreciated. The authors wish to thank Ralph Browne, Tyler Ley, and Augustine Ramirez for arranging access to field sites.

Table A 2-1 - Concrete properties

Item	Content	Material Description
Cement	426 lb./yd.^{3}	TXI - Type I/II
Class F Fly Ash	168 lb./yd.^{3}	Coleto Creek
Coarse Aggregate	1874 lb./ yd.^{3}	1" Siliceous River Gravel
Fine Aggregate	1158 lb./ yd.^{3}	Natural Sand
Air Entraining Admixture	1.26 oz/ cwt.	Master Builders AE 90
Mid Range Water Reducer	4.1 oz/ cwt.	Master Builders Polyheed 997
Water Reducer / Retarder	2.73 oz/ cwt.	Pozzolith 300R
Ice	60 lb./ yd.^{3}	
Water	147.9 lb./ yd.^{3}	
Jobsite Measured Air Content	9.00%	
Jobsite Measured Slump	7.5"	
Water/cementitious materials ratio	0.35	

Table A 2-2 - Tested concrete properties

Concrete Age (days)	Compressive Strength (psi)	Splitting Tensile Strength (psi)	Elastic Modulus (psi)	Permeability (Coulombs)
4	4330	570	-	-
28	6020	670	5.67×10^6	-
91	6730	670	-	865

Table A 2-3 - Location of iButtons on temperature bar 1 on dolphin 6

iButton #	Distance from North Side Formwork	Distance from West Side Formwork	Distance vertically from precast panel
1	6' - 3"	6' - 3"	1' - 9"
2	5' - 3"	6' - 3"	1' - 8"
3	4' - 3"	6' - 3"	1' - 7"
4	3' - 3"	6' - 3"	1' - 6"
5	2' - 3"	6' - 3"	1' - 5"
6	1' - 3"	6' - 3"	1' - 5"
7	0' - 9"	6' - 3"	1' - 5"
8	0' - 3"	6' - 3"	1' - 5"

Table A 2-4 - Location of iButtons on temperature bar 2 on dolphin 6

iButton #	Distance from North Side Formwork	Distance from West Side Formwork	Distance vertically from precast panel
1	7' - 8"	5' - 2"	0' - 8.5"
2	7' - 8"	5' - 2"	1' - 8.5"
3	7' - 8"	5' - 2"	2' - 8.5"
4	7' - 8"	5' - 2"	3' - 8.5"
5	7' - 8"	5' - 2"	4' - 8.5"
6	7' - 8"	5' - 2"	5' - 8.5"
7	7' - 8"	5' - 2"	6' - 2.5"
8	7' - 8"	5' - 2"	6' - 8.5"

Table A 2-5 - Location of iButtons on temperature bar 3 on dolphin 6

iButton #	Distance from South Side Formwork	Distance from West Side Formwork	Distance vertically from precast panel
1	0' - 2"	4' - 9"	1' - 6"
2	0' - 5"	4' - 9"	1' - 6"
3	1' - 2"	4' - 9"	1' - 6"
4	1' - 6"	0' - 0"	5' - 3"

Table A 2-6 - Location of iButtons on temperature bar 4 on dolphin 7

iButton #	Distance from South Side Formwork	Distance from East Side Formwork	Distance vertically from precast panel
1	4' - 3"	6' - 2"	1' - 8"
2	4' - 3"	5' - 2"	1' - 8"
3	4' - 3"	4' - 2"	1' - 8"
4	4' - 3"	3' - 2"	1' - 8"
5	4' - 3"	2' - 2"	1' - 8"
6	4' - 3"	1' - 2"	1' - 8"
7	4' - 3"	0' - 8"	1' - 8"
8	4' - 3"	0' - 2"	1' - 8"

Table A 2-7 - Temperature data summary for dolphins 6 and 7

Concrete Member	Maximum Temperature Recorded (°F)	Maximum Temperature Difference Recorded (°F)
Dolphin 6	145.4	72
Dolphin 7	123.8	45.9

Figure A 2-1 - Dolphins 8, 9, and 10 before side formwork was placed

Figure A 2-2 - Top view of concrete being placed in dolphin 6

Figure A 2-3 - Dolphin 6 with formwork

Figure A 2-4 - Temperature bar 1 after installation

Figure A 2-5 - Temperature bar 2 after installation

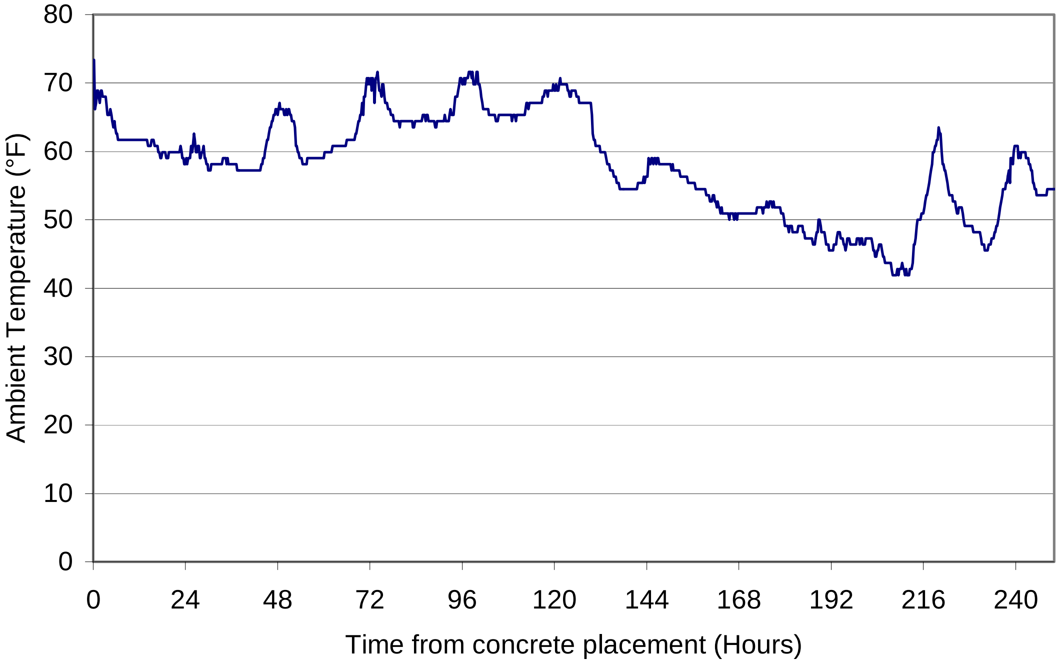

Figure A 2-6 - Ambient temperature data

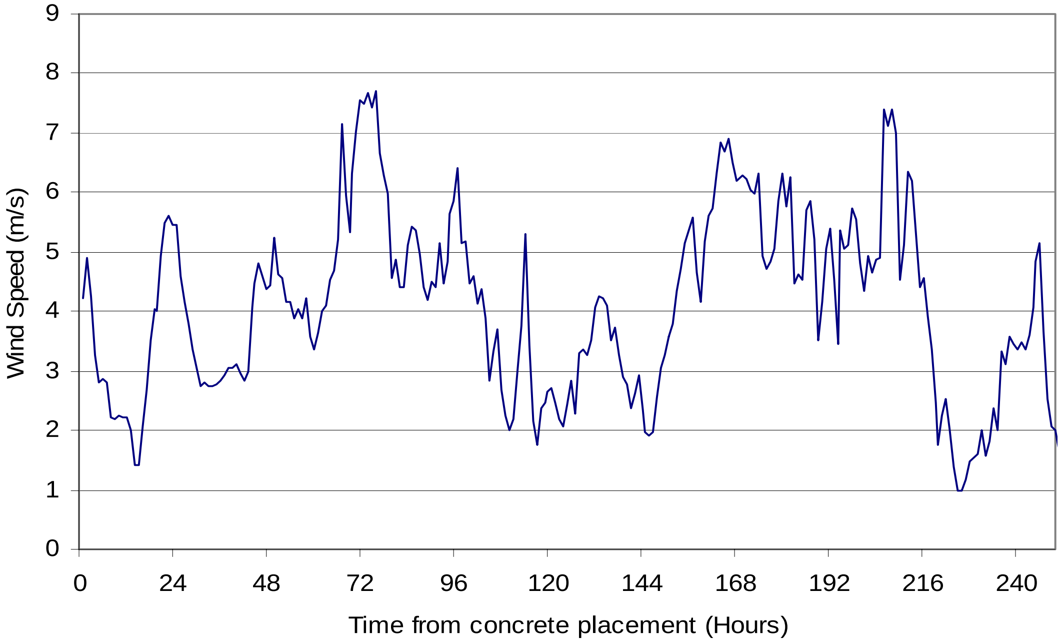

Figure A 2-7 - Wind speed data

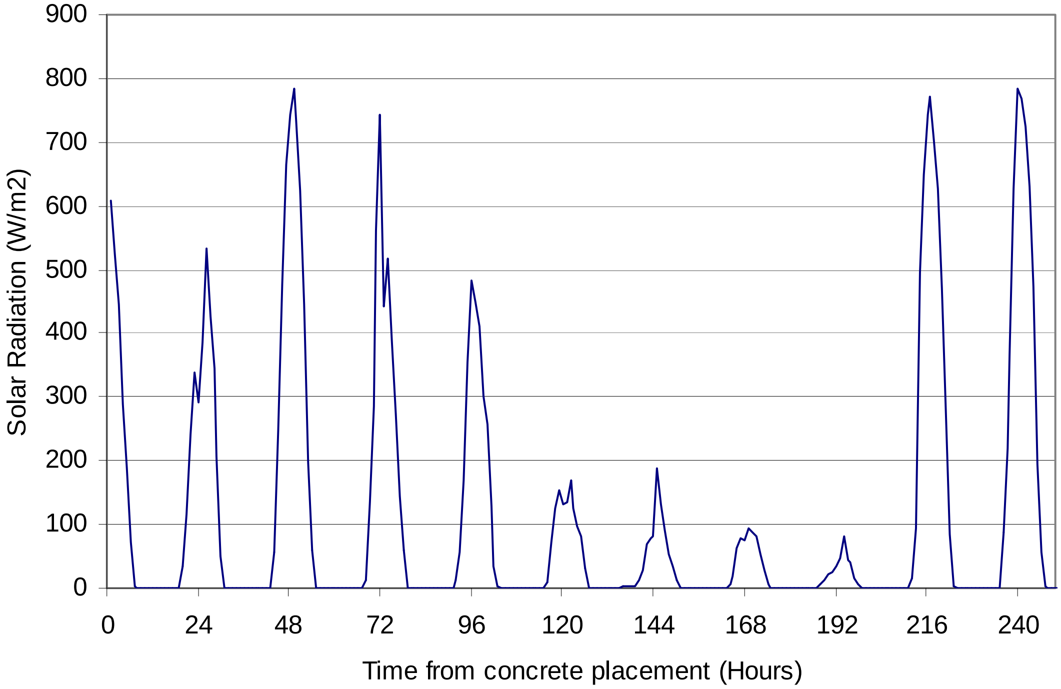

Figure A 2-8 - Solar radiation data

Figure A 2-9 - Weather station on sandbar in construction yard

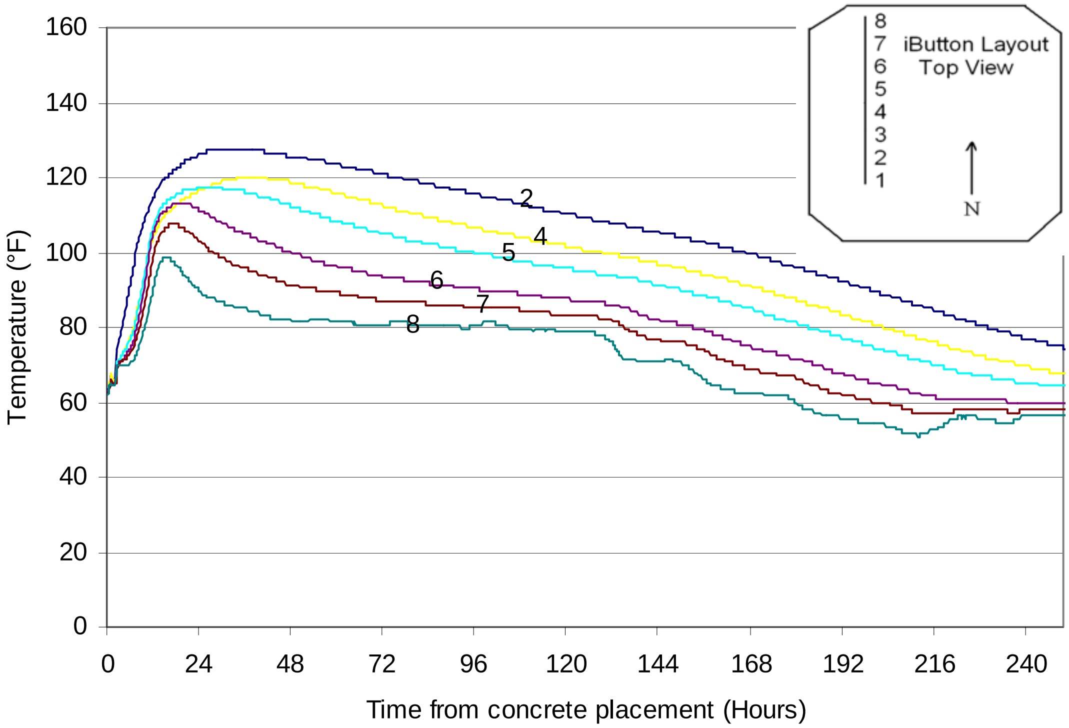

Figure A 2-10 - Data from temperature bar 1 on dolphin 6

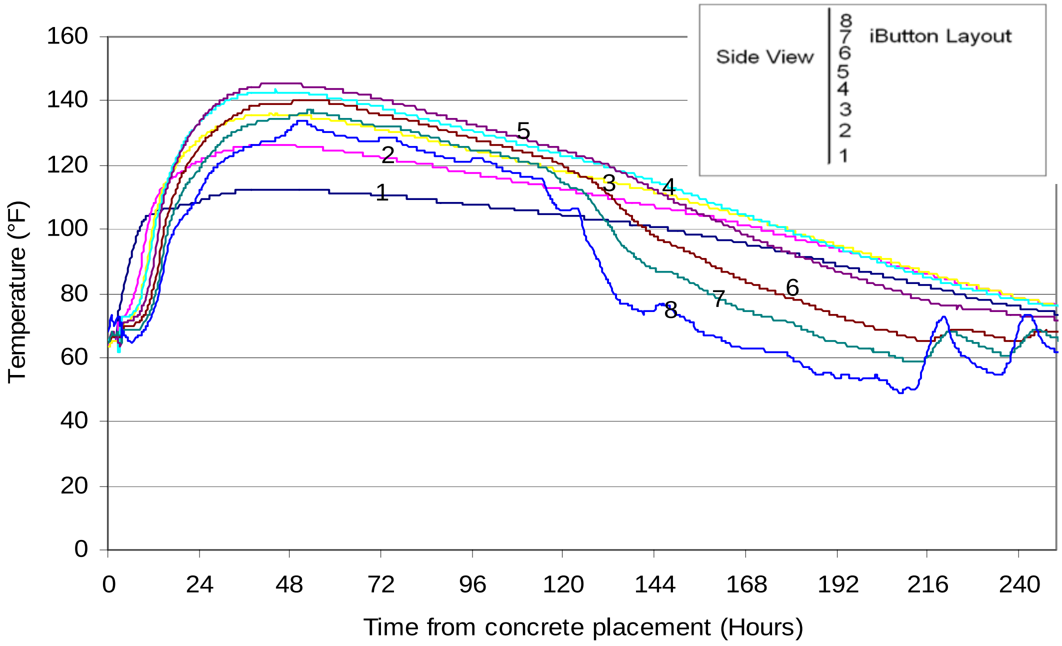

Figure A 2-11 - Data from temperature bar 2 on dolphin 6

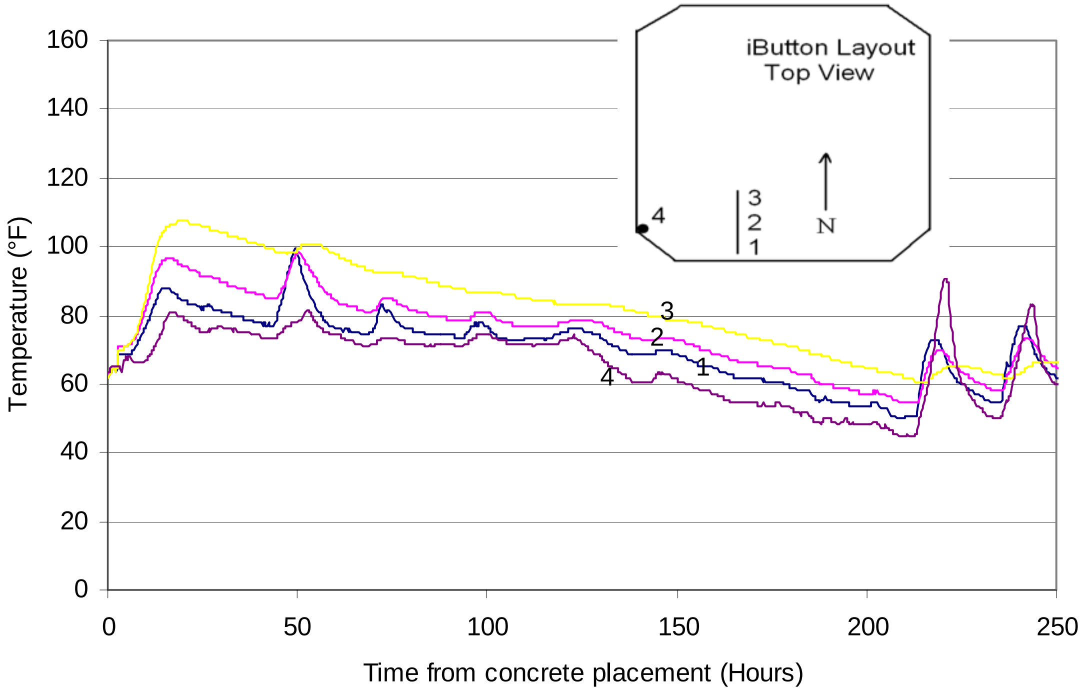

Figure A 2-12 - Data from temperature bar 3 on dolphin 6

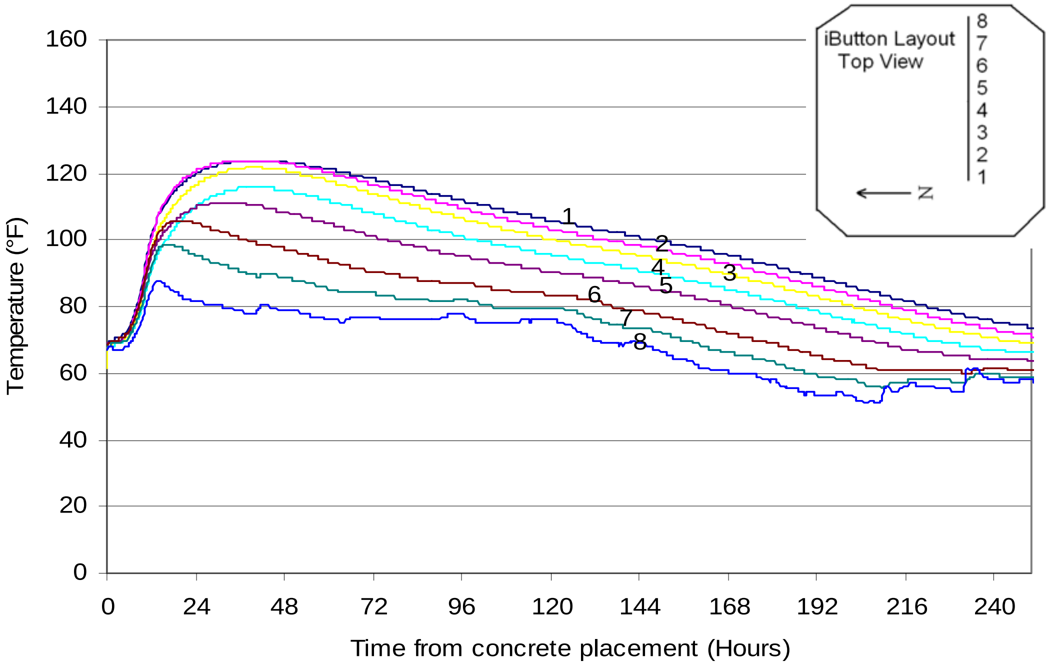

Figure A 2-13 - Data from temperature bar 4 on dolphin 7

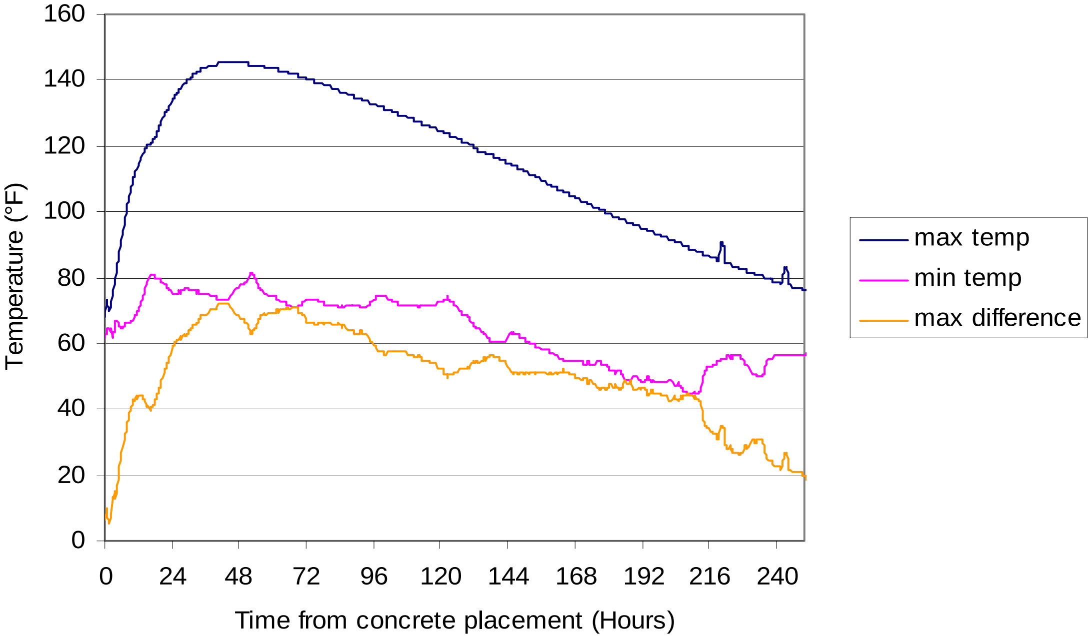

Figure A 2-14 - Maximum temperature, minimum temperature and maximum temperature difference at any location in dolphin 6

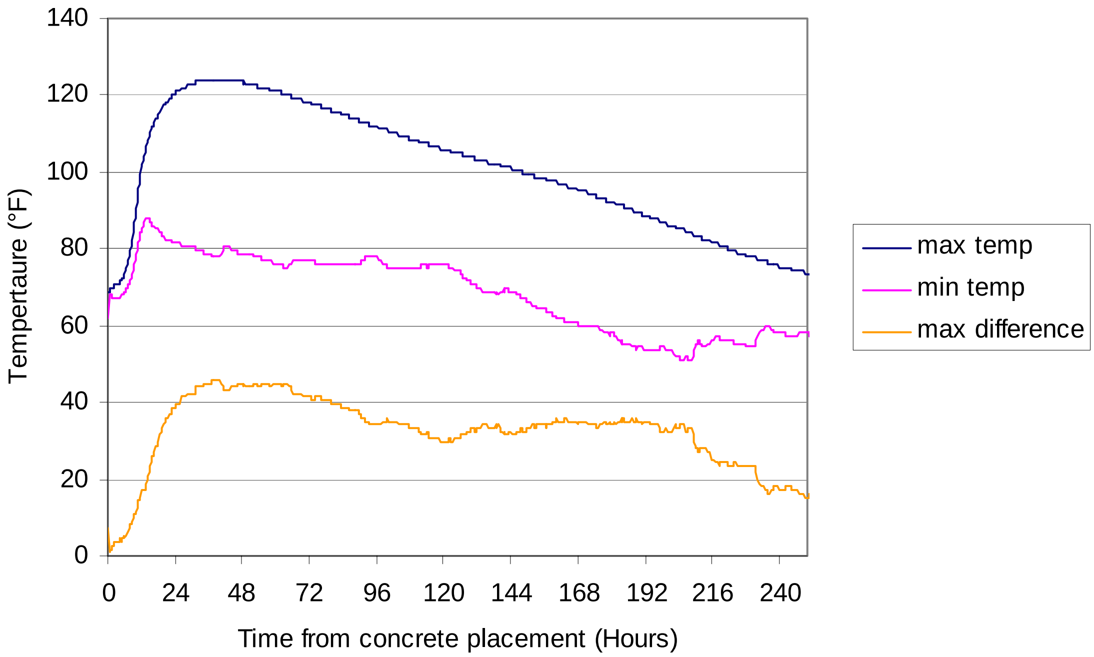

Figure A 2-15 - Maximum temperature, minimum temperature and maximum temperature difference at any location in dolphin 7

APPENDIX A-3 SCOTT ST. BRIDGE IN WICHITA FALLS

A-3.1 Introduction

As part of TxDOT project 4563 a graphical, user-friendly computer program is being developed to predict the in-place temperature development of concrete members during curing. Each construction project uses different combinations of formwork, architectural form liners, concrete raw materials and curing techniques. In addition, environmental conditions during concrete placement and curing differ for every placement. To assure good results, as many of these variations as possible must be used in the model calibration.

The Scott St. bridge in Wichita Falls that crosses the F W and D Railroad and Old Iowa Park Highway is being rebuilt. The new bridge is a 7 span bridge made up of six bent caps and two abutments. The project goes from Jefferson Street to 0.8 miles east of Junction US 287. Bent cap 6 on this project was selected for instrumentation because of the type of aggregate used, location, member type, project accessibility and type of formwork used. The field site was instrumented over March 31 – April 12, 2004.

A-3.2 Bent Cap Construction

The bent cap had a rectangular cross section. Figure A 3-1 shows the view looking southward of bent cap 6 during concrete placement. The bent cap cross-section dimensions were 3’-3” by 3’-3". The bent cap was supported by 5 circular columns. The columns were 3’-0” in diameter and were spaced 18’-6” off center. The forms were made from ¾” thick plywood. The formwork, walkway, and railings were supported by 4”x4” wood joists 12” off center resting on steel beams.

The prime contractor was Jay-Reese Contractors, Inc. City Concrete supplied the concrete. Table A 3-1 shows the concrete mixture properties. Table A 3-2 shows the tested concrete properties. Figure A 3-2 shows the concrete being placed. Concrete placement on the bent cap started at approximately 8:00 am on March 31st. Forms were removed on April 5th. The maximum in-place fresh concrete temperature was 75°F. No curing methods were used after forms were removed.

A-3.3 Instrumentation

Thermochron iButtons®[3] made by Dallas Semiconductors (Dallas Semiconductor, 2003) were used to measure and log the bent cap in-place temperature. Thermochron iButtons record the temperature in increments of 0.9°F and have an accuracy of ±1.8 °F (Dallas Semiconductor, 2003). The procedures for preparing the iButtons for installation were similar to those used in an earlier TxDOT study (Ramaiah, 2002). Wires were soldered onto the iButtons to allow external access to the iButton data. After the wires were attached, the iButtons were coated with epoxy to prevent water damage. To speed-up installation, series of iButtons were attached to ½” diameter acrylic dowels with duct tape. These prefabricated “temperature bars” were placed in bent cap 6 immediately before the concrete was placed. Temperature bars 1-4 were installed on a vertical cross section between the first and second column. Figure A 3-3 shows temperature bars 1-4 installed. Temperature bar 5 was installed at the western end of the bent cap to capture any end effects on the bent cap heat transfer. Figure A 3-4 shows temperature bar 5 installed in bent cap 6. Table A 3-3 to Table A 3-8 show the location of temperature bars 1-6, respectively. Temperature bar 6 was not taped to an acrylic dowel. Instead, the three iButtons on temperature bar 6 were tied to rebar within

---

[3] iButton® is a registered trademark of Dallas Semiconductor

½” of the formwork to capture any effect of the horizontal bracing of the formwork on the heat transfer.

A-3.4 Weather Data

Weather data were acquired using a Campbell Scientific weather station. The weather station had instrumentation to record relative humidity, and temperature, solar radiation, precipitation, wind speed and wind direction. Ambient temperature was also recorded using an iButton that was taped to the bottom of the weather station data logger box. Figure A 3-5 to Figure A 3-7 show the temperature, wind speed and solar radiation as measured by the weather station. Figure A 3-8 compares the temperature data measured by the weather station to the temperature data measured by the iButton taped to the bottom of the weather station. The weather station was placed in the contractor’s construction yard, which was located adjacent to the construction site. Figure A 3-9 shows a picture of the weather station in the construction yard.

A-3.5 Concrete Temperature Data Acquired

The Thermocron iButtons were programmed to measure and log the temperature every 15 minutes. Figure A 3-10 to Figure A 3-13 show the data acquired from temperature bars 1-4, respectively. The data from temperature bar 5 was lost. A possible reason for the corruption of the iButtons in temperature bar 5 is that one of the iButtons was not epoxied properly, allowing concrete pore water to reach an iButton. Figure A 3-14 shows the temperature variance vertically along the south side formwork. Figure A 3-15 shows the maximum temperature anywhere, minimum temperature anywhere and maximum temperature difference recorded anywhere in the bent cap. The maximum temperature and maximum temperature difference recorded were 128.3°F and 27.9°F respectively. The maximum temperature in the cap was recorded by iButton 4 on temperature bar 1.

Figure A 3-16 shows the effect that member orientation can have on the concrete temperature. The south side of the member received more solar radiation because of the orientation of the sun, resulting in higher surface temperatures. The south side data were recorded by iButton 1 on temperature bar 4. The north side data were recorded by iButton 1 on temperature bar 3. The maximum temperature difference between the south side temperature data and the north side temperature data is 14.4°F. The R^2 value comparing the south side temperature to the north side temperature is 0.959. This shows that even though the difference between the north side temperature and south side temperature can at times be great, an average value can be used in modeling solar radiation with only a small loss in accuracy.

A-3.6 Summary

Temperature sensors were placed in bent cap 6 of the Scott St. Bridge reconstruction in Wichita Falls before concrete placement to record the temperature development due to the heat of hydration of the concrete. The maximum temperature and maximum temperature difference recorded anywhere in the cap were 128.3°F and 27.9°F respectively. The temperature data collected will be used to calibrate the concrete temperature prediction model being developed as part of TxDOT project 4563.

A-3.7 Acknowledgements

The advice and assistance of the TxDOT Bridge Division and TxDOT Wichita Falls office is greatly appreciated. The authors wish to thank Ralph Browne, Tyler Ley, Doug Beer and Scott Reaves for arranging access to field sites.

Table A 3-1- Concrete Properties

Item	Content	Material Description
Cement	423 lb./yd.^{3}	TXI Ty I/II - Midlothian
Class C Fly Ash	107 lb./yd.^{3}	Oklaunion
Coarse Aggregate	1868 lb./ yd.^{3}	1" Crushed Granite
Fine Aggregate	1226 lb./ yd.^{3}	Granite Sand
Air Entraining Admixture	0.5 OZ/ cwt.	Darex II
Water Reducer / Retarder	4.0 OZ/ cwt.	WRDA 35
Water	212 lb./ yd.^{3}	
Jobsite Measured Air Content	5.50%	
Jobsite Measured Slump	3"	
Water/cementitious ratio	0.4	

Table A 3-2 - Tested Concrete Properties

Concrete Age	Compressive Strength (psi)	Splitting Tensile Strength (psi)	Elastic Modulus (psi)
2 day	2300	300	-
7 day	3360	380	-
28 day	4430	470	4134000
91 day	4950	-	-

Table A 3-3 - Location of iButtons on temperature bar 1

iButton #	Distance from North Side Formwork	Distance from West Side Formwork	Distance vertically from bottom formwork
1	1' - 8"	15' - 11"	0' - 0"
2	1' - 8"	15' - 11"	0' - 5"
3	1' - 8"	15' - 11"	0' - 10"
4	1' - 8"	15' - 11"	1' - 8"

Table A 3-4 - Location of iButtons on temperature bar 2

iButton #	Distance from North Side Formwork	Distance from West Side Formwork	Distance vertically from bottom formwork
1	1' - 9"	15' - 11"	3' - 2"
2	1' - 9"	15' - 11"	2' - 9"
3	1' - 9"	15' - 11"	2' - 4"
4	1' - 9"	15' - 11"	1' - 6"

Table A 3-5 - Location of iButtons on temperature bar 3

iButton #	Distance from North Side Formwork	Distance from West Side Formwork	Distance vertically from bottom formwork
1	0' - 0"	15' - 11"	1' - 9"
2	0' - 5"	15' - 11"	1' - 9"
3	0' - 10"	15' - 11"	1' - 9"
4	1' - 8"	15' - 11"	1' - 9"

Table A 3-6 - Location of iButtons on temperature bar 4

iButton #	Distance from North Side Formwork	Distance from West Side Formwork	Distance vertically from bottom formwork
1	3' - 3"	15' - 11"	1' - 9"
2	2' - 10"	15' - 11"	1' - 9"
3	2' - 5"	15' - 11"	1' - 9"
4	1' - 7"	15' - 11"	1' - 9"

Table A 3-7 - Location of iButtons on temperature bar 5

iButton #	Distance from North Side Formwork	Distance from West Side Formwork	Distance vertically from bottom formwork
1	1' - 7.5"	0' - 0"	0' - 8"
2	1' - 7.5"	0' - 6"	0' - 9.75"
3	1' - 7.5"	1' - 0"	0' - 11.5"
4	1' - 7.5"	2' - 0"	1' - 3"
5	1' - 7.5"	3' - 0"	1' - 6.5"
6	1' - 7.5"	4' - 0"	1' - 10"

Table A 3-8 - Location of iButtons on temperature bar 6

iButton #	Distance from North Side Formwork	Distance from West Side Formwork	Distance vertically from bottom formwork
1	3' - 2.5"	15' - 11"	2' - 1"
2	3' - 2.5"	15' - 11"	2' - 7"
3	3' - 2.5"	15' - 11"	3' - 0"

Figure A 3-1 - Southward view of bent cap 6 during concrete placement

Figure A 3-2 - Concrete being placed by pump at bent cap 6

Figure A 3-3 - Temperature bars 1-4 installed in bent cap 6

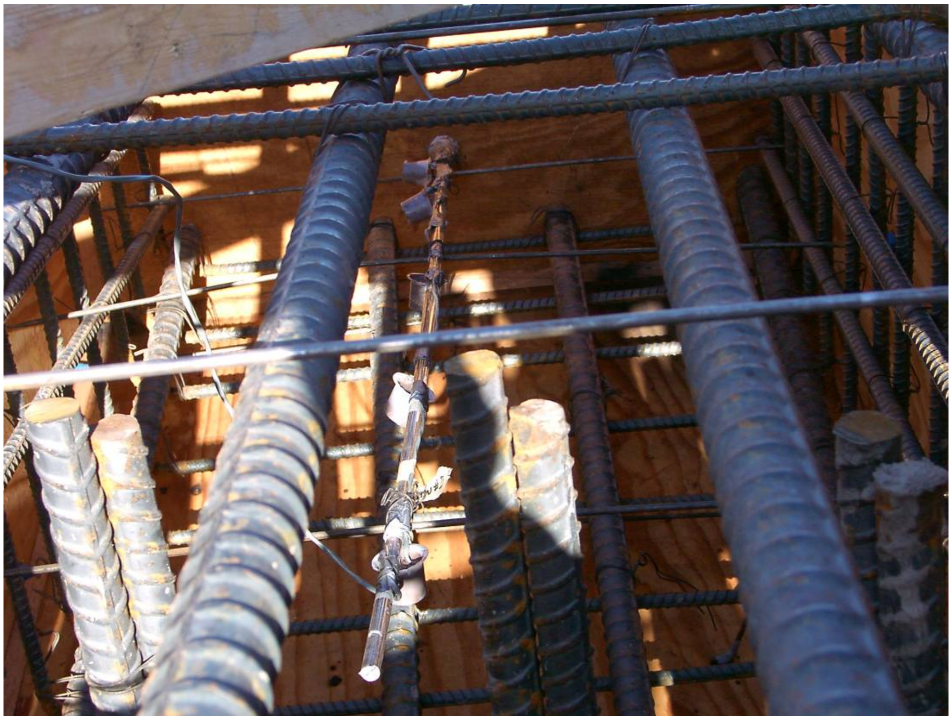

Figure A 3-4 - Temperature bar 5 installed in bent cap 6

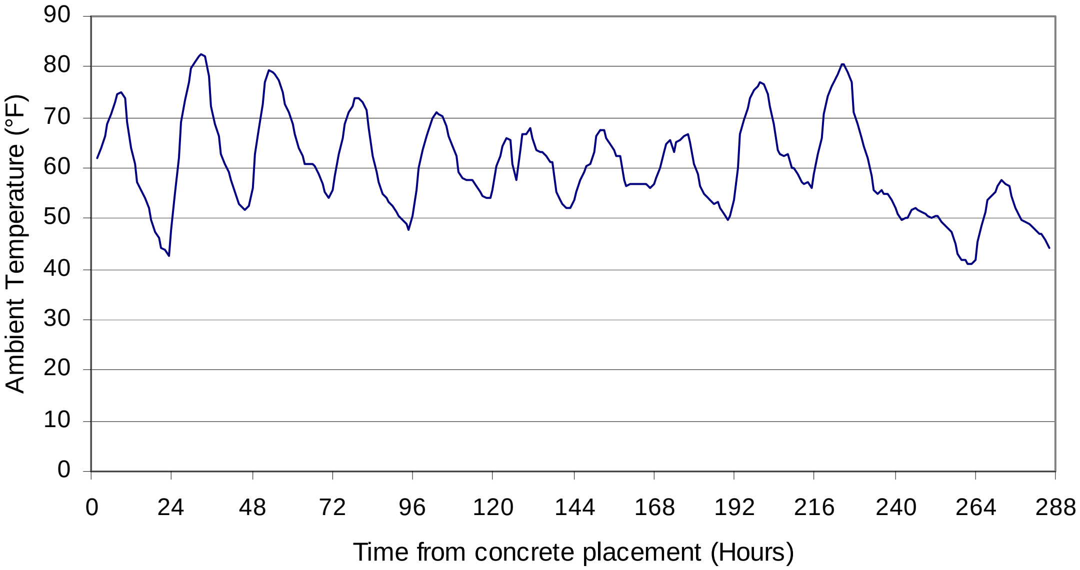

Figure A 3-5 - Ambient temperature recorded by weather station

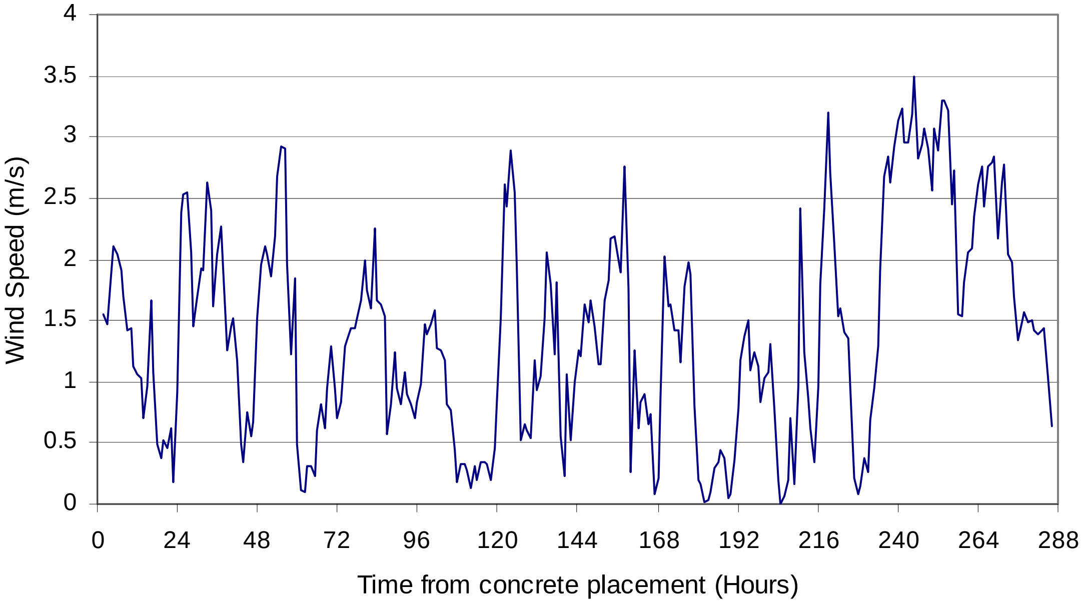

Figure A 3-6 - Wind speed data measured by weather station

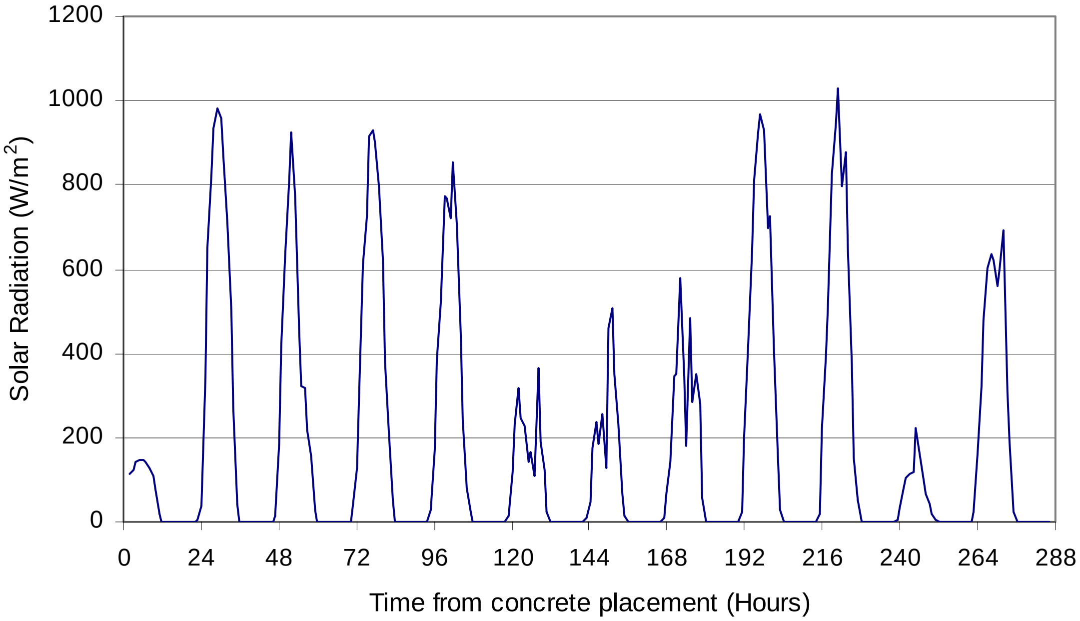

Figure A 3-7 - Solar radiation measured by weather station

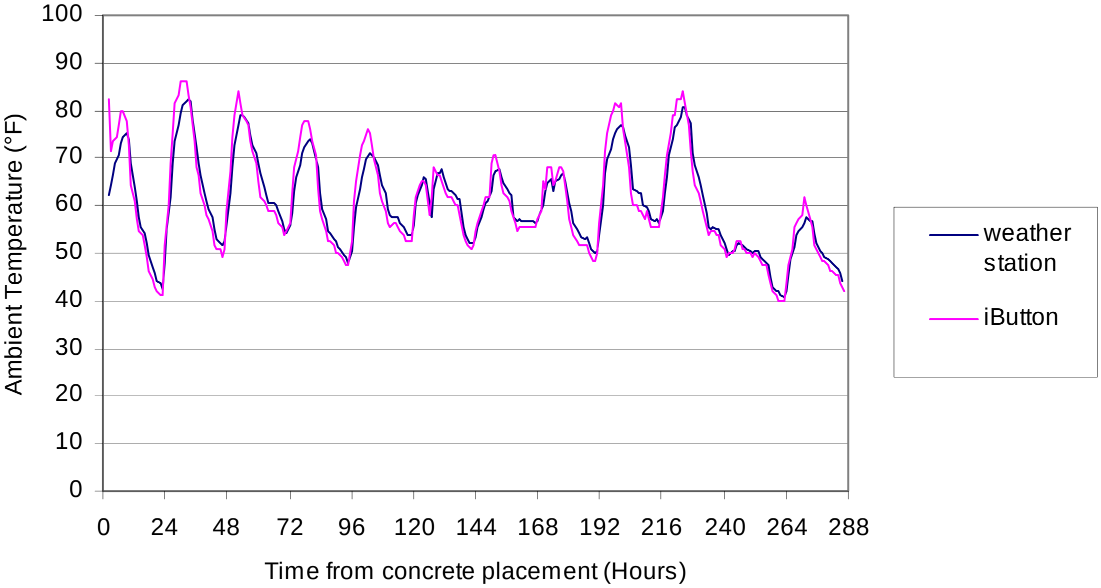

Figure A 3-8 - Comparison of weather station temperature data to iButton temperature data

Figure A 3-9 - Weather station set up in contractor’s yard

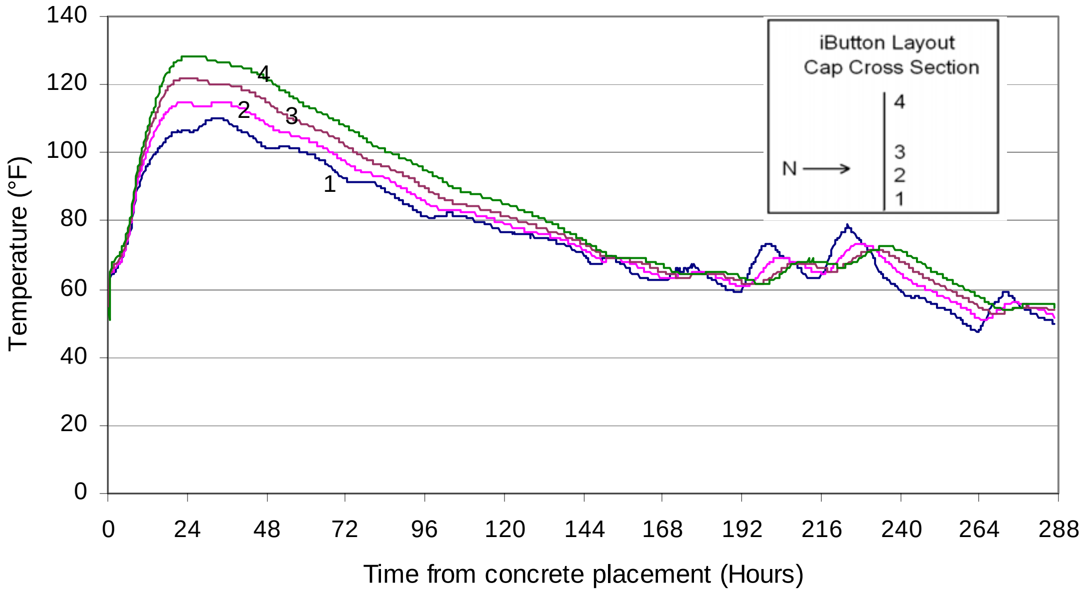

Figure A 3-10 - Data from temperature bar 1

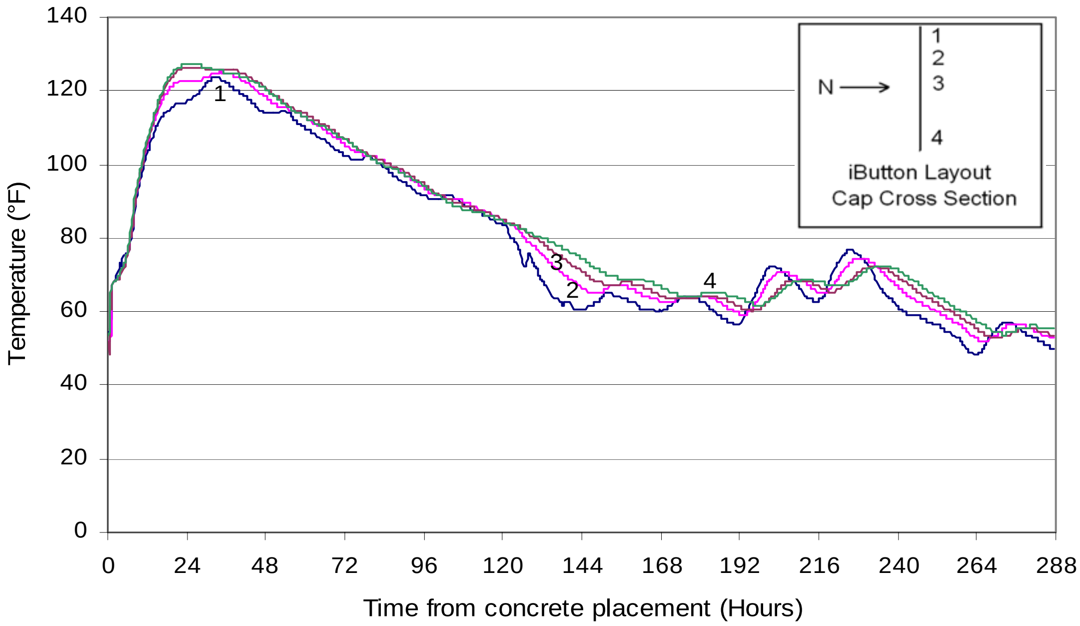

Figure A 3-11 - Data from temperature bar 2

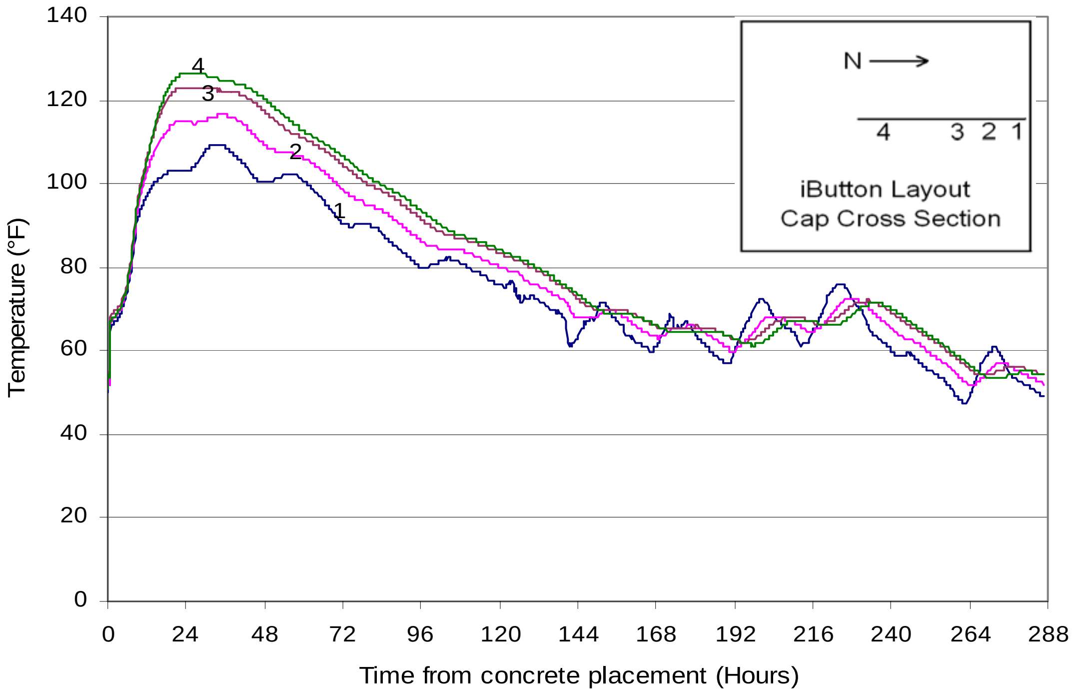

Figure A 3-12 - Data from temperature bar 3

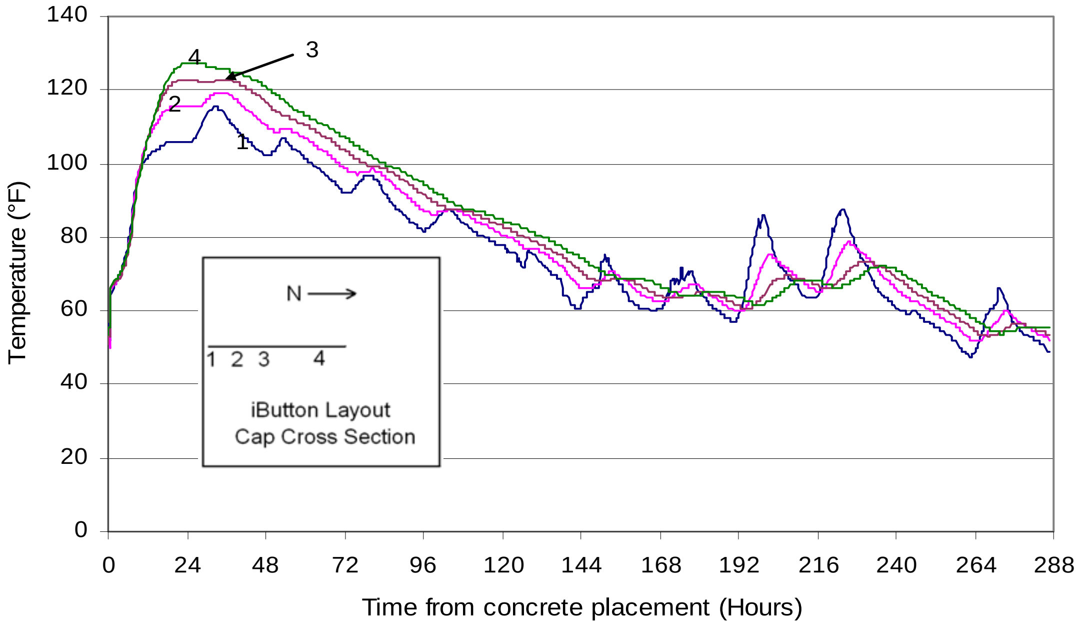

Figure A 3-13 - Data from temperature bar 4

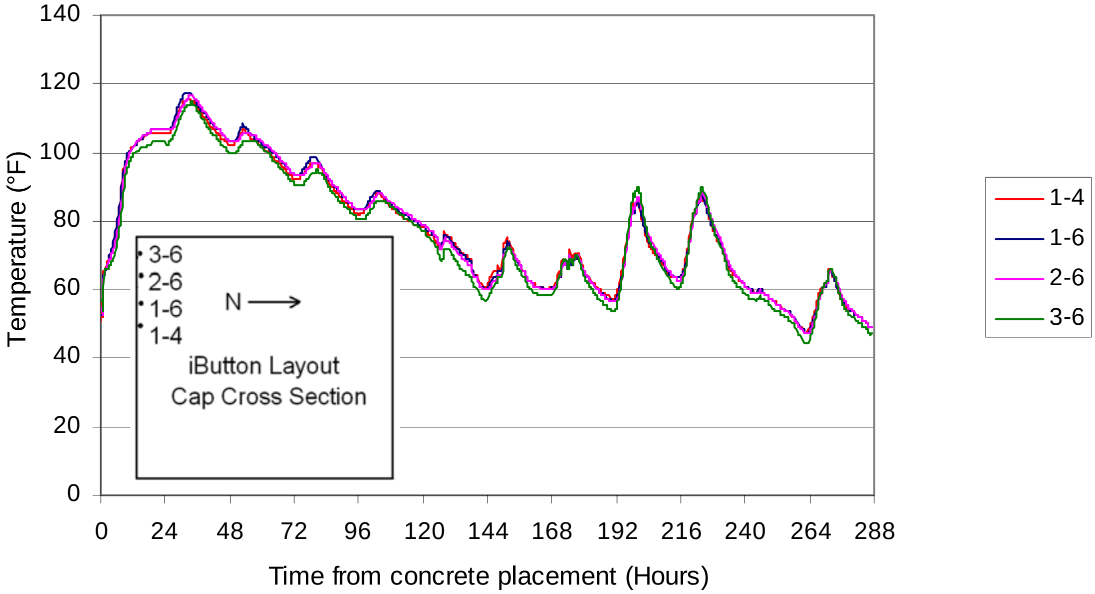

Figure A 3-14 - Data from temperature bar 6 and outside iButton on temperature bar 4

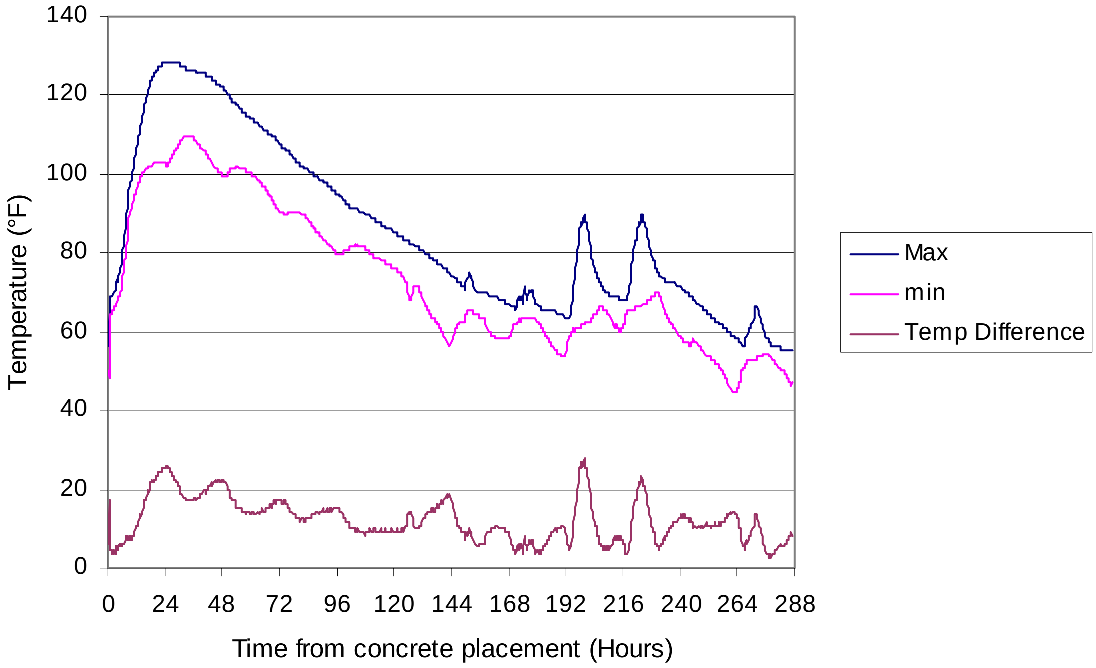

Figure A 3-15 - Maximum and minimum temperatures anywhere recorded in bent cap 6

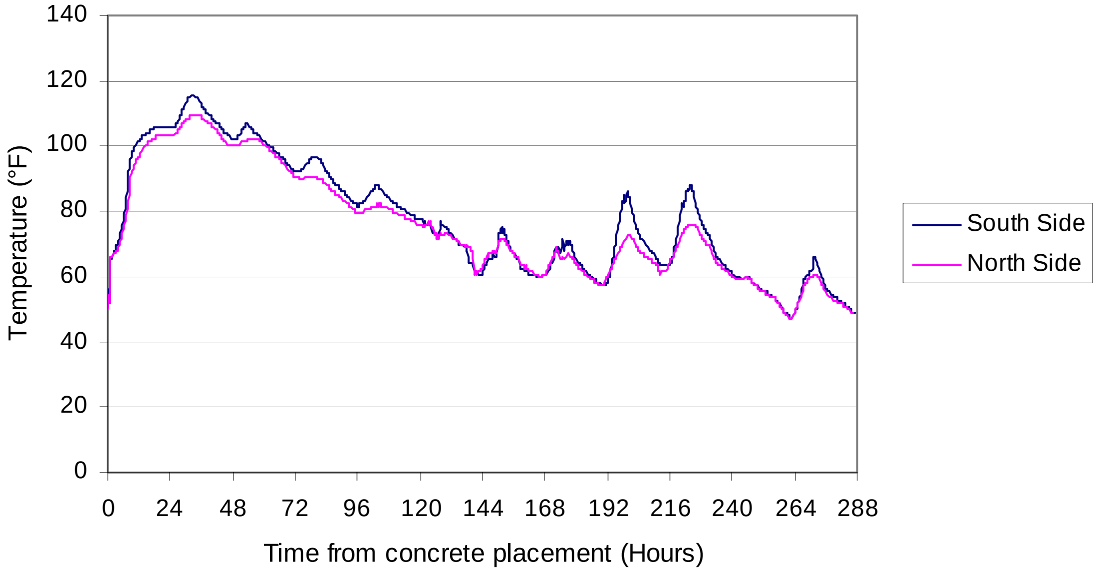

Figure A 3-16 - South side vs. north side data

APPENDIX A-4 SH 45

A-4.1 Introduction

As part of TxDOT project 4563, a graphical user-friendly computer program is being developed to predict the in-place temperature development of concrete members during curing. Each construction project uses different combinations of formwork, architectural form liners, concrete raw materials and curing techniques. In addition, environmental conditions during concrete placement and curing differ for every placement. To assure good results, as many of these variations as possible must be used in the model calibration.

The Central Texas Turnpike System (CTTS) began construction in 2002 to improve traffic and safety on I-35 in the Austin area. The CTTS contains parts of three different roads, SH 45, SH 130 and Loop 1. The construction on SH 45 is broken into 9 sections (Texas Department of Transportation, 2002). The instrumentation was performed on sections 4a and 4b of SH 45. A total of three concrete members were instrumented, a T-shaped bent cap, a rectangular column and a column pedestal (which closely resembles a footing). The concrete members were selected for temperature instrumentation because of the type of materials used, weather conditions expected, project accessibility and formwork used.

A-4.2 Construction Details

Archer Western Contractors was the prime contractor and placed the concrete. Transit Mix Concrete and Materials Co. designed the concrete mix and supplied the concrete. Semi-adiabatic calorimetry was also performed on a sample taken on-site. The results of the semi-adiabatic calorimetry are reported elsewhere (Poole, 2007).

A-4.2.1 T-SHAPED BENT CAP

The T-shaped bent cap was supported by 2 rectangular columns as shown in Figure A 4-1. Figure A 4-2 shows the bent cap's cross-section dimensions. The top section of the cap used ¾" thick Betofilm for the formwork. Betofilm is made of birch and spruce plywood coated with a brown phenolic film. The coating is resistant to moisture and weak alkalis (WISA Wood Products, 2000). Horizontal struts were used to brace the betofilm at 10" O.C. The strut dimensions were made from wood that had dimensions of 5 $^{5}/_{8}$" x 2 $^{5}/_{8}$". For architectural reasons, the bottom of the cap was formed using cut Styrofoam covered with a thin piece of Betofilm. Figure A 4-3 shows a picture of two Styrofoam cutouts similar to those used. Figure A 4-4 summarizes the type of formwork that was used.

The concrete for the bent cap was a TxDOT Class C concrete mix. Table A 4-1 shows the concrete properties. Table A 4-2 shows the tested concrete properties. The concrete placement on the bent cap started at approximately 8:00 a.m. on June 5th. A concrete sample was taken from the fourth truck to test the fresh temperature, air content, slump, and make cylinders. The in-place fresh concrete temperature was 84°F. The side forms were removed at approximately 2:00 pm on June 7, 2004 (about 54 hours after concrete placement).

A-4.2.2 RECTANGULAR COLUMN

The rectangular column was placed in two 40 foot lifts. Because of safety and convenience, the instrumentation was placed on the first lift. The column cross-sectional dimensions were 8'-6" by 10'-0". Figure A 4-5 shows a picture of the red forms used. Custom Ashlar Elasto-Tex form liners made by the Symons Corp. were used on the

North and South sides of the column. Concrete placement began at 8:30 am on June 11th, 2004. A TxDOT Class F concrete mix was used. Table A 4-3 shows the concrete properties. Table A 4-4 shows the tested concrete properties. A concrete sample was taken from the second truck that arrived on site to test the concrete fresh temperature, air, slump, and make cylinders. The concrete fresh temperature was 72ºF. The forms were removed on June 21st, 2004 at 11:30 am, 243 hours after the concrete was placed.

A-4.2.3 PEDESTAL

The pedestal dimensions were 9’-6” by 10’-6” by 5’-6” high. Concrete placement began at 9:45 am on June 11th, 2004. A class F concrete mix was used. The concrete sample taken from the column was assumed to be representative of the concrete used on the pedestal because the concrete came from the same batch plant on the same day using the same mixture proportions. Wood forms were used on the pedestal, with custom Ashlar Elasto-Tex form liners made by Symons© used on the North and East sides. The pedestal was placed on top of a concrete footing. A cure blanket was placed on top of the footing after the top surface was finished. The forms were stripped at an unknown time after the final temperature reading was taken on June 25th, 2004. Figure A 4-6 shows a picture of the footing before concrete placement.

A-4.3 Instrumentation

Thermochron iButtons®[4] made by Dallas Semiconductors (Dallas Semiconductor, 2003) were used to measure and log the bent cap, column, and pedestal in place temperatures. Thermochron iButtons record the temperature in increments of 0.9°F and have an accuracy of ±1.8 °F (Dallas Semiconductor, 2003). The procedures for preparing the iButtons for installation were similar to those used in an earlier TxDOT

---

[4] iButton® is a registered trademark of Dallas Semiconductor

study (Ramaiah, 2002) and are documented in Appendix B. Wires were soldered onto the iButtons to allow external access to the iButton data. After the wires were attached, the iButtons were coated with epoxy to prevent water damage. To speed-up installation, series of iButtons were attached to ½" diameter acrylic dowels with duct tape. These prefabricated "temperature bars" were placed in the concrete members before the concrete was placed.

A-4.3.1 T-SHAPED BENT CAP

Temperature bars 1-5 were installed in the bent cap on June 4th. Figure A 4-7 shows the location of the reference point used to locate the iButtons. Table A 4-5 to Table A 4-9 show the location of temperature bars 1-5 with respect to the reference point. Figure A 4-8 shows temperature bar 4 after installation. Temperature bars 1, 2 and 3 were placed far enough away from the north-south ends of the cap to avoid end-effect heat transfer. Temperature bars 1 and 3 were placed to capture the temperature profiles on the cap corbel. Temperature bar 2 was used to record the effects that wood horizontal cross bracing can have on the temperature. Temperature bar 4 was placed to investigate the effect that the end of the cap can have on the cap temperature. Temperature bar 5 was placed to capture the temperature profile in the top section of the T-shaped cap.

A-4.3.2 COLUMN

Temperature bars 6-8 were installed on the column on June 9th, 2004. Temperature bar 6 was placed vertically on the east side of the column to investigate the heat transfer properties of the horizontal form struts. Temperature bar 7 was placed vertically on the north side to investigate the insulating properties of the form liners. Temperature bar 8 was placed vertically in the core of the column, with one iButton touching the footing. Table A 4-10 to Table A 4-12 show the location of each iButton on temperature bars 6-8 in relation to the bottom northeast corner of the column. Temperature readings were also taken from iButtons placed in the column by the contractor, although the exact location of each of those iButtons in the column was not measured.

A-4.3.3 PEDESTAL

Temperature bars 9-10 were installed in the pedestal on June 7th, 2004. Temperature bar 9 was placed horizontally on the east side of the pedestal. Temperature bar 10 was placed vertically in the pedestal to measure the vertical profile in the pedestal. Table A 4-13 to Table A 4-14 show the location of each iButton on temperature bars 9-10 in relation to the bottom northeast corner of the pedestal.

A-4.4 Weather Data

Weather data were acquired using a Campbell Scientific weather station. The weather station had instrumentation to record relative humidity, temperature, solar radiation, precipitation, wind speed and wind direction. The weather station was placed outside of Building 18B at the Pickle Research Center at the University of Texas because there were no practical locations available at the construction site. The Pickle Research Center is located approximately 9 miles south of the construction site

A-4.4.1 T-SHAPED BENT CAP

Figure A 4-9 to Figure A 4-12 show the temperature, relative humidity, wind speed and solar radiation measured for the T-shaped bent cap. The time shown on the graphs is from the start of concrete placement for the cap.

A-4.4.2 COLUMN

Figure A 4-13 to Figure A 4-16 show the temperature, relative humidity, wind speed and solar radiation measured for the column. The time shown on the graphs is from the start of concrete placement for the column.

A-4.4.3 PEDESTAL

Figure A 4-17 to Figure A 4-20 show the temperature, relative humidity, wind speed and solar radiation measured for the pedestal. The time shown on the graphs is from the start of concrete placement for the pedestal.

A-4.5 Concrete Temperature Data Acquired

All Thermocron iButtons were programmed to measure and log the temperature every 15 minutes.

A-4.5.1 T-SHAPED BENT CAP

Figure A 4-21 to Figure A 4-25 show the data acquired from temperature bars 1-5. Figure A 4-26 shows the maximum temperature, minimum temperature and maximum temperature difference recorded in the T-shaped cap. The maximum temperature and maximum temperature difference recorded in the cap were 153.5°F and 65.7°F, respectively. The maximum temperature recorded in the cap was recorded by iButton 4 on temperature bar 5 and by iButton 6 on temperature bar 4. A visual inspection for cracking of the cap was made 5 days after concrete placement. Even though the temperature difference on the cap was high, no cracks were found.

A-4.5.2 COLUMN

Figure A 4-27 to Figure A 4-29 show the data acquired from temperature bars 6-8. Figure A 4-30 shows the data acquired from the iButtons placed by the contractor.

Figure A 4-31 shows the maximum temperature, minimum temperature and maximum temperature difference recorded in the column. The maximum temperature and maximum temperature difference recorded in the column were 163.4°F and 60.3°F respectively. The maximum temperature recorded in the column was recorded by an iButton placed by the contractor. The maximum difference between the temperatures recorded on temperature bar 6 was 6.3ºF. The maximum difference between the temperatures recorded on temperature bar 7 was 3.6 ºF. A visual inspection for cracking of the cap was made after the forms were removed. Even though the temperature difference on the cap was high, no cracks were found.

A-4.5.3 PEDESTAL

Figure A 4-32 to Figure A 4-33 show the data acquired from temperature bars 9-10. Figure A 4-34 shows the maximum temperature, minimum temperature and maximum temperature difference recorded in the column. The maximum temperature and maximum temperature difference recorded in the column were 165.2°F and 43.2°F, respectively. The maximum temperature recorded in the column was recorded by an iButton placed by the contractor.

A-4.6 Summary

Temperature sensors were placed in a T-shaped bent cap, a column, and a pedestal were instrumented on SH 45 between June 4th, 2004 and June 25th, 2004. They were installed to record the temperature development due to the heat of hydration of the concrete. Table A 4-15 shows the maximum temperatures and temperature differences recorded in each concrete member. The temperature data collected will be used to calibrate the concrete temperature prediction model being developed as part of TxDOT project 4563.

A-4.7 Acknowledgements

The advice and assistance of the TxDOT Bridge Division and the Central Texas Turnpike Authority is greatly appreciated. The authors wish to thank Ralph Browne, and Tyler Ley, and Rob Crowson for arranging access to field sites.

Table A 4-1– Class C concrete properties

Item	Content	Material Description
Cement	409 lb./yd.^{3}	TXI - Type I/II
Class F Fly Ash	143 lb./yd.^{3}	Big Brown
Coarse Aggregate	1749 lb./ yd.^{3}	1" Crushed Limestone
Fine Aggregate	1255 lb./ yd.^{3}	Natural Sand
Air Entraining Admixture	1.27 oz/ cwt.	Master Builders AE 90
Water Reducer / Retarder	2.74 oz/ cwt.	Pozzolith 200N
Water Reducer / Retarder	0.87 oz/ cwt.	Pozzolith 961R
Water	260.4 lb./ yd.^{3}	
Jobsite Measured Air Content	6.5%	
Jobsite Measured Slump	5"	
Water/cementitious materials ratio	0.47	

Table A 4-2 – Class C tested concrete properties

Concrete Age	Compressive Strength (psi)	Splitting Tensile Strength (psi)	Elastic Modulus (psi)	Permeability (Coulombs)
3 day	3680	390	-	-
7 day	4550	470	-	-
28 day	6040	-	3940000	-
91 day	6450	690	-	2585

Table A 4-3 – Class F column concrete

Item	Content	Material Description
Cement	503 lb./yd.^{3}	TXI - Type I/II
Class F Fly Ash	179 lb./yd.^{3}	Big Brown
Coarse Aggregate	1745 lb./ yd.^{3}	1" Crushed Limestone
Fine Aggregate	1081 lb./ yd.^{3}	Natural Sand
Air Entraining Admixture	1.1 oz/ cwt.	Master Builders AE 90
Water Reducer / Retarder	2.3 oz/ cwt.	Pozzolith 200N
Water Reducer / Retarder	0.7 oz/ cwt.	Pozzolith 961R
Water	279.2 lb./ yd.^{3}	
Jobsite Measured Air Content	6.4%	
Jobsite Measured Slump	4.25"	
Water/cementitious ratio	0.41	

Table A 4-4 - Class F Tested Concrete Properties

Concrete Age	Compressive Strength (psi)	Splitting Tensile Strength (psi)	Elastic Modulus (psi)
1 day	1890	220	-
7 day	4890	560	-
28 day	6530	830	5939000
91 day	7310	730	-

Table A 4-5 - Location of iButtons on temperature bar 1 on the T-shaped bent cap

iButton #	Distance horizontally from reference point	Distance vertically from reference point
1	0’ - 0.75”	5’ - 11”
2	0’ - 3.75”	5’ - 11”
3	0’ - 6.75”	5’ - 11”
4	0’ - 9.75”	5’ - 11”
5	1’ - 0.75”	5’ - 11”

Table A 4-6 - Location of iButtons on temperature bar 2 on the T-shaped bent cap

iButton #	Distance horizontally from reference point	Distance vertically from reference point
1	2’ - 3”	3’ - 7”
2	2’ - 3”	3’ - 4”
3	2’ - 3”	3’ - 1”
4	2’ - 3”	2’ - 10”
5	2’ - 3”	2’ - 7”

Table A 4-7 - Location of iButtons on temperature bar 3 on the T-shaped bent cap

iButton #	Distance horizontally from reference point	Distance vertically from reference point
1	1’ - 1”	7’ - 1.25”
2	1’ - 1”	6’ - 10.25”
3	1’ - 1”	6’ - 7.25”
4	1’ - 1”	6’ - 4.25”
5	1’ - 1”	6’ - 1.25”

Table A 4-8 - Location of iButtons on temperature bar 4 on the T-shaped bent cap

iButton #	Distance horizontally from reference point	Distance vertically from reference point	Distance from the south end of the cap
1	3’ - 7.5”	5’ - 11”	0’ - 2.5”
2	3’ - 7.5”	5’ - 11”	1’ - 2.5”
3	3’ - 7.5”	5’ - 11”	2’ - 2.5”
4	3’ - 7.5”	5’ - 11”	3’ - 2.5”
5	3’ - 7.5”	5’ - 11”	4’ - 2.5”
6	3’ - 7.5”	5’ - 11”	5’ - 2.5”

Table A 4-9 - Location of iButtons on temperature bar 5 on the T-shaped bent cap

iButton #	Distance horizontally from reference point	Distance vertically from reference point	Distance from the south end of the cap
1	3’ - 2.5”	0’ - 4”	24’ - 4”
2	3’ - 2.5”	0’ - 10”	24’ - 4”
3	3’ - 2.5”	2’ - 4”	24’ - 4”
4	3’ - 2.5”	5’ - 4”	24’ - 4”

Table A 4-10 - Location of iButtons on temperature bar 6

iButton #	Distance south from northeast corner of column	Distance west from northeast corner of column	Distance vertically from top of footing
1	2' - 5.5"	0' - 1"	7' - 9"
2	2' - 5.5"	0' - 1"	7' - 5"
3	2' - 5.5"	0' - 1"	7' - 1"
4	2' - 5.5"	0' - 1"	6' - 9"
5	2' - 5.5"	0' - 1"	6' - 5"

Table A 4-11 - Location of iButtons of temperature bar 7

iButton #	Distance south from northeast corner of column	Distance west from northeast corner of column	Distance vertically from top of footing
1	0' - 2"	3' - 9"	7' - 6"
2	0' - 2"	3' - 9"	7' - 1"
3	0' - 2"	3' - 9"	6' - 8"
4	0' - 2"	3' - 9"	6' - 3"
5	0' - 2"	3' - 9"	5' - 10"

Table A 4-12 - Location of iButtons on temperature bar 8

iButton #	Distance south from northeast corner of column	Distance west from northeast corner of column	Distance vertically from top of footing
1	3' - 10"	5' - 11.5"	0
2	3' - 10"	5' - 11.5"	1' - 6"
3	3' - 10"	5' - 11.5"	3' - 6"
4	3' - 10"	5' - 11.5"	5' - 6"

Table A 4-13 - Location of iButtons on temperature bar 9

iButton #	Distance south from northeast corner of pedestal	Distance west from northeast corner of pedestal	Distance vertically from top of footing
1	5' - 3"	0' - 1.5"	2' - 2"
2	5' - 3"	0' - 4.5"	2' - 2"
3	5' - 3"	0' - 7.5"	2' - 2"
4	5' - 3"	0' - 10.5"	2' - 2"
5	5' - 3"	1' - 1.5"	2' - 2"

Table A 4-14 - Location of iButtons on temperature bar 10

iButton #	Distance south from northeast corner of pedestal	Distance west from northeast corner of pedestal	Distance vertically from top of footing
1	5' - 10"	4' - 0"	0' - 0"
2	5' - 10"	4' - 0"	1' - 6"
3	5' - 10"	4' - 0"	3' - 0"
4	5' - 10"	4' - 0"	5' - 0"

Table A 4-15 - Temperature data summary for dolphins 6 and 7

Concrete Member	Maximum Temperature Recorded (°F)	Maximum Temperature Difference Recorded (°F)
T-shaped bent cap	153.5	65.7
Column	163.4	60.3
Pedestal	165.2	43.2

Figure A 4-1- T-shaped bent cap

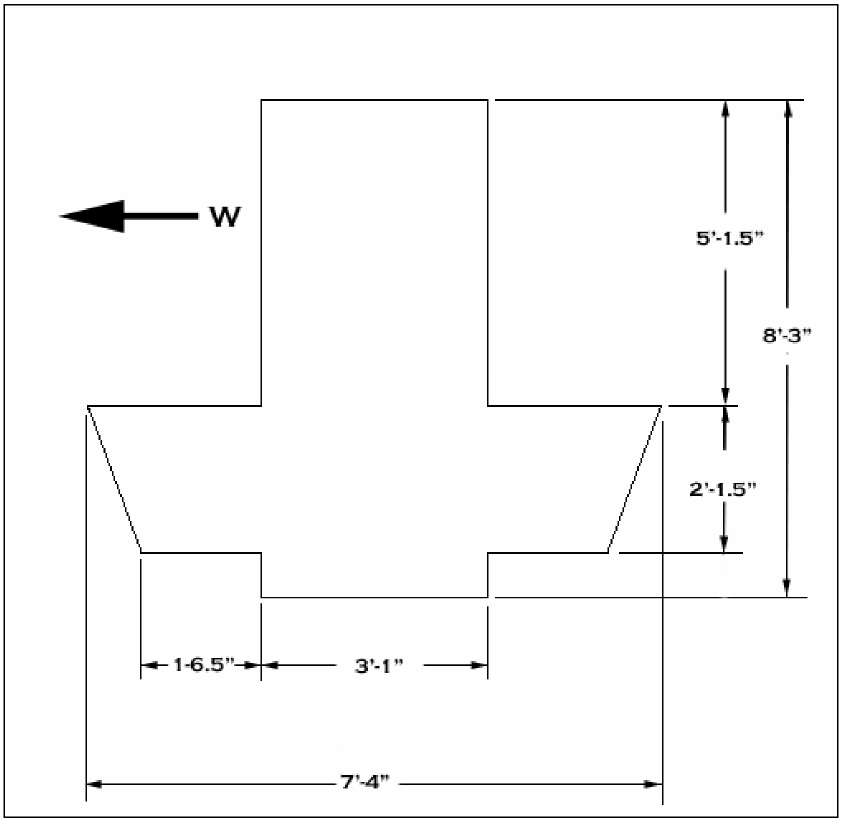

Figure A 4-2 - T-shaped cap dimensions

Figure A 4-3 - Styrofoam cutouts used for formwork

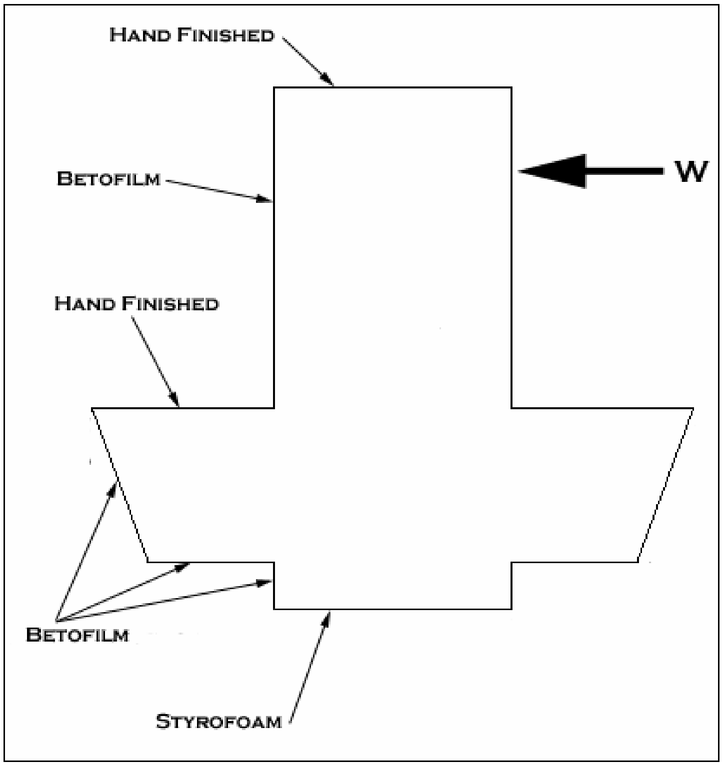

Figure A 4-4 - Formwork Summary

Figure A 4-5 - Section of Symons forms similar to that used on the column

Figure A 4-6 - Pedestal before concrete placement

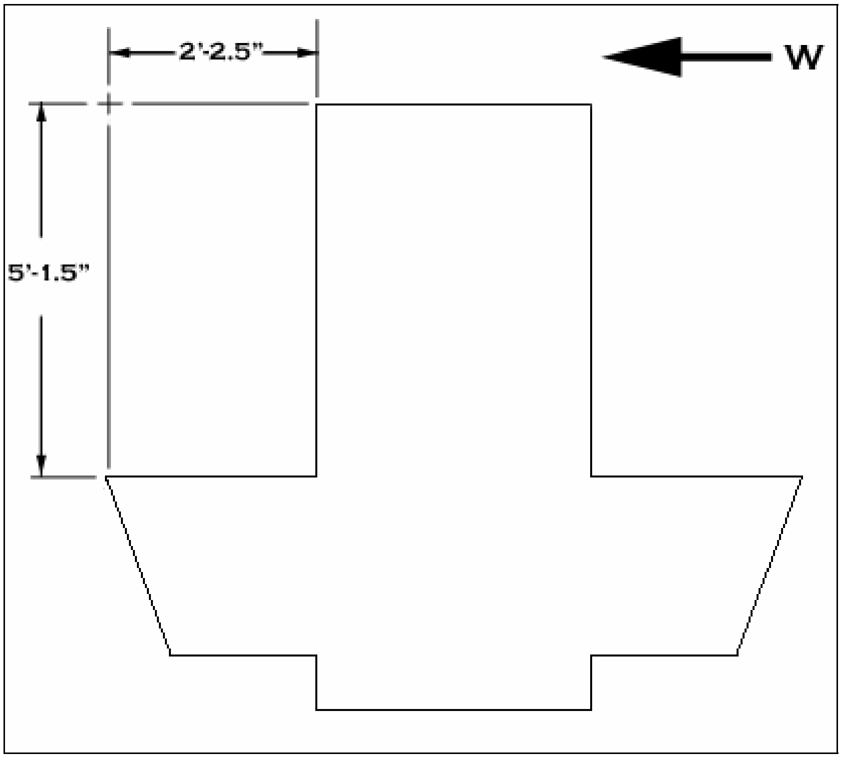

Figure A 4-7 - Location of point used as reference to identify iButton locations


Figure A 4-8 - Temperature bar 4 after installation

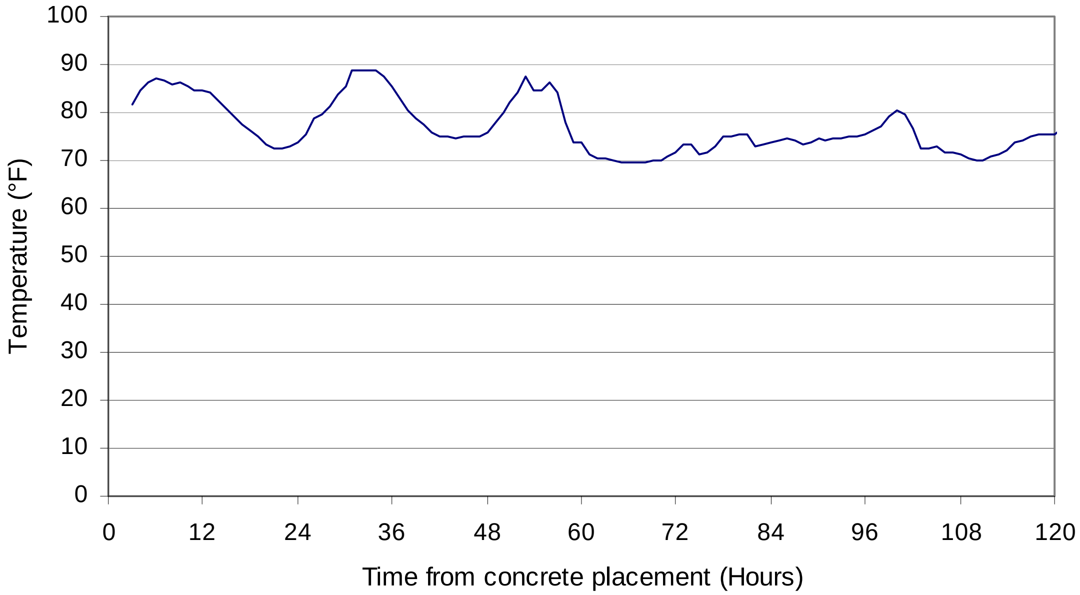

Figure A 4-9 - Ambient temperature data for T-shaped bent cap

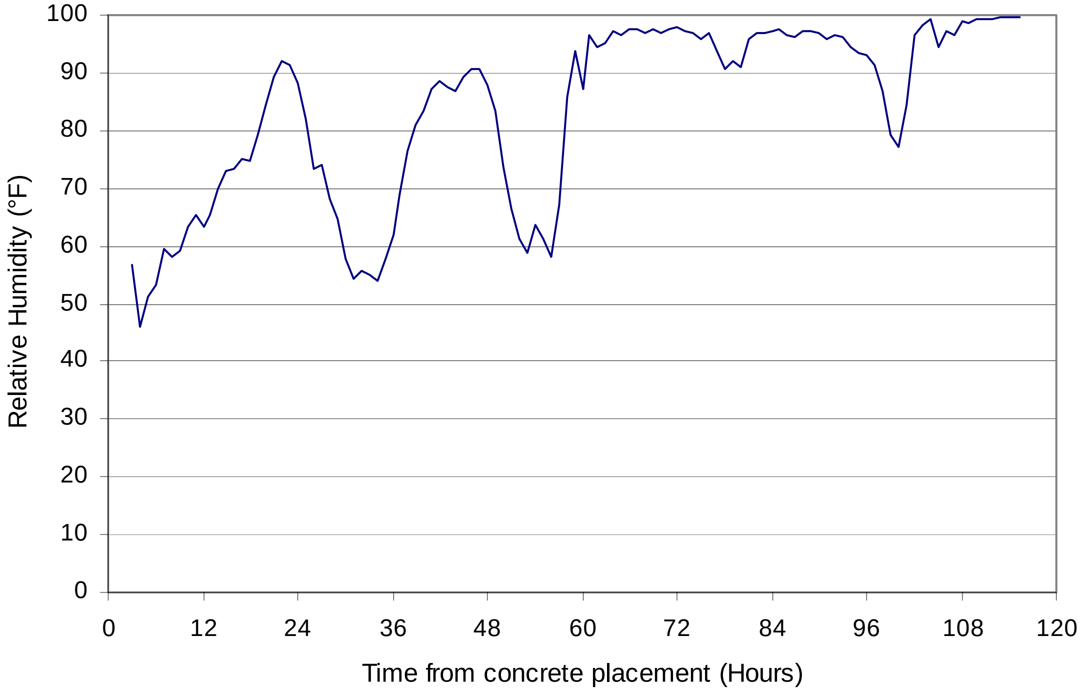

Figure A 4-10 - Relative humidity data for T-shaped bent cap

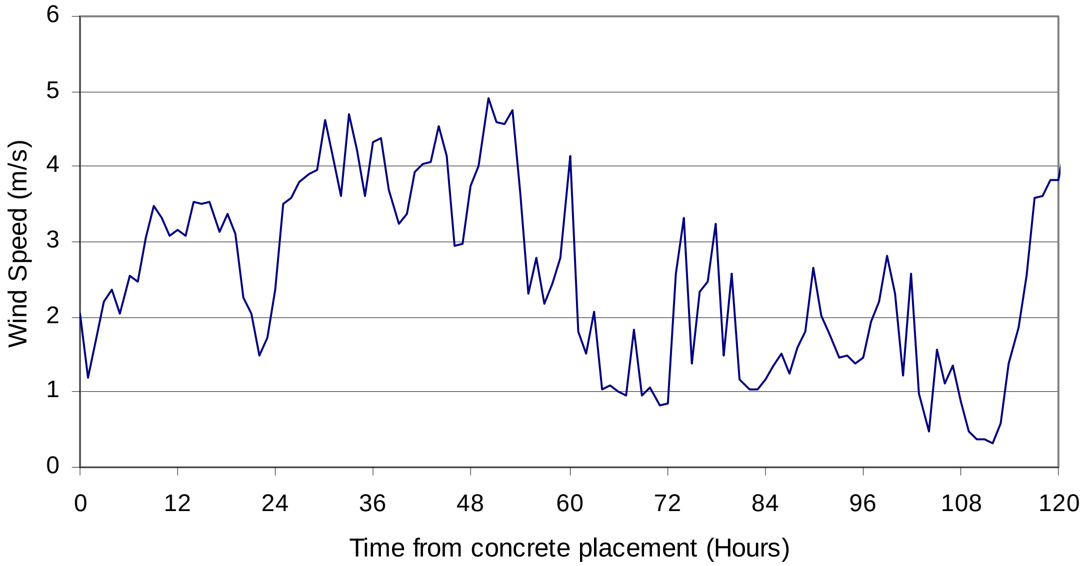

Figure A 4-11 - Wind speed data for T-shaped bent cap

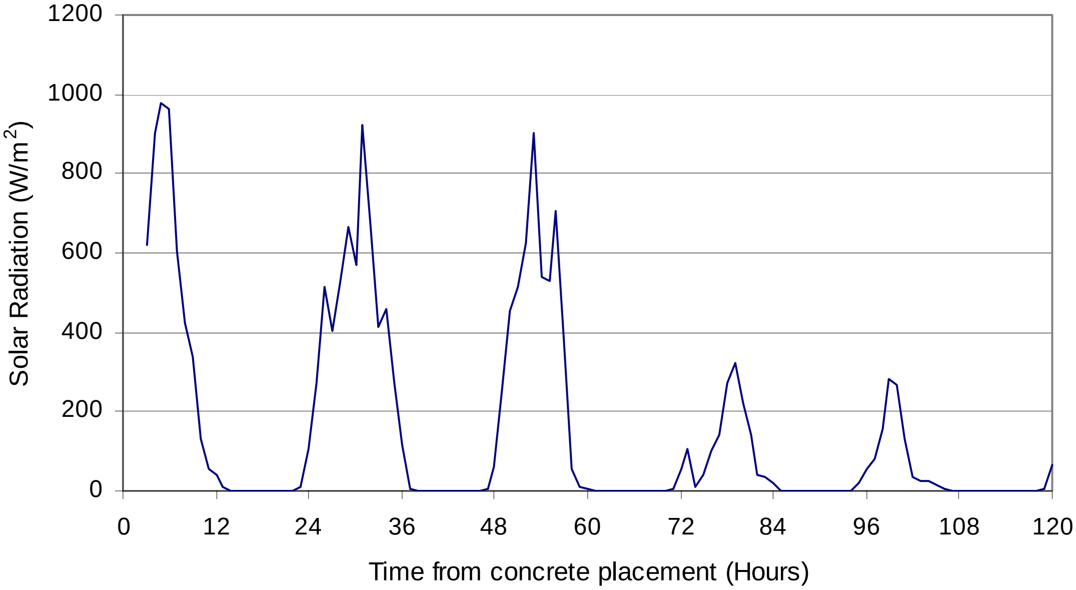

Figure A 4-12 - Solar radiation data for T-shaped bent cap

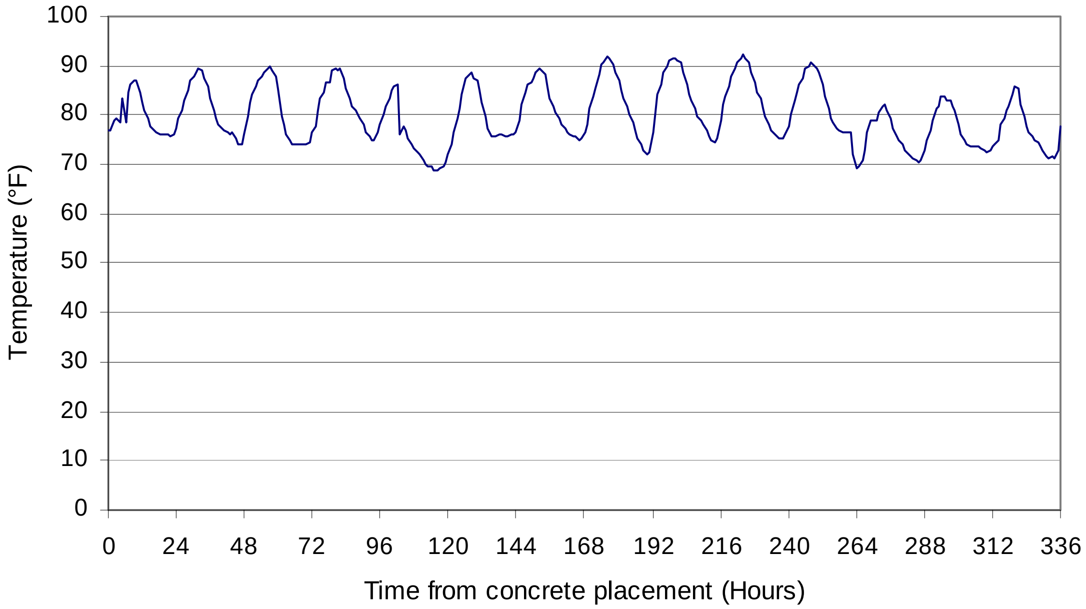

Figure A 4-13 - Ambient temperature data for column

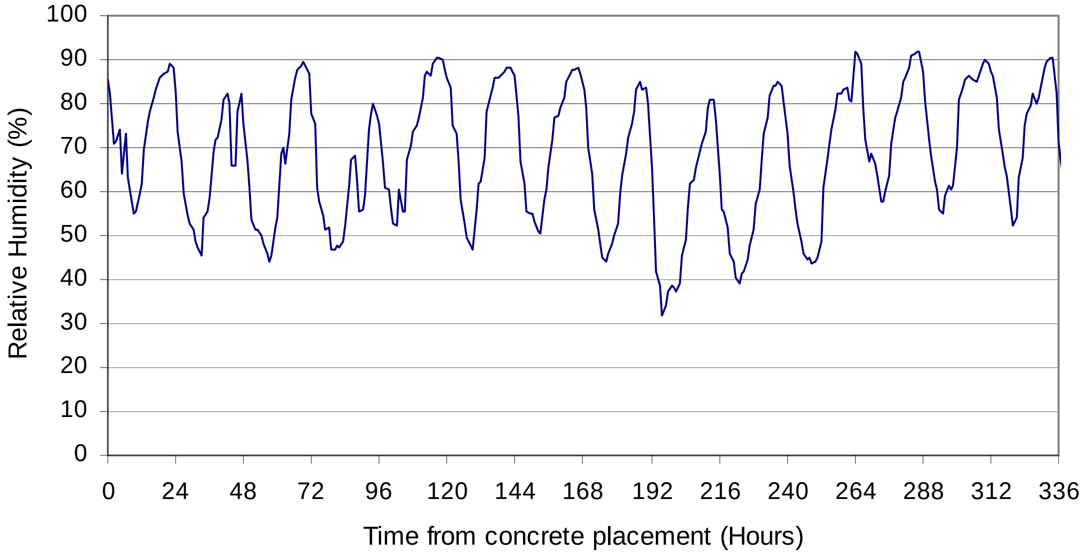

Figure A 4-14 - Relative humidity data for column

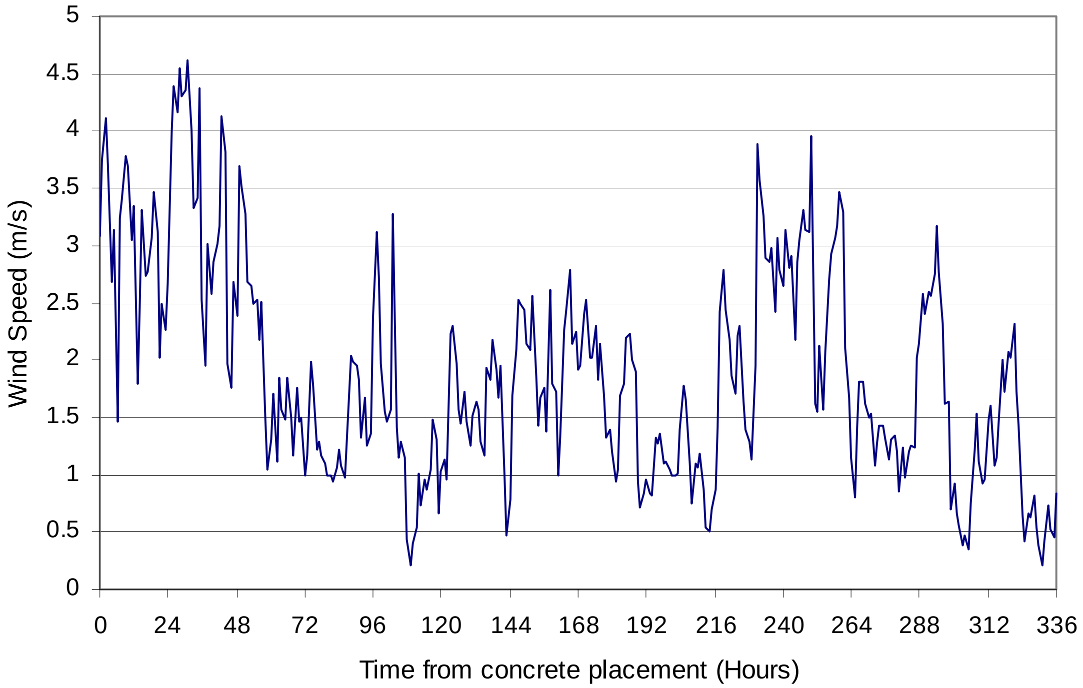

Figure A 4-15 - Wind speed data for column

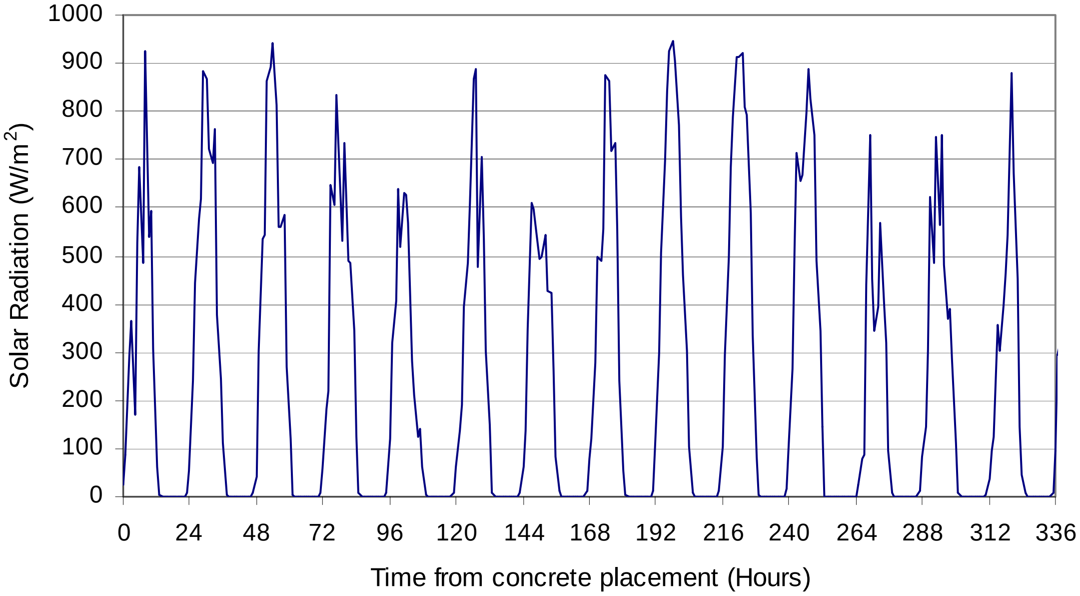

Figure A 4-16 - Solar radiation data for column

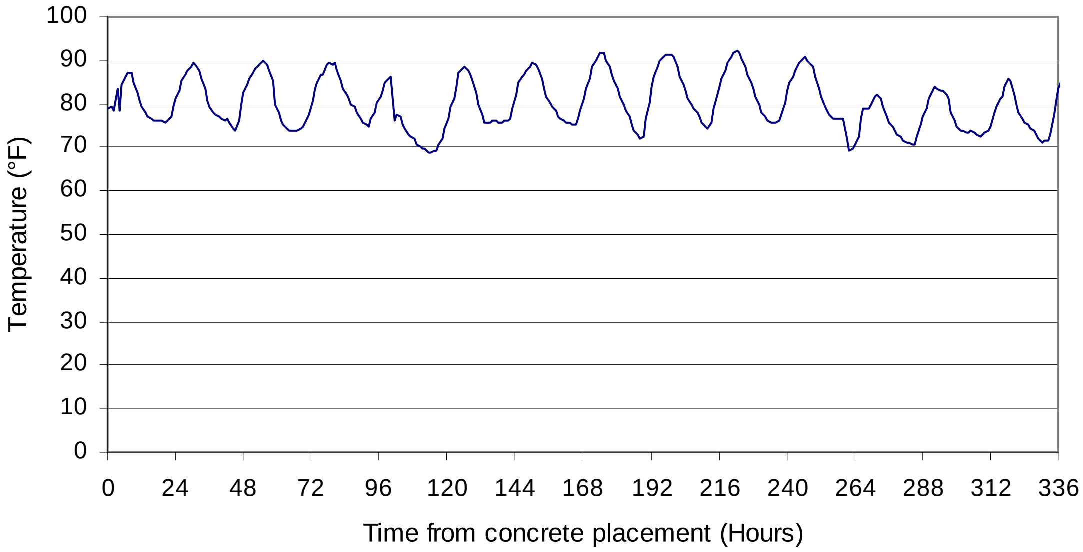

Figure A 4-17 – Ambient temperature data for pedestal

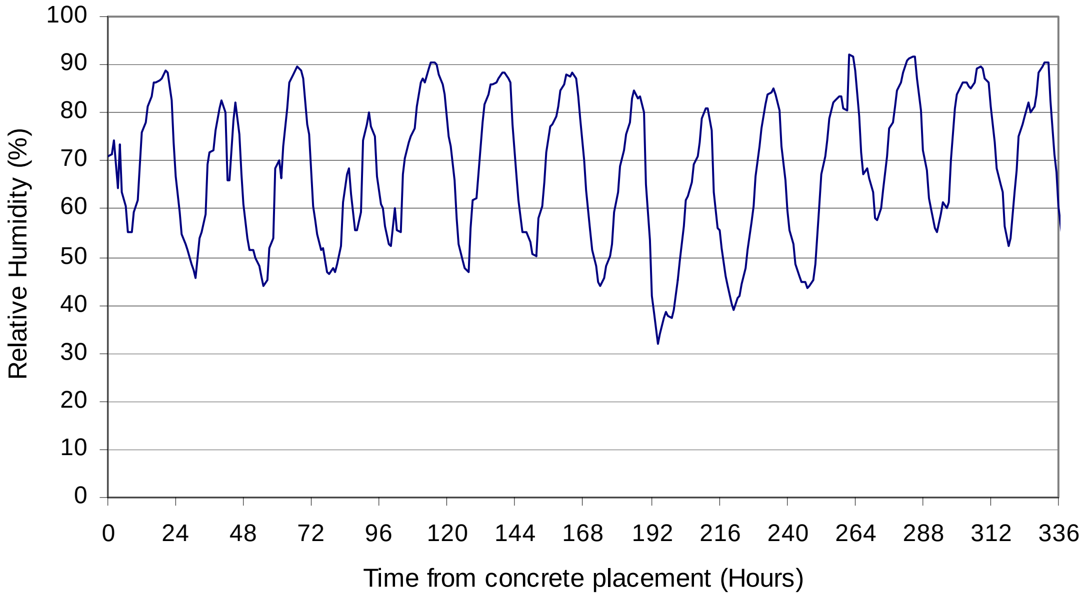

Figure A 4-18 - Relative humidity data for pedestal

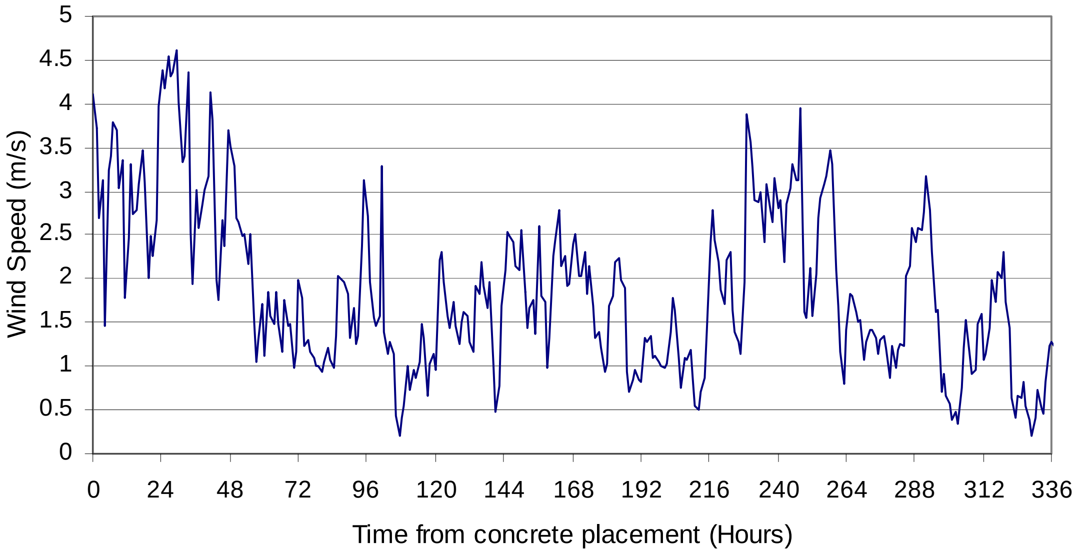

Figure A 4-19 - Wind speed data for pedestal

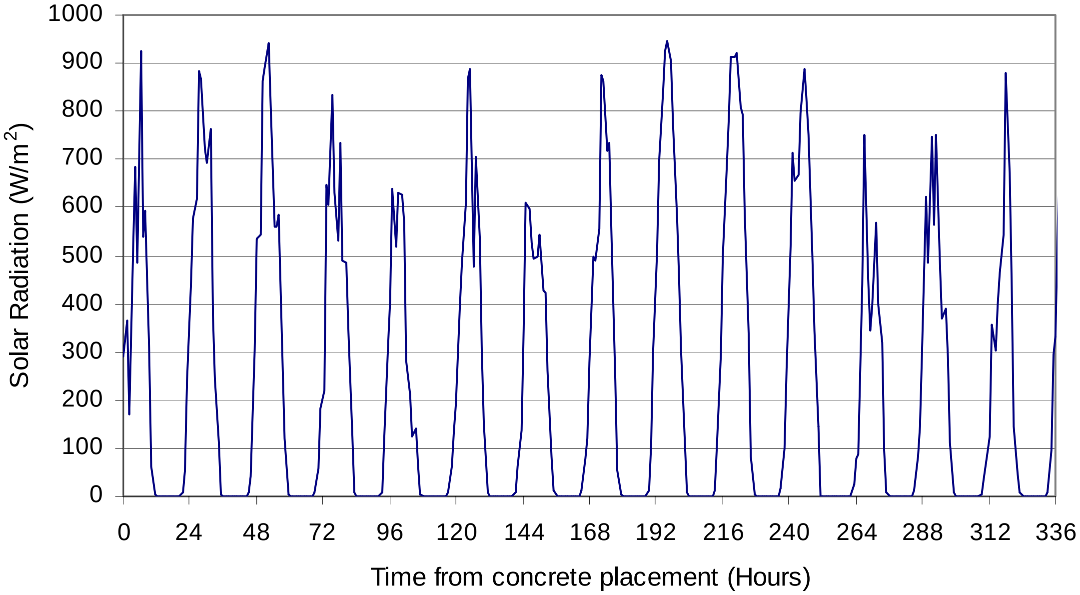

Figure A 4-20 - Solar radiation data for pedestal

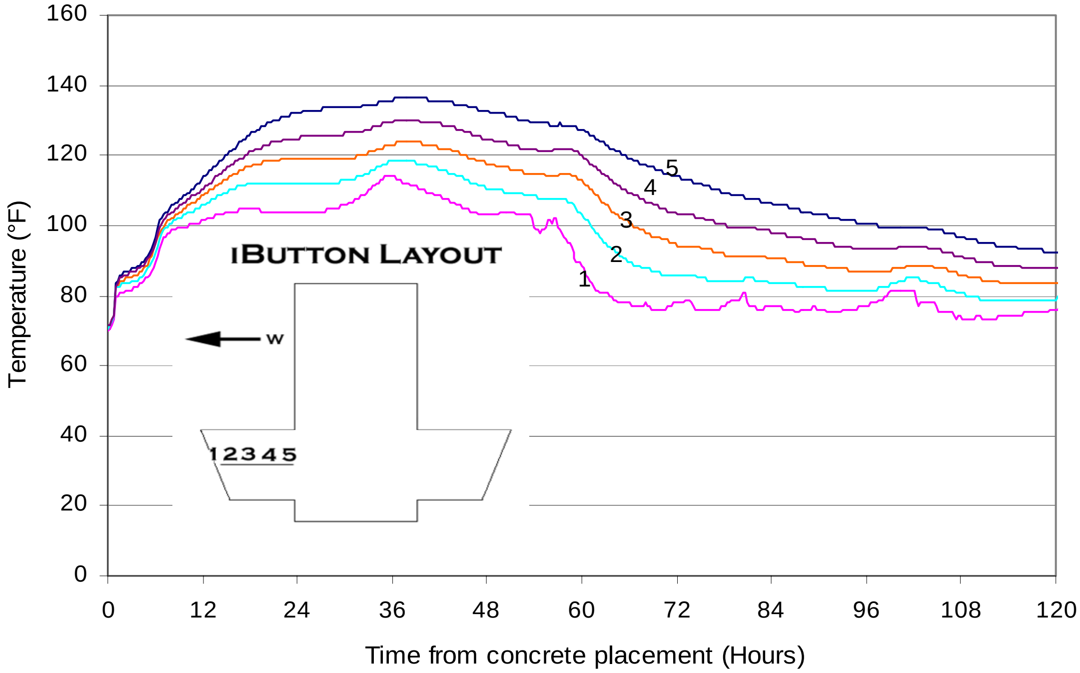

Figure A 4-21 - Data from temperature bar 1 on T-shaped bent cap

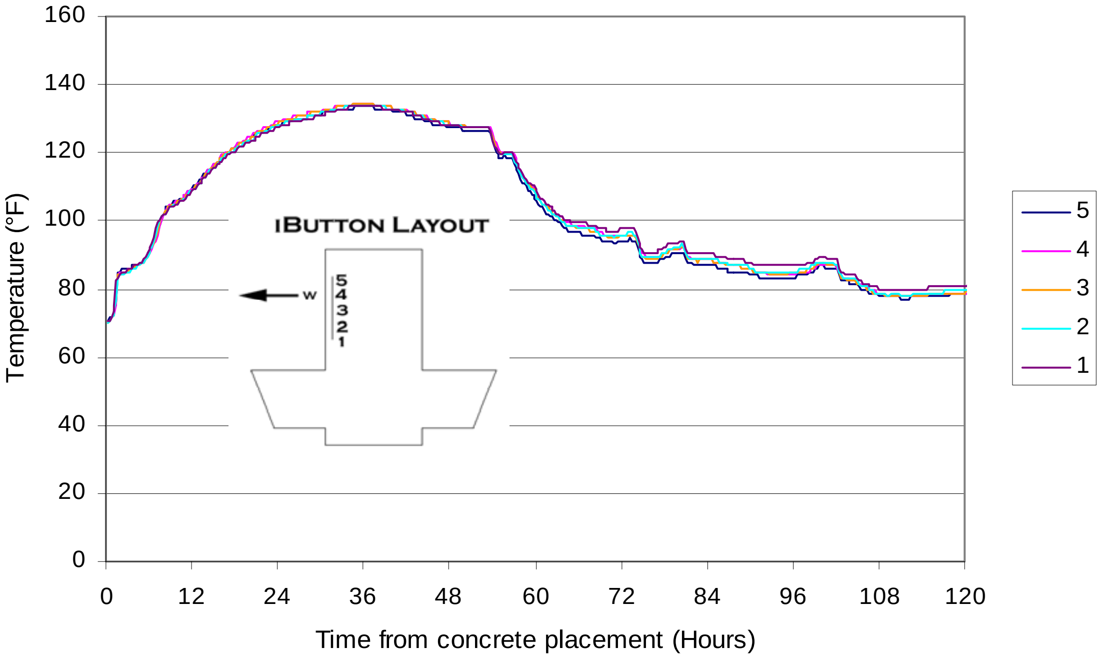

Figure A 4-22 - Data from temperature bar 2 on the T-shaped bent cap

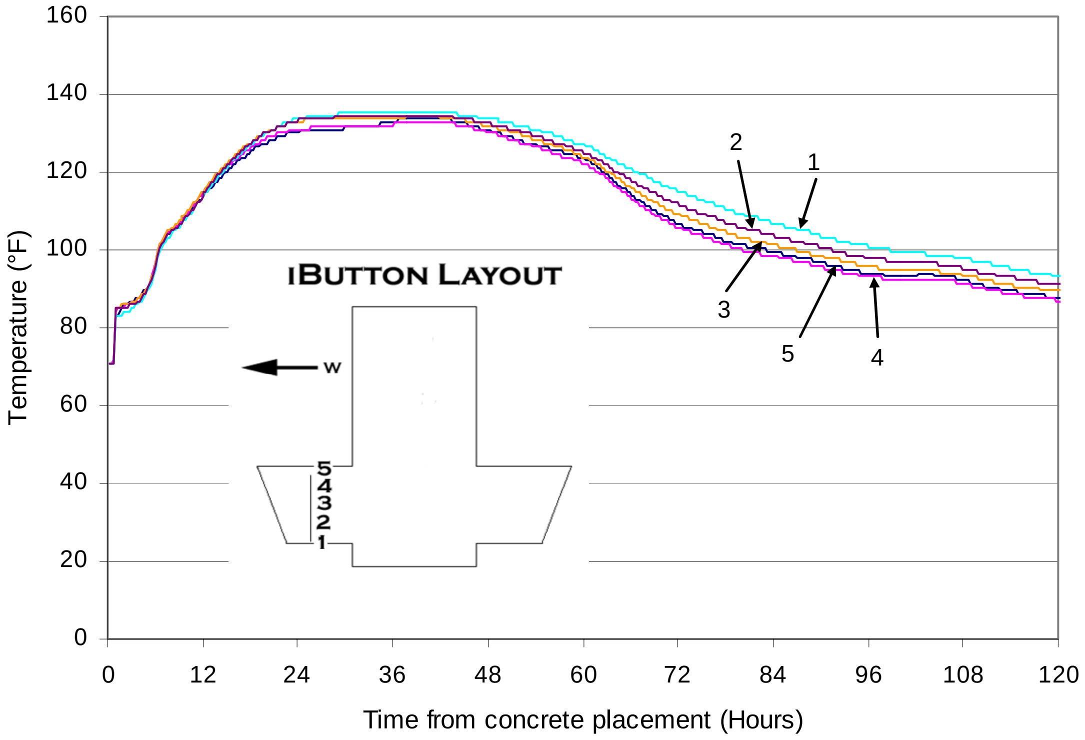

Figure A 4-23 - Data from temperature bar 3

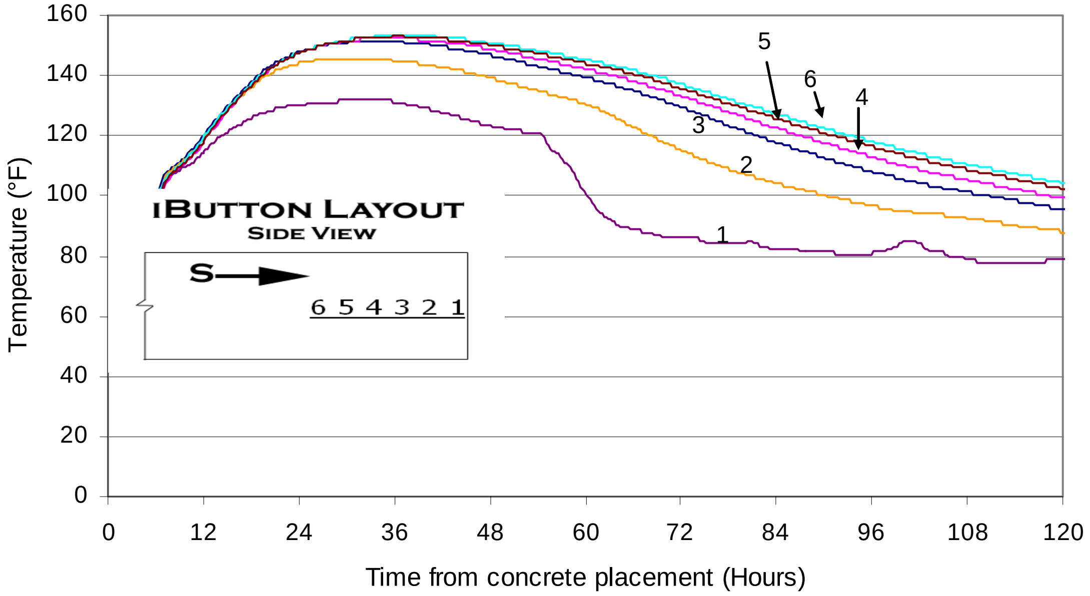

Figure A 4-24 - Data from temperature bar 4

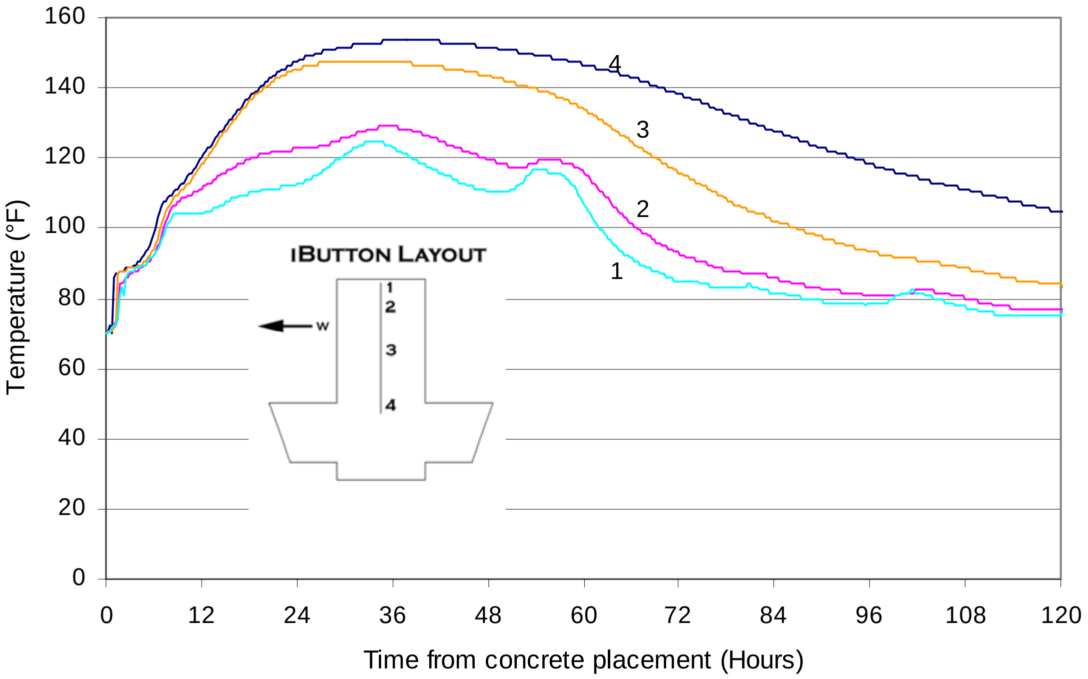

Figure A 4-25 - Data from temperature bar 5 on the T-shaped bent cap

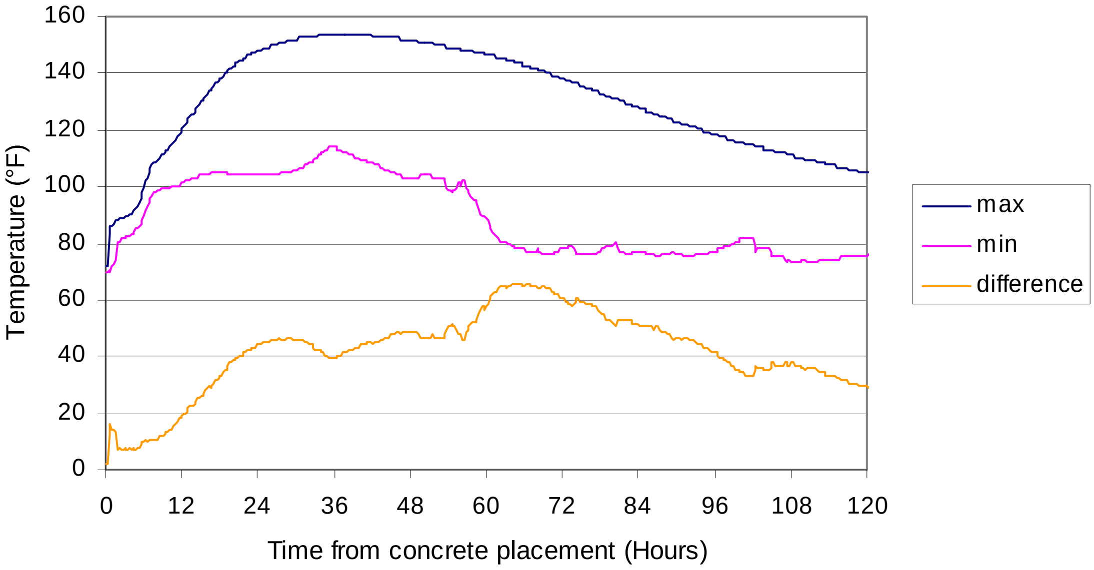

Figure A 4-26 - Maximum, minimum and maximum temperature difference recorded in T-shaped bent cap

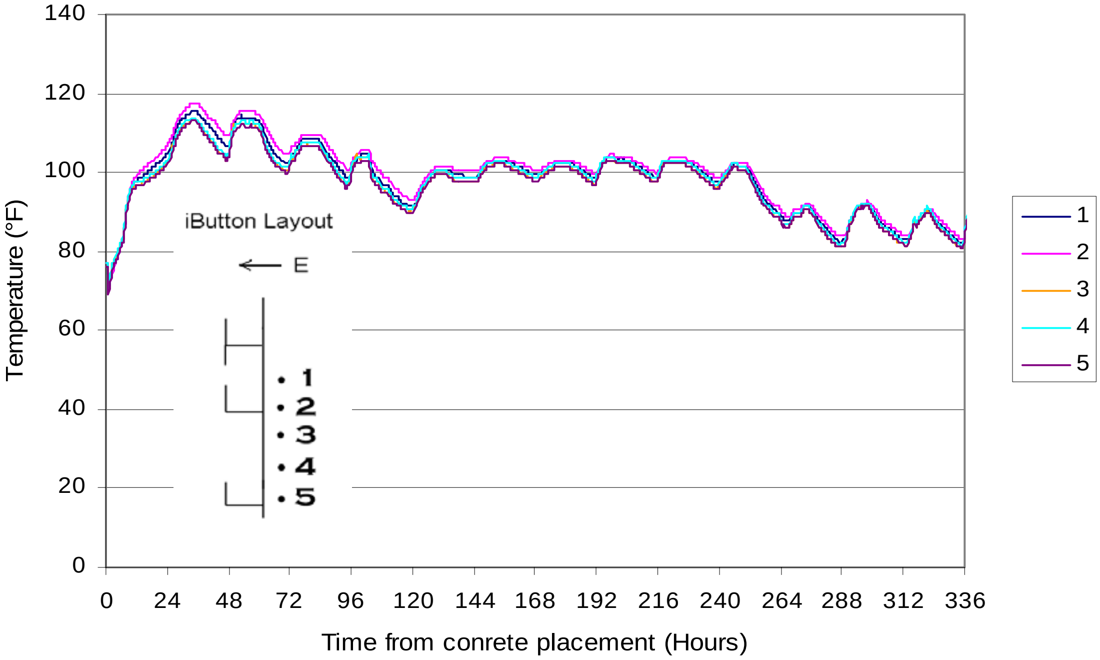

Figure A 4-27 – Temperature data from temperature bar 6

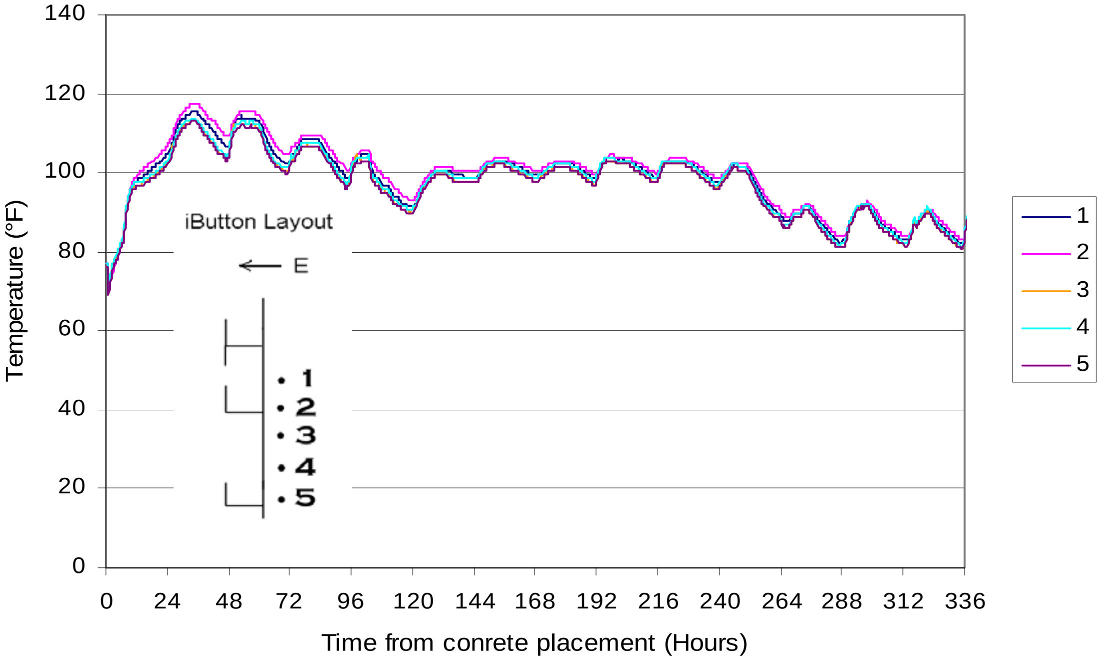

Figure A 4-28 - Temperature data from temperature bar 7

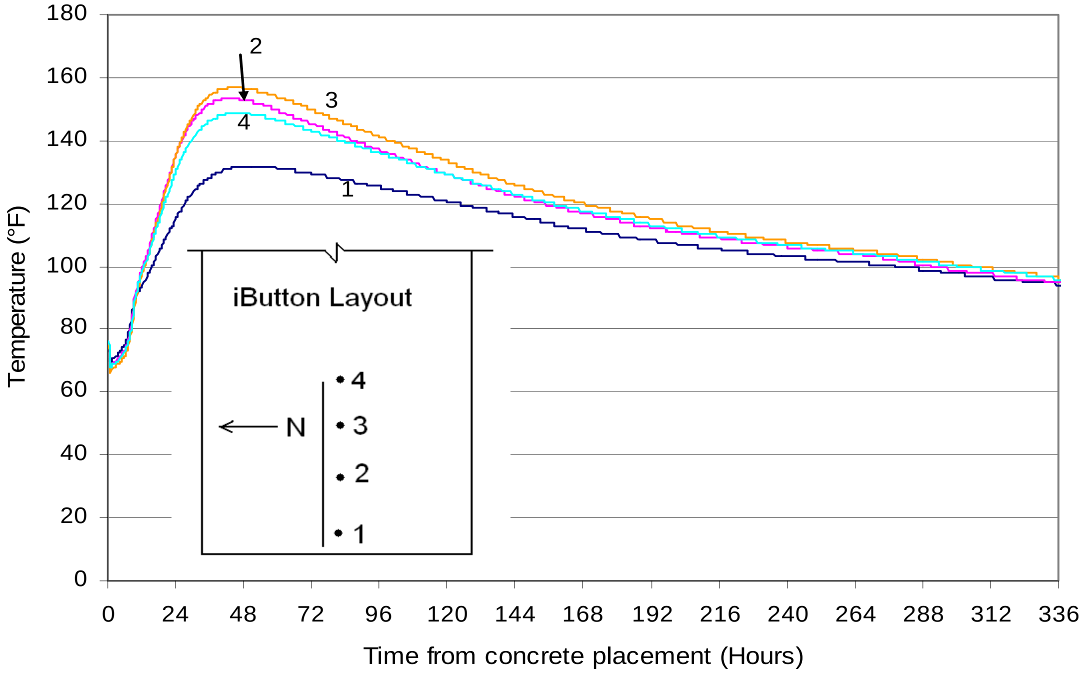

Figure A 4-29 - Temperature data from temperature bar 8

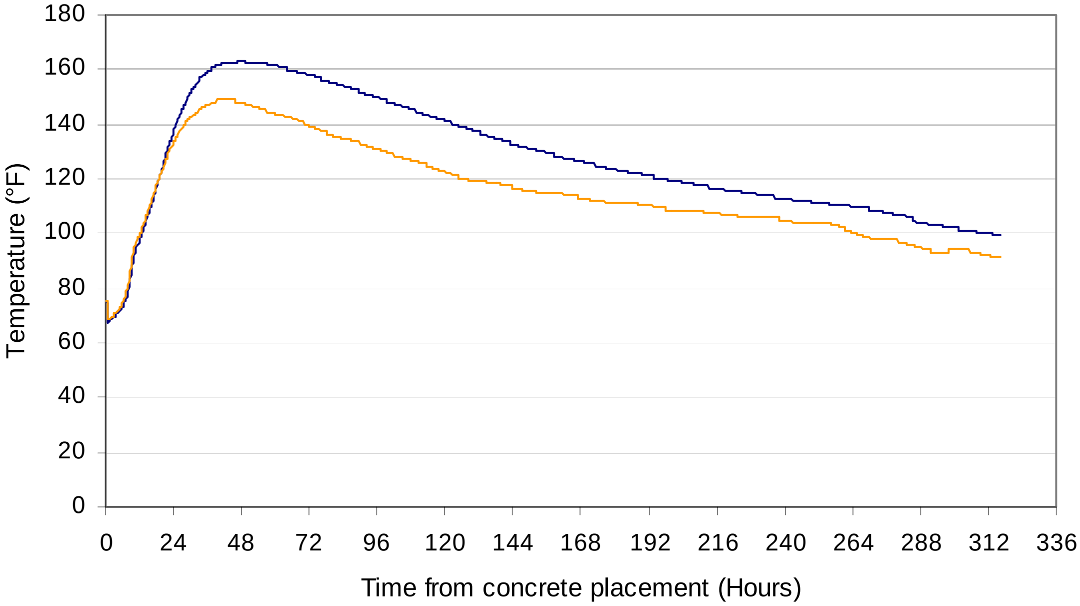

Figure A 4-30 - Data collected from iButtons placed by contractor

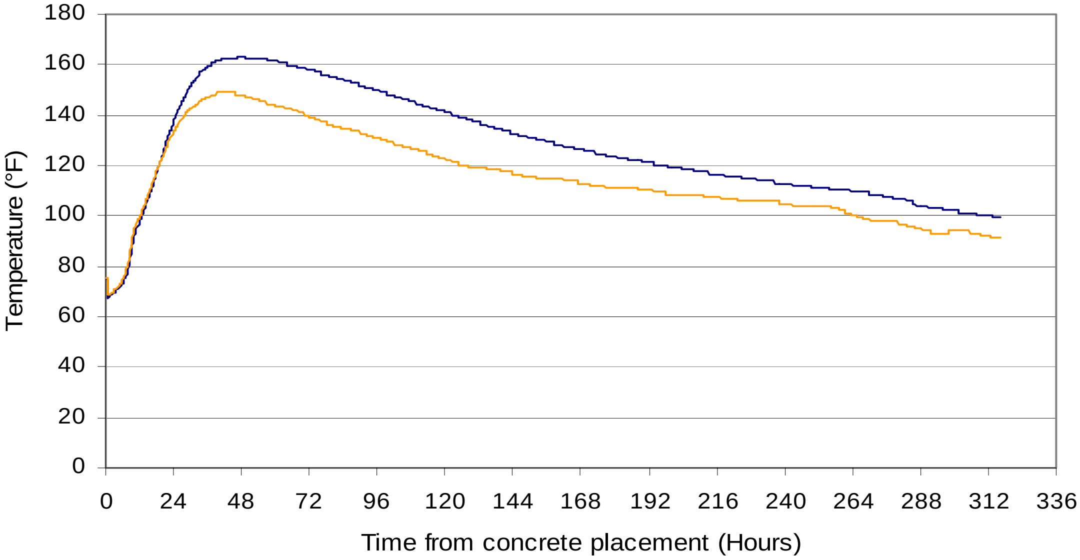

Figure A 4-31 - Maximum temperature, minimum temperature, and maximum temperature difference recorded in column

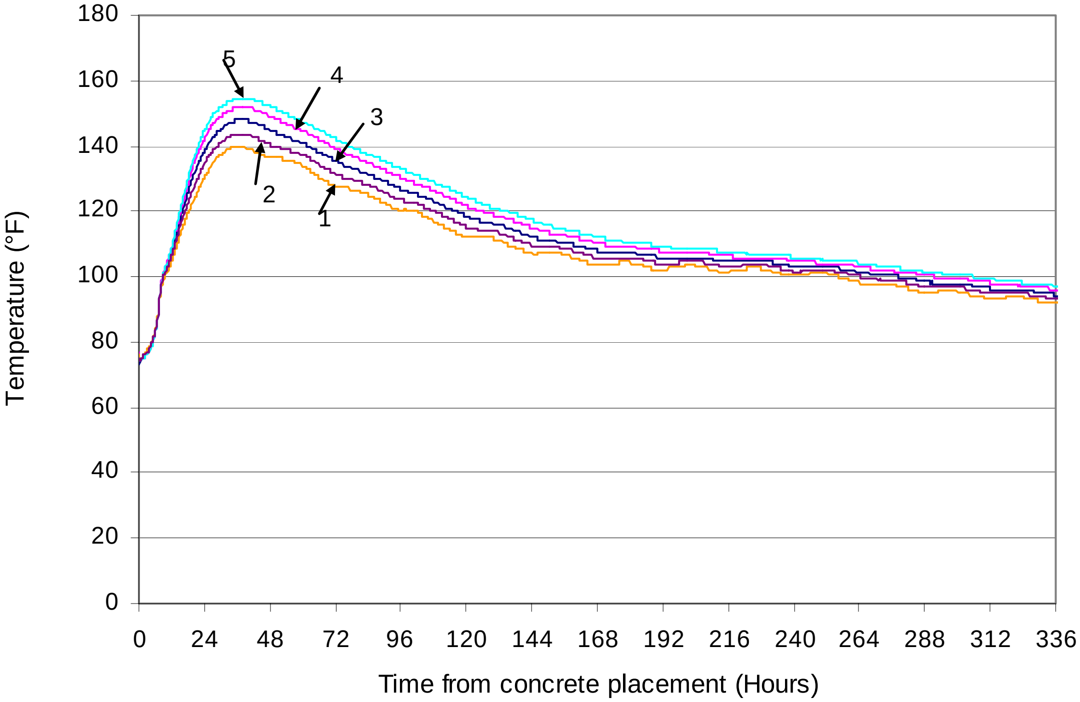

Figure A 4-32 - Temperature data from temperature bar 9

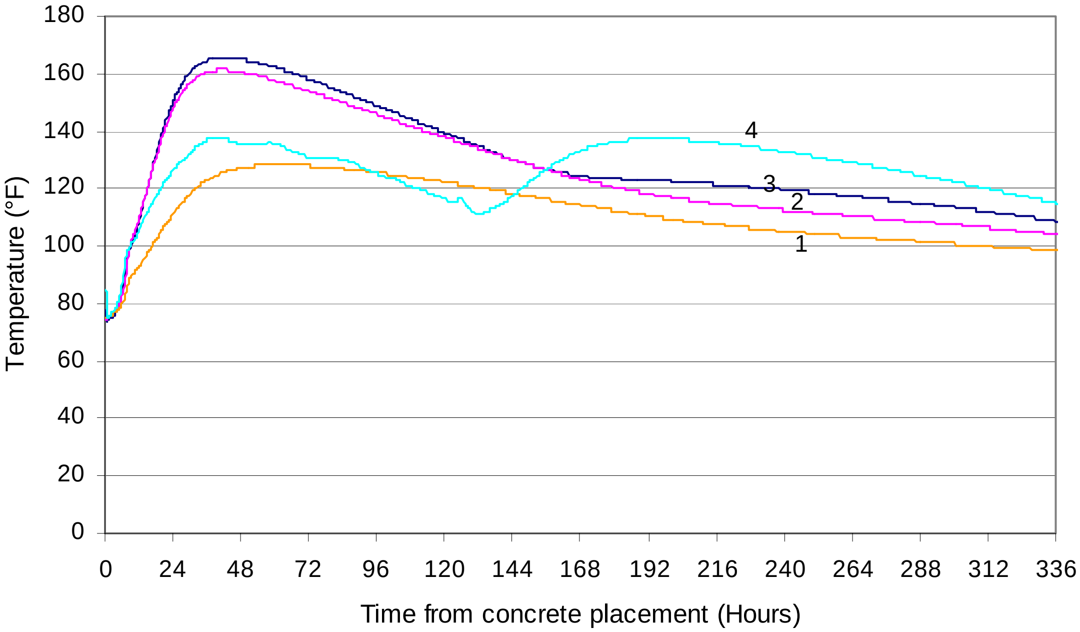

Figure A 4-33 - Temperature data from temperature bar 10

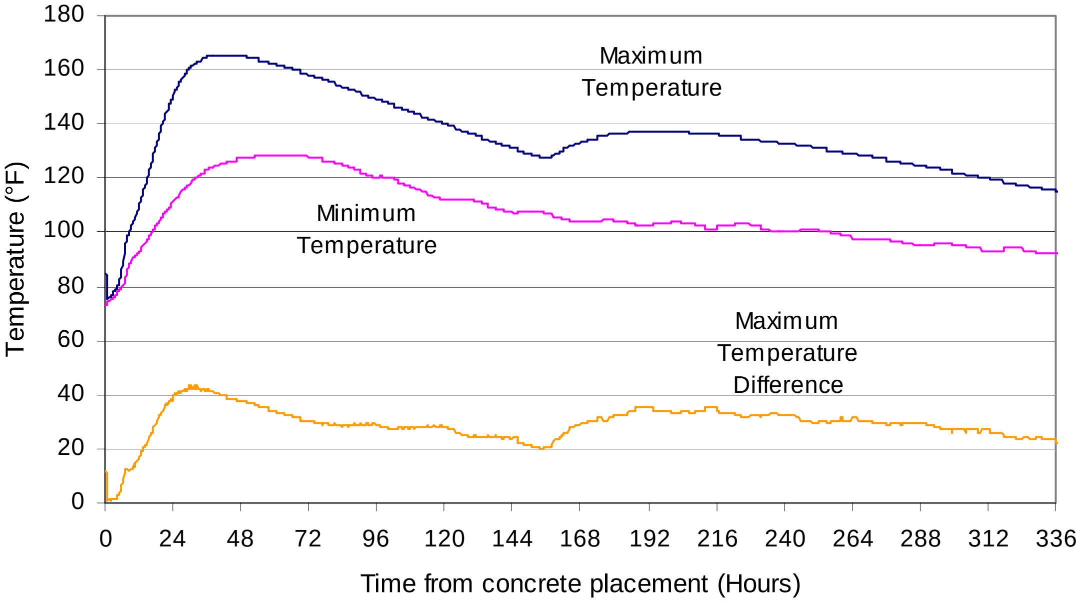

Figure A 4-34 - Maximum temperature, minimum temperature, and maximum temperature difference

APPENDIX A-5 GALVESTON CAUSEWAY

A-5.1 Introduction

As part of TxDOT project 4563, a graphical user-friendly computer program is being developed to predict the in-place temperature development of concrete members during curing. Each construction project uses different combinations of formwork, architectural form liners, concrete raw materials and curing techniques. In addition, environmental conditions during concrete placement and curing differ for every placement. To assure good results as many of these variations as possible must be used in the model calibration.

Inspections performed in 1997 on the causeway linking Galveston Island to the mainland showed that the bridge was deficient in several areas. Over 50 of the causeway's precast beams had significant cracks and showed potential for corrosion. The Texas Department of Transportation decided to replace the causeway with a wider, safer bridge. Construction began in 2003 on the new causeway. Instrumentation was performed on the Bent 28 footing. The concrete members were selected for temperature instrumentation because of the type of materials used, weather conditions expected, project accessibility, formwork used, project location, and member size.

A-5.2 Construction Details

Traylor Bros., Inc. was the prime contractor and placed the concrete. Dorsett Bros. Concrete Supply, Inc. designed the concrete mix and supplied the concrete. Semi-adiabatic calorimetry was also performed on a sample taken on-site. The results of the semi-adiabatic calorimetry are reported elsewhere (Poole, 2007).

The bent 28 footing was placed on top of a seal slab in the Galveston Bay on August 9, 2004. A coffer dam was used to facilitate the formwork erection, reinforcing steel placement, and concrete placement. The footing was 6'-6" deep by 13'-6" wide by 66'-0" long. Light blue steel forms were used. The footing was placed on top of a concrete seal slab.

Table A 5-1 shows the concrete properties. Table A 5-2 shows the tested concrete properties. The concrete placement on the footing started at approximately 5:30 a.m. on August 9th. A concrete sample was taken from the concrete pump inlet at approximately 5:45. The in place fresh concrete temperature was 79°F. Curing blankets and black plastic tarps were placed on top of the footing, as seen in Figure A 5-1. Formwork and curing blankets were removed after the temperature instrumentation of the footing was completed.

A-5.3 Instrumentation

Thermochron iButtons®[5] made by Dallas Semiconductors (Dallas Semiconductor, 2003) were used to measure and log the dolphin in place temperature. Thermochron iButtons record the temperature in increments of 0.9°F and have an accuracy of ±1.8 °F (Dallas Semiconductor, 2003). The procedures for preparing the iButtons for installation were similar to those used in an earlier TxDOT study (Ramaiah, 2002). Wires were soldered onto the iButtons to allow external access to the iButton data. After the wires were attached, the iButtons were coated with epoxy to prevent water damage. To speed-up installation, series of iButtons were attached to ½" diameter acrylic dowels with duct tape. These prefabricated "temperature bars" were placed in the concrete members before the concrete was placed.

---

[5] iButton® is a registered trademark of Dallas Semiconductor

Temperature bars 1-4 were installed in the footing at 3:30 am on August 9th, 2004. Table A 5-3 to Table A 5-6 show the location of temperature bars 1-4 with. Figure A 5-2 shows temperature bar 3 after installation. Temperature bars 1, 2 and 3 were placed horizontally in the footing to capture the temperature profiles of the north, south and east sides of the footing. Temperature bar 4 was placed to capture vertical temperature profile of the footing. Temperature bars 1, 2, and 4 were placed a far enough away from the east end of the footing to avoid end effects.

A-5.4 Weather Data

Weather data were acquired using a Campbell Scientific weather station. The weather station had instrumentation to record relative humidity, temperature, solar radiation, precipitation, wind speed and wind direction. The weather station was placed in the construction yard at the Village of Tiki Island.

Figure A 5-3 to Figure A 5-6 show the temperature, relative humidity, wind speed and solar radiation measured for the footing. The weather station experienced technical difficulties on the first day of instrumentation. Weather data for the first day of instrumentation were provided by Bill Nichtberger of nichtberger.com. The time shown on the graphs is from the start of concrete placement for the footing.

A-5.5 Concrete Temperature Data Acquired

All Thermocron iButtons were programmed to measure and log the temperature every 15 minutes. Figure A 5-7 to Figure A 5-10 show the data acquired from temperature bars 1-4. Figure A 5-11 shows the maximum temperature, minimum temperature and maximum temperature difference recorded in the T-shaped cap. The maximum temperature and maximum temperature difference recorded in the cap were

135.5°F and 41.4°F respectively. The maximum temperature recorded in the cap was recorded by iButtons 2 and 3 on temperature bar 4.

A-5.6 Summary

Temperature sensors were placed in the bent 28 footing of the Galveston Causeway construction. The concrete footing was instrumented on IH 45 between August 9th, 2004 and August 18th. They were installed to record the temperature development due to the heat of hydration of the concrete. The maximum temperature recorded in the footing was 135.5 °F, and the maximum temperature difference recorded in the footing was 41.4 °F. The temperature data collected are being used to calibrate the concrete temperature prediction model being developed as part of TxDOT project 4563.

A-5.7 Acknowledgements

The advice and assistance of the TxDOT Bridge Division and the Central Texas Turnpike Authority is greatly appreciated. The authors wish to thank Ralph Browne, and Tyler Ley, and Robert Dick for arranging access to field sites. The authors also wish to thank Bill Nichtberger for providing weather data.

Table A 5-1– Class C concrete properties

Item	Content	Supplier
Cement	282 lb./yd.^{3}	Holcim Midlothian - Type I/II
Class F Fly Ash	224 lb./yd.^{3}	Big Brown
Coarse Aggregate	1869 lb./ yd.^{3}	1" Siliceous River Gravel
Fine Aggregate	1337 lb./ yd.^{3}	Natural Sand
Air Entraining Admixture	0.59 oz/ cwt.	Eucon Air 40
Water Reducer / Retarder	4.94 oz/ cwt.	EUCON LR
Water Reducer / Retarder	8-12 oz/ cwt.	EUCON SP
Water	175 lb./ yd.^{3}	
Jobsite Measured Slump	4.75"	
Water/cementitious ratio	0.35	

Table A 5-2 – Class C tested concrete properties

Concrete Age	Compressive Strength (psi)	Splitting Tensile Strength (psi)	Elastic Modulus (psi)	Permeability (Coulombs)
28 day	4800	630	5120000	-
91 day	6050	730	-	560

Table A 5-3 - Temperature bar 1 iButton locations

iButton #	Distance west from east side of pedestal	Distance south from north side of pedestal	Distance vertically from top of footing
1	-	0' - 3"	1' - 11.5"
2	-	0' - 6"	1' - 11.5"
3	-	0' - 9"	1' - 11.5"
4	-	0' - 12"	1' - 11.5"
5	-	0' - 15"	1' - 11.5"

Table A 5-4 - Temperature bar 2 iButton locations

iButton #	Distance west from east side of pedestal	Distance north from south side of pedestal	Distance vertically from top of footing
1	-	0' - 0.5"	1' - 11"
2	-	0' - 6.5"	1' - 11"
3	-	1' - 0.5"	1' - 11"
4	-	1' - 6.5"	1' - 11"

Table A 5-5 - Temperature bar 3 iButton locations

iButton #	Distance west from east side of pedestal	Distance south from north side of pedestal	Distance vertically from top of footing
1	0' - 2"	7' - 6"	1' - 8"
2	1' - 2"	7' - 6"	1' - 8"
3	2' - 2"	7' - 6"	1' - 8"
4	3' - 8"	7' - 6"	1' - 8"

Table A 5-6 - Temperature bar 4 iButton locations

iButton #	Distance west from east side of pedestal	Distance north from south side of pedestal	Distance vertically from top of footing
1	-	5' - 9"	6' - 6"
2	-	5' - 9"	4' - 6"
3	-	5' - 9"	2' - 6"
4	-	5' - 9"	0' - 6"

Figure A 5-1 - Bent 28 footing curing conditions

Figure A 5-2 - Temperature bar 3 after installation

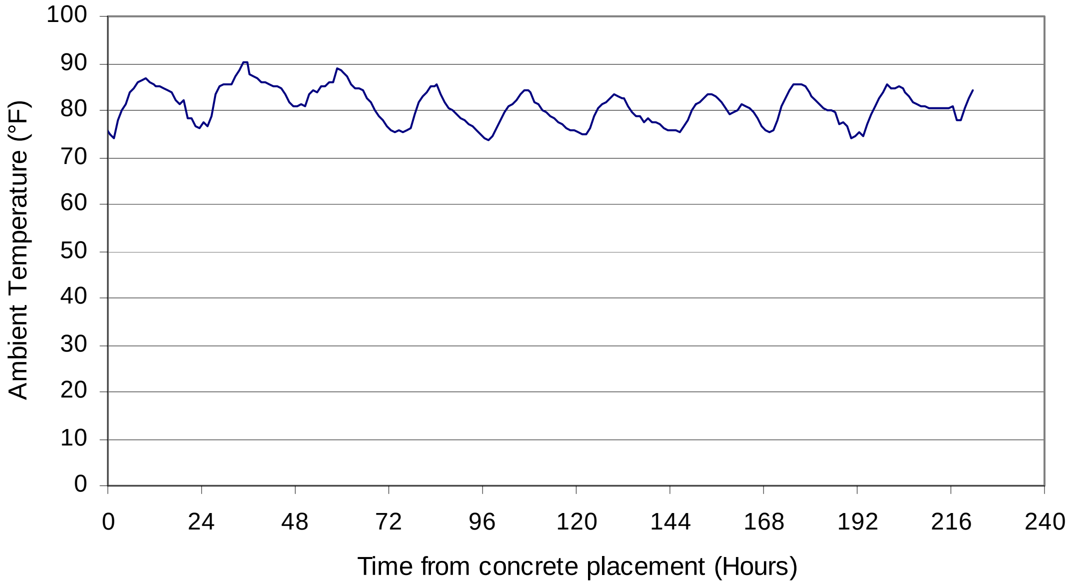

Figure A 5-3 - Ambient temperature data

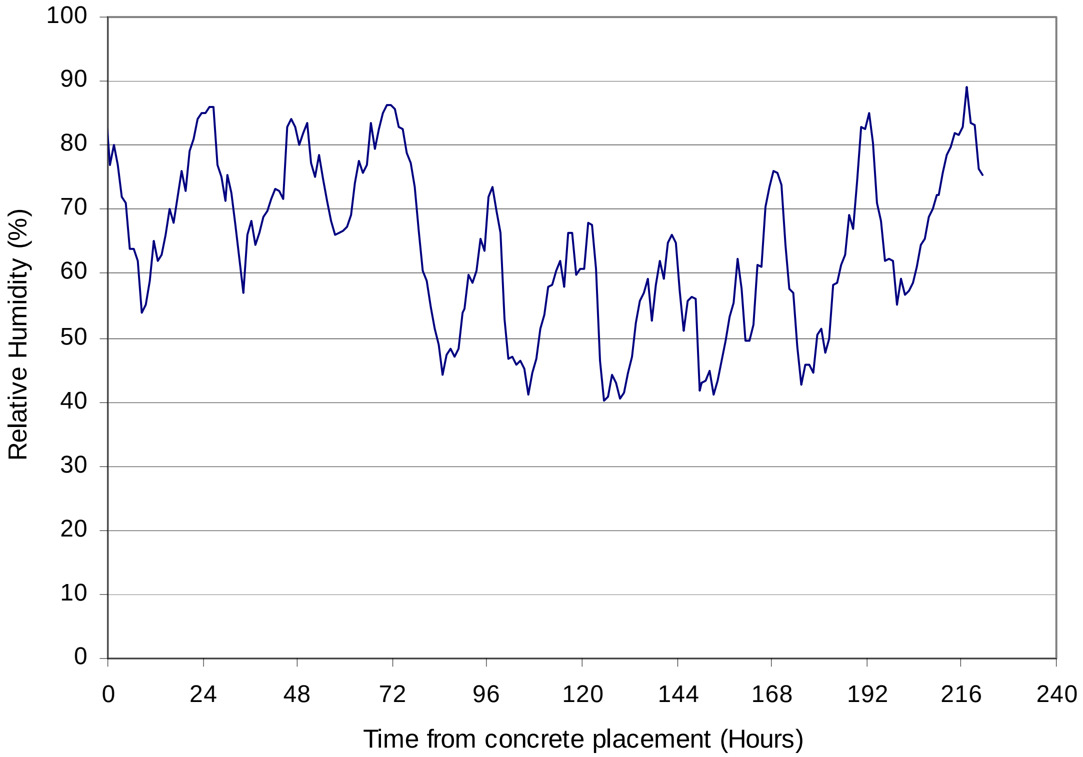

Figure A 5-4 - Relative humidity data

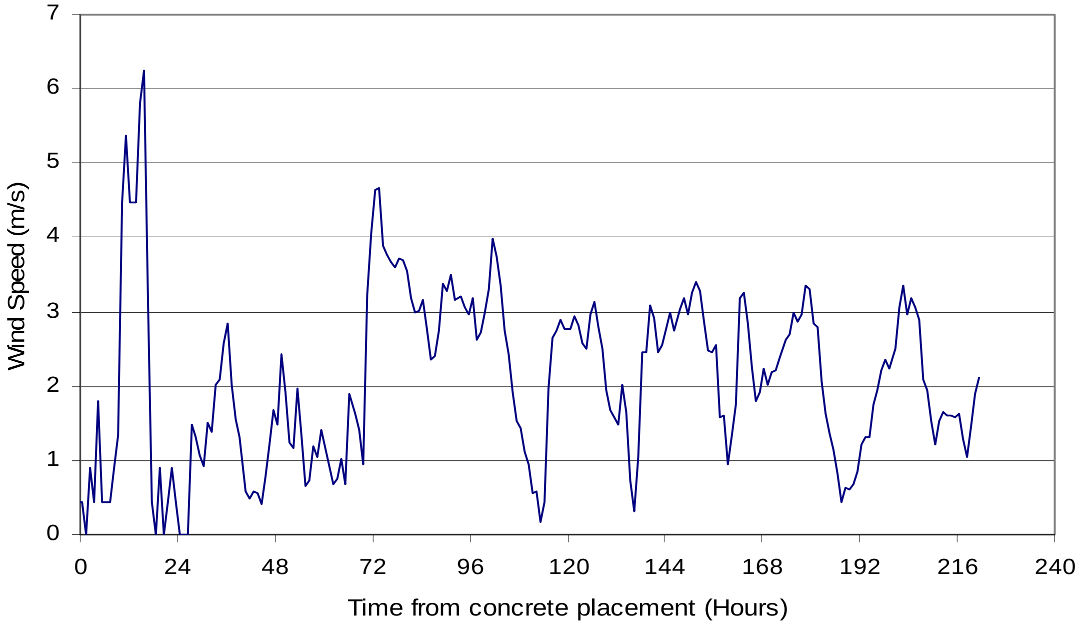

Figure A 5-5 - Wind speed data

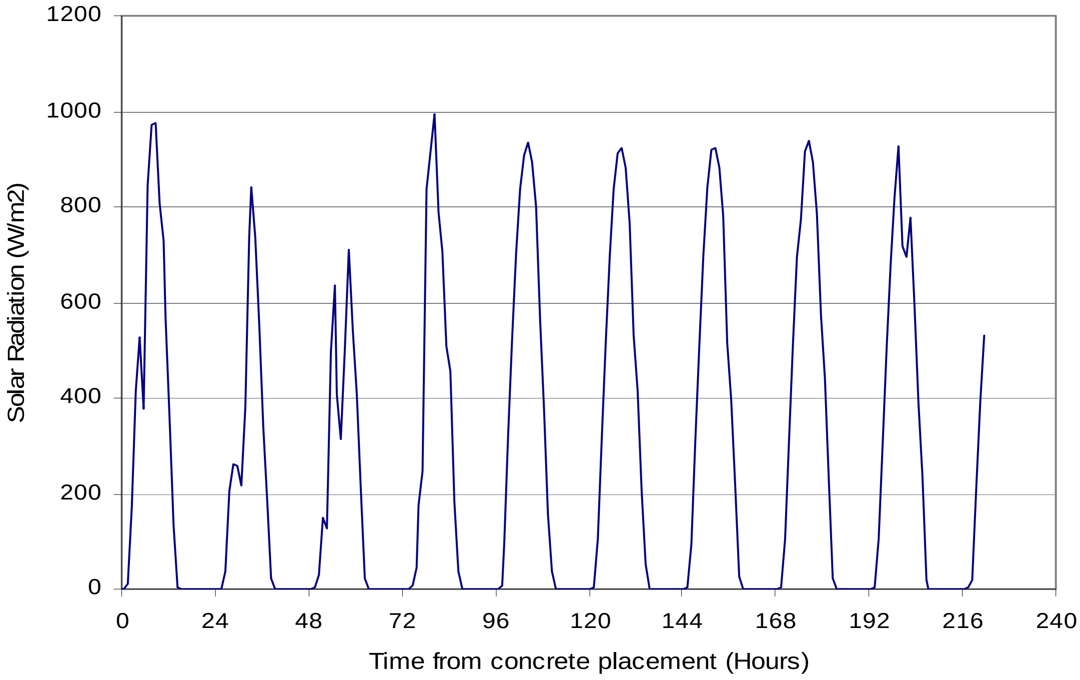

Figure A 5-6 - Solar radiation data

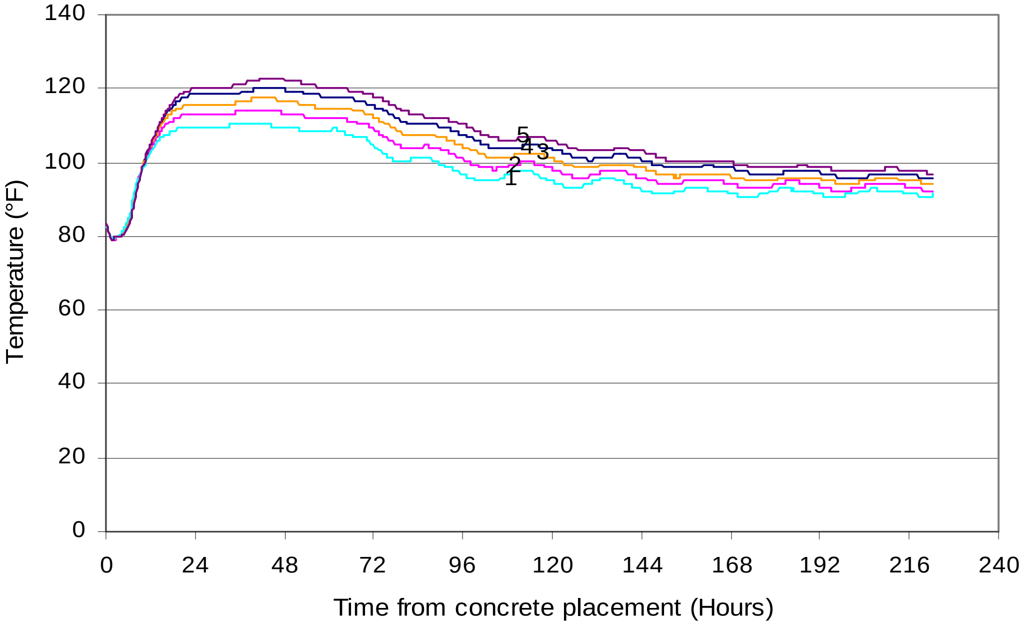

Figure A 5-7 – Data from temperature bar 1

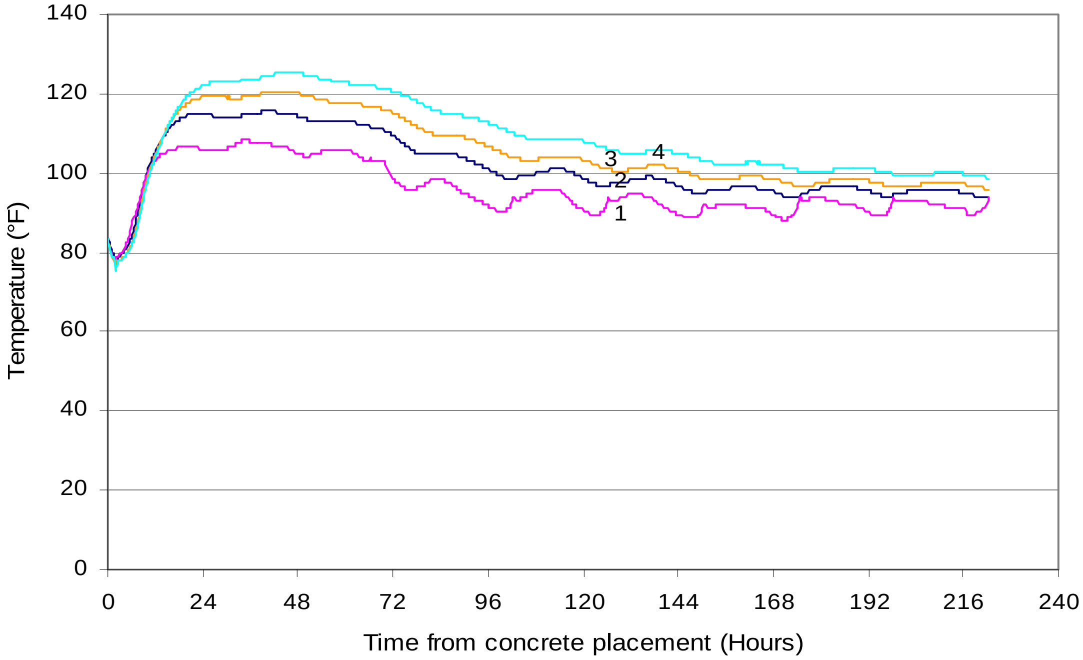

Figure A 5-8 - Data from temperature bar 2

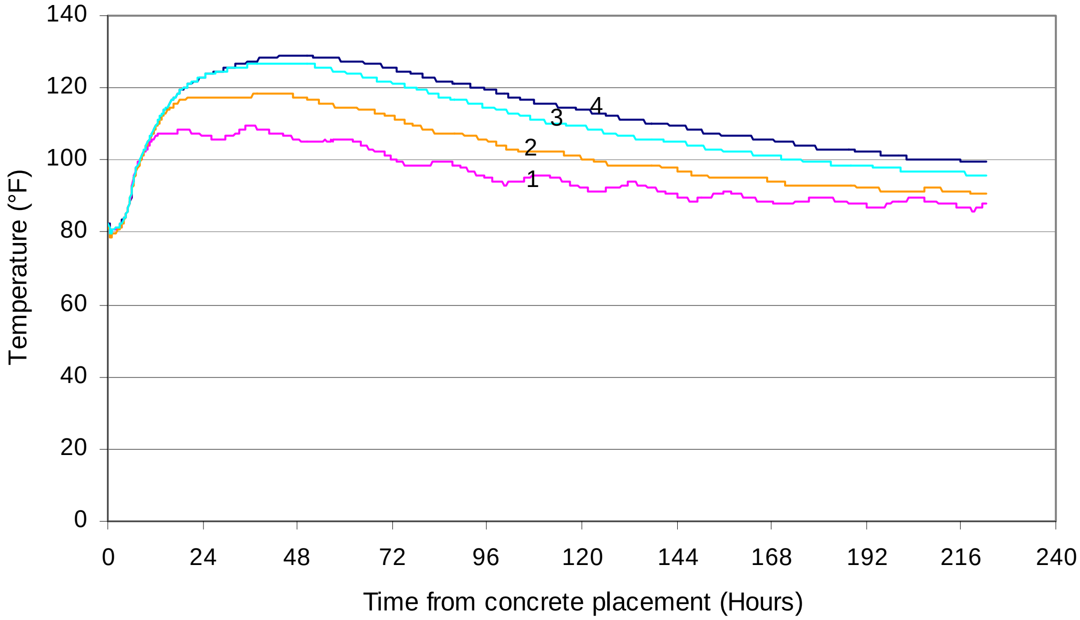

Figure A 5-9 - Data from temperature bar 3

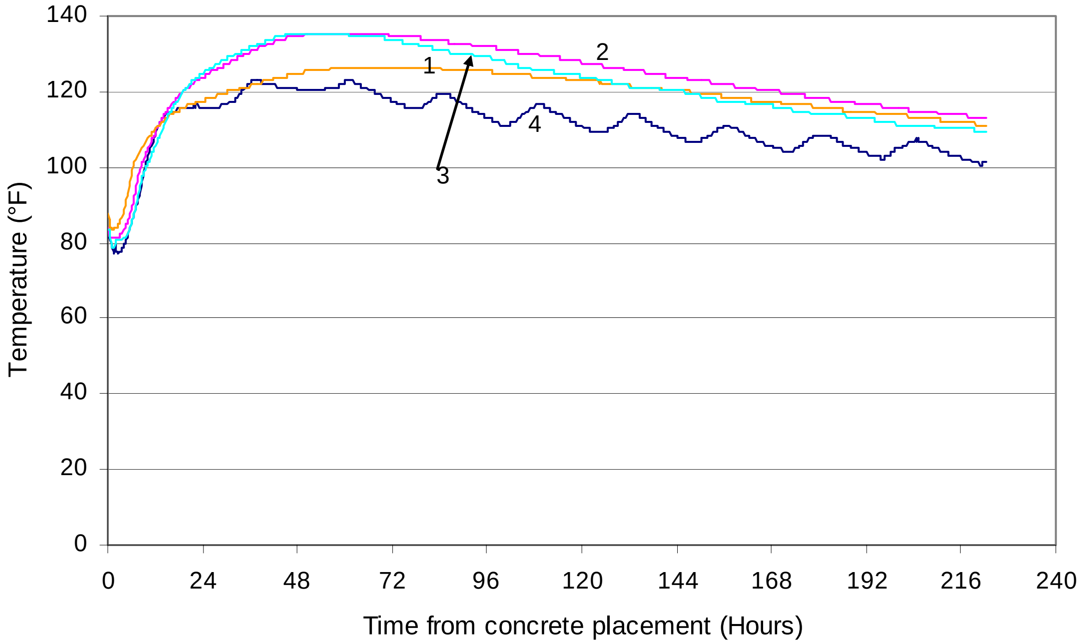

Figure A 5-10 - Data from temperature bar 4

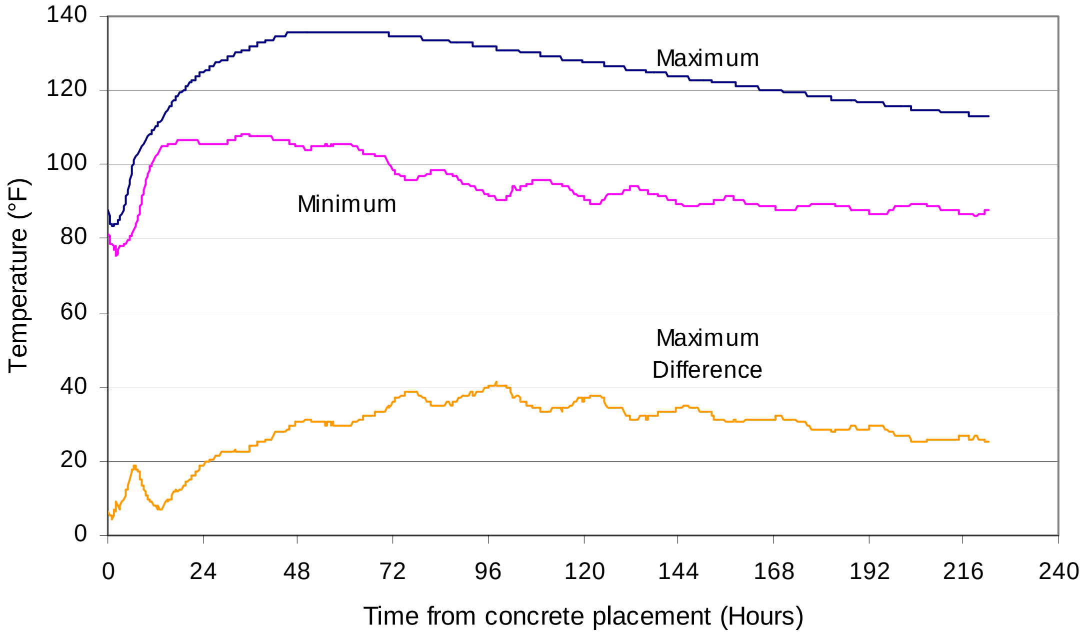

Figure A 5-11 - Maximum temperature, minimum temperature, and maximum temperature difference recorded in footing

APPENDIX A-6 QUEEN ISABELLA CAUSEWAY SEPTEMBER 2004

A-6.1 Introduction

As part of TxDOT project 4563, a graphical user-friendly computer program is being developed to predict the in-place temperature development of concrete members during curing. Each construction project uses different combinations of formwork, architectural form liners, concrete raw materials and curing techniques for concrete. In addition, environmental conditions during concrete placement and curing differ for every placement. To assure accurate results for the model, data from as many of these variations as possible must be captured and used in the model calibration.

On September 15, 2001 a barge ran into the Queen Isabella Causeway. The impact destroyed a 240 ft. section of the bridge, killing 8 people and cutting off the only road to South Padre Island. As part of a three point plan to improve bridge safety, mass concrete dolphins were built to form a “bumper” around the bridge piers (The Associated Press 2003). As part of this project, temperature instrumentation was performed on two dolphins at the Queen Isabella Causeway on February 4-16. Two more dolphins at the Queen Isabella Causeway were instrumented from September 9-23 to the compare the effects of hot summer weather to cold winter weather on the concrete heat transfer.

A-6.2 Dolphin Construction

The dolphin’s dimensions were 16’ square by 9’ in depth. The dolphins were supported by nine piers that elevate the dolphins a few feet above the water line. A 2’ thick precast panel was used as a stay-in-place bottom formwork. The remaining 7’ thick sections were placed by a pump truck from the bridge. Figure A 6-1 shows dolphin 10 before the formwork was placed. Figure A 6-2 shows dolphin 9 with the formwork in place.

Orion Construction was the prime contractor and placed the concrete. Transit Mix Concrete and Materials Co. designed the concrete mix and supplied the concrete. Table A 6-1 shows the concrete mix design and fresh properties. Table A 6-2 shows the tested, hardened concrete properties. Semi-adiabatic calorimetry was also performed on a sample taken on-site and is reported on elsewhere (Poole 2007).

Concrete placement on dolphin 10 started at approximately 4:15 a.m. on September 10th, 2004. Concrete placement on dolphin 9 started at about 5:45 a.m. on September 10th, 2004. Forms were removed on September 14th, 2004. The in-place fresh concrete temperature was 75°F. No insulating curing methods were used after forms were removed.

A-6.3 Instrumentation

Thermochron iButtons®[6] made by Dallas Semiconductor (Dallas Semiconductor 2003) were used to measure and log the dolphin in-place temperature. Thermochron iButtons record the temperature in increments of 0.9°F and have an accuracy of ±1.8 °F (Dallas Semiconductor 2003). The procedures for preparing the iButtons for installation were similar to those used in an earlier TxDOT study (Ramaiah, 2002). Wires were soldered onto the iButtons to allow external access to the iButton data. After the wires were attached, the iButtons were coated with epoxy to prevent water damage. To speed-up installation, series of iButtons were attached to ½" diameter acrylic dowels with duct tape. These prefabricated "temperature bars" were placed in dolphins 9 and 10 the day

---

[6] iButton® is a registered trademark of Dallas Semiconductor

before concrete was placed. Temperature bars 1-3 were installed on dolphin 10 while temperature bars 4-7 were installed on dolphin 9. Table A 6-3 to Table A 6-9 show the locations of temperature bars 1-7. Figure A 6-3 shows temperature bars 2 and 3 after installation. Figure A 6-4 shows temperature bar 4 after installation.

A-6.4 Weather Data

Weather data were acquired using a Campbell Scientific weather station. The weather station has instrumentation to record relative humidity, temperature, solar radiation, precipitation, wind speed and wind direction. Ambient temperature was instead recorded using an iButton that was taped to the bottom of the weather station data logger box. Figure A 6-5 to Figure A 6-9 show the temperature, relative humidity, wind speed, rainfall and solar radiation measured. The time shown on the graphs is from the start of concrete placement for dolphin 10. The concrete for dolphin 9 was placed one and a half hours after dolphin 10. The weather station was placed on a sand bar next to the barge dock at the contractor's construction yard.

A-6.5 Concrete Temperature Data Acquired

The Thermochron iButtons were programmed to measure and log the temperature every 15 minutes. Figure A 6-10 to Figure A 6-16 show the data acquired from temperature bars 1-7. Figure A 6-17 shows the maximum temperature, minimum temperature and maximum temperature difference recorded in dolphin 10. The maximum temperature and maximum temperature difference recorded in dolphin 10 were 147.2°F and 45°F respectively. The maximum temperature recorded in dolphin 10 was recorded by iButton 6 on temperature bar 1 and iButtons 5 and 6 on temperature bar 3. Figure A 6-18 shows the maximum temperature, minimum temperature and maximum temperature difference recorded in dolphin 9. The maximum temperature and maximum temperature difference recorded in dolphin 9 were 149.9°F and 55.8°F, respectively. The maximum temperature recorded in dolphin 9 was recorded by iButtons 5 and 6 on temperature bar 5.

A visual inspection for cracking of dolphins 9 and 10 was made 13 days after concrete placement. Restraint cracking was found on both dolphins 9 and 10. Figure A 6-19 shows a restraint crack on dolphin 9 that starts near the corner. The cracks extended several feet towards the center of the dolphin on the top and several feet vertically downward on the sides. The steep temperature drop recorded at the top surface of both dolphins between 76 hrs and 81 hrs coincides with a large amount of rain being recorded by the weather station. The cool rain may have thermally shocked the top concrete surface. Thermal shock is when the concrete surface is rapidly cooled, resulting in surface cracking (ACI 2071.R 1996).

A-6.6 Summary

Temperature sensors were placed in dolphins 9 and 10 of the Queen Isabella Causeway on September 9th, the day before concrete placement. They were installed to record the temperature development due to the heat of hydration of the concrete. Table A 6-10 shows the maximum temperatures and temperature differences recorded in each dolphin. Both dolphins show similar temperature development because they were cast on the same day from the same concrete mixture proportions at the same location. The same pattern of restraint cracks were found on both dolphins thirteen days after concrete placement. The restraint cracking was probably caused by thermal shock during a rainstorm. The temperature data collected will be used to calibrate the concrete temperature prediction model being developed as part of TxDOT project 4563.

A-6.7 Acknowledgements

The advice and assistance of the TxDOT Bridge Division and TxDot McAllen office is greatly appreciated. The authors wish to thank Ralph Browne, Tyler Ley, Luiz Gonzales, and Augustine Ramirez for arranging access to field sites.

.

Table A 6-1- Concrete properties

Item	Content	Material Description
Cement	422 lb./yd.^{3}	TXI - Type I/II
Class F Fly Ash	189 lb./yd.^{3}	Coleto Creek
Coarse Aggregate	1872 lb./ yd.^{3}	1" Siliceous River Gravel
Fine Aggregate	1188 lb./ yd.^{3}	Natural Sand
Air Entraining Admixture	1.33 oz/ cwt.	Master Builders AE 90
Mid Range Water Reducer	3.95 oz/ cwt.	Master Builders Polyheed 997
Water Reducer / Retarder	2.42 oz/ cwt.	Pozzolith 300R
Jobsite Measured Air Content	8.500%	
Jobsite Measured Slump	5.25"	
Water/cementitious material ratio	0.35	

Table A 6-2 - Tested concrete properties

Concrete Age (days)	Compressive Strength (psi)	Splitting Tensile Strength (psi)	Elastic Modulus (psi)	Permeability (Coulombs)
28	4130	450	4,707,000	-
91	-	-	-	850

Table A 6-3 - iButton locations for temperature bar 1 on dolphin 10

iButton #	Distance from North Side Formwork	Distance from East Side Formwork	Distance vertically from precast panel
1	4' - 6"	10' - 2"	0' - 0"
2	4' - 6"	10' - 2"	1' - 0"
3	4' - 6"	10' - 2"	2' - 0"
4	4' - 6"	10' - 2"	3' - 0"
5	4' - 6"	10' - 2"	4' - 0"
6	4' - 6"	10' - 2"	5' - 0"
7	4' - 6"	10' - 2"	6' - 0"
8	4' - 6"	10' - 2"	6' - 11"

Table A 6-4 - iButton locations for temperature bar 2 on dolphin 10

iButton #	Distance from North Side Formwork	Distance from East Side Formwork	Distance vertically from precast panel
1	0' -1"	5' - 10"	1' - 5.5"
2	1' - 6"	5' - 10"	1' - 5.5"
3	3' - 0"	5' - 10"	1' - 5.5"
4	4' - 0"	5' - 10"	1' - 5.5"
5	5' - 0"	5' - 10"	1' - 5.5"
6	6' - 0"	5' - 10"	1' - 5.5"
7	7' - 0"	5' - 10"	1' - 5.5"

Table A 6-5 - iButton locations for temperature bar 3 on dolphin 10

iButton #	Distance from North Side Formwork	Distance from East Side Formwork	Distance vertically from precast panel
1	4' -8"	6' - 2"	0' - 0"
2	4' -8"	6' - 2"	1' - 0"
3	4' -8"	6' - 2"	2' - 0"
4	4' -8"	6' - 2"	3' - 0"
5	4' -8"	6' - 2"	4' - 0"
6	4' -8"	6' - 2"	5' - 0"
7	4' -8"	6' - 2"	6' - 0"
8	4' -8"	6' - 2"	6' - 9"

Table A 6-6 - iButton locations for temperature bar 4 on dolphin 9

iButton #	Distance from North Side Formwork	Distance from East Side Formwork	Distance vertically from precast panel
1	7' - 1"	0' - 0.5"	4' - 5"
2	7' - 1"	0' - 3.5"	4' - 5"
3	7' - 1"	0' - 6.5"	4' - 5"
4	7' - 1"	0' - 9.5"	4' - 5"
5	7' - 1"	1' - 0.5"	4' - 5"

Table A 6-7 - iButton locations for temperature bar 5 on dolphin 9

iButton #	Distance from North Side Formwork	Distance from East Side Formwork	Distance vertically from precast panel
1	6 '- 0"	5' - 10"	0' - 0"
2	6' - 0"	5' - 10"	1' - 0"
3	6' - 0"	5' - 10"	2' - 0"
4	6' - 0"	5' - 10"	3' - 0"
5	6' - 0"	5' - 10"	4' - 0"
6	6' - 0"	5' - 10"	5' - 0"
7	6' - 0"	5' - 10"	6' - 0"
8	6' - 0"	5' - 10"	7' - 0"

Table A 6-8 - iButton locations for temperature bar 6 on dolphin 9

iButton #	Distance from North Side Formwork	Distance from East Side Formwork	Distance vertically from precast panel
1	4' - 6.5"	5' - 10"	4' - 6"
2	3' - 0.5"	5' - 10"	4' - 6"
3	1' - 6.5"	5' - 10"	4' - 6"
4	1' - 0.5"	5' - 10"	4' - 6"
5	0' - 6.5"	5' - 10"	4' - 6"
6	0' - 0.5"	5' - 10"	4' - 6"

Table A 6-9 - iButton locations for temperature bar 7 on dolphin 9

iButton #	Distance from North Side Formwork	Distance from East Side Formwork	Distance vertically from precast panel
1	6' - 2"	9' - 11"	0' - 0"
2	6' - 2"	9' - 11"	1' - 0"
3	6' - 2"	9' - 11"	2' - 0"
4	6' - 2"	9' - 11"	3' - 0"
5	6' - 2"	9' - 11"	4' - 0"
6	6' - 2"	9' - 11"	5' - 0"
7	6' - 2"	9' - 11"	6' - 0"
8	6' - 2"	9' - 11"	6' - 10"

Table A 6-10 - Temperature data summary for dolphins 11 and 12

Concrete Member	Maximum Temperature Recorded (°F)	Maximum Temperature Difference Recorded (°F)
Dolphin 9	149.9	55.8
Dolphin 10	147.2	45


Figure A 6-1 - Dolphin 10 before the formwork placement


Figure A 6-2 - Dolphin 9 after formwork placement

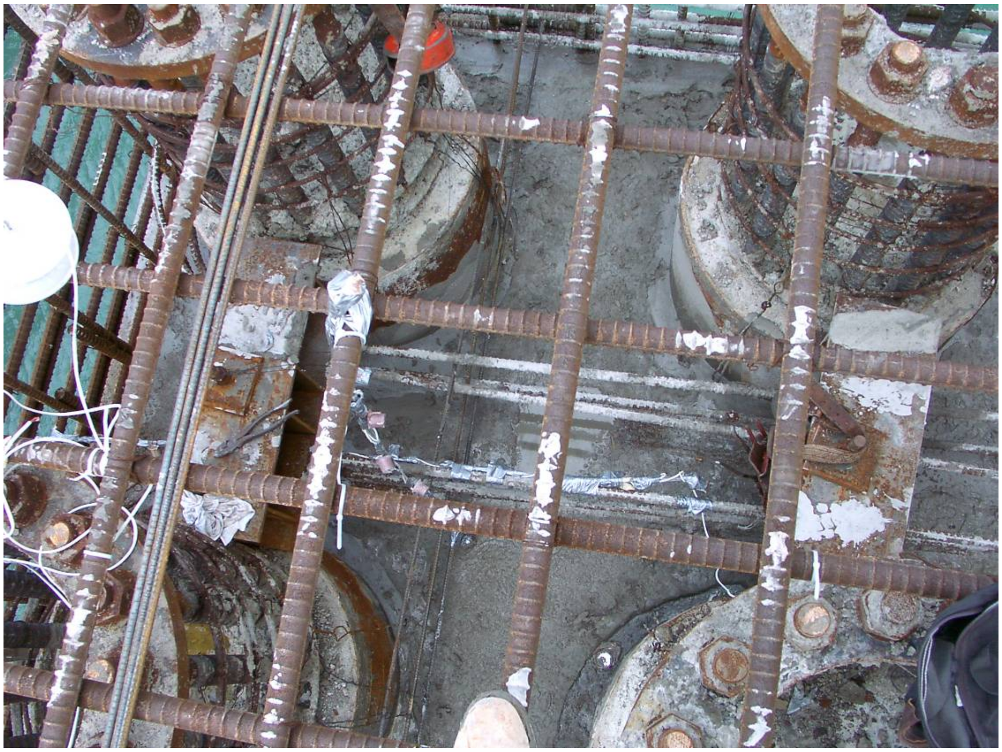

Figure A 6-3 - Temperature bars 2 and 3 on dolphin 10 after installation

Figure A 6-4 - Temperature bar 4 on dolphin 9 after installation

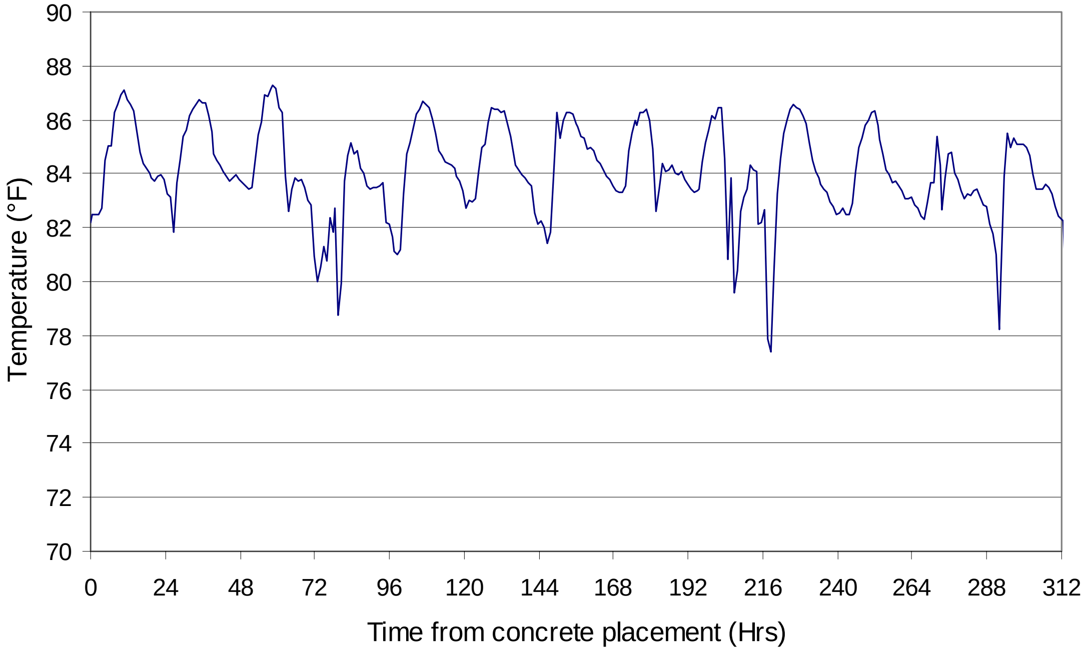

Figure A 6-5 - Ambient temperature data

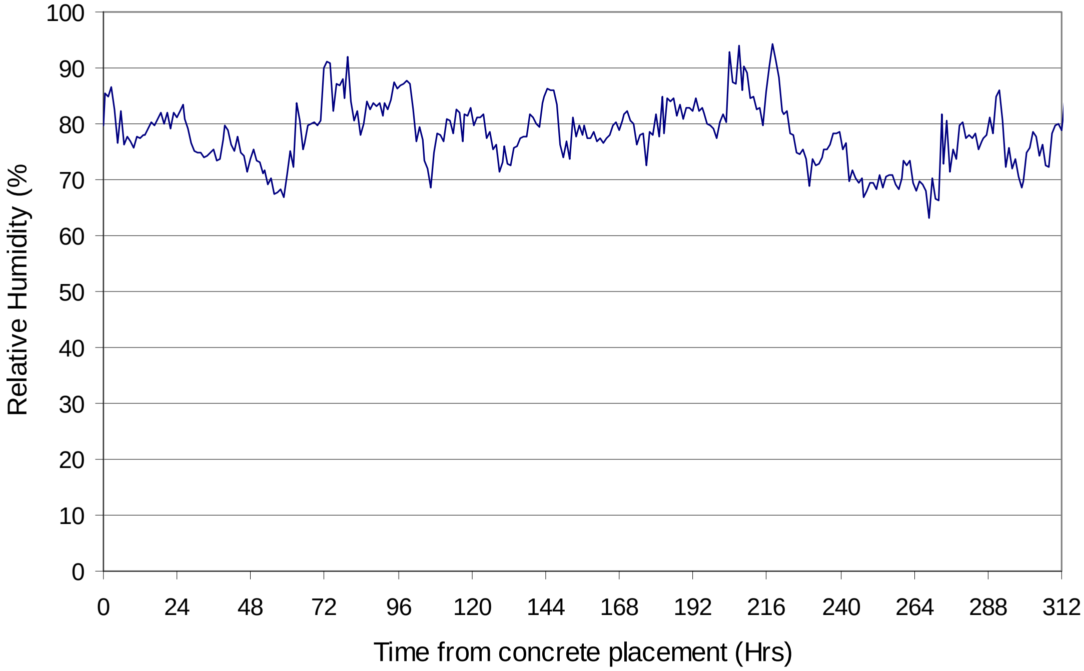

Figure A 6-6 - Relative humidity data

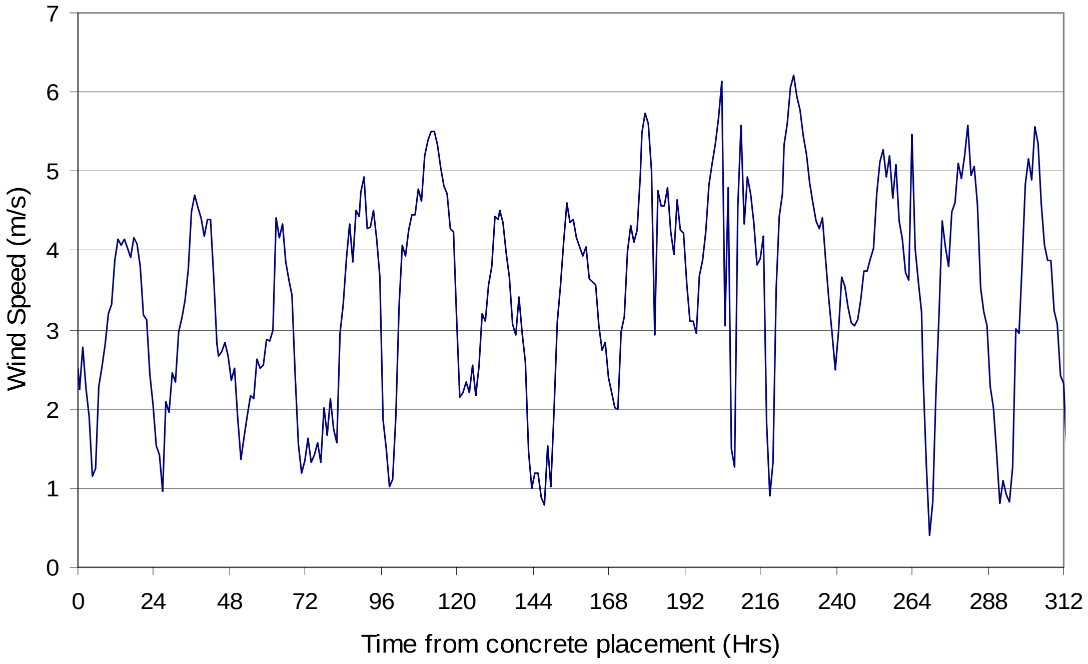

Figure A 6-7 - Wind speed data

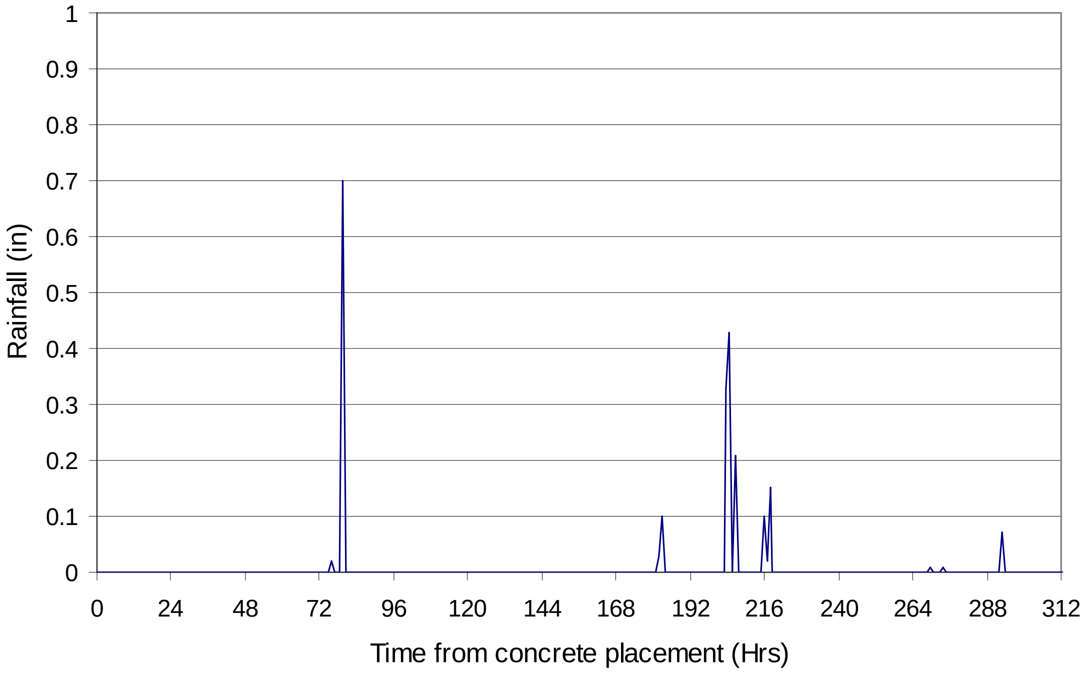

Figure A 6-8 - Rainfall data

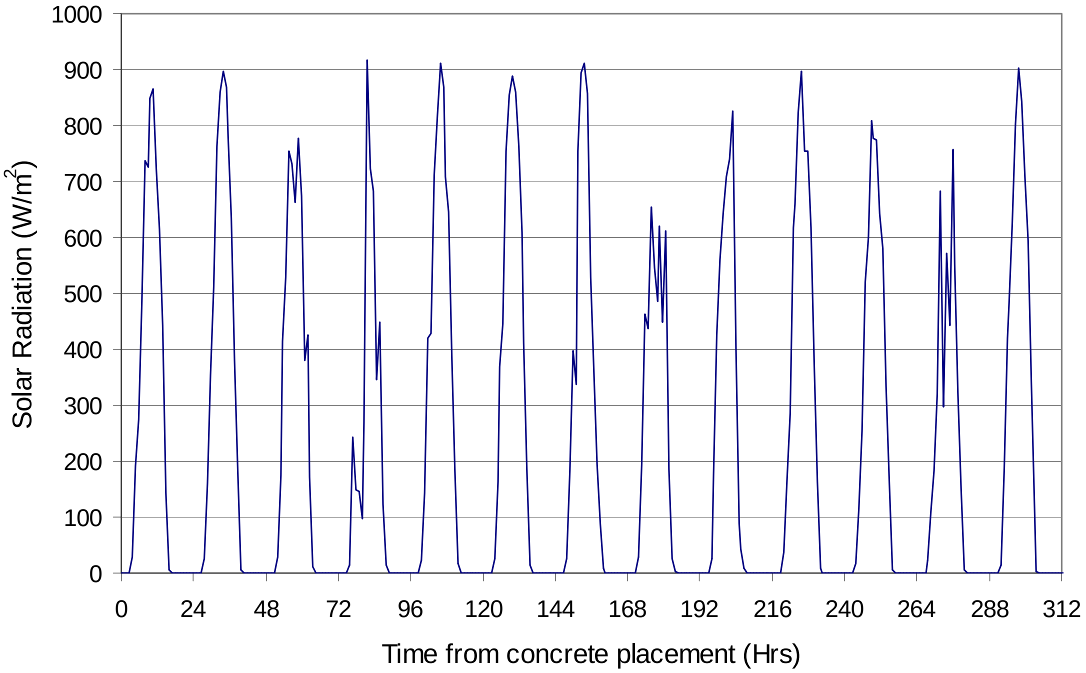

Figure A 6-9 - Solar radiation data

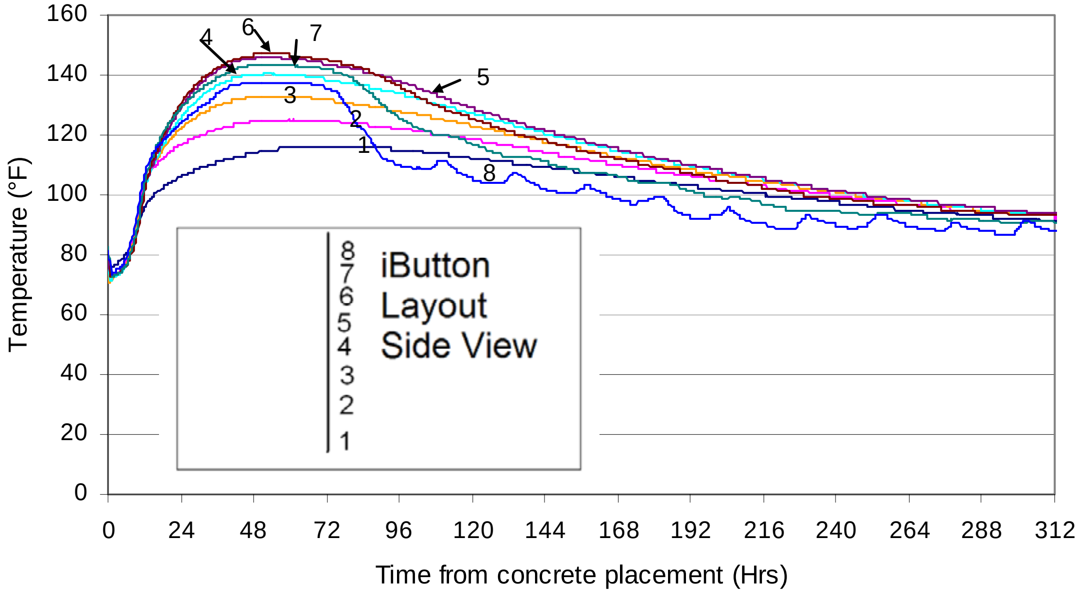

Figure A 6-10 - Temperature bar 1 data

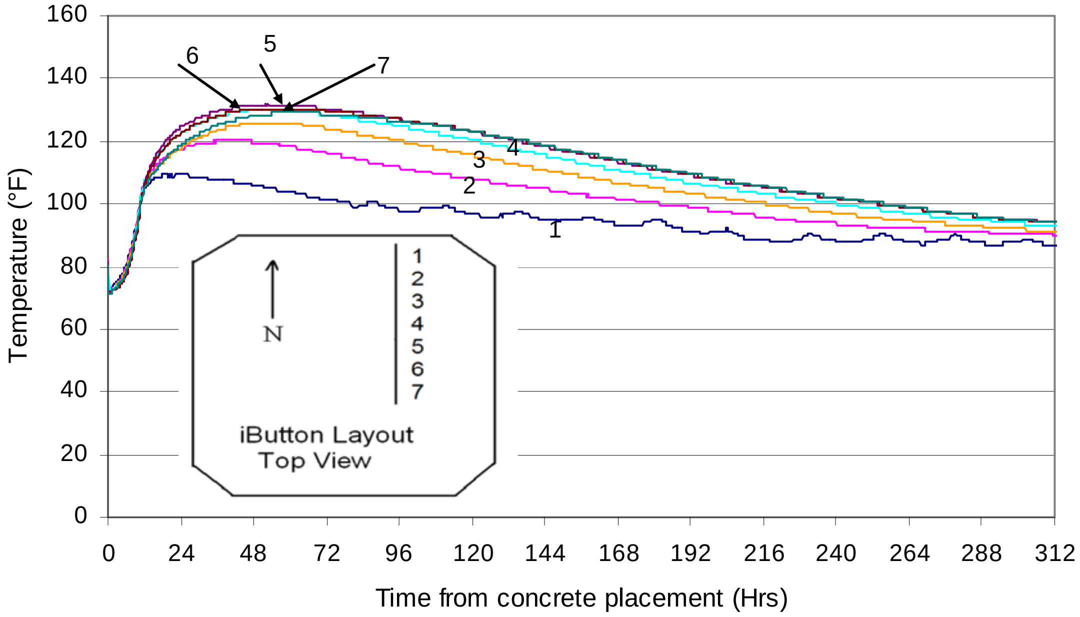

Figure A 6-11 - Temperature bar 2 data

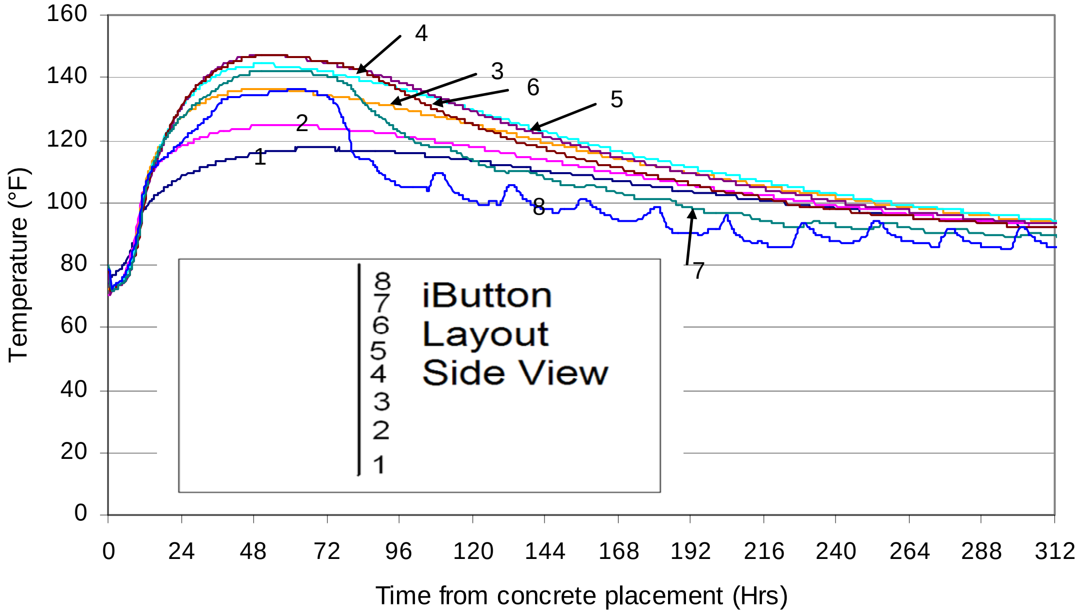

Figure A 6-12 - Temperature bar 3 data

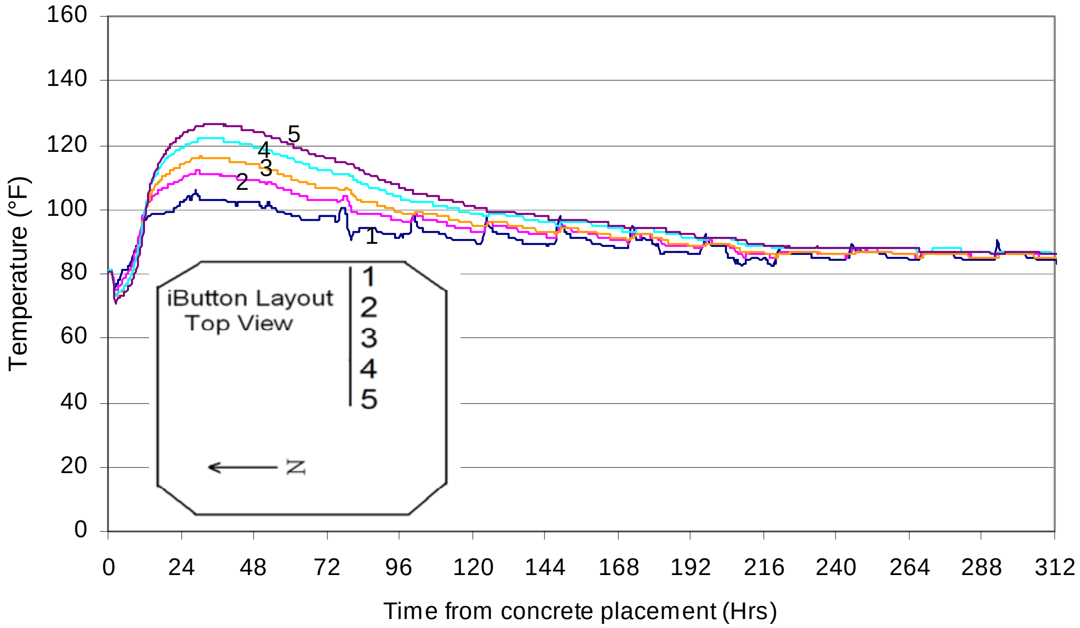

Figure A 6-13 - Temperature bar 4 data

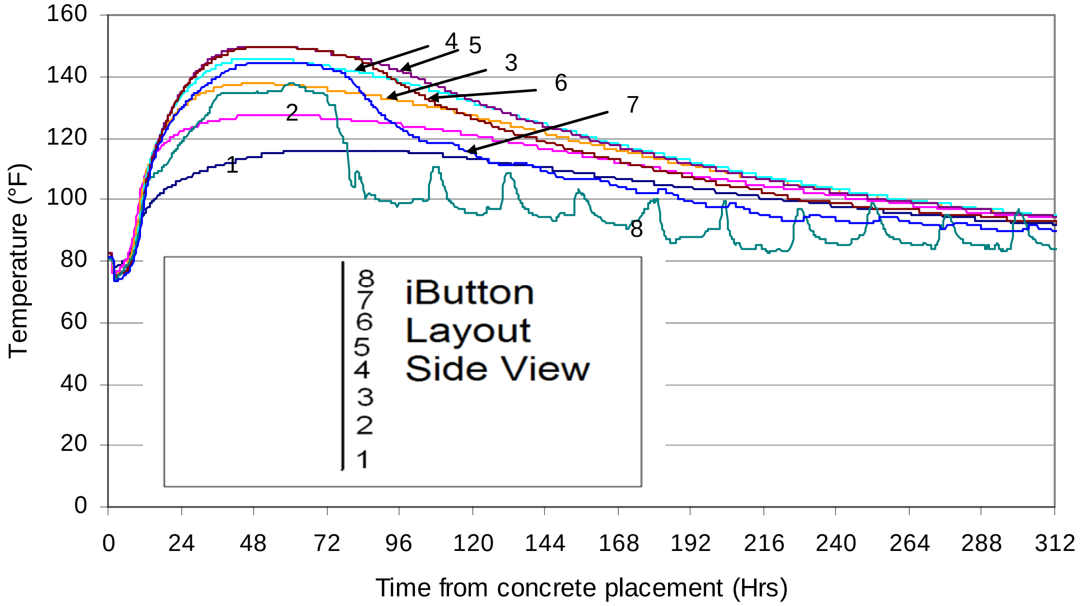

Figure A 6-14 - Temperature bar 5 data

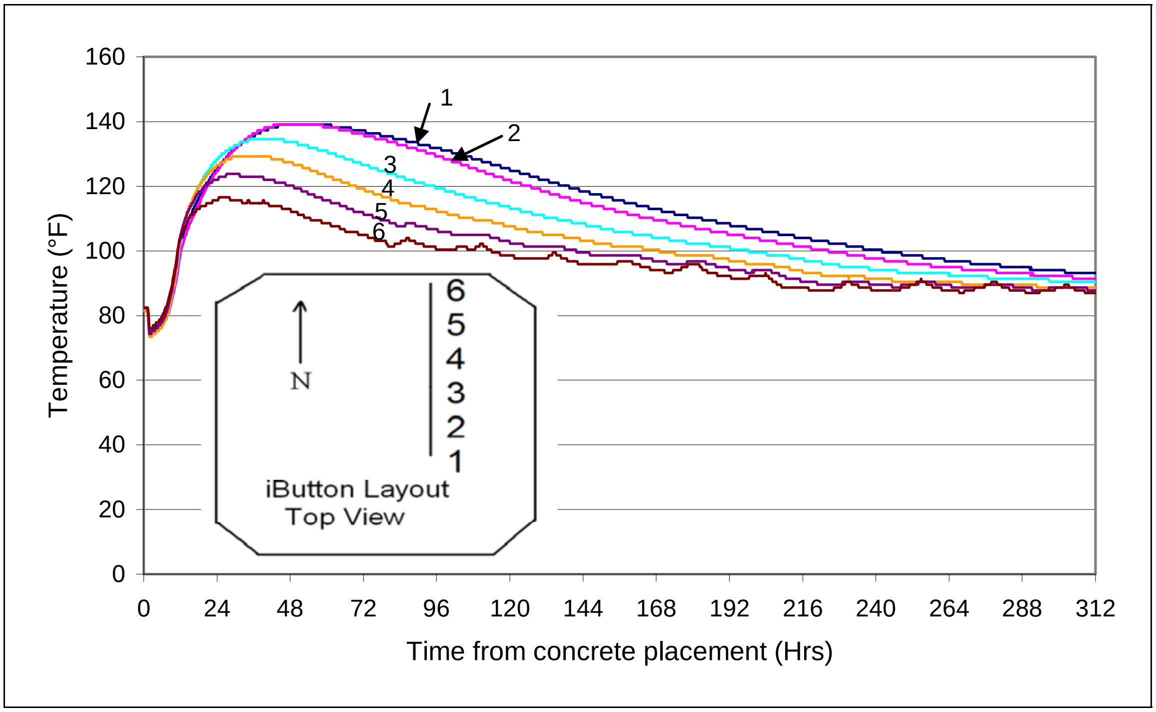

Figure A 6-15 - Temperature bar 6 data

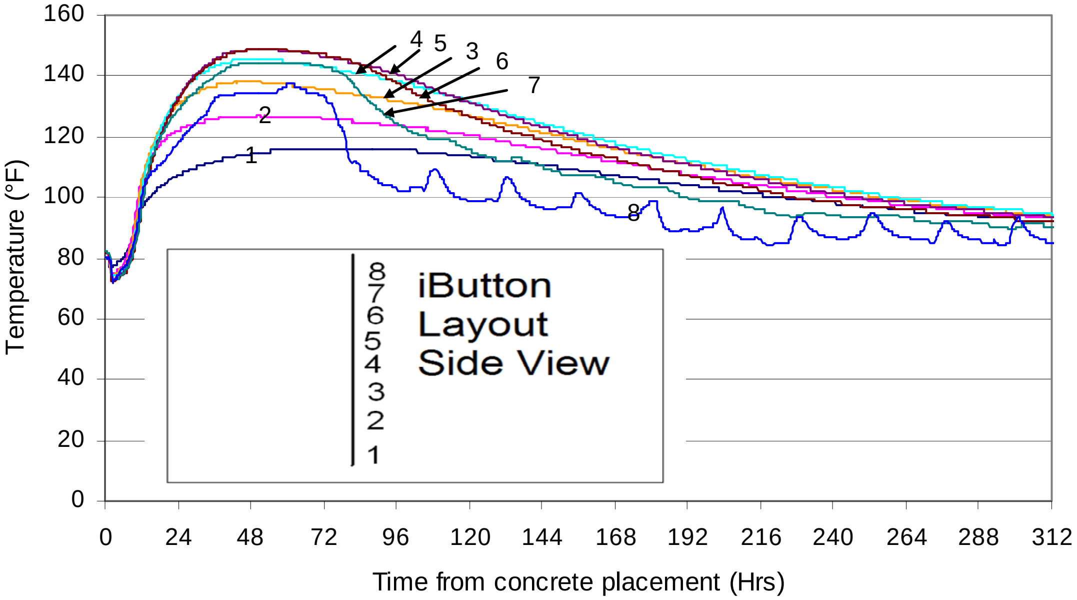

Figure A 6-16 - Temperature bar 7 data

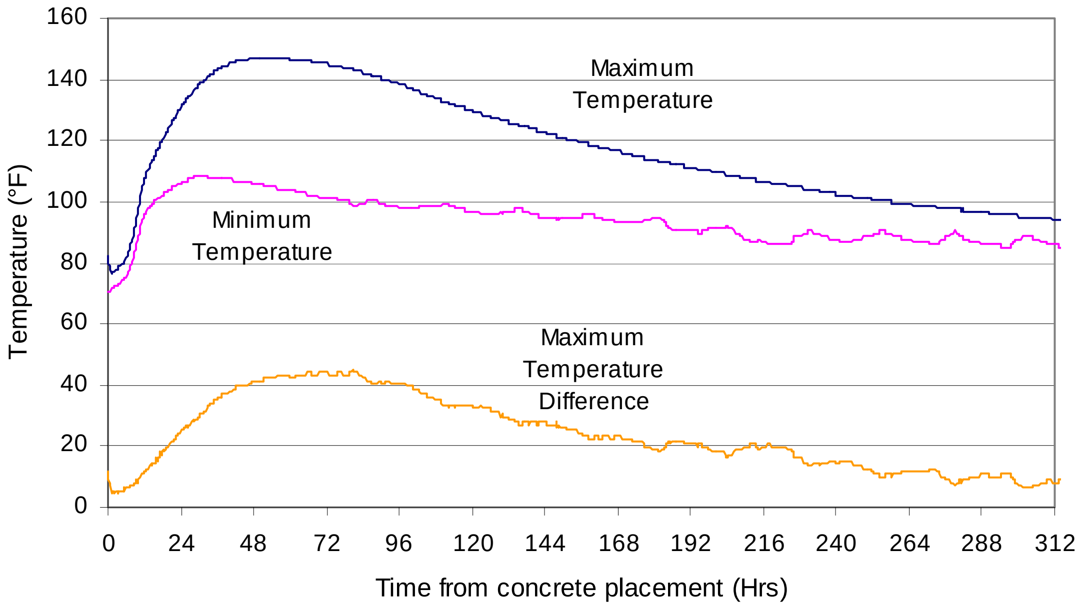

Figure A 6-17 – Maximum temperature, minimum temperature, and maximum temperature difference recorded in dolphin 10

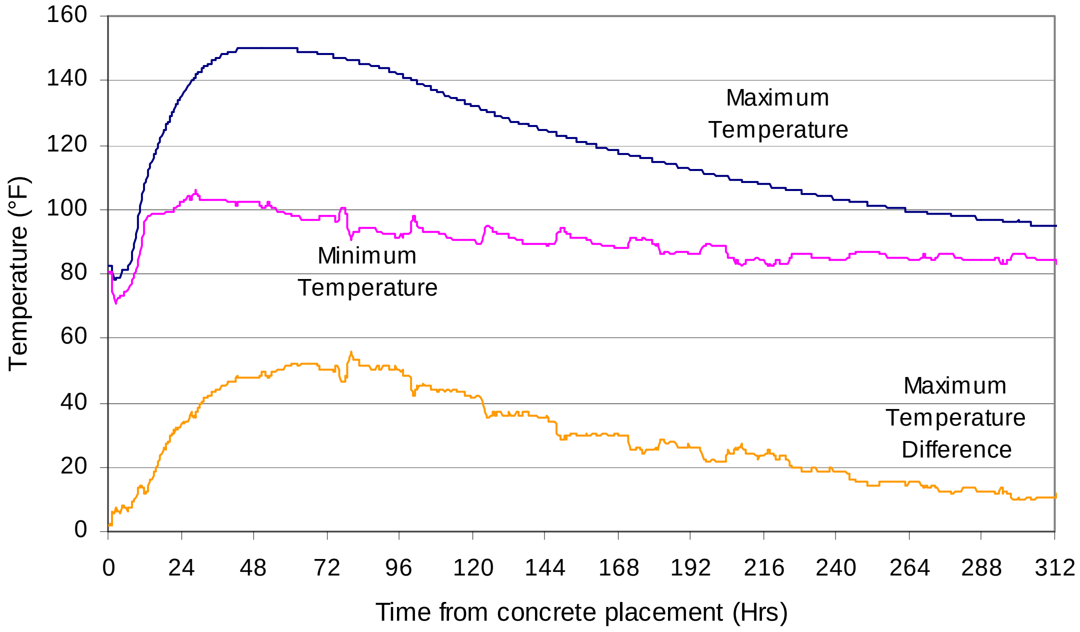

Figure A 6-18 - Maximum temperature, minimum temperature, and maximum temperature difference recorded in dolphin 9

Figure A 6-19 - Restraint crack on the top surface of dolphin 9

APPENDIX A-7 EL PASO PILASTER

A-7.1 Introduction

As part of TxDOT project 4563, a graphical user-friendly computer program is being developed to predict the in-place temperature development of concrete members during curing. Each construction project uses different combinations of formwork, architectural form liners, concrete raw materials and curing techniques for concrete. In addition, environmental conditions during concrete placement and curing differ for every placement. To assure accurate results for the model, data from as many of these variations as possible must be captured and used in the model calibration.

As part of the project several pilasters (faux columns built for architectural purposes) of different sizes were constructed to improve the appearance of I-10. A mass pilaster was selected for temperature instrumentation to capture the effect of low relative humidity and ground granulated blast furnace slag (GGBFS) on concrete temperature development.

A-7.2 Footing Construction

The dimensions of the part of the pilaster that was instrumented are 9’ by 6’ by 5’ 6” deep. The pilaster was placed in three sequences. The first sequence was placing the solid bottom portion. Foam was placed in the center of the second concrete section to reduce the amount of concrete used in the middle section of the pilaster. In the third construction sequence, a solid concrete cap was placed on top of the second concrete section. Figure A 7-1 shows the construction sequences used for the pilaster. The pilaster is located within a few feet of a retaining wall, as shown in Figure A 7-2.

J.D. Abrams was the prime contractor and placed the concrete. Jobe Concrete Products, Inc. designed and supplied the concrete mixture. Table A 7-1 shows the concrete mixture design and fresh properties. Semi-adiabatic calorimetry was performed at the job-site. Results from the semi-adiabatic calorimetry are reported elsewhere (Poole 2007)

Concrete placement on the footing began at approximately 9:15 a.m. on February 22nd, 2005. Heaters were placed at the top of the formwork and point down during the first two nights of curing. Forms were removed sometime after the last temperature readings were taken. The in-place fresh concrete temperature was 69°F.

A-7.3 Instrumentation

Thermochron iButtons®[7] made by Dallas Semiconductor (Dallas Semiconductor, 2003) were used to measure and log the dolphin in-place temperature. Thermochron iButtons record the temperature in increments of 0.9°F and have an accuracy of ±1.8 °F (Dallas Semiconductor, 2003). The procedures for preparing the iButtons for installation were similar to those used in an earlier TxDOT study (Ramaiah, 2002). Wires were soldered onto the iButtons to allow external access to the iButton data. After the wires were attached, the iButtons were coated with epoxy to prevent water damage. To speed-up installation, series of iButtons were attaced to ½” diameter acrylic dowels with duct tape. These prefabricated “temperature bars” were placed in the footing in the morning of February 15th, 2005. Five temperature bars were placed in the footing. Table A 7-2 to 6 show the location of each ibutton in the pilaster. Figure A 7-3 shows the pilaster during installation.

---

[7] iButton® is a registered trademark of Dallas Semiconductor

A-7.4 Weather Data

Weather data were acquired using a Campbell Scientific weather station. The weather station has instrumentation to record relative humidity, temperature, precipitation, solar radiation, wind speed, and wind direction. Figure A 7-4 to Figure A 7-8 show the temperature, relative humidity, wind speed, solar radiation, and rainfall. The time shown on the graphs is from the start of concrete placement for the footing. The weather station was placed a few hundred yards away from the pilaster at the job trailer.

A-7.5 Concrete Temperature Data Acquired

The Thermochron iButtons were programmed to measure and log the temperature every 15 minutes. Figure A 7-9 to Figure A 7-13 show the data acquired from temperature bars 1-5. Figure A 7-14 shows the maximum temperature, minimum temperature and maximum temperature difference recorded in the footing. The maximum temperature and maximum temperature difference recorded in the footing were 130.1°F and 65.7°F respectively. The maximum temperature recorded in the footing was recorded by iButton 4 on temperature bar 1.

A-7.6 Summary

Temperature sensors were placed in the mass footing before concrete placement on April 22nd. They were installed to record the temperature development due to the heat of hydration of the concrete. The maximum temperature and maximum temperature difference recorded in the footing were 130.1°F and 65.7°F respectively. The temperature data collected are being used to calibrate the concrete temperature prediction model being developed as part of TxDOT project 4563.

A-7.7 Acknowledgements

The advice and assistance of the TxDOT Bridge Division is greatly appreciated. The authors wish to thank Ralph Browne and Tomas Saenz for arranging access to field sites.

Table A 7-1 - Concrete properties

Item	Content	Material Description
Cement	305 lb./yd.^{3}	Type I/II
Ground Granulated Blast Furnace Slag	278 lb./yd.^{3}	Grade 120
Coarse Aggregate	1680 lb./ yd.^{3}	1" Siliceous River Gravel
Fine Aggregate	1258 lb./ yd.^{3}	Natural Sand
Air Entraining Admixture	0.5 oz/ cwt.	AEA - 40
Water Reducer	4.7 oz/ cwt.	X-15
Jobsite Measured Air Content	%	
Jobsite Measured Slump	"	
Design w/cm	0.43	

Table A 7-2 - iButton locations for temperature bar 1

iButton #	Distance from North Side Formwork	Distance from East Side Formwork	Distance Vertically from Bottom of Footing
1	6' - 0"	3' - 1"	3' - 8"
2	4' - 6"	3' - 1"	3' - 8"
3	3' - 0"	3' - 1"	3' - 8"
4	1' - 6"	3' - 1"	3' - 8"
5	0' - 0"	3' - 1"	3' - 8"

Table A 7-3 - iButton locations for temperature bar 2

iButton #	Distance from North Side Formwork	Distance from West Side Formwork	Distance Vertically from Bottom of Footing
1	4' - 6"	0' - 0"	3' - 8"
2	4' - 6"	1' - 6"	3' - 8"
3	4' - 6"	3' - 0"	3' - 8"
4	4' - 6"	4' - 6"	3' - 8"
5	4' - 6"	6' - 0"	3' - 8"

Table A 7-4 - iButton locations for temperature bar 3

iButton #	Distance from North Side Formwork	Distance from East Side Formwork	Distance Vertically from Bottom of Footing
1	3' - 2"	4' - 6"	0' - 0"
2	3' - 2"	4' - 6"	1' - 0"
3	3' - 2"	4' - 6"	2' - 0"
4	3' - 2"	4' - 6"	3' - 0"
5	3' - 2"	4' - 6"	4’ - 0”

Table A 7-5 - iButton locations for temperature bar 4

iButton #	Distance from North Side Formwork	Distance from East Side Formwork	Distance Vertically from Bottom of Footing
1	1' - 9"	4' - 6"	4' - 0"
2	1' - 9"	4' - 6"	3' - 0"
3	1' - 9"	4' - 6"	2' - 0"
4	1' - 9"	4' - 6"	1' - 0"
5	1' - 9"	4' - 6"	0’ - 0”

Table A 7-6 - iButton locations for temperature bar 5

iButton #	Distance from North Side Formwork	Distance from East Side Formwork	Distance Vertically from Bottom of Footing
1	0' - 6"	4' - 6"	5' - 0"
2	0' - 6"	4' - 6"	4' - 6"
3	0' - 6"	4' - 6"	3' - 0"
4	0' - 6"	4' - 6"	1' - 6"
5	0' - 6"	4' - 6"	0’ - 0”

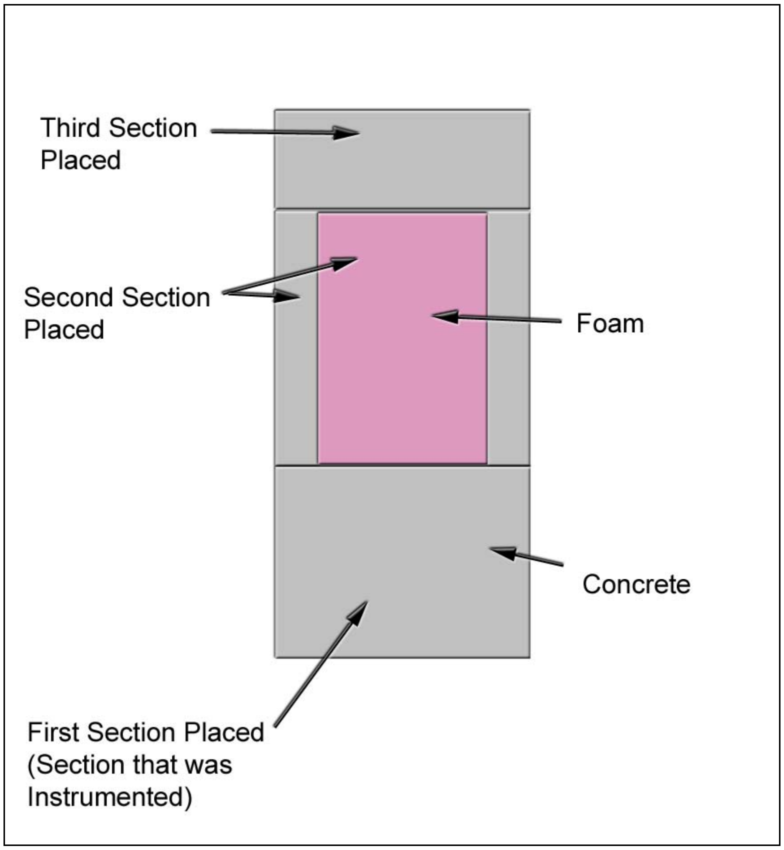

Figure A 7-1 - Pilaster construction sequences

Figure A 7-2 - Pilaster next to retaining wall

Figure A 7-3 – Pilaster during temperature bar installation

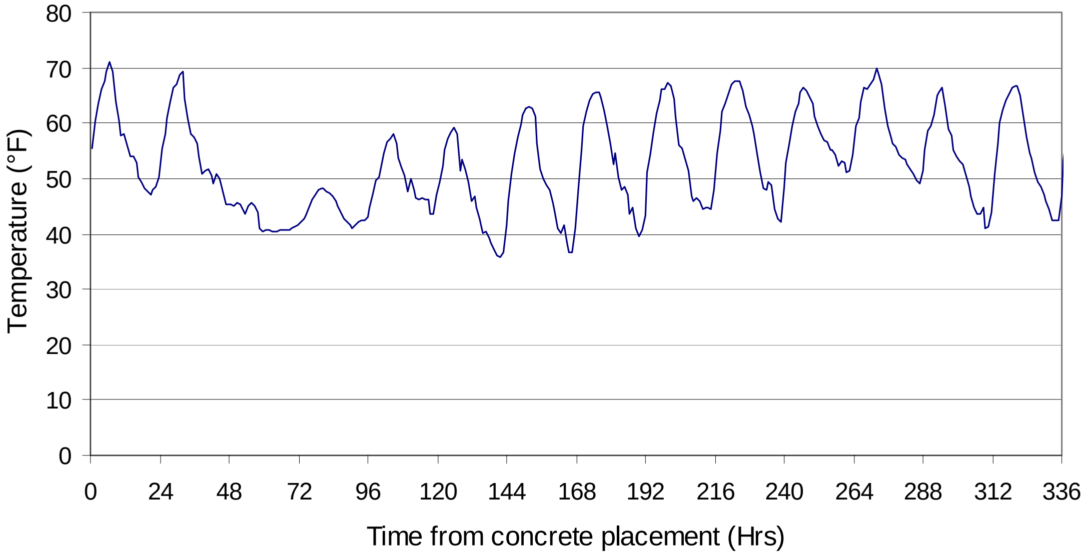

Figure A 7-4 - Ambient temperature data

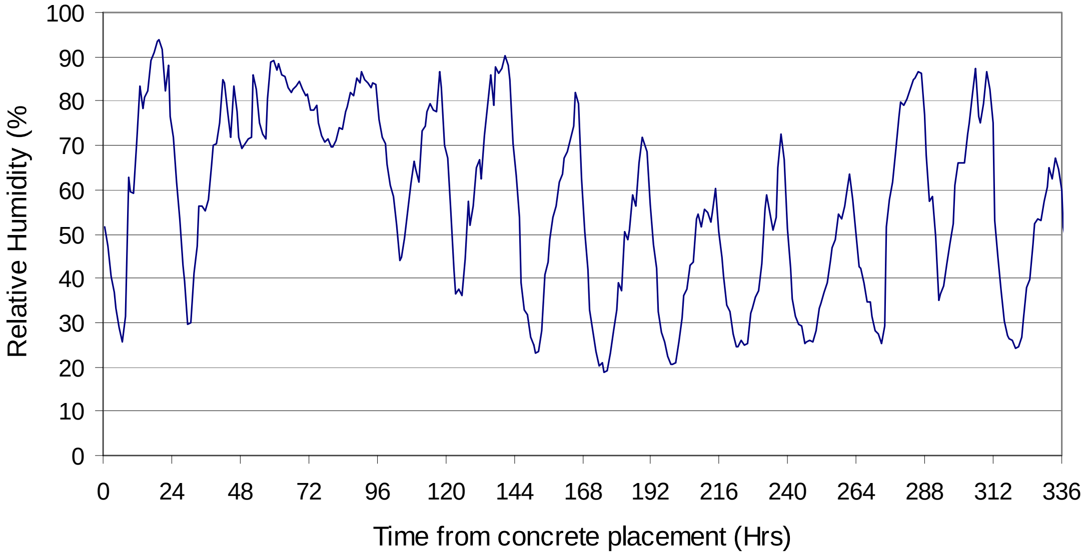

Figure A 7-5 - Relative humidity data

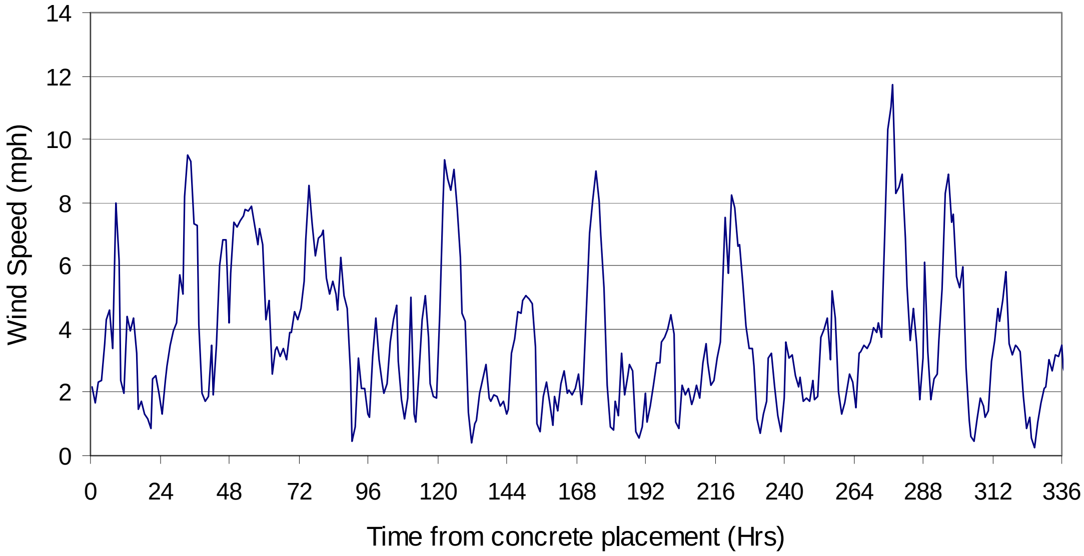

Figure A 7-6 - Wind speed data

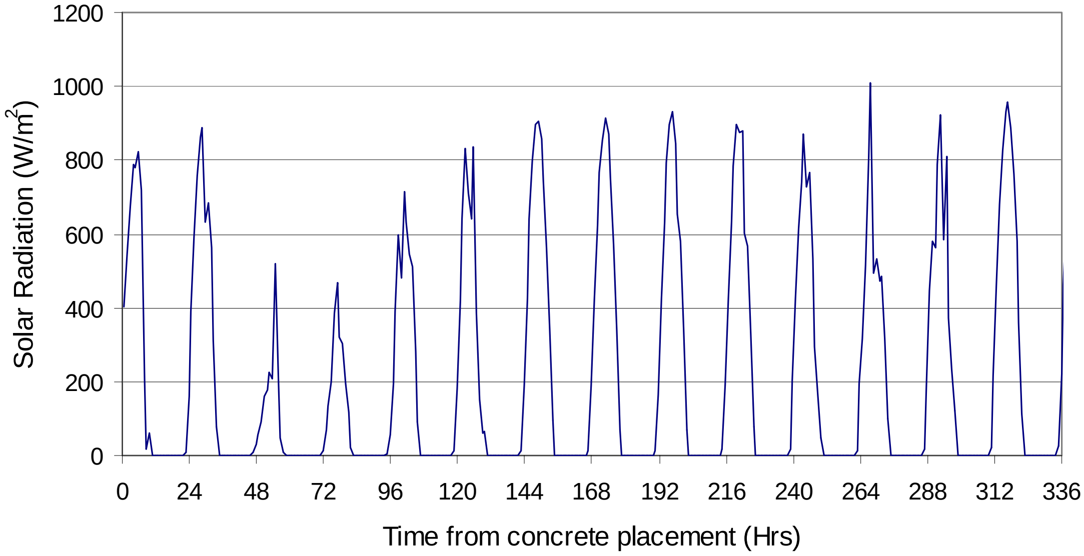

Figure A 7-7 - Solar radiation data

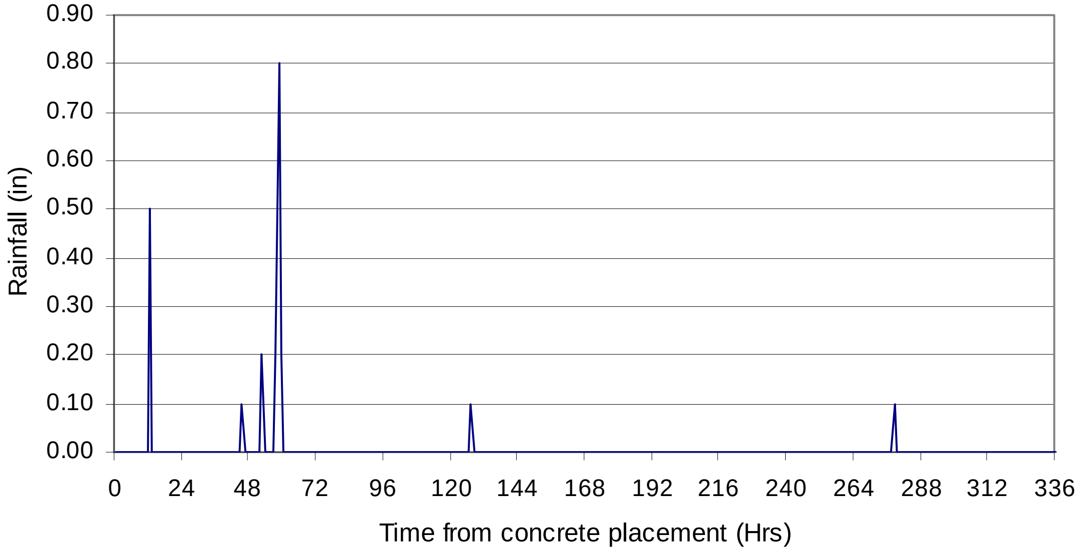

Figure A 7-8 - Rainfall data

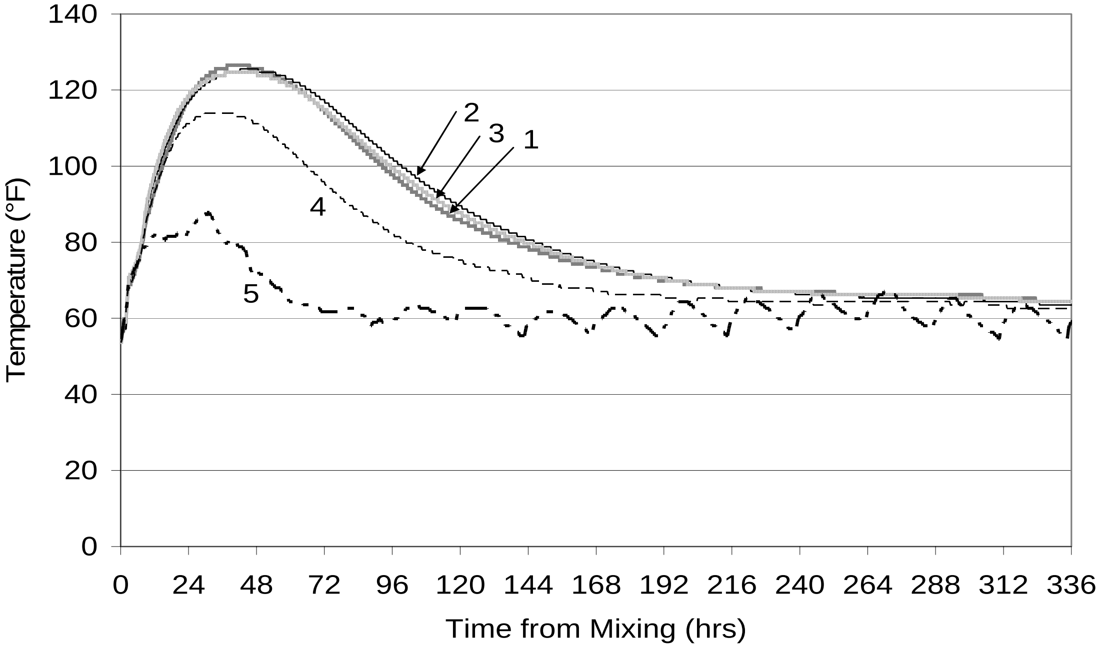

Figure A 7-9 – Measured temperature in temperature bar 1

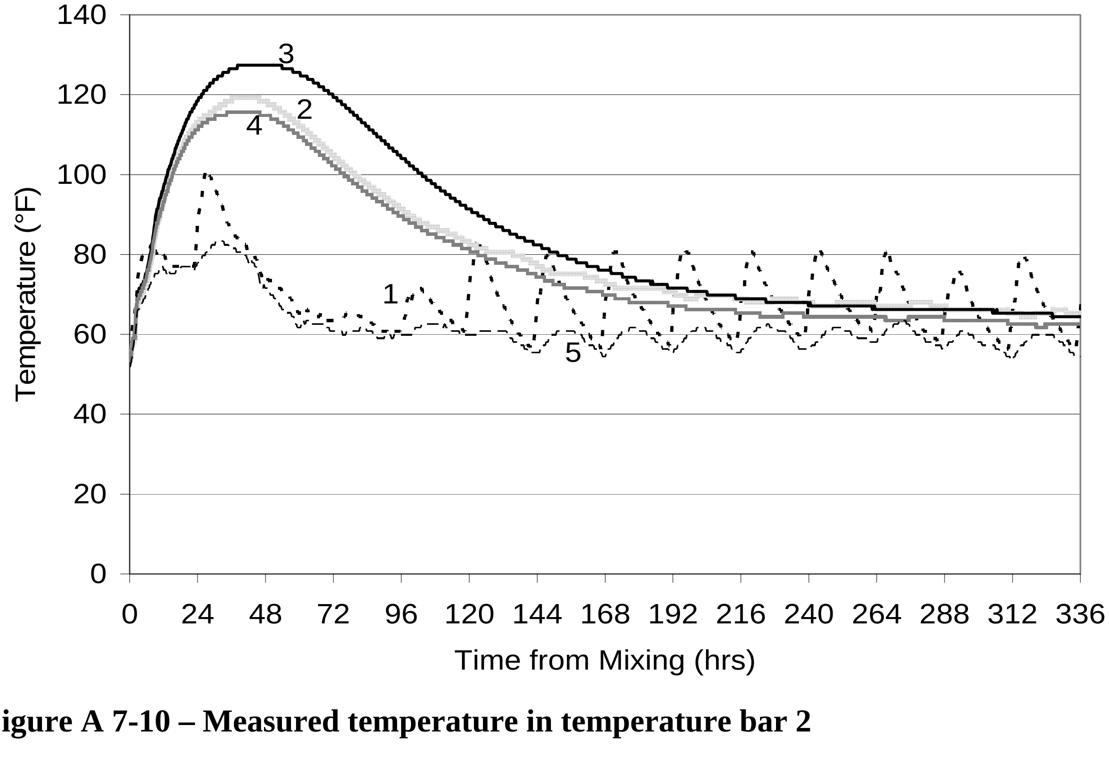

Figure A 7-10 – Measured temperature in temperature bar 2

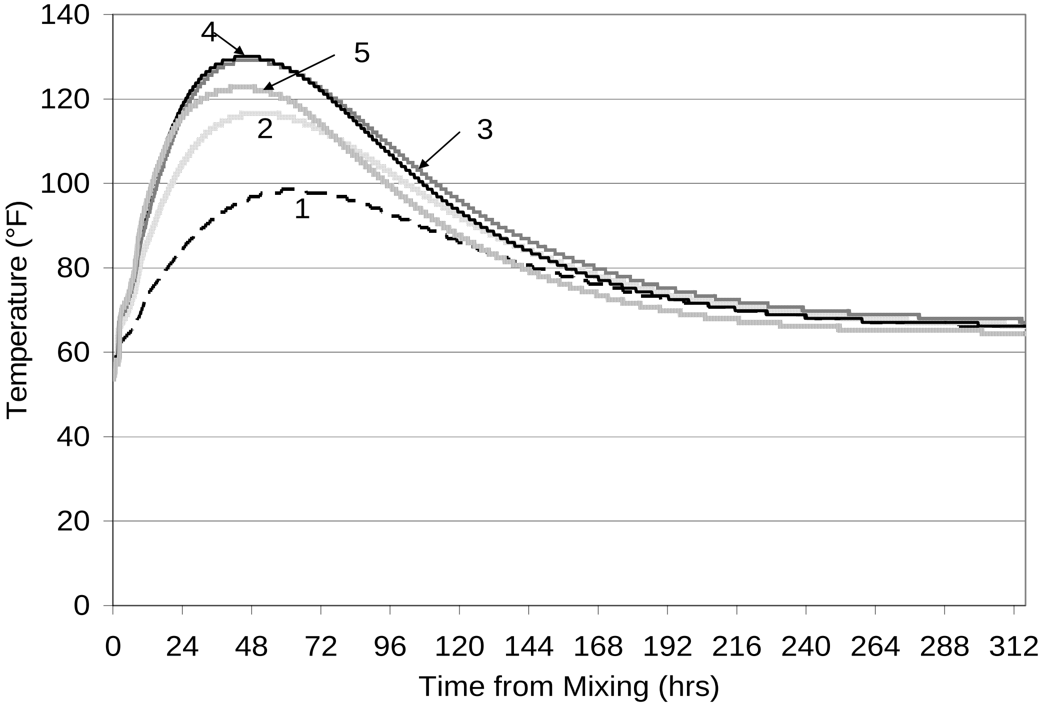

Figure A 7-11 – Measured temperature in temperature bar 3

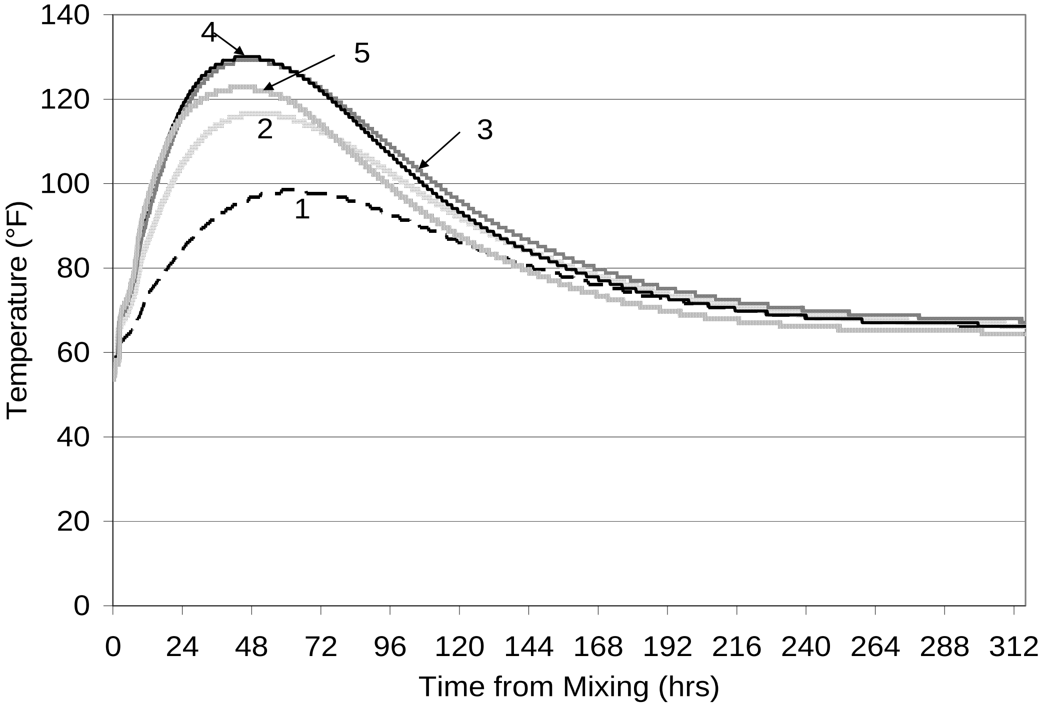

Figure A 7-12 - Measured temperature in temperature bar 4

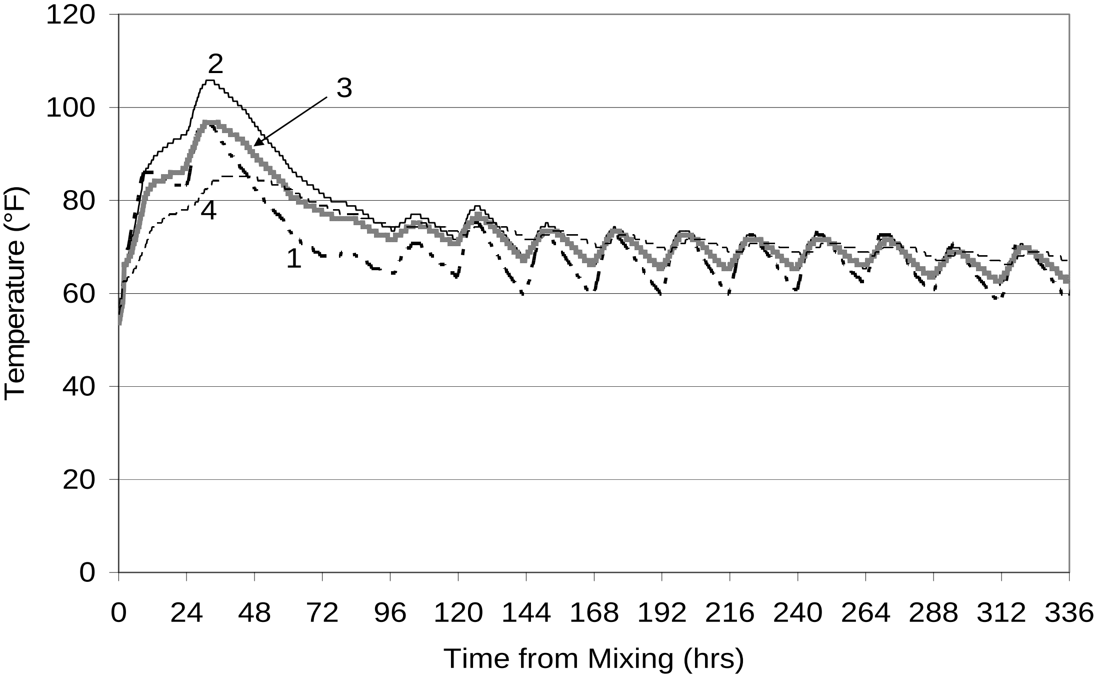

Figure A 7-13- Measured temperature in temperature bar 5

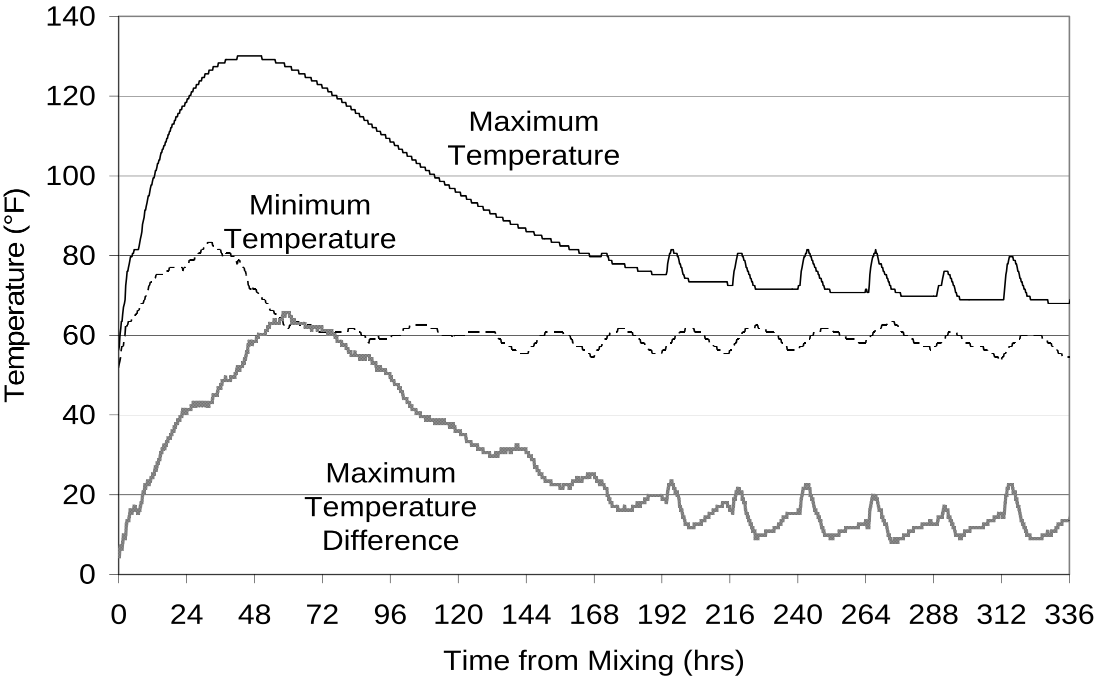

Figure A 7-14 – Maximum temperature, minimum temperature, and maximum temperature difference recorded in dolphin 10

APPENDIX A-8 I-35 AND BEN WHITE

A-8.1 Introduction

As part of TxDOT project 4563, a graphical user-friendly computer program is being developed to predict the in-place temperature development of concrete members during curing. Each construction project uses different combinations of formwork, architectural form liners, concrete raw materials and curing techniques for concrete. In addition, environmental conditions during concrete placement and curing differ for every placement. To assure accurate results for the model, data from as many of these variations as possible must be captured and used in the model calibration.

The I35 and TX-71/US-290 (Ben White Blvd.) interchange is being built to alleviate traffic congestion in south Austin. Construction on the five level stack began in February of 2000 (Ben White Bulletin, 2000). The mass footing instrumented on this project is located between the southbound I-35 access road and I-35. The column that will sit on top of the footing instrumented will be built as part of a future phase of construction.

A-8.2 Footing Construction

The footing's dimensions are 60' long by 20' wide by 10' deep. The footing is supported by three drilled shafts. The east end of the footing has a depth of 6', sloping downward to the maximum depth of 10' in the middle of the footing. To construct the side formwork and shoring, steel beams were driven into the ground on the sides of the excavated footing. Steel sheets were placed between beams. Steel beams were welded inside the formwork for bracing. Plastic was taped on the inside of the steel forms to allow for easy formwork removal. After concrete placement, a tarp canopy was placed above the footing to shade the footing. Figure A 8-1 shows footing before the concrete was placed. Figure A 8-2 shows the footing after concrete placement.

J.D. Abrams was the prime contractor and placed the concrete. J.D. Abrams also designed and supplied the concrete mixture. Table A 8-1 shows the concrete mixture design and fresh properties. Semi-adiabatic calorimetry was performed at the job-site. Results from the semi-adiabatic calorimetry are reported elsewhere (Poole 2007).

Concrete placement on the footing began at approximately 10:00 p.m. on April 14th, 2005. The tarp canopy was taken down on April 17th, 2005. Forms were removed sometime after the last temperature readings were taken. The in-place fresh concrete temperature was 69°F. Cure blankets were placed on top of the footing and were kept in place until after the last temperature readings were taken.

A-8.3 Instrumentation

Thermochron iButtons®[8] made by Dallas Semiconductor (Dallas Semiconductor, 2003) were used to measure and log the in-place temperature in the footing. Thermochron iButtons record the temperature in increments of 0.9°F and have an accuracy of ±1.8 °F (Dallas Semiconductor, 2003). The procedures for preparing the iButtons for installation were similar to those used in an earlier TxDOT study (Ramaiah, 2002). Wires were soldered onto the iButtons to allow external access to the iButton data. After the wires were attached, the iButtons were coated with epoxy to prevent water damage. To speed-up installation, series of iButtons were attaced to ½" diameter acrylic dowels with duct tape. These prefabricated "temperature bars" were placed in the footing in the morning of April 14th, 2005. Three temperature bars were placed in the footing. An additional iButton was taped onto the formwork, but experienced technical

---

[8] iButton® is a registered trademark of Dallas Semiconductor

problems during the instrumentation. Valid temperature readings were only obtained for the iButtons on the three temperature bars. Table A 8-2 and Table A 8-3 show the iButton locations in the footing. Figure A 8-3 shows temperature bar 3 after installation.

A-8.4 Weather Data

Weather data were acquired using a Campbell Scientific weather station. The weather station has instrumentation to record relative humidity, temperature, precipitation, wind speed, and wind direction. Figure A 8-4 to Figure A 8-6 show the temperature, relative humidity, wind speed. The time shown on the graphs is from the start of concrete placement for the footing. The weather station was located at Bldg 18B at the Pickle Research Campus at the University of Texas at Austin, about 10 miles north of the footing.

A-8.5 Concrete Temperature Data Acquired

The Thermochron iButtons were programmed to measure and log the temperature every 15 minutes. Figure A 8-7 to Figure A 8-9 show the data acquired from temperature bars 1-3. Figure A 8-10 shows the maximum temperature, minimum temperature and maximum temperature difference recorded in the footing. The maximum temperature and maximum temperature difference recorded in the footing were 149.9°F and 65.7°F respectively. The maximum temperature recorded in the footing was recorded by iButton 4 on temperature bar 2.

A visual inspection for cracking of the footing was made 7 days after concrete placement. Because the cure blankets were still in place, however, a thorough inspection for cracks was not possible. No visible surface cracks were found at the locations checked.

A-8.6 Summary

Temperature sensors were placed in the mass footing at the I35 and TX-71/US-290 (Ben White Blvd) interchange the morning of the concrete placement on April 14, 2005. They were installed to record the temperature development due to the heat of hydration of the concrete. The maximum temperature and maximum temperature difference recorded in the footing were 149.9°F and 65.7°F respectively. No visible signs of cracking were found. The temperature data collected will be used to calibrate the concrete temperature prediction model being developed as part of TxDOT project 4563.

A-8.7 Acknowledgements

The advice and assistance of the TxDOT Bridge Division is greatly appreciated. The authors wish to thank Ralph Browne, Keith Taylor, and Bill Braswell for arranging access to field sites.

Table A 8-1 - Concrete properties

Item	Content	Material Description
Cement	395 lb./yd.^{3}	TXI - Type I/II
Class F Fly Ash	145 lb./yd.^{3}	Jewett
Coarse Aggregate	1745 lb./ yd.^{3}	1" Limestone
Fine Aggregate	1199 lb./ yd.^{3}	Natural Sand
Air Entraining Admixture	0.4 oz/ cwt.	PaveAir
Retarder	0.3 oz/ cwt.	Masterpave RI
Water Reducer	4.4 oz/ cwt.	Masterpave
Jobsite Measured Air Content	4.25%	
Jobsite Measured Slump	4"	
Design w/cm	0.47	

Table A 8-2 - iButton locations for temperature bar 1

iButton #	Distance from South Side Formwork	Distance from East Side Formwork	Distance Vertically from Top of Footing
1	10' - 4"	28' - 0"	10' - 0"
2	10' - 4"	28' - 0"	7' - 6"
3	10' - 4"	28' - 0"	6' - 0"
4	10' - 4"	28' - 0"	4' - 0"
5	10' - 4"	28' - 0"	1' - 10"

Table A 8-3 - iButton locations for temperature bar 2

iButton #	Distance from South Side Formwork	Distance from West Side Formwork	Distance Vertically from Top of Footing
1	9' - 9"	8' - 6"	0' - 2"
2	9' - 9"	8' - 6"	1' - 8"
3	9' - 9"	8' - 6"	3' - 2"
4	9' - 9"	8' - 6"	5' - 2"
5	9' - 9"	8' - 6"	7' - 1"

Table A 8-4 - iButton locations for temperature bar 3

iButton #	Distance from North Side Formwork	Distance from East Side Formwork	Distance Vertically from Top of Footing
1	0' - 7"	28' - 0"	0' - 5"
2	0' - 7"	28' - 0"	2' - 5"
3	0' - 7"	28' - 0"	4' - 5"
4	0' - 7"	28' - 0"	6' - 5"

Figure A 8-1 - Footing before concrete placement

Figure A 8-2 - Footing after placement

Figure A 8-3 - Temperature bars 2 and 3 on dolphin 10 after installation

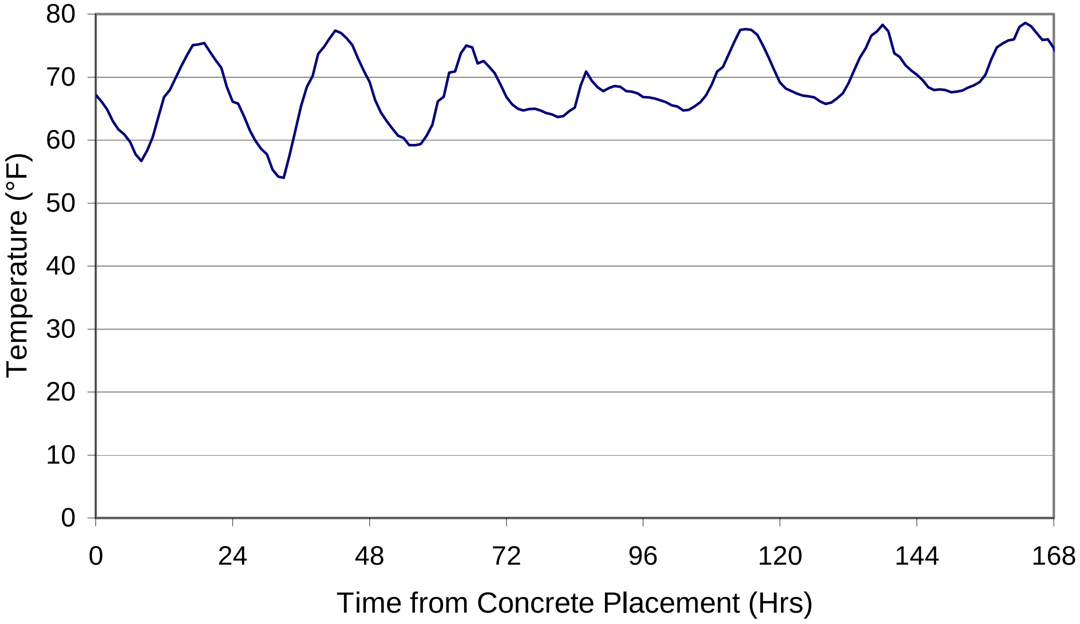

Figure A 8-4 - Ambient temperature data

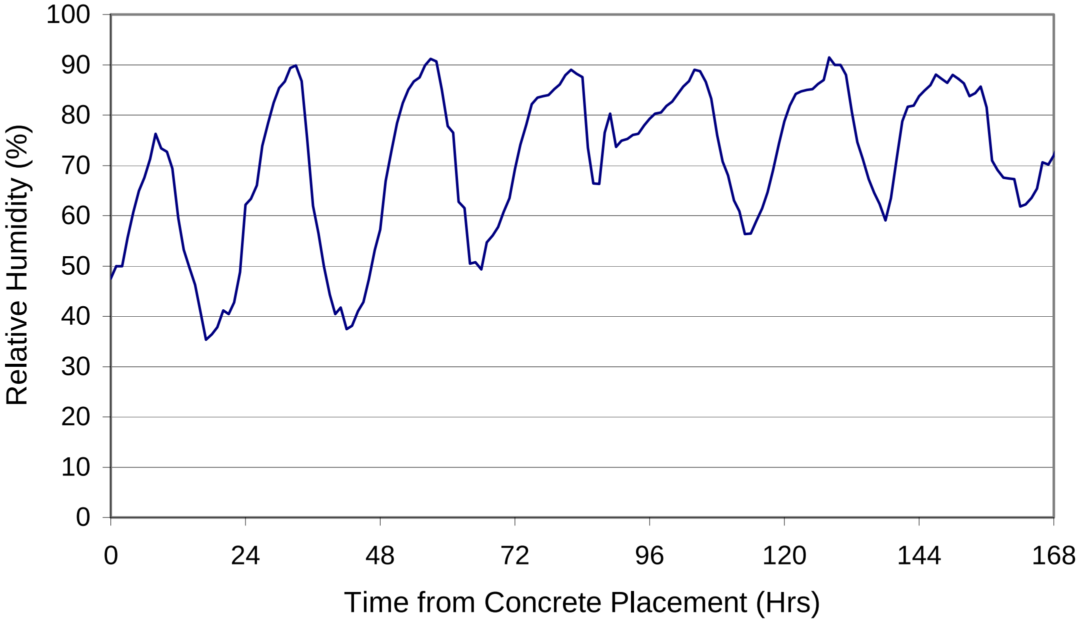

Figure A 8-5 - Relative humidity data

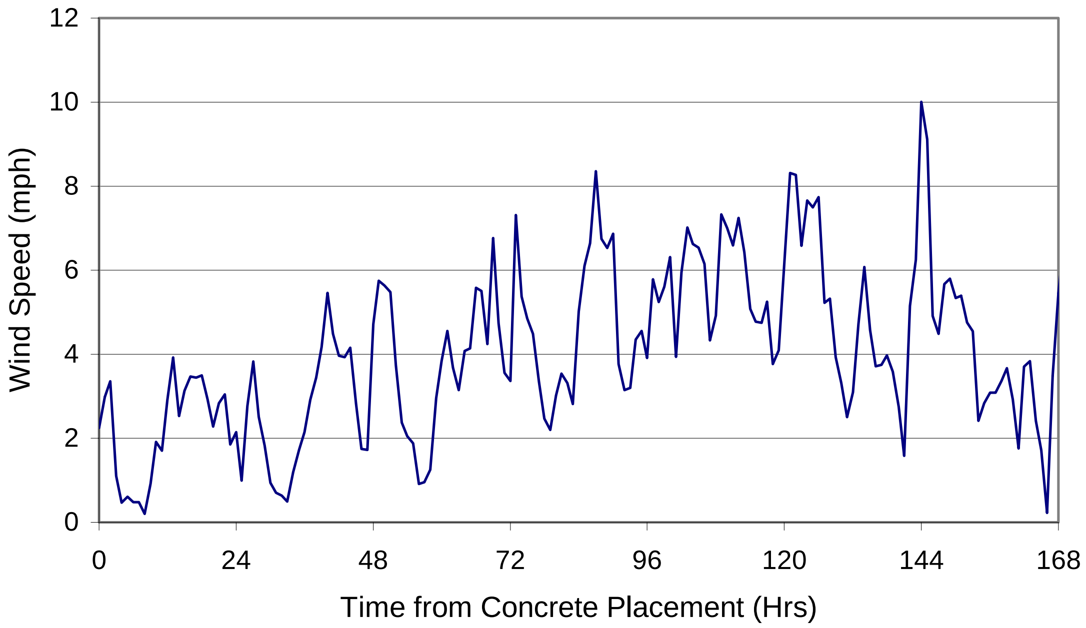

Figure A 8-6 - Wind speed data

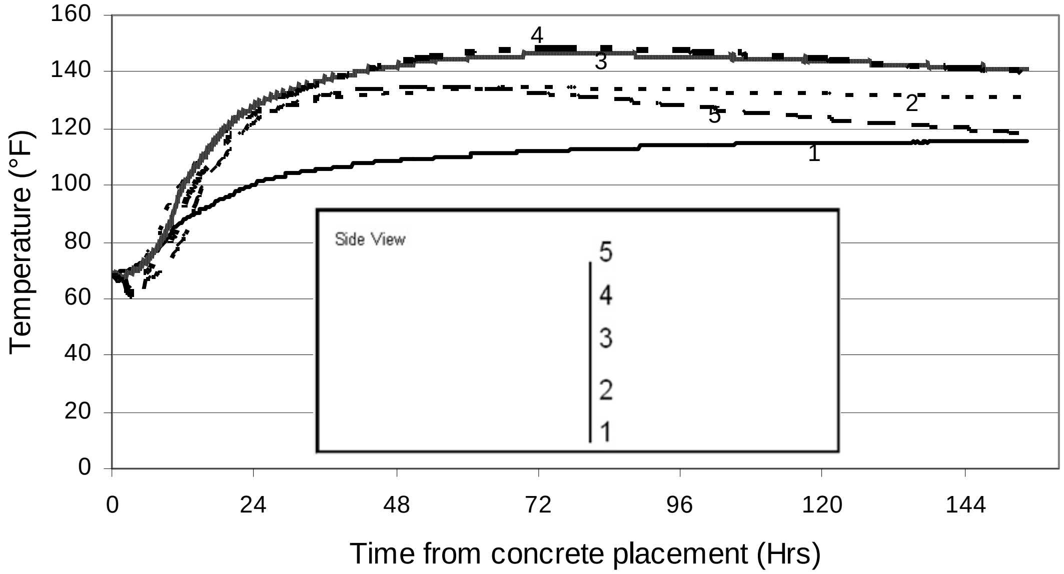

Figure A 8-7 - Temperature bar 1 data

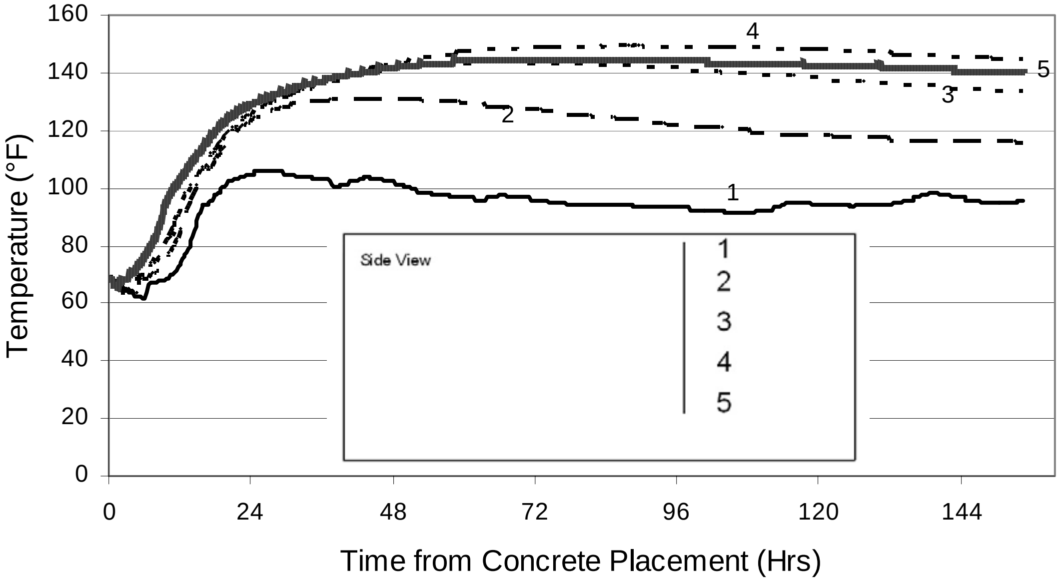

Figure A 8-8 - Temperature bar 2 data

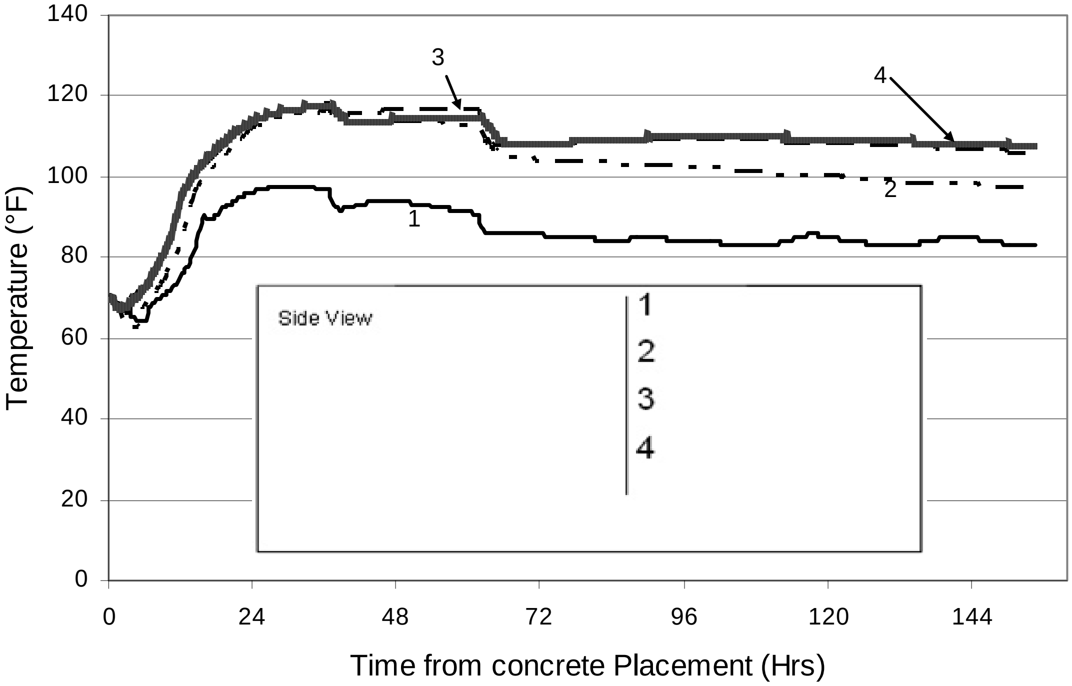

Figure A 8-9 - Temperature bar 3 data

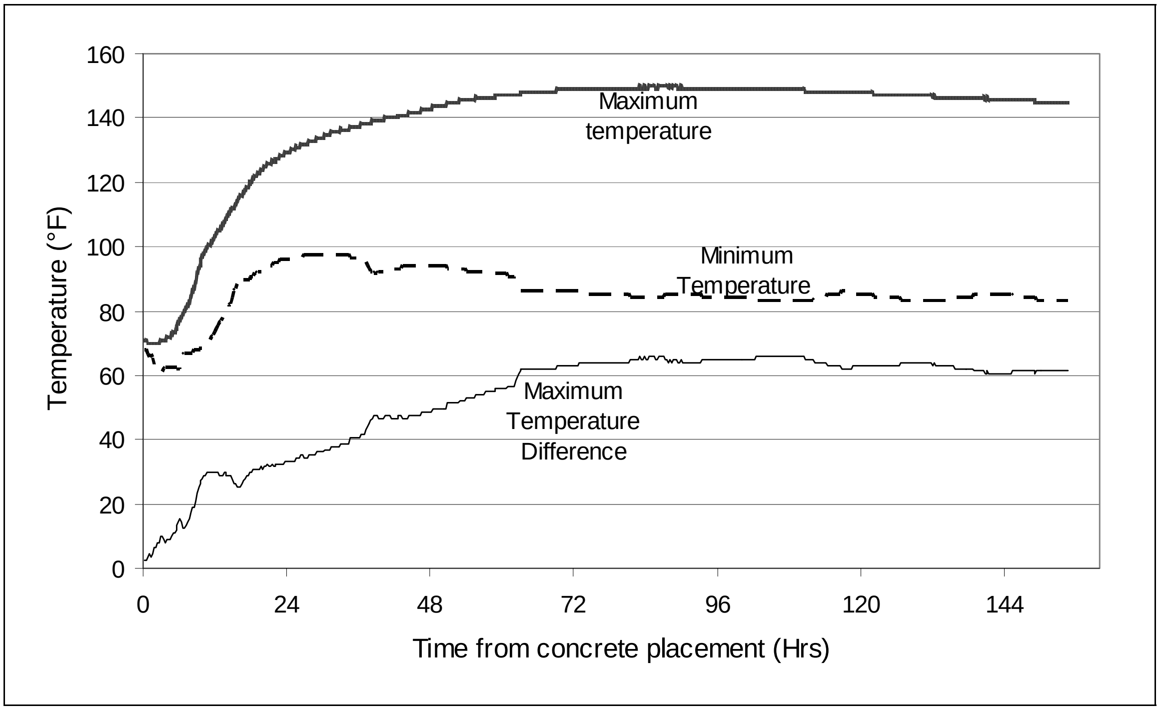

Figure A 8-10 – Maximum temperature, minimum temperature, and maximum temperature difference recorded in dolphin 10

APPENDIX A-9 FERGUSON BRIDGE DECK

A-9.1 Introduction

As part of TxDOT project 4563, a graphical user-friendly computer program is being developed to predict the in-place temperature development of concrete members during curing. A bridge deck temperature prediction module has been added to the program. The module includes options for modeling bridge decks made with precast concrete panels, permanent metal deck forms, and removable wood forms. In addition, the software allows the user to model different combinations of environmental conditions, concrete placement and curing conditions. To assure accurate results for the model, data from as many of these variations as possible must be captured and used in the model calibration.

A 120 foot long, single span bridge is being built behind the Ferguson Structural Engineering Laboratory at the University of Texas at Austin for researching the effects of fracture of a steel tub girder on the bridge. The bridge was instrumented with temperature sensors for use as part of the model calibration.

A-9.2 Footing Construction

The bridge deck dimensions are 120’ long by 23’ – 4” wide by 8” deep. The bridge deck is supported by two steel tub girders that were removed from a bridge in Houston, shipped to the Ferguson Structural Engineering Laboratory and repaired. Permanent metal deck forms were used above and between the girders, while ¾” plywood was used to form the overhangs. Figure A 9-1 shows bridge deck before the concrete was placed. Figure A 9-2 shows the bridge deck during concrete placement.

Jay-Reese Contractors, Inc. was the prime contractor and placed the concrete. Transit Mix Concrete and Materials Co. designed and supplied the concrete. Table A 9-1 shows the concrete mixture design and fresh properties. Semi-adiabatic calorimetry was performed at the job-site. Results from the semi-adiabatic calorimetry are reported elsewhere (Poole 2007).

Concrete placement on the footing began at approximately 7:00 a.m. on August 17th, 2006. Liquid nitrogen was used to comply with the fresh temperature specifications. The in-place fresh concrete temperature was 83°F. Cure blankets and black plastic were placed on top of the bridge deck and were kept in place for 10 days.

A-9.3 Instrumentation

Thermochron iButtons®9 made by Dallas Semiconductor (Dallas Semiconductor, 2003) were used to measure and log the dolphin in-place temperature. Thermochron iButtons record the temperature in increments of 0.9°F and have an accuracy of ±1.8 °F (Dallas Semiconductor, 2003). The procedures for preparing the iButtons for installation were similar to those used in an earlier TxDOT study (Ramaiah, 2002). Wires were soldered onto the iButtons to allow external access to the iButton data. After the wires were attached, the iButtons were coated with epoxy to prevent water damage. To speed-up installation, series of iButtons were attached to ½" diameter acrylic dowels with duct tape. These prefabricated "temperature bars" were placed in the bridge deck on July 21, 2006. Seven temperature bars were placed in the footing. Valid temperature readings were only obtained for the iButtons on temperature bars 2 – 7.

Table A 9-2 to Table A 9-6 show the location of the iButtons in the bridge deck. Figure A 9-3 shows temperature bar 2 after installation. Temperature bar 4 was above a

---

[9] iButton® is a registered trademark of Dallas Semiconductor

steel girder. Temperature bar 2 was above the overhang. iButtons 1 and 2 on temperature bar 3 were above the overhang, while iButtons 3-5 were above the steel girder. Temperature bars 5-7 were between the two steel girders.

A-9.4 Weather Data

Weather data were acquired using a Campbell Scientific weather station. The weather station has instrumentation to record relative humidity, temperature, precipitation, solar radiation, wind speed and wind direction. Figure A 9-4 to Figure A 9-7 show the temperature, relative humidity, wind speed, and solar radiation. The time shown on the graphs is from the start of concrete placement for bridge deck. The weather station was located a few hundred yards from the bridge deck at Bldg 18B at the Pickle Research Campus at the University of Texas at Austin.

A-9.5 Concrete Temperature Data Acquired

The Thermochron iButtons were programmed to measure and log the temperature every 15 minutes. Figure A 9-8 to Figure A 9-13 show the data acquired from temperature bars 2-7. The largest variation in temperature seen in each temperature bar occurred in temperature bar 3. This is because one of the iButtons was located against the side forms, iButton 2 was located on the overhang, and the other three iButtons were located above a steel tub girder. Figure A 9-14 shows iButton 3 on temperature bar 4, which is above a steel tub girder, and iButton 3 on temperature bar 6, which is located between the two steel tub girders. There was a small difference between the two temperatures recorded because of the different heat transfer conditions directly underneath the bridge deck. Part of the difference in temperature between days 5-11 may be attributed to a large stack of materials placed directly over temperature bar 6, as shown in Figure A 9-15.

A-9.6 Summary

Temperature sensors were placed in the bridge deck at the Ferguson Structural Engineering Laboratory for the concrete placement on August 17th, 2006. They were installed to record the temperature development due to the heat of hydration of the concrete and the environment. The temperature data collected will be used to calibrate the concrete bridge deck temperature prediction model being developed as part of TxDot project 4563.

A-9.7 Acknowledgements

The advice and assistance of the TxDOT Bridge Division is greatly appreciated. The authors wish to thank Dr. Karl Frank, Timothy Barnard, and Catherine Hovell for arranging access to the field site.

Table A 9-1 - Concrete properties

Item	Content	Material Description
Cement	439 lb./yd.^{3}	TXI - Type I/II
Class F Fly Ash	149 lb./yd.^{3}	Limestone Plant - Jewett, TX
Coarse Aggregate	1900 lb./ yd.^{3}	1" Dolomitic Limestone
Fine Aggregate	1286 lb./ yd.^{3}	Natural Sand
Air Entraining Admixture	0.3 oz/ cwt.	AE 90
Water Reducer / Retarder	2.9 oz/ cwt.	Pozzolith 80
Jobsite Measured Air Content	2.6%	
Jobsite Measured Slump	3"	
Design w/cm	0.45	

Table A 9-2 - iButton locations for temperature bar 2

iButton #	Distance from South Side	Distance from East Side	Distance Vertically from Form
1	9’ - 3"	0' - 11"	0' – 7.5"
2	9’ - 3"	0' - 11"	0' – 3.5"
3	9’ - 3"	0' - 11"	0’ – 0”

Table A 9-3 - iButton locations for temperature bar 3

iButton #	Distance from South Side	Distance from East Side	Distance Vertically from Form
1	13’ – 8”	0’ – 0”	0' - 4"
2	13’ – 8”	1’ – 0”	0' - 4"
3	13’ – 8”	2’ – 0”	0' - 4"
4	13’ – 8”	3’ – 0”	0' - 4"
5	13’ – 8”	4’ – 0”	0' - 4"

Table A 9-4 - iButton locations for temperature bar 4

iButton #	Distance from South Side	Distance from West Side	Distance Vertically from Form
1	9’ - 3"	15’ – 1”	0' - 4"
2	9’ - 3"	16’ – 1”	0' - 4"
3	9’ - 3"	17’ – 1”	0' - 4"
4	9’ - 3"	18’ – 1”	0' - 4"
5	9’ - 3"	19’ – 1”	0' - 4"

Table A 9-5 - iButton locations for temperature bar 5

iButton #	Distance from South Side	Distance from East Side	Distance Vertically from Form
1	29’ - 8"	11’ – 4”	0' - 0"
2	29’ - 8"	11’ – 4”	0' - 3"
3	29’ - 8"	11’ – 4”	0' - 7"

Table A 9-6 - iButton locations for temperature bar 6

iButton #	Distance from South Side	Distance from West Side	Distance Vertically from Form
1	9’ - 3"	9’ – 6”	0' - 4"
2	9’ - 3"	10’ – 6”	0' - 4"
3	9’ - 3"	11’ – 6”	0' - 4"
4	9’ - 3"	12’ – 6”	0' - 4"
5	9’ - 3"	13’ – 6”	0' - 4"
6	9’ - 3"	14’ – 6”	0' - 4"

Table A 9-7 - iButton locations for temperature bar 7

iButton #	Distance from South Side	Distance from East Side	Distance Vertically from Form
1	27’ - 10"	10’ – 11”	0' - 0"
2	27’ - 10"	10’ – 11”	0' – 3.5"
3	27’ - 10"	10’ – 11”	0' - 7"

Figure A 9-1 – Bridge deck before concrete placement

Figure A 9-2 - Footing after placement

Figure A 9-3 - Temperature bar 2 on the bridge deck after installation

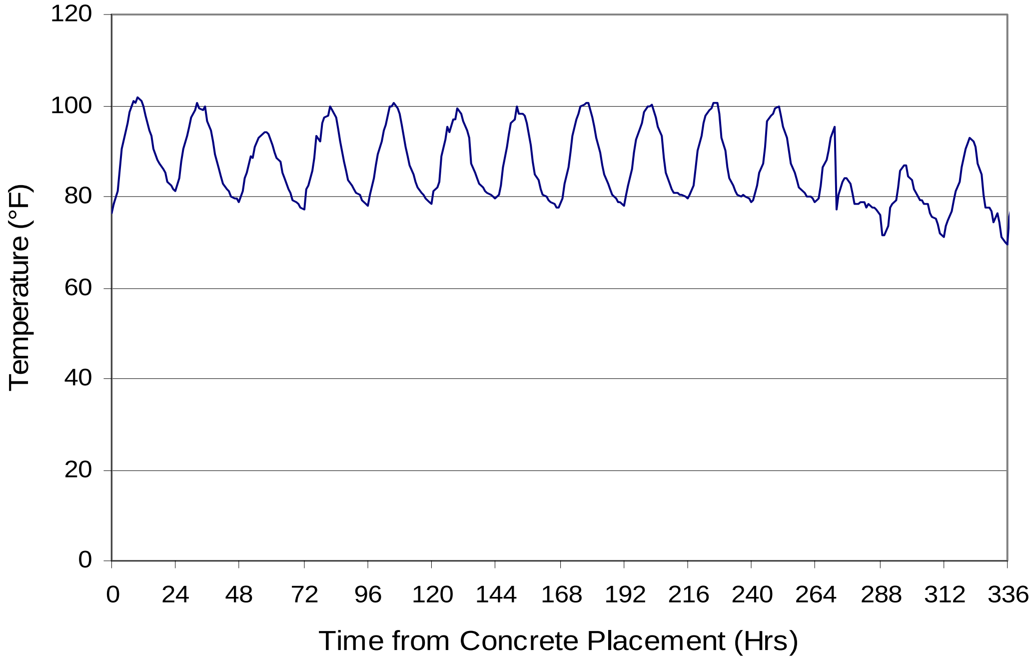

Figure A 9-4 - Ambient temperature data

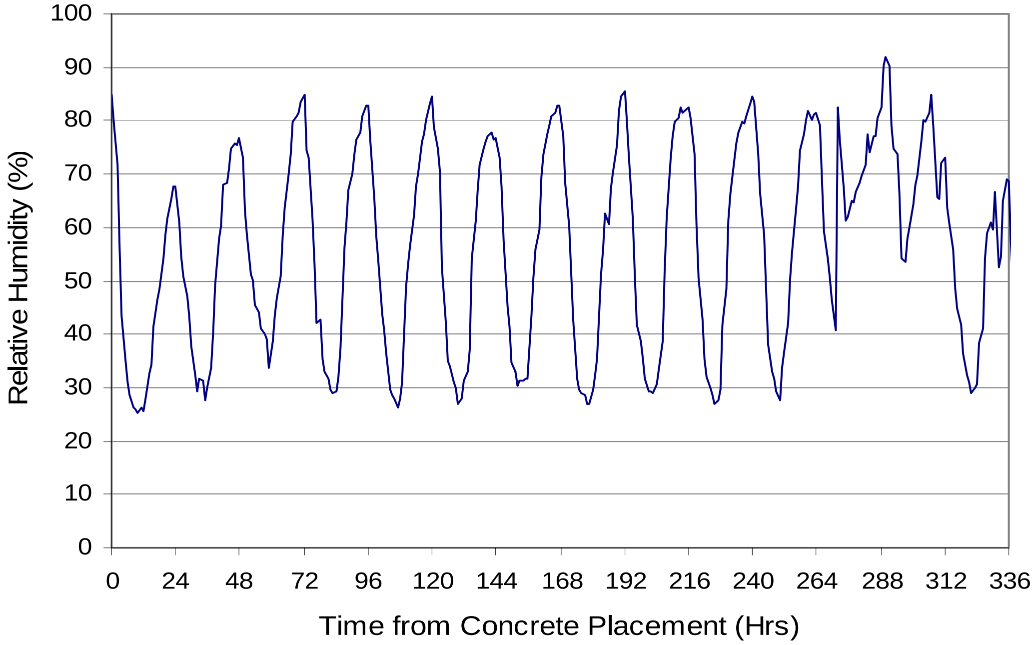

Figure A 9-5 - Relative humidity data

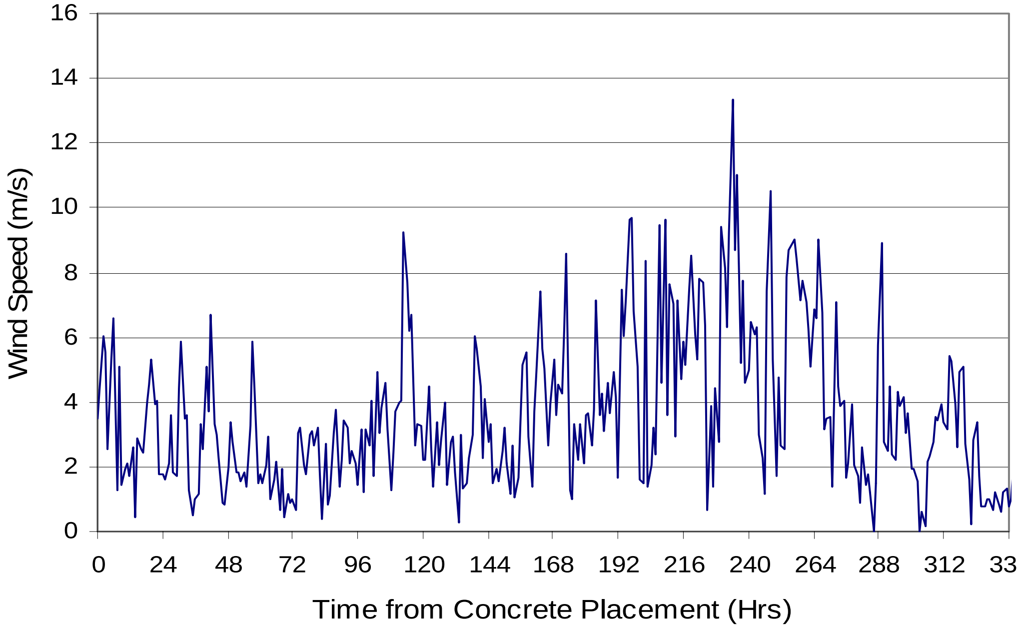

Figure A 9-6 - Wind speed data

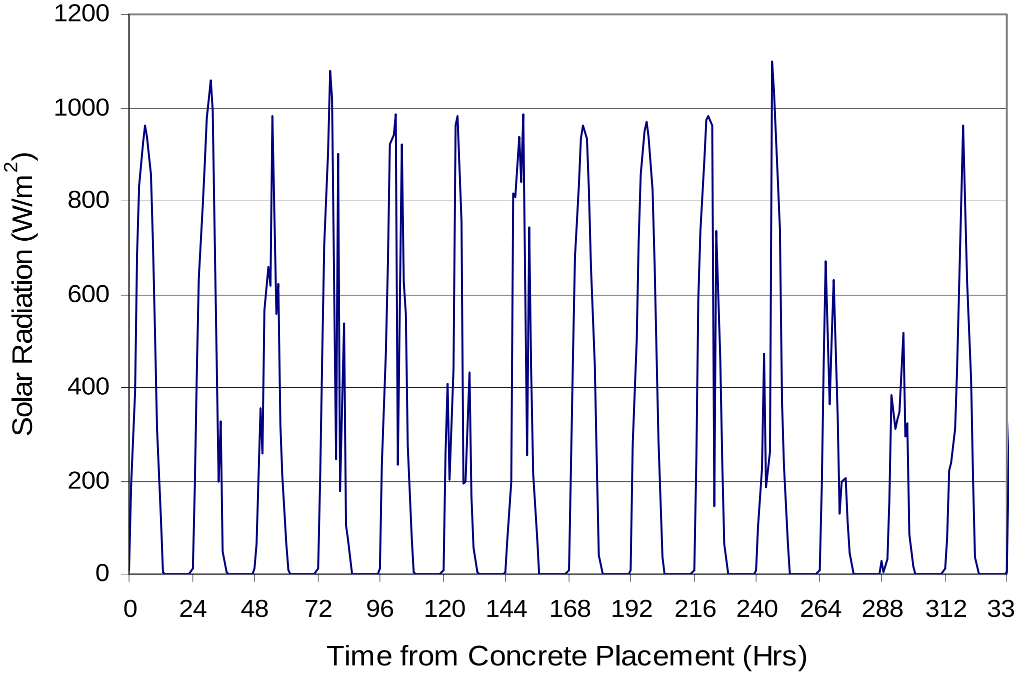

Figure A 9-7 – Solar radiation data

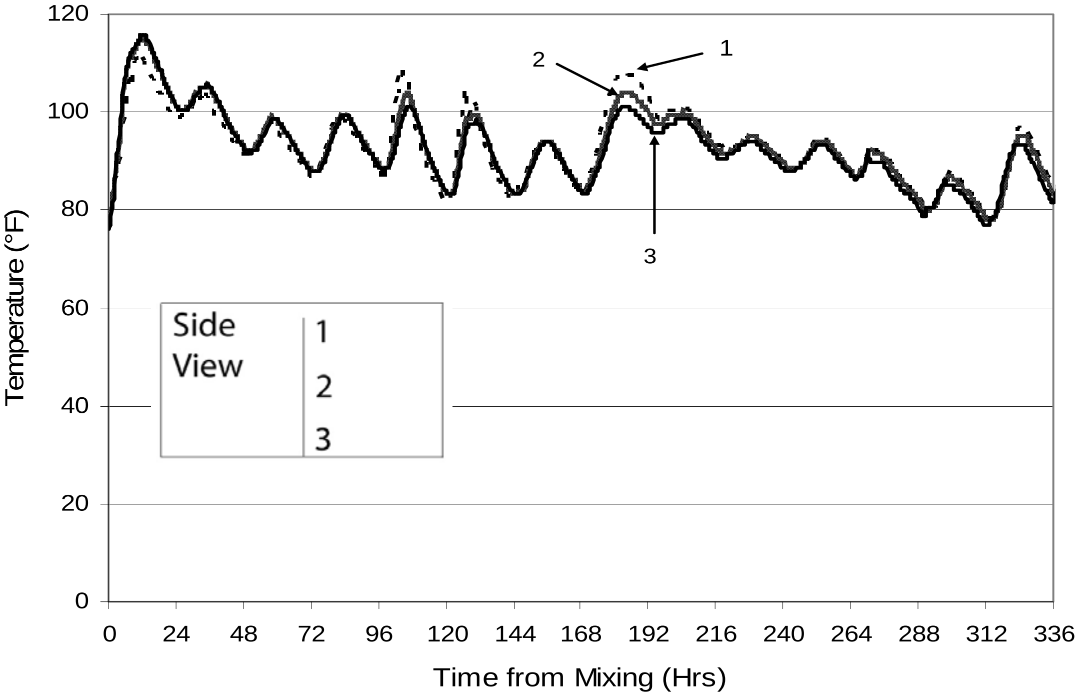

Figure A 9-8 - Temperature bar 2 data

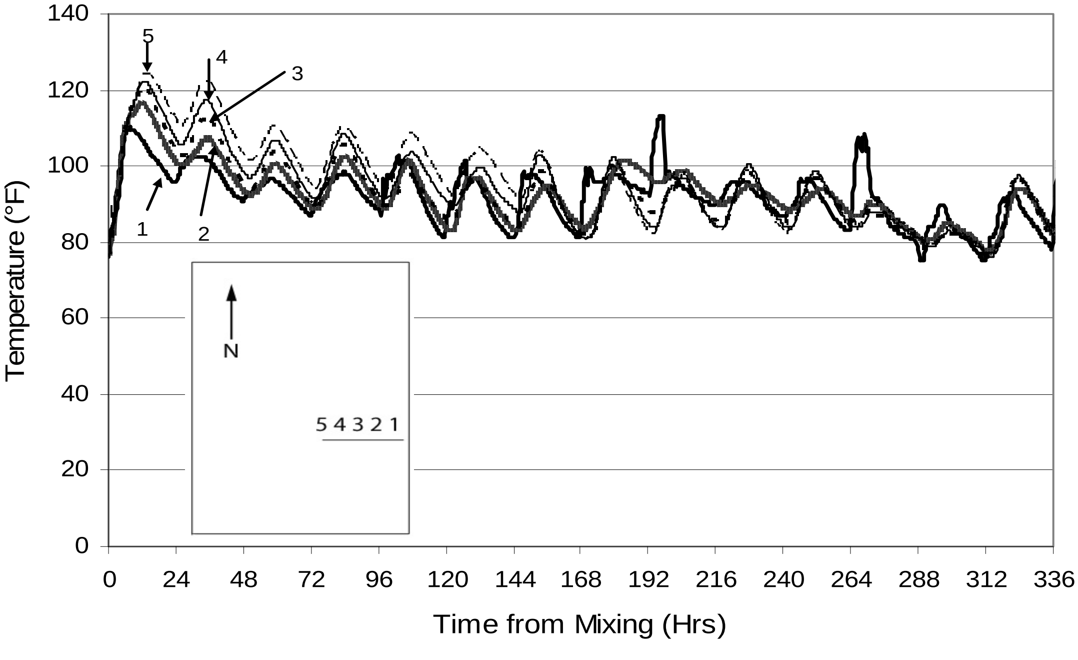

Figure A 9-9 - Temperature bar 3 data

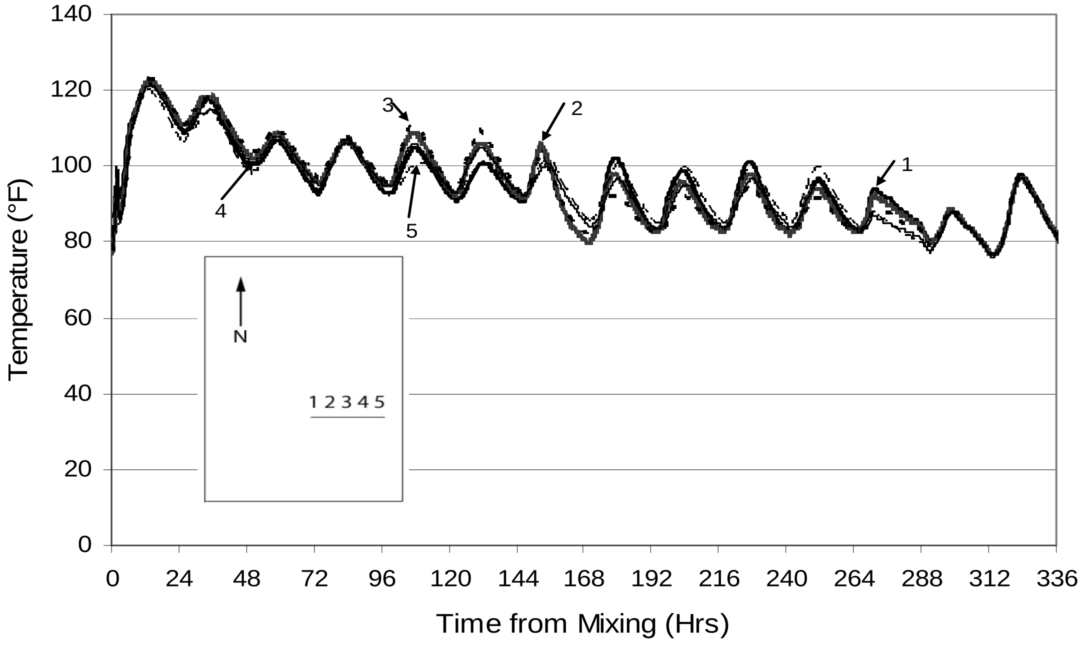

Figure A 9-10 - Temperature bar 4 data

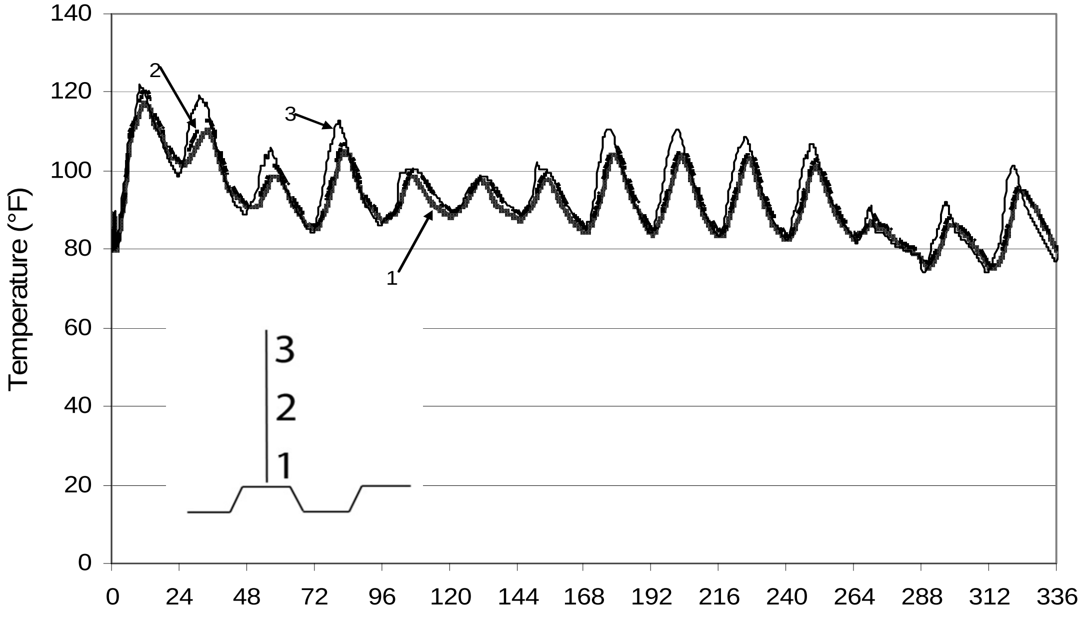

Figure A 9-11 – Temperature bar 5 data

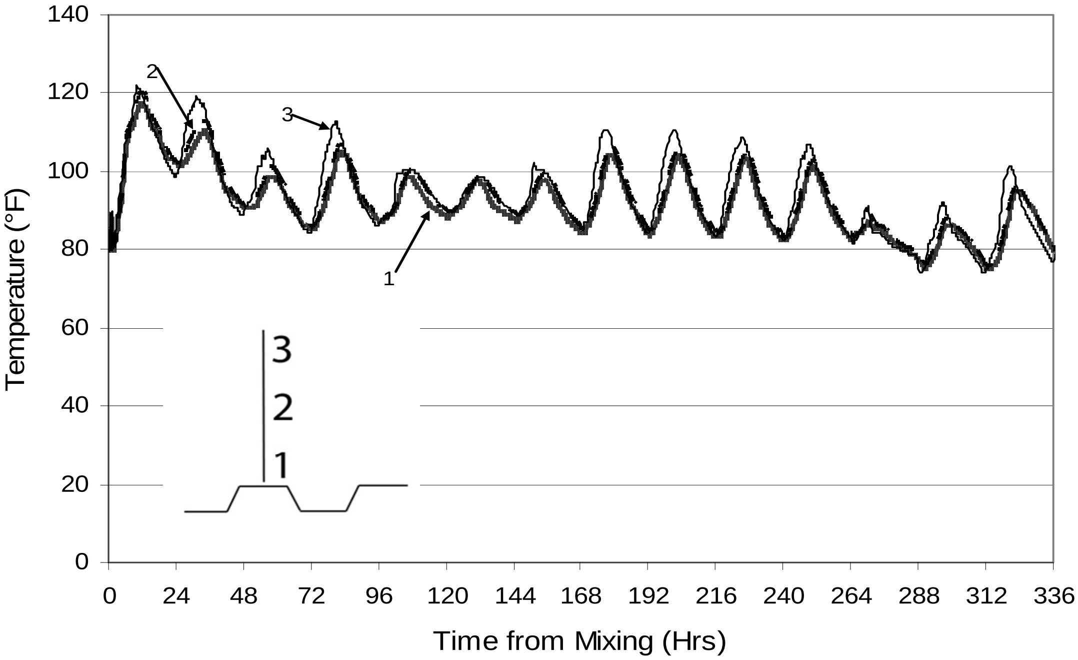

Figure A 9-12 – Temperature bar 6 data

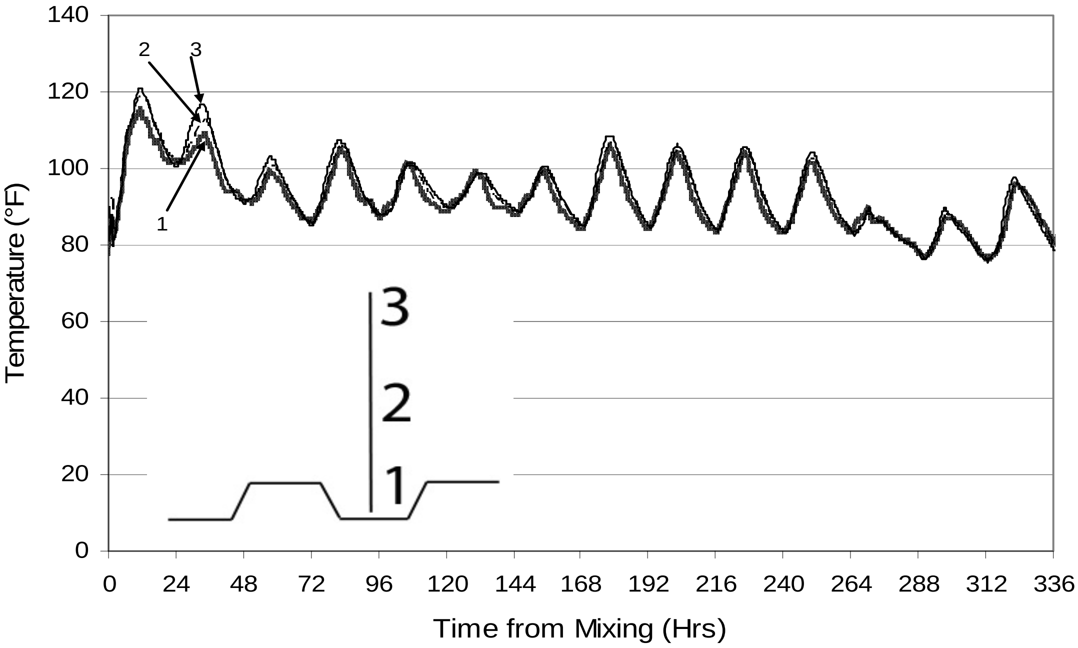

Figure A 9-13 – Temperature bar 7 data

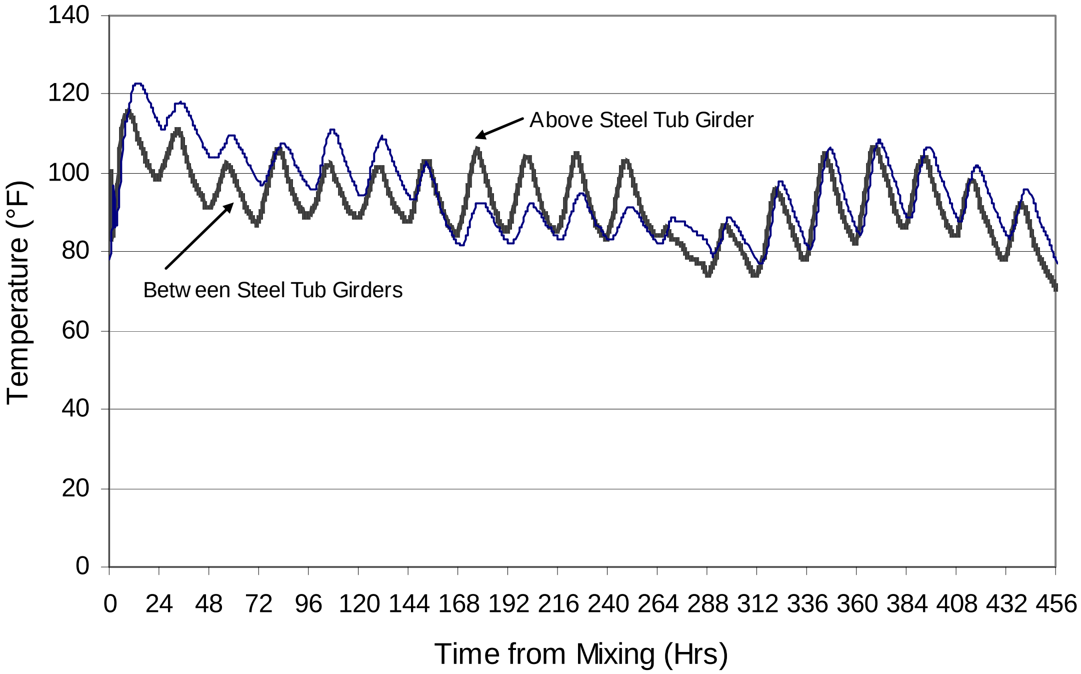

Figure A 9-14 – Temperatures recorded in iButton 3 of temperature bar 6 (between the steel tub girders) and iButton 3 of temperature bar 4 (above the steel tub girder)

Figure A 9-15 - Large stack of building materials placed over the location of temperature bar 6

APPENDIX B

How to Use iButtons in Concrete

APPENDIX B-1 HOW TO USE IBUTTONS IN CONCRETE

B-1.1 Introduction

Many jobs in Texas now require contractors to measure temperature gradients in mass concrete elements. Contractors need a cheap and reliable method of collecting these temperature data. They also need to employ a device that will not interfere with construction practices.

The iButton®[1] (Dallas Semiconductor Corp.) is a convenient and rather inexpensive temperature-recording device that has mainly been used in the food industry. It has an internal data logger, which eliminates the need for external data logging devices that can be inconvenient and unreliable at job sites. It can easily be programmed for users' individual needs. The iButton can be used to take and record temperature data inside concrete elements. With some adaptation, the data can be accessed externally so that the iButton does not have to be removed.

Previous projects have explored ibutton use in pavements. Work done on TxDOT project 1700 showed that iButtons can give accurate, reliable results in pavements. For project 1700, control slab tests were done comparing embedded iButton readings to embedded thermocouple readings. The iButton readings correlated very well to the thermocouple readings (Ramaiah, 2002). The Transtec Group also successfully used iButtons on the airfield at the Des Moines International Airport (Dallas Semiconductor, 2002). A similar method of preparing iButtons can be used to instrument mass concrete elements.

---

[1] iButton® is a registered trademark of Dallas Semiconductor.

This report shows how to prepare the iButtons for installation in a mass concrete element. The iButtons need to be modified in two ways for use as temperature recording devices in mass concrete elements. The first modification entails attaching wires so that data can be accessed externally. The second modification involves protecting the iButtons from moisture and impacts. The report also contains a form to be filled out by contractors with information about any temperature data submitted for use by the 4563 project team.

B-1.2 Items needed for wire attachment

Figure 1 shows a picture of the items needed to solder wires onto an iButton. The names of the numbered items in Figure B 1-1 are shown in Table 1. It is through these wires that you can send and receive signals from a laptop computer to the iButton.

B-1.3 Attaching the iButton

There are three steps in attaching wires onto iButtons: preparing the iButton surface, preparing the wires and attaching the wires onto the iButton.

B-1.3.1 PREPARING THE IBUTTON® SURFACE

Solder tends to not bond well with the smooth stainless steel finish of iButtons. In order for the solder to form a bond to the iButton, you must roughen the iButton® surface with a knife. Scratch both sides of the iButton® surface with the utility knife as shown in Figure B 1-2.

The iButton® also has dirt and other surface films that prevent the solder from bonding. The Tip Tinner and Cleaner will help remove the dirt. Use the electronics screwdriver to scratch off some of the Tip Tinner and Cleaner as seen in Figure B 1-3, leaving a powder. Tilt the container to collect some of the powder. Use the end of the screwdriver to scoop out some of the powder onto the surface of the iButton. Figure B 1-4 shows some of the Tip Tinner and Cleaner on top of the iButton.

After putting powdered Tip Tinner and Cleaner on the iButton surface, make sure that the surface of the soldering iron is hot and has been tinned. Next, touch the tip of the hot soldering iron onto the part of the iButton surface covered with powder. Rub the tip of the soldering iron on the iButton surface until some of the solder on the soldering iron bonds to the iButton. Caution: do not leave the soldering iron on the surface of the iButton for extended periods of time; excessive heat can damage the iButton. Repeat the process for the both sides of the iButton.

B-1.3.2 PREPARING THE WIRES

First, strip away the end of the wire jacket and insulation as seen in Figure B 1-5. On both wires, expose approximately a quarter of an inch. Next, put a small amount of Rosin Soldering Flux on each wire end. The Rosin Soldering Flux may be placed on the wire by dipping the tip of the wire in the Rosin Soldering Flux tube, as shown in Figure B 1-6. After coating the wire tips, touch the end of the wire to the hot, tinned soldering iron. This will coat the end of the wire with solder.

B-1.3.3 ATTACHING THE WIRES ONTO THE IBUTTON

Now the iButton is ready for wire attachment. Choose which wire will be attached onto which side of the iButton. It does not matter which side, as long as it is consistent with the sides chosen on the other iButtons attached in the same series.

First, touch the prepared wire onto the prepared surface of the iButton as shown in Figure B 1-7. Touch the Rosin Core Solder onto the hot soldering iron long enough to build up excess solder on the soldering iron. Now, hold the wire on the iButton and place the soldering iron on top of the wire. Keep the soldering iron on the wire long enough to melt all of the solder on the iButton and wire as shown in Figure B 1-8. Press the wire down in the solder until the wire is covered in solder. Once again, do not hold the soldering iron to the iButton for an excessive amount of time. Take the soldering iron away from the connection, and allow the solder to cool until it hardens.

After one wire has been soldered, solder the other wire onto the reverse side of the iButton in the same manner. Caution: when soldering the wire onto the side of the iButton with the black gasket, make sure that no part of that bare wire touches any part of the outside of the black gasket. This will cause your wires to short. After soldering on both wires, the iButton® should look like the one shown in Figure B 1-9.

B-1.4 Protecting the iButton

Two methods of protecting the iButton from impact and water damage have been used. Each method has its own unique advantages and disadvantages. The two methods are dipping the iButton in a two-part epoxy and potting the iButton in a two-part epoxy.

B-1.4.1 EPOXY DIP

The first method of protecting iButtons is to dip them in a two-part epoxy. The first step is to mix the epoxy parts together according to the manufacturer’s instructions. Caution: protective gloves should be worn when handling the uncured epoxy. Next, dip or brush epoxy onto the iButton, completely covering the iButton and the exposed part of the wires. After the iButton is covered in epoxy, the iButton must be hung to cure. Care must be taken to insure that no part of the coated iButton touches anything else; the epoxy will bond to whatever it touches. After the epoxy cures according to the manufacturer’s instructions, the iButton may be programmed and put into service.

B-1.4.2 EPOXY POTTING

IButtons can be potted in epoxy instead of merely using a coating. To pot the iButton, the first step is to mix the epoxy as stated above. The next step is to fill a small cup or mold with the epoxy, as seen in Figure B 1-10. Next, place the iButton in the epoxy as seen in Figure B 1-11. Finally, make sure that the iButton and any bare wire are completely covered by epoxy, as seen in Figure B 1-12. Leave the iButton in the epoxy until the epoxy has cured (refer to the manufacturer's instructions).

The advantages of the potting method are greater iButton protection, ease of use, and durability. The disadvantages of the potting method are the size (the potted iButton could be too big for use in thin elements like pavements, where great control over placement is needed).

B-1.5 Retrieving Data

To download iButton data onto a laptop computer, a Universal 1-Wire COM Port Adapter sold by Dallas Semiconductor Corp. (Dallas Semiconductor, 2003) is needed. The port adapter has a telephone wire plug on one end. A modified telephone cable should be plugged into the Port Adapter. The other end of the Port Adapter plugs into the laptop.

B-1.5.1 MODIFIED TELEPHONE WIRE

To make the modified telephone cable, first cut off one of the ends. Next, strip off about one inch of the end of the insulating jacket. Next, strip off about three-quarters of an inch of insulation from two of the wires in the telephone cable. Twist one of the stripped wires together with the bare wire of one of the alligator clips. Repeat for the other stripped wire. Each connection can be soldered, or just wrapped in electrical tape.

Figure B 1-13 shows a picture of the modified telephone wire plugged into the Port Adapter.

B-1.6 Contractor Mass Concrete Temperature Instrumentation Form

When any mass concrete temperature data are sent to the University of Texas Concrete Durability Center, a completed Mass Concrete Temperature Instrumentation Form must accompany the data. The following form contains a copy of the Mass Concrete Temperature Instrumentation Form.

Mass Concrete Temperature Instrumentation Form

Send this form with temperature data on disk to:
Kyle Riding • 10100 Burnett Rd. Bldg 18B • Austin TX, 78758-4497 • (512) 471-4555 (fax)

General Information

Type of Concrete Member
(Check only one)

☐ Rectangular Column
☐ Rectangular Footing
☐ Partly Submerged Rect. Footing
☐ Rectangular Bent Cap
☐ T-Shaped Bent Cap
☐ Circular Column

☐ Concrete Member is submerged
☐ If Footing, Embankment was used as Form

Brand and type of Formwork Used: __________
Date of Concrete Placement: ______________
If Footing, type of subbase (type of soil or rock) __________

Please attach a drawing of the member with dimensions (including measured dimensions of where temperature instrumentation was placed. A photocopy of the member plans with a north arrow and hand drawn locations and dimensions of temperature instrumentation are sufficient.)

Concrete Mix Design

Cement Content: _________ lb/yd^3
Fly Ash Content: _________ lb/yd^3
Slag Content: ___________ lb/yd^3
Additional SCM: _________ lb/yd^3
Coarse Agg. Content: _____ lb/yd^3
Fine Agg. Content: _______ lb/yd^3
Air Content: _____________ %

Type and Brand of Cement: ________
Fly Ash Source: _________________
Slag Supplier and Grade: __________
Type and Brand of SCM: __________
Type of Coarse Agg.: _____________
Type of Fine Agg.: _______________

List all Chemical Admixtures used and the dosages used: _____________________
____

____
Water to Binder Ratio: _____________

Construction Techniques

☐ Cure Blanket Used
☐ Plastic Cover Used on Element

Plastic Wrap Color: _____________
Time of Form Removal (Hrs from Start of Concrete Placement): __________________
Describe Cure Method After Form Removal: _________________________________

Weather Conditions

Day (starting with day of concrete placement)	Max Temp	Min Temp	Max. Relative Humidity	Min. Relative Humidity	Average Cloud Cover*	Max Wind Speed	Rainfall
Day 1							
Day 2							
Day 3							
Day 4							

* For average cloud cover, pick a number based on the average amount of cloud cover for the day, with 0 being sunny, 50 being partly cloudy and 100 being overcast
** Go to www.weather.com for the 4-day weather forecast

Please attach a copy of the cement/ fly ash certificates (mill sheets).

Table B 1-1- List of items needed to solder wires onto iButtons

Item #	Item Description
1	18 AWG Thermostat Wire with 0.008 PVC Insulation and 0.018 PVC Jacket
2	Wire cutters
3	Rosin-Core Solder for PC Work
4	Thermochron iButton
5	Soldering Iron
6	RadioShack Non-Spill Paste Rosin Soldering Flux®
7	Utility Knife (with a clean blade)
8	RadioShack Tip Tinner and Cleaner®
9	Small flat-head screwdriver, made for electronics
10 (not pictured)	Wire strippers (optional)

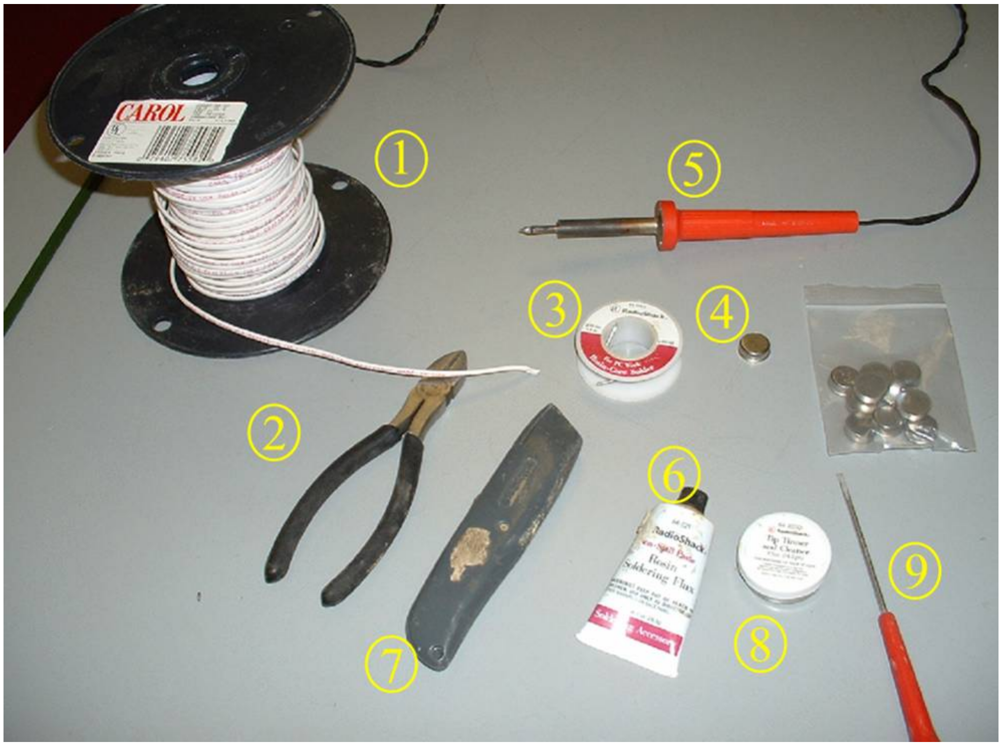

Figure B 1-1- Picture of items needed to solder wires onto an iButton

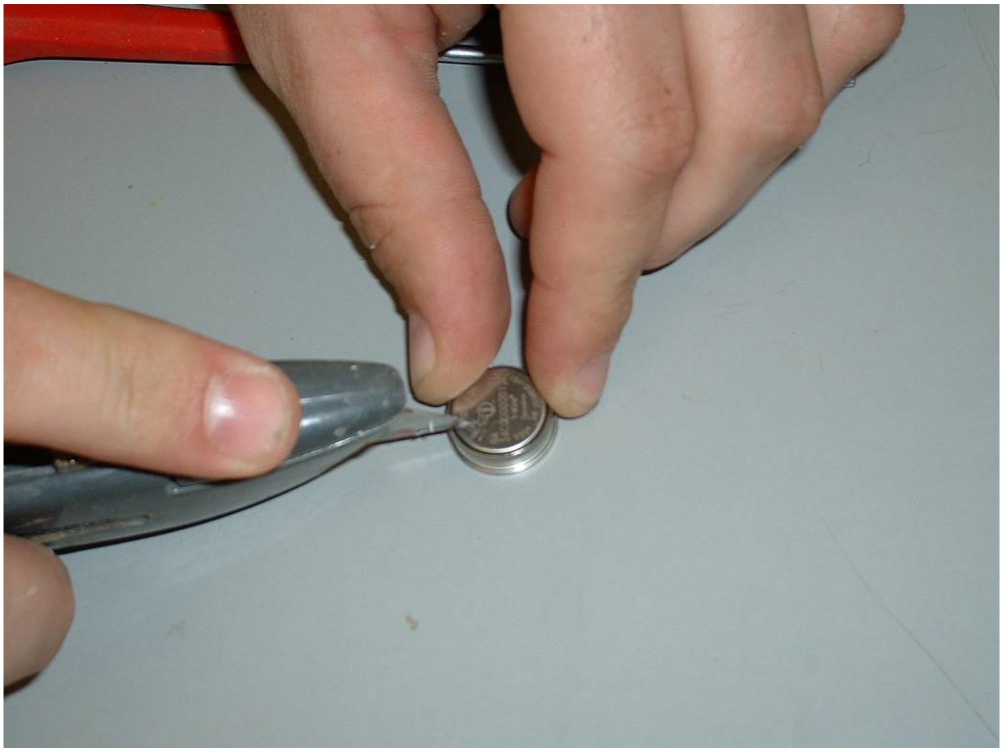

Figure B 1-2 - Scratching the iButton® surface with a utility knife

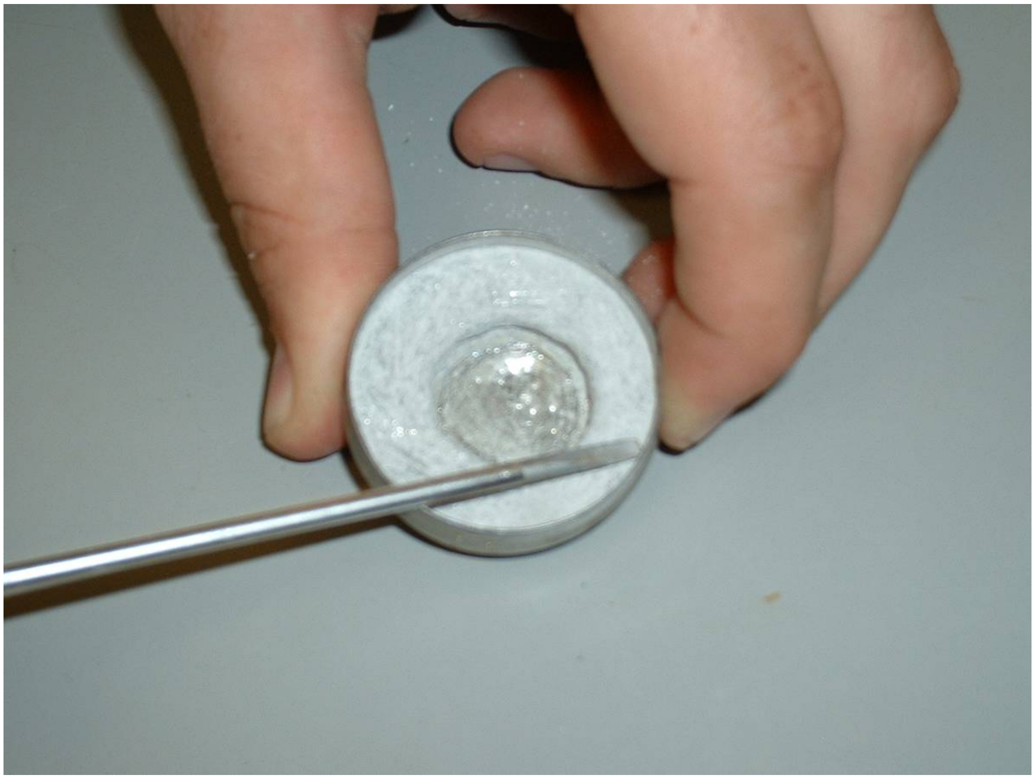
Figure B 1-3 -Scratching off some of the Tip Tinner and Cleaner with the Screwdriver, forming a powder


Figure B 1-4 - Picture of powdered Tip Tinner and Cleaner on an iButton

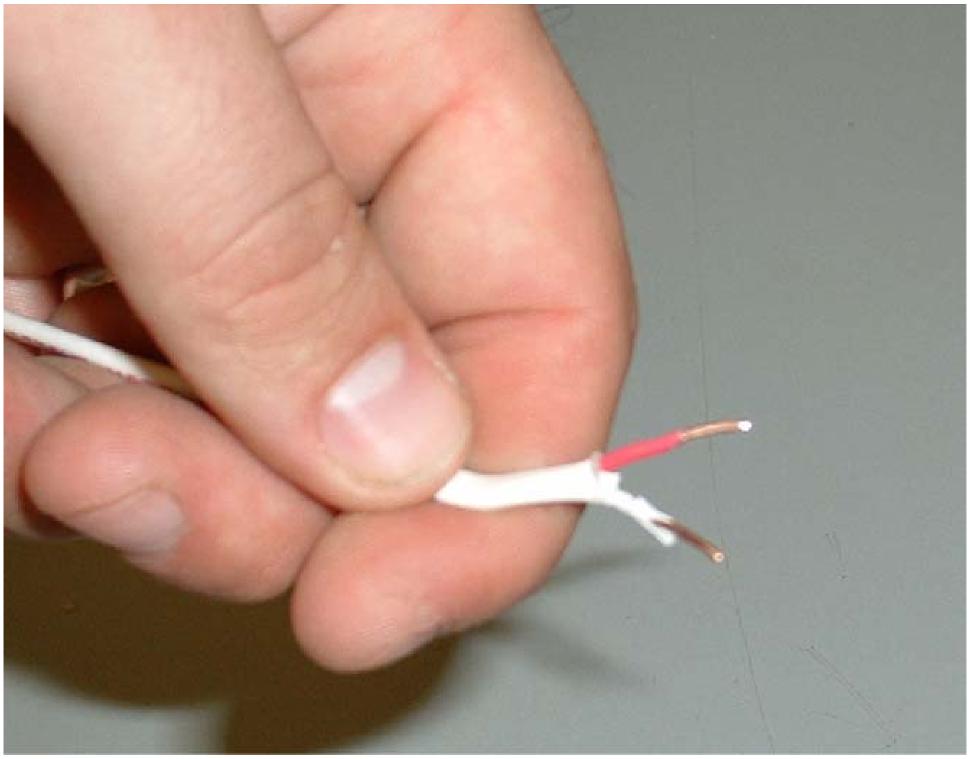

Figure B 1-5 - Close-up picture of the stripped wire ends

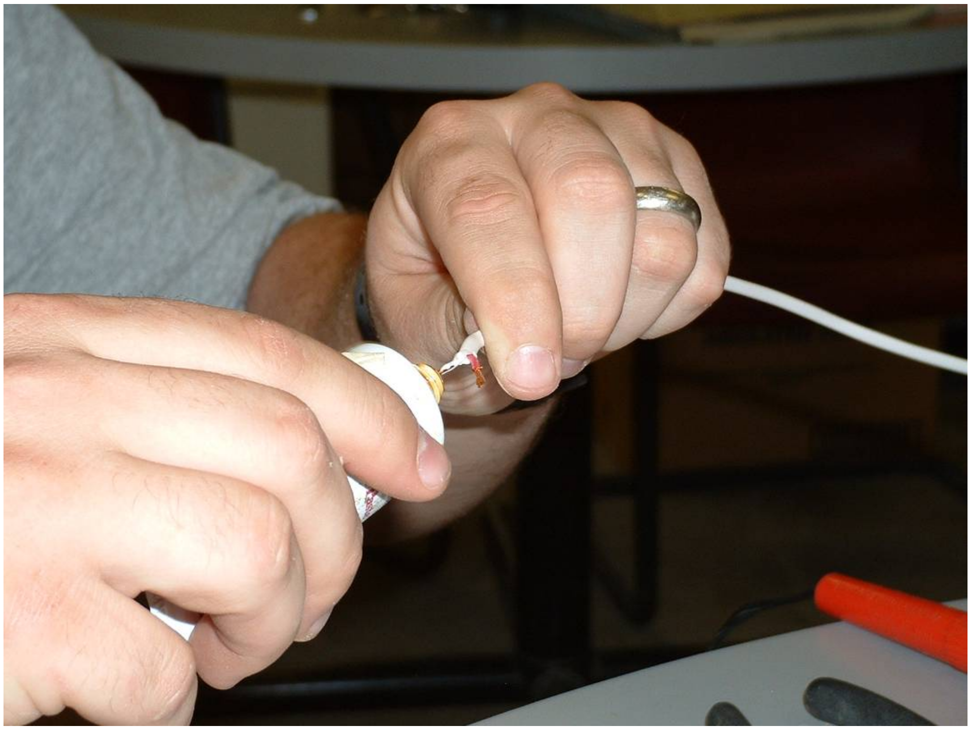

Figure B 1-6 - Dipping the ends of the wires into the Rosin Soldering Flux tube

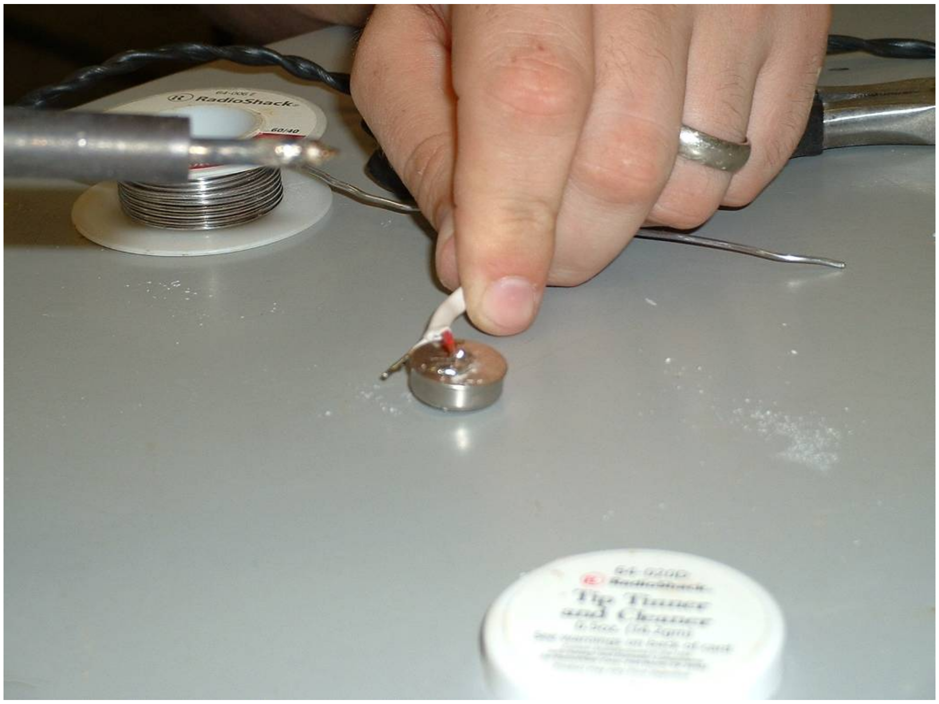

Figure B 1-7 - Placing the prepared wire on the prepared iButton surface

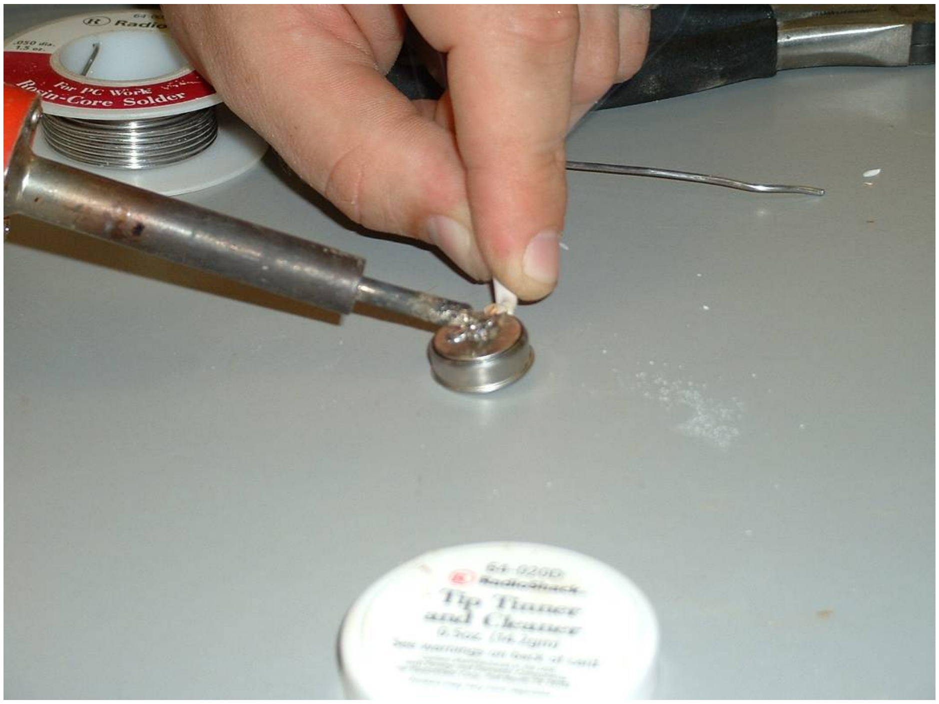

Figure B 1-8 - Touching the wire with the soldering iron long enough to melt the solder on the iButton - making sure that there is enough solder on the iButton to cover the wire

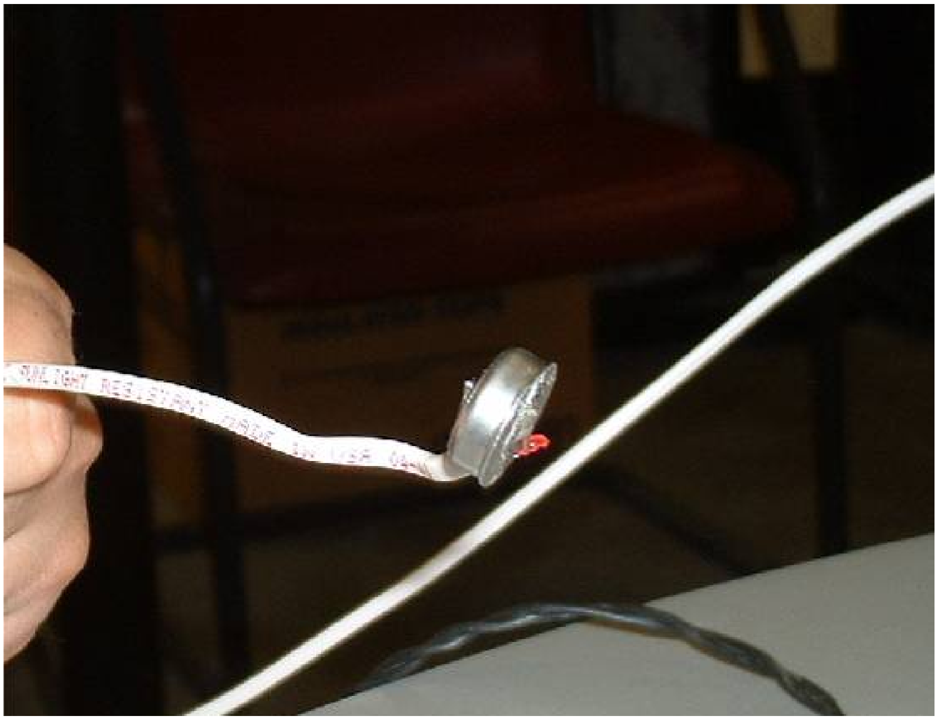

Figure B 1-9 - IButton with attached wires

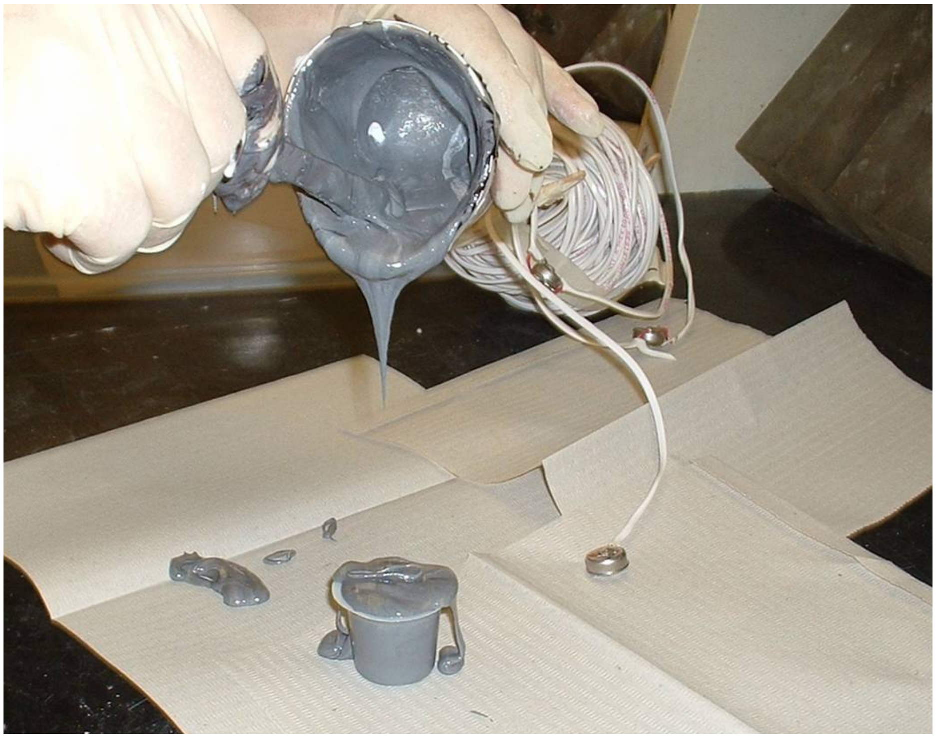

Figure B 1-10 - Filling the cup with epoxy

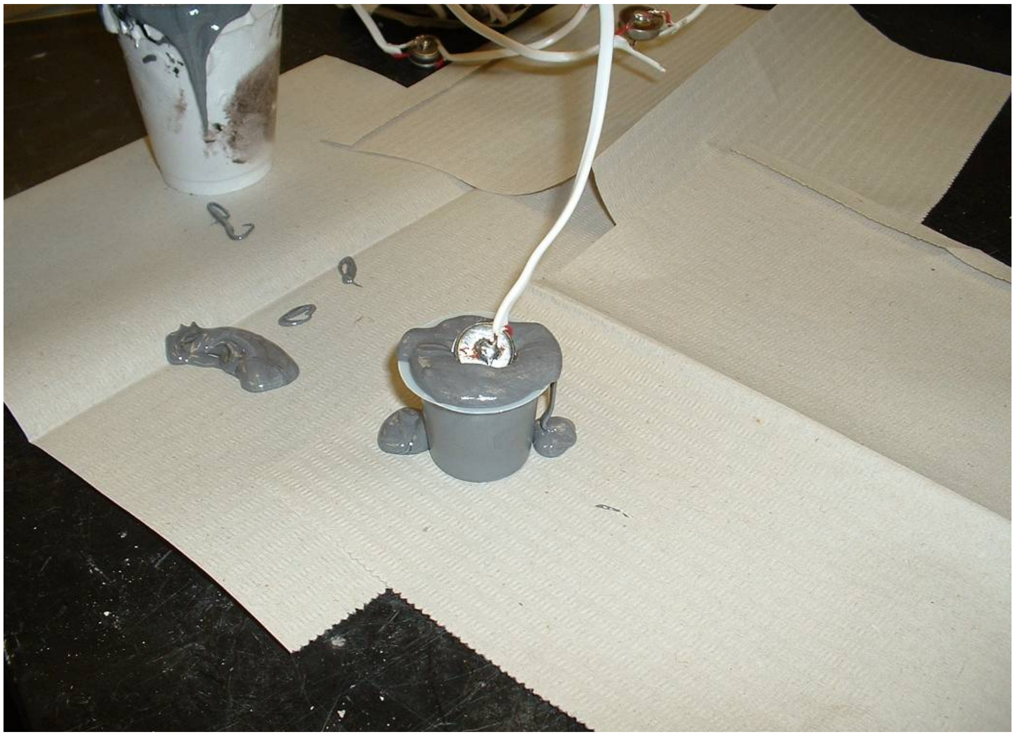
Figure B 1-11 - Placing the iButton® in the epoxy

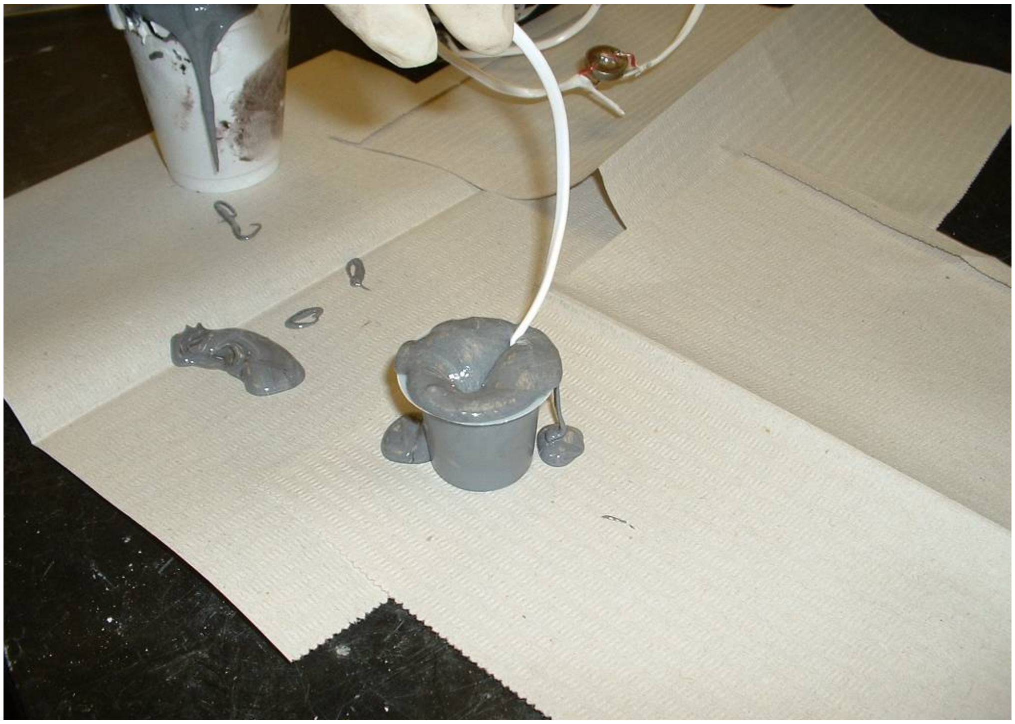
Figure B 1-12 - Completely covering the iButton and bare wire in epoxy

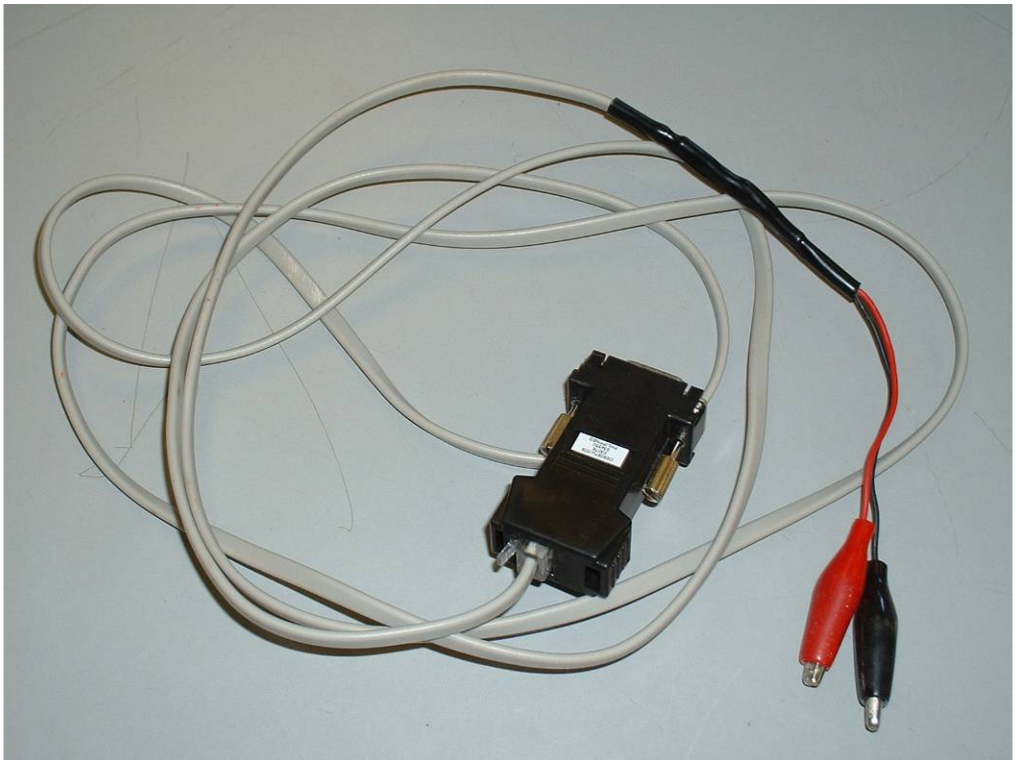

Figure B 1-13 - Modified telephone wire plugged into Port Adapter

APPENDIX C

ConcreteWorks Operator's Manual

CHAPTER C-1   CONCRETEWORKS OPERATOR'S MANUAL

C-1.1 Introduction To Using ConcreteWorks

ConcreteWorks is a suite of Windows®-based concrete technology programs intended to be used by engineers, researchers, inspectors, contractors and precasters already familiar with concrete materials and construction practices. The first program in the series is the self-titled *ConcreteWorks* program. *ConcreteWorks* is a concrete durability design tool that may be used to predict temperature development, thermal stress cracking probability, or the concrete chloride service life for various concrete members, as explained in the software introduction. *ConcreteWorks* is meant to be used by operators described above that have a working knowledge of concrete behavior. It is recommended that *ConcreteWorks* users thoroughly read the background information on the software to understand some of the limitations and the assumptions made in the software.

Mix Proportions is a program that assists the user in concrete mixture design and proportioning. *Mix Proportions* is based on the procedures outlined in ACI 211 (1991) and National Highway Institute (NHI) Course 15123 (Hover, 2003). This user manual provides help and explanations on how to use the program *ConcreteWorks*. No warranty of the accuracy of results calculated by any of the *ConcreteWorks* programs is given or implied.

C-1.1.1 INSTALLATION

To install *ConcreteWorks*, the target computer must be running the Microsoft .NET Framework v2.0. The .NET Framework can be installed by running the program dotnetfx.exe. The program dotnetfx.exe can be downloaded for free from the site http://www.microsoft.com/downloads/details.aspx?FamilyID=0856eacb-4362-4b0d-8edd-aab15c5e04f5&displaylang=en

The system requirements needed to install dotnetfx.exe can be found at:

http://www.microsoft.com/downloads/details.aspx?FamilyID=0856eacb-4362-4b0d-8edd-aab15c5e04f5&displaylang=en#Requirements

Once the target computer is running the .NET Framework, you may install *ConcreteWorks*. To install *ConcreteWorks* from CD, start by inserting the *ConcreteWorks* CD. The computer should automatically detect *ConcreteWorks*, and open the Installation Wizard. If the computer does not automatically start the installation process then open The "My Computer" window. Next, open the folder of the CD containing *ConcreteWorks*. Then double click the *Setup* icon. The program should then start the Installation Wizard. To install *ConcreteWorks* from a zip file downloaded from the internet, first unzip the file. After the file has been unzipped, click run when prompted to open up the installation wizard.

The installation wizard will guide you through all of the necessary steps to install the *ConcreteWorks* suite of programs. The first screen is the installation welcome screen. Click the *Next* button to continue with the installation. The second screen contains the End-User License Agreement (EULA). Click the *I Agree* button if you agree with the terms of the EULA, and then click *Next.* If you do not agree with the terms of the EULA, click *I Do Not Agree* and then *Cancel*, ending the installation process. The software will not install unless you signify that you agree to the terms of the EULA by clicking *I Agree*. The next screen contains four check boxes corresponding to states, as seen in

Figure C 1-1- Installation screen three, which weather files to install. The installation wizard will install the weather files of all the states whose corresponding box is checked. As explained in Section C-1.2.2.4, inputting the closest city to the construction project is essential to accuracy of the program calculations.

Internet Explorer is required to be installed on the computer to access the official *ConcreteWorks* website from *ConcreteWorks* as described in Section C-1.4.7.1. Failure to have Internet Explorer installed on the computer could result in an error and/or the program crashing.

Adobe Reader® is also required to be installed on the computer to access the *ConcreteWorks User Manual* as described in Section C-1.4.7.2. Failure to have Adobe Reader® installed on the computer could result in an error and / or the program crashing.

C-1.1.2 NAVIGATING THE PROGRAM

There are two methods of opening a new or saved file in *ConcreteWorks*. The first method is to click on the *New File* or *Open Existing File* toolbar button. The second method is to click *New* or *Open* under the *File* Menu. Figure C 1-2 shows a zoomed in view of the upper left side of *ConcreteWorks*. The red arrows point to the different menus and toolbars available in *ConcreteWorks*. If a file is already open, the program will prompt to save the current file. If the *Yes* button is clicked, the program follows the save procedure outlined in Section C-1.4.4. If a file is not already open, the program will prompt the user for a filename and location, as described in Section C-1.4.3.

There are also two methods of changing the current input/results screen in *ConcreteWorks*. The navigation toolbar found at the top of the program allows the user to quickly navigate between input/results screens. Each button when clicked, displays the corresponding input/results screen. Clicking on the *Next* button displays the next chronological input screen. Clicking the *Back* button displays the previous screen shown. The navigation toolbar shows the order the screens are displayed.

For more information on the printing features found in the *File* menu, see Section C-1.4.1. See Section C-1.4.6 for more information on the *Tools* menu and Section C-1.4.7 for more information on the *Help* menu.

C-1.2 Inputs

C-1.2.1 MEMBER TYPE

When a new file is selected, the user is prompted to select the type of member to analyze. In ConcreteWorks v2.0, the user may select from four basic types of concrete members: mass concrete, bridge decks, pavements, or precast beams. The analysis options available for each type of concrete member is shown in Table 9-1 of Chapter 9. The input screens available will depend on the type of member selected, and will only be shown if needed. For example, the *Corrosion Inputs* screen is not available when the user selects the *Precast Concrete* member type because *ConcreteWorks* does not contain a chloride service life module for precast beams. The inputs for all member types will be explained together in the manual with the implication that if the input is not applicable for a particular member type, it will simply not be shown in the software. Additionally, the *next* and *back* buttons will show the next input screen available in the same order as the order of inputs shown in the input screen navigation toolbar shown in Figure C 1-2.

C-1.2.2 GENERAL INPUTS

The basic model settings and project inputs are all done in the *General Inputs* screen, as seen in Figure C 1-3. The *General Inputs* screen is the first screen shown after opening a new or saved file, which is why there's not a *Back* button shown. Changing the inputs in the *General Inputs* screen will fundamentally change other data entered later in the program. Changing the *placement date, analysis duration*, or *project location* will cause the weather data to change, even if maximum or minimum values have been entered earlier.

C-1.2.2.1 Units

There are many inputs in *ConcreteWorks* that can be entered in either English units or Metric (S.I.) units. The English units system is the default units system in *ConcreteWorks*. When the system of units is changed, the program will prompt the user to change all values or cancel to stay in the current unit system. If the user chooses to change the values entered, the program assumes that the user entered the correct values for the old unit system, and will then multiply the entered values by the appropriate conversion factor for the new unit system. The *Chloride Units* input allows the user to select to perform the chloride service life calculations by % Chlorides by mass of concrete, or by mass per unit volume. The chloride surface concentration inputs in the *Corrosion Inputs* will be in the units chosen, as will the steel chloride threshold at corrosion initiation values, and the initial chloride concentration values.

C-1.2.2.2 Project Time and Date

The *Placement Time* box allows the user to enter the time concrete placement is started on the element being analyzed. If the cross-section being analyzed is a horizontal cross-section (such as a column), then the user should input the time concrete is placed at the particular cross-section being analyzed. The default time is 7:00 a.m.

The *Placement Date* is entered by clicking on the number corresponding to the date of concrete placement. The month or year of placement can be changed by either clicking on the appropriate arrow or by clicking on the month or year. The default date is the current date.

Accurate results in *ConcreteWorks* depend on the user entering the correct time and date. Even if the minimum and maximum weather data is entered later in the program, the correct date and time must still be entered. The shape of the weather data plots are extracted from thirty-year average data. Because of the changing sunrise and sunset times, every day has fundamentally different shape of the weather data plot. Entering the correct maximum and minimum weather data later in the program will give the correct overall magnitude for the weather data plots, but will not change the weather data's fundamental shape.

C-1.2.2.3 Analysis Setup

ConcreteWorks predicts the temperature development of a concrete cross-section for the number of days selected under the *Analysis Duration* option. The default number of days is seven. The *Chloride Service Life Analysis Duration* input allows the user to select the number of years that are used to calculate the chloride ingress into the concrete. If the steel chloride threshold has not been exceeded during the time period selected for the *Chloride Service Life Analysis Duration*, then the results will show that the time to corrosion initiation will be greater than the *Chloride Service Life Analysis Duration*.

C-1.2.2.4 Project Location

Under the *Project Location* option, the user should select the closest city to the construction site that has a similar climate. Besides using the drop-down list of cities to select the project location, cities in the currently selected state can be selected by clicking on the city name in the city map. When installed, *ConcreteWorks* automatically installs weather data files for seventeen Texas cities (as shown on the map on the *General Inputs* screen). The files are located in the same folder as the *ConcreteWorks* application. Weather files for states other than Texas may be installed during the installation process. This is done by checking on the box corresponding to the state desired found on installation screen 3, as seen in Figure C 1-1 and described in Section C-1.1.1. Weather files for other cities will also be detected automatically and added to the available cities list by placing a copy of the weather file in the same folder as *ConcreteWorks*. *ConcreteWorks* automatically detects all weather files located in the same folder as *ConcreteWorks*, and adds them to the drop-down list of available cities. Caution: only genuine *ConcreteWorks* weather files can be recognized by *ConcreteWorks*. Other weather files may cause an error in the program.

C-1.2.3 SHAPE INPUTS

ConcreteWorks can predict the temperature distribution for several types of mass concrete elements. All available concrete shapes available according to the type of concrete member selected are listed in the *Shape Inputs* screen.

C-1.2.3.1 Available Shapes

ConcreteWorks has the capability of predicting temperature development in six unique mass concrete member types, four types of bridge decks, and four precast beam shapes. ConcreteWorks also has a pavement temperature prediction built in, but because there is only one concrete pavement type allowed, the shape inputs screen is not shown when pavement member types are selected. The shapes available were selected in cooperation with TxDOT engineers to reflect the most common types used in Texas. Figure C 1-4 shows the mass concrete shapes available in the *Available Shapes* frame. Figure C 1-5 shows the four types of bridge deck types available in the *Shape Inputs* screen, while Figure C 1-6 shows the precast beam types available. When a shape is checked, a picture of the shape is shown to the right for confirmation. Once the desired shape is selected, proceed to the next screen.

C-1.2.4 MEMBER DIMENSIONS

Each unique concrete cross-section type will display a different picture and inputs on the *Member Dimensions* screen. All shapes however, use the same basic format. Figure C 1-7 shows the *Member Dimensions* screen for the Rectangular Column member.

C-1.2.4.1 Dimensions

Each shape will require the user to enter the member cross-sectional dimensions. All dimensions input will correspond to the same dimensions on the picture on the left side. Because the program's focus is on transportation related concrete (bridges and pavements), *ConcreteWorks* limits the size of some member dimensions. The Rectangular Column, Rectangular Footing, Partially Submerged Rectangular Footing, and Rectangular Bent Cap have minimum dimensions of three feet each. The Circular Column has a minimum diameter of three feet. The T-Shaped Bent Cap has a minimum seat height of nine inches and a minimum top width of 1.5 feet. The overall cap height must also be 1.5 feet taller than the seat, and the overall cap width must be 1.5 feet greater than the top width. If an invalid dimension is entered, an error will appear when the user attempts to calculate the member temperature development using the *Calculate Temperatures* button on the *Input Check* screen. Member dimension limits for decks and pavements are enforced by the numeric-up-down control used to input the dimension. The *Overall Deck Thickness* is limited to 14 in., while the *Precast Panel Thickness* are limited to 8 in. The *Pavement Thickness*, *Subbase 1 Thickness*, and *Subbase 2 Thickness* are all limited to 24 in.

Pavement analysis are broken up into different layers with different material properties, as shown in Figure C 1-8. Users may select up to two types of subbase materials, in addition to the pavement and subgrade. The subgrade material is assumed to extend infinitely beneath the subbase layer(s). Pavement layer dimensions and types are not changed in *ConcreteWorks* until the user clicks on the *Re-Draw Pavement System* button. The figure to the right of the pavement dimensions inputs will then update, allowing the user to check the currently selected inputs.

C-1.2.4.2 Submerged

Some of the available member types have the option of being submerged in water. This means that the cross-section being modeled is completely immersed in water. One example of when the submerged option would be selected is when a column is placed in a lake or ocean.

C-1.2.4.3 Soil on the Sides

Some member types have the option of modeling soil on the sides of the member. This option is selected when earthwork is used instead of formwork. Figure C 1-9 shows an example of the type of member that would have soil on the sides used instead of formwork.

C-1.2.4.4 Cross-Sections analyzed

Temperature predictions are in some cases based on one or two-dimensional cross-sections of the member. When *ConcreteWorks* does not calculate the temperature distribution for a direction in a concrete member, the program assumes that there is no heat loss in that direction (i.e., perfectly insulated). For example, with the rectangular column, *ConcreteWorks* calculates the temperature profile of a horizontal cross-section of the column. The program assumes that there is no heat loss from the top of the column to the air or from the bottom of the column to the footing. This assumption is a valid assumption for the vertical middle of the column, and becomes less accurate towards the ends in the column.

When the user selects to analyze a rectangular footing or partially submerged rectangular footing in three dimensions, the temperature distribution in the footing is calculated for all three directions. Calculating the temperature in three dimensions can give slightly better results in some cases, but significantly increases the calculation run time. The user only has the option of calculating the footing temperature in three dimensions when the user does not select soil on the sides of the footing. When the user selects to calculate a two dimensional cross-section of the footing temperatures, as seen in Figure C 1-10, the width side is used in calculations. The length dimension entered is then ignored. The user should enter the smaller dimension of the two horizontal footing dimensions in the width text box.

C-1.2.4.5 Precast Panel Inputs

When the user selects a *Generic User Defined Bridge* on the *Shape Inputs* screen, then the user has the option of selecting to use a precast panel and the number of mats of steel. Figure C 1-11 shows the *Bridge Deck Dimensions Inputs* screen when the *Generic User Defined Bridge* deck type is selected. When the user selects to use two mats of steel and a precast panel, the bottom mat of steel is assumed to be made of prestressed strands.

C-1.2.5 MIXTURE PROPORTIONS

The *Mixture Proportions* screen is where the user inputs the concrete batch information, as seen in Figure C 1-12. If blended cement is used, the user should enter the fly ash and cement quantities separately, as if they were added to the concrete completely separate.

C-1.2.5.1 Mix Proportion Inputs

All information found in the *Mix Proportion Inputs* area must be inputted correctly for the program to generate a heat signature curve for the concrete. Mixture information is entered by the amount of weight of a particular material for every unit volume (pounds per cubic yard for English units, kilograms per cubic meter for SI units). The aggregate contents are entered assuming the aggregate is saturated surface dry (SSD). The water is entered based on total amount of free water available for hydration (aggregate moisture not absorbed + water/ice added).

C-1.2.5.2 Supplementary Cementing Materials

The *Supplementary Cementing Materials* (SCM) frame is where SCMs are input. To include an SCM in the batch, check the box corresponding to the particular SCM. Enter in the amount of SCM used in the batch. The program defaults the free lime content of the ASTM Class C fly ash to twenty-nine percent and the ASTM Class F fly ash to nineteen percent. These values can be changed if the free lime content of the fly ash used is known. To remove the SCM from the batch, simply uncheck the corresponding box or set the amount used to zero.

C-1.2.5.3 Calculated Mixture Proportions

The *Calculated Mixture Proportions* frame displays calculated mixture ratios based on the current values entered. The *Sacks of Cement*/volume quantity is based on the total number of 94 pound sacks of cementitious materials used in the batch (cement + SCMs) per cubic yard/meter. The number of *Gallons of water per sack/liters per sack* figure is the amount of water per sack of cementitious materials. The density of the water is assumed to be 1g/cm^3 (62.43 lb/ft^3). The *Water/Cement Ratio* is equal to the water content entered divided by the cement content. The *Water/Cementitious Ratio* is equal to the water content entered divided by cementitious materials content.

C-1.2.5.4 Chemical Admixture Inputs

Chemical admixtures are entered by checking on the admixture. To simplify mixture proportion inputs, typical values of chemical admixture doses are assumed as shown in Table 9-5.

C-1.2.5.5 Bottom Panel Mixture Proportions

When a bridge deck member type with precast panels is selected, the user may change the bottom panel mixture proportions by clicking the button *Click to Change Bottom Panel Mixture Proportions*. When this button is clicked, an input screen similar to the *Mixture Proportion Inputs* screen is shown. Figure C 1-13 shows the *Precast Panel Mixture Proportions Inputs* screen that is displayed. Here, the user may enter the mixture proportions used in the precast panel concrete. There are two visible differences between the *Mixture Proportion Inputs* screen and the *Precast Panel Mixture Proportions Inputs* screen. The first is the title shown on the blue form bar. The second is that the button on the lower right hand corner is the *Next* button on the *Mixture Proportion Inputs* screen, while on the *Precast Panel Mixture Proportions Inputs* screen is the *OK* button. The *OK* button, when clicked, will return the user to the *Mixture Proportion Inputs* screen. Although the precast panel is assumed to not generate any heat, the concrete diffusion coefficients used in the chloride service life analysis is determined from the concrete panel mixture proportions.

C-1.2.6 CONCRETE MIXTURE PROPORTIONING

If the user needs help with the concrete mixture design and proportioning, the user may click on the *Go to Design of Mixture* Proportion button on the lower right corner of the *Mixture Proportions* screen, as seen in Figure C 1-12. The *Design of Mixture Proportion* screen will appear, as seen in Figure C 1-14. The *Design of Mixture Proportion* screen guides the user through the mixture proportioning steps as found in ACI 211 (1991) and NHI Course 15123 (Hover, 2003). For a more detailed presentation of the mixture proportioning procedure and limitations, please refer to ACI 211 (1991). The most important thing to remember about the mixture proportion calculations is that they are only designed to create the proportions for making and testing a trial batch. The calculations in the *Design of Mixture Proportions* screen can never be used as a substitute for local knowledge of material properties or for trial batches. This is designed to be a user-friendly tool as the first step in designing mixtures for field applications.

The *Cancel* button on the *Design of Mixture Proportion* screen sends the user back to the *Mix Proportions Inputs* screen without any changes being made to the material weights. The *OK* button sends the user back to the *Mixture Proportions Inputs* screen, changing the material weights to those shown in the *Final Volume Calculations*. When a chemical admixture is checked in the *Water Adjustment* tab, the admixture is then checked on the *Mix Proportions Inputs* screen. When the *High-Range Water Reducer (Type F)* box is checked in the *Design of Mixture Proportion* screen, *ConcreteWorks* assumes that a Napthalene-based admixture is used.

C-1.2.6.1 General Mix Information

The *General Mix Information* tab of the *Design of Mixture Proportion* screen displays all of the general material specifications. If not entered manually, the *w/cm ratio* is calculated from the *Target Strength* shown in the *Strength Requirement* frame, the air content, and any minimum w/cm ratios imposed by selecting a severe exposure condition from ACI 318-05 Tables 4.2.2 or 4.3.1.

The target strength is calculated by default on the specified f'_c increased by either a prescribed amount from ACI 318-05 Table 5.3.2.2 or using the standard deviation and ACI 318-05 Tables 5.3.1.2. and 5.3.2.1. If fewer than 15 tests were used to determine the standard deviation or a standard deviation for the concrete compressive strength is not known, then ACI 318-05 Table 5.3.2.2 is used. If fewer than 30 tests were used to determine the concrete standard deviation, then a multiplication factor is applied to the standard deviation according to ACI 318-05 Table 5.3.1.2.

C-1.2.6.2 Aggregate Properties

The *Aggregate Properties* tab allows the user to either input the aggregate properties or calculated some of the inputs needed from an aggregate sieve analysis. Figure C 1-15 shows the *Aggregate Properties* tab. *Sieve Analysis Data* for each aggregate type used should be entered as percent passing. Additionally, the percent of each aggregate used should be input as percent of the coarse or fine aggregate used, not the total amount of aggregates used. When the *Update Agg. Properties* button is clicked, the combined *Coarse Aggregate Specific Gravity*, combined *Fine Aggregate Specific Gravity*, and *Maximum Size Aggregate* inputs are updated. Additionally, the aggregate gradation charts are updated when the *Update Agg. Properties* button is clicked. An error is generated when the user enters a percent passing value that is larger than that from a larger size sieve, when the sum of coarse aggregate percent used values does not equal 100 percent, or when the sum of fine aggregate percent used values does not equal 100 percent.

C-1.2.6.3 Water Adjustment

The *Water Adjustment* tab contains tracking bars that let the user adjust the water requirements for the concrete by moving the tracking bar values, as seen in Figure C 1-16. To use a water reducer, check the corresponding box on the *Water Adjustment* tab. Then move the track bar value to correspond to the water reduction gained from that particular admixture. The values used for maximum and minimum water reduction for all factors come from the NHI Course 15123 (Hover, 2003). A local knowledge of the water reduction properties for all the materials is extremely important. The quality of the concrete mixture designed will depend greatly on the accuracy of the inputs. Trial batches should always be made to verify the slump and strength properties of the concrete.

The *Adjusted Water Content* shown in the *Paste Content* frame is calculated based on the desired slump, the percent air, the aggregate gradation, and any water requirement adjustments made in the *Water Adjustment* tab (as described in Section C-1.2.6.3). The cementitious material content is calculated by dividing the *Adjusted Water Content* by the *w/cm ratio*.

C-1.2.6.4 Final Volume Calculations

The final volume calculations for the concrete mixture are calculated based on the aggregate properties, cement content, adjusted water content, mineral admixture replacement, and air content. The batch weights per yard of concrete are shown in the *Final Weights* frame. The pie graph shows the percent of each material in the concrete mixture by volume. Figure C 1-17 shows the *Final Volume Calculations* tab. When the total calculated paste content exceeds 30% by volume a warning appears to warn the user that the concrete mixture may be more susceptible to drying shrinkage. This does not preclude the use of the concrete mixture, but caution should be used for concrete members with a high surface area-to-volume ratio when exposed to low relative humilities.

C-1.2.6.5 Material Properties

The material characteristics are entered in the *Material Properties* screen. Figure C 1-18 shows the *Material Properties* screen. To manually override the default cement chemistry and hydration parameters, check the corresponding boxes and enter in the desired values, as seen in Figure C 1-19.

C-1.2.6.6 Cement Chemical/ Physical Properties

The *Cement Chemical/Physical Properties* frame is where the cement type, composition and physical properties are entered. To change the cement properties to those for the cement used, check the *Check to manually enter cement chemical/physical properties* box. If the user unchecks the *Check to manually enter cement chemical/physical properties box*, the cement properties revert back to the default values for the cement type selected. When the Bogue method is selected under the *Cement Analysis Method* found in the *Tools* menu, the Bogue values and oxide contents for the cement properties are displayed. If the Rietveld method is selected instead of the Bogue method, then the cement composition phases corresponding to that method is displayed. Actual cement properties estimated using the Bogue method can be found on mill sheets shipped with the cement.

C-1.2.6.7 Hydration Calculation Properties

Hydration Calculation Properties are based on equations developed as part of Texas Department of Transportation (TxDOT) research project 0-4563, and are described in section 9.3.1.5. Different models that describe the Hydration Calculation Properties are used depending on whether the Bogue method of the Rietveld method is used to define the cement properties. If the user has performed a semi-adiabatic calorimetry test on the concrete mixture used, then the calculated hydration properties can be changed by checking the *Check to manually enter hydration properties* box. When the *Check to manually enter hydration properties* box is checked, the hydration parameters do not change when the mixture proportions is changed or the cement type changes. The semi-adiabatic calorimetry test performed to determine hydration parameter equations for *ConcreteWorks* Version 2.0 came from mixes that used Texas materials. Low alkali cements were used in a majority of tests, and thus the hydration parameters for any mix containing a large amount of alkalis may not be as accurate. In the case that the concrete material properties deviate substantially from those used in Texas, a semi-adiabatic calorimetry test should be performed to determine the hydration parameters.

C-1.2.6.8 Aggregate Factors

Choose the type of coarse and fine aggregates used in the concrete batch. Up to three coarse aggregates types can be blended, while up to two fine aggregate types may be used. The user may change the number of coarse aggregates blended by changing the number in the *# of Coarse Aggregate Types* drop down menu, and the number of fine aggregates blended by changing the number in the *# of Fine Aggregate Types* drop down menu. When more than one type of aggregate type is selected to be blended, additional corresponding drop down menus will appear that prompt the user for the type of additional aggregate used. The coefficient of thermal expansion (CTE) and material thermal properties are calculated based on the mixture proportions and the coarse aggregate types. The coefficient of thermal expansion and material thermal properties may be input by the user if a hardened concrete coefficient of thermal expansion test, hardened concrete thermal conductivity test, or aggregate specific heat test is performed. The combined aggregate Cp value shown in Figure C 1-18 is the Ca parameter shown in

Equation 9-24. It is highly recommended that the user perform a hardened concrete coefficient of thermal expansion test on the concrete mixture to be used as the thermal stresses calculated are very sensitive to the concrete coefficient of thermal expansion. When the checkbox *Check to Manually Enter the Concrete Coefficient of Thermal Expansion and Thermal Properties* is unchecked, the concrete CTE and thermal properties revert to default values as calculated according to the chosen aggregate types.

C-1.2.7 MECHANICAL PROPERTIES INPUTS

The Mechanical Properties Inputs screen allows the user to input the type of maturity method used, the maturity – strength relationships, and the early age creep parameters as shown in Figure C 1-20.

C-1.2.7.1 Maturity Functions

The *Maturity Functions* frame allows the user to select between the Nurse-Saul method of maturity and the Equivalent Age method, both as described in ASTM C 1074 (2004). For the Nurse-Saul method, a reference temperature of 0°C is used when metric units are selected and 0°F is used as the reference temperature when English units are selected. If the user has a maturity curve already calculated for the given concrete mixture, the user may enter the a and b strength parameters according to the equation shown on the *Materials Inputs* screen. The *Check to calculate thermal stresses when temperatures are calculated* checkbox must be checked for the software to calculate the concrete member cracking probability failure classification. When thermal stresses are to be calculated, the equivalent age maturity method must be used. The elastic modulus and splitting tensile strength equations are calculated from the concrete compressive strength fit parameters entered. At a minimum, the compressive strength – maturity relationship must be entered for the concrete mixture proportions and materials used. The accuracy of the thermal cracking probability analysis increases when the elastic modulus and splitting tensile strength are measured and input in the software.

C-1.2.7.2 Early Age Creep Parameters

The concrete early age creep is calculated using the Modified Linear Logarithmic Model (MMLM) described in section 9.4.4. The early age creep parameters for the MLLM are calculated from the mixture proportions and material properties entered. Different equations are used, depending on whether the Bogue method or the Rietveld method is selected as describe in section 9.4.4.1.

C-1.2.8 CONSTRUCTION INPUTS

The *Construction Inputs* screen is where the construction related options are entered. Each type of concrete member will have different construction options to choose from. *ConcreteWorks* will automatically display the needed inputs based on the other options selected by the user such as member type or if the member is submerged. Do not be alarmed if a particular set of inputs does not appear with the particular choices made. If you change the member shape or submerged status, the available construction inputs will change. Dramatically different results will be calculated for even small mistakes, such as the form type, or blanket insulation. Figure C 1-21 shows the *Construction Inputs* screen for a rectangular column.

C-1.2.8.1 Concrete Placement Temperature

The *Estimated Placement Temperature* is the temperature of the concrete when it arrives on the jobsite. The concrete placement temperature can be calculated three ways.

The first way is to click on the *Calculate* button. After it is clicked, the *Raw Material Temperature Inputs* screen will pop up. The temperature of the cementitious materials, aggregates, and water must be entered. Aggregate moisture contents and absorptions must also be entered. Optionally, ice may be entered if it is used in the batch. The *OK* button will not work until all of the required information is entered. After all of the required information is entered and the *OK* button is clicked, the calculated placement temperature will be displayed in the *Estimated Placement Temperature* box. *ConcreteWorks* uses the ACI 305 model for predicting the fresh concrete temperature (ACI 305R, 1991). When the *Mixture Proportion* inputs are changed, the predicted fresh concrete temperature will also change, if all of the required inputs are entered in the *Raw Material Temperature Inputs* screen. Note: If all of the required inputs in the *Mixture Proportion Inputs* screen are not entered, *ConcreteWorks* will not be able to calculate the fresh concrete temperature.

The second way is to calculate the concrete placement temperature from the ambient temperature. In this method, the concrete fresh temperature is estimated as the ambient temperature at the time of placement.

The third way to enter the concrete placement temperature is to check the *Check here to manually enter Fresh Concrete Placement Temperature* box. After the box has been checked, the user may enter the concrete placement temperature in the *Estimated Placement Temperature* box. If the *Check here to manually enter Fresh Concrete Placement Temperature* box is checked, the value in the *Estimated Placement Temperature* box will only change when manually entered by the user.

C-1.2.8.2 Formwork

The *Concrete age at Form Removal* input requires the user to input the concrete age when formwork is removed (at the cross-section being analyzed), starting from the time the concrete was first mixed. The form type and form color must also be input in their corresponding boxes.

C-1.2.8.3 Surrounding Temperature

If the element selected is a footing or the element is submerged, the *Construction Inputs* screen will have inputs for the soil temperature and water temperature. The soil temperature refers to the average soil temperature for the time being modeled. A good estimate of the soil temperature for most footings is the average of the maximum and minimum ambient temperatures during the time period in question. The water temperature refers to the temperature of the water surrounding a concrete element. For example, if a column was being placed in a lake, the user would enter the average lake water temperature for that time period.

C-1.2.8.4 After Forms Are Stripped

The *After Forms Are Stripped* area asks the user to input what kind of curing methods are applied to the member after the forms are removed. *ConcreteWorks* requires the user to enter a time in the box *Time between form removal and curing method applied* if a cure method is checked. If the user enters a delay time, but does not check a cure method box, *ConcreteWorks* assumes that no cure methods are used. The user cannot check both the *Black Plastic* option and the *White or Clear Plastic* option at the same time. If for some reason, both types of plastic are used in construction, the user should check the type of plastic used as the outside layer. All curing methods applied after forms are stripped are assumed to remain on the concrete member until the end of the analysis duration. The default time between removing forms and applying the cure method is one hour.

C-1.2.8.5 Footing Inputs

When a footing is selected as the member type, the *Footing Inputs* frame becomes visible on the *Construction Inputs* screen, as seen in Figure C 1-22. The input *Type of footing subbase* asks the user to select the type of soil or rock on which the footing is built. If a plastic sheet is also used in curing, the user should select which color plastic is used. If both types of plastic are used, the user should select the color of the plastic placed on top. The input *Concrete age when cure blanket is placed* is the number of hours between concrete placement time and when cure methods are applied (the cure methods applied to the top before form removal). This input allows the concrete to set before placing the cure blankets on top of the footing.

If the sides of the footing are shaded from the sun because of scaffolding or the ground, the user should check the input *Footing Sides Shaded*.

C-1.2.8.6 Bent Cap Inputs

The user must select which type of form is used for the bottom of the bent cap. This allows the user to use different forms for the sides and bottom of a bent cap. For example, the user could select steel forms for the sides of the bent cap, and wood for the bottom. If the user selects *Precast Concrete* for the bottom form of the cap, the *Precast Concrete Section Thickness* input box appears, as seen in Figure C 1-23. The default cap bottom form type is steel. The default precast concrete thickness is two feet. The *Concrete age when cure blanket is placed* is the number of hours between concrete placement time and when cure methods are applied (the cure methods applied to the top before form removal). This input allows the concrete to set before placing the cure blankets on top of the bent cap. If a plastic is used on top of the cure blanket before form removal, the user should select which color plastic is used. If more then one color of plastic is used, the user should select the plastic placed on top.

C-1.2.8.7 Bridge Deck Inputs

ConcreteWorks assumes that a cure blanket is used on top of bridge decks. The user may additionally select to use a layer of plastic on top of blanket, the time the blanket is placed, and the concrete age when the the cure blanket is removed. If wood forms are selected for the bridge deck, the user may additionally specify the concrete age at the wood form removal, as shown in Figure C 1-24.

C-1.2.8.8 Precast Concrete Construction Inputs

Precast concrete members allow the user to specify a tarp or blanket to be used on the member sides. When the a tarp or blanket is used on the sides of the precast beam, the same R-value is used for the blanket on the top and sides of the beam. The software also allows the user to select the subbase underneath the precast member, and the age when the cure method is started. The cure method is assumed to end when the forms are removed.

C-1.2.8.9 Pavement Construction Inputs

ConcreteWorks asks the user to input the type of cure method used as shown in Figure C 1-25. The other pavement curing options depends on the curing method selected, and may ask the user for the application rate, the time of cure method application and removal, and the cure method color.

C-1.2.8.10 Blanket Insulation R-Value

The *Blanket Insulation R-Value* frame allows the user to select the R-Value of all cure blankets used during the concrete member construction. The R-Value is a measure of the blanket's thermal insulation. A high R-Value indicates a good insulator. Recommended R-values are 3 in^2-hr-F/BTU for a thick, good quality cure blanket and 1 in^2-hr-F/BTU for burlap or worn cure blankets.

C-1.2.8.11 Form Liners

The *Form Liners* frame asks the user to input which sides of the member use form liners. The width and depth sides correspond to the width and depth sides input in the *Member Dimensions* screen. *ConcreteWorks* assumes that the form liners are solid rubber reusable form liners (such as the Symons brand Elasto-Tex™[1] form liner).

---

[1] The Elasto-Tex™ trademark belongs to the Symons Co.

C-1.2.9 ENVIRONMENT INPUTS

The *Environment Inputs* screen is where all weather inputs are entered. All weather inputs are entered in tables that function similar to cells in a spreadsheet. *ConcreteWorks* requires that the user enter one more day than the number of days selected for analysis. The first day entered is the day selected as for the project date. Default values are the average thirty-year weather data for the days selected for each individual city. When the user changes the *Placement Date*, *Temperature Analysis Duration*, or project location on the *General Inputs* screen, the environment inputs are automatically updated to the thirty-year average values. The environmental inputs will always be updated, even if the user checks the boxes to input maximum and minimum weather values manually. Care should be taken to manually input environment values last. Clicking on the table headings will sort the table by the values of the column clicked on. The overall data will not be affected by sorting the data.

C-1.2.9.1 Temperature

The maximum and minimum temperature for each day is shown in the table on the *Temperature* tab. Default values can be overridden by checking the *Check to manually enter temperature data* input. Next, click on the table cell desired, and change the maximum or minimum value. Figure C 1-26 shows the *Environment Inputs* screen with the *Temperature* tab selected.

C-1.2.9.2 Relative Humidity

The maximum and minimum relative humidity for each day are shown in the table on the *Relative Humidity* tab. Default values can be overridden by checking the

Check to manually enter humidity data box. Next, click on the table cell desired, and change the maximum or minimum value.

C-1.2.9.3 Percent Cloud Cover

Average daily cloud cover value for each day is shown in the table on the *Percent Cloud Cover* tab. Default values can be overridden by checking the *Check to manually enter cloud cover data* box. Next, click on the table cell desired, and change the average cloud cover value. Enter cloud cover according to the scale shown. A zero cloud cover value is entered for sunny conditions, 50 for partly cloudy, and 100 for overcast. Figure C 1-27 shows the *Environment Inputs* screen with the *Percent Cloud Cover* tab selected.

C-1.2.9.4 Wind Speed

Maximum wind speed value for each day is shown in the table on the *Wind Speed* tab. Default values can be overridden by checking the *Check to manually enter wind speed data* box. Next, simply click on the table cell desired, and change the maximum wind speed value.

C-1.2.9.5 Yearly Temperature

The yearly temperature profile is calculated based on the number of temperature points per year selected as shown in Figure C 1-28. Additionally, under the input *Temperature Value to Use*, users can select to use the average temperature values, the average temperature plus one standard deviation, or the average plus two standard deviations. The yearly temperature profile is used in calculating the chloride service life. The estimated chloride service life is not very sensitive to the number of data point per year selected, but is moderately affected by using the average temperature plus one or two standard deviations.

C-1.2.9.6 Summary Graphs

The *Summary Graphs* tab can display the updated weather data on a graph. All plots start at 1:00 a.m. on the project date selected. The *Temperature* button shows a plot of temperature data with time. The *Humidity* button displays the relative humidity data with time. The *Wind Speed* tab shows a plot of wind speed with time. The *Solar Radiation* tab shows a plot of solar radiation with time. The solar radiation values are calculated based on the cloud cover data and relative humidity data. Figure C 1-29 shows the *Environment Inputs* screen with the *Summary Graphs* tab selected. The graph shown in Figure C 1-29 is a plot of the temperature.

C-1.2.10 INPUT CHECK

The Input Check screen shows the values that have been entered. This is the chance for the user to see if any mistakes were made in the inputs section of ConcreteWorks. Anytime a user enters a character not allowed, ConcreteWorks assumes the value of the input to be zero. For example, if the user types “78u” on the Cement Content input in the Mixture Proportion Inputs screen, the Input Check screen would show that the cement content is “0”. Figure C 1-30 shows the Input Check screen. Notice the default values are highlighted green, and the questionable values are highlighted red.

C-1.2.10.1 Default Check

Anytime the user chooses to use the default program value for an input, the *Input Check* screen will highlight that value in green. This feature makes it easy for the user to see how many entries the user actually made.

C-1.2.10.2 Questionable Values

Anytime the user enters a value that the program deems questionable, *ConcreteWorks* highlights that value red. Just because *ConcreteWorks* deemed the value questionable, does not always mean that the program will not calculate temperature profiles for the element. A red value simply means that the user should check to make sure that the value is indeed what the user wanted. Caution: questionable values can (but not always) cause instability in *ConcreteWorks* or give unrealistic results. This feature makes it easy for the user to quickly scan the *Input Check* screen for common mistakes in entering data. Table C 1-1 shows which values are considered questionable by *ConcreteWorks*.

C-1.3 Results

C-1.3.1 RESULTS SUMMARY

After clicking the *Calculate Temperatures* button on the *Input Check* screen, *ConcreteWorks* will begin performing model calculations for the member type selected. A progress bar will appear in the lower left corner or the *Results* screen, showing the calculations progress. If a serious error was made in entering an input, a message box will appear telling the user the error. The *Results* screen has a different heading, depending on the type of member shape chosen.

C-1.3.1.1 Mixture Checks

The *Mix Checks* tab shows a summary table of the calculated results, as seen in Figure C 1-31. The first section in the *Mix Checks* table states the set of specifications used to check the calculated results (for example, the TxDOT 2004 specifications), the maximum temperature in the concrete member during the analysis period, the maximum temperature difference at time t anywhere in the concrete member, and whether the concrete mixture meets the specifications selected for alkali silica reactivity. The second section in the *Mix Checks* table tells the user the time to corrosion initiation and damage estimated in the concrete member. The last section gives the cracking probability classification. The cracking probability classification criterion is explained in section 9.4.5. A low or moderate cracking probability classification does not guarantee that the structural member will be free of cracks. A low cracking probability classification only indicates that the probability of cracking is lower than if the concrete cracking probability classification were moderate, high or very high. Any classification, including the low cracking probability classification includes some chance that cracking will occur. When the TxDOT 2004 specification is selected, the maximum temperature difference line in the *Mix Checks* table will be highlighted red if the value exceeds 35°F, the maximum temperature in the member line will be highlighted if the value exceeds 158°F, and the alkali-aggregate reactivity line will be highlighted red if the concrete does not meet TxDOT specification 420 (Texas Department of Transportation, 2004).

C-1.3.1.2 Max-Min Graph

The *Max-Min Graph* tab shows the user a graph of the important calculated values with time, as seen in Figure C 1-32. The values shown are: the maximum temperature anywhere in the concrete member at each point in time, the minimum temperature anywhere in the concrete member at each point in time, the maximum temperature difference in the concrete member at each point in time, and the ambient temperature.

C-1.3.1.3 Animation

The *Animation* tab allows the user to view an animated chart of the concrete member, as seen in Figure C 1-33. The *Animate* button shows the charts and starts the animation from the start of concrete placement. The *Stop Animation* button stops the animation. *ConcreteWorks* animates the calculated property checked in the *What to animate?* frame. If no compressive strength parameters are entered in the *Material Properties* screen (see Section C-1.2.7.1), then the *Comp. Strength* button will be disabled. The *CircularColumnfinite* screen does not show a three dimensional animation of the concrete temperature. Instead, the *CircularColumnfinite* screen will show a two dimensional animated graph of the temperature on the column diameter cross-section. When the cracking failure classification is calculated, the animation will also display a bar at the bottom of the animation that will show the cracking classification at that point in time that is being animated.

C-1.3.1.4 Maturity

The *Maturity* tab contains a graph that shows the calculated maximum, minimum, and maximum maturity difference for the concrete member, as seen in Figure C 1-34. The maturity is calculated from the strength parameters chosen on the *Material Inputs* screen (see Section C-1.2.7.1). The calculated maturity is only an estimate, and only applies when the maturity parameters entered are from same concrete mixture as the one entered.

C-1.3.1.5 Compressive Strength

The *Compressive Strength* tab shows the maximum compressive strength, minimum concrete strength, and the average compressive strength of the concrete member, as seen in Figure C 1-35. The average compressive strength is a weighted average of the compressive strength in the member. This means that the compressive strength of the concrete member is integrated, and then divided by the total area. The compressive strength is calculated using the calculated concrete temperature, the calculated concrete maturity (see Section C-1.3.1.4), and the compressive strength parameters entered on the *Mechanical Properties Input* screen (see Section C-1.2.7.1). If the user does not enter the compressive strength parameters in the *Mechanical Properties Input* screen, the concrete compressive strength is not calculated. The compressive strength graph on the *Compressive Strength* tab is then not visible.

C-1.3.1.6 Chloride Concentration at the Steel

As part of the chloride service life analysis, ConcreteWorks calculates the chloride concentration at the steel. When the chloride concentration reaches the chloride threshold level, corrosion is considered to have initiated. The chloride concentration at the steel level value will turn orange once corrosion exceeds the chloride threshold level, as shown in Figure C 1-36.

C-1.3.1.7 Cracking Probability Classification

The cracking probability classification at different times is plotted as a bar chart, with the maximum temperature difference plotted as a blue line on the same graph to show how the temperature gradient in the concrete affects the cracking probability classification. Figure C 1-37 shows the graph used to show the cracking probability classification and maximum temperature difference. The bar color shown for the cracking probability classification corresponds to the classification shown at the bottom of the chart. The methodology used to determine the cracking probability classification is discussed in section 9.4.5. A green color corresponds to a low cracking probability classification, yellow to moderate, orange to high, and red to a very high cracking probability classification.

C-1.3.2 RESULTS SCREEN BUTTONS

The buttons found on the *Results* screen give the user choices on how to view and manipulate the calculated temperature data.

C-1.3.2.1 Show Comparison Chart

The *Show Comparison Chart* button displays a form that allows users to compare the results from different analysis runs as seen in Figure C 1-38. The *Show Comparison Chart* screen is to allow the user to compare calculated maximum temperatures, maximum temperature differences, cracking probability classifications, and chloride concentration levels at the steel from one model calculation run to another. Graphs comparing the results will also be displayed. The *Print Chart* button on the *Comparison Chart* screen will print the comparison chart results and charts on the *Comparison Chart*. A pdf report of the printout will be created when the user clicks on the *PDF Comparisons* button, and will prompt the user for a location to the save the pdf file. The user may name an analysis run by typing in a name under the *Series Name* textbox, selecting the number of the analysis run in the *Selected Analysis Number* input, and clicking on the *Update Series Name* button. When a user selects the *Delete Series* button, the analysis run number selected under the *Selected Analysis Number* will be deleted.

C-1.3.2.2 Export Temperature Data

To export the temperature data calculated, click on the *Export Temperature Data* button on the *Results* screen. *ConcreteWorks* saves the data in an ASCII text file when the extension .txt is used. *ConcreteWorks* will also save the data as an excel spreadsheet when the extension .xls is used. Data will be shown for discrete points in the member with time. The default file extension for data exported is ".xls".

C-1.3.2.3 Cross-Section to be Displayed

ConcreteWorks only displays data in the graphs from two dimensional cross-sections. When a footing temperature distribution is calculated in three dimensions, the user may change which cross-section is shown in the graphs by changing the *Cross-Section Number to be Displayed* value, and then clicking on the *Display new cross-section* button, as seen in Figure C 1-39. The *Mix Checks* values are calculated for the full three dimensional temperature distributions, however, and will not change when the *Display new cross-section* button is clicked. The temperature data exported when the *Export Temperature Data* button is clicked (as explained in Section C-1.3.2.2) only exports the temperature data from the two dimensional cross-section currently selected.

C-1.4 Program Features

C-1.4.1 PRINTING

While the *Results* screen is displayed, the user can print out the results and inputs entered in a report format.

C-1.4.1.1 Print

To print the report, click *Print* under the *File* menu.

C-1.4.1.2 Print Preview

To see of preview of the printed report, click *Print Preview* under the *File* menu, as seen in Figure C 1-40. The report may be printed from the *Print Preview* window by clicking on the *Print* button in the *Print Preview* window.

C-1.4.1.3 Page Setup

The *Page Setup* screen allows the user to select which graphs to print in the report. The *Page Setup* dialog can be opened by clicking on *Page Setup* under the *File* menu. If compressive strength parameters are not entered in the *Mechanical Properties* screen, then the *Compressive Strength* graph will not print, even if the user selects to print it on the *Page Setup* dialog. The *Page Setup* dialog can be seen in Figure C 1-41.

C-1.4.2 EXPORT

The *ConcreteWorks* inputs and results can be exported to a pdf file. The pdf file exported is similar to the printed reports. To make the pdf report, select “pdf” from the “Export to” option under the *File* menu. The software will then prompt the user for a location to save the pdf file. It may take a few minutes for the software to generate the pdf file. After the file has been generated and saved, *ConcreteWorks* will display a message that the pdf file was generated.

ConcreteWorks also contains an option to export the inputs to SiteManager™. SiteManager™ is an AASHTOWare® product used by several state departments of transportation. The export to SiteManager™ function in *ConcreteWorks* will create an xml file that can be used to import *ConcreteWorks* inputs into SiteManager™. For more information on the procedure to import the xml file generated by *ConcreteWorks*, contact the Texas Department of Transportation.

C-1.4.3 SAVE AS

To save the inputs entered in a new file, click *Save As* under the *File* menu. The default file extension for an inputs file is ".dat".

C-1.4.4 SAVE FILE

To save a currently opened file, click the *Save* button, or click *Save* under the *File* menu. If the *Save* button is clicked and the file has not previously been saved, the program will prompt for a name and location.

C-1.4.5 CHANGE DEFAULTS

Click the *Change Defaults* item under the *File* menu to change the default values used for inputs to custom values. All values entered in the *Change Defaults* screen are input in English units, but are displayed in the correct units in the inputs section of *ConcreteWorks* the next time a new file is opened. All units stay the same in the *Change Defaults* screen, except for the *a* and *b* strength parameters under the *Mechanical Properties* tab. The *a* and *b* parameters change units depending on the type of maturity function chosen under the same tab. The *Material Inputs* tab on the *Change Defaults* screen is seen on Figure C 1-42.

C-1.4.6 TOOLS MENU

The *Tools* menu contains a few options that increase the power and versatility of ConcreteWorks. The first is the analysis method used to calculate the cement chemical properties. To select the Bogue method of determining the cement composition, select *Bogue (ASTM C 150 2005)* under the *Cement Analysis Method* under the *Tools* menu. To select the Rietveld method of determining the cement chemistry, select *Rietveld* under the *Cement Analysis Method* under the *Tools* menu. Different equations are used to determine the concrete heat of hydration and early age concrete creep properties based on the cement analysis method selected, as explained in sections 9.3.1.5 and 9.4.4.1.

The specification used in the results check section can be changed by selecting the desired specification from the *Specifications Used* option under the *Tools* menu. *ConcreteWorks* currently only contains the 2004 specifications for the Texas Department of Transportation. If the *Basic ASR and DEF* specification is selected, *ConcreteWorks* will check to see if the predicted maximum temperature exceeds 158°F, and if the minimum amounts of SCMs prescribed by TxDOT in the 2004 specification are used. If the minimum amounts of SCMs are not used, then a warning that more investigations should be done is shown. Caution should be used in interpreting this check for alkali-silica reaction (ASR). Specifications that require the use of minimum amounts of supplementary cementing materials or maximum cement alkali levels to reduce the likelihood of ASR do not guarantee that this deleterious reaction will be prevented. Alkali silica reaction is highly dependent on the aggregate type, type and quantity of supplementary cementing materials, alkali loading, and exposure environment.

C-1.4.7 HELP MENU

The *Help* menu provides the user with useful information about the *ConcreteWorks* program.

C-1.4.7.1 About ConcreteWorks

When the user clicks on the *About ConcreteWorks* item under the *Help* menu, a splash screen appears with information on the *ConcreteWorks* version being used, a link to the official *ConcreteWorks* website, www.texasconcreteworks.com, and a button that shows the End-User License Agreement. When the link to the official *ConcreteWorks* website is clicked, *ConcreteWorks* uses Internet Explorer® to navigate to the website. This is the reason that Internet Explorer is required for using *ConcreteWorks* as described in Section C-1.1.1.

C-1.4.7.2 View User Manual

When the user clicks on the *View User Manual* item under the *Help* menu, the *ConcreteWorks* User Manual is opened as a new Adobe Reader® process. This is the reason that Adobe Reader® is required for using *ConcreteWorks* as described in Section C-1.1.1.

C-1.5 Input Sensitivities

ConcreteWorks asks the user to input a lot of data. To receive a correct answer, the user must enter correct data. Some of the data needed may be hard to obtain. Other data have less of an effect on the calculated results and performance of the model. This section contains some comments on these input sensitivities.

C-1.5.1 ENVIRONMENT INPUTS SENSITIVITY

All of the *Environment Inputs* directly affect the way heat is transferred to or from the concrete member to the surrounding environment. Of the four types of environmental inputs, the temperature inputs have the greatest impact on the resulting temperature distribution in the element. The relative humidity and cloud cover inputs have a moderate effect on the data. A percent cloud cover value within 30% is generally acceptable. The wind data can also have a moderate effect on the calculated temperatures.

C-1.5.2 RUN SPEED

The run speed of the program is one of the biggest concerns to many designers. The six biggest factors in the run speed of the program are:

1. The computer speed and computer RAM

2. Analysis duration – A 14-day duration takes longer to run than a 5 day duration. When a thermal stress analysis is performed, the analysis duration has a very large impact on the run time. Because of the numerical methods used, an analysis duration of 4 days may have a run time several times that of a 3 day analysis, instead of the expected 33% longer runtime.

3. Member size – the larger the element, the longer the run-time

4. Concrete age at form removal - the greater the time before form removal, the greater the run-time

5. Cure method after form removal - if a cure blanket is used after form removal, the run-time is longer
6. Three dimensional analysis greatly increases the run-time compared to a two dimensional analysis.

C-1.6 Troubleshooting

C-1.6.1 INSTALLATION PROBLEMS

If more than one version of the .NET Framework is installed, errors may occur during installation or when the *ConcreteWorks* is started. To resolve the issue, try deleting the folder containing the old version of the .NET Framework, usually found in the directory C:\WINDOWS\Microsoft.NET\Framework. Before installing or deleting any files or folders, make sure that the owner of the computer or appropriate network administrator is contacted to obtain permission and / or assistance.

C-1.6.2 SCREEN SETTINGS

The screen settings on the computer running *ConcreteWorks* may adjust the programs appearance. Some of the buttons may be cut off or not visible. The problem may be corrected by either manually resizing the program windows or adjusting the screen settings on the computer. To adjust the screen settings on the computer, open up the display settings window by right clicking on the desktop. Then click on the *Settings* tab. Then adjust the screen resolution for optimal software viewing.

C-1.7 Acknowledgements

This program was made possible through funding provided by the Texas Department of Transportation. The advice of the following individuals is appreciated: Ralph Brown, Tyler Ley, Moon Won, Brian Merrill, Charles Gaskin, David Head, Doug Beer, J.C. Liu, John Vogel, and Tom Yarbrough.

Table C 1-1- Values deemed questionable by ConcreteWorks

Input	If the input is less than this value	If the input is greater than this value
Rectangular Column Width or Depth	3'	30'
Rectangular Footing Width, Length or Depth	3'	90'
Rectangular Bent Cap Width or Depth	3'	30'
T Shaped Bent Cap Width	3'	15'
T Shaped Bent Cap Height	3'	15'
Circular Column Diameter	3'	15'
Cement Content	100#	1200#
Water Content	100#	1200#
Coarse Aggregate Content	100#	4000#
Fine Aggregate Content	100#	4000#
Air Content	0%	10%
Class C Fly Ash Content	0#	1200#
Class C Fly Ash CaO	20%	30%
Class F Fly Ash Content	0#	1200#
Class F Fly Ash CaO	0%	20%
Slag Content	0#	1200#
Silica Fume Content	0#	1200#
Ultra Fine Fly Ash	0#	1200#
Any Bogue Compound Content	0%	100%
Any Bogue Compound that does not meet ASTM C 150		
C_3A	1%	
Blaine Fineness	280(m^2/kg)	1000(m^2/kg)
Alkali Content	0%	100%

Fresh Concrete Placement Temperature	32°F	212°F
PCC age at form removal	0 hrs	
Delay between removing forms and cure method application	0	
Hydration Parameter alpha	0	1

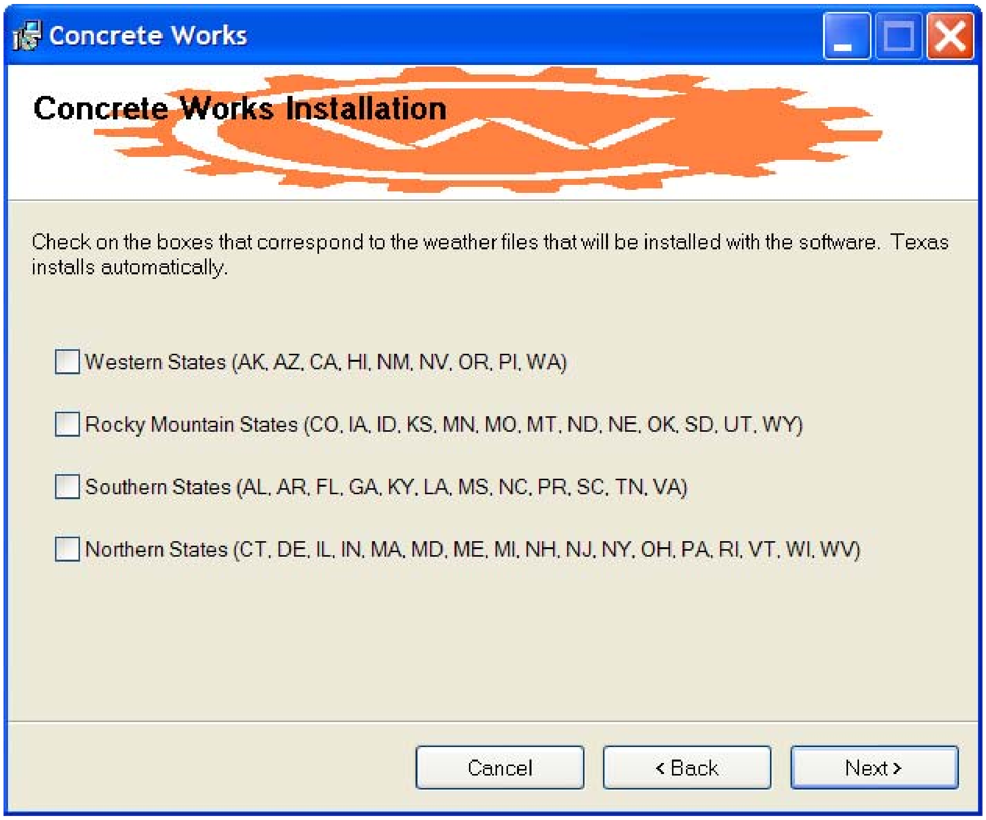

Check on the boxes that correspond to the weather files that will be installed with the software. Texas installs automatically.

☐ Western States (AK, AZ, CA, HI, NM, NV, OR, PI, WA)

☐ Rocky Mountain States (CO, IA, ID, KS, MN, MO, MT, ND, NE, OK, SD, UT, WY)

☐ Southern States (AL, AR, FL, GA, KY, LA, MS, NC, PR, SC, TN, VA)

☐ Northern States (CT, DE, IL, IN, MA, MD, ME, MI, NH, NJ, NY, OH, PA, RI, VT, WI, WV)

Figure C 1-1- Installation screen three, which weather files to install

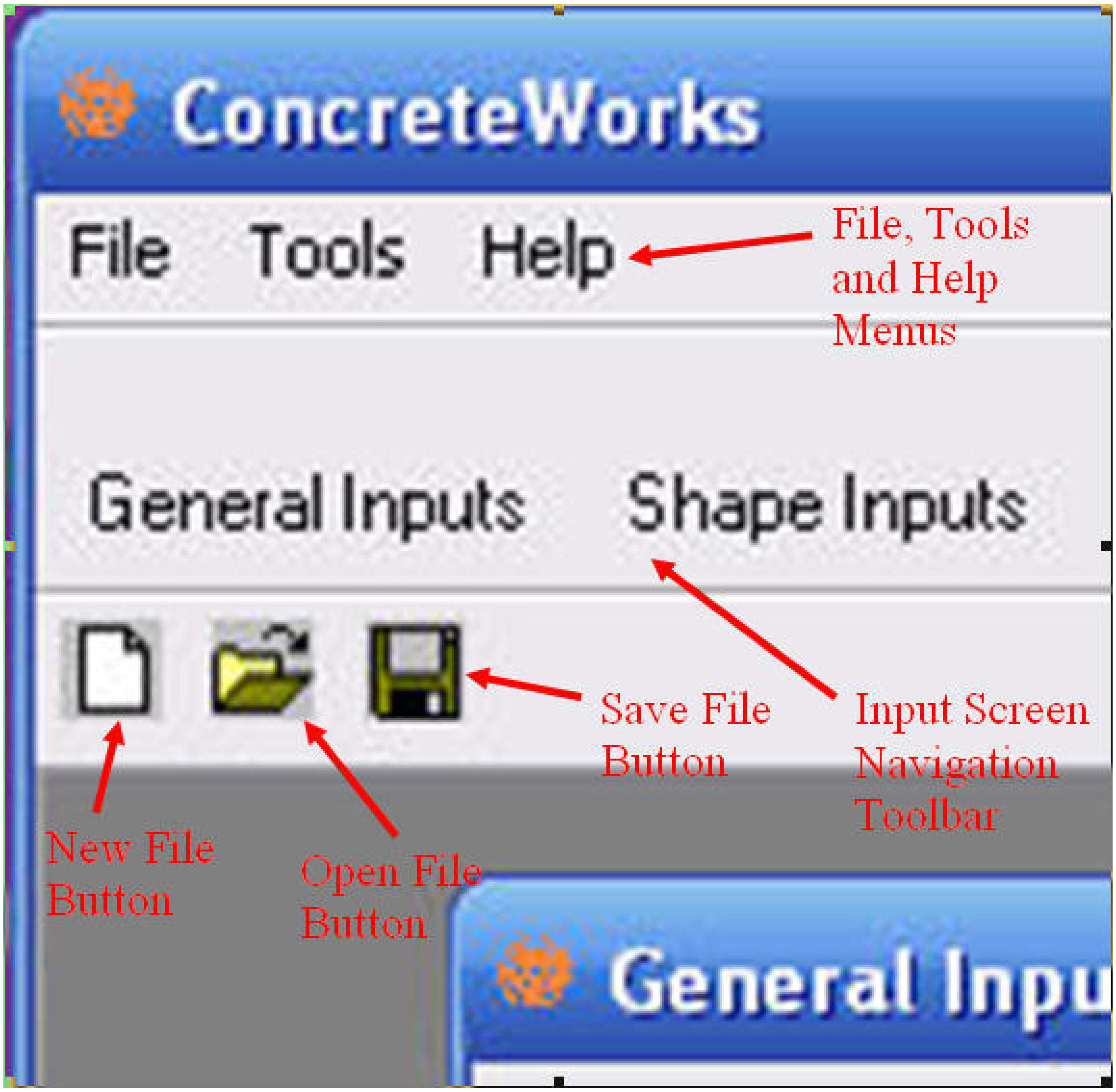

Figure C 1-2 - Close up view of toolbars and menus

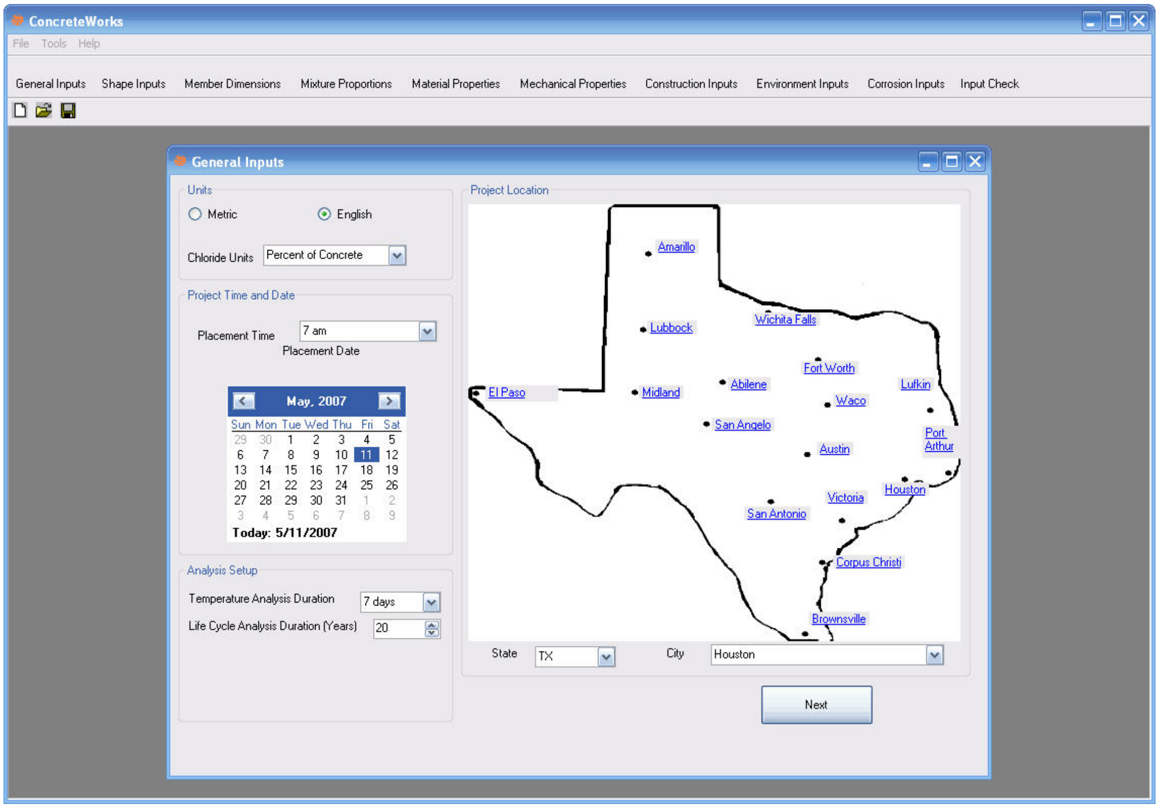

Units

○ Metric ● English

Chloride Units: Percent of Concrete

Project Time and Date

Placement Time: 7 am

Placement Date

Sun	Mon	Tue	Wed	Thu	Fri	Sat
29	30	1	2	3	4	5
6	7	8	9	10	11	12
13	14	15	16	17	18	19
20	21	22	23	24	25	26
27	28	29	30	31	1	2
3	4	5	6	7	8	9

May, 2007

Today: 5/11/2007

Analysis Setup

Temperature Analysis Duration: 7 days

Life Cycle Analysis Duration (Years): 20

Project Location

State: TX

City: Houston

Figure C 1-3 - *General Inputs* screen

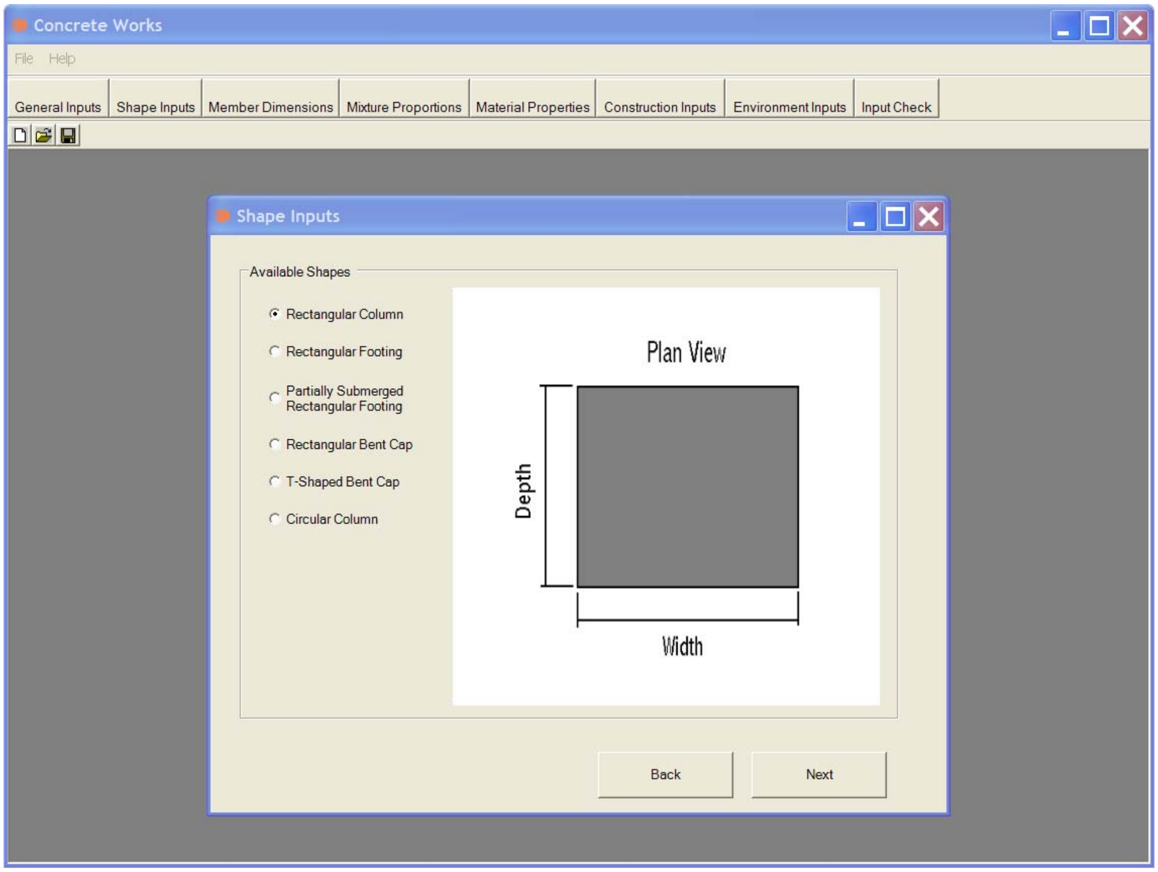

● Rectangular Column
○ Rectangular Footing
○ Partially Submerged Rectangular Footing
○ Rectangular Bent Cap
○ T-Shaped Bent Cap
○ Circular Column

Figure C 1-4 - *Shape Inputs* screen for mass concrete member types

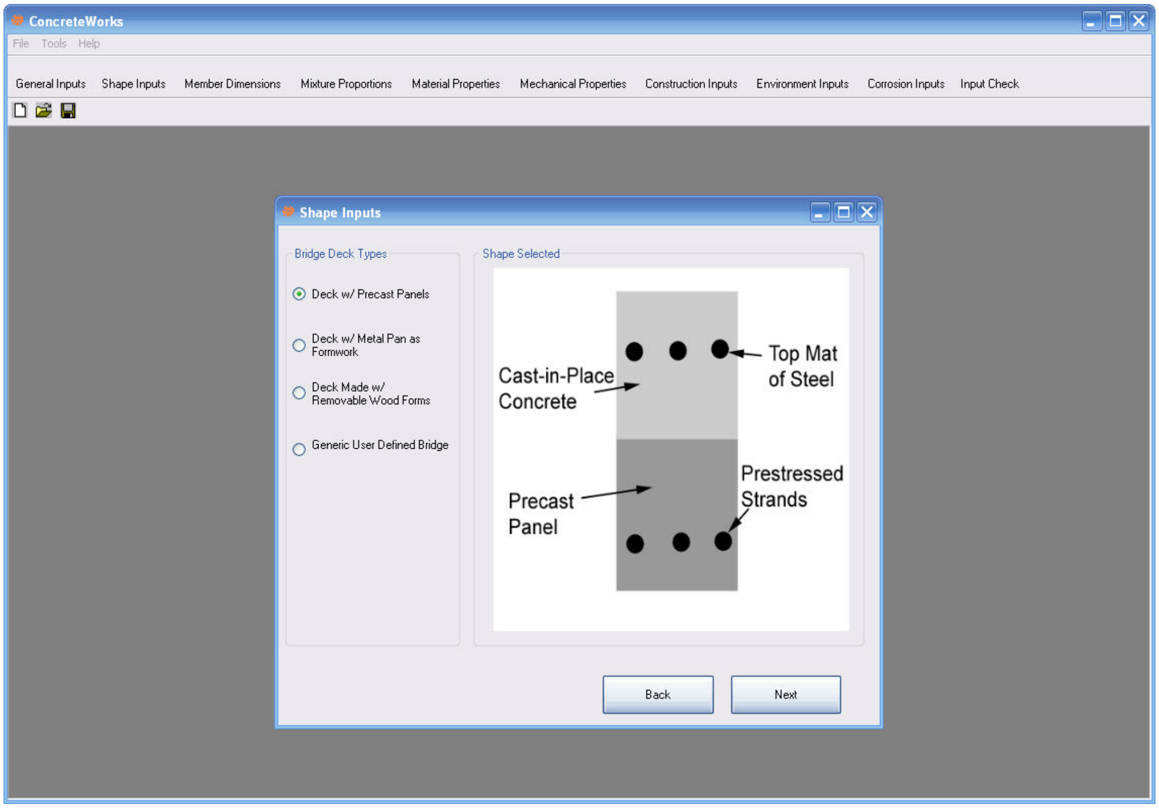

Bridge Deck Types

● Deck w/ Precast Panels

○ Deck w/ Metal Pan as Formwork

○ Deck Made w/ Removable Wood Forms

○ Generic User Defined Bridge

Figure C 1-5 - Shape Inputs screen for bridge deck member types

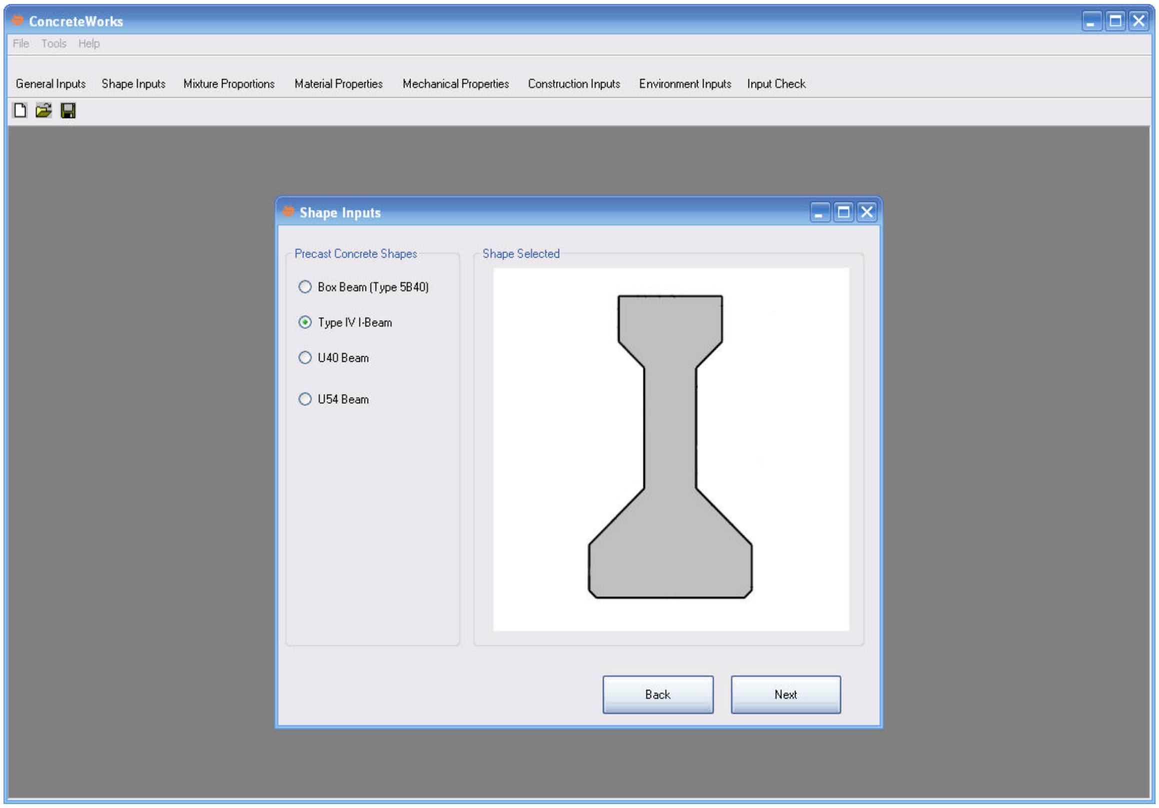

Precast Concrete Shapes

○ Box Beam (Type 5B40)
● Type IV I-Beam
○ U40 Beam
○ U54 Beam

Figure C 1-6 - Shape Inputs screen for precast beam member types

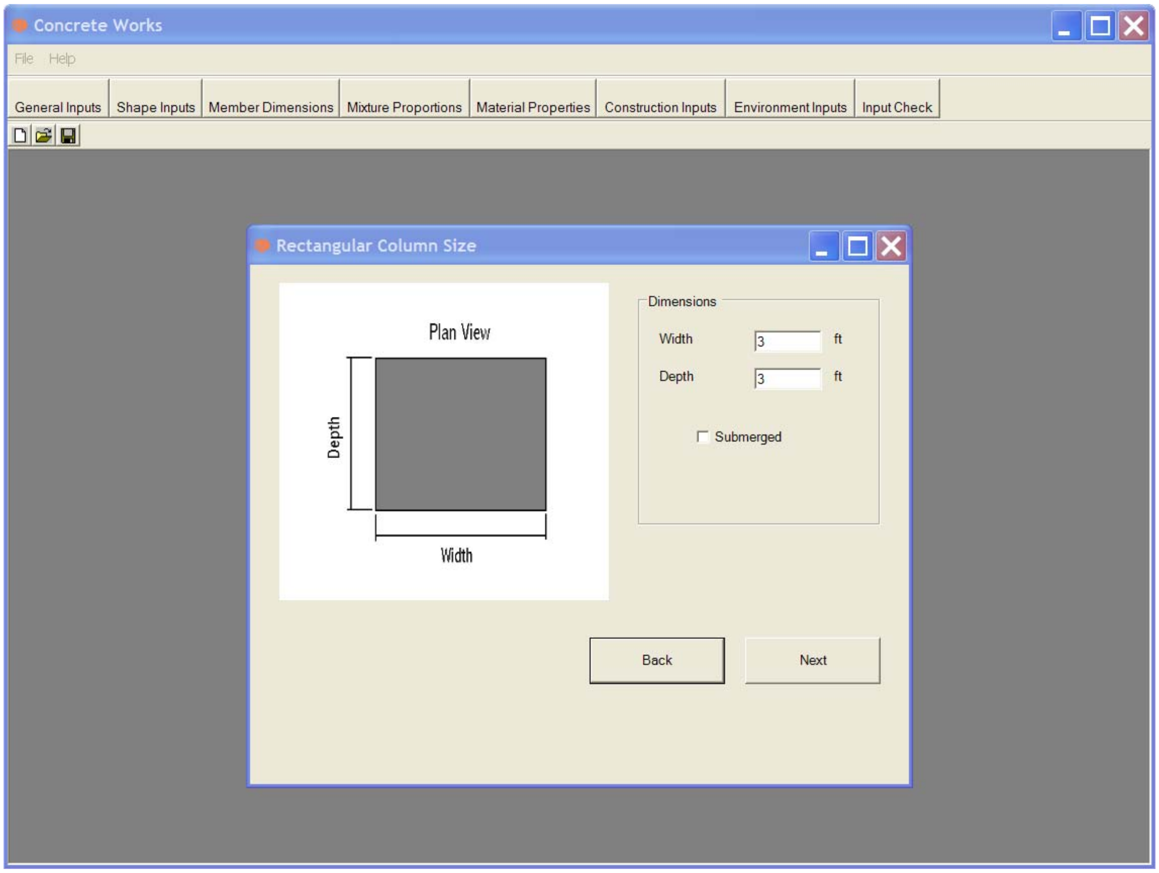

Dimensions

Width 3 ft

Depth 3 ft

☐ Submerged

Figure C 1-7 - *Member Dimensions* screen for the Rectangular Column element

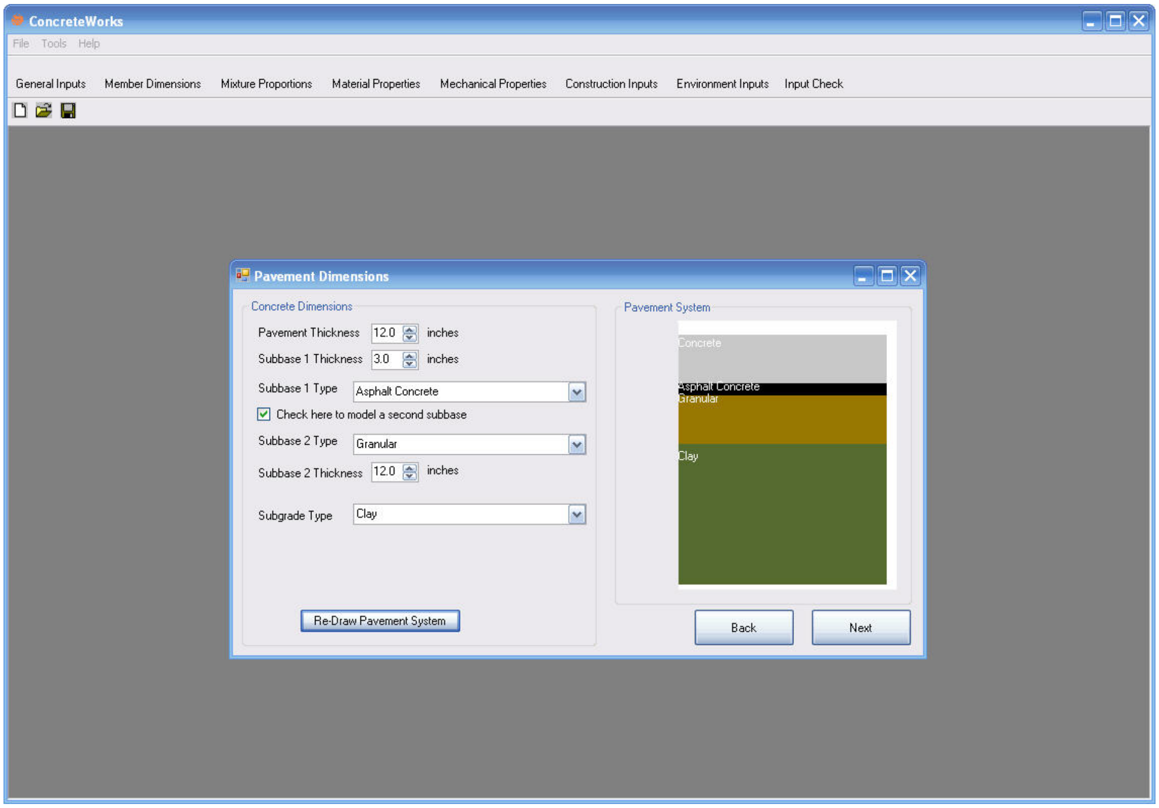

Concrete Dimensions

Pavement Thickness 12.0 inches

Subbase 1 Thickness 3.0 inches

Subbase 1 Type Asphalt Concrete

☑ Check here to model a second subbase

Subbase 2 Type Granular

Subbase 2 Thickness 12.0 inches

Subgrade Type Clay

Figure C 1-8 - Pavement Dimensions Input Screen

Figure C 1-9 - Example of a footing that would use the *Soil on the Sides* option

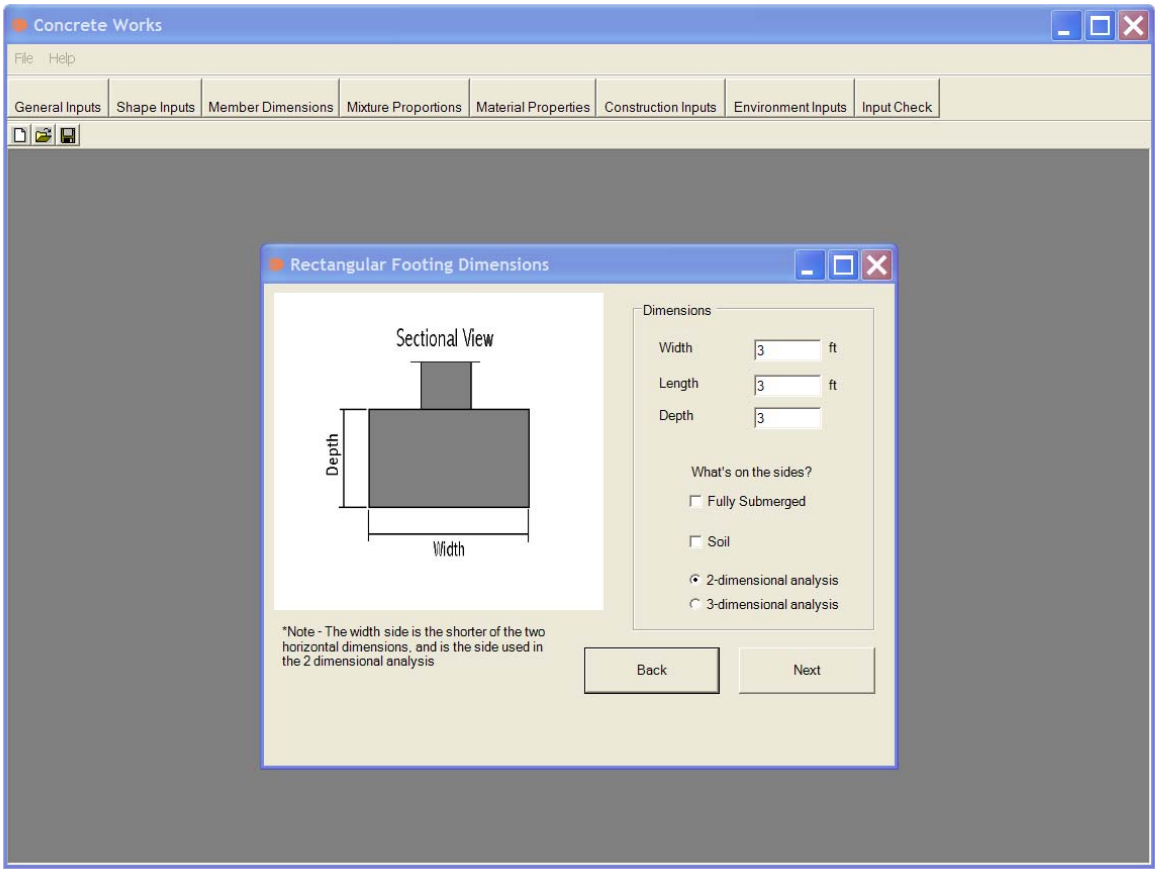

Dimensions

Width 3 ft

Length 3 ft

Depth 3

What's on the sides?

☐ Fully Submerged

☐ Soil

● 2-dimensional analysis

○ 3-dimensional analysis

*Note - The width side is the shorter of the two horizontal dimensions, and is the side used in the 2 dimensional analysis

Figure C 1-10 - *Rectangular Footing* screen with Two Dimensional Analysis Selected

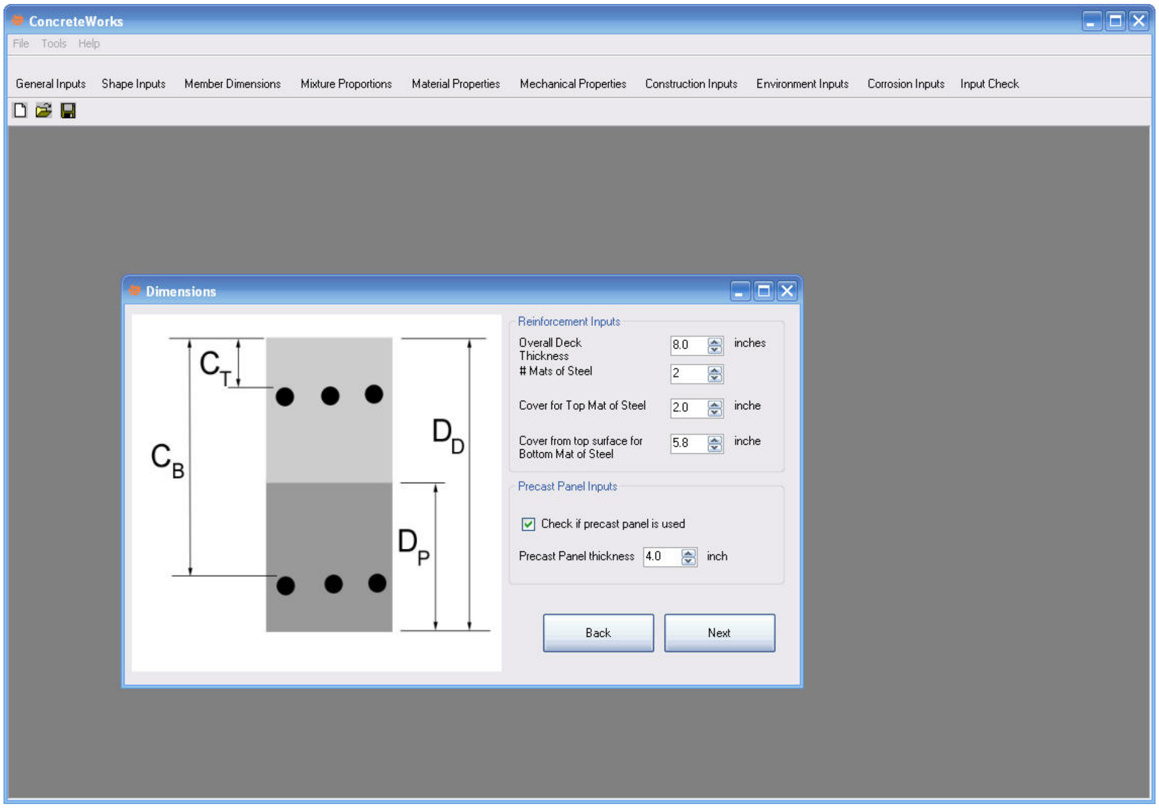

Reinforcement Inputs

Overall Deck Thickness 8.0 inches

Mats of Steel 2

Cover for Top Mat of Steel 2.0 inche

Cover from top surface for Bottom Mat of Steel 5.8 inche

Precast Panel Inputs

☑ Check if precast panel is used

Precast Panel thickness 4.0 inch

Figure C 1-11 - Bridge Deck Dimensions Input Screen when the Generic User Defined Bridge Deck Type is Selected

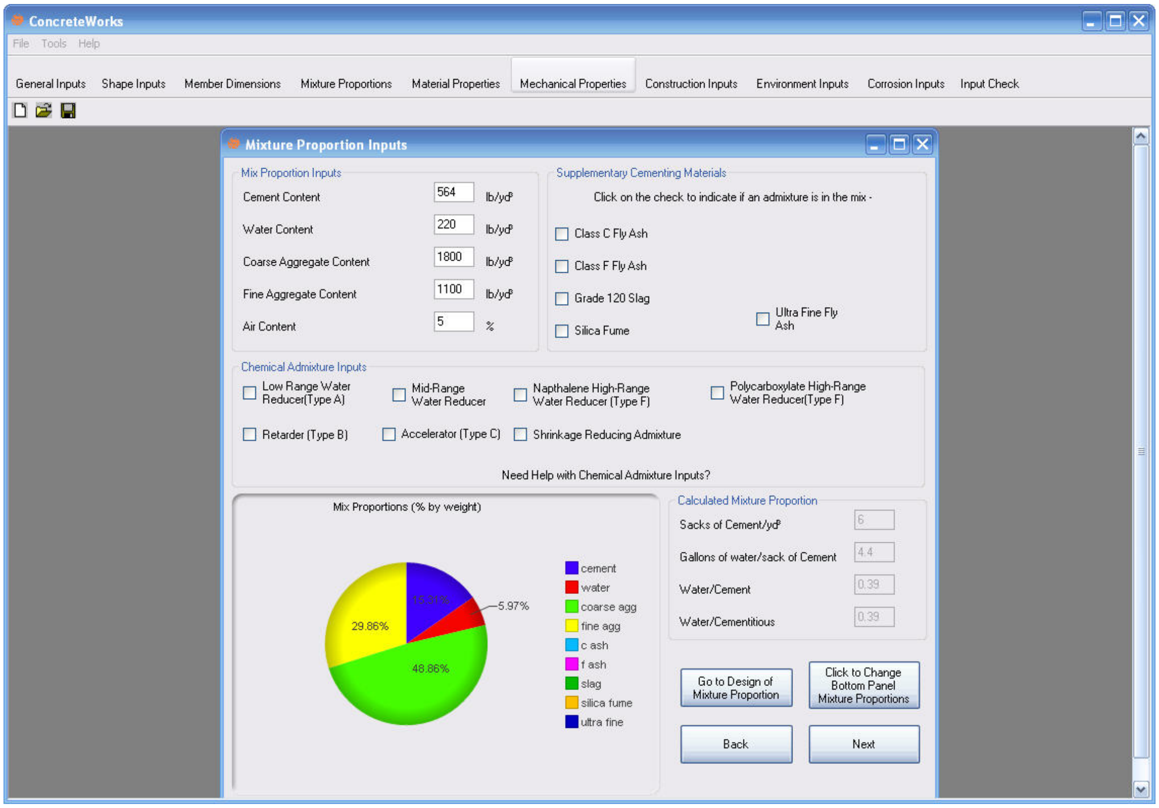

Mix Proportion Inputs

Cement Content	564	lb/yd³
Water Content	220	lb/yd³
Coarse Aggregate Content	1800	lb/yd³
Fine Aggregate Content	1100	lb/yd³
Air Content	5	%

Supplementary Cementing Materials

Click on the check to indicate if an admixture is in the mix -

☐ Class C Fly Ash
☐ Class F Fly Ash
☐ Grade 120 Slag
☐ Silica Fume
☐ Ultra Fine Fly Ash

Chemical Admixture Inputs

☐ Low Range Water Reducer(Type A)
☐ Mid-Range Water Reducer
☐ Napthalene High-Range Water Reducer (Type F)
☐ Polycarboxylate High-Range Water Reducer(Type F)
☐ Retarder (Type B)
☐ Accelerator (Type C)
☐ Shrinkage Reducing Admixture

Need Help with Chemical Admixture Inputs?

Calculated Mixture Proportion

Sacks of Cement/yd³	6
Gallons of water/sack of Cement	4.4
Water/Cement	0.39
Water/Cementitious	0.39

Figure C 1-12 - *Mixture Proportion Inputs* Screen when a Bridge Deck Member Type is Selected with Precast Panels

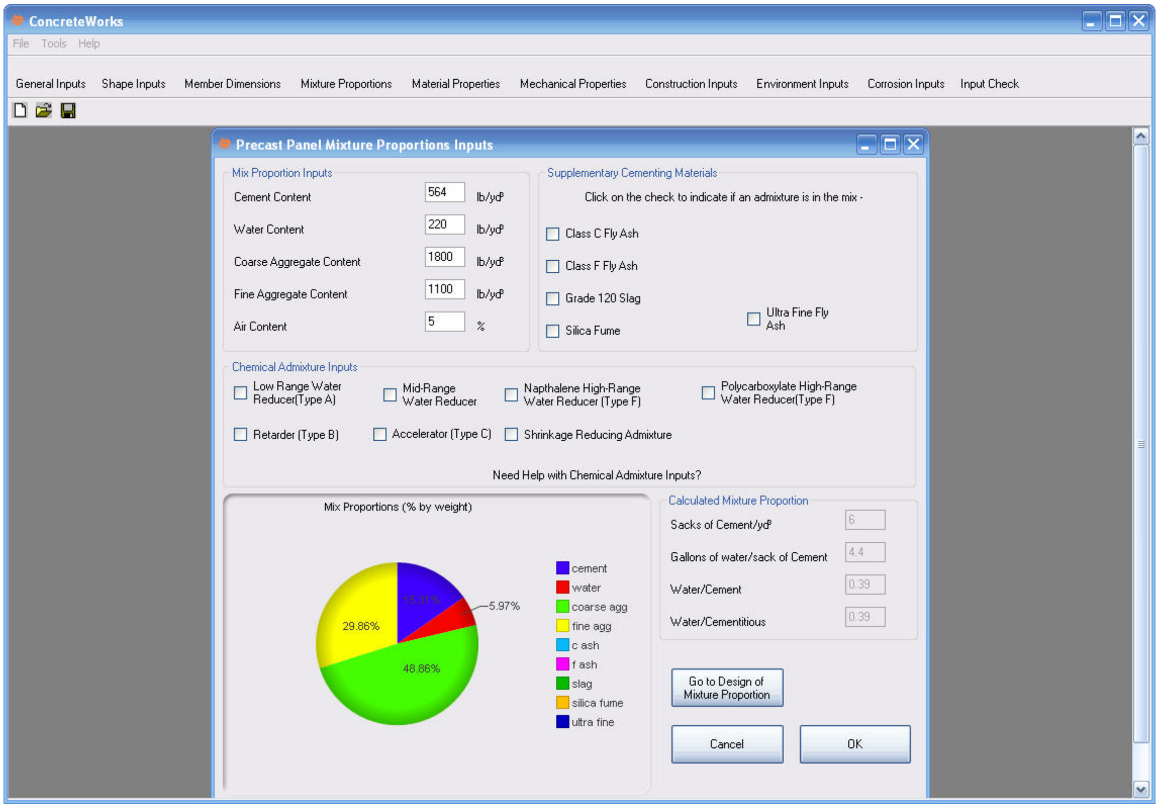

Mix Proportion Inputs

Cement Content 564 lb/yd^3

Water Content 220 lb/yd^3

Coarse Aggregate Content 1800 lb/yd^3

Fine Aggregate Content 1100 lb/yd^3

Air Content 5 %

Supplementary Cementing Materials

Click on the check to indicate if an admixture is in the mix -

☐ Class C Fly Ash

☐ Class F Fly Ash

☐ Grade 120 Slag

☐ Silica Fume

☐ Ultra Fine Fly Ash

Chemical Admixture Inputs

☐ Low Range Water Reducer(Type A)

☐ Mid-Range Water Reducer

☐ Napthalene High-Range Water Reducer (Type F)

☐ Polycarboxylate High-Range Water Reducer(Type F)

☐ Retarder (Type B)

☐ Accelerator (Type C)

☐ Shrinkage Reducing Admixture

Need Help with Chemical Admixture Inputs?

Calculated Mixture Proportion

Sacks of Cement/yd^3 6

Gallons of water/sack of Cement 4.4

Water/Cement 0.39

Water/Cementitious 0.39

Figure C 1-13 - Precast Panel Mixture Proportions Inputs Screen

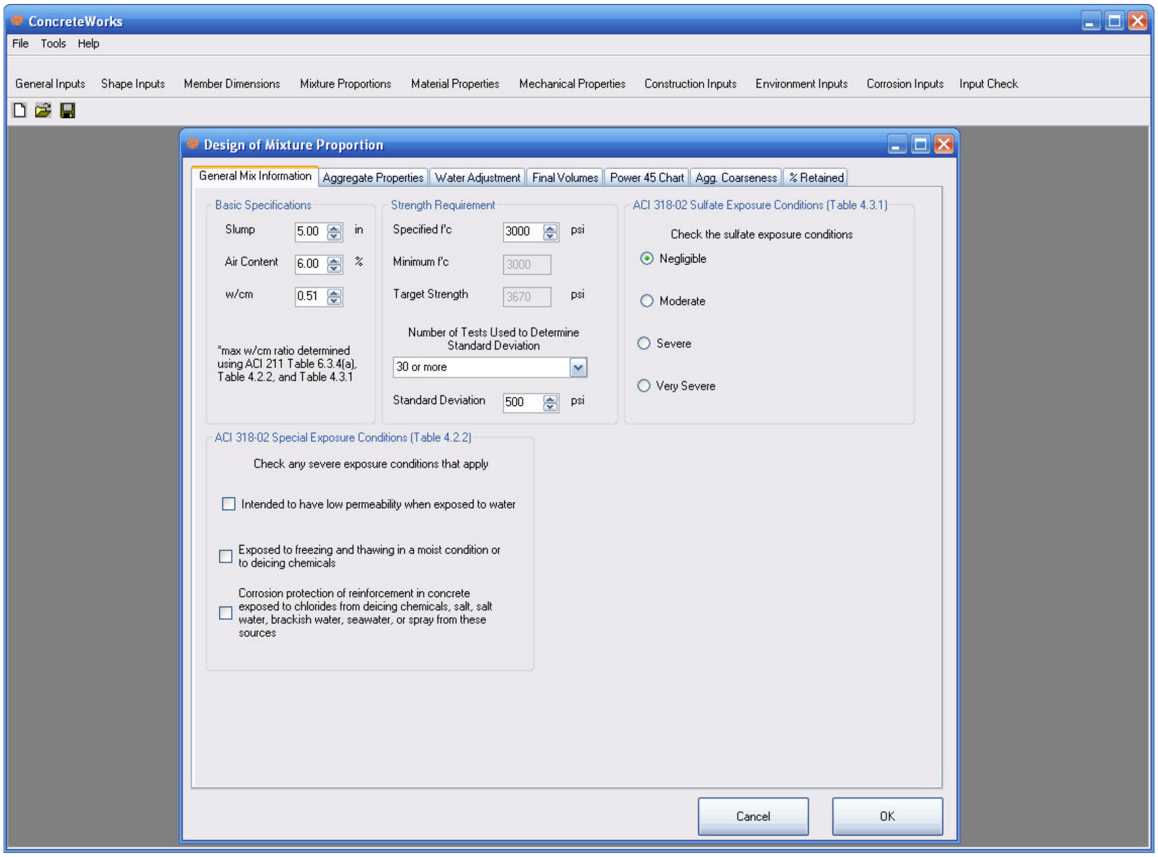

Basic Specifications

Slump 5.00 in

Air Content 6.00 %

w/cm 0.51

*max w/cm ratio determined using ACI 211 Table 6.3.4(a), Table 4.2.2, and Table 4.3.1

Strength Requirement

Specified f'c 3000 psi

Minimum f'c 3000

Target Strength 3670 psi

Number of Tests Used to Determine Standard Deviation: 30 or more

Standard Deviation 500 psi

ACI 318-02 Sulfate Exposure Conditions (Table 4.3.1)

Check the sulfate exposure conditions

● Negligible

○ Moderate

○ Severe

○ Very Severe

ACI 318-02 Special Exposure Conditions (Table 4.2.2)

Check any severe exposure conditions that apply

☐ Intended to have low permeability when exposed to water

☐ Exposed to freezing and thawing in a moist condition or to deicing chemicals

☐ Corrosion protection of reinforcement in concrete exposed to chlorides from deicing chemicals, salt, salt water, brackish water, seawater, or spray from these sources

Figure C 1-14 - *Design of Mixture Proportion* Screen - General Mix Information Inputs

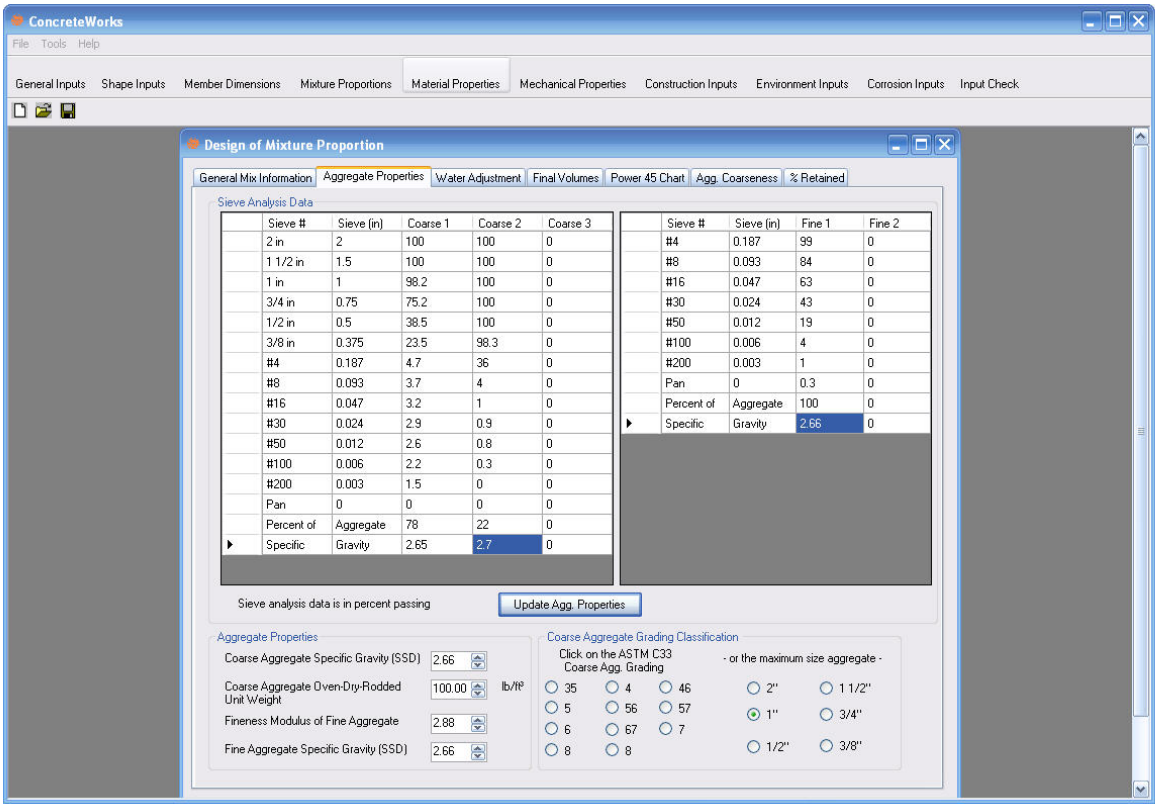

Sieve Analysis Data

	Sieve #	Sieve (in)	Coarse 1	Coarse 2	Coarse 3
	2 in	2	100	100	0
	1 1/2 in	1.5	100	100	0
	1 in	1	98.2	100	0
	3/4 in	0.75	75.2	100	0
	1/2 in	0.5	38.5	100	0
	3/8 in	0.375	23.5	98.3	0
	#4	0.187	4.7	36	0
	#8	0.093	3.7	4	0
	#16	0.047	3.2	1	0
	#30	0.024	2.9	0.9	0
	#50	0.012	2.6	0.8	0
	#100	0.006	2.2	0.3	0
	#200	0.003	1.5	0	0
	Pan	0	0	0	0
	Percent of	Aggregate	78	22	0
▶	Specific	Gravity	2.65	2.7	0

	Sieve #	Sieve (in)	Fine 1	Fine 2
	#4	0.187	99	0
	#8	0.093	84	0
	#16	0.047	63	0
	#30	0.024	43	0
	#50	0.012	19	0
	#100	0.006	4	0
	#200	0.003	1	0
	Pan	0	0.3	0
	Percent of	Aggregate	100	0
▶	Specific	Gravity	2.66	0

Sieve analysis data is in percent passing

Aggregate Properties

Coarse Aggregate Specific Gravity (SSD) 2.66
Coarse Aggregate Oven-Dry-Rodded Unit Weight 100.00 lb/ft³
Fineness Modulus of Fine Aggregate 2.88
Fine Aggregate Specific Gravity (SSD) 2.66

Coarse Aggregate Grading Classification

Click on the ASTM C33 Coarse Agg. Grading
○ 35 ○ 4 ○ 46
○ 5 ○ 56 ○ 57
○ 6 ○ 67 ○ 7
○ 8 ○ 8

- or the maximum size aggregate -
○ 2" ○ 1 1/2"
● 1" ○ 3/4"
○ 1/2" ○ 3/8"

Figure C 1-15 - Aggregate Properties Tab on the Design of Mixture Proportions Inputs Screen

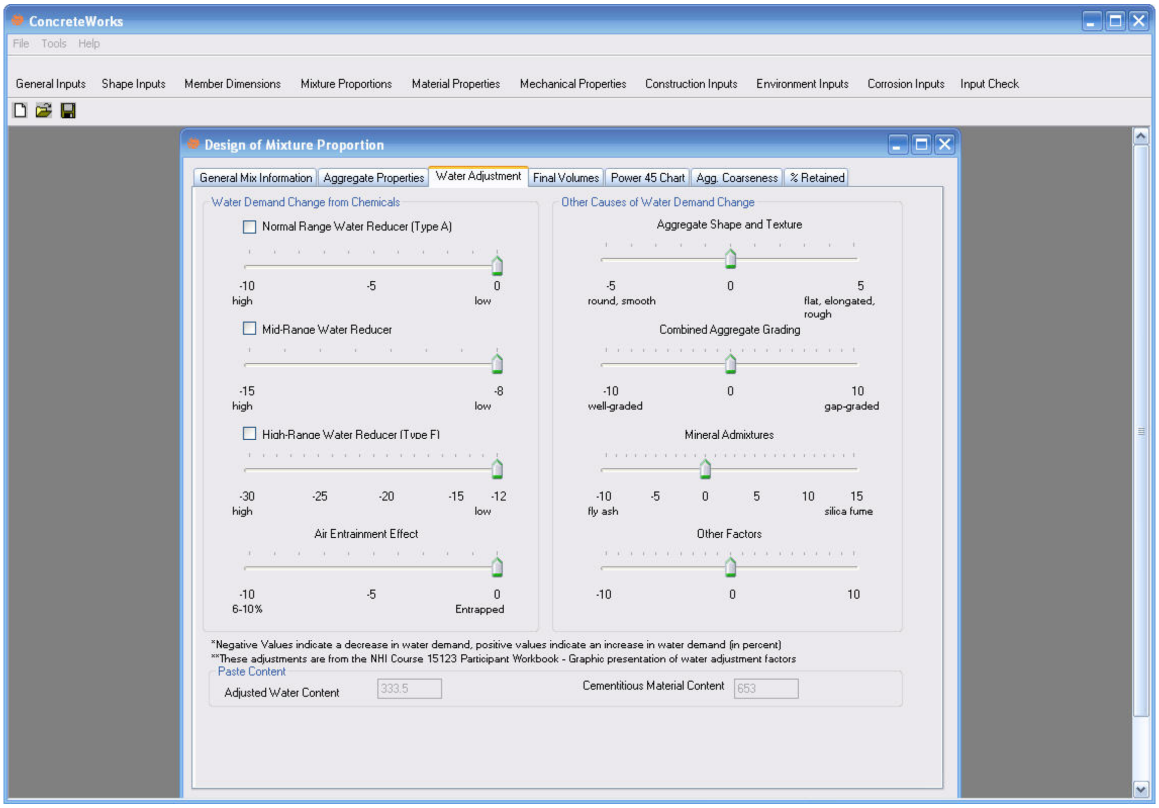

☐ Normal Range Water Reducer (Type A)

☐ Mid-Range Water Reducer

☐ High-Range Water Reducer (Type F)

*Negative Values indicate a decrease in water demand, positive values indicate an increase in water demand (in percent)

**These adjustments are from the NHI Course 15123 Participant Workbook - Graphic presentation of water adjustment factors

Adjusted Water Content: 333.5

Cementitious Material Content: 653

Figure C 1-16 - ***Water Adjustment*** **tab on the** ***Design of Mixture Proportion*** **screen**

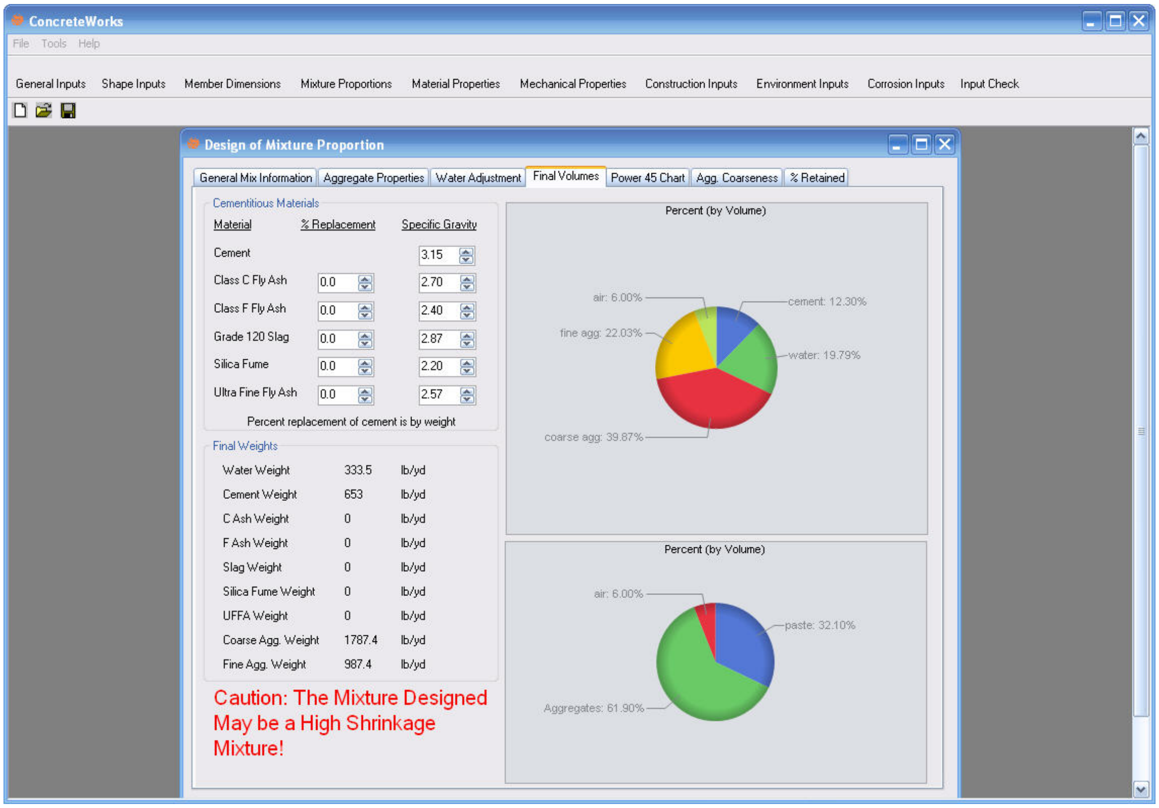

Cementitious Materials

Material	% Replacement	Specific Gravity
Cement		3.15
Class C Fly Ash	0.0	2.70
Class F Fly Ash	0.0	2.40
Grade 120 Slag	0.0	2.87
Silica Fume	0.0	2.20
Ultra Fine Fly Ash	0.0	2.57

Percent replacement of cement is by weight

Final Weights

Water Weight	333.5	lb/yd
Cement Weight	653	lb/yd
C Ash Weight	0	lb/yd
F Ash Weight	0	lb/yd
Slag Weight	0	lb/yd
Silica Fume Weight	0	lb/yd
UFFA Weight	0	lb/yd
Coarse Agg. Weight	1787.4	lb/yd
Fine Agg. Weight	987.4	lb/yd

Caution: The Mixture Designed May be a High Shrinkage Mixture!

Figure C 1-17 - ***Final Volume*** **tab of the** ***Design of Mixture Proportion*** **screen**

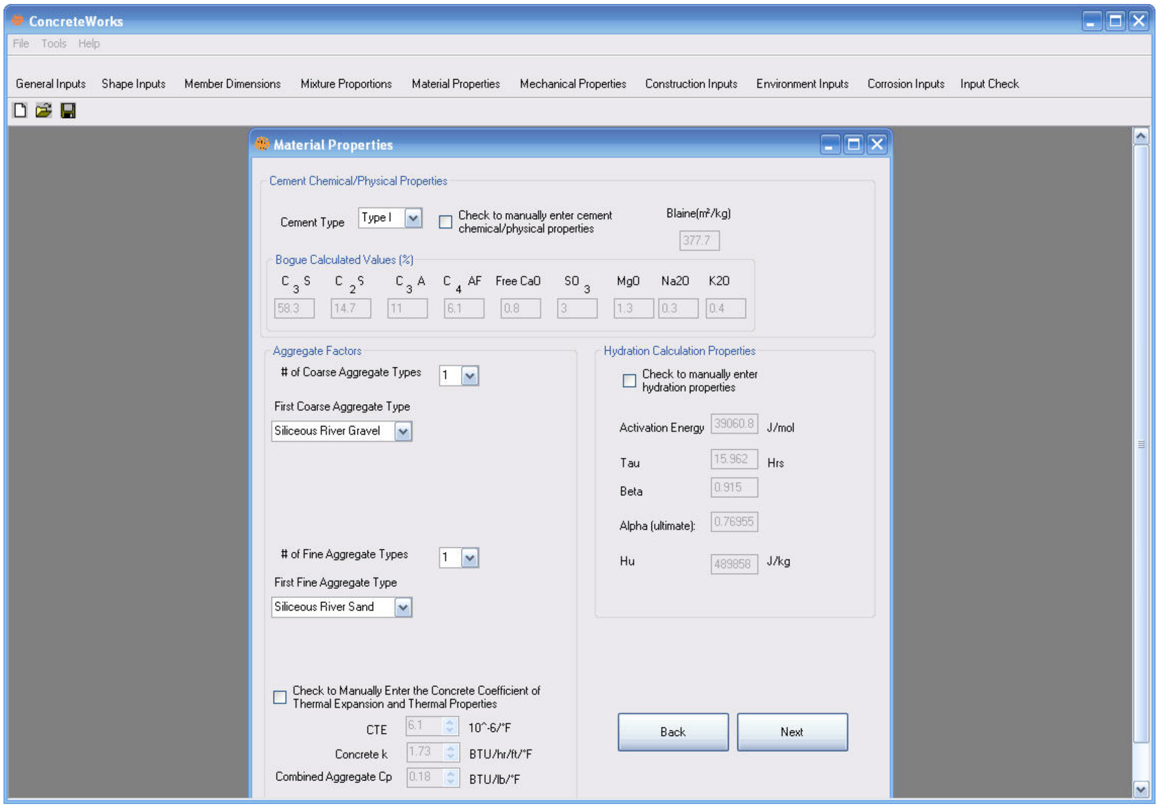

Cement Chemical/Physical Properties

Cement Type: Type I

☐ Check to manually enter cement chemical/physical properties

Blaine(m²/kg): 377.7

Bogue Calculated Values (%)

C_3S	C_2S	C_3A	C_4AF	Free CaO	SO_3	MgO	Na2O	K2O
58.3	14.7	11	6.1	0.8	3	1.3	0.3	0.4

Aggregate Factors

\# of Coarse Aggregate Types: 1

First Coarse Aggregate Type: Siliceous River Gravel

\# of Fine Aggregate Types: 1

First Fine Aggregate Type: Siliceous River Sand

☐ Check to Manually Enter the Concrete Coefficient of Thermal Expansion and Thermal Properties

CTE: 6.1 10^-6/°F

Concrete k: 1.73 BTU/hr/ft/°F

Combined Aggregate Cp: 0.18 BTU/lb/°F

Hydration Calculation Properties

☐ Check to manually enter hydration properties

Activation Energy: 39060.8 J/mol

Tau: 15.962 Hrs

Beta: 0.915

Alpha (ultimate): 0.76955

Hu: 489858 J/kg

Figure C 1-18 - *Material Properties* screen

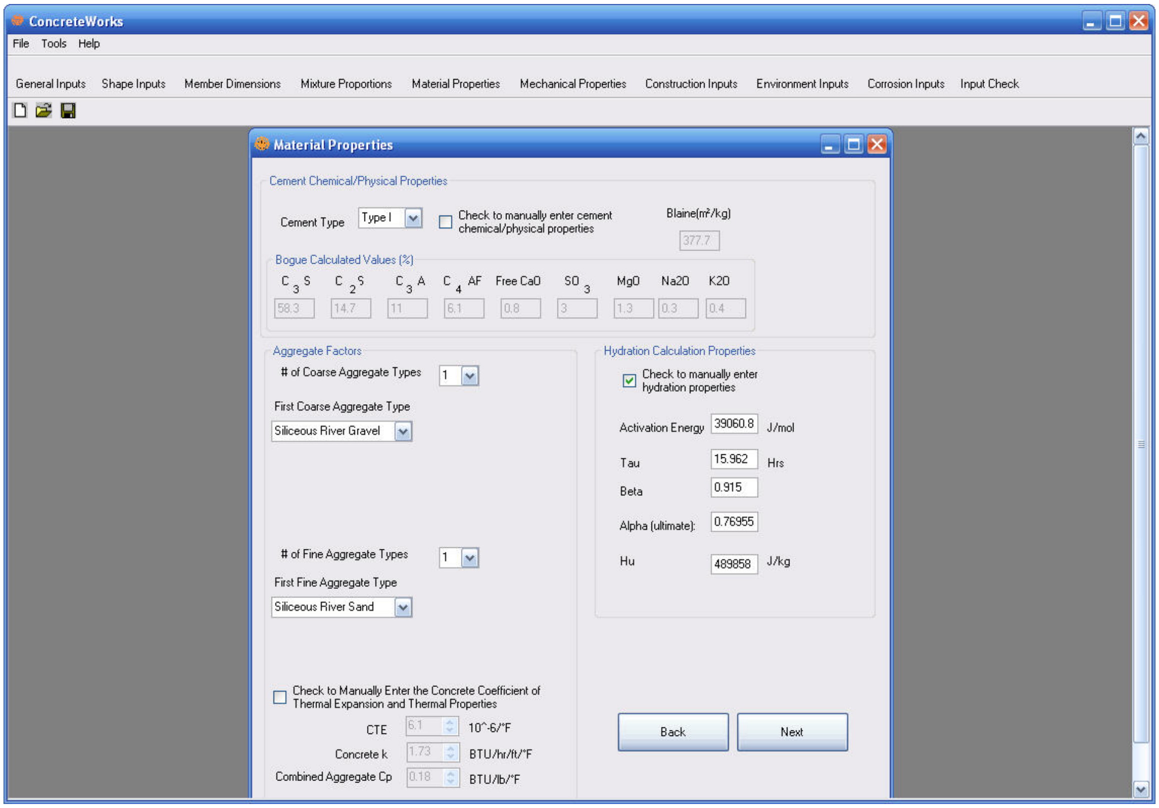

Cement Chemical/Physical Properties

Cement Type: Type I

☐ Check to manually enter cement chemical/physical properties

Blaine(m²/kg): 377.7

Bogue Calculated Values (%)

C_3S	C_2S	C_3A	C_4AF	Free CaO	SO_3	MgO	Na2O	K2O
58.3	14.7	11	6.1	0.8	3	1.3	0.3	0.4

Aggregate Factors

# of Coarse Aggregate Types: 1

First Coarse Aggregate Type: Siliceous River Gravel

# of Fine Aggregate Types: 1

First Fine Aggregate Type: Siliceous River Sand

☐ Check to Manually Enter the Concrete Coefficient of Thermal Expansion and Thermal Properties

CTE: 6.1 10^-6/°F

Concrete k: 1.73 BTU/hr/ft/°F

Combined Aggregate Cp: 0.18 BTU/lb/°F

Hydration Calculation Properties

☑ Check to manually enter hydration properties

Activation Energy: 39060.8 J/mol

Tau: 15.962 Hrs

Beta: 0.915

Alpha (ultimate): 0.76955

Hu: 489858 J/kg

Figure C 1-19 - ***Material Inputs*** **screen with manual adjustment checkboxes checked**

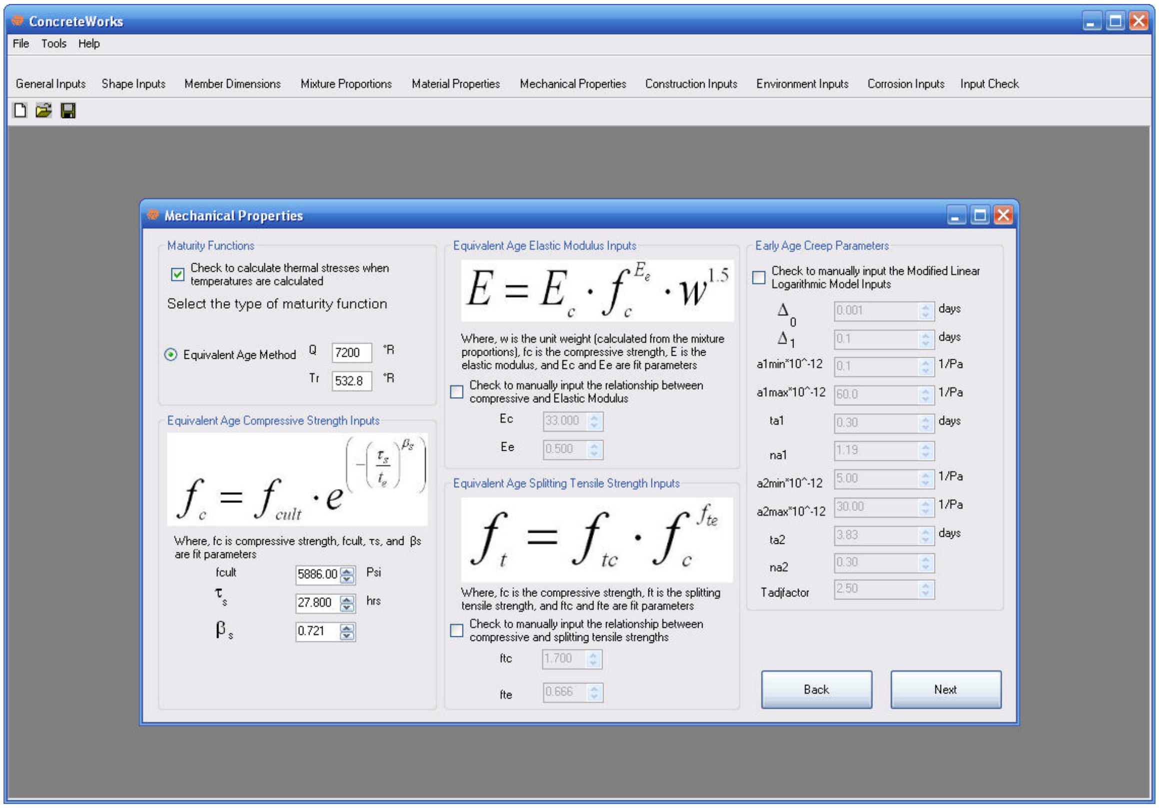

Maturity Functions

☑ Check to calculate thermal stresses when temperatures are calculated

Select the type of maturity function

● Equivalent Age Method

Q 7200 °R

Tr 532.8 °R

Equivalent Age Compressive Strength Inputs

$$f_c = f_{cult} \cdot e^{\left(-\left(\frac{\tau_s}{t_e}\right)^{\beta_s}\right)}$$

Where, fc is compressive strength, fcult, τs, and βs are fit parameters

fcult 5886.00 Psi

τ_s 27.800 hrs

β_s 0.721

Equivalent Age Elastic Modulus Inputs

$$E = E_c \cdot f_c^{E_e} \cdot w^{1.5}$$

Where, w is the unit weight (calculated from the mixture proportions), fc is the compressive strength, E is the elastic modulus, and Ec and Ee are fit parameters

☐ Check to manually input the relationship between compressive and Elastic Modulus

Ec 33.000

Ee 0.500

Equivalent Age Splitting Tensile Strength Inputs

$$f_t = f_{tc} \cdot f_c^{f_{te}}$$

Where, fc is the compressive strength, ft is the splitting tensile strength, and ftc and fte are fit parameters

☐ Check to manually input the relationship between compressive and splitting tensile strengths

ftc 1.700

fte 0.666

Early Age Creep Parameters

☐ Check to manually input the Modified Linear Logarithmic Model Inputs

Δ_0 0.001 days

Δ_1 0.1 days

a1min*10^-12 0.1 1/Pa

a1max*10^-12 60.0 1/Pa

ta1 0.30 days

na1 1.19

a2min*10^-12 5.00 1/Pa

a2max*10^-12 30.00 1/Pa

ta2 3.83 days

na2 0.30

Tadjfactor 2.50

Figure C 1-20 - Mechanical Properties Inputs

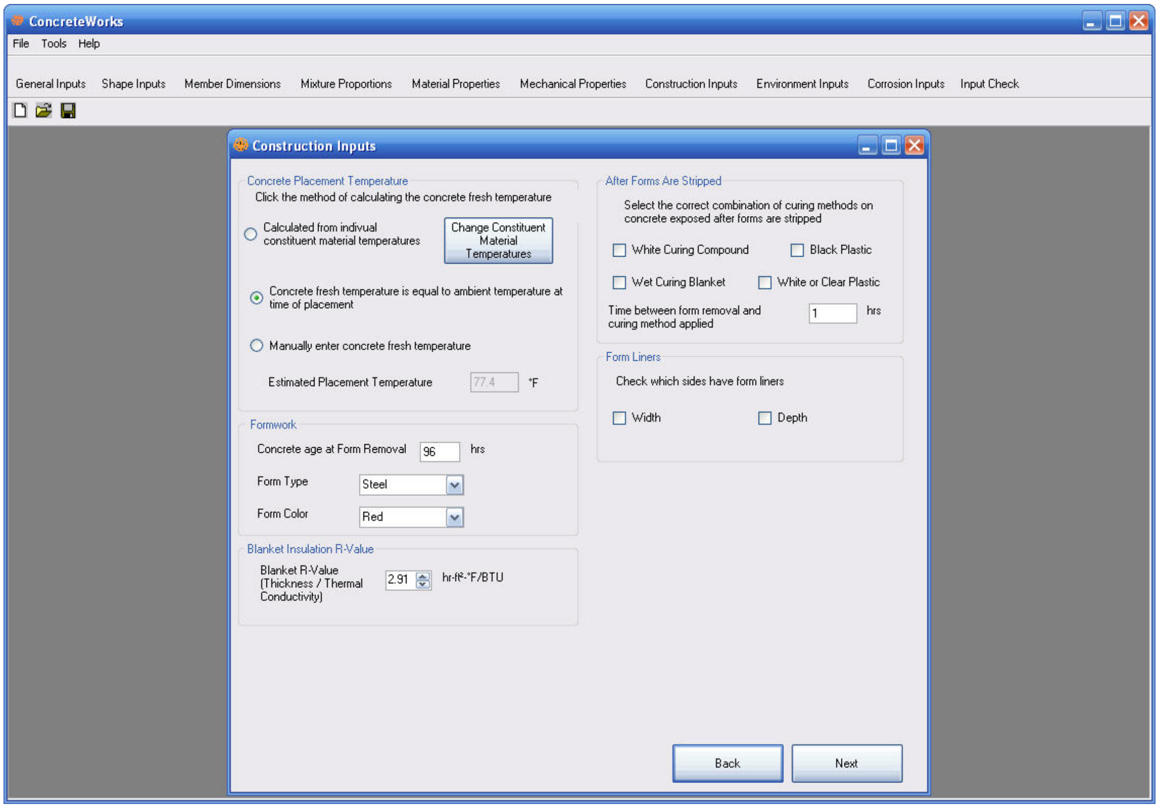

Concrete Placement Temperature

Click the method of calculating the concrete fresh temperature

○ Calculated from indivual constituent material temperatures

● Concrete fresh temperature is equal to ambient temperature at time of placement

○ Manually enter concrete fresh temperature

Estimated Placement Temperature 77.4 °F

Formwork

Concrete age at Form Removal 96 hrs

Form Type Steel

Form Color Red

Blanket Insulation R-Value

Blanket R-Value (Thickness / Thermal Conductivity) 2.91 hr-ft²-°F/BTU

After Forms Are Stripped

Select the correct combination of curing methods on concrete exposed after forms are stripped

☐ White Curing Compound ☐ Black Plastic

☐ Wet Curing Blanket ☐ White or Clear Plastic

Time between form removal and curing method applied 1 hrs

Form Liners

Check which sides have form liners

☐ Width ☐ Depth

Figure C 1-21 - ***Construction Inputs*** **screen for a rectangular column**

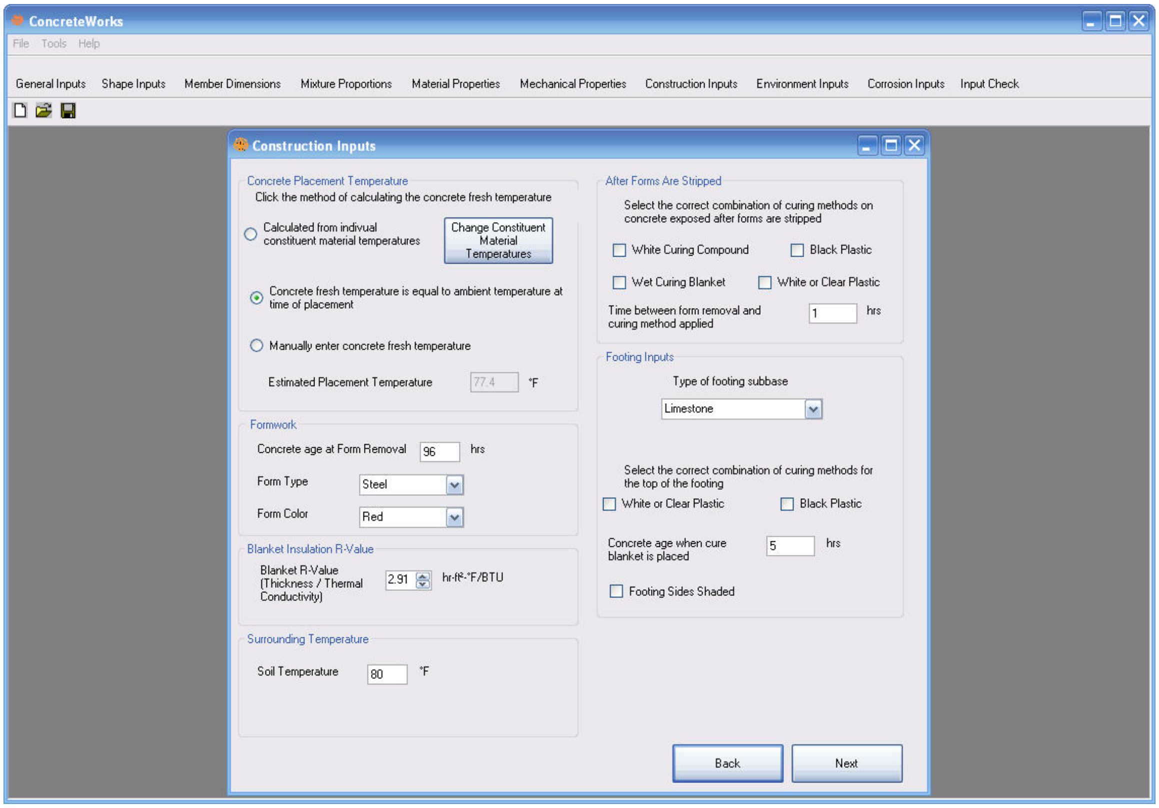

Concrete Placement Temperature

Click the method of calculating the concrete fresh temperature

○ Calculated from indivual constituent material temperatures

● Concrete fresh temperature is equal to ambient temperature at time of placement

○ Manually enter concrete fresh temperature

Estimated Placement Temperature 77.4 °F

Formwork

Concrete age at Form Removal 96 hrs

Form Type Steel

Form Color Red

Blanket Insulation R-Value

Blanket R-Value (Thickness / Thermal Conductivity) 2.91 hr-ft²-°F/BTU

Surrounding Temperature

Soil Temperature 80 °F

After Forms Are Stripped

Select the correct combination of curing methods on concrete exposed after forms are stripped

☐ White Curing Compound ☐ Black Plastic

☐ Wet Curing Blanket ☐ White or Clear Plastic

Time between form removal and curing method applied 1 hrs

Footing Inputs

Type of footing subbase Limestone

Select the correct combination of curing methods for the top of the footing

☐ White or Clear Plastic ☐ Black Plastic

Concrete age when cure blanket is placed 5 hrs

☐ Footing Sides Shaded

Figure C 1-22 - *Construction Inputs* screen shown when the rectangular footing member shape is chosen

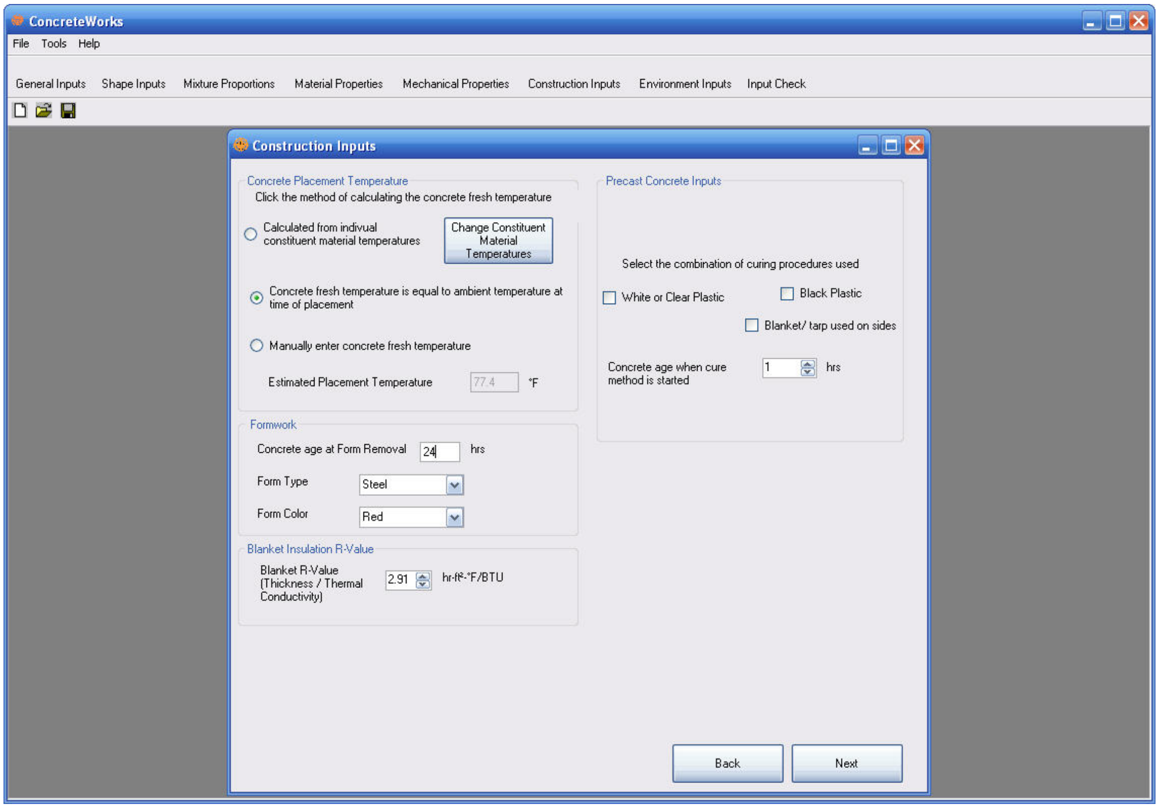

Concrete Placement Temperature

Click the method of calculating the concrete fresh temperature

○ Calculated from indivual constituent material temperatures

● Concrete fresh temperature is equal to ambient temperature at time of placement

○ Manually enter concrete fresh temperature

Estimated Placement Temperature 77.4 °F

Formwork

Concrete age at Form Removal 24 hrs

Form Type Steel

Form Color Red

Blanket Insulation R-Value

Blanket R-Value (Thickness / Thermal Conductivity) 2.91 hr-ft²-°F/BTU

Precast Concrete Inputs

Select the combination of curing procedures used

☐ White or Clear Plastic

☐ Black Plastic

☐ Blanket/ tarp used on sides

Concrete age when cure method is started 1 hrs

Figure C 1-23 - *Construction Inputs* screen for a rectangular bent cap with pre-cast concrete selected as the bottom form

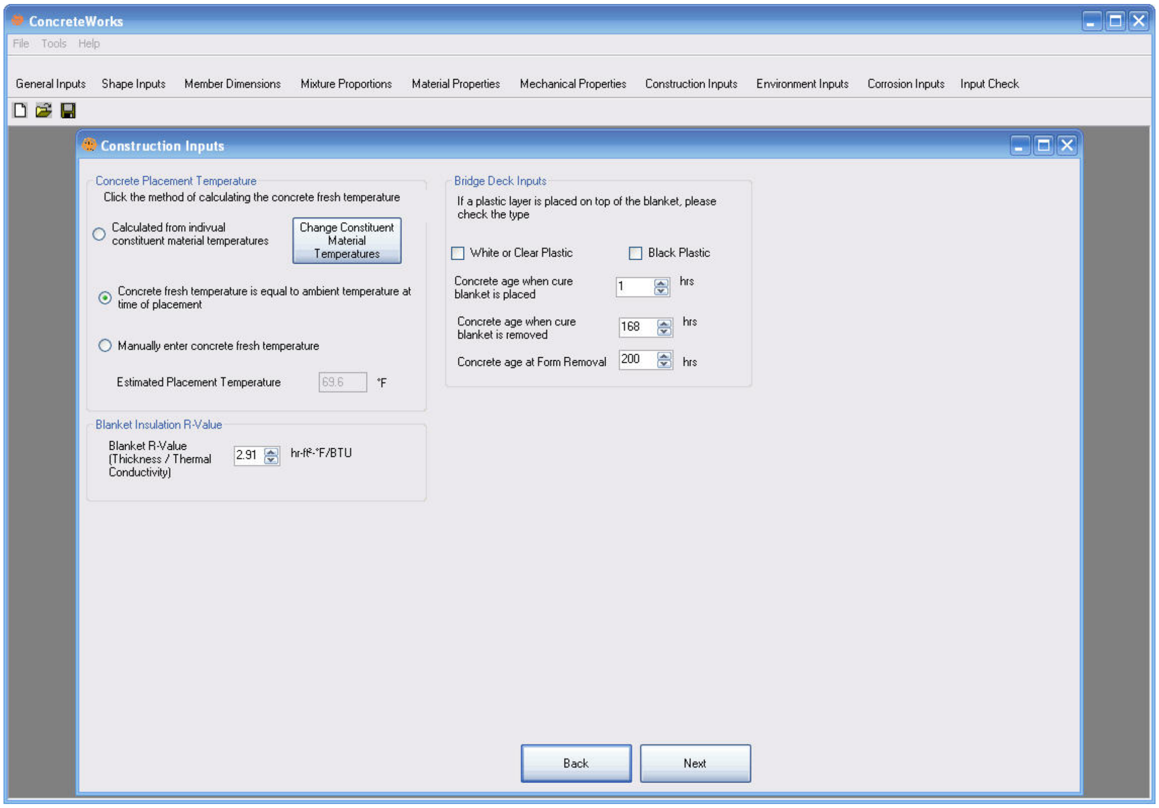

Concrete Placement Temperature

Click the method of calculating the concrete fresh temperature

○ Calculated from indivual constituent material temperatures

● Concrete fresh temperature is equal to ambient temperature at time of placement

○ Manually enter concrete fresh temperature

Estimated Placement Temperature 69.6 °F

Blanket Insulation R-Value

Blanket R-Value (Thickness / Thermal Conductivity) 2.91 hr-ft²-°F/BTU

Bridge Deck Inputs

If a plastic layer is placed on top of the blanket, please check the type

☐ White or Clear Plastic ☐ Black Plastic

Concrete age when cure blanket is placed 1 hrs

Concrete age when cure blanket is removed 168 hrs

Concrete age at Form Removal 200 hrs

Figure C 1-24 - Bridge Deck Inputs when Wood forms are Selected

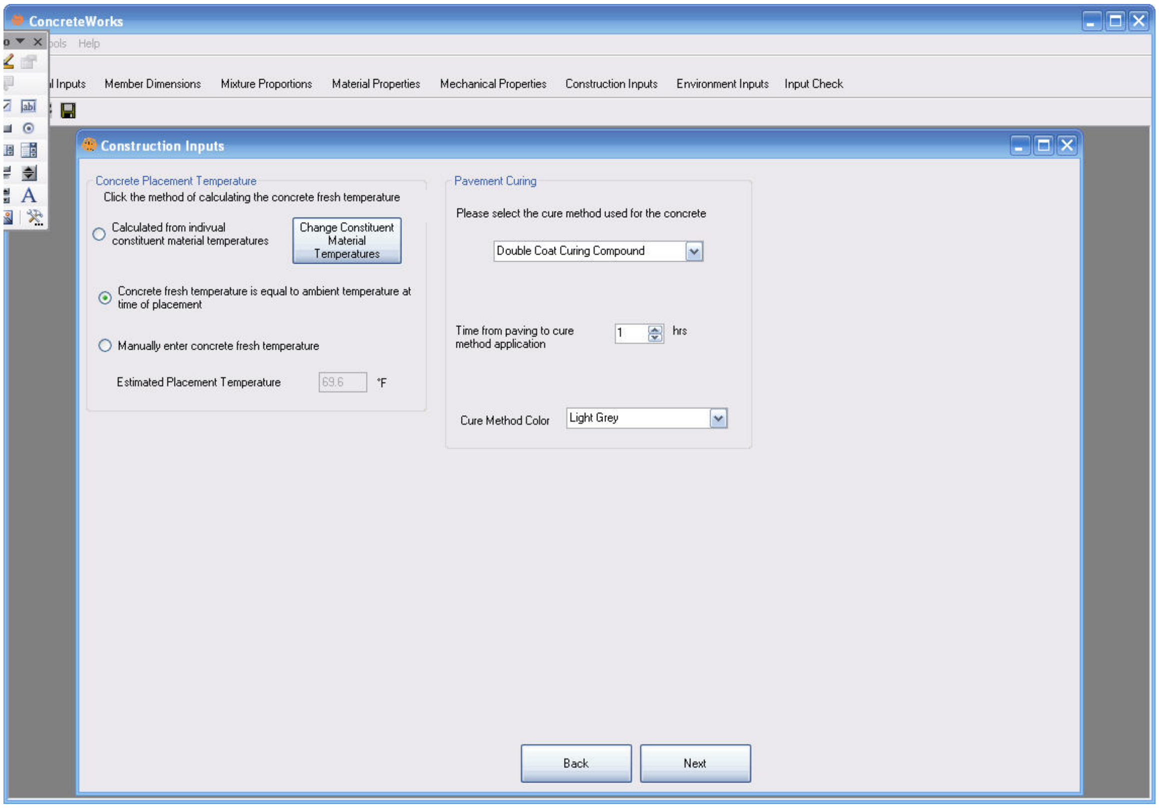

Concrete Placement Temperature

Click the method of calculating the concrete fresh temperature

○ Calculated from indivual constituent material temperatures

● Concrete fresh temperature is equal to ambient temperature at time of placement

○ Manually enter concrete fresh temperature

Estimated Placement Temperature 69.6 °F

Pavement Curing

Please select the cure method used for the concrete

Double Coat Curing Compound

Time from paving to cure method application 1 hrs

Cure Method Color Light Grey

Figure C 1-25 - Pavement Construction Inputs

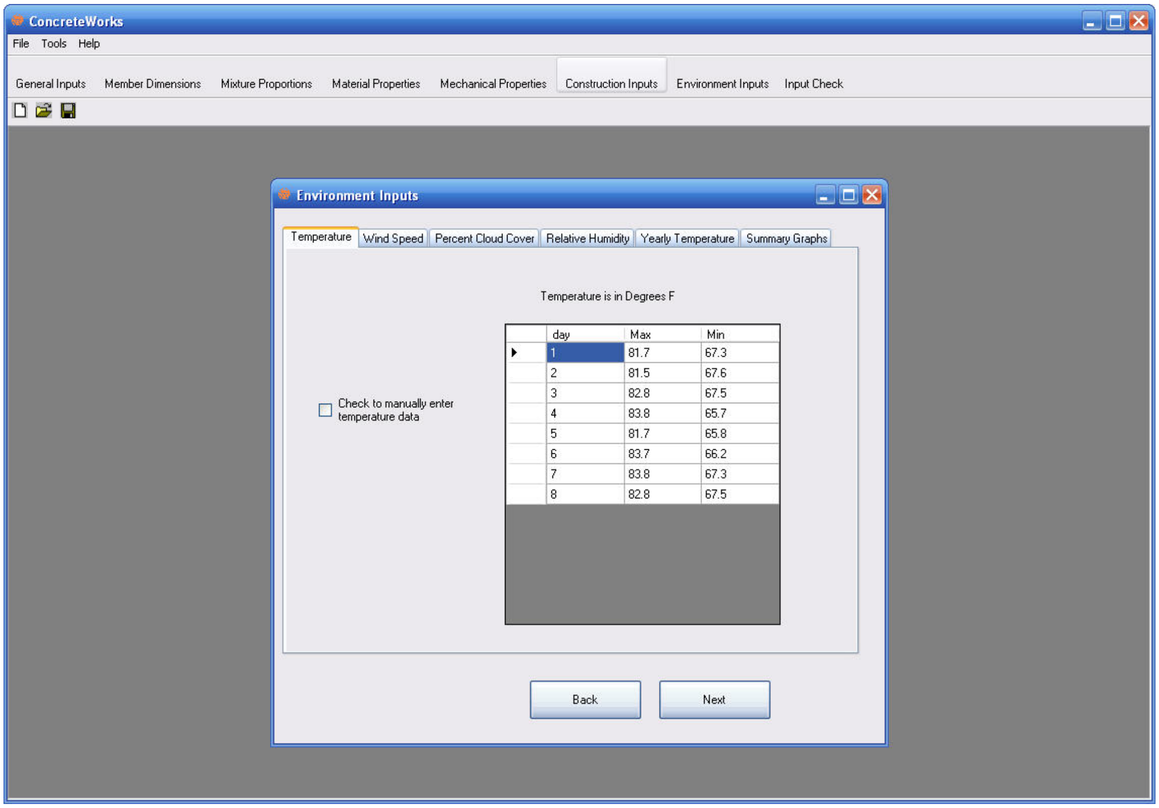

Temperature is in Degrees F

☐ Check to manually enter temperature data

day	Max	Min
1	81.7	67.3
2	81.5	67.6
3	82.8	67.5
4	83.8	65.7
5	81.7	65.8
6	83.7	66.2
7	83.8	67.3
8	82.8	67.5

Figure C 1-26 - *Temperature* tab on the *Environment Inputs* screen

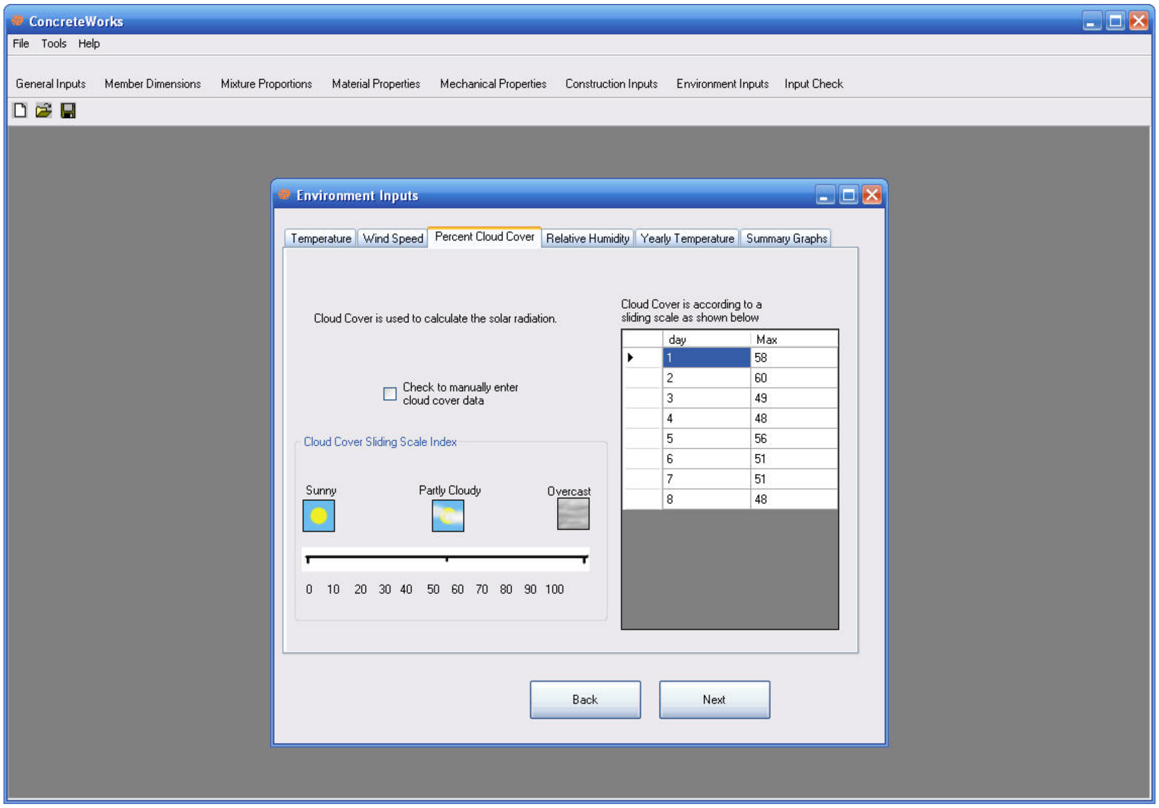

Cloud Cover is used to calculate the solar radiation.

☐ Check to manually enter cloud cover data

Cloud Cover is according to a sliding scale as shown below

day	Max
1	58
2	60
3	49
4	48
5	56
6	51
7	51
8	48

Figure C 1-27 - *Percent Cloud Cover* tab on the *Environment Inputs* screen

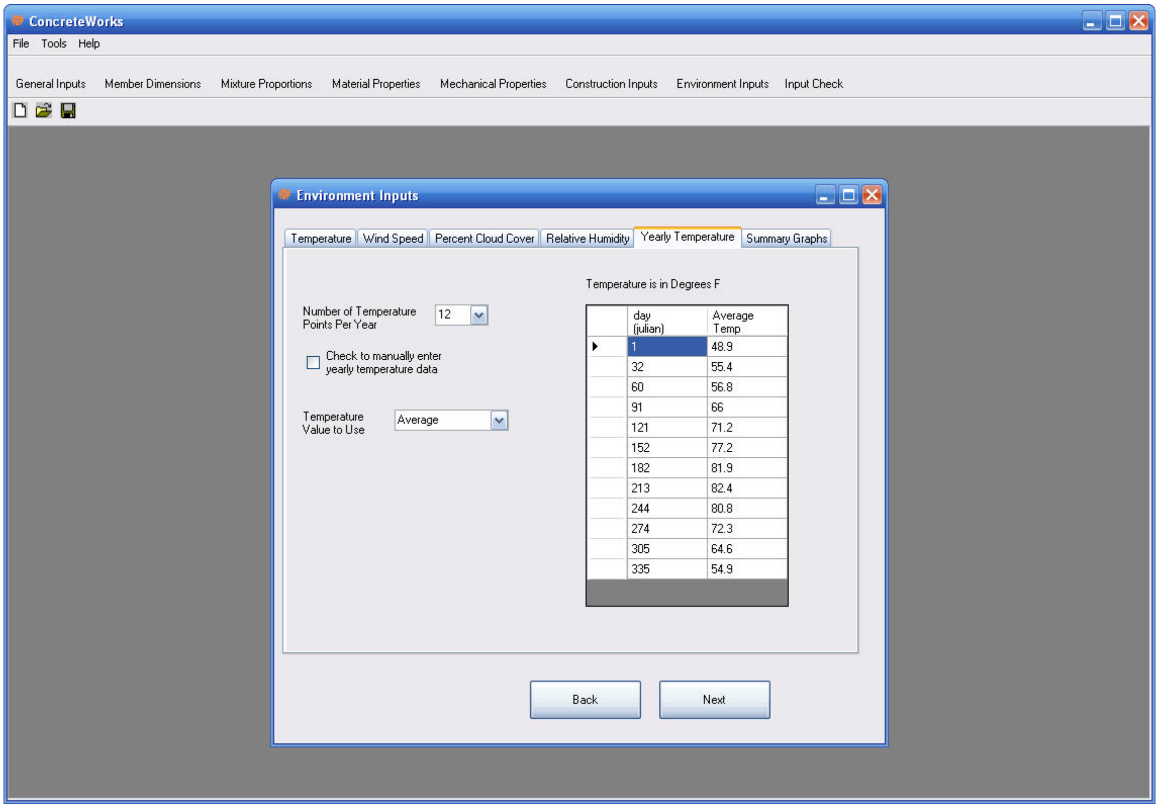

Temperature is in Degrees F

Number of Temperature Points Per Year: 12

☐ Check to manually enter yearly temperature data

Temperature Value to Use: Average

day (julian)	Average Temp
1	48.9
32	55.4
60	56.8
91	66
121	71.2
152	77.2
182	81.9
213	82.4
244	80.8
274	72.3
305	64.6
335	54.9

Figure C 1-28 - Yearly Temperature Inputs

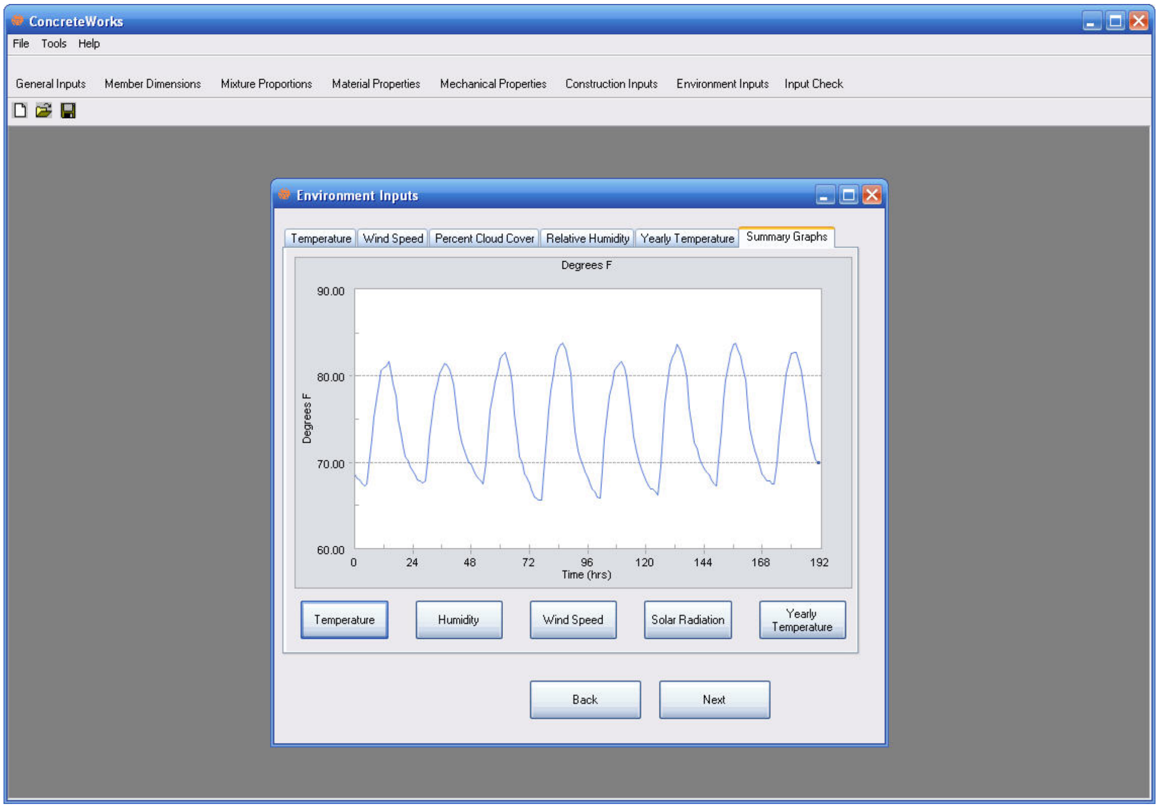

Figure C 1-29 - *Summary Graphs* tab on the *Environment Inputs* screen - the temperature graph is currently displayed

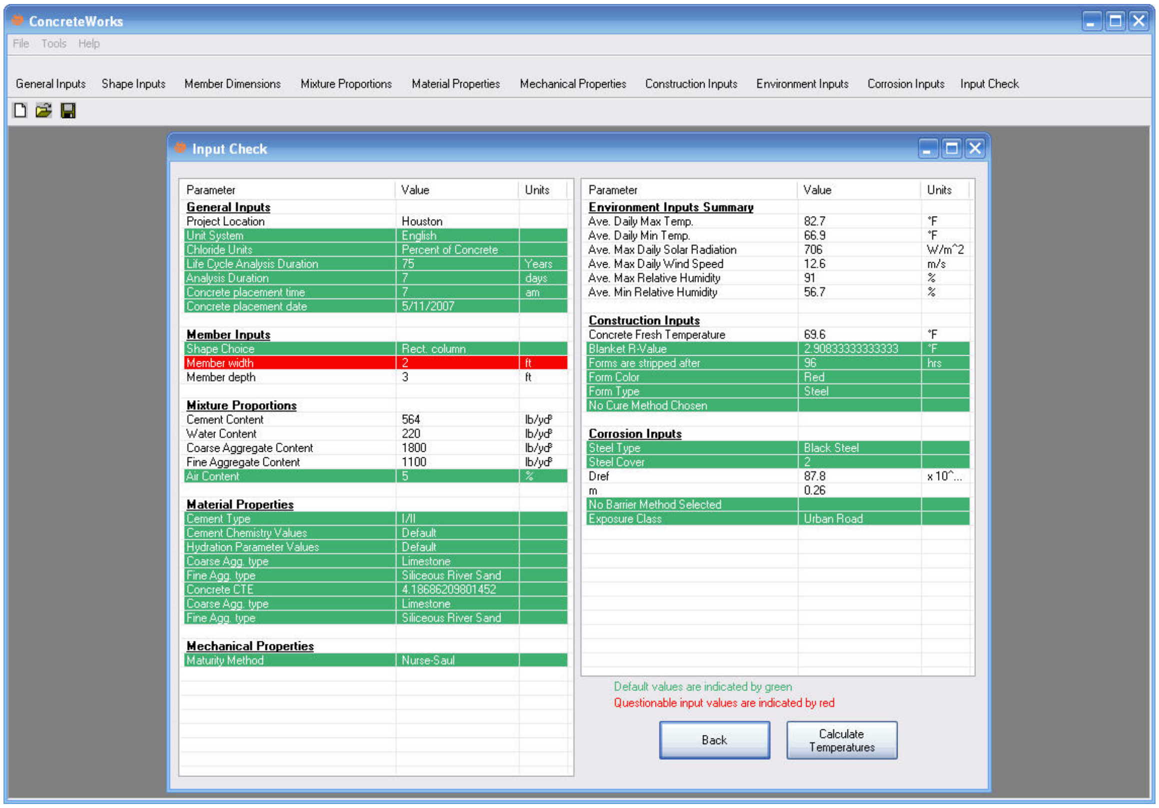

Parameter	Value	Units
General Inputs		
Project Location	Houston	
Unit System	English	
Chloride Units	Percent of Concrete	
Life Cycle Analysis Duration	75	Years
Analysis Duration	7	days
Concrete placement time	7	am
Concrete placement date	5/11/2007	
Member Inputs		
Shape Choice	Rect. column	
Member width	2	ft
Member depth	3	ft
Mixture Proportions		
Cement Content	564	lb/yd^3
Water Content	220	lb/yd^3
Coarse Aggregate Content	1800	lb/yd^3
Fine Aggregate Content	1100	lb/yd^3
Air Content	5	%
Material Properties		
Cement Type	I/II	
Cement Chemistry Values	Default	
Hydration Parameter Values	Default	
Coarse Agg. type	Limestone	
Fine Agg. type	Siliceous River Sand	
Concrete CTE	4.18686209801452	
Coarse Agg. type	Limestone	
Fine Agg. type	Siliceous River Sand	
Mechanical Properties		
Maturity Method	Nurse-Saul	

Parameter	Value	Units
Environment Inputs Summary		
Ave. Daily Max Temp.	82.7	°F
Ave. Daily Min Temp.	66.9	°F
Ave. Max Daily Solar Radiation	706	W/m^2
Ave. Max Daily Wind Speed	12.6	m/s
Ave. Max Relative Humidity	91	%
Ave. Min Relative Humidity	56.7	%
Construction Inputs		
Concrete Fresh Temperature	69.6	°F
Blanket R-Value	2.90833333333333	°F
Forms are stripped after	96	hrs
Form Color	Red	
Form Type	Steel	
No Cure Method Chosen		
Corrosion Inputs		
Steel Type	Black Steel	
Steel Cover	2	
Dref	87.8	x 10^...
m	0.26	
No Barrier Method Selected		
Exposure Class	Urban Road	

Default values are indicated by green

Questionable input values are indicated by red

Figure C 1-30 - *Input Check* Screen

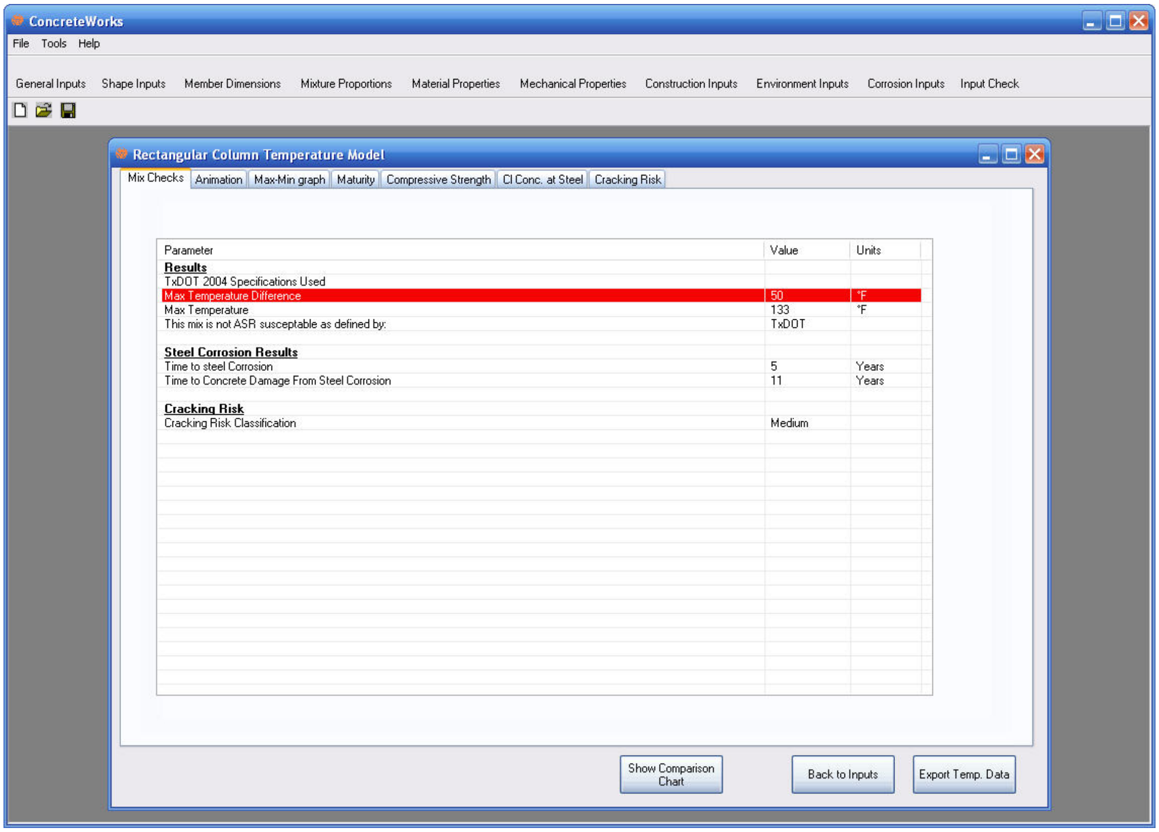

Parameter	Value	Units
Results		
TxDOT 2004 Specifications Used		
Max Temperature Difference	50	°F
Max Temperature	133	°F
This mix is not ASR susceptable as defined by:	TxDOT	
Steel Corrosion Results		
Time to steel Corrosion	5	Years
Time to Concrete Damage From Steel Corrosion	11	Years
Cracking Risk		
Cracking Risk Classification	Medium	

Figure C 1-31 - ***Mix Checks*** **tab shown on the** ***Rectangular Column Temperature Model*** **screen**

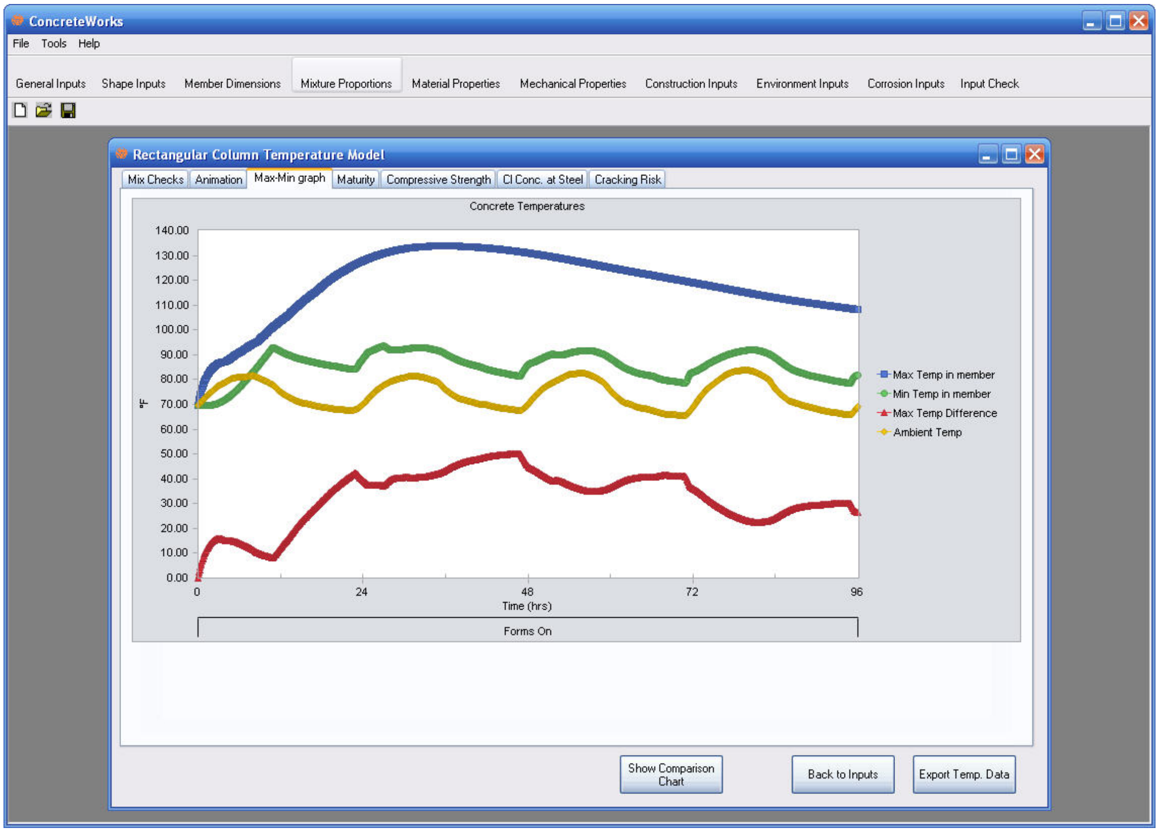

Figure C 1-32 - ***Max-Min Graph*** **tab as shown on the** ***Rectangular Column Temperature Model*** **screen**

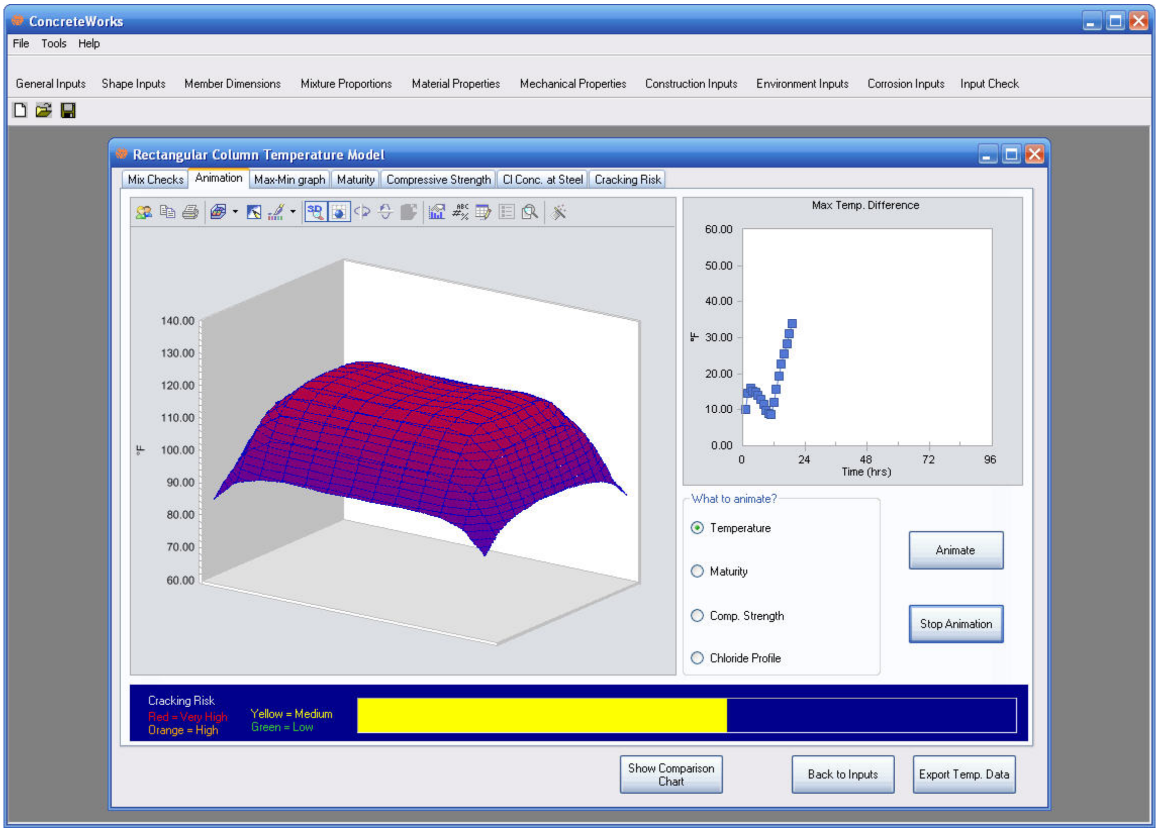

What to animate?

● Temperature

○ Maturity

○ Comp. Strength

○ Chloride Profile

Figure C 1-33 - *Animation* tab as shown on the *Rectangular Column Temperature Model* screen

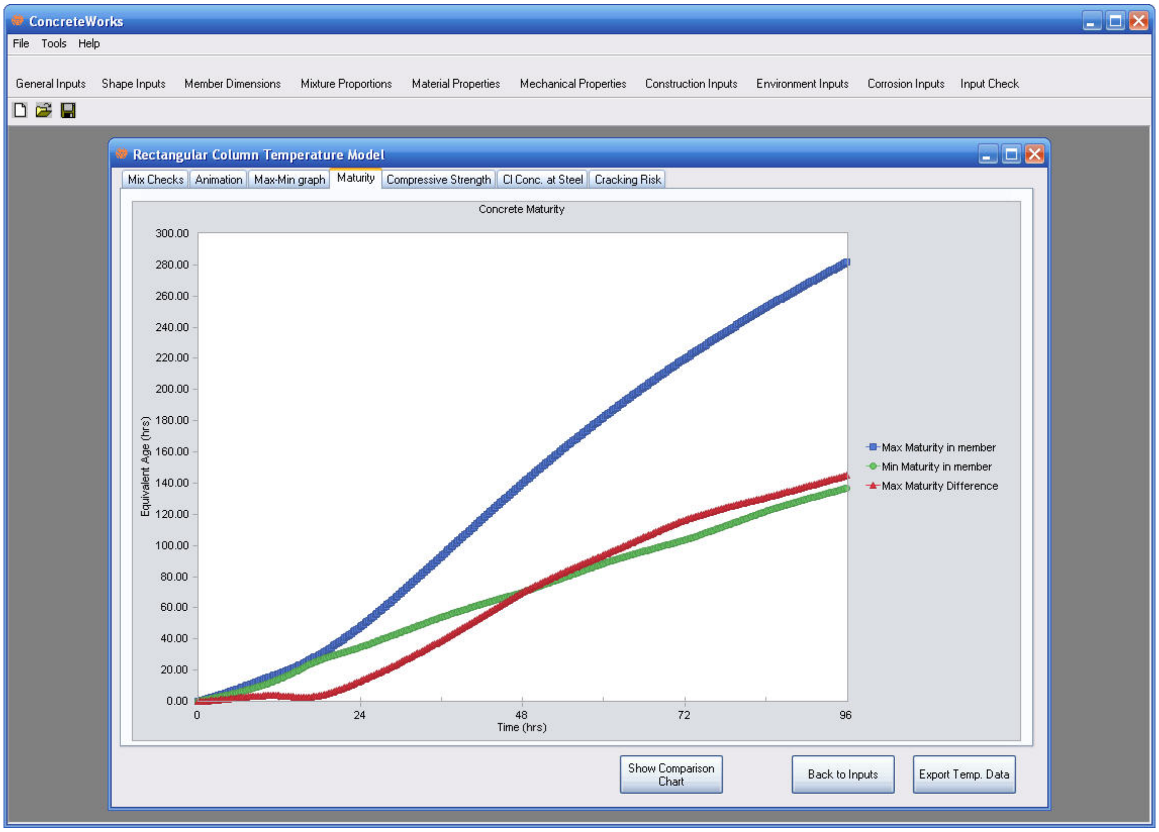

Figure C 1-34 - ***Maturity*** **tab as shown on the** ***Rectangular Column Temperature Model*** **screen**

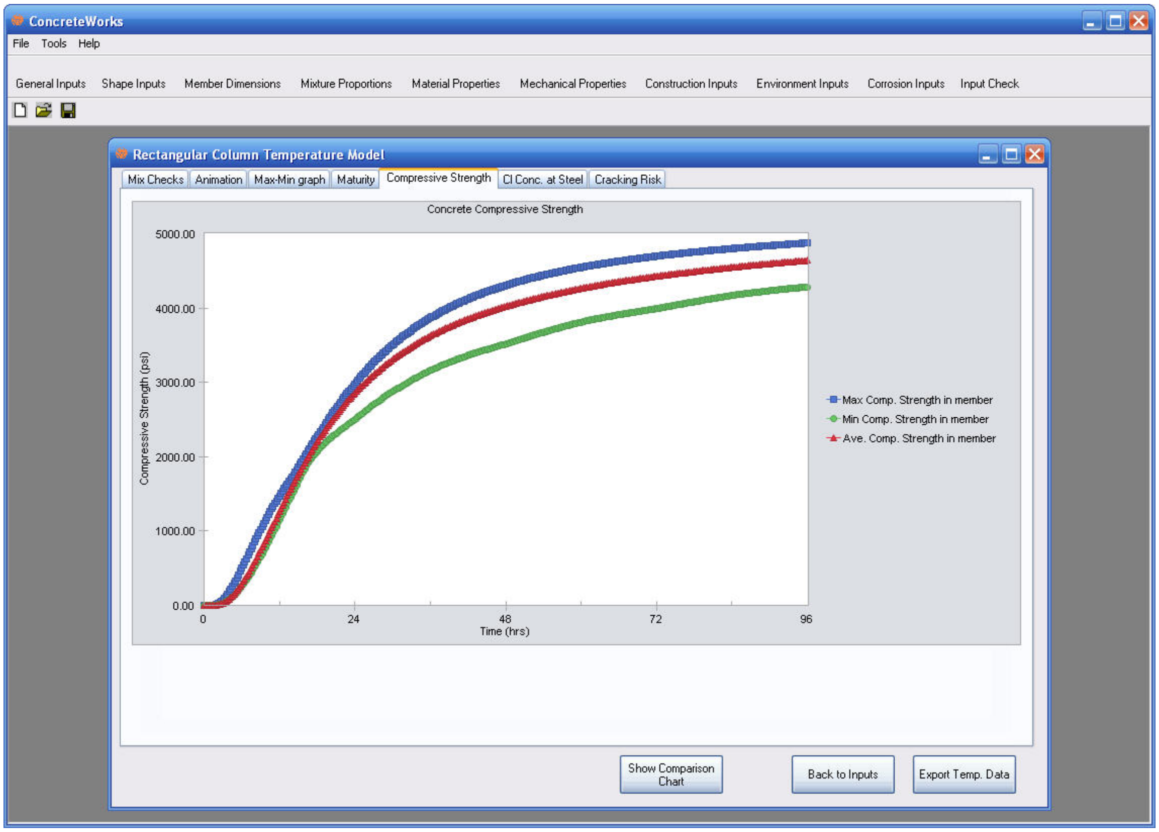

Figure C 1-35 - ***Compressive Strength*** **tab with compressive strength calculated as shown on the** ***Rectangular Column Temperature Model*** **screen**

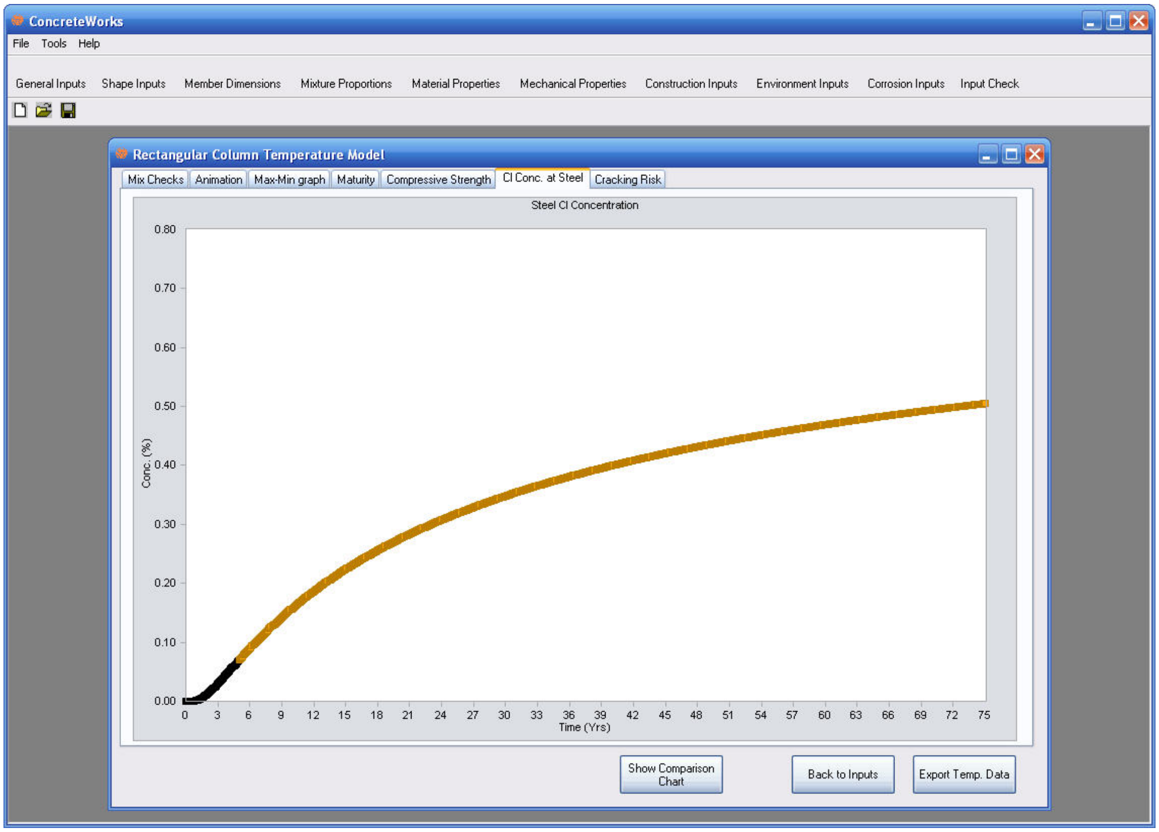

Figure C 1-36 - Graph of Chloride Concentration at Steel

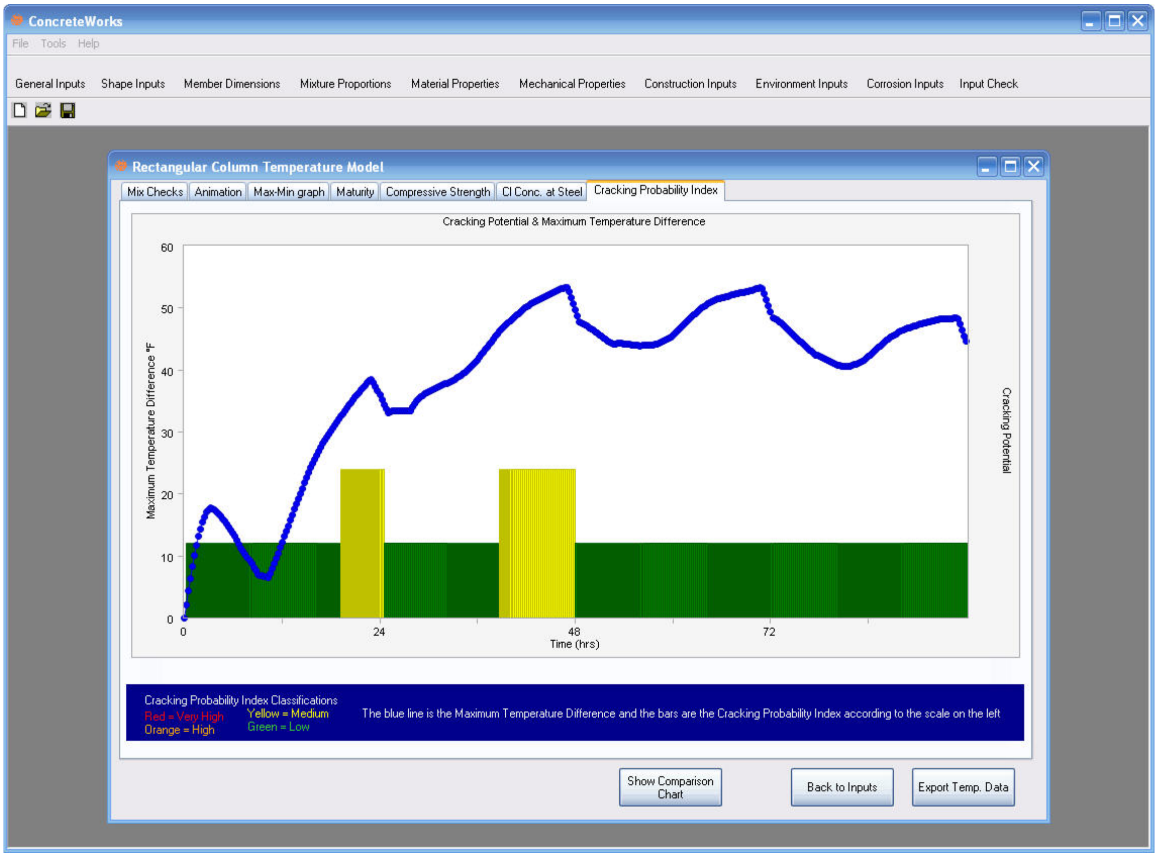

Cracking Probability Index Classifications

Red = Very High

Orange = High

Yellow = Medium

Green = Low

The blue line is the Maximum Temperature Difference and the bars are the Cracking Probability Index according to the scale on the left

Figure C 1-37 - Cracking Probability Classification Chart

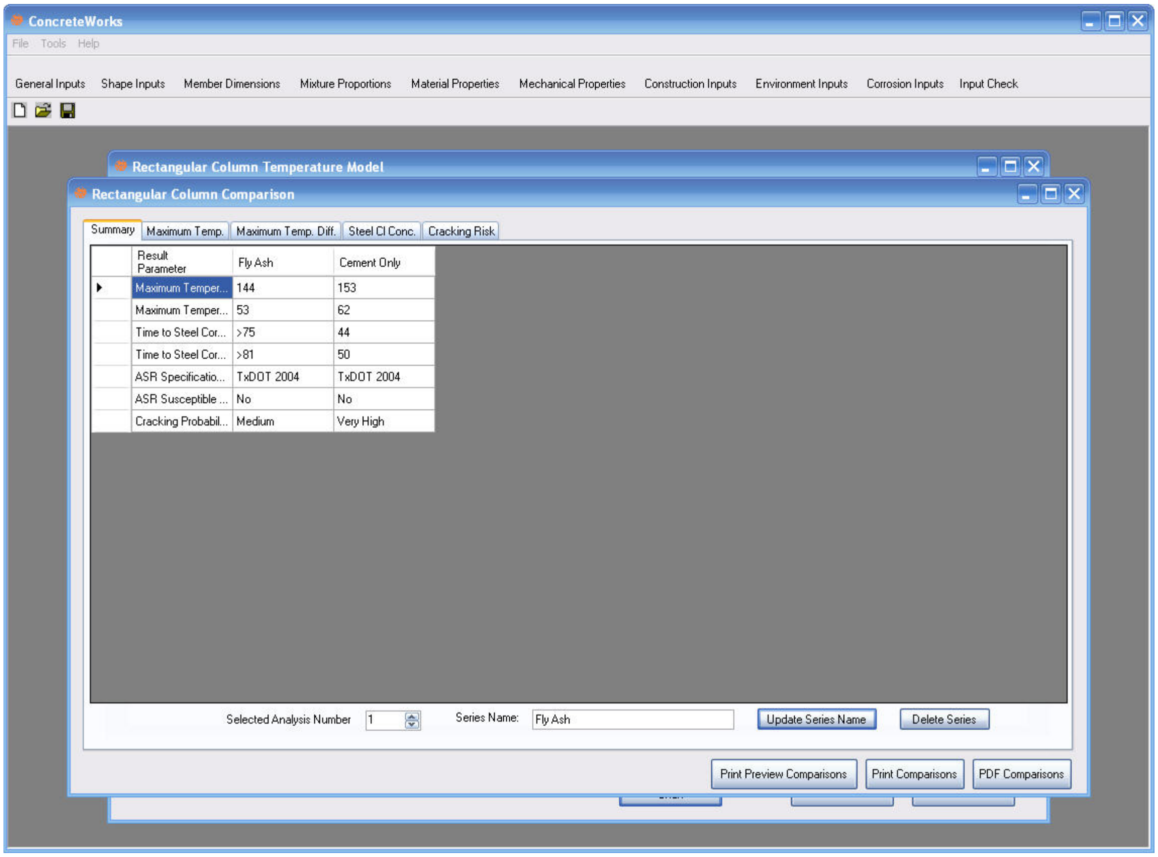

Result Parameter	Fly Ash	Cement Only
Maximum Temper...	144	153
Maximum Temper...	53	62
Time to Steel Cor...	>75	44
Time to Steel Cor...	>81	50
ASR Specificatio...	TxDOT 2004	TxDOT 2004
ASR Susceptible ...	No	No
Cracking Probabil...	Medium	Very High

Selected Analysis Number: 1

Series Name: Fly Ash

Figure C 1-38 - *Comparison Chart* screen

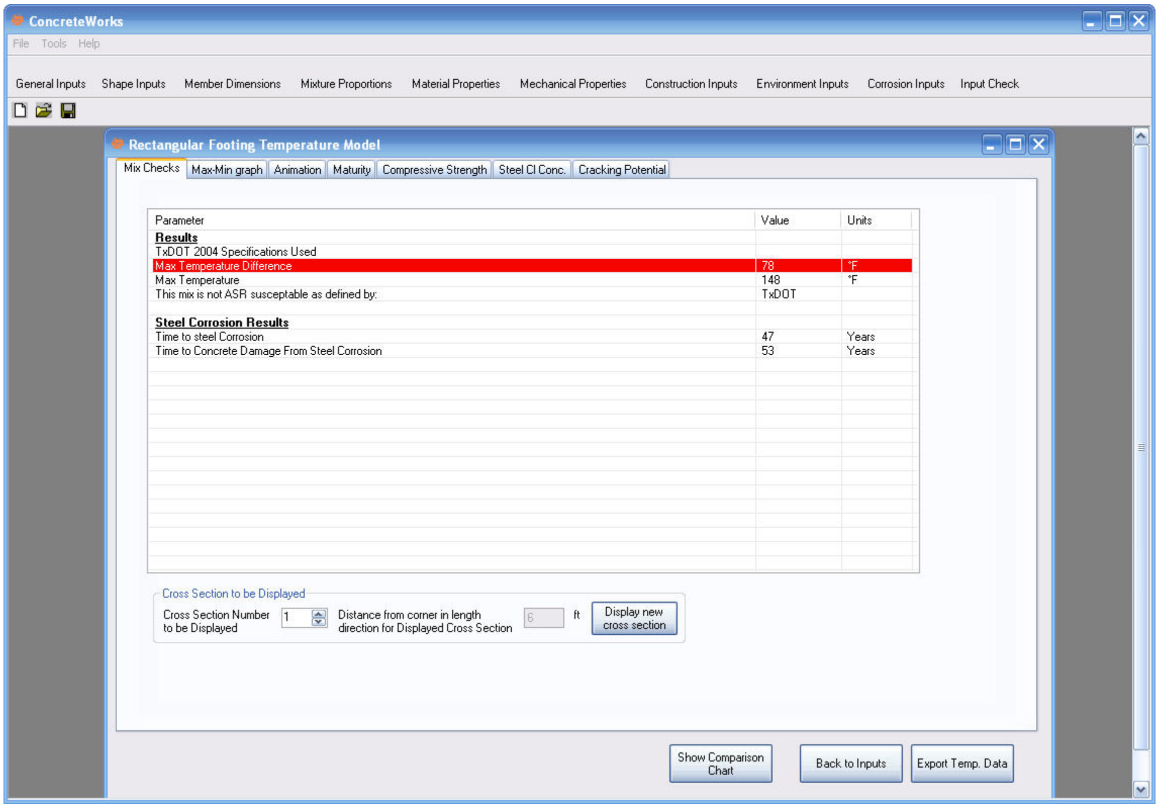

Parameter	Value	Units
Results		
TxDOT 2004 Specifications Used		
Max Temperature Difference	78	°F
Max Temperature	148	°F
This mix is not ASR susceptable as defined by:	TxDOT	
Steel Corrosion Results		
Time to steel Corrosion	47	Years
Time to Concrete Damage From Steel Corrosion	53	Years

Cross Section to be Displayed

Cross Section Number to be Displayed: 1

Distance from corner in length direction for Displayed Cross Section: 6 ft

Figure C 1-39 - ***Rectangular Footing Results*** **screen with the** ***Cross-Section to be Displayed*** **frame showing**

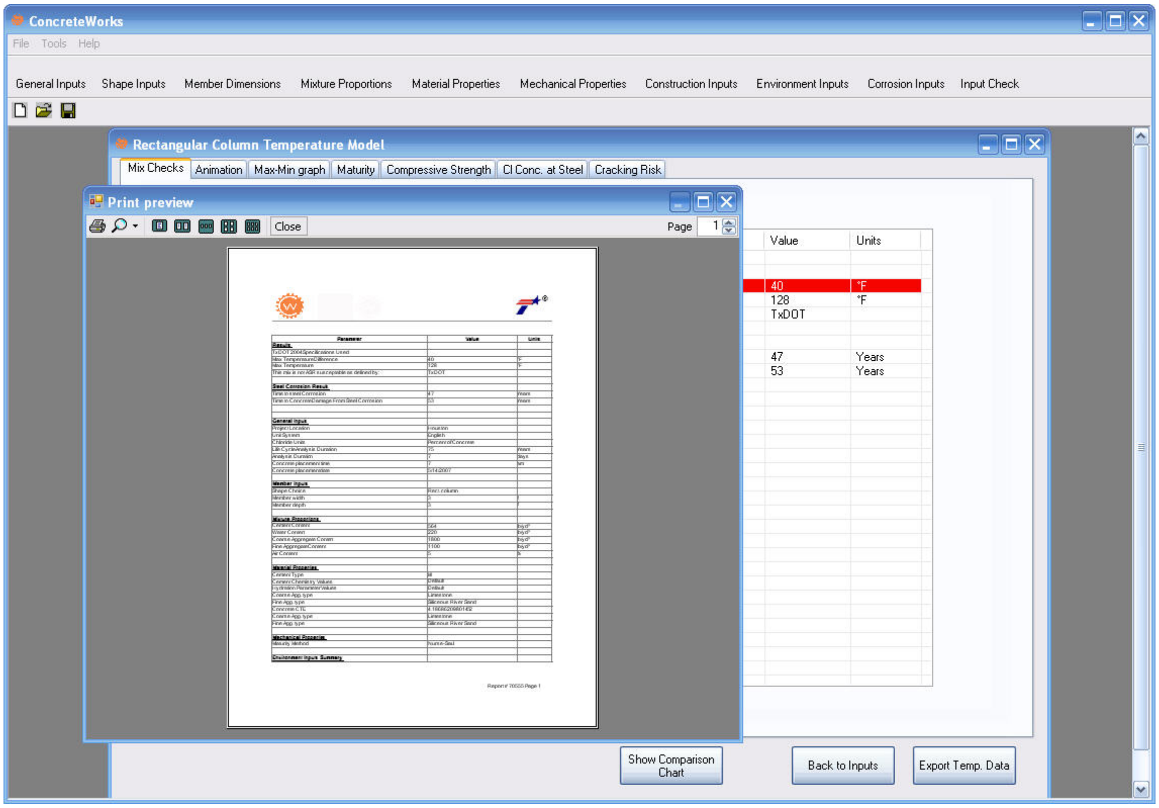

Value	Units
40	°F
128	°F
TxDOT	
47	Years
53	Years

Figure C 1-40 - *Print Preview* screen

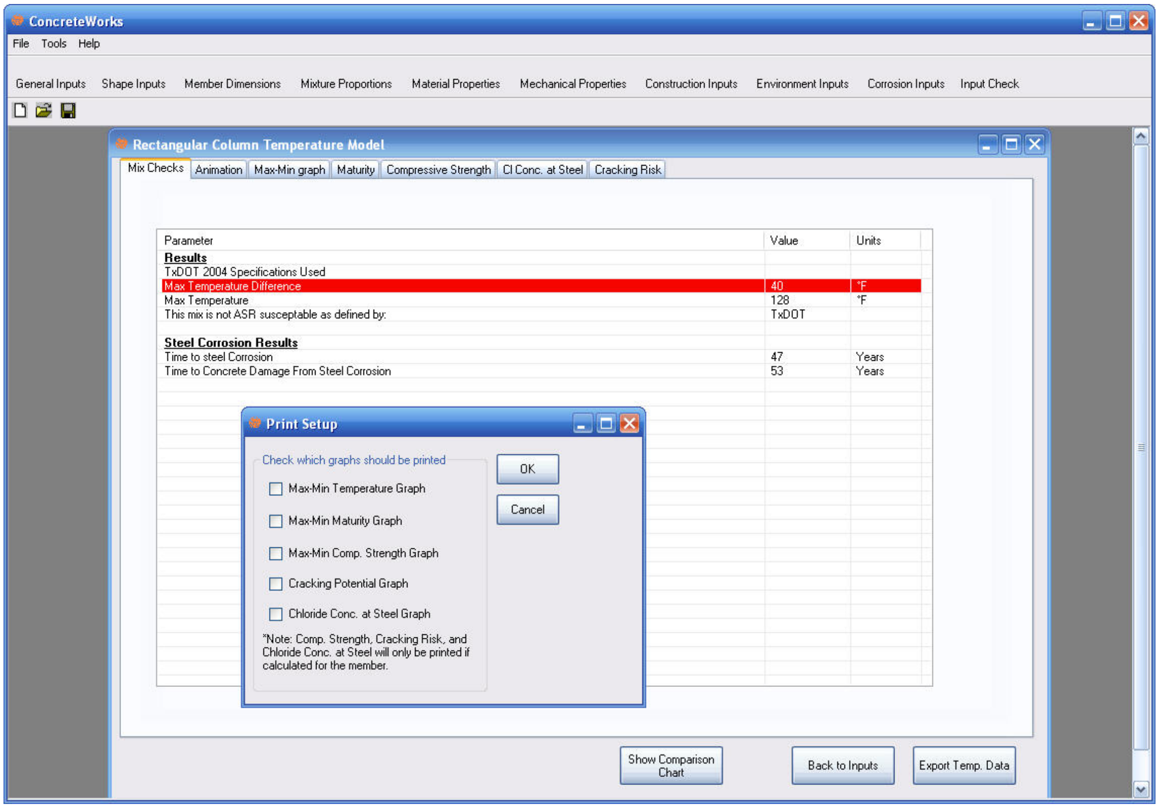

Parameter	Value	Units
Results		
TxDOT 2004 Specifications Used		
Max Temperature Difference	40	°F
Max Temperature	128	°F
This mix is not ASR susceptable as defined by:	TxDOT	
Steel Corrosion Results		
Time to steel Corrosion	47	Years
Time to Concrete Damage From Steel Corrosion	53	Years

Check which graphs should be printed

☐ Max-Min Temperature Graph

☐ Max-Min Maturity Graph

☐ Max-Min Comp. Strength Graph

☐ Cracking Potential Graph

☐ Chloride Conc. at Steel Graph

*Note: Comp. Strength, Cracking Risk, and Chloride Conc. at Steel will only be printed if calculated for the member.

Figure C 1-41 - *Page Setup* dialog

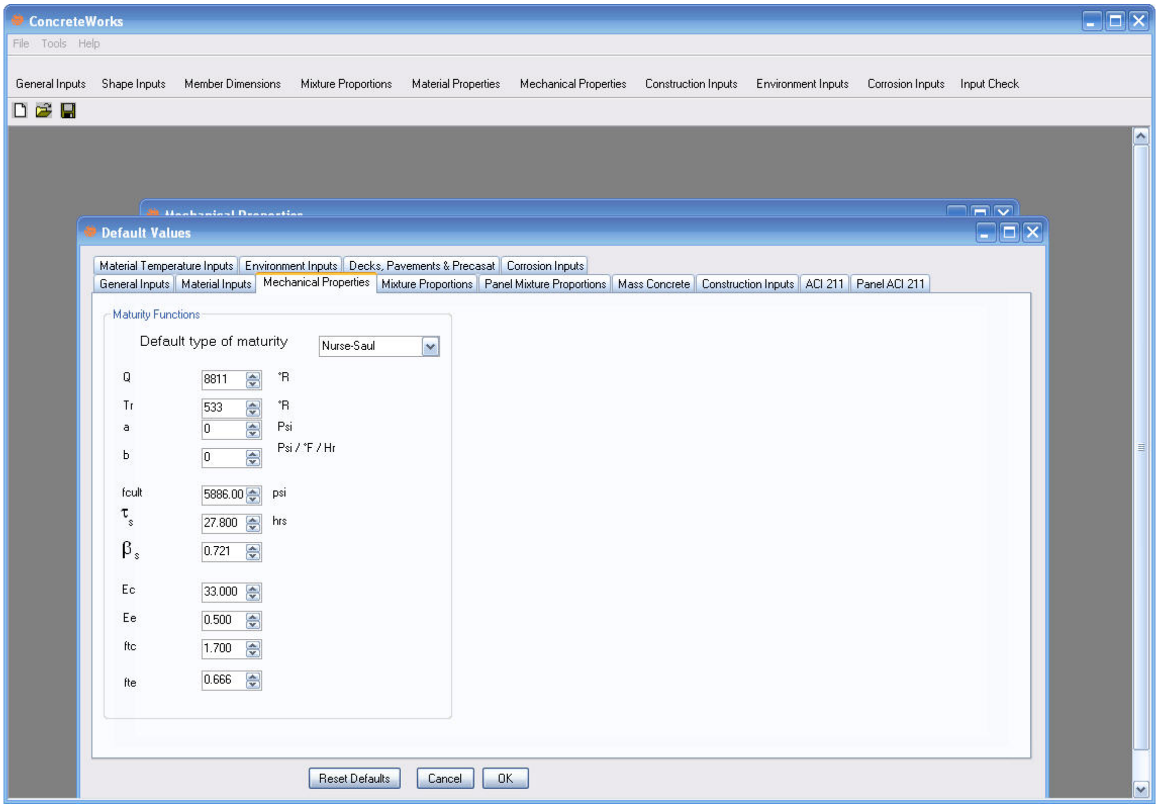

Default type of maturity: Nurse-Saul

Q: 8811 °R

Tr: 533 °R

a: 0 Psi

b: 0 Psi / °F / Hr

fcult: 5886.00 psi

τ_s: 27.800 hrs

β_s: 0.721

Ec: 33.000

Ee: 0.500

ftc: 1.700

fte: 0.666

Figure C 1-42 - *Material Inputs* tab on the *Change Defaults* screen

References

AASHTO, (2001). "Proposed Standard Test Method for the Coefficient of Thermal Expansion of Hydraulic Cement Concrete." AASHTO TP-60-00, *American Association of State Highway and Transportation Officials*..

AASHTO, (2002). AASHTO Designation T 259-02, "Standard Method of Test for Resistance of Concrete to Chloride Ion Penetration," AASHTO Standard Specification, American Association of State Highway and Transportation Officials, Washington, DC.

AASHTO, (2005). "Coefficient of Thermal Expansion of Hydraulic Cement Concrete," AASHTO TP 60-00, *American Association of State Highway Transportation* Officials, Washington, DC, 7 pp.

Abrams, D., (1918). "Effect of Time of Mixing on the Strength and Wear of Concrete," ACI Journal Proceedings, Vol. 14, No. 6, pp. 22-92.

ACI Building Code Committee, (2005). "Building Code Requirements for Structural Concrete (ACI 318-05) and Commentary (ACI 318R-05)," American Concrete Institute, Farmington Hills, MI, 430 pp.

ACI Committee 207, (1996). "Mass Concrete," ACI 207.1R, American Concrete Institute, Farmington Hills, Mich., 42 pp.

ACI Committee 207, (1995). "Effect of restraint, volume change, and reinforcement on cracking in massive concrete," ACI 207.2R, American Concrete Institute, Farmington Hills, Mich., pp. 3-10.

ACI Committee 209, (1992). "Prediction of Creep, Shrinkage, and Temperature Effects in Concrete Structures," ACI 209R, American Concrete Institute, Farmington Hills, Mich., 47 pp.

ACI Committee 211, (1991). "Standard Practice for Selecting Proportions for Normal, Heavyweight, and Mass Concrete, ACI 211.1R, American Concrete Institute, Farmington Hills, Mich., 38 pp.

ACI Committee 222, (2001). "Protection of Metals in Concrete Against Corrosion," ACI 222R, American Concrete Institute, Farmington Hills, Mich., 41 pp.

ACI Committee 305R, (1991). “Hot Weather Concreting – Reported by ACI Committee 305,” American Concrete Institute, Farmington Hills, Michigan, 20 pp.

Al-Fadhala, M., and Hover, K.C., (2001). “Rapid Evaporation from Freshly Cast Concrete and the Gulf Environment,” Construction and Building Materials, Vol. 15, pp. 1-7.

Altoubat, S.A., (2000). “Early Age Stresses and Creep-Shrinkage Interaction of Restrained Concrete,” Doctoral Thesis, the University of Illinois at Urbana-Champaign, 221 pp.

Arıoglu, N., Girgin, Z.C., and Arıoglu, E., (2006). “Evaluation of Ratio between Splitting Tensile Strength and Compressive Strength for Concretes up to 120 MPa and its Application in Strength Criterion,” ACI Materials Journal, Vol. 103, No. 1, pp. 18-24.

Anson, M.; and Newman, K., (1966). "The effect of mix proportions and method of testing on Poisson's ratio for mortars and concretes," Magazine of Concrete Research, V. 18, No. 56, pp. 115-130.

Arup, H.; Sørensen, B.; Frederiksen, J.; and Thaulow, N., (1993. “The Rapid Chloride Permeation Test – An Assesment,” Corrosion93, The NACE Annual Conference and Corrosion Show, Paper 334, 11 pp.

ASCE, (2005). “Report Card for America’s Infrastructure: Bridges,” http://www.asce.org/reportcard/2005/page.cfm?id=22, American Society of Civil Engineers, Accessed May 2007.

ASHRAE, (1993). “1993-ASHRAE Handbook,” American Society of Heating, Refrigerating and Air-Conditioning Engineers, Incorporated, Atlanta.

ASTM C 33, (2003). “Standard Specification for Concrete Aggregates,” *ASTM International*, West Conshohocken, PA., 11 pp.

ASTM C 39, (2005). Standard Test Method for Compressive Strength of Cylindrical Concrete Specimens. *ASTM International*, West Conshohocken, PA.

ASTM C 78, (2002). “Standard Test Method for Flexural Strength of Concrete (Using Simple Beam with Third-Point Loading,” ASTM International, West Conshohocken, PA, 3 pp.

ASTM C 105, (2005). “Standard Specification for Portland Cement,” ASTM International, West Conshoocken, PA., 8 pp.

ASTM C 150, (2005). Standard Specification for Portland Cement. *ASTM International*, West Conshohocken, PA.

ASTM C 204, (2005). "Standard Test Method for Fineness of Hydraulic Cement by Air Permeability Apparatus," ASTM International, West Conshoocken, PA., 10 pp.

ASTM C 403, (2005). "Standard Test Method for Time of Setting of Concrete Mixtures by Penetration Resistance," *ASTM International*, West Conshohocken, PA., 6 pp.

ASTM C 469, (2002). "Standard Test Method of Static Modulus of Elasticity and Poisson's Ratio of Concrete in Compression," *ASTM International*, West Conshohocken, PA., 4 pp.

ASTM C 494, (1999). "Standard Specification for Chemical Admixtures for Concrete," ASTM International, West Conshohocken, Pa., 9 pp.

ASTM C 496, (2004). Standard Test Method for Splitting Tensile Strength of Cylindrical Concrete Specimens. *ASTM International*, West Conshohocken, PA.

ASTM C 512, (2002). "Standard Test Method for Creep of Concrete in Compression," ASTM International, West Conshoocken, PA, 3 pp.

ASTM C 618, (2003). "Standard Specification for Coal Fly Ash and Raw or Calcined Natural Pozzolan for Use in Concrete," ASTM International, West Conshohocken, Pa., 3 pp.

ASTM C 680, (2004). "Standard Practice for Estimate of the Heat Gain or Loss and the Surface Temperatures of Insulated Flat, Cylindrical, and Spherical Systems by Use of Computer Programs," American Society for Testing and Materials, Pennsylvania.

ASTM C 989, (2005). "Standard Specification for Ground Granulated Blast-Furnace Slag for Use in Concrete and Mortars," ASTM International, West Conshohocken, Pa., 5 pp.

ASTM C 1074, (2004). "Standard Practice for Estimating Concrete Strength by the Maturity Method," ASTM International, West Conshoocken, PA, 9 pp.

ASTM C 1202, (2005). "Standard Test Method for Electrical Indication of Concrete's Ability to Resist Chloride Ion Penetration," ASTM International, Pennsylvania, 6 pp.

ASTM C 1365, (1998). Standard Test Method for Determination of Proportion of Phases in Portland Cement and Portland-Cement Clinker Using X-Ray Powder Diffraction Analysis. *ASTM International*, West Conshohocken, PA.

ASTM C 1556, (2004). “Standard Test Method for Determining the Apparent Chloride Diffusion Coefficient of Cementitious Mixtures by Bulk Diffusion,” American Society for Testing and Materials, Pennsylvia, 7 pp.

Barber, E.S., (1957). “Calculation of Maximum Pavement Temperatures from Weather Reports,” Bulletin 168, Highway Research Board, Washington, D.C., pp. 1-8.

Bažant, Z., (1972). “Numerical Determination of Long-Range Stress History from Strain History in Concrete,” *Materials and Structures*, RILEM, Paris, Vol. 5, No. 27, pp. 135-141.

Bažant, Z, and J. Chern., (1985). “Triple Power Law for Concrete Creep,” *Journal of Engineering Mechanics*, Vol. 111, No. 1, pp. 63-83.

Bažant, Z.P., and Panula, L., (1978). “Practical Prediction of Time-Dependent Deformations of Concrete Part IV: Temperature Effect on Basic Creep,” Matériaux et Constructions, Vol. 11, No. 66, pp. 424-434.

Beaudoin, J.J; and Liu, Z., (2000). “The Permeability of Cement Systems to Chloride Ingress and Related Test Methods,”Cement, Concrete and Aggregates, Vol. 22, No. 1, June, pp. 16-23.

Ben White Bulletin, (2000). Austin District Office, Texas Department of Transportation, “Ben White-IH35 Project Underway,” 4 pp.

Bentz, E.C., and Thomas, M.D.A., (2001). “Life-365 Service Life Prediction Model™: User Manual,” 57 pp.

Bernard, O.; Ulm, F.; and Lemarchand, E., (2003). "A multiscale micromechanics-hydration model for the early-age elastic properties of cement-based materials," Cement and Concrete Research, V 33, pp. 1293–1309.

Bjøntegaard, O., (1999). "Thermal Dilation and Autogenous Deformation as Driving Forces to Self-Induced Stresses in High Performance Concrete," Doctoral Thesis, Division of Structural Engineering, The Norwegian University of Science and Technology, 256 pp.

Brooks, A.G., Schindler, A.K., and Barnes, R.W., (2007). “The Maturity Method Evaluated for Various Cementitious Materials,” ASCE Materials Journal, In press.

Brutsaert, W., (1975). “On a Derivable formula for longwave radiation from clear skies,” Water Resources Research, Vol. 11, pp. 742-744.

Byfors, J. (1980). "Plain Concrete at Early Ages," Research 3:80, Swedish Cement and Concrete Research Institute, Stockholm, Sweden.

Cannon, R.W., Tuthill, L., Schrader, K., and Tatro, S.B., (1992). "Cement – When to Say When!" Concrete International, Vol. 14, No. 1, pp. 52-54.

Carino, N.J., and Lew, H.S., (1982). "Re-examination of the Relation Between Splitting Tensile and Compressive Strength of Normal Weight Concrete," ACI Journal, Vol. 79, No. 3, pp. 214-218.

Carino, N.J.; and Tank, R.C., (1992). "Maturity functions for concretes made with various cements and admixtures," ACI Materials Journal, Vol. 89, No. 2, pp. 188-196.

Clear, R.D.; Gartland, L.; and Winkelmann, F.C., (2003). "An empirical correlation for the outside convective air-film coefficient for horizontal roofs," Energy and Buildings, Vol. 35, pp. 797-811.

Dallas Semiconductor, (2002). Applications: Total Environmental Management for Paving. 1 Aug. 2003 <http://db.maxim-ic.com/iButton/applications/index.cfm?Action=DD&id=27>.

Dallas Semiconductor, (2003). Thermocron iButton. 27 Feb. 2003. 15 July 2003 <http://pdfserv.maxim-ic.com/arpdf/DS1921L-F5X.pdf>.

Day, R.L., (1992). "The Effect of Secondary Ettringite Formation on the Durability of Concrete: A Literature Analysis," Research and Development Bulletin RD108T. Portland Cement Association, Skokie, IL, pp. 59, 83-84.

De Schutter, G, Taerwe, L., (1996). "Degree of hydration-based description of mechanical properties of early age concrete," Materials and Structures, V. 29, July, pp. 335-344.

Devore, J.L., (1995). "Probability and Statistics for Engineering and the Sciences," 4th ed. Duxbury Press, New York, 743 pp.

Eberhardt, M., Lokhorst, S.J., and van Breugel, K., (1994). "On the Reliability of Temperature Differentials as a Criterion for the Risk of Early-Age Thermal Cracking," Rilem Report 25, Thermal Cracking in Mass Concrete, Edited by R. Springenschmid, E & FN Spon, London, pp. 353-360.

Emanuel and Hulsey, (1977). "Prediction of the Thermal Expansion Coefficient of Concrete," Journal of the American Concrete Institute, Vol. 74, No. 4, pp. 149-155.

Emborg, M., (1989). “Thermal Stresses in Concrete Structures at Early Ages,” *Doctoral Thesis*, Luleå University of Technology, Division of Structural Engineering, 280 pp.

Emborg, M., (1998a). “Developing Early Age Mechanical Behaviour.” *Rilem Report 15, Prevention of Thermal Cracking in Concrete at Early Ages*, Edited by R. Springenschmid, E & Fn Spon, London, UK, 76-148.

Emborg, M., (1998b). “Models and Methods for Computation of Thermal Stresses,” In *Rilem Report 15, Prevention of Thermal Cracking in Concrete at Early Ages*, Edited by R. Springenschmid, E & Fn Spon, London, pp. 179-230.

Feldman, R.; Chan, G.; Brouseau, R.; and Tumidajski, P., (1993). “An Investigation of the Rapid Chloride Permeability Test,” Proceedings of the Third Canadian Symposium on Cement and Concrete, Ottawa, August 3-4, pp. 279-306.

Feldman, R.; Prudencio, L.R.; and Chan, G., (1999). “Rapid chloride permeability test on blended cement and other concretes: correlations between charge, initial current and conductivity,” Construction and Building Materials, Vol. 13, pp. 149 – 154.

Feldstein, Dan, (1997), “Galveston causeway needs to be replaced,” Houston Chronicle, November 3, 1997, http://www.chron.com/content/chronicle/page1/97/11/04/causeway.html

Freedman J.M.; Fitzjarrald, D.R.; Moore, K.E.; and Sakai, R.K., (2001). “Boundary Layer Clouds and Vegetation-Atmosphere Feedbacks,” Journal of Climate, V. 14, pp. 180-197.

Freiesleben Hansen, P. and Pedersen, J., (1985). “Curing of Concrete Structures,” CEB Information Bulletin 166, May, 42 p.

Gajda, J., and VanGeem, M., (2002). “Controlling Temperatures in Mass Concrete,” Concrete International, Vol. 24, No. 1, pp. 58-62.

Ge, Z., (2006). “Predicting Temperature and Strength Development of the Field Concrete,” Doctoral Dissertation, Iowa State University.

Gilliland, J.A.; and Dilger, W.H., (1997). “Modeling Concrete Temperature Measured During Construction of the Confederation Bridge,” Proceedings of the Annual Conference of the Canadian Society for Civil Engineering, Sherbrooke, Québec, May 27-30, pp. 187-196.

Glisic, B., (2000). “Fibre Optic Sensors and Behavior in Concrete at Early Age,” Thesis No. 2186, Swiss Federal Institute of Technology, Lausanne, p. 113.

Grasley, Z.C., (2006). "Measuring and Modeling the Time-Dependent Response of Cementitious Materials to Internal Stresses," Doctoral Thesis, The University of Illinois at Urbana Champaign, 238 pp.

Hashida, H., and Yamazaki, N., (2002). "Deformation Composed of Autogenous Shrinkage and Thermal Expansion due to Hydration of High-Strength Concrete and Stress in Reinforced Structures," Proceedings of the Third International Research Seminar on Self-Desiccation and its Importance in Concrete Technology, Edited by B. Persson and G. Fagerlund, Lund, Sweden, June 14-15, pp. 77-92.

Hedlund, H., (2000). "Hardening Concrete: Measurements and evaluation of non-elastic deformation and associated restraint stresses," *Doctoral Thesis*, Luleå University of Technology, Division of Structural Engineering, 394 pp.

Hover, K., (2003). "NHI Course 15123 – Highway Materials Engineering: Portland Cement Concrete Module – Participant Workbook,".

Hover, K.C., (2006). "Evaporation of Water from Concrete Surfaces," ACI Materials Journal, Vol. 103, No. 5, pp. 384-389.

Hermansson, A., (2001). "Mathematical Model for Calculation of Pavement Temperatures," Transportation Research Record, Vol. 1764, pp. 180-188.

Incropera, F.P.; and Dewitt, D.P., (2002). Fundamentals of Heat and Mass Transfer, John Wiley & Sons, Inc., New York, p. 931.

Jensen, O.M.,and Hansen, P.F., (1999). "Influence of temperature on autogenous deformation and relative humidity change in hardening cement paste," Cement and Concrete Research, V 29, PP. 567-575.

Jensen, O.M., and Hansen, P.F., (2001). "Water-entrained cement-based materials – I. Principles and theoretical background," Cement and Concrete Research, Vol. 31, No. 4, pp. 647- 654.

Johnson, R.A., (2000). Miller & Freund's Probability and Statistics for Engineers, Sixth Edition, Upper Saddle River, NJ, Prentice Hall, Inc., 622 pp.

Justnes, H.; T. Hammer, B. Ardoullie, E. Hendrix, D. Van Gemert, k. Overmeer, and E. Sellevold., (1999). "Chemical Shrinkage of Cement Paste, Mortar and Concrete," *Autogenous Shrinkage of Concrete*, edited by Ei-ichi Tazawa, E&FN Spon, London, pp. 211-220.

Kada, H.; Lachemi, M.; Petrov, N.; Bonneau, O.; and Aïtcin, P.C., (2002). "Determination of the coefficient of thermal expansion of high performance concrete from initial setting," Materials and Structures, Vol. 35, No. 245, pp. 35-41.

Kadlečeck Sr., V., Modrý, S., and Kadlečeck Jr., V., (2002). "Size Effect of Test Specimens on Tensile Splitting Strength of Concrete: General Relation," Materials and Structures, Vol. 35, No. 1, pp. 28-34.

Kanstad, T., Ø. Bjøntegaard, E. Sellevold, T. Hammer, and P. Fidjestol., (2001). "Effects of Silica Fume on Crack Sensitivity," Concrete International, Vol. 23, No. 12, pp. 53-59.

Khan, A.A., (1995). "Concrete Properties and Thermal Stress Analysis of Members at Early Ages," Ph.D. Dissertation, Department of Civil Engineering, McGill University, July, 215 pp.

Khan, A.A., Cook, W.D., and Mitchell, D., (1998). "Thermal Properties and Transient Thermal Analysis of Structural Members During Hydration," ACI Materials Journal, Vol. 95, No. 3, pp. 293-303.

Krauss, P.D., and Rogalla, E.A., (1996). Transverse Cracking in Newly Constructed Bridge Decks, NCHRP Report 380, Transportation Research Board, National Research Council, Washington, D.C..

Larson, M., (2003). "Thermal Crack Estimation in early Age Concrete – Models and Methods for Practical Application," *Doctoral Thesis*, Luleå University of Technology, Division of Structural Engineering, 190 pp.

Levinson, R.; and Akbari, H., (2002). "Effects of composition and exposure on the solar reflectance of Portland cement concrete," Cement and Concrete Research, Vol. 32, pp. 1679 – 1698.

Lura, P.; K. van Breugel, and I. Maruyama., (2001). "Effect of Curing Temperature and Type of Cement on Early-age Shrinkage of High-Performance Concrete," *Cement and Concrete Research*, V. 31, pp. 1867-1872.

Lydon, F.D., and Balendran, R.V., (1986). "Some Observations on Elastic Properties of Plain Concrete," Cement and Concrete Research, Vol. 16, No. 3, pp. 314-324.

Ma, W.; Sample, D.; Martin, R.; and Brown, P., (1994). "Calorimetric Study of Cement Blends Containing Fly Ash, Silica Fume, and Slag at Elevated Temperatures," Cement, Concrete, and Aggregates, Vol. 16, pp. 93-99.

Mangold, M., (1994). "Thermal Prestress of Concrete by Surface Cooling," *Rilem Report 25, Thermal Cracking in Concrete at Early Ages*, Edited by R. Springenschmid, E & Fn Spon, London, UK, 265-272.

Mangold, M. (1998). “Methods for Experimental Determination of Thermal Stresses and Crack Sensitivity in the Laboratory.” *Rilem Report 15, Prevention of Thermal Cracking in Concrete at Early Ages*, Edited by R. Springenschmid, E & Fn Spon, London, UK, 26-39.

Meyers, S.L., (1950). “Thermal Expansion Characteristics of Hardened Cement paste and of Concrete,” Proceedings, Highway Research Board, Vol. 30, pp. 193-203.

Mindess, S., Young, J.F., and Darwin, D., (2003). Concrete, 2nd Ed., Pearson Education, Inc., Upper Saddle River, NJ, 644 pp.

Mitchell, L.J., (1953). “Thermal Expansion Tests on Aggregates, Neat Cement, and Concretes,” Proceedings, ASTM, V. 53, pp. 963-977.

Naik, T.R., and S. Singh., (1997). “Influence of Fly Ash on Setting and Hardening Characteristics of Concrete Systems,” *ACI Materials Journal*, Vol. 94, No. 5, pp. 355-360.

National Climatic Data Center, (1993). “Solar and Meteorological Surface Observational Network CDROM,” Version 1.0.

National Climatic Data Center, (2003). “NSRDB Synoptic Format-CDROM Format,” 12 pp.

Oluokun, F.A., Burdette, E.G., and Deatherage, J.H., (1991). “Splitting Tensile Strength and Compressive Strength Relationship at Early Ages,” ACI Materials Journal, Vol. 88, No. 2, pp. 115-121.

Patankar, S.V., (1980). Numerical Heat Transfer and Fluid Flow, McGraw-Hill Book Company, New York, p. 30-66.

Paulini, P., and Gratl, N., (1994). “Stiffness Formation on Early Age Concrete,” In *Rilem Report 25, Thermal Cracking in Mass Concrete*, E & FN Spon, London, pp. 153-160.

Pauw, A., (1960). “Static Modulus of Elasticity of Concrete as Affected by Density,” ACI Journal Proceedings, Vol. 57, No. 6, Dec., pp. 679-687.

Poole, J.L., (2007). “Modeling Temperature Sensitivity and Heat Evolution of Concrete,” Doctoral Dissertation, The University of Texas at Austin, 299 pp.

Poole, J.L., Riding, K.A., Folliard, K.J., Juenger, M.C.G., and Schindler, A.K., (2007a). “Methods for Calculating Activation Energy for Portland Cement,” ACI Materials Journal, Vol. 104, No. 1, pp. 303-311.

Poole, J.L.; Riding, K.A.; Folliard, K.J.; Juenger, M.G.; and Schindler, A.K., (2007b). ”Hydration Study of Cementitious Materials Using Semi-Adiabatic Calorimetry,”ACI Special Publication 241CD Concrete Heat Development: Monitoring, Prediction & Management, Edited by K. Wang & A. Schindler, paper SP-241-5.

Ramaiah, S.V..; Dossey, T.; and B.F. McCullough, (2002). “An Investigation of the Thermacron© I-button for Early-Age and Long-Term Temperature,” TRB 2002 Annual Meeting CD-ROM, 19 pp.

Raphael, J.M., (1984). “Tensile Strength of Concrete,” ACI Journal, Vol. 81, No. 2, pp. 158-165.

Riding, K.A., Poole, J.L., Schindler, A.K., Juenger, M.G., and Folliard, K.J. (2006). “Evaluation of Temperature Prediction Methods for Mass Concrete Members**.”** *ACI Materials Journal*, 103(5), 357-365.

Riding, K.A., Poole, J.L., Juenger, M.G., Schindler, A.K., and Folliard, K.J., (2007a). “Calorimetry Performed On-Site: Methods and Uses,” *ACI Special Publication 241CD Concrete Heat Development: Monitoring, Prediction & Management*, Edited by K. Wang & A. Schindler, paper SP-241-3.

Riding K.A., Poole J.L., Schindler A.K., Juenger M.G., and Folliard K.J., (2007b). “Temperature Boundary Condition Models for Concrete Bridge Members,” *ACI Materials Journal*, Vol. 104, No. 4, pp. 379-387.

Rietveld, H.M., (1969). “A Profile Refinement Method for Nuclear and Magnetic Structure,” *Journal of Applied Crystallography*, Vol. 2, pp. 65-71.

RILEM Technical Committee 119-TCE, (1998). “Adiabatic and Semi-Adiabatic Calorimetry to Determine the temperature Increase in Concrete due to Hydration Heat of Cement,” RILEM Report 15, Prevention of Thermal Cracking in Concrete at Early Ages, Edited by R. Springenshmid, E & FN Spon, London, pp. 315-330.

Rostasy, F.S.; Gutsch, A.; and Laube, M., (1993). "Creep and Relaxation of Concrete at Early Ages - Experiments and Mathematical Modeling," Creep and Shrinkage of Concrete, Edited by Z.P. Bazant and I. Carol, E & Fn Spon, London, pp. 453-458.

Rostásy, F.S., Tanabe, T., and Laube, M., (1998). “Assessment of External Restraint,” Rilem Report 15, Prevention of Thermal Cracking in Concrete at Early Ages, Edited by R. Springenschmid, E & FN Spon, London, UK, pp. 149-177.

Scali, M.J.; Chin, D.; and Berke, N.S., (1987). “Effect of Microsilica and Fly Ash Upon the Microstructure and Permeability of Concrete,” Proceedings of the Ninth

International Conference on Cement Microscopy, Reno, NV, April 5-9, pp. 375-397.

Shilstone, J.M. Sr., and Shilstone, J.M. Jr., (2002). "Performance-Based Concrete Mixtures and Specifications for Today," Concrete International, Vol. 24, No. 2, pp. 80-83.

Schindler, A.K., (2002). "Concrete Hydration, Temperature Development, and Setting at Early-Ages," Doctoral Dissertation, The University of Texas at Austin, 530 pp.

Schindler, A.K., (2004). "Effect of Temperature on Hydration of Cementitious Materials", ACI Materials Journal Vol. 101, No. 1, pp. 72-81.

Schindler, A.K. and Folliard**,** K.J., (2005). "Heat of Hydration Models for Cementitious Materials," ACI Materials Journal, Vol. 102, No. 1, pp. 24-33.

Schöppel, K., M. Plannerer, and R. Springenschmid., (1994). "Determination of Restraint Stresses and of Material Properties During Hydration of Concrete with the Tempertaure-Stress-Testing Machine," In *Rilem Report 25, Thermal Cracking in Mass Concrete*, E & FN Spon, London, pp. 153-160.

Schöppel, K., and R. Springenschmid., (1994). "The Effect of Thermal Deformation, Chemical Shrinkage and Swelling on Restraint Stresses in Concrete at Early ages," In *Rilem Report 25, Thermal Cracking in Mass Concrete*, E & FN Spon, London, pp. 213-220.

Sellevold, E.J. and Bjøntegaard, O., (2006). "Driving Forces to Cracking in Hardenging Concrete: Thermal and Autogenous Deformations," Proceedings of the 2nd International Symposium on Advances in Concrete through Science and Engineering, Sept. 11-13, 2006, Quebec City, Canada, pp. 125-139.

Shah, S.P., Swartz, S.E., and Ouyang, C., (1995). Fracture Mechanics of Concrete: Applications of Fracture Mechanics to Concrete, Rock and Other Quasi-Brittle Materials, Wiley, New York, 591 pp..

Siegel, R.; and Howell, J.R, (1992). Thermal Radiation Heat Transfer, Hemisphere Pub. Corp., Washington D.C., 1072 pp.

Springenschmid, R. and R. Breitenbücher., (1998). "Influence of Constituents, Mix Proportions and Temperature on Cracking Sensitivity of Concrete," In *Rilem Report 15, Prevention of Thermal Cracking in Concrete at Early Ages*, Edited by R. Springenschmid, E & Fn Spon, London, pp. 40-50.

Springenschmid, R., Brietenbücher, R., and Mangold, M., (1994). “Development of the Cracking Frame and the Temperature-Stress Testing Machine,” In *Rilem Report 25, Thermal Cracking in Mass Concrete*, E & FN Spon, London, pp. 153-160.

Stanish, K. D., R. D. Hooton, and M. D. A Thomas, (2000). “Testing the Chloride Penetration Resistance of Concrete: A Literature Review,” FHWA Contract DTFH61-97-R-00022. University of Toronto, Toronto, Ontario, Canada. June. 31 pp.

The Associated Press, (2003). Queen Isabella Causeway gets greater protection . 5 Nov. 2003. Amarillo Globe News. 19 Mar. 2004 <http://www.amarillonet.com/stories/091403/tex_queenisabella.shtml>.

Texas Department of Transportation, (2002). Texas Tollways.com. 8 June 2004 <http://www.texastollways.com/tta/index.asp>.

Thomas, J.J., and Jennings, H.M., (2006). “A Colloidal Interpretation of Chemical Aging of the C-S-H Gel and its Effects on the Properties of Cement Paste,” *Cement and Concrete Research*, Vol. 36, No. 1, pp. 30-38.

Tuthill, L., and Cordon, W.A., (1955). “Properties and Uses of Initially Retarded Concrete,” *Journal of the American Concrete Institute*, Vol. 27, No. 3, pp. 273-286.

Tuutti, K., (1982). “Corrosion of Steel in Concrete,” Swedish Cement and Concrete Research Institute, Report No. 4-82.

TxDOT, (2004). “Special Provision 421 – Hydraulic Cement Concrete,” Texas Department of Transportation.

USDOT, (2006). “Reduced Congestion Strategic Goal,” http://www.dot.gov/stratplan2011/redcong.htm,http://www.dot.gov/stratplan2011/redcong.htm United States Department of Transportation, Accessed May 2007.

van Breugel, K., (1998). “Prediction of Temperature Development in Hardening Concrete,” RILEM Report 15, Prevention of Thermal Cracking in Concrete at Early Ages, Edited by R. Springenshmid, E & FN Spon, London, pp. 51- 75.

van Breugel, K, and Lokhorst, S.J., (2001). “Stress-Based Crack Criterion as a Basis for Prevention of Through-Cracks in Concrete Structures at Early Ages,” Early Age Cracking in Cementitious Systems, Edited by A. Bentur and K. Kovler, Haifa, Israel, March 12-14, pp. 229-236.

Viviani, M., (2005). “Monitoring and Modeling of Construction Materials During Hardening,” Doctoral Thesis, Swiss Federal Institute of Technology, Lausanne, Switzerland, 172 pp.

Walenta, G., and Füllman, T., (2004). “Advances in Quantitative XRD Analysis for Clinker, Cements, and Cementitious Additions,” *Advances in X-Ray Analysis*, Vol. 47, pp. 287-296.

Walker, S., Bloem, D.L., and Mullen, W.G., (1952). “Effects of Temperature Changes on Concrete as Influenced by Aggregates,” Journal of the American Concrete Institute, Vol. 48, pp. 661-679.

Watt Engineering, Ltd, (1978). “On the Nature and Distibution of Solar Radiation,” U.S. Department of Energy, U.S. Government Printing Office Stock No. 016-000-00044-5, p. 57.

Westman, G., (1999). “Concrete Creep and Thermal Stresses,” *Doctoral Thesis*, Luleå University of Technology, Division of Structural Engineering, 301 pp.

Whigham, J., (2005). “Evaluation of Restraint Stresses and Cracking in Early-Age Concrete with the Rigid Cracking Frame,” Master’s Thesis, Auburn University, p. 169, 192.

Whiting, D., (1981). “Rapid Determination of the Chloride Permeability of Concrete,” Final Report No. FHWA/RD-81/119, Federal Highway Administration, NTIS No. PB 82140724.

WISA Wood Products. (2000). Kymmene Corporation. 9 June 2004 <http://fikyrsk13.upm-kymmene.com/sch/internet/schintern3.nsf/71e61a4d7077d9f ec225689a00444eb7/9412d4ec143d0b94c225696e005056c3?OpenDocument>.

Wojcik, G.S., (2004). “Effects of Atmospheric and Construction Conditions on Concrete Equivalent Ages,” ACI Materials Journal, V. 101, No. 5, pp. 376-384.

Wojcik, G.S.; and Fitzjarrald, D.R., (2001). “Energy Balances of Curing Concrete Bridge Decks,” Journal of Applied Meteorology, Vol. 40, No. 11, pp. 2003-2025.

Yamakawa, H, H. Nakauchi, T. Kita, and H. Onuma., (1986). “A Study of the Coefficient of Thermal Expansion of Concrete,” *Transactions of the Japan Concrete Institute*, V. 8, pp. 111-118.

Yoshitake, I., Nagai, S., Tanimoto, T., and Hamada, S., (2002). “Simple Estimation of the Ground Water Temperature and Snow Melting Process,” Proceedings of The

11th Standing International Road Weather Commission, Sapporo, Japan, January 26-28, 8 pp.

Zhao, T.J.; Zhou, Z.H.; Zhu, J.Q.; and Feng, N.Q., (1998). "An Alternating Test Method for Concrete Permeability," Cement and Concrete Research, Vol. 28, No. 1, pp. 7-12.

Vita

Kyle Austin Riding was born in Baltimore, MD on May 5, 1978 to Don and Donna Riding. He graduated from Edison High School in Fresno, CA in 1996. He then enrolled in Brigham Young University where he received a Bachelor of Science in Civil Engineering. In September, 2002 he entered graduate school at the University of Texas at Austin, where he worked as a graduate research assistant for Dr. Kevin Folliard and Maria Juenger at the Concrete Durability Center. He received a Master's of Science in Engineering degree from the University of Texas at Austin in 2004.

Permanent address: 1254 E. Vartikian, Fresno CA 93710

This dissertation was typed by the author.